SYNTHESIS AND CHARACTERIZATION OF CHALCONE BASED 1,2,3-TRIAZOLE VIA CuAAC REACTION AND THEIR APPLICATION AS CHEMOSENSORS

Thesis Submitted for the Award of the Degree of

DOCTOR OF PHILOSOPHY (Ph.D.)

in

Chemistry

By

Riddima Singh
Registration number: 12109118

Supervised By

Dr. Jandeep Singh (19394)

School of Chemical Engineering and

Physical Sciences (Associate Professor)

Lovely Professional University,

Phagwara, Punjab

Co-Supervised by

Dr. Gurpreet Kaur

Assistant Professor, GGN

Khalsa College, Ludhiana, Punjab

LOVELY PROFESSIONAL UNIVERSITY
PUNJAB

2025

DECLARATION

I, hereby declared that the presented work in the thesis entitled "**SYNTHESIS AND CHARACTERIZATION OF CHALCONE BASED 1,2,3-TRIAZOLE VIA CuAAC REACTION AND THEIR APPLICATION AS CHEMOSENSORS**" in fulfillment of degree of **Doctor of Philosophy (Ph.D.)** is outcome of research work carried out by me under the supervision of Dr. Jandeep Singh, working as Associate Professor in the School of Chemical Engineering and Physical Sciences and Dr. Gurpreet Kaur, working as Assistant Professor in GGN Khalsa College, Ludhiana, India. In keeping with general practice of reporting scientific observations, due acknowledgements have been made whenever work described here has been based on findings of other investigators. This work has not been submitted in part or full to any other University or Institute for the award of any degree.

(Signature of Scholar)

Name of the scholar: Riddima Singh

Registration No.: 12109118

Department/school: School of Chemical Engineering and Physical Sciences,

Lovely Professional University, Punjab, India

CERTIFICATE

This is to certify that the work reported in the Ph. D. thesis entitled **"SYNTHESIS AND CHARACTERIZATION OF CHALCONE BASED 1,2,3-TRIAZOLE VIA CuAAC REACTION AND THEIR APPLICATION AS CHEMOSENSORS"** submitted in fulfillment of the requirement for the award of degree of **Doctor of Philosophy (Ph.D.)** in the School of Chemical Engineering and Physical Sciences, is a research work carried out by Riddima Singh, Registration No. 12109118, is bonafide record of his original work carried out under mysupervision and that no part of thesis has been submitted for any other degree, diploma orequivalent course.

(Signature of Supervisor)

Dr. Jandeep Singh

Associate Professor in Chemistry

School of Chemical Engineering
and Physical Sciences,
Lovely Professional University,
Phagwara, Punjab-144001

(Signature of Co-Supervisor)

Dr. Gurpreet Kaur

Assistant Professor in Chemistry

GGN Khalsa College, Ludhiana

Abstract

'Click Chemistry' a concept introduced by Sir Karl Barry Sharpless in 2001, transformed the chemical synthesis by enabling efficient, selective, and direct product formation of complex molecules. Click Chemistry has gained significant attention, with CuAAC emerging as one of the most widely used synthetic approaches due to its modularity, broad applicability, high yield and stereospecificity. These key advantages make it highly efficient for synthesizing 1,4-disubstituted 1,2,3-triazoles via the cycloaddition of a terminal alkyne and an organic azide, catalyzed by a Cu(I) catalyst. The reaction is regioselective, tolerates a wide range of functional groups, and operates under mild, environment friendly conditions, making it indispensable in modern synthetic chemistry. The remarkable ability of this synthetic methodology to rapidly synthesize structurally diverse 1,2,3 triazole derivatives have paved the way for new avenues for the creation of complex molecules with tailored functionalities.

Chalcones, characterized by their unsaturated ketone structure, offer a versatile platform for functionalization, due to the presence of carbonyl group and extended conjugation, making them sensitive to the changes in their environment. These features are particularly useful in synthesizing ion sensors, where chalcone backbone can be modified to enhance selectivity and sensitivity. Incorporating the 1,2,3-triazole ring into chalcone structure via CuAAC further expands the versatility of these molecules, as the chalcone-based 1,2,3-triazoles represent a unique class of hybrid molecules that combine the photophysical properties of chalcones with the chemical diversity of 1,2,3-triazoles, resulting in compounds with enhanced fluorescence and metal-binding capabilities, thereby making them valuable tools in environmental monitoring and biological systems.

The chalcone based 1,2,3-triazole derivatives have great significance in the metal ion detection. Metal ion detection is crucial for monitoring environmental pollution, ensuring food safety, and diagnosing various health conditions. Reliable detection methods allow for the identification of trace metal concentration in samples, providing insights into their physiological roles and potential toxic effects. The presence of nitrogen in the 1,2,3 triazole structure, these sensors undergo specific structural changes upon binding with metal ion, often resulting in noticeable shifts, observed by UV-Visible/or fluorescence spectrophotometer, allowing for sensitive and selective metal ion detection. Therefore, due to the efficiency and reliability of CuAAC for regioselective synthesis of 1,2,3-triazole, this method was chosen as

a core approach in this research. Based on the literature review of the chalcone based 1,2,3-triazoles via 'CuAAC' methodology, following are the main objectives of the proposed research work.

1) Synthesis of new chalcone based 1,2,3–triazole derivatives via Cu(I) catalysed alkyne azide cycloaddition reaction.

2) Characterization of the synthesized novel compounds by spectroscopic techniques like IR, NMR (^{1}H, ^{13}C) and mass spectrometry.

3) Exploring ion sensing behaviour of the synthesized 1,2,3–triazole derivatives using different spectroscopic techniques.

A total of six chalcone-based 1,2,3-triazole derivatives were synthesized via 'CuAAC' and characterized using a different spectroscopic technique like IR, ^{1}H NMR, ^{13}C NMR and mass spectrometry. These chalcone appended 1,2,3-triazole derivatives were subsequently employed as selective chemosensors.

Chalcones, known for their conjugated carbonyl system and chromophoric properties, serves as essential precursors for synthesizing a variety of bioactive molecules. In this thesis, chalcones are modified to form chalcone based alkynes, which acted as a key molecule for the synthesis of 1,2,3-triazole derivatives. The chalcone was synthesised by the reaction of an aldehyde and a ketone in the presence of potassium hydroxide as a base and ethanol as a solvent. The synthesis of terminal alkyne was carried out through nucleophilic substitution of a propargyl group onto chalcone containing labile protons, preferably amino groups, in the presence of a base like K_2CO_3. To quench the reaction, ice-cold water was added and the product was separated by filtration of precipitates or solvent extraction for liquid products. For the synthesis of organic azide, starting material like benzyl chloride was reacted with sodium azide (NaN_3) at a temperature range 85-90 °C to yield the organic azide. The organic azide was subsequently subjected to a 'CuAAC' with terminal alkynes, leading to the efficient synthesis of chalcone-based 1,4-disubstituted 1,2,3-triazoles. The synthesized compounds were characterized using a range of spectroscopic techniques, including IR, ^{1}H NMR, ^{13}C NMR and mass spectrometry.

The ion-sensing capabilities of chalcone-based 1,2,3-triazole derivatives were assessed using UV-Visible and fluorescence spectroscopy for various metal ions such as Cr(III), Mn(II), Fe(III), Fe(II), Zn(II), Pb(II), Hg(II), Cd(II), Ce(III), Ba(II), Ca(II), Mg(II),Na(I), K(I), Cu(II), Ni(II), Co(II), in appropriate solvents. The changes in the absorption and emission responses of the newly synthesized chalcone-based 1,2,3-triazole derivatives upon metal ion binding,

highlighting their selectivity towards various metal ions, are presented in this thesis through series of graphs and figures to assess the chemosensing potential. Additionally, analytical parameters such as the stoichiometric ratio, association constant (K_a), limit of detection (LoD), and limit of quantification (LoQ) of the sensors towards certain metal ions were calculated and presented.

Acknowledgement

I am deeply humbled as I pen these acknowledgments, a small reflection of the immense gratitude I feel for all those whose contributions have shaped this doctoral journey. First and foremost, I offer my heartfelt thanks to **Lord Shiva**, whose divine guidance and inspiration have provided me with the strength and motivation to delve into the world of knowledge.

I am profoundly grateful to my esteemed supervisors, **Dr. Jandeep Singh and Dr. Gurpreet Kaur,** whose exceptional wisdom and insight have been pivotal in guiding me through this academic journey. Your steadfast mentorship, thoughtful advice, and unwavering support have not only enriched my academic path but also molded my intellectual growth. Your dedication to excellence has inspired me to become a more capable and insightful individual.

To my parents, **Mr. Vivek Singh Atwal and Mrs. Meenakshi Atwal,** whose blessings and unconditional love have been my guiding light through the challenges of academia, I owe everything. Your sacrifices, unwavering belief in my potential, and constant encouragement have been the foundation upon which my achievements rest. My gratitude extends to my brother, **Er. Rishit Atwal**, and the entire family, whose endless support has been invaluable in both difficult times and moments of celebration.

To my dear friends, both old and new, your friendship has provided much-needed balance and support throughout this rigorous academic journey. I would like to express my heartfelt gratitude to my research colleague and dear friend, **Dr. Gurleen Singh**, for his stimulating discussions, intellectual insights, and shared moments of laughter, all of which have brought vitality to this journey. I am also deeply thankful to my research colleagues, **Miss Nancy George** and **Dr. Parveen Saini** for their valuable contributions and support, which have enriched this experience.

To the Almighty, my respected supervisors, my family, friends, and research colleagues, your influence and support have left an indelible mark on this journey, continuously driving me toward greater knowledge and enlightenment.

Riddima Singh

TABLE OF CONTENTS

Chapter II: Review of Literature

Part B: Analysis of Photophysical data

LIST OF FIGURES, SCHEMES AND TABLES

FIGURES

Content

Chapter I

SCHEMES

Content

Chapter III

TABLES

Contents

Chapter II

LIST OF ABBREVIATIONS

STANDARD UNITS

Abbreviation	Meaning
%	Percentage
°C	Degree Celsius
Å	Angstrom
atm	Atmosphere
cm	Centimeter
equiv.	Equivalent(s)
et al.	Latin for 'and others'
g	Gram(s)
h	Hours(s)
Hz	Hertz
K	Kelvin
Kcal/mol	Kilocalories per mole
MHz	Megahertz
min	Minute(s)
ml	Millilitre(s)
mmol	Millimole(s)
mol	Mole(s)
mp	Melting Point
nm	Nanometer(s)
ppm	Parts Per Million

Miscellaneous

Abbreviation	Meaning
m	Multiplet
s	Singlet
stirr	Stirring
t	Triplet
TLC	Thin layer chromatography
UV	Ultraviolet
w/v	Weight /Volume
NMR	Nuclear magnetic resonance
rt	Room temperature
MS	Mass spectrum
LCMS	Liquid chromatography mass spectrum
IR	Infrared
J	Coupling constant
H	Hydrogen
d	Doublet
dd	Doublet of doublet
CuAAC	Copper(I)-catalyzed alkyne azide cycloaddition
μM	Micro molar
μw	Microwave
δ	Delta
ε_{max}	Molar absorptivity coefficient
λ_{em}	Emission wavelength
λ_{ex}	Excitation wavelength
λ_{max}	Wavelength of maximum absorption

Chapter I

Introduction

This section of the thesis explains the key terminologies, methodologies, and recent advancements related to the undertaken research, which will be detailed in subsequent chapters. It provides an in-depth review of the existing literature, specifically, it outlines the important aspects considered when addressing the identified research gap and integrated to form a comprehensive and conclusive study. This study not only contextualizes the research within the scientific field but also elucidates the approach employed to bridge the proposed research gap.

1.1. Organic Chemistry

Organic compounds play central part in the production of many materials including synthetic fibres[1], pharmaceuticals, dyes, fertilizers, cosmetics, fuels, etc.[2,3] that can range from simple hydrocarbons, to alcohols, amines, and ketones, giving them distinct chemical characteristics.[4,5] The study of heterocyclic compounds—wherein, one or more than one carbon atoms in a ring are substituted by other elements like nitrogen, oxygen, sulphur, etc. became crucial, as these structures are integral to many biological molecules and pharmaceuticals.[6]

1.2. Heterocyclic Compounds

Half of the reported organic compounds are encompassed under the category of 'heterocyclic' compounds,[7,8] having aromatic as well as non-aromatic ring structures.[9,10] Heterocyclic compounds are capable of exhibiting aromaticity[11], provided that the ring structure meets the requisite criteria such as having a certain number of electrons that allows for a continuous overlap of p-orbitals, and making them more stable as compared to non-aromatic heterocycles.[12,13] The structural properties of heterocyclic compounds are crucial for predicting their behaviour, reactivity, and chemical interactions, including electrophilic or nucleophilic substitutions, catalysis, and coordination chemistry. Furthermore, in biological interactions, these compounds play important roles in enzyme-substrate interactions, receptor binding, and metabolic processes, influencing their function in biological systems.[14–17]

1.2.1. Classification of Heterocyclic Compounds

Heterocyclic compounds can be classified based on aromaticity, electronic properties, or functional group interactions as well as can be grouped based upon their natural or synthetic accessibility.[10] Additionally, heterocyclic compounds can also be classified based on several criteria like size of the ring, the type of heteroatoms, and the saturation level of the ring, as illustrated in **figure 1.1** and **figure 1.2**.

➢ **By Ring Size**

The heterocyclic compounds can be systematically categorized based on their ring size, including 3 to 6-membered, and fused heterocycles, which significantly influence their chemical reactivity as well as properties.[18] 3-Membered heterocycles often possess significant ring strain, leading to high reactivity and unique chemical behaviour whereas 4-membered heterocycles also experience ring strain and exhibit distinct reactivity patterns useful in organic synthesis and medicinal chemistry. 5-Membered heterocycles include well-known compounds such as pyrrole, furan, triazole, thiophene, etc are crucial structural components for various

antibacterials. Six-membered heterocycles, such as aromatic pyridine and non-aromatic piperidine, generally have lower ring strain, resulting in a balance of stability and reactivity that makes them versatile in chemical synthesis and pharmacological application.[14–17] Fused heterocycles, involving two or more rings sharing common atoms, such as indole and quinoline, often exhibit unique properties that are not present in their parent ring structure, offering enhanced stability and complex reactivity profiles suitable for advanced material sciences and drug development.[19,20]
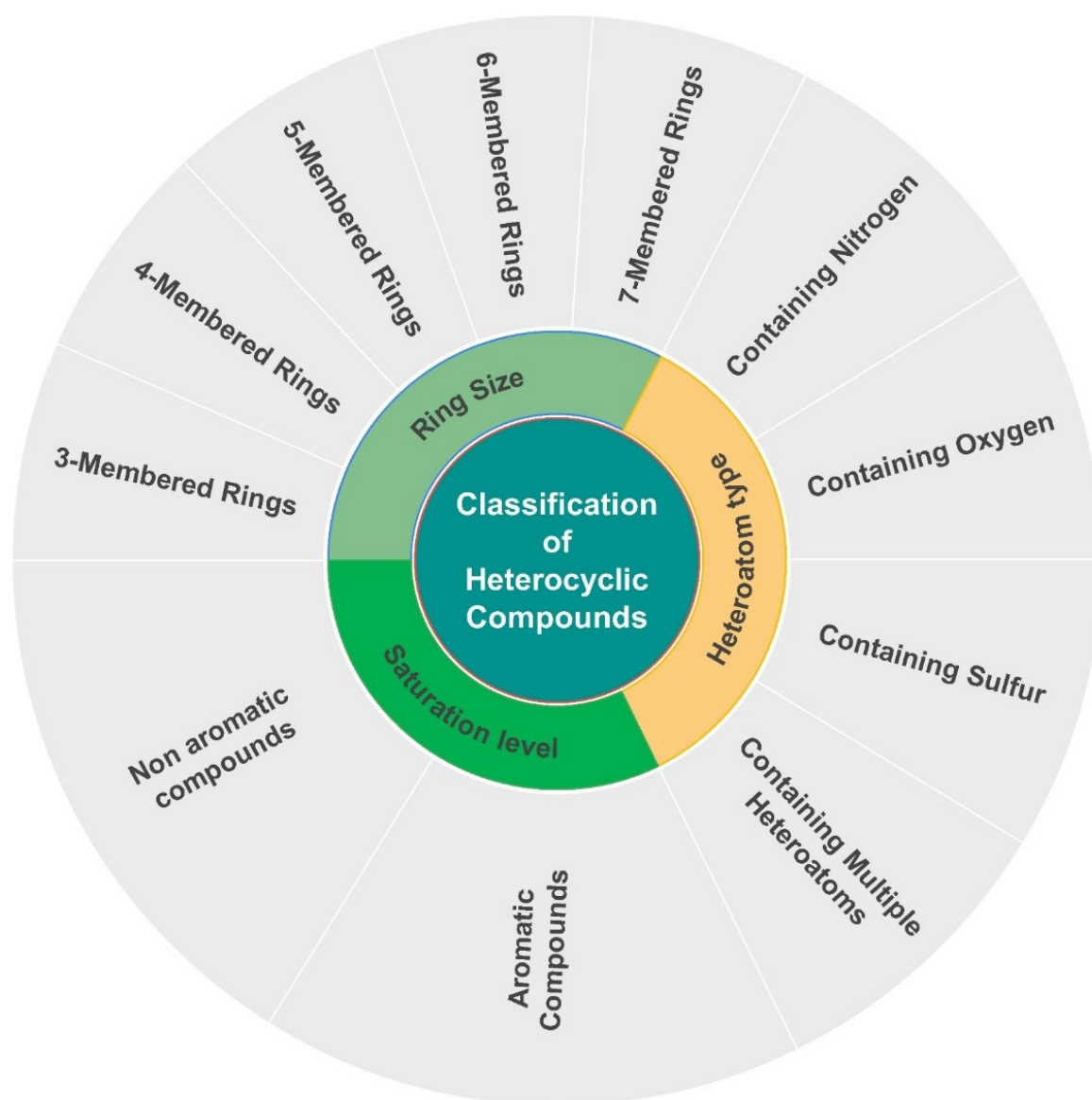
Figure 1.1: An illustration of the classification of heterocyclic compounds based on ring size, heteroatom type, and saturation level[14–17]
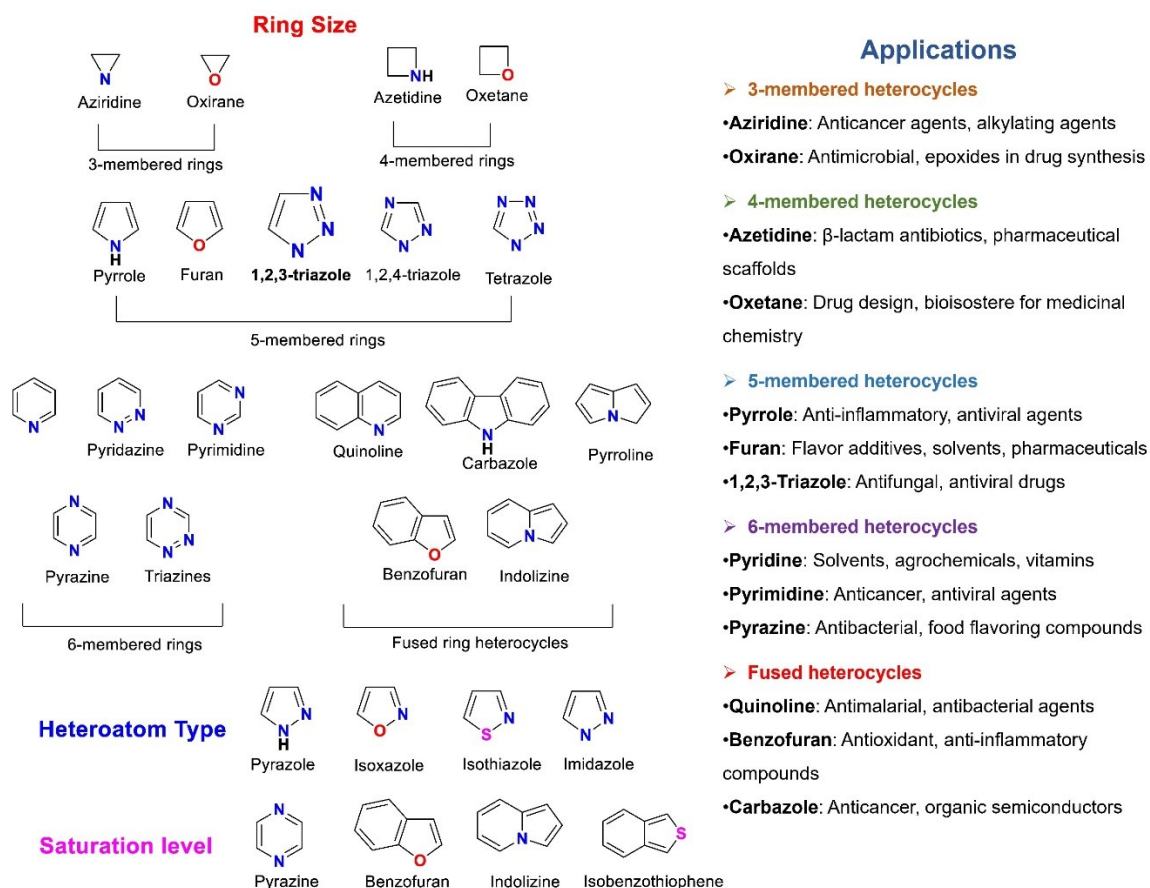
Figure 1.2: Illustrate the hierarchical classification of heterocyclic compounds according to ring size, heteroatom type, and saturation level and their applications[10,14]

> **By Heteroatom Type**

Heterocyclic compounds can also be classified based upon the type and number of heteroatoms present in the ring and thus play noteworthy role in the determination of their chemical properties and regulate their reactivity.[21,22] For instance, 1) nitrogen heterocycles include pyrrole, pyridine, indole, quinoline, etc. are particularly significant in medicinal chemistry; 2) Oxygen containing heterocycles include furan, benzofuran, etc. are known for their roles in both natural products and synthetic materials like conducting polymers, resins, agrochemicals and pharmaceuticals.[23–25] 3) Similarly, sulphur containing heterocycles like thiophene, benzothiophene, and thiazoles, and are important in various chemical industries like organic semiconductors, agrochemicals and dyes. Furthermore, the number of heteroatoms within the ring also impacts the properties of these compounds such as imidazole, which contains two nitrogen atoms in five-membered rings, and pyrimidine, which features two nitrogen atoms in a six-membered ring, exhibits distinct electronic and steric hindrance characteristics.[26,27]

➤ **By Saturation Level**

The saturation level of the ring/aromaticity is another crucial factor in the classification of heterocyclic compounds[16,28] such as five or six-membered rings with one or multiple heteroatoms. These heterocycles have unique chemical properties, such as enhanced stability and distinct reactivity patterns, making them essential in various applications, including pharmaceuticals, agrochemicals, and organic electronics, whereas non-aromatic heterocycles do not have fully conjugated π-system and include compounds like tetrahydrofuran (THF), piperidine, etc.[29–31]

1.2.2. Synthesis of different Heterocyclic Compounds

The synthesis of heterocyclic compounds follows key synthetic strategies like Diels-Alder reaction[32], involving the cycloaddition of a conjugated diene with a suitable dienophile, which can include heteroatoms to produce compounds like pyran or thiopyran.[33,34] The Hantzsch reaction synthesizes dihydropyridines via three-component condensation of aldehydes, β-keto esters, and ammonia or amines.[35] Additionally, Pechmann condensation allows for the synthesis of flavonoids, which are polycyclic compounds containing heterocycles, through the reaction of phenols with β-keto esters in the presence of acid catalysts.[36] The Mannich reaction leads to the formatoion of β-amino carbonyl compounds, which can further cyclize into nitrogen-containing heterocycles such as piperidines.[37–39] The CuAAC reaction, is another powerful approach for constructing heterocycles like 1,2,3-triazole derivatives exclusively.[40,41] The synthetic methodology is known for its efficiency and versatile production of N-based heterocyclic compounds, which have been proved to be crucial for advancements in diverse research areas like pharmaceuticals, material science, agriculture, bioconjugation, nanotechnology, and environmental science.[42]

1.3. Click Chemistry

The term 'Click Chemistry' was coined by Sir Karl Barry Sharpless to describe a set of reactions that are highly reliable and efficient that form the basis for synthesizing a wide variety of complex molecules from relatively small molecules using benign reaction conditions.[43] The process exhibits distinctive properties such as modularity, wide scope, high yield, use of benign solvents, and simple product isolation. If purification is required, non-chromatographic methods such as crystallization should be used, ensuring that the product remains stable under physiological conditions. (**figure 1.3**). This approach is driven by a strategy that promotes irreversible connections between the substrates involved in the reactions.[44,45] These conditions are advantageous for ensuring the practicality and broad applicability of click reactions, especially in organic solvents which are of high significance in polymer and material

science.[46,47] The 'CuAAC' reaction serves as a reliable, efficient, simple and robust molecular linking methodology; this has gained widespread application in organic synthesis due to its ability to facilitate the creation of desirable compounds with precise control and high selectivity.[48]
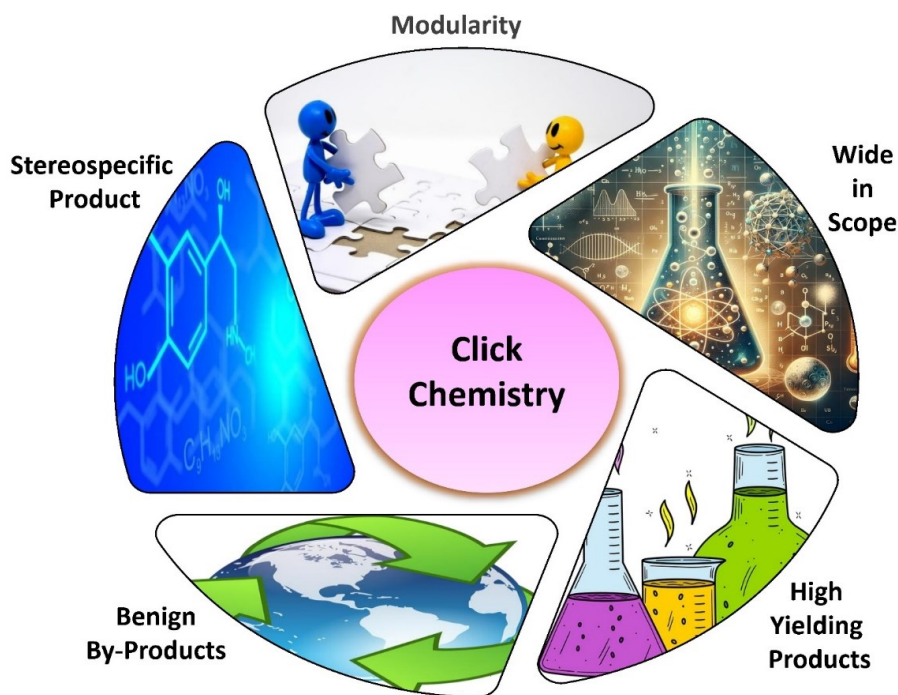
Figure 1.3: Depicting key characteristics of Click Chemistry methodology

1.3.1. Historical Background

1.3.1.1. 1,3-Dipolar Cycloaddition – A key reaction in synthetic chemistry

The Huisgen 1,3-dipolar cycloaddition reaction, pioneered by Rolf Huisgen in the early 1960s, stands as a pivotal evolutionary development in 3+2 cycloaddition reaction that involves the reaction between a 1,3-dipole and a dipolarophile to form five-membered heterocycles (**figure 1.4**).[49] The 1,3-dipoles are generally three-atom π-electrons systems represented by zwitterion octet resonance structures, which undergoes cycloaddition with multiple bond system, termed as 'dipolarophile'. Common examples of 1,3-dipoles include nitrile imines, azomethine ylides, and diazo compounds, whereas compounds such as alkenes and alkynes are encompassed under dipolarophiles. The mechanism of 1,3-dipolar cycloaddition involves the concerted overlap of the frontier molecular orbitals of the 1,3-dipole and the dipolarophile. 1,3-Dipolar cycloaddition reactions are extensively utilized in the synthesis of natural products, pharmaceuticals, and advanced materials such as the synthesis of isoxazoles, pyrazoles, and

1,2,3-triazoles-scaffolds found in many bioactive compounds.[50–52] The integration of alkyne and azide components into a diverse array of substituents presents significant advantages for the 1,3-dipolar cycloaddition reaction. However, the reaction was plagued for more than 40 years due to the lack of selectivity, yielding a mixture of 1,4 and 1,5-regioisomers. Additionally, this reaction requires high temperature and the separation of two isomers becomes challenging.[53]
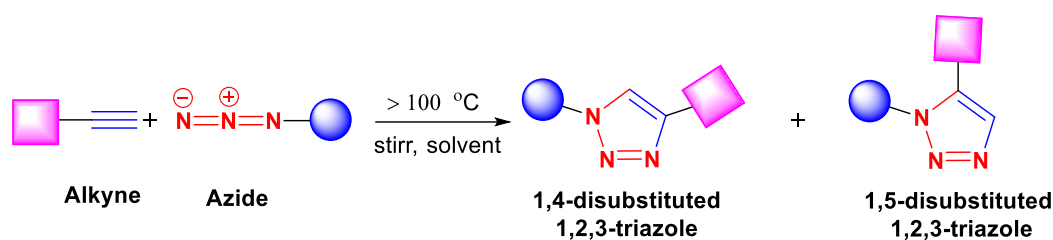
Figure 1.4: A schematic representation of the Huisgen cycloaddition reaction[54]

1.3.1.2. Development of 'CuAAC': A Variant of the Huisgen Reaction

The development of 'CuAAC', a variant of the Huisgen reaction, has revolutionized the synthetic chemistry by providing a reliable, high-yielding, and regioselective methodology for constructing 1,4-disubstituted 1,2,3-triazoles. Developed independently by Dr. Morten Meldal and Dr. Karl Barry Sharpless in the early 2000s,[55,56] the reaction involves the use of Cu(I) species as the catalyst which not only enhances the rate of the reaction but also leads to the regioselective synthesis of 1,4-disubstituted 1,2,3-triazoles (**figure 1.5**), thereby overcoming the limitations of the Huisgen Cycloaddition. This reaction is widely used in bioconjugation, materials science, and polymer chemistry due to its robustness and broad substrate scope.[57,58] The development of metal-catalyzed and organocatalytic variants has enabled the reaction to proceed under milder conditions, enhancing functional group tolerance and increasing the reaction's applicability.[59,60]
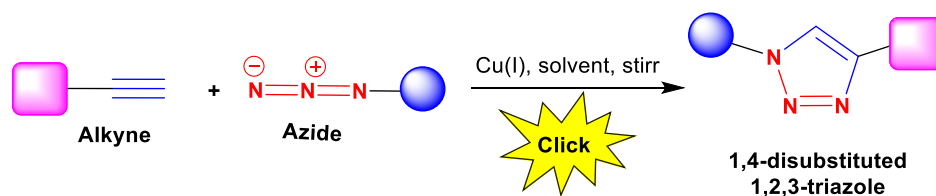
Figure 1.5: A schematic representation of 'CuAAC' reaction for the synthesis of 1,4-disubstituted 1,2,3-triazole[54]

1.3.2. Mechanism of CuAAC

Sharpless and co-workers proposed a mononuclear mechanism for CuAAC,[61] The reaction initiates with the deprotonation of the terminal alkyne, followed by its complexation with the copper(I) catalyst, leading to the formation of a Cu(I)-acetylide complex. This is followed by the coordination of the organic azide to the same copper centre, positioning the azide in close proximity to the acetylide. A nucleophilic attack occurs, forming a C-N bond between the azide and the alkyne, which leads to the formation of a six-membered metalacyclic intermediate. This transformation involves a two-electron oxidation of the copper from Cu(I) to Cu(III). After the formation of the Cu(III) metallacycle, the structure undergoes a ring contraction and is accompanied by the reduction of the copper from the +3 oxidation state back to the +1 state to form Cu(I)-triazolide complex. In the final step, the triazolide complex undergoes deprotonation, releasing the copper catalyst and yielding the final 1,4-disubstituted 1,2,3-triazole product. The copper(I) species is now free to re-enter the catalytic cycle, facilitating further reactions[62] (**figure 1.6**). The whole mechanism is briefly explained sequentially in the following steps:
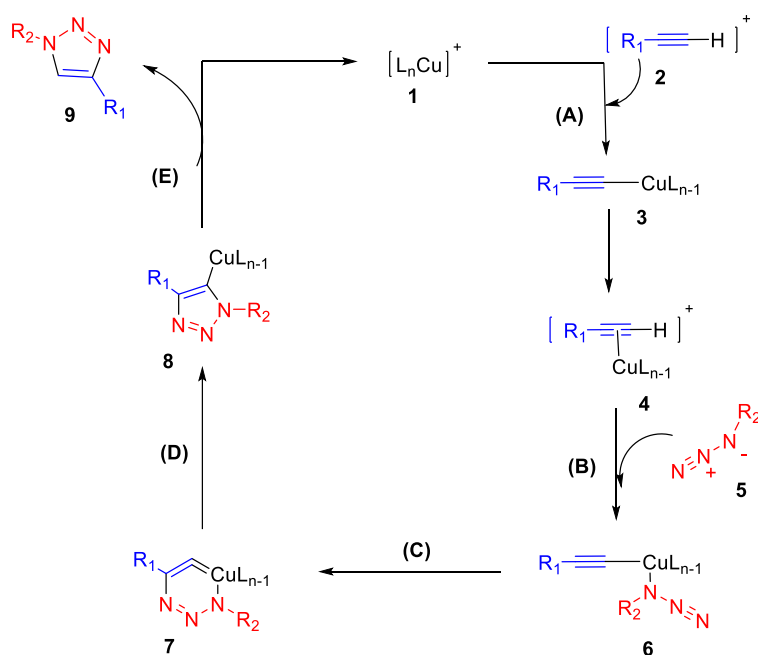
Figure 1.6: Illustrating the mononuclear mechanism of CuAAC proposed by Sharpless *et al.*[62]

(A) Formation of Cu(I)-acetylide complex.

(B) Coordination of the organic azide to the copper(I)-acetylide complex.

(C) Formation of six-membered Cu(III)-metallacyclic intermediate.

(D) Ring contraction and reduction of Cu from +3 to +1 to form a cuprous triazolide complex.

(E) Formation of the 1,4-disubstituted 1,2,3-triazole.

With the advancement in research studies, a binuclear mechanism was reported by Finn and Fokin showing two copper atoms binding to the alkyne on different positions forming π – complex followed by the azide nucleophilic attack leading to the formation of six-membered rings. The product was then obtained by the new C-N bond formation.[61,63] The proposed mechanism (**figure 1.7**) is envisioned through the following steps:

(A) σ, π-dicopper-acetylide complex is formed.

(B)   The azide group is coordinated with the dicopper-acetylide complex via one Cu(I) and the alkylated nitrogen, leading to the synthesis of the ternary complex.

(C)   Oxidation of second Cu(I) from +1 to +3, resulting in the formation of a metallacycle.

(D)   Ring contraction, yielding the Cu(I)-triazolide complex, accompanied by the reduction of Cu(III) to Cu(I).

(E)   Protonation of triazolide complex, producing 1,2,3-triazole moiety.
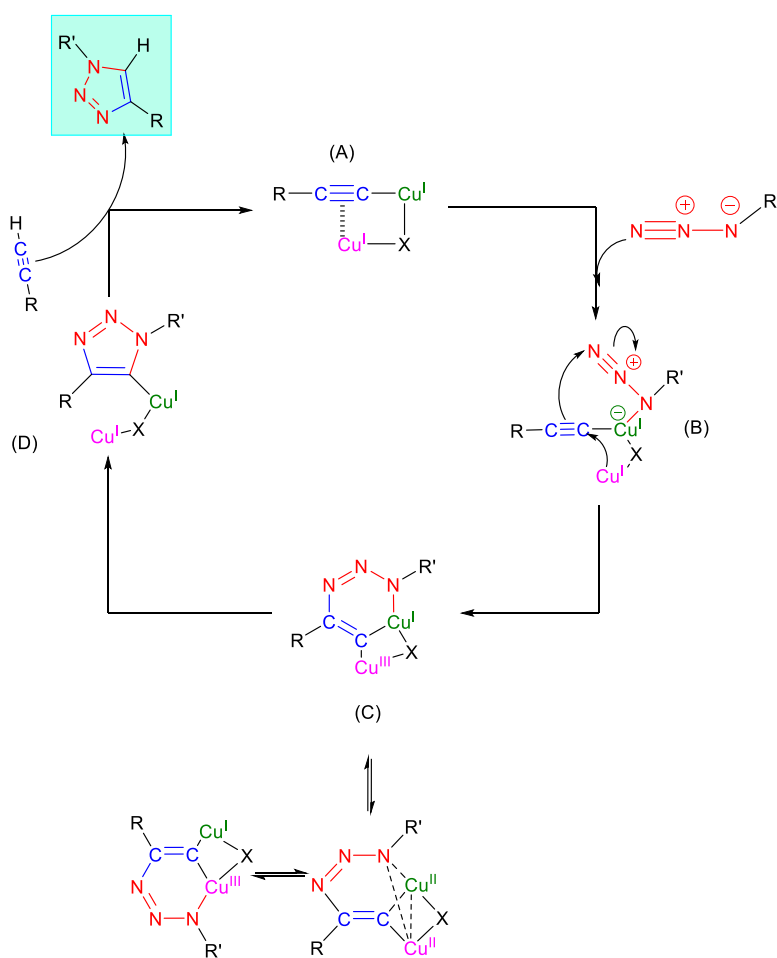
Figure 1.7: An illustration of the binuclear mechanism of CuAAC proposed by Finn and Folkin[63]

1.4. Various substituents for click reactions

The synthesis of 1,4-disubstituted 1,2,3-triazole derivatives via click reactions has garnered extensive attention in the literature, with a wide array of methodologies developed to incorporate various substituents onto the 1,2,3-triazole backbone. These 1,2,3-triazole derivatives often utilize different structural frameworks such as Schiff bases, chalcones, dendrimers, polymers, etc,[64–66] commonly containing aromatic substituents, particularly benzene rings functionalized with electron-donating groups (-OCH$_3$, -OH, etc.) and/or electron-withdrawing groups (-NO$_2$, -CN, halogens, etc.)[67,68] Moreover, the inclusion of heterocyclic rings, like pyridine, provides additional opportunities for functionalization and fine-tuning of the chemical reactivity and coordination abilities of the 1,2,3-triazole derivatives.[69] Furthermore, more complex substituents, such as dendritic or polymeric structures, allow for the development of highly functionalized 1,2,3-triazole systems with enhanced solubility, stability, and multifunctional properties.[70] Overall, the strategic selection of substituents for click reactions enables tailored physical, chemical, and electronic properties of 1,2,3-triazoles, making them suitable for a wide range of applications, including metal ion detection, drug development, and materials science.[71]

1.4.1. Chalcones

Chalcones are a class of organic compounds belonging to the flavonoid family with the core structure of Ar-CO-CH=CH-Ar' linked together by a three-carbon α, β-unsaturated carbonyl system, wherein Ar and Ar' are aromatic rings which can be either the same or different and may contain various substituents.[72]
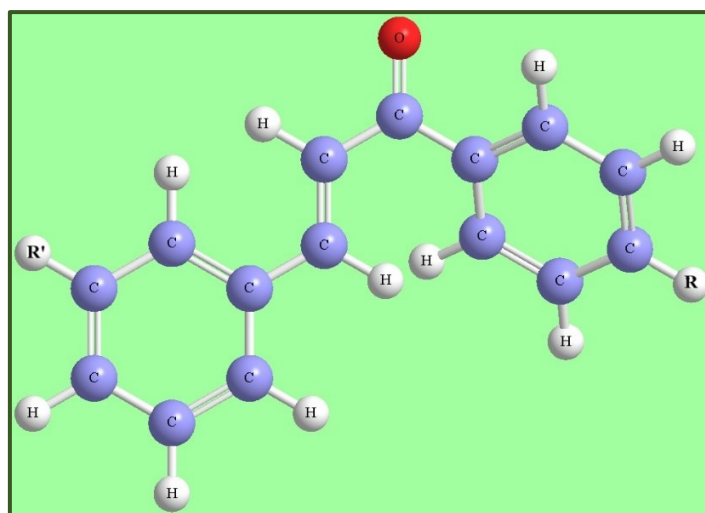
Figure 1.8: A depiction of the 3-dimensional structure of an α, β-unsaturated carbonyl system chalcone) [72]

9

In this structure, the C=O is conjugated with the double bond (CH=CH), which can be further conjugated with the aromatic rings (**figure 1.8**). This extended conjugation in α, β-unsaturated carbonyl system imparts distinct electronic and photophysical properties to chalcones such as conjugation and planarity that enhance the stability and reactivity, having significant biological and chemical properties, making them valuable in pharmaceuticals, agrochemicals, and materials science.[73,74]

1.4.2. Methods for synthesizing chalcones

There are various methods reported in literature for the synthesis of chalcones such as the carbonylated Heck coupling reaction, where aryl halides are coupled with alkenes in the presence of a palladium catalyst and carbon monoxide, resulting in the formation of chalcone derivatives with carbonyl functionality.[75] The Sonogashira isomerization coupling offers a versatile approach for synthesizing chalcones by reacting terminal alkynes with aryl halides under copper and palladium co-catalysis. This reaction can lead to alkyne-containing chalcones, which may undergo isomerization to form conjugated enones, expanding the scope of chalcone derivatives.[76] Similarly, the Suzuki-Miyaura coupling involves the cross-coupling of aryl boronic acids with aryl halides in the presence of a palladium catalyst, providing a highly functional group-tolerant route to biaryl chalcones.[77] In addition, solid acid catalyst-mediated reactions are also used for chalcone synthesis. Heterogeneous acid catalysts such as zeolites, montmorillonite, and sulfated zirconia promote the condensation of aldehydes and ketones, offering environmentally friendly alternatives that are easy to recover and reuse.[78] One of the most widely used methods is the Claisen-Schmidt condensation, which involves the reaction of an aromatic aldehyde with an acetophenone under basic conditions to form chalcones through aldol condensation followed by dehydration. This method is simple and provides high yields, making it ideal for both laboratory and industrial-scale production.[79]

1.4.3. The Claisen-Schmidt Condensation Reaction

The Claisen-Schmidt condensation reaction is a widely employed method for synthesizing chalcones, involving the condensation of an aromatic aldehyde with an aromatic ketone possessing at least one α-hydrogen with another carbonyl compound in the presence of a base or acid catalyst to form β-hydroxy aldehydes (aldols) or β-hydroxy ketones.[80] This fundamental carbon-carbon bond-forming reaction proceeds via the enolate ion, which reacts with the carbonyl compound to form the aldol product. Subsequent dehydration of the aldol product yields a chalcone (**figure 1.9**). In the synthesis of chalcones, the base (commonly NaOH or KOH) abstracts the α-hydrogen of the ketone to form an enolate ion, which then

10

attacks the carbonyl carbon of the aromatic aldehyde, forming a β-hydroxy ketone (aldol). This β-hydroxy ketone undergoes base-catalyzed or acid-catalyzed dehydration to form the chalcone. This reaction is efficient and typically occurs at room temperature or mild heating, with dehydration often facilitated by heating, making it a valuable method for producing chalcones.[81,82]
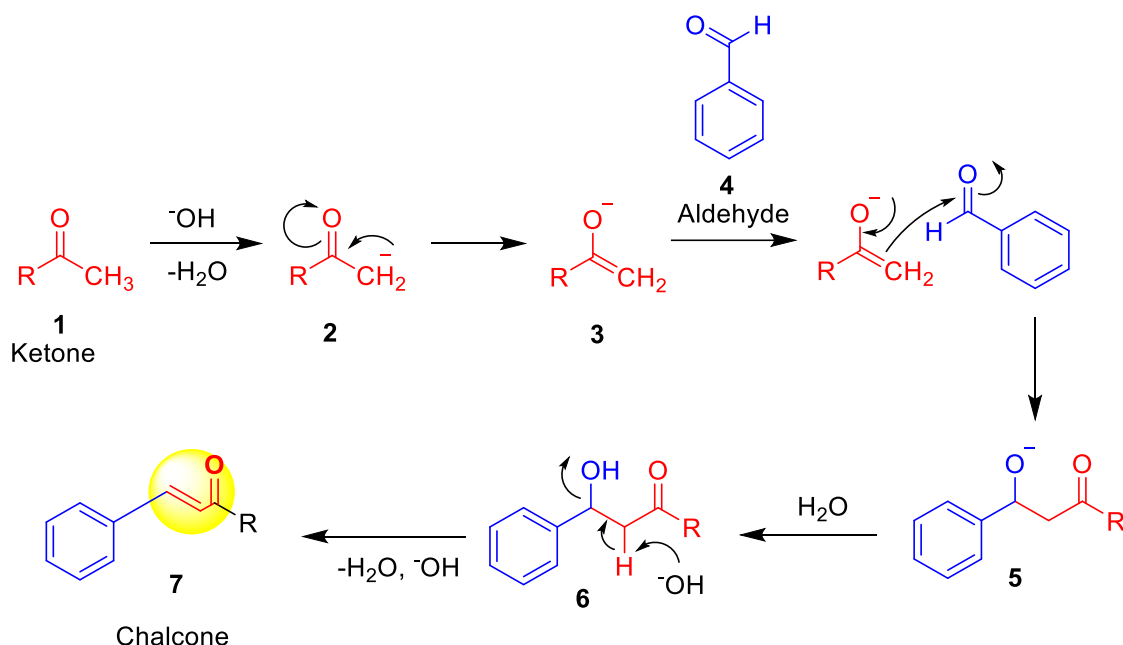
Figure 1.9: Mechanism of Claisen-Schmidt Condensation reaction [79]

1.5. Click-Derived Chalcone Based 1,2,3-Triazoles

Chalcone derivatives, distinguished by their α, β-unsaturated carbonyl systems, represent a versatile class of compounds commended for their extensive range of biological activities and pronounced fluorescence.[83] By using click chemistry to combine these chalcone derivatives with 1,2,3-triazoles, it improves their intrinsic properties that lead to the development of chalcone-based 1,2,3-triazoles with superior functionality.[84] This synthesis, particularly through the CuAAC reaction, yields compounds that not only retain but augment the desirable traits of both the parent structures. Moreover, the combination of the electron-rich 1,2,3-triazole ring with chalcone's conjugated system facilitates strong π-π interactions and hydrogen bonding, thereby contributing to the stability and robustness of the material in solid-state applications, as it leads to enhanced electron delocalization across the entire molecule. This extended conjugation results in improved electronic and optical properties, including increased fluorescence and enhanced charge transport characteristics.

1.6. Applications of 1,2,3-triazole derivatives

The 1,2,3-triazole derivatives have attracted substantial interest in the scientific community due to their unique structural and electronic properties. Their ability to engage in diverse chemical reactions and form stable complexes makes them integral in various fields of research and industry such as in medicinal chemistry as key scaffolds for drug development, and in materials science, polymer synthesis, and organic electronics. Significantly, their key applications are in metal ion detection, anion sensing, biological and environmental monitoring, medicinal chemistry, material science, and catalysis as elaborated below and illustrated in **figure 1.10**. Furthermore, their structural stability and ease of functionalization enable the development of advanced materials and innovative solutions across multiple domains,[71,85]
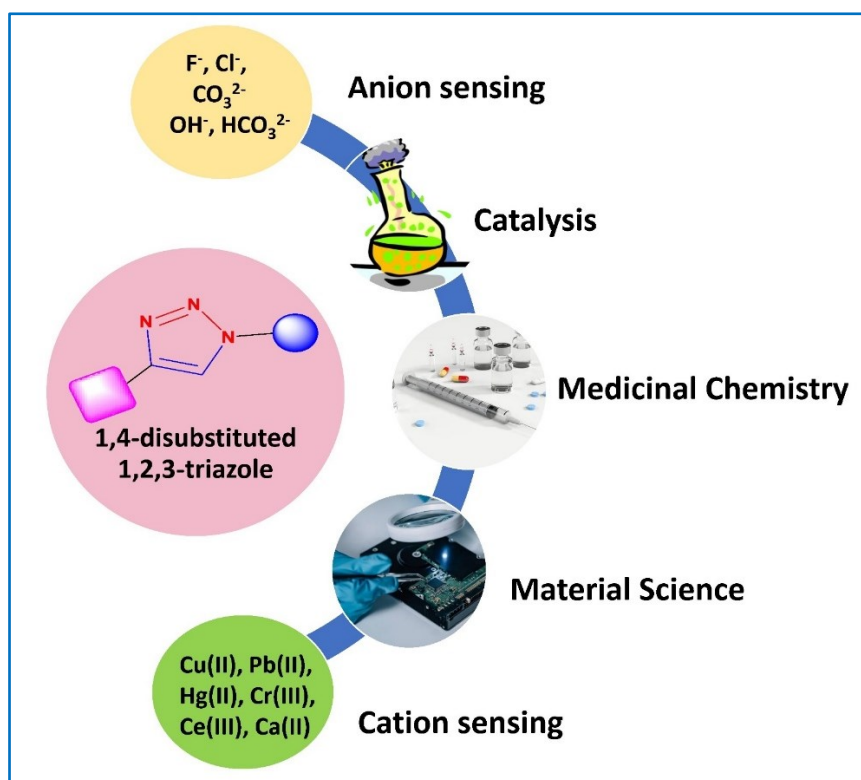
Figure 1.10: Highlighting the versatility of 1,2,3-triazoles[71,85]

➢ **Metal Ion Detection**

The 1,2,3-triazole tailored chemosensors have demonstrated remarkable efficacy in the recognition of metal ions, an area of considerable importance due to the environmental and biological implications of metal ion contamination. The nitrogen atoms within the 1,2,3-triazole ring exhibit a strong propensity to coordinate with metal ions, which induces measurable changes in the sensor's optical or electrochemical properties.[86] This coordination

is facilitated by the electron-rich nature of the 1,2,3-triazole ring, which can interact with electron-deficient metal ions. For instance, 1,2,3-triazole-based sensors have been successfully developed for the detection of copper, mercury, lead, zinc, cobalt, magnesium, manganese, aluminum, iron, barium, calcium, chromium, cerium etc., known for their toxicity, when present in excess to cause severe environmental and health issues. The sensitivity and selectivity of 1,2,3-triazole-based sensors make them indispensable tools in environmental and biological monitoring; and is typically achieved using UV-Visible and fluorescence spectroscopy.[87] To verify metal ion recognition through UV and/or fluorescence, the absorption/emission spectrum of the pure 1,2,3-triazole-based sensor in the solution phase is compared with the spectrum of the solution of the sensor in which a particular metal ion has been introduced, focusing on shifts in absorption maxima and intensity changes. The complexation of the sensor molecules with the metal ions can alter the energy gap between the ligand's ground and excited states, leading to a shift in the absorption peak or changes in its intensity. Therefore, these techniques efficiently allow for the monitoring of changes in absorbance or emission spectra upon binding with metal ion, enabling the accurate and reliable detection of trace metal ions.[84]

> **Anion Sensing**

The detection of anions such as fluoride, chloride, iodide, nitrate, sulfate, carbonate, cyanide, bicarbonate, and phosphate are critical due to their potential harmful effects when present in excess in environmental and biological systems. These anions can disrupt ecological balance, contribute to water contamination, or pose direct toxicological risks to human health.[89] For example, cyanide and fluoride are highly toxic even at trace levels, making their sensitive detection crucial for public safety. Similarly, elevated levels of phosphate and nitrate can lead to eutrophication, causing significant environmental degradation in aquatic ecosystems.[90] The 1,2,3-triazole ring is particularly effective in detecting these anions through hydrogen bonding or electrostatic interactions, leading to measurable signal changes in sensors. This interaction is largely driven by the electron density provided by the nitrogen atoms in the 1,2,3-triazole ring. Furthermore, electron-donating substituents attached to the 1,2,3-triazole structure enhance the formation of stable complexes with anions, improving the sensitivity and selectivity of detection.[91]

➢ **Biological and Environmental Applications**

In addition to metal ion and anion sensing, 1,2,3-triazole-based chemosensors have found extensive applications in biological and environmental monitoring.[92] In biological systems, these sensors are utilized for the detection of biomolecules such as proteins, nucleic acids, and small metabolites.[93,94] The 1,2,3-triazole ring's ability to form stable interactions with a variety of biomolecules underpins its utility in medical diagnostics and therapeutic monitoring.[95,96] For example, 1,2,3-triazole-based sensors can aid in disease diagnosis by detecting specific biomarkers such as estrogen related receptor α for therapeutic treatment of breast cancer[97], protein biomarkers associated with neurodegenerative diseases, nucleic acids linked to genetic disorders, metabolites indicative of metabolic disease like diabetes. Moreover, in environmental applications, 1,2,3-triazole-based sensors can be employed for the detection of pollutants and toxins such as pesticides, organic contaminants, heavy metals, etc. in soil and water samples.[98,99]

➢ **Medicinal Chemistry**

The incorporation of 1,2,3-triazoles into drug molecules has been widely explored due to their bio-isosteric properties for various functional groups, such as amides, esters, and heterocycles. This means it can replace these groups in drug molecules without significantly altering their biological activity, while often improving stability, solubility, and binding properties.[93] For example, in peptide-based drugs, the 1,2,3-triazole ring can be used to mimic the planar structure of amide bonds, while being resistant to enzymatic hydrolysis. The 1,2,3-triazole ring is also capable of forming hydrogen bonds through its nitrogen atoms, which enhances its interaction with biological macromolecules, such as proteins and nucleic acids. This hydrogen bonding ability allows 1,2,3-triazole-based drugs to form strong, selective interactions with active sites of enzymes, receptors, and other biomolecular targets.[100] As a result, the 1,2,3-triazole-containing drugs can exhibit higher binding affinity and specificity, leading to more effective inhibition or activation of biological pathways. These interactions are particularly important in designing drugs for targeting enzymes, such as kinases or proteases, and receptors involved in disease mechanisms. The 1,2,3- triazole ring's high stability and ability to form hydrogen bonds make it a valuable scaffold in medicinal chemistry.[101] The 1,2,3-triazole-containing compounds have shown promising results in the development of antiviral, antibacterial, antifungal, and anticancer agents owing to the fact that the 1,2,3-triazole

moiety can improve the solubility, metabolic stability, and target specificity of drugs, leading to more effective treatments with fewer side effects.[102]

➢ **Material Science**

1,2,3-triazoles have also found applications in material science, particularly in the development of advanced polymers and nanomaterials. The 1,2,3-triazole ring can impart unique mechanical, thermal, and electronic properties to materials, making them suitable for various applications such as thermal stability in fire resistant materials, high-performance polymers, anticorrosion coatings.[103] For example, 1,2,3-triazole-based polymers exhibit excellent thermal stability and mechanical strength, which are desirable characteristics for materials used in aerospace, automotive, and electronics industries. 1,2,3-triazole-containing materials have been employed in the fabrication of organic light-emitting diodes (OLEDs), solar cells, and sensors, demonstrating their versatility and potential for innovation.[104–106]

➢ **Catalysis**

The catalytic applications of di-substituted 1,2,3-triazole derivatives have gained significant attention, particularly in organic synthesis. These 1,2,3-triazole-based ligands and catalysts have demonstrated efficiency in facilitating several key reactions, including cross-coupling, oxidation, and reduction processes. The electron-rich nature of the 1,2,3-triazole ring enables it to stabilize transition states and reactive intermediates during these catalytic reactions, thereby enhancing both reaction efficiency and selectivity.[107] Specifically, 1,2,3-triazoles play an essential role in palladium-catalyzed cross-coupling reactions (such as Suzuki, Heck, and Sonogashira couplings), where they serve as ligands to stabilize the active palladium species, improving catalyst longevity and activity. Additionally, 1,2,3-triazole-based ligands have been employed in oxidation reactions like the aerobic oxidation of alcohols and reduction processes such as the hydrogenation of alkenes, where the 1,2,3-triazole ring helps modulate the electronic environment of the metal center.[108] Moreover, 1,2,3-triazole-based catalysts have shown particular value in enantioselective synthesis, where controlling stereochemistry is critical. The tunability of the 1,2,3-triazole scaffold allows for precise adjustment of electronic and steric properties, enabling the development of chiral 1,2,3-triazole ligands that can steer the reaction towards high enantioselectivity. These properties make them indispensable in asymmetric catalysis, facilitating reactions such as asymmetric hydrogenations.[109]

1.7. Overview of Chemosensors

Chemosensors, often referred to as chemical sensors, are molecular entities that can detect and respond to chemical substances, converting chemical information into an analytically useful signal. Sensor consists of a recognition element that interacts specifically with the target analyte, and a transducer that converts the chemical interaction into a measurable signal, such as optical, electrical, or thermal signals, an optical device consists of a light source and a detector.[110,111] The advancement of chemosensors has significantly revolutionized various fields such as environmental monitoring, medical and healthcare industries, the food and beverage industry, etc., to enable the detection of pollutants at trace levels and pathogens in biological samples for ensuring better management and protection of ecosystem by providing tools for real-time monitoring and analysis with high sensitivity and specificity.[112] The development of chemosensors, molecular devices capable of detecting chemical species with high selectivity and sensitivity, has become increasingly important in various fields such as environmental monitoring, medical diagnostics, and chemical analysis.[113] Chemosensors can be categorized based on specific interactions between the recognition element and the target analyte:

➢ Electrochemical interactions: These involve redox reactions or changes in electrical properties (e.g., impedance, conductivity) upon binding of the analyte to the sensor's surface. These interactions can lead to measurable changes that correlate directly with the concentration of the target analyte, making electrochemical chemosensors highly sensitive tools for detection of ions, gases, and organic molecules due to their high sensitivity and simplicity. The ability to operate in diverse conditions, including aqueous and non-aqueous environments, further enhances their applicability. The rapid response time and real-time monitoring capabilities of these sensors make them invaluable in scenarios where timely detection is crucial, such as in emergency response situations or continuous health monitoring.[114]

➢ Optical interactions: Optical interactions in chemosensors are characterized by observable changes in properties such as absorbance, fluorescence, phosphorescence, or refractive index upon the binding of an analyte. Optical chemosensors are particularly favored in analytical chemistry for their high specificity, which allows for the selective detection of target molecules even in complex mixtures. These sensors enable real-time, non-invasive analysis, making them ideal for applications in biological systems, environmental assessments, and industrial processes. Techniques such as fluorescence resonance energy transfer (FRET) are commonly employed in optical sensing applications.[115]

➤ Mass-sensitive interactions: Mass-sensitive interactions form the basis of a different category of chemosensors that rely on detecting changes in mass resulting from analyte binding. These changes can be measured using advanced techniques such as piezoelectric sensors or surface acoustic wave (SAW) devices, which translate mass changes into electrical signals. These sensors are particularly adept at detecting large biomolecules, such as proteins and nucleic acids, making them invaluable in biochemical and biomedical applications. For instance, the binding of a large analyte to the sensor surface induces a measurable shift in frequency or amplitude, allowing for quantitative analysis of biomolecular interactions.[116]

1.7.1. Metal ion sensors

Metal ion sensors typically operate based on specific interactions between the sensor and target metal ions, often utilizing mechanisms such as coordination, chelation, or electrochemical processes. The design of these sensors incorporates selective ligands that bind to particular metal ions, ensuring high specificity and minimizing interference from other species present in the sample.[117] For example, chemosensors based on 1,2,3-triazole derivatives can form stable complexes with transition metals like copper, mercury, lead, zinc, cobalt, magnesium, manganese, aluminum, iron, barium, calcium, chromium, cerium etc, allowing for the selective detection of these ions in complex matrices such as biological fluids or environmental water samples.[118]

These sensors typically consist of three main components: a recognition site/receptor, a signaling unit, and a linker or spacer that connects these two parts[119], as depicted in **figure 1.11**. The recognition site is the core of the sensor, responsible for the selective binding of the target metal ion, often incorporating specific ligands or functional groups like amines, thiols, carboxylates, or heterocyclic rings that interact strongly with the metal ion through coordination bonds.[120] The design of the recognition site is important for the selectivity of the sensor, tailored to match the size, charge, and coordination preferences of the target metal ion. The signaling unit, which produces a detectable signal upon metal binding, can be a fluorophore, chromophore, or any other moiety that undergoes a measurable change in response to metal binding.[86] The linker or spacer connects the recognition site and the signaling unit, playing a crucial role in ensuring that the binding event at the recognition site can effectively induce a change in the signaling unit. The binding of the metal ion induces a conformational or electronic change in the sensor molecule, transmitted through the linker to the signaling unit, leading to an alteration in its properties.[106,107]
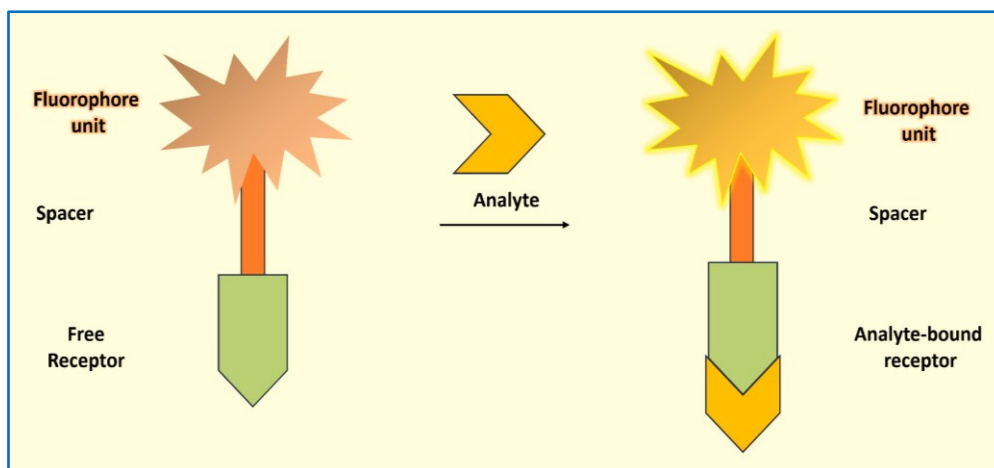
Figure 1.11: A pictorial representation of the components of a chemosensor and their specific functions in the detection of an analyte[119]

1.8. Elucidating Chemosensing Mechanisms: Advanced Spectroscopic Insights from UV-Visible and Fluorescence Analysis

The determination of chemosensing behavior through spectroscopic analysis, particularly utilizing UV-visible and fluorescence spectroscopy, is an essential approach for understanding and characterizing the interactions between chemosensors and their target analytes. This technique provides critical insights into the electronic and optical properties of chemosensors, allowing for the elucidation of their sensitivity, selectivity, and overall performance in detecting various chemical species.[123,124] For example, a 1,2,3-triazole decorated imino-phenol sensor was reported for the selective detection of Zn(II) and Cu(II).[125]
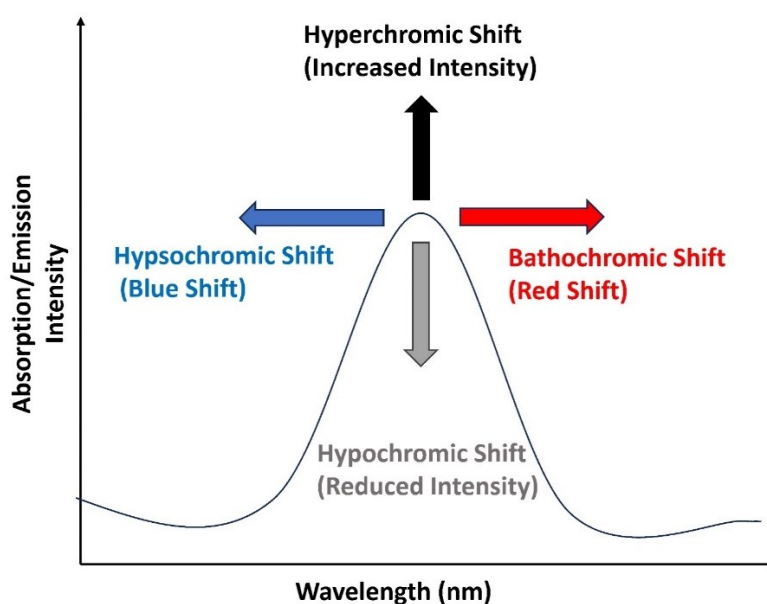
Figure 1.12: Illustrating the significant spectral changes observed in absorption and emission spectra upon binding of the chemosensor with an analyte[126]

18

UV-visible spectroscopy is a powerful tool for analyzing the chemosensing behavior of compounds, as it measures the absorbance or transmittance of light in the ultraviolet and visible regions of the electromagnetic spectrum. This method is particularly effective in monitoring changes in the electronic transitions of molecules, which can occur upon interaction with analytes.[85] When a chemosensor binds to a target molecule, it often results in the change of the of the electronic environment, leading to shifts in the absorption spectra (**figure 1.12**). These shifts, which can be in the form of hypsochromic or bathochromic shifts, provide quantitative data on the binding affinity and stoichiometry of the sensor-analyte complex. By analyzing these spectral changes, researchers can determine the effective concentration range and detection limits of the chemosensor, which are critical parameters for its practical applications.[69,126]

Fluorescence spectroscopy, on the other hand, measures the changes in the emission of light by a substance that has interacted with the electromagnetic radiations. This technique is highly sensitive and is capable of detection of even little changes in the environment of the fluorescent molecules. In the context of chemosensing, fluorescence spectroscopy is frequently employed to observe changes in the emission intensity or wavelength upon binding of the sensor to an analyte,[127] and the phenomenon of fluorescence quenching or enhancement is often indicative of specific interactions between the sensor and the target molecule. Quenching occurs when the presence of an analyte leads to a decrease in fluorescence intensity, while enhancement results in an increase in fluorescence emission.
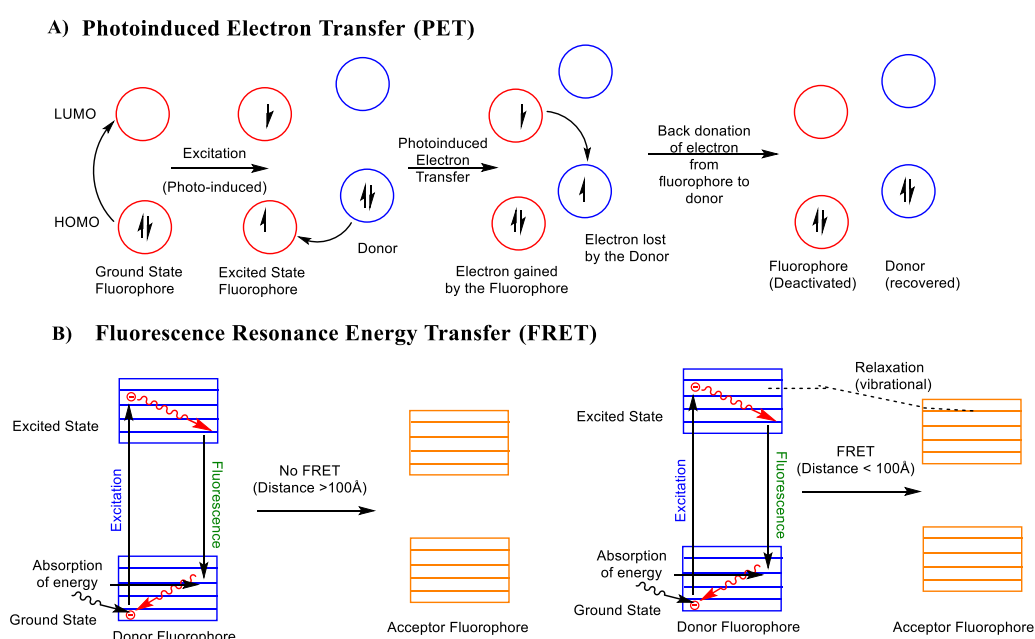
Figure 1.13: An illustration of the process of (A) Photo-induced Electron Transfer (PET) and (B) Förster resonance energy transfer (FRET)[87]

19

These changes are typically attributed to mechanisms such as photoinduced electron transfer (PET), Förster resonance energy transfer (FRET) **(figure 1.13)**, or changes in the local environment of the fluorophore.[128–130] The combination of UV-visible and fluorescence spectroscopy allows for a comprehensive analysis of chemosensing behavior. UV-Visible spectroscopy provides information on the ground-state electronic transitions and helps in understanding the initial interaction mechanisms, while fluorescence spectroscopy offers insights into the excited-state dynamics and the subsequent changes in the sensor's optical properties. This dual approach is particularly beneficial in studying complex systems where multiple interaction pathways might be involved. For example, the detection of metal ions using a 1,2,3-triazole-based chemosensor can be elucidated by observing both the absorbance changes in the UV-Visible spectra and the fluorescence response, providing a robust understanding of the sensing mechanism.[131]

1.9. Conclusion

In summary, heterocyclic compounds, characterized by their ring structures, are crucial in organic chemistry due to their extensive occurrence and diverse applications. With the advent of Click Chemistry, i.e. the concept of highly efficient and modular chemical reactions introduced to construct complex molecules through heteroatom bond formation, has revolutionized synthetic methodologies. A cornerstone of click chemistry is the Huisgen 1,3-dipolar cycloaddition reaction, a seminal development by Rolf Huisgen. This reaction laid the groundwork for the CuAAC, a variant that has become a quintessence of regioselective and high-yielding synthesis, enabling the construction of 1,2,3-triazoles with remarkable precision and efficiency. 1,2,3-Triazole derivatives have found extensive utility across various domains, including medicinal chemistry, materials science, and chemosensing. These heterocyclic compounds exhibit unique structural and electronic properties, making them ideal candidates for the development of chemosensors. Chalcone-linked 1,2,3-triazole moieties in particular, combine the advantageous attributes of chalcones and 1,2,3-triazoles, resulting in compounds with good fluorescence and metal ion recognition activities, which are crucial for sensitive and selective detection of analytes. The study of chemosensing behavior through advanced spectroscopic techniques, such as UV-visible and fluorescence spectroscopy, provides profound insights into the chemosensor behavior, revealing binding affinity, stoichiometry, and interaction mechanisms. These techniques facilitate comprehensive analyses of both ground-state and excited-state dynamics in sensor-analyte interactions.

References

1. G. Patrick, Organic Chemistry: A Very Short Introduction, Oxford University Press, Oxford, 2017, pp. 1–140.

2. N. J. Keighley, Introduction to Organic and Medicinal Chemistry, CRC Press, Boca Raton, 2024, pp. 1–300.

3. M. Moghaddam and L. Mehdizadeh, in Soft Chemistry and Food Fermentation, eds. A. M. Grumezescu and A. M. Holban, Academic Press, Cambridge, 2017, pp. 379–419.

4. H. Wilkes, R. Jarling and J. Schwarzbauer, in Hydrocarbons, Oils and Lipids: Diversity, Origin, Chemistry and Fate, ed. H. Wilkes, Springer International Publishing, Cham, 2020, pp. 3–48.

5. V. Ya. Lee and A. Sekiguchi, *Angew. Chem., Int. Ed.*, 2007, **46,** 6596–6620.

6. N. Kerru, L. Gummidi, S. Maddila, K. K. Gangu and S. B. Jonnalagadda, *Molecules,* 2020, **25,** 1909.

7. E. Kabir and M. Uzzaman, *Results Chem.,* 2022, **4**, 100606.

8. O. Ebenezer, M. A. Jordaan, G. Carena, T. Bono, M. Shapi and J. A. Tuszynski, *Int. J. Mol. Sci.,* 2022, **23**, 8117.

9. M. A. Shalaby, A. M. Fahim and S. A. Rizk, *RSC Adv.,* 2023, **13**, 14580–14593.

10. D. Hamid, N. Safir, I. Sodani, Y. Salih, H. Ibrahim, I. Al Sammarraie and M. Khudair, 2023, **4**, 72–80.

11. M. Lõkov, S. Tshepelevitsh, A. Heering, P. Plieger, R. Vianello and I. Leito, *Eur. J. Org. Chem.,* 2017, **2017,** 4475–4489.

12. H.-H. Zong, C. Yao, C. Q. Sun, J.-G. Zhang and L. Zhang, *Molecules*, 2020, **25**, 3232.

13. M. A. Quraishi, D. S. Chauhan and V. S. Saji, *J. Mol. Liq.,* 2021, **341**, 117265.

14. K. Dze, *Int. J. Res. Appl. Sci. Eng. Technol.,* 2020, **8,** 36–56.

15. G. Zhussupova and A. Zhussupova, *Procedia - Soc. Behav. Sci.*, 2015, **191,** 1247–1254.

16. Y. Volkova, S. Baranin and I. Zavarzin, *Adv. Synth. Catal.,* 2021, **363**, 40–61.

17. A. Rusu, I.-M. Moga, L. Uncu and G. Hancu, *Pharmaceutics,* 2023, **15**, 2554.

18. M. M. Heravi and V. Zadsirjan, *RSC Adv.*, 2020, **10**, 44247–44311.

19. M.-M. Li, X. Chen, Y. Deng and J. Lu, *RSC Adv*., 2021, **11,** 38060–38078.

20. I. Ameziane El Hassani, K. Rouzi, H. Assila, K. Karrouchi and M. Ansar, *Reactions,* 2023, **4,** 478–504.

21. A. Mermer, T. Keles and Y. Sirin, *Bioorg. Chem.,* 2021, **114**, 105076.

22. G. C. Dos Santos, L. M. Martins, B. A. Bregadiolli, V. F. Moreno, L. C. Da Silva-Filho and B. H. S. T. Da Silva, *J. Heterocycl. Chem.,* 2021, **58,** 2226–2260.

23. A. Amin, T. Qadir, P. K. Sharma, I. Jeelani and H. Abe, Curr. Med. Chem., 2022, **29,** 1234-1250.

24. T. Qadir, A. Amin, P. K. Sharma, I. Jeelani and H. Abe, Curr. Med. Chem., 2022, **29,** 1120-1135.

25. R. B. Vlocskó, G. Xie and B. Török, *Molecules,* 2023, **28,** 4153.

26. A. Kumar, A. K. Singh, H. Singh, V. Vijayan, D. Kumar, J. Naik, S. Thareja, J. P. Yadav, P. Pathak, M. Grishina, A. Verma, H. Khalilullah, M. Jaremko, A.-H. Emwas and P. Kumar, *Pharmaceuticals,* 2023, **16,** 299.

27. R. W. Sidwell and J. T. Witkowski, Antiviral Res., 2019, 162, 5-21,

28. Z. Lei, W. Chang, H. Guo, J. Feng and Z. Zhang, *Molecules,* 2023, **28,** 3012.

29. L. K. M. O. Goni, M. A. Jafar Mazumder, M. A. Quraishi and M. Mizanur Rahman, *Chem. Asian J.*, 2021, **16,** 1324–1364.

30. J. Toldo, O. El Bakouri, M. Solà, P.-O. Norrby and H. Ottosson, *ChemPlusChem,* 2019, **84,** 712–721.

31. B. Zhao, B. Prabagar and Z. Shi, *Chem*, 2021, **7**, 2585–2634.

32. M.-C. Ríos and J. Portilla, *Chemistry*, 2022, **4**, 940–968.

33. G. Blond, M. Gulea and V. Mamane, *Curr. Org. Chem.*, 2016, **20**, 1–10.

34. M. A. Jordan and A. J. Frontier, *RSC Adv.*, 2017, 7, 10716-10740.

35. M. Babu, K. Keyan, S. Srinivasan, K. Eluri, M. Elumalai and S. Sivannan, *Carbon Resour. Convers.,* 2020, **3,** 36-46.

36. M. M. Heravi, S. Khaghaninejad and M. Mostofi, *Adv. Heterocycl. Chem.*, 2014, **112**, 1–50.

37. A. Trowbridge, S. M. Walton and M. J. Gaunt, *Chem. Rev.*, 2020, **120**, 2613–2692.

38. U. Dhawa, N. Kaplaneris and L. Ackermann, *Org. Chem. Front.*, 2021, **8**, 4886–4913.

39. Á. Molnár, *Coord. Chem. Rev.*, 2024, **504**, 215668.

40. M. Choury, A. Basilio Lopes, G. Blond and M. Gulea, *Molecules*, 2020, **25**, 3147.

41. H. Nada, A. Elkamhawy and K. Lee, *Molecules*, 2021, **26**, 553.

42. V. Kumar, K. Lal, Naveen and R. K. Tittal, *Catal. Commun.*, 2023, **176**, 106629.

43. H. C. Kolb, M. G. Finn and K. B. Sharpless, *Angew. Chem. Int. Ed.*, 2001, **40**, 2004–2021.

44. A. K. Agrahari, P. Bose, M. K. Jaiswal, S. Rajkhowa, A. S. Singh, S. Hotha, N. Mishra and V. K. Tiwari, *Chem. Rev.*, 2021, **121**, 7638–7956.

45. G. S. Kumar and Q. Lin, *Chem. Rev.*, 2021, **121**, 6991–7031.

46. J. Kaur, M. Saxena and N. Rishi, *Bioconjug. Chem.*, 2021, **32**, 1455–1471.

47. H. Y. Yoon, D. Lee, D.-K. Lim, H. Koo and K. Kim, *Adv. Mater.*, 2022, **34**, 2107192.

48. G. Singh, N. George, R. Singh, G. Singh, J. D. Kaur, G. Kaur, H. Singh and J. Singh, *ACS Omega*, 2022, **7**, 39159–39168.

49. C. Nájera, J. M. Sansano and M. Yus, *Org. Biomol. Chem.*, 2015, **13**, 8596–8636.

50. R. Huisgen, *Angew. Chem., Int. Ed.* 1968, **7**, 321–328.

51. R. Huisgen, *Angew. Chem., Int. Ed.* 1963, **2**, 565–598.

52. R. Huisgen, *Angew. Chem., Int. Ed.* 1963, **2**, 633–645.

53.   M. Breugst and H.-U. Reissig, *Angew. Chem., Int. Ed.*, 2020, **59**, 12293–12307.

54.   M. Danese, M. Bon, G. Piccini and D. Passerone, *Phys. Chem. Chem. Phys.*, 2019, **21**, 19281–19287.

55.   D. Bauer, S. M. Sarrett, J. S. Lewis and B. M. Zeglis, *Nat. Protoc.*, 2023, **18**, 1659–1668.

56.   S. Sharma, F. Gallou and S. Handa, *Green Chem.*, 2024, **26**, 6289–6317.

57.   C. Wang, D. Ikhlef, S. Kahlal, J.-Y. Saillard and D. Astruc, *Coord. Chem. Rev.* 2016, **316**, 1–20.

58..   M. Meldal and F. Diness, *Trends Chem.*, 2020, **2**, 569–584.

59   X.-P. He, Y.-L. Zeng, Y. Zang, J. Li, R. A. Field and G.-R. Chen, *Carbohydr. Res.*, 2016, **429**, 1–22.

60.   X. Wang, B. Huang, X. Liu and P. Zhan, *Drug Discov. Today*, 2016, **21**, 118–132.

61.   L. Li and Z. Zhang, *Molecules*, 2016, **21**, 1393.

62.   V. O. Rodionov, S. I. Presolski, D. D. Díaz, V. V. Fokin and M. G. Finn, *J. Am. Chem. Soc.*, 2007, **129**, 12705–12712.

63.   Y. Özkılıç and N. Ş. Tüzün, *Organometallics*, 2016, **35**, 2589–2599.

64.   R. Singh, G. Singh, N. George, G. Singh, P. Malik, H. Singh, G. Kaur and J. Singh, *RSC Adv.*, 2024, **14**, 15374–15390.

65.   A. Afrin, A. Jayaraj, M. S. Gayathri and C. A. S. P, *Sens. Diagn.*, 2023, **2**, 988–1076.

66.   R. M. Arnold, N. E. Huddleston and J. Locklin, *J. Mater. Chem.*, 2012, **22**, 19357.

67.   M. M. Alam, *Archiv. der. Pharmazie.*, 2022, **355**, 2100158.

68.   M. Stanitska, N. Pokhodylo, R. Lytvyn, E. Urbonas, D. Volyniuk, S. Kutsiy, K. Ivaniuk, V. Kinzhybalo, P. Stakhira, R. Keruckiene, M. Obushak and J. V. Gražulevičius, *ACS Omega*, 2024, **9**, 14613–14626.

69.   Sudheer, V. Kumar, P. Kumar and R. Gupta, *New J. Chem.*, 2020, **44**, 13285–13294.

70.   P. Rajakumar, S. Raja, C. Satheeshkumar, S. Ganesan, P. Maruthamuthu and S. A. Suthanthiraraj, *New J. Chem.*, 2010, **34**, 2247.

71.   D. P. Vala, R. M. Vala and H. M. Patel, *ACS Omega*, 2022, **7**, 36945–36987.

72.   M. Rudrapal, J. Khan, A. A. B. Dukhyil, R. M. I. I. Alarousy, E. I. Attah, T. Sharma, S. J. Khairnar and A. R. Bendale, *Molecules*, 2021, **26**, 7177.

73.   G. Rajendran, D. Bhanu, B. Aruchamy, P. Ramani, N. Pandurangan, K. N. Bobba, E. J. Oh, H. Y. Chung, P. Gangadaran and B.-C. Ahn, *Pharmaceuticals (Basel)*, 2022, **15**, 1250.

74.   C. Zhuang, W. Zhang, C. Sheng, W. Zhang, C. Xing and Z. Miao, *Chem. Rev.*, 2017, **117**, 7762–7810.

75.   X.-F. Wu, H. Neumann, A. Spannenberg, T. Schulz, H. Jiao and M. Beller, *J. Am. Chem. Soc.*, 2010, **132**, 14596–14602.

76..   R. Chinchilla and C. Nájera, *Chem. Soc. Rev.*, 2011, **40**, 5084–5121.

77.   M. A. Selepe and F. R. Van Heerden, *Molecules*, 2013, **18**, 4739–4765.

78.   M. Rueping, T. Bootwicha, H. Baars and E. Sugiono, *Beilstein J. Org. Chem.*, 2011, **7**, 1680–1687.

79.   G. D. Yadav and D. P. Wagh, *ChemistrySelect*, 2020, **5**, 9059–9085.

80.   C. L. Perrin and K.-L. Chang, *J. Org. Chem.*, 2016, **81**, 5631–5635.

81.   A. Jawad, M. Salih, T. abd-alameer al Zubaidi, N. Obaid and N. Aljamali, 2019, **5**, 16–27.

82.   S. Mandal, S. Mandal, S. K. Ghosh, A. Ghosh, R. Saha, S. Banerjee and B. Saha, *Synth. Commun.,* 2016, **46**, 1327–1342.

83.   N. A. A. Elkanzi, H. Hrichi, R. A. Alolayan, W. Derafa, F. M. Zahou and R. B. Bakr, *ACS Omega*, 2022, **7**, 27769–27786.

84.   P. Prasher and M. Sharma, *Medchemcomm*, 2019, **10**, 1302–1328.

85.   S. Kumar, B. Lal and R. K. Tittal, *Green Chem.*, 2024, **26**, 1725–1769.

86.   F. Ahmed and H. Xiong, *Dyes Pigm.,* 2021, **185**, 108905.

87.   G. Singh, N. George, R. Singh, G. Singh, Sushma, G. Kaur, H. Singh and J. Singh, *Appl. Organomet. Chem.* **2023,** e6897.

88.   B. Shen and Y. Qian, *Sens. Actuators B: Chem.* 2017, **239**, 226–234.

89.   J. J. Bryant and U. H. F. Bunz, *Chemistry – An Asian Journal*, 2013, **8**, 1354–1367.

90.   D. A. Erzunov, G. V. Latyshev, A. D. Averin, I. P. Beletskaya and N. V. Lukashev, *Eur. J. Org. Chem.*2015, **2015**, 6289–6297.

91.   D. Ghosh, S. Rhodes, K. Hawkins, D. Winder, A. Atkinson, W. Ming, C. Padgett, J. Orvis, K. Aiken and S. Landge, *New J. Chem.*, 2014, **39**, 295–303.

92.   P. Rani, K. Lal, Aruna, R. Shrivastava and V. D. Ghule, *J. Mol. Struct.* 2020, **1203**, 127437.

93.   N. Agouram, E. M. El Hadrami and A. Bentama, *Molecules*, 2021, **26**, 2937.

94.   D. Baraniak and J. Boryski, *Biomedicines*, 2021, **9**, 628.

95.   H.-Y. Guo, Z.-A. Chen, Q.-K. Shen and Z.-S. Quan, *J. Enzyme Inhib. Med. Chem.* 2021, **36**, 1115–1144.

96.   M. Rajasekar, C. Narendran, J. Mary, M. Sivakumar and M. Selvam, *Results Chem.,* 2024, **7**, 101543.

97.   S. Xu, X. Zhuang, X. Pan, Z. Zhang, L. Duan, Y. Liu, L. Zhang, X. Ren and K. Ding, *J. Med. Chem.*, 2013, **56**, 4631–4640.

98.   D. Ghosh, A. Atkinson, J. Gibson, H. Subbaiahgari, W. Ming, C. Padgett, K. S. Aiken and S. M. Landge, *Sensors*, 2023, **23**, 7000.

99.   C.-W. Huang, C. Lin, M. K. Nguyen, A. Hussain, X.-T. Bui and H. H. Ngo, *Bioengineered*, **14**, 58–80.

100.   D. N. Kumari, S. V. Reddy, A. S. Kumar, D. B. Rao, M. Al-Madani and S. Al-Shaibani, *Molecules*, 2020, **25,** 1-12.

101.   D. Lengerli, K. Ibis, Y. Nural and E. Banoglu, Expert Opin. *Drug Discov.,* 2023, **18,** 123-134.

102.   S. A. Khan, M. J. Akhtar, U. Gogoi, D. U. Meenakshi and A. Das, *Pharmaceuticals*, 2023, **16**, 179.

103.   J. Huo, H. Hu, M. Zhang, X. Hu, M. Chen, D. Chen, J. Liu, G. Xiao, Y. Wang and Z. Wen, *RSC Adv.*, 2017, **7**, 2281–2287.

104.   P. S. Gribanov, A. N. Philippova, M. A. Topchiy, D. A. Lypenko, A. V. Dmitriev, S. D. Tokarev, A. F. Smol'yakov, A. N. Rodionov, A. F. Asachenko and S. N. Osipov, *Molecules*, 2024, **29**, 2151.

105.   M. Aydemir, G. Haykır, A. Battal, V. Jankus, S. K. Sugunan, F. B. Dias, H. Al-Attar, F. Türksoy, M. Tavaslı and A. P. Monkman, *Org. Electr.*, 2016, **30**, 149–157.

106.   M. K. Kim, J. Kwon, T.-H. Kwon and J.-I. Hong, *New J. Chem.*, 2010, **34**, 1317–1322.

107.   M. Zurro and O. G. Mancheño, *Chem. Rec.*, 2017, **17**, 485–498.

108.   J. Lauko, P. H. J. Kouwer and A. E. Rowan, *J. Heterocycl. Chem.*, 2017, **54**, 1677–1699.

109.   R. Singh, G. Singh, N. George, G. Singh, S. Gupta, H. Singh, G. Kaur and J. Singh, *Catalysts*, 2023, **13**, 130.

110.   V. Naresh and N. Lee, *Sensors*, 2021, **21**, 1109.

111.   J. Baranwal, B. Barse, G. Gatto, G. Broncova and A. Kumar, *Chemosensors*, 2022, **10**, 363.

112.   M. Banu and C. Ungureanu, *Coatings*, 2023, **13**, 486.

113.   Y. Shi, W. Zhang, Y. Xue and J. Zhang, *Chemosensors*, 2023, **11**, 226.

114.   G. Maduraiveeran, M. Sasidharan and V. Ganesan, *Biosens. Bioelectron.* 2018, **103**, 113–129.

115.   P. Gruber, M. P. C. Marques, N. Szita and T. Mayr, *Lab Chip*, 2017, **17**, 2693–2712.

116.   A. N. Kursunlu and E. Güler, *J. Mol. Struct.* 2017, **1134**, 345–349.

117.   X. Xu, S. Yang, Y. Wang and K. Qian, *Green Anal. Chem.* 2022, **2**, 100020.

118. N. Ullah, M. Chohan, I. Khan and A. Qurashi, *Trends Anal. Chem.,* 2018, **105,** 44-56.

119. F. Caroleo, G. Magna, M. L. Naitana, L. Di Zazzo, R. Martini, F. Pizzoli, M. Muduganti, L. Lvova, F. Mandoj, S. Nardis, M. Stefanelli, C. Di Natale and R. Paolesse, *Sensors*, 2022, **22**, 2649.

120. N. Kwon, Y. Hu and J. Yoon, *ACS Omega*, 2018, **3**, 13731–13751.

121. *Inorganica Chimica Acta*, 2023, **551**, 121470.

122. C. Guo, A. C. Sedgwick, T. Hirao and J. L. Sessler, *Coord. Chem. Rev.*, 2021, **427**, 213560.

123. I. J. Kim, Y. Xu and K. H. Nam, *Molecules*, 2022, **27**, 2922.

124. A. S. Tanwar, R. Parui, R. Garai, M. A. Chanu and P. K. Iyer, *ACS Meas. Sci. Au*, 2022, **2**, 23–30.

125. S. Ghosh, N. Baildya and K. Ghosh, *New J. Chem.*, 2021, **45**, 10923–10929.

126. W. Mäntele and E. Deniz, *Spectrochim. Acta A: Mol. Biomol. Spectrosc.*, 2017, **173**, 965–968.

127. V. Kumar, P. Kumar, S. Kumar, D. Singhal and R. Gupta, *Inorg. Chem.*, 2019, **58**, 10364–10376.

128. G. Das, B. Garai, T. Prakasam, F. Benyettou, S. Varghese, S. K. Sharma, F. Gándara, R. Pasricha, M. Baias, R. Jagannathan, N. Saleh, M. Elhabiri, M. A. Olson and A. Trabolsi, *Nat. Commun.*, 2022, **13**, 3904.

129. A. Kaur, P. Kaur and S. Ahuja, *Anal. Methods*, 2020, **12**, 5532–5550.

130. H. Niu, J. Liu, H. M. O'Connor, T. Gunnlaugsson, T. D. James and H. Zhang, *Chem. Soc. Rev.*, 2023, **52**, 2322–2357.

131. C. J. Fossum, B. O. V. Johnson, S. T. Golde, A. J. Kielman, B. Finke, M. A. Smith, H. R. Lowater, B. F. Laatsch, S. Bhattacharyya and S. Hati, *ACS Omega*, 2023, **8**, 44820–44830.

Chapter II

Review of literature

This section offers a thorough review of the methodologies, including a detailed analysis of the existing literature on chalcones, terminal alkynes, organic azides and 1,4-disubstituted 1,2,3-triazoles, employed for chemosensing along with an overview of the spectroscopic methods for characterizing the synthesized molecules, addressing all phases involved in their potential use as chemosensors.

2.1. Click chemistry

The term 'Click' refers to a chemical process that is highly efficient, selective, and results the product formation in a single step[1], a concept introduced by Sir Karl Barry Sharpless and his colleagues in 2001 as 'Click Chemistry'.[2] The significance of this breakthrough was further highlighted in 2022, when Sir Karl Barry Sharpless, along with Prof. Carolyn Bertozzi and Sir Morten Meldal, were awarded the Noble Prize for developing Click chemistry and Biorthogonal Chemistry.[3] Under moderate reaction conditions, Click chemistry has developed into a versatile tool offering a quick and simple method for joining two molecular fragments. The synthetic methodology involves the use of benign solvents, is insensitive to oxygen and moisture, generates minimal waste and allows for easy product isolation.[4] Owing to these substantial attributes, Click Chemistry has found extensive applications **(figure 2.1)** in pharmaceutical sciences and drug delivery, playing a crucial role in the synthesis of bioactive compounds and the development of drug delivery systems, particularly through target-guided synthesis.[5,6]
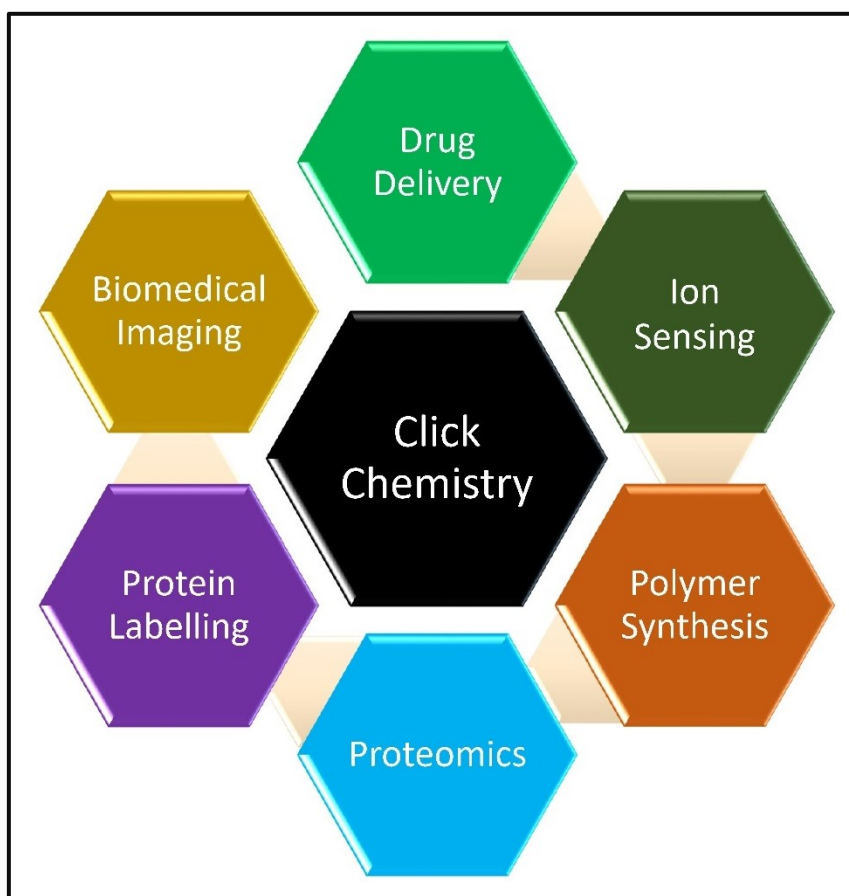
Figure 2.1: An illustrative representation of applications of click chemistry

In polymer sciences, Click reactions are utilized for post polymerization modifications, facilitating the design of functionalized polymers for advanced materials and biomedical applications[7]. Beyond these areas, Click Chemistry has gained importance in bioconjugation, enabling the attachment of biomolecules to synthetic materials, often used in imaging techniques and protein labelling. In cell biology and proteomics, Click reactions have been employed for the creation of fluorogenic probes.[8,9] Moreover, Click Chemistry is increasingly applied in material science, nanotechnology and even environmental chemistry, where it aids in the development of sensors, surface modifications, and the synthesis of environmentally benign materials.[10]

In recent years, the development of various 'Click' based approaches has expanded the scope of organic reactions with some notable Click reactions, include CuAAC, Inverse Electron Demand Diels–Alder reaction (IEDDA), Thiol-ene reactions, Thiol-yne reactions, Strain-Promoted Azide-Alkyne Cycloaddition (SPAAC), Strain-Promoted Alkyne-Nitrone Cycloaddition (SPANC), and Staudinger ligation.[11,12] Click Chemistry has garnered considerable interest, with the CuAAC being recognized as the most implemented synthetic methodology encompassed under Click Chemistry due to its key features of modularity, wide scope, high yields, stereospecific nature; and due to these desirable properties it is widely used for the synthesis of heterocyclic molecular structures with desired functions.[9]

2.2. The 1,2,3-triazole derivatives

The CuAAC is a significant reaction in Click Chemistry, owing to its role in synthesizing 1,4-disubstituted 1,2,3-triazole derivatives with 100% conversion rate and high purity by facilitating a 3+2 cycloaddition reaction of a terminal alkyne and an organic azide in the presence of a Cu(I) catalyst under mild reaction conditions.[13,14.] The 1,4-disubstituted 1,2,3-triazoles feature two nitrogen atoms (N3 and N2) with lone pairs, enabling diverse supramolecular interactions. These include anion complexation through hydrogen or halogen bonds, often assisted by charge, and metal coordination using their nitrogen atoms in anionic, neutral, or cationic forms, as well as carbanionic and mesoionic carbene donors.[15–17] Furthermore, their capacity to form hydrogen bonds, engage in dipole-dipole interactions, and participate in π-stacking has increased their importance in medicinal chemistry, as these interactions boost binding affinity to biological targets and improve solubility.[18,19] The literature is abundant with several methodologies for the formation of 1,2,3-triazole derivatives incorporating different structural frameworks such as Schiff bases[20,21], chalcones[22,23], dendrimers[24], polymers[25] and organic derivatives[26] as a backbone structure **(figure 2.2)** in order

to achieve diverse functional properties. These frameworks can accommodate different substituent groups such as aromatic rings, electron withdrawing/ donating groups (-OCH$_3$, -OH, Cl, Br, -NO$_2$) on aromatic rings, heteroatomic rings (such as Pyridine) etc., which significantly influence their properties.[27,28] Among the mentioned structural frameworks, chalcone skeleton is notable due to its ease of modification, strong π-conjugation, and an inherent ability to enhance interactions with metal ions, making it an ideal moiety for designing highly sensitive and selective chalcone based 1,2,3-triazole-based metal ion sensors.
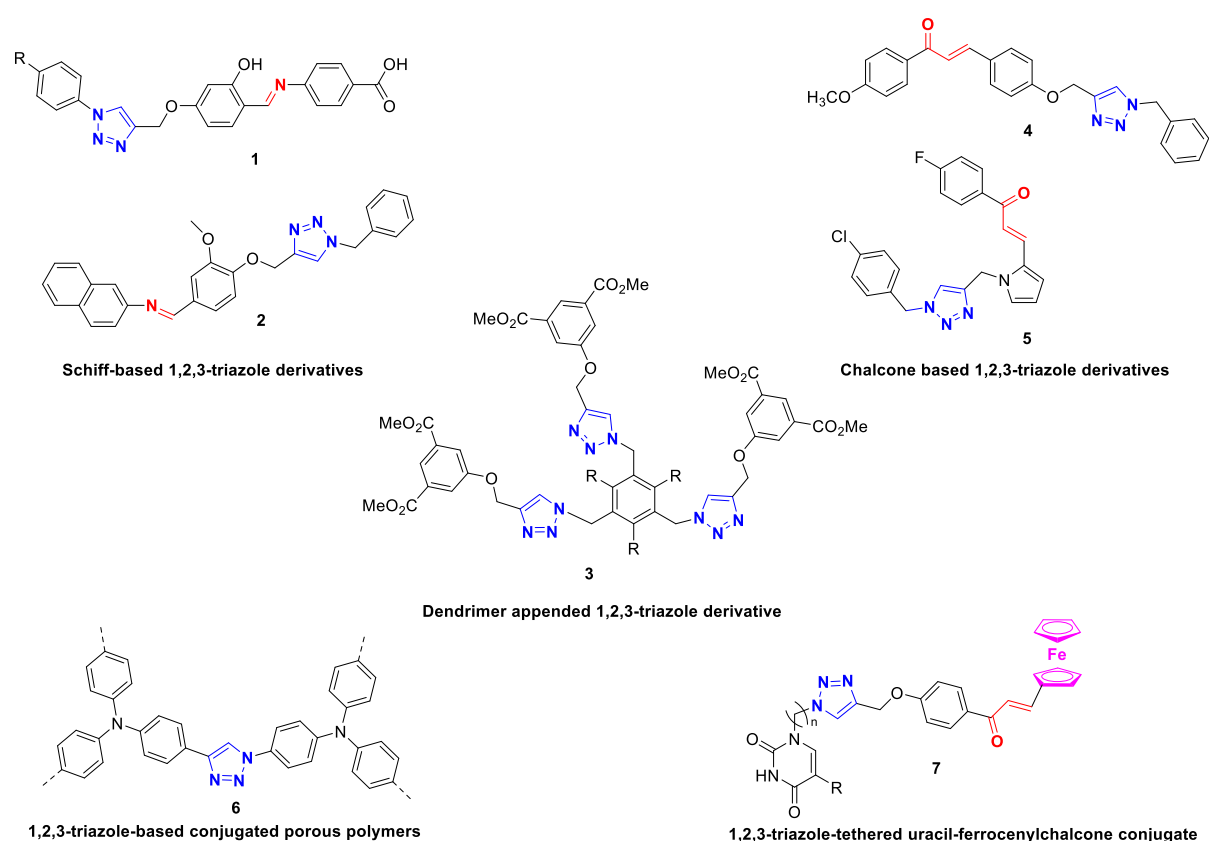
Figure 2.2: An illustration of 1,2,3-triazole derivatives having different structural frameworks[1–7]

2.3. Chalcones

Chalcones are particularly advantageous as a skeleton for designing chemosensors due to their distinctive α, β-unsaturated ketone structure, which provides a versatile framework for functionalization and modification. The conjugated system of chalcones, consisting of two aromatic rings linked by a three-carbon α,β-unsaturated carbonyl group, facilitates strong electronic interactions that are crucial for sensor development.[29] This structural arrangement allows for fine tuning of optical properties; for example, electron donating groups and electron

withdrawing groups can increase the electron density of the conjugated system as well as enhance selectivity for specific analytes by altering the electronic environment and fluorescence characteristics.[30] The planarity of chalcones ensures efficient π conjugation, which is essential for maximizing fluorescence and enhancing sensor performance. Extended conjugation within the chalcone structure can lead to a redshift in emission/absorption spectra. The incorporation of carbonyl group can facilitate effective anion detection by forming stable hydrogen-bonded complexes, which alter the fluorescence properties.[31,32] Furthermore, for metal ion detection, chalcones can be modified by integrating heteroatoms such as nitrogen, oxygen etc., can co-ordinate with metal ions, providing selective binding sites and enhances sensor's efficiency in detecting specific metal ions.[33]

2.3.1. Chalcone tethered 1,2,3-triazoles

Chalcone tethered 1,2,3-triazole compounds represent a fascinating class of hybrid molecules that synergistically integrate the structural and electronic attributes of chalcones with distinct functionalities of 1,2,3-triazoles.[34] The chalcone scaffold, characterized by its extensive conjugation significantly enhances the photophysical properties of these hybrids, offering a highly customizable platform for fluorescence-based applications.[35] Meanwhile, the 1,2,3-triazole ring, introduced as a robust, five-membered heterocycle that is capable of integrating with a variety of metal ions and biomolecules, thereby enriching the synthesized moieties with significant functional capabilities.[36]

Incorporating the 1,2,3-triazole moiety into the chalcone architecture not only imparts additional structural stability but also provides strategic coordination sites for metal ion binding, thereby rendering these hybrids particularly suitable for applications in sensing and catalysis.[37] Moreover, these hybrid molecules also pave the way for the development of multifunctional materials, utilizing the complementary properties of the chalcone and 1,2,3-triazole moieties. For instance, the capability to show strong absorptive and emissive properties of chalcones can be effectively coupled with the 1,2,3-triazole's metal-chelation capabilities, resulting in sophisticated sensors capable of both detecting and responding to specific analytes.[38] Additionally, the modular approach of Click Chemistry enables the facile synthesis of diverse chalcone-tethered 1,2,3-triazole derivatives, allowing for precise tailoring of their properties to meet specific application requirements.[39] The synthesis of chalcone-tethered 1,2,3-triazoles via 'CuAAC' reaction, is generally carried out in the following 4 steps:

1. Synthesis of chalcone derivatives

2. Synthesis of terminal alkynes from the chalcones
3. Synthesis of organic azides
4. Synthesis of chalcone-based 1,2,3-triazole derivatives

2.3.2. Synthesis of chalcone

Chalcones are aromatic enones **(figure 2.3)** and are regarded as open-chain flavonoids, possessing a simple chemistry that allows for a wide range of replacements via simple synthetic methodologies. The crucial step in their synthesis technique usually involves the condensation of two aromatic systems, each containing nucleophilic and electrophilic groups, resulting in the formation of chalcone scaffolds. They exhibit a broad range of biological activities, including antibacterial, antifungal, antiparasitic, antioxidant, anti-inflammatory, antimalarial, antitumor, analgesic, and antidepressant effects.[29,30,40] The following are some of the several sets of reactions for chalcone synthesis that have been documented in the literature:
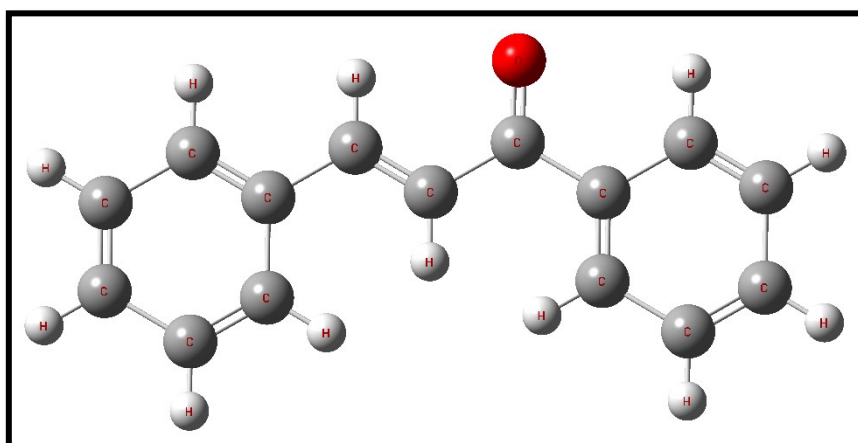
Figure 2.3: A pictorial representation of basic backbone structure of chalcones[29]

2.3.2.1. Carbonylated heck coupling reaction

The carbonylated heck coupling process involves the synthesis of chalcones by the carbonylated vinylation of a phenyl halide with styrene. This reaction involves the presence of carbon monoxide and utilizes palladium (Pd) as a catalyst. Wu *et al.* first developed the method for the synthesis of chalcone **11** via the carbonylated vinylation of halides **8** with styrene **10** in the presence of carbon monoxide **9**, catalyzed by Pd, yield ranging from 41 to 90% **(figure 2.4)**. This approach allows for the simple production of a variety of building blocks, starting from readily available aryl halides and olefins.[41]
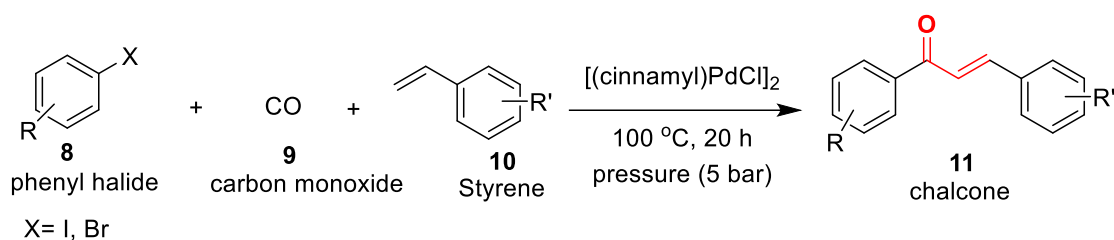
Figure 2.4: Synthesis of chalcone via carbonylative vinylation of phenyl halides with styrene[41]

2.3.2.2. Coupling reaction

The synthesis of chalcone **14** was carried out through a coupling reaction between benzaldehyde **12** and phenylacetylene **13** with yield ranging from 60-90 %. This reaction was conducted in the presence of HBr and the ionic liquid 1-butyl-3-methyl-1H-imidazolium 4-methylbenzenesulfonate (BmimOTs), under conditions of 100 °C for 12 hours **(figure 2.5)**.[42]
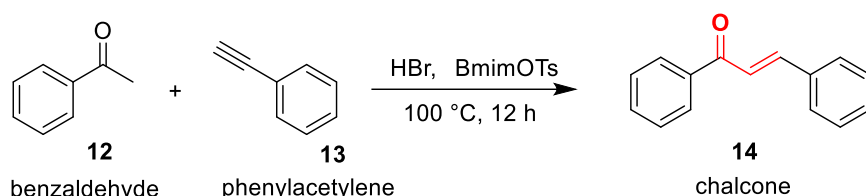
Figure 2.5: Synthesis of chalcone via coupling reaction[42]

2.3.2.3. Sonogashira isomerization coupling

The Sonogashira isomerization coupling process was used to synthesize chalcone **17** with the good yield of 41- 96 % by reacting equimolar amounts of an electron-deficient phenyl halide **15** with propargyl alcohol **16** under microwave irradiations, catalyzed by $PdCl_2(PPh_3)_2$ and THF as the solvent **(figure 2.6)**.[43]
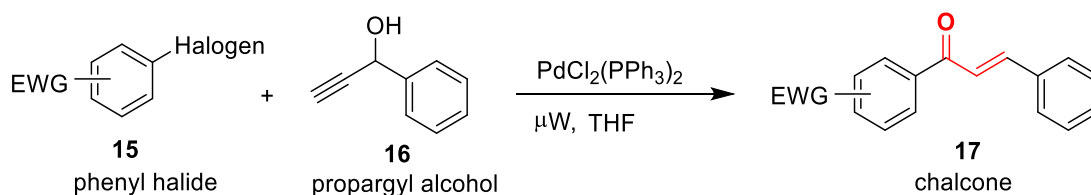
Figure 2.6: Sonogashira isomerization coupling reaction for the synthesis of chalcone (EWG: electron withdrawing group)[43]

2.3.2.4. Suzuki-Miyaura reaction

The Suzuki-Miyaura coupling process is another method for synthesizing chalcone **14** by the coupling of benzoyl chloride **18** with styrylboronic acid **19** using $Pd(PPh_3)_4$, $CsCO_3$, and anhydrous toluene **(figure 2.7 a)**. Alternatively, synthesis of chalcone can be carried out via

coupling of phenylboronic acid **20** with cinnamoyl chloride **21** under the same reaction conditions using Pd(PPh₃)₄, CsCO₃, and anhydrous toluene **(figure 2.7 b)** having a good yield of 68-93 %.[44]
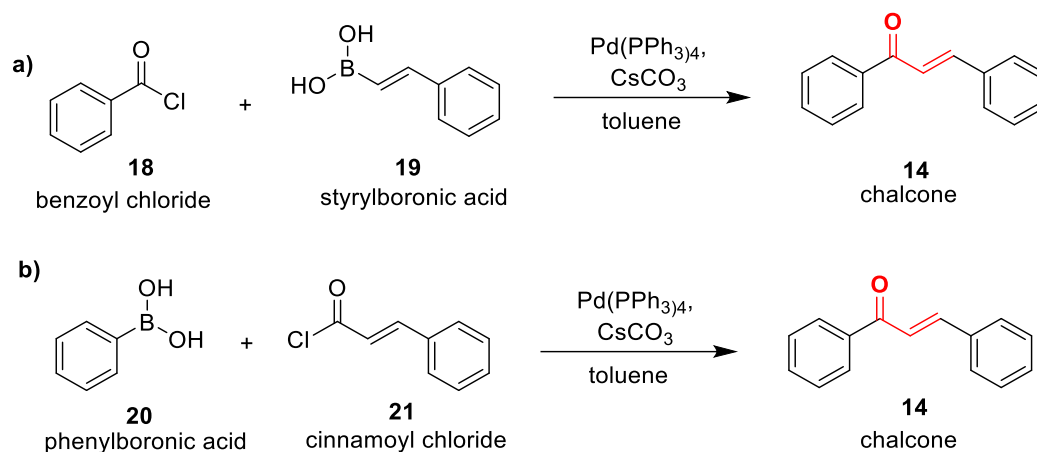
Figure 2.7: Suzuki-Miyaura coupling reaction for the synthesis of chalcone **a)** the coupling of benzoyl chloride with styrylboronic acid **b)** the coupling of phenylboronic acid with cinnamoyl chloride[44]

2.3.2.5. Solid acid catalyst mediated reaction

The synthesis of chalcone **14** has also been achieved using a heterogenous solid acid catalyst methodology, wherein, equimolar quantities of benzaldehyde **12** and phenylacetylene **13** were combined using 1,2-dichloroethane as the solvent, with exposure to microwave irradiation and the yield of the product was in the range of 30- 91% **(figure 2.8)**. The reaction utilized Amberlyst-15, an ion exchange resin, as the heterogenous solid catalyst.[45]
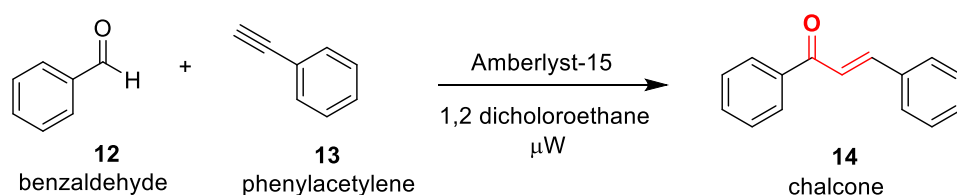
Figure 2.8: Chalcone synthesis via microwave-assisted coupling of benzaldehyde and phenylacetylene using Amberlyst-15 in 1,2-dichloroethane[45]

2.3.2.6. Claisen-Schmidt reaction

Alarcon *et al.* gave the green synthesis of chalcone **24** from Claisen Schmidt condensation with substituted benzaldehyde **22** and acetophenone **23** using ethanol as a solvent at room temperature **(figure 2.9)**.[46]
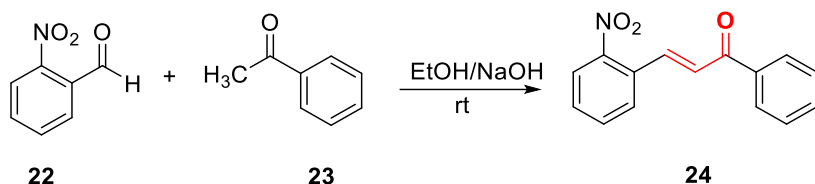
Figure 2.9: Synthesis of chalcone from substituted benzaldehyde and acetophenone[46]

Sharma and co-workers gave the synthesis of α, β unsaturated carbonyl compound from 5-substituted salicylic acid **25**, which was acetylated with acetic anhydride and concentrated sulfuric acid to form an intermediate **26**. The intermediate **26** was then heated at 160 ⁰C in a Fries rearrangement process with anhydrous aluminium chloride to transfer the acetyl group from the 2-position to the 3-position, yielding 3-acetyl salicylic acid intermediate **27**. To get the target chalcone **28**, the intermediate **27** was subjected to a Claisen– Schmidt condensation reaction with different aryl aldehydes at room temperature using NaOH as presented in **figure 2.10**.[47] The yield of the products obtained was in the range of 27- 94 %.
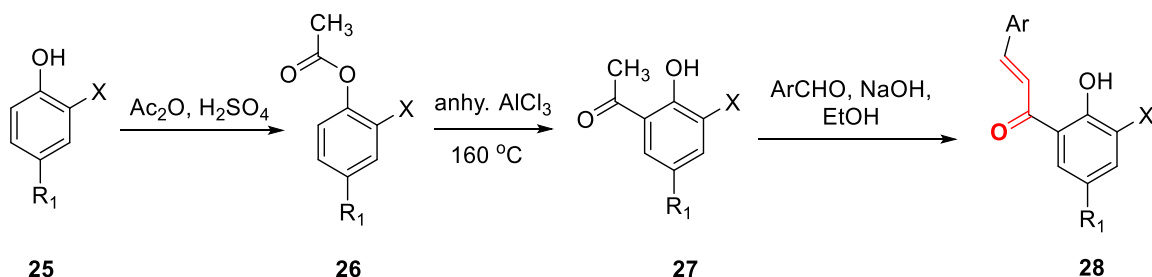
Figure 2.10: Synthesis of target chalcone 5-substituted salicylic acid (X = COOH)[47]

Jacob *et al.* gave the synthesis of chalcones having high yield of 90% via a Claisen-Schmidt condensation reaction **(figure 2.11)**, wherein acetophenone (1-phenylethan-1-one) **23** underwent a reaction with substituted benzaldehyde **29** in the presence of acetic acid, potassium hydroxide, and ethanol, maintained on ice for 24 hours, resulting in the formation of chalcone **30** (2E-1,3-diphenylprop-2-en-1-one).[48]
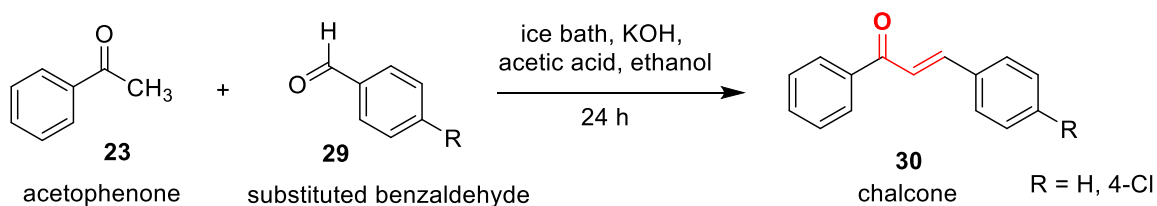
Figure 2.11: Synthesis of chalcone via Claisen-Schmidt condensation in acidic medium[48]

Sandip *et al.* synthesized a chalcone derivative **23** with high yield ranging between 53-94 % and good antioxidant properties utilizing the traditional Claisen-Schmidt condensation method, wherein, substituted benzaldehyde **17** and acetophenone **16** were used in the presence of methanol as a solvent and sodium hydroxide as a base at ambient temperature for a duration of 45 minutes **(figure 2.12)**.[49]
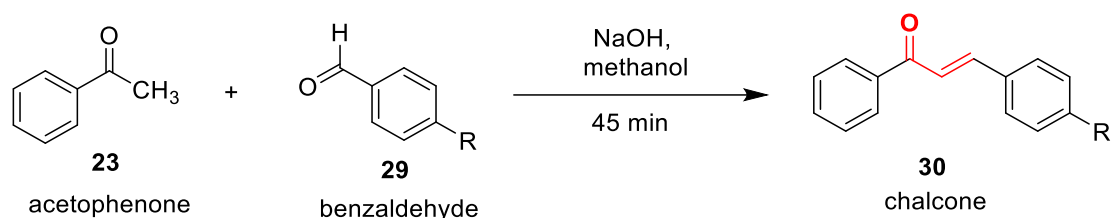
Figure 2.12: Synthesis of chalcone using sodium hydroxide via Claisen-Schmidt condensation[49]

Among various methods reported in the literature, the Claisen-Schmidt condensation stands out as one of the best approaches for synthesizing chalcones due to its simplicity, efficiency, and versatility. This reaction involves the base-catalyzed condensation of benzaldehyde and acetophenone derivatives, offering a straightforward route to produce chalcones with excellent yields. One of the key advantages is the mild reaction conditions, as it typically only requires a common base such as sodium hydroxide or potassium hydroxide, avoiding the need for expensive or hazardous reagents. Additionally, the reaction can be conducted in standard solvents like ethanol or methanol, making it both cost-effective and environmentally friendly. The process is highly efficient, often completing in just a few hours, and allows for easy purification of the product.

2.3.3. Synthesis of terminal alkyne

Alkynes are a significant class of compounds which are widely used as precursor for the formation of heterocycles. They are divided into two types: terminal alkynes and internal alkynes. Terminal alkynes (R-C≡C-H), particularly valuable as precursors in the synthesis of internal alkynes,[50,51] are characterized by an alkyl group connected to the sp-hybridized carbon atom of a triple bond situated at the terminal position of a carbon chain. Moreover, because of its distinctive electrical characteristics and adaptability, the C≡C bond has been used as a fundamental component in biological and material science application.[52] Additionally, terminal alkynes can be produced through a variety of techniques employing diverse starting materials under varying conditions, some of which are discussed below:

2.3.3.1. Carbene rearrangement

Hijfte and his team synthesised different terminal alkynes **33** via the combination of aldehydes **31** with carbon tetrabromide, produced vinyl dibromides **32.** These vinyl dibromides, when refluxed with magnesium in THF, successfully formed terminal alkynes **(figure 2.13)**. The reaction is driven by the negative reduction potential of magnesium, which facilitates electron transfer to the vinyl dibromide. This method suggests that magnesium is an effective alternative base, which are prone to cause undesirable side reactions, and its consistently produce terminal alkynes with high yields ranging from 75 % to 95 %.[53]

$R = C_6H_5, C_6H_5CH(CH_3)$
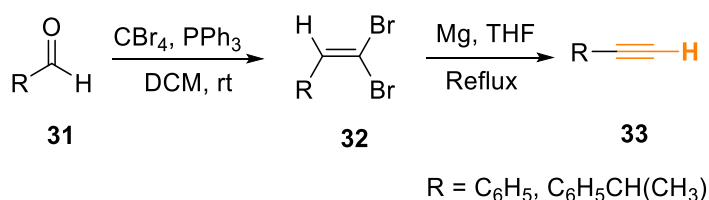
Figure 2.13: Depicting the synthesis of terminal alkyne via the reaction of aldehyde[53]

By refluxing acetoxynitrosamide **34** in THF, terminal alkynes can be produced with high yields in the range of 77 % to 97 %. The process involves the generation of carbene **36**, which then undergoes rearrangement to form the terminal alkyne **33 (figure 2.14)**. This approach is versatile, suitable for synthesizing terminal alkynes with either aryl or alkyl substituents.[54]

$R = Ph, C_6H_{19}$
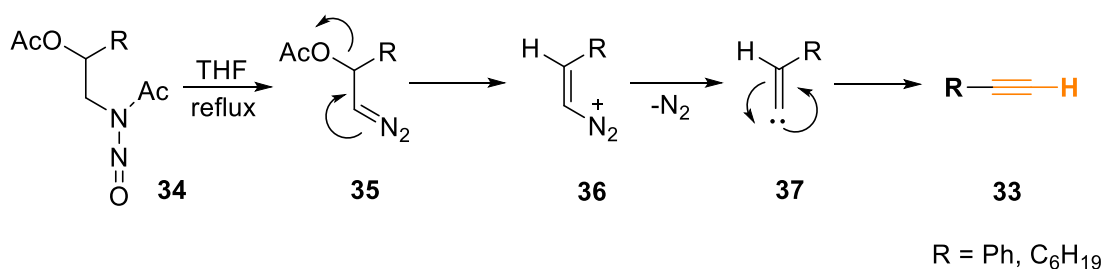
Figure 2.14: Synthesis of terminal alkynes with alkyl and aryl substituents[54]

2.3.3.2. α, β-eliminations

Kuang *et al.* demonstrated the decarboxylation and dehalogenation of 3-aryl-2,3-dibromopropanoic acid **34** using K_2CO_3 as the base to synthesize terminal alkynes **35**. The reaction was conducted at 115 °C in DMSO and proceeded smoothly, showing compatibility with a broad range of heteroaryl and aryl substituents, whether they are electron withdrawing

or electron donating **(figure 2.15)**.[55] Its consistently produce terminal alkynes with high yields ranging from 68- 95%.
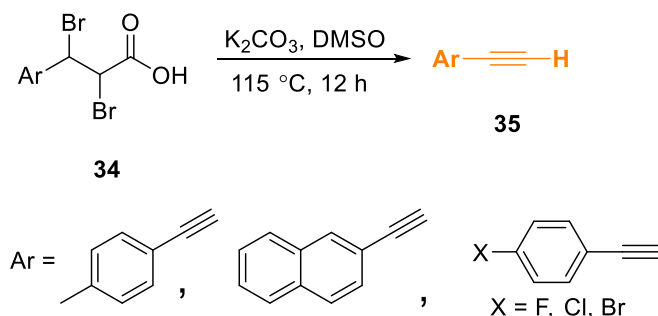
Figure 2.15: Synthesis of terminal alkyne from dibromopropanoic acid[55]

Singh and coworkers developed a method for synthesizing terminal alkyne from gem-dibromoalkenes **32** using Na_2S as the reagent. The reaction occurs at room temperature (20 – 40 °C) and does not require a base, proceeds efficiently in air with yields ranging from 65 % to 83% **(figure 2.16)**. This approach successfully produced terminals alkyne **33** from a variety of gem-dibromoalkenes, including heteroatomic, aromatic and aliphatic types.[56]
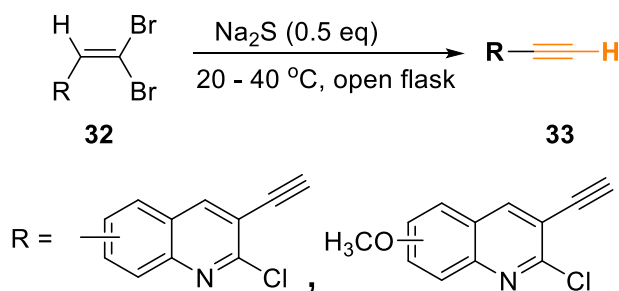
Figure 2.16: Synthesis of terminal alkyne from gem-dibromoalkene[56]

2.3.3.3. Miscellaneous Reactions

As illustrated in **figure 2.17**, Bestmann *et al.* suggested the synthesis of terminal alkyne **33** by treating aldehydes **36** with Ohira–Bestmann reagent (a phosphate derivative) **37** in the presence of K_2CO_3 and methyl alcohol.[57]
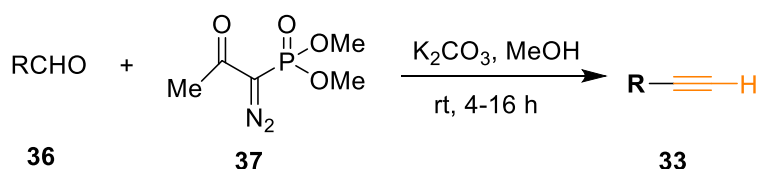
Figure 2.17: Synthesis of terminal alkyne by treating aldehyde with the Ohira–Bestmann reagent[57]

The direct synthesis of alkynes **40** under moderate circumstances was made possible by dehydrogenating and dehydrating alcohols **38** with SO_2F_2 **39** in potassium carbonate and DMSO as solvent was used **(figure 2.18)** with yields ranging from 77-92%. Cu(I)–catalyzed alkyne–azide cycloaddition can be employed directly with the alkyne produced.[58]
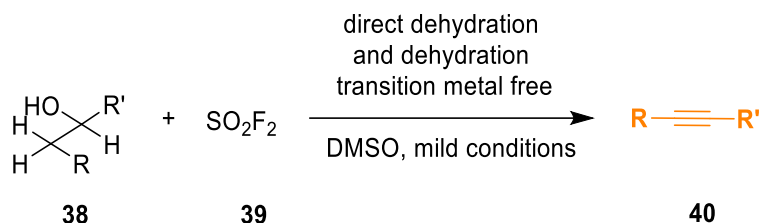
Figure 2.18: Dehydration and dehydrogenation of alcohols[58]

The kursunlu research group described synthesis of the di-alkyne **42 (figure 2.19)** via the propargylation of phenolic O-H groups in compound **41**, employing potassium carbonate as a base and dimethylformamide (DMF) as thr solvent.[59]
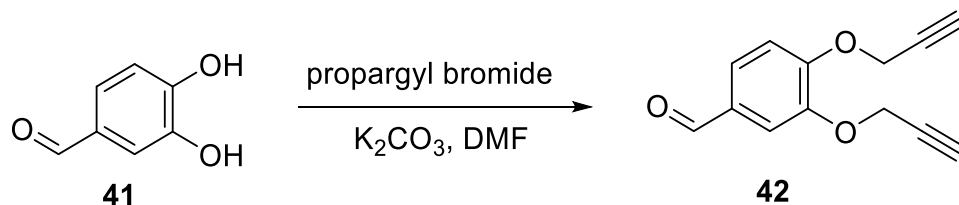
Figure 2.19: Synthesis of di-alkyne via propargylation of O-H group[59]

El. Azab *et al.* reported the synthesis of terminal alkyne **44** by propargylation of O-H group in compound **43**, employing DMF as solvent and potassium carbonate as base **(figure 2.20).** After 6 hours of stirring along with refluxing, a 75% of the yield of the final product was attained.[60]
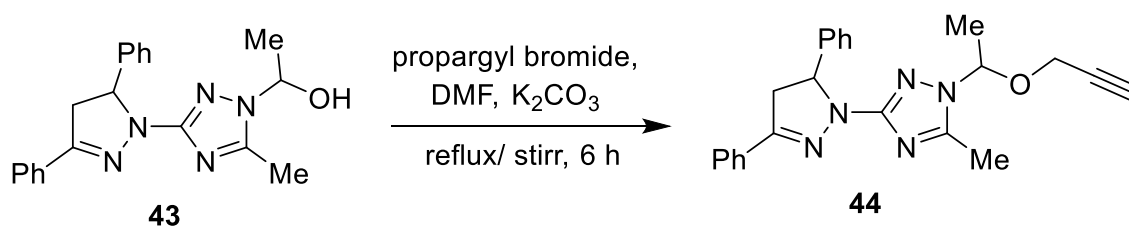
Figure 2.20: Synthesis of terminal alkyne reported by El. Azab and research group[60]

2.3.3.4. Synthesis of chalcone based terminal alkyne

Guantai *et al.* reported the alkylation reaction involving vanillin **45** with propargyl bromide using DMF in the presence of K_2CO_3 to obtain an acetylenic intermediate **46**. The reaction between acetylenic intermediate and acetone is carried out to in the presence of sodium hydroxide as base to form the next intermediate **47**. Afterwards, an appropriate benzaldehyde

was added in the presence of dioxane and under optimum reaction conditions the final product **48** was obtained in yield ranging between 31-88 % **(figure 2.21).**[61]
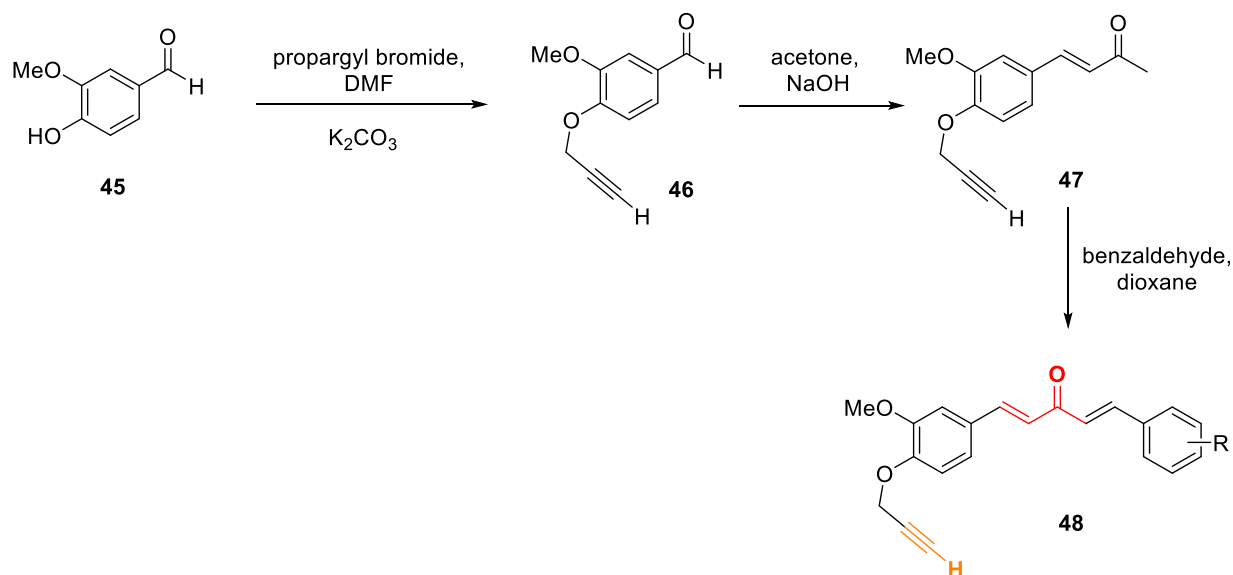
Figure 2.21: Synthesis of alkyne reported by Guantai research group[61]

Similarly, Singh and co-workers initiated the propargylation of 4-hydroxyacetophenone **49** in the presence of potassium carbonate as a base and acetone as a solvent to get terminal alkyne **51** with good yield ranging from 71 -81 %, which was then followed by aldol condensation with ferrocene carboxaldehyde **52** in the presence of ethanol and sodium hydroxide to obtain O-propargylated ferrocenyl chalcone **53** as represented in **figure 2.22**.[62]
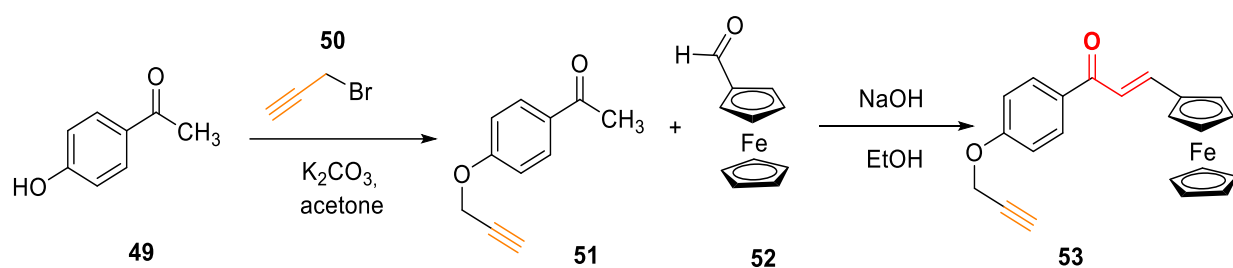
Figure 2.22: Synthesis of O-propargylated ferrocenyl chalcone[62]

Nagameni research group designed a chalcone derivative featuring propargyl group. Initially, the O-substituted phenylketone **54** derivative was reacted with propargyl bromide **46** and via a nucleophilic substitution process terminal alkyne **51** was synthesized. Then, the alkyne **55** and 3-bromo acetophenone **56** were reacted in the presence of methanol and 50% potassium hydroxide to form chalcone derivative **57** as represented in **figure 2.23**.[63] The

resulting chalcone derivative **57,** incorporating the propargyl group, serves as a versatile intermediate for further functionalization and could be explored for various applications, including in the development of organic sensors.
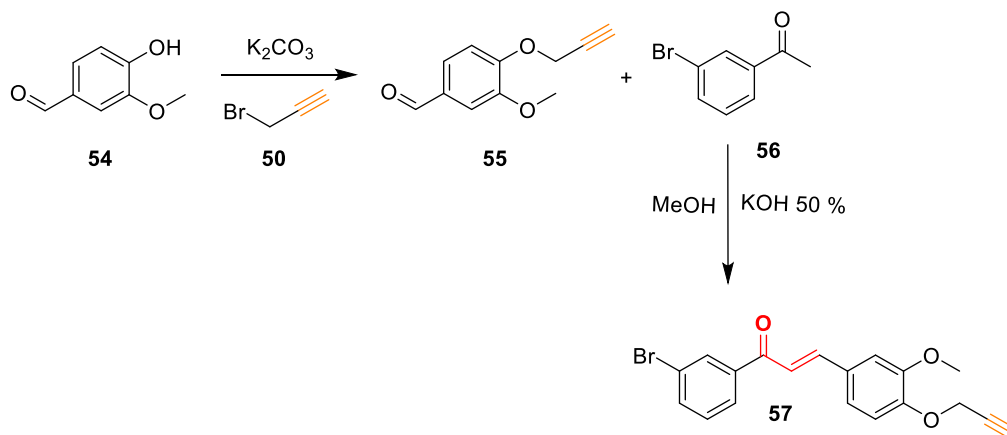
Figure 2.23: Synthesis of chalcone based alkyne from O-substituted phenylketone derivative[63]

A review of the literature highlights several methods for synthesizing terminal alkynes as mentioned above. By utilizing chalcones with labile protons (such as -OH, -NH$_2$) can also be used for the synthesis of terminal alkynes. The method involves the reaction of chalcone based reactant with propargyl bromide in solvents like N,N-dimethylformamide, acetone, and acetonitrile, along with bases such as potassium carbonate. This approach is advantageous for its high yield potential, normal laboratory conditions and does not require expensive equipments or harsh reaction conditions.

2.3.4. Synthesis of an organic azide

Organic azides were synthesized over a century ago, and have been valued for their exceptional reactivity, making them indispensable in various chemical reactions such as amine synthesis, azide- azide homocoupling, photochemistry, and the synthesis of heterocycles like 1,2,3-triazoles. Phenyl azide **59** was the first organic azide to be synthesized by Peter Griess in 1864 **(figure 2.24)**, and marks a significant milestone in the history of organic chemistry.[64] This discovery not only expanded the understanding of azide compounds but also laid the foundation for further exploration into their unique reactivity. The earliest methods of producing these compounds relied on hazardous materials such as hydrogen azides, which posed significant safety risks due to their volatility, toxicity, and explosive nature.[65] However, advancements in synthetic chemistry have led to the development of safer, more practical azidation techniques that avoid the use of such dangerous chemicals.[66] One of the most widely

adopted methods is the SN2-azidation reaction, where sodium azide is used to react with alkyl halides, acyl halides or aryl halides.[67,68] This approach is favoured for its efficiency and simplicity, particularly in producing aryl azides, which are highly stable and conjugated, making them crucial precursors in organic chemistry. These properties have broadened the application of organic azides in various fields, including biology and industry, where they serve as photoaffinity labels, cross linkers in photoresistors, and activators of polymer surfaces under light exposure. The shift toward modern azidation methods has not only improved laboratory safety but also expanded the utility of organic azides in scientific research, polymer industry, material science, agriculture and pharmaceuticals.[69,70]
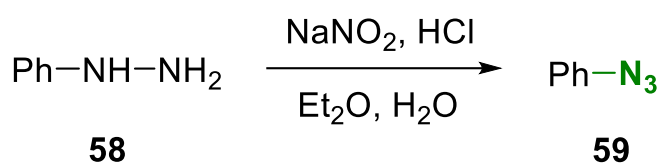
Figure 2.24: Synthesis of phenyl azide **52** from phenylhydrazine[64]

Jiang *et al.* developed a fully automated and reproducible method for converting primary amines **60** into organic azides **62** using prepacked capsules that contain all required reagents, including imidazole-1-sulfonyl azide tetrafluoroborate **61 (figure 2.25)**. Once the primary amine is manually loaded into the reaction vessel, the entire reaction and product isolation process runs automatically, with no further user input, producing the desired organic azide in high purity.[71]
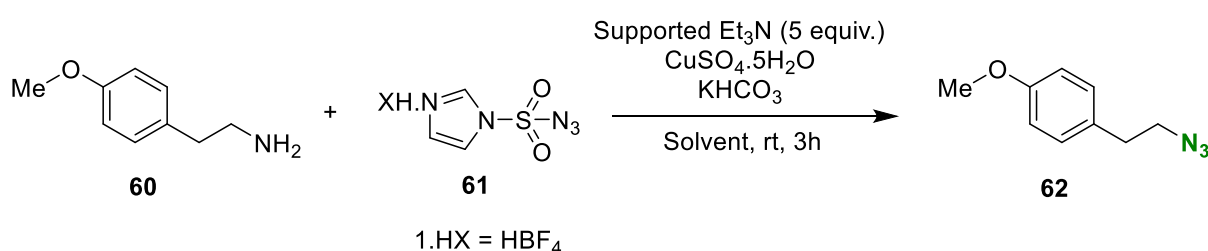
Figure 2.25: Synthesis of organic azide from primary amine[71]

Kitamura *et al.* described a method for directly synthesizing organic azides **65** from alcohols **63** using 2-azido-1,3-dimethylimidazolium hexafluorophosphate (ADMP) **64** as the azide transfer agent. By employing 1,8-diazabicyclo(5.4.0)undec-7-ene (DBU) as the base, the reaction was completed in 10 minutes at room temperature, achieving high yields of 65 % to 96 % **(figure 2.26 a)**.[72] Similarly, when a primary amine **66** was used as the starting material

with ADMP **64** and N,N-dimethyl-4-aminopyridine (DMAP) as the base, the reaction yielded products with yields ranging from 63 % to 94 % **(figure 2.26 b),** demonstrating the effectiveness of the base and amine in promoting the reaction and providing good to excellent yields under these conditions.[73]

(a)
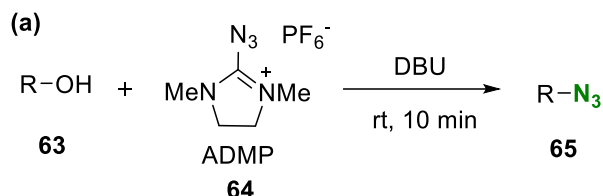
R = (E)-PhCH=CHCH$_2$, Ph(CH$_2$)$_3$, *n*-octyl

(b)
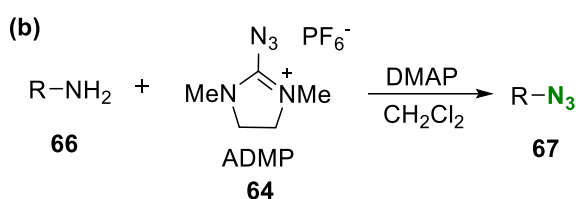
R = Ph, 4-MeOC$_6$H$_4$, 1-naphthyl

Figure 2.26: Synthesis of organic azide by reacting **(a)** alcohol with ADMP and DBU as the base; and **(b)** primary amine with ADMP and DMAP as the base[72,73]

Synthesis of organic azide **69** by nucleophilic substitution of aryl halide **68** by sodium azide (method A) is reported by Qiang hu *et al*. Another efficient way to synthesis azides is conversion of aniline **70** into aryldiazonium salt **71** and then to aryl azide **69** as shown in **(figure 2.27)** is method B. Alternative method C, for the synthesis of organic azide with high yields of 71- 92 %, is the reaction of organometallic reagent **72** with tosyl azide.[74]
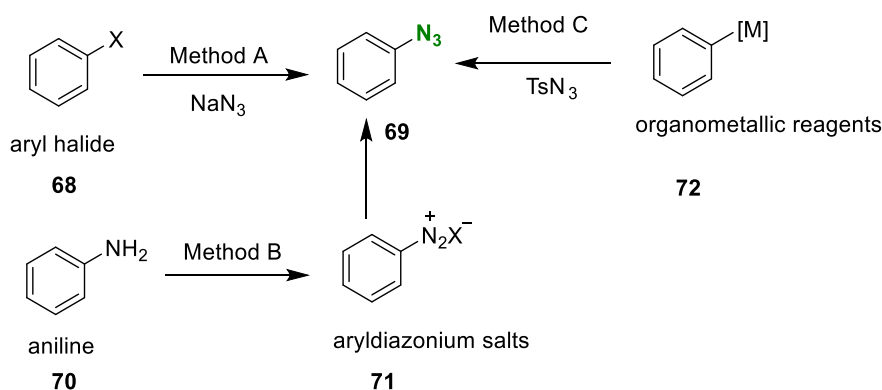
Figure 2.27: Synthesis of organic azide by nucleophilic substitution of aryl halide[74]

The Gavenonis research group reported a method to convert 2,6-dimesityphenyliodide **73** into its corresponding azide **74** with a 96 % yield. The process involved the reaction of 2,6-

dimesityphenyliodide with *n*-BuLi at 0 °C in hexane, followed by the addition of p-toluenesufonyl azide to the resulting lithium salt. This reaction produced the azide as red-orange crystals. **(figure 2.28)**.[75] The high yield and simple procedure make this method a valuable approach for synthesizing azides from aryl iodides.
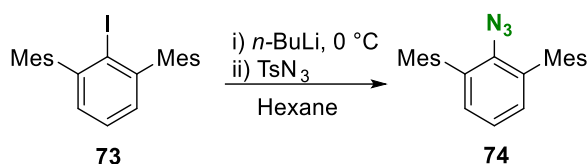
Figure 2.28: Synthesis of an azide based on 2,6-dimesitylphenyliodide by Gavenonis research group[75]

Kim *et al.* described a well-established method for producing various aromatic azides **76** by using substituted hydrazine **75** in combination with nitrosyl ions or their precursors, achieving outstanding yields of 84 % to 95 % **(figure 2.29)**.[76]
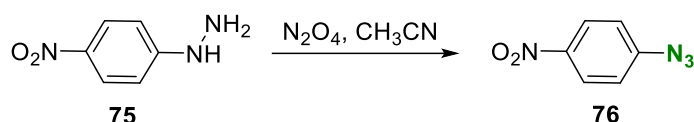
Figure 2.29: Synthesis of azide based on nitrosyl-hydrazine[76]

2.3.5. Synthesis of 1,2,3-triazole via CuAAC reaction

The 1,2,3-triazoles are versatile heterocycles that have become substantial molecular scaffolds in modern organic synthesis, particularly through the 'CuAAC'. The reaction selectively produces 1,4-disubstitution 1,2,3-triazole derivatives with high yields, stereospecificity, and under mild conditions, often in benign solvents.[16,77] The following section lists several reported studies on the cycloaddition of terminal alkynes and organic azides for the synthesis of 1,2,3-triazoles.

2.3.5.1 Synthesis of 1,2,3-triazole having different substituents via CuAAC methodology

Eoin P. McCarney *et al.* synthesized 1,4-(dipyridin-2-yl)-1,2,3-triazole **79** with 69 % yield by mixing 2- ethynylpyridine **78** and 2-azidopyridine **77** in the presence of toluene as a solvent and tetrakis(acetonitrile)copper(I)hexafluorophosphate as a catalyst at 90 °C for 48 h as shown in **figure 2.30**.[78]
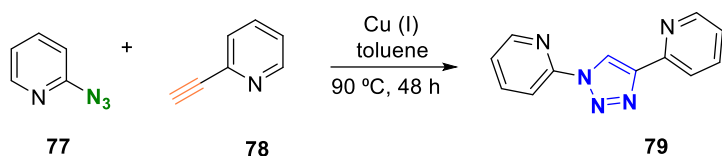
Figure 2.30: Synthesis of 1,4-(dipyridin-2-yl)-1,2,3-triazole[78]

Shaily and colleagues developed a 1,2,3-triazole-linked derivative **82** by initially transforming 4-hydroxycoumarin into its respective alkyne **80** and azide **81** in individual steps. Thereafter, $CuSO_4.5H_2O$/ Na ascorbate was employed as a catalyst to merge these intermediated through a cycloaddition reaction, a compound **89** obtained with yield 88% where two coumarin units are connected via a 1,2,3-triazole bridge **(figure 2.31)**.[79]
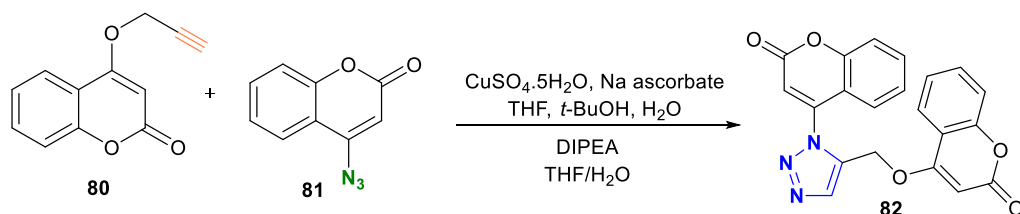
Figure 2.31: The synthesis of a probe based on coumarin-linked 1,2,3-triazole[79]

Ghosh *et al.* reported a newly synthesized 1,2,3-triazole decorated imino-phenol compound **84** with yield of 57%, using $CuSO_4.5H_2O$/ Na ascorbate as a catalyst and water as the solvent medium to carry out the reaction **(figure 2.32)**. The compound was then utilized for metal ion sensing of Zn^{2+}, Cu^{2+} and picric acid.[80]
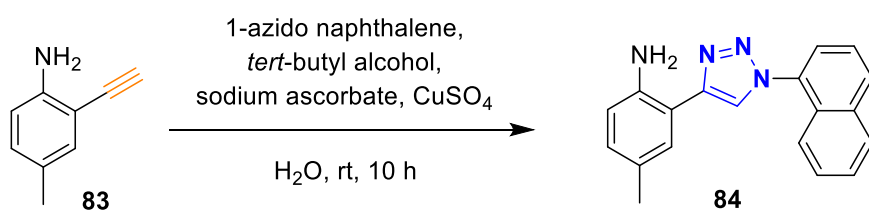
Figure 2.32: Synthesis of 1,2,3-triazole decorated imino-phenol compound[80]

Similarly, Ghosh *et al.* reported the synthesis of 1,4-diaryl-1,2,3-triazole **86** through CuAAC methodology, utilizing phenylacetylene **13** and hydroxy substituted azide **85** in the presence of $CuSO_4.5H_2O$/ Na ascorbate as a catalyst. The obtained compound **93** with yield of 74%**,** bearing a phenol moiety has an ability to act as a fluorescence chemo sensor **(figure 2.33)**[81]
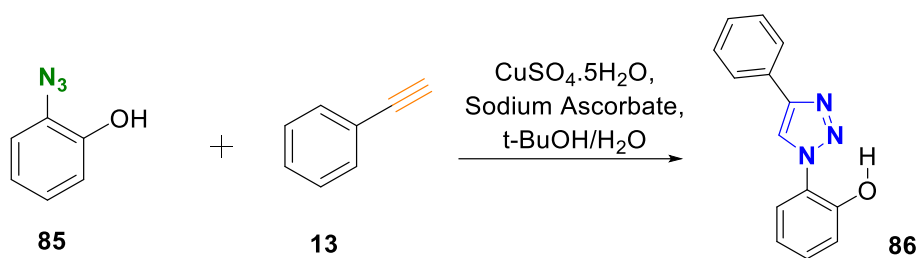
Figure 2.33: Synthesis of 1,2,3 triazole through click chemistry[81]

Joshi research group described the synthesis of coumarin-1,2,3-triazole-based chemosensor **89** probe having yield of 79% by linking amino acyl O-propargyl esters **87** with 4-azidomethyl-7-hydroxycoumarin **88** through a cycloaddition reaction, facilitated by a Cu(I) catalyst at ambient temperature **(figure 2.34)**.[82]

Pg = -OCOC(CH$_3$), -OCOCH$_2$C$_6$H$_5$
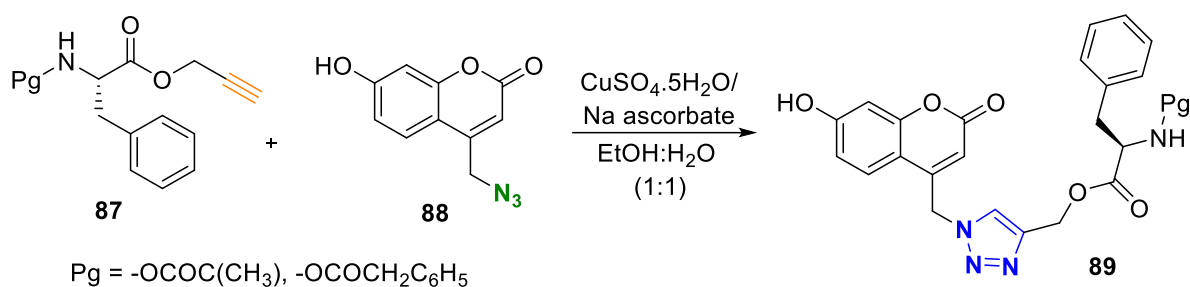
Figure 2.34: Synthesis of coumarin-1,2,3-triazole based chemosensors[82]

2.3.5.2 Synthesis of 1,2,3-triazole having chalcone as a backbone via CuAAC methodology

Nagaraja *et al.* reported the synthesis of pyrazole embedded 1,2,3 triazole **92** by mixing aryl acetylene **91** with 1-(p-azidophenyl)-3-(3-methyl-1-phenyl-5-(otolyloxy)-1H-pyrazol-4-yl)-prop-2-en-1-one **90** in the presence of CuSO$_4$.5H$_2$O/ NaASc as a catalyst. The reaction mixture was agitated for 10 to 12 hours at room temperature in order to get the intended product with a good yield of 67–77% as demonstrated in the **figure 2.35**.[83]
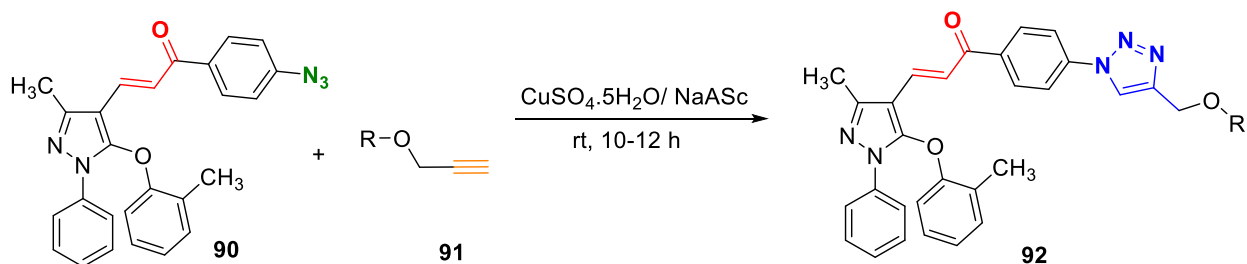
Figure 2.35: Synthetic route for synthesis of 1,2,3- triazole[83]

Similarly, P. Rajakumar *et al.* reported the efficient synthesis of a 1,2,3-triazole derivative **(95)** through a CuAAC reaction involving chalconated alkyne **(93)** and bis-azide **(94).** The reaction was carried out in the presence of $CuSO_4 \cdot 5H_2O$ and sodium ascorbate, using a tert-butanol and water mixture (1:1) as the solvent system at room temperature, as illustrated in **figure 2.36**. The process yielded a 1,2,3-triazole-based dendrimer product with an impressive yield of 92%, showcasing the efficiency and practicality of this synthetic approach.[84]
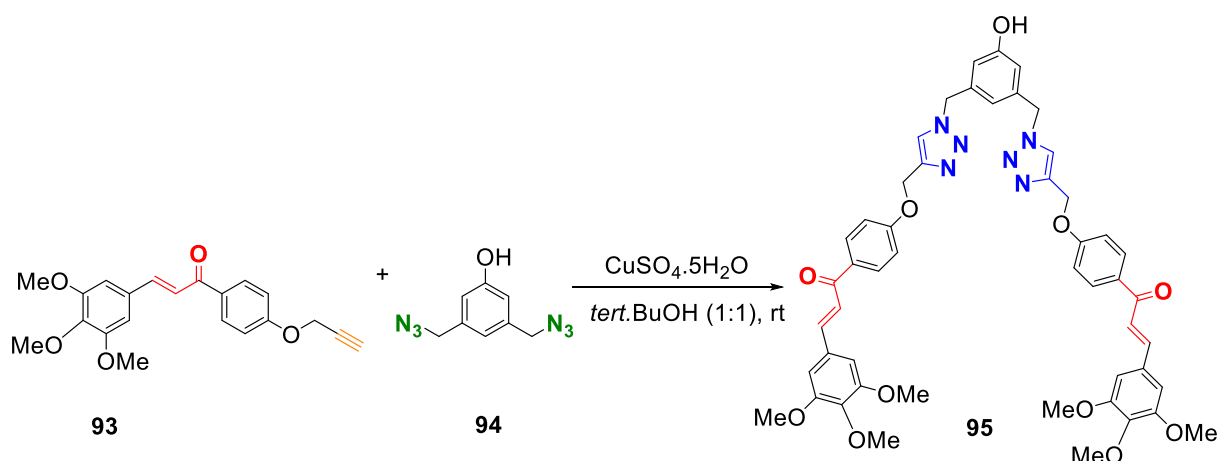
Figure 2.36: Synthesis of 1,2,3 triazole from bis azide[84]

Yadav and colleagues reported the synthesis of substituted 1,2,3-triazoles **(98)** with a yield of 75% through a CuAAC reaction. The reaction involved a chalcone-based alkyne and a fluorinated azide, utilizing copper nanoparticles as the catalyst. Water was used as the solvent while the mixture was agitated for four hours at 70 °C as depicted in **figure 2.37.** This method highlights an efficient and environmentally friendly approach to synthesizing fluorinated 1,2,3-triazoles with moderate to high yields.[85]

R' = NO$_2$, OCH$_3$, Br
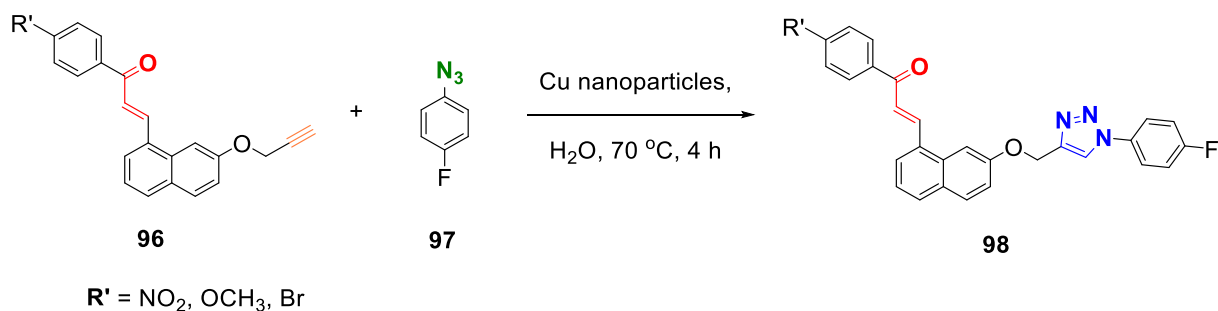
Figure 2.37: Synthesis of chalcone based 1,2,3-triazole[85]

Singh and their research group described the synthesis of Schiff base-chalcone-functionalized bis(1,2,3-triazolyl-y-propyltriethoxysilanes) **(101)** through an efficient "Click Silylation" approach. The reaction employed CuBr(PPh₃)₃ as a catalyst and a mixture of tetrahydrofuran (THF) and triethylamine (TEA) as the solvent system. The process was carried out at 60 °C for 6 hours, resulting in excellent yields ranging from 90% to 96%, as illustrated in **figure 2.38.** This method demonstrates a highly effective strategy for the synthesis of functionalized triazole-based silane derivatives.[86]
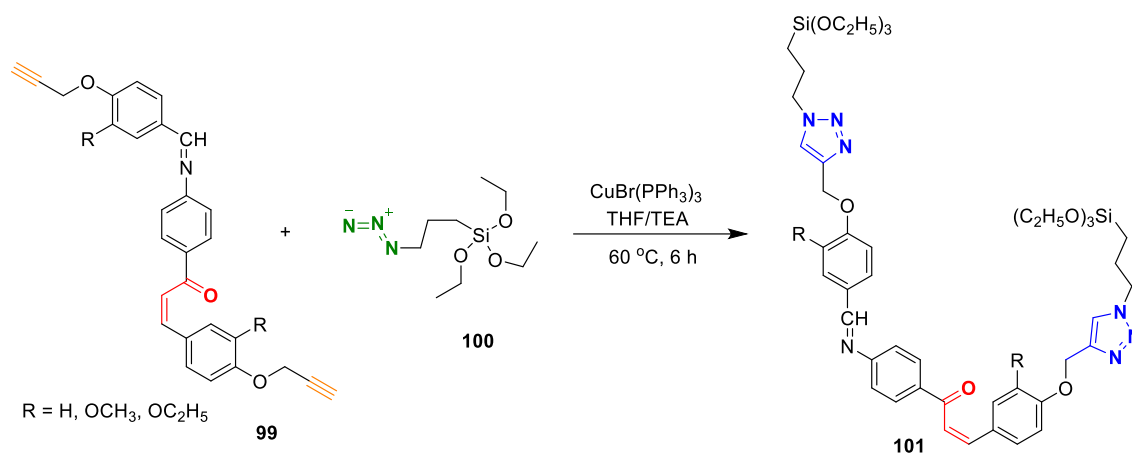
Figure 2.38: Synthesis of Schiff base – chalcone functionalised bis (1,2,3-triazolyl-y-propyltriethoxysilanes) using an efficient "Click Silylation" method[86]

The extensive literature on the synthesis of 1,2,3-triazoles through Cu-catalyzed azide-alkyne cycloaddition (CuAAC) underscores its superiority as a highly efficient and versatile methodology in organic synthesis. CuAAC has gained widespread recognition due to its ability to facilitate the regioselective formation of 1,4-disubstituted triazoles under mild conditions with excellent yields. The development of advanced catalytic systems, particularly Cu(I) coordination complexes, has significantly enhanced the scope and utility of this reaction. Complexes such as [CuBr(PPh₃)₃] have proven to be highly effective catalysts, offering improved stability for Cu(I) species and minimizing the risk of oxidation to Cu(II), which can otherwise diminish catalytic activity. The bulky ligands in these complexes stabilize the active Cu(I) center, allowing for smooth catalytic cycles and minimizing the formation of unwanted byproducts.

2.4. Exploring synthesized compounds via spectroscopic approach

Spectroscopic analysis is essential for the thorough characterization of synthesized products, providing critical validation of their formation and integrity. Various analytical

techniques are employed to confirm the identity and purity of compounds. Infrared (IR) spectroscopy, NMR spectroscopy (both ^{1}H and ^{13}C), and mass spectrometry are commonly used to identify functional groups, confirms molecular structures, and determine molecular weights.

Additionally, fundamental analytical methods, such as determining melting points and performing CHN analysis, further verify the synthesis and purity of the products. Physical inspection, including observation of color, texture etc. also contributes to the overall examination of the synthesized materials.

2.4.1. Infrared (IR) spectroscopy

IR spectroscopy provides valuable insights into the vibrational modes of molecules, making it a crucial tool for identifying functional groups and characterizing molecular structures. A sample absorbs IR radiations within the $4000 - 400$ cm^{-1} range, specific functional groups can be identified based on their characteristic absorption peaks.[87] For instance, In the infrared (IR) spectrum of chalcones, several distinct peaks are observed due to the functional groups present in the structure. The carbonyl group (C=O) in chalcones produces a strong and characteristic peak typically in the 1750–1650 cm^{-1} range, with chalcones commonly showing absorption near 1660–1680 cm^{-1} due to conjugation with the double bond. The C=C stretching vibrations of the α,β-unsaturated carbonyl system are observed around 1680–1600 cm^{-1}. Primary amines typically display two distinct peaks in the 3300–3500 cm^{-1} region, corresponding to symmetric and asymmetric N–H stretching vibrations. These two peaks are generally weaker and broader compared to O–H stretching. Additionally, primary amines exhibit a bending vibration (N–H bend) around 1600–1580 cm^{-1}. The C-H stretching appears above 3000 cm^{-1} for aromatic compounds and between $3000 - 2850$ cm^{-1} for aliphatic compounds. In alkynes, triple bonds (C≡C) show absorption in $2250 - 2100$ cm^{-1} range. Additionally, the fingerprint region below 1500 cm^{-1} offers a complex pattern of peaks that further aids in the detailed structural elucidation of molecules.[88,89]

2.4.2. NMR spectroscopy

Nuclear magnetic resonance (NMR) spectroscopy is a widely used analytical technique used to determine the structure of molecules by analyzing the behaviour of certain nuclei (usually hydrogen and carbon) in reaction to a strong magnetic field. When placed in a magnetic field, these nuclei resonate at specific frequencies which are determined by its

specific chemical surroundings, including the electronegativity of adjacent atoms or the type of bonding present.[90] Through the measurement of these frequencies, nuclear magnetic resonance (NMR) may provide comprehensive structural information, including the nature of atom bonds, the quantum number of atoms in comparable surroundings, and even spatial configurations. Hence, NMR has emerged as a crucial method for studying the structure of both simple and complicated molecules. In organic chemistry, there are two main types of NMR spectroscopy commonly used: Proton NMR (^{1}H NMR) and Carbon-13 NMR (^{13}C NMR), provides distinct understanding of the molecular structure.[91]

2.4.2.1. Proton NMR (^{1}H)

^{1}H NMR spectroscopy focuses on the detection of hydrogen atoms (protons) in a molecule. Due to the abundance of hydrogen in organic compounds, each proton in a molecule experiences a unique environment, leading to the distinctive chemical shifts. The chemical shift of a proton provides crucial insights on its electronic surroundings such as specifying its proximity to electronegative atoms or π-systems (double bonds, aromatic rings, or triple bonds), while the splitting pattern provides insights into the number of adjacent protons.[91] The protons located in the close proximity to electronegative atoms experience deshielding, and the signal appears at high chemical shift value (downfield), while the protons in electron rich environment (shielded protons) resonate at lower chemical shift values (upfield). For instance, ^{1}H NMR of a terminal alkyne, a signal in the region of $\delta = 1.7 - 2.7$ ppm corresponds to alkynyl protons, whereas the peaks emerging at $\delta = 7 - 8$ ppm are suggestive of protons attached to a 1,2,3-triazole ring/or aromatic groups.[92] The Protons on a methylene group (–CH$_2$) adjacent to nitrogen typically resonate between 2.5-3.5 ppm, as the nitrogen withdraws electron density, causing deshielding. The protons of the α,β-unsaturated carbonyl system (C=C) typically resonate between 7.2-8.0 ppm. The β-proton (closer to the carbonyl group) usually appears downfield (around 7.5-8.0 ppm) due to the deshielding effect of the carbonyl group, while the α-proton appears slightly upfield, around 7.2-7.5 ppm. These shifts can vary depending on the substitution on the aromatic rings and the overall molecular structure.

2.4.2.2. Carbon-13 NMR (^{13}C)

^{13}C NMR provides information on the carbon skeleton of a molecule. Since, ^{13}C is less abundant in nature, it requires higher sensitivity and longer acquisition time than ^{1}H NMR; therefore, produces distinct signals in the NMR spectrum. The chemical shift range of ^{13}C NMR is much wider than that of ^{1}H NMR, typically from 0 to 220 ppm. Carbons in different

environments (e.g., alkanes, alkenes, aromatics, carbonyls) exhibit distinct shifts, making it easier to identify functional groups and carbons. For example, sp^3 hybridized carbons typically resonate at lower values (0 – 50 ppm), while sp^3 hybridized carbons, such as those in aromatic systems, resonate at higher values (100 – 150 ppm). The carbon of the carbonyl group (C=O) resonates at 185 – 220 ppm. The proton decoupled ^{13}C NMR spectrum displayed signal corresponding to the carbon with attached hydrogen of the 1,4-disubstituted 1,2,3-triazole at around 120 ppm.[93,94]

2.4.3. Mass spectrometry

Mass spectrometry is a versatile analytical technique that ionizes chemical compounds to generate charged molecules or fragments, which are then measured by their mass-to-charge (m/z) ratio. This method is widely used for applications such as reaction monitoring, structural characterization, and determining the molecular mass of unknown substances.[95] By analyzing the resulting spectrum, where peaks correspond to different ion masses and abundances, the mass spectrometer identifies the molecular mass of the compound from the peak with the highest m/z ratio.[96] The principle of mass spectrometry enables precise molecular weight determination and structural elucidation, making it crucial in chemistry, biochemistry, pharmaceuticals, and environmental chemistry. When integrated with various chromatographic techniques like gas chromatography (GC) or liquid chromatography (LC), mass spectrometry delivers a thorough analysis of complex samples. GC or LC firsts separates the components of a mixture based on their chemical properties, such as volatility or solubility. Following separation, mass spectrometry measures the mass to charge ratios of the individual components. The molecular ion peak (M^+) represents the ion formed by the removal of one electron from the molecule, corresponding to the molecular weight of the compounds. The base ion peak is the most intense peak, represents the most stable and abundant fragment ion. The M+1 peak results from the presence of isotopes, such as carbon-13, adding one atomic mass unit (amu) to the molecular ion. Similarly, the M+2 peak often arises due to isotopes like chlorine-37 or bromine-81. The M+23 peak in mass spectrometry typically indicates the presence of a sodium ion (Na^+) adduct. This combination allows for the detection of trace level analytes and facilitates accurate quantification of each component.[97,98]

2.5. Utilization of Chalcone-based 1,2,3-triazoles in Chemosensing

Over the past few decades, 1,2,3-triazole-based ligands have been extensively investigated for their ability to detect ions, particularly for cations using absorption and

emission spectroscopy across various solvent systems. The unique electronic properties of the 1,2,3-triazole ring, often in combination with other functional groups, enhances the selectivity and senstivity of these ligands, making them highly effective in identifying and quantifying specific metal ions in complex media.[86] As a result, 1,2,3-triazole based sensors have become indispensable tools in analytical chemistry, contributing to advancements in environmental monitoring, biological studies, and industrial applications.[34]

Singh *et al.* reported a highly sensitive and selective 1,2,3-triazole appended organosilicon sensor **102** featured an azo dye **(figure 2.39).** The CH_3CN/H_2O (4:1) solvent was used for the photophysical investigations, which were conducted using UV-visible spectroscopy, Cu(II) and Fe(II) ions detection utilizing. According to estimates, the sensor's limit of detection for Cu(II) and Fe(II) was 0.12 µM and 0.11 µM, respectively..[99]
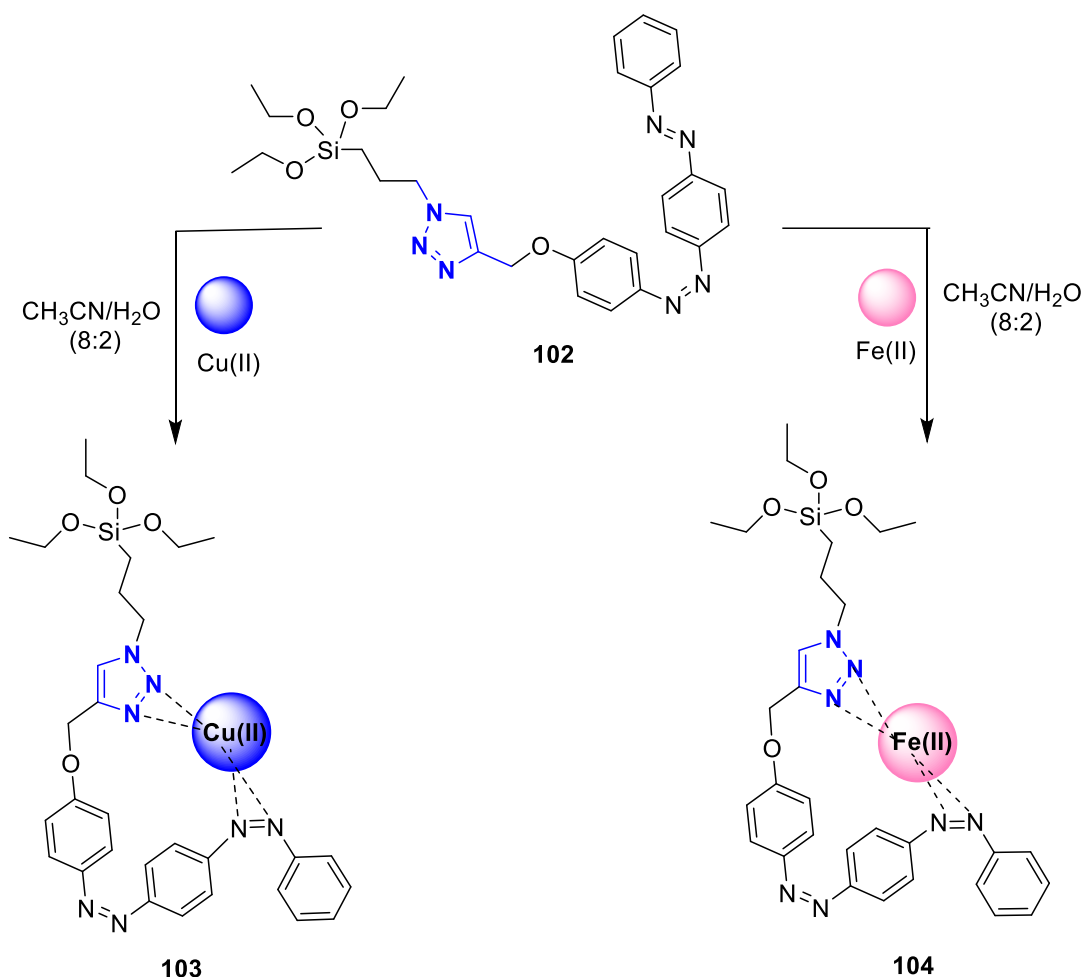
Figure 2.39: 1,2,3-triazole appended organosilicon sensor for the selective detection of Cu(II) and Fe(II) ions[99]

Kaur *et al.* reported the synthesis of a triazole linked naphthalimide-ferrocenyl-chalcone (TNFC) **105** derivative as a potentiometric sensor specifically for the detection of Cu(II) ions **(figure 2.40)**, comprehensively evidenced by UV-Vis and fluorescence spectroscopy. The sensor exhibited the detection limit of 0.79 μM.[32]
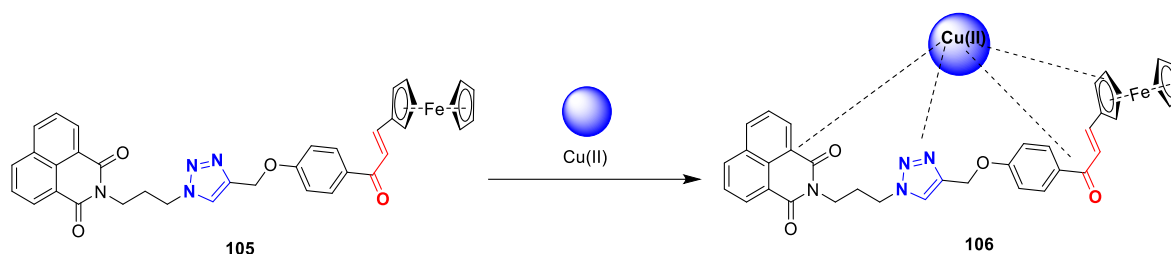
Figure 2.40: A triazole linked naphthalimide-ferrocenyl-chalcone (TNFC) derivative was synthesised as a potentiometric sensor designed in particular for the detection of Cu(II) ion[32]

Rathinam and colleague described the click reaction between a rhodamine alkyne derivatives and 11-azidoundecan-1-ol using a CuSO₄/Na ascorbate catalytic system in tBuOH/H₂O, resulting in the formation of a 1,2,3-triazole **107** based receptor for the specific detection of Cu(II) and Fe(III) ions **(figure 2.41)**.[100]
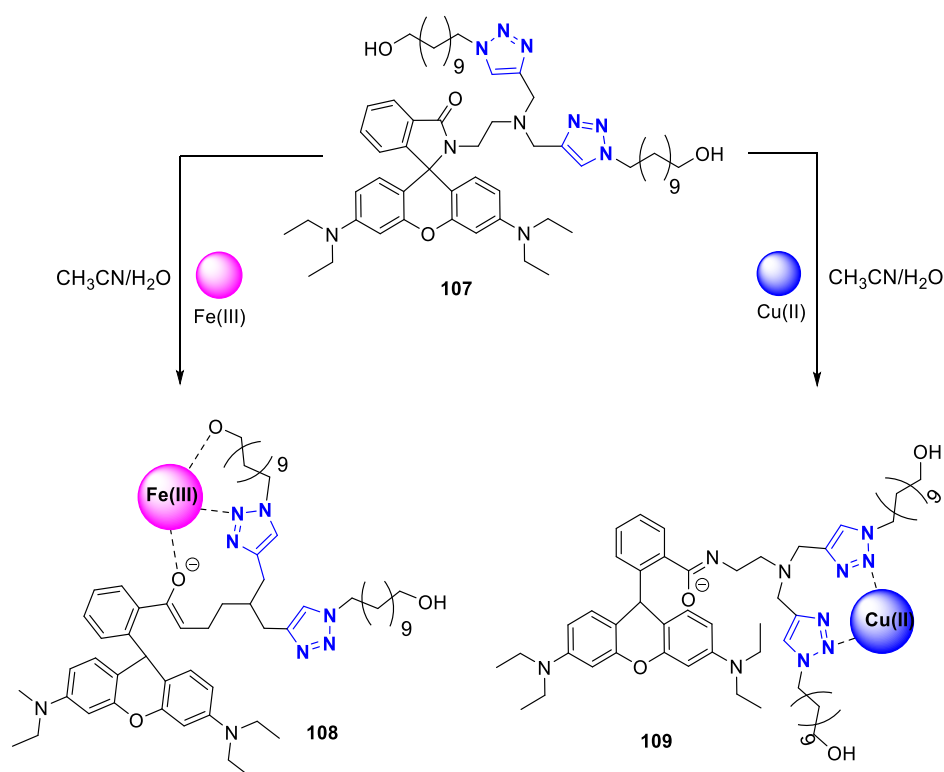
Figure 2.41: Development of a receptor based on 1,2,3-triazole for the selective detection of Cu(II) and Fe(III) ions[100]

Wahab's research group developed new optical sensors for detecting heavy metals by preparing a novel organic linker [4-(1-(2-(2,4-dinitrophenyl)hydrazineylidene)-5-phenylpenta-2,4-dien-1-yl)-1-(4-methoxyphenyl)-5-methyl-1H-1,2,3-triazole] **110**. This new linker was employed to detect various metal ions, including Cu^{2+}, Zn^{2+}, Cr^{3+}, Co^{2+}, Cd^{2+}, and Hg^{2}. Notably, the linker demonstrated high sensitivity and selectivity towards Hg^{2}, with a binding stoichiometry of 1:1 **(figure 2.42)**.[101]
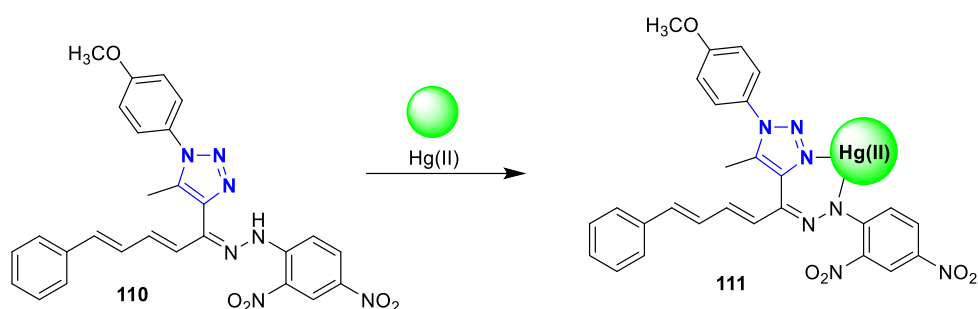
Figure 2.42: The synthesis of an optical sensor specifically designed for the targeted detection of Hg(II) ions[101]

A research publication by Singh and co-workers reported the cationic chemo sensing capabilities of chalconyl-triazole caged organosilicon complexes were reported using the o-, m-, and p-isomeric units. The absorption spectra as well as molar absorptivity constant reveal significant variability in UV-vis spectral analyses. The ortho isomer of chalcone based 1,2,3-triazole silatrane (CTS) **112**, operating as double ion fluorescence sensors for Cu^{2+} and Ni^{2+} ions, shows effective sensing **(figure 2.43)**. Organosilicon compounds have been employed to actively detect Cu^{2+} and Ni^{2+} ions in a solvent combination that includes water.[102]
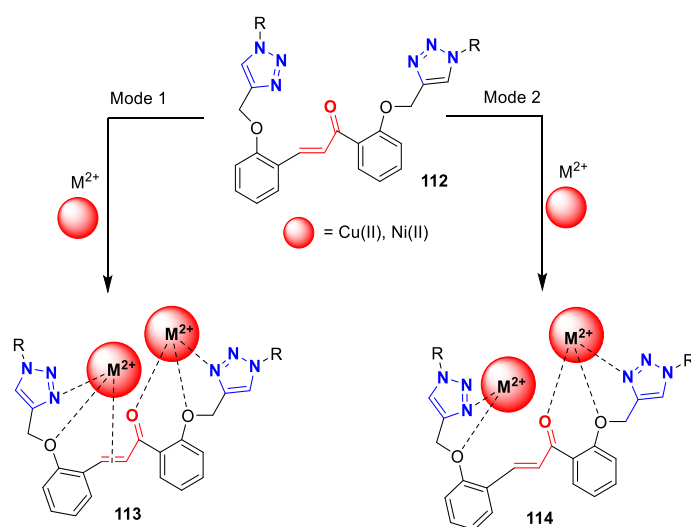
Figure 2.43: organosilicon compounds caged with chalconyl-triazole were investigated for the detection of Cu(II), Ni(II) ions[102]

A tripropargylamine pyrene azide click adduct-based ratiometric fluorescent 'on-off' Zn(II) chemosensor **115 (figure 2.44)** was reported by Ingale and colleagues. The observed ratiometric shift in emission, characterized by an augmentation in monomer emission and reduction in excimer emission, suggests the presence of Zn(II) selectivity in the fluorescence 'on-off' sensor and the detection limit was 0.2 μM.[103]
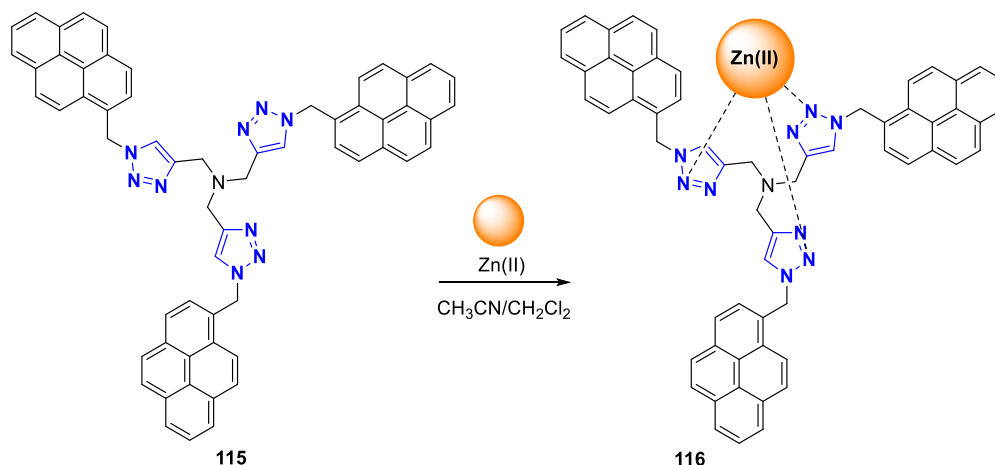
Figure 2.44: Pyrene-linked tris-1,2,3-triazole amine sensor for the detection of Zn(II) ions[103]
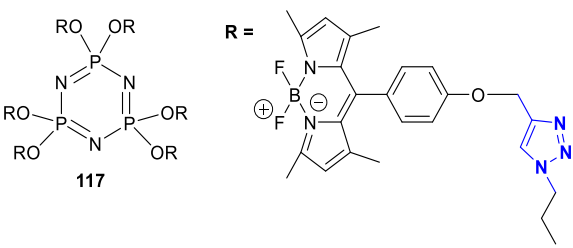
2.6. UV-Visible and Fluorescence spectroscopy
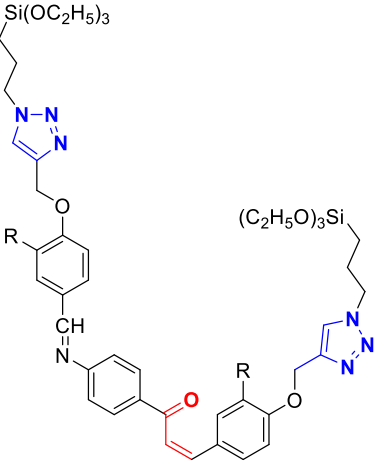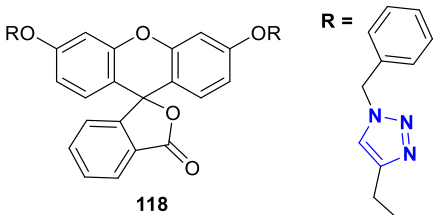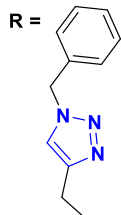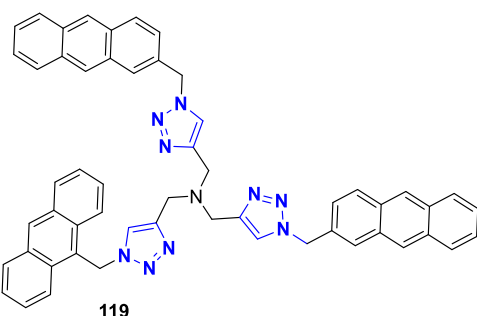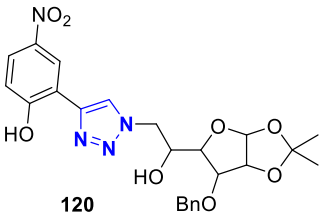
UV-visible spectroscopy is a widely used analytical technique that measures the absorption of light in the ultraviolet (200-400 nm) and visible (400-800 nm) regions. The principle of this technique is based on the excitation of electrons from lower energy states to higher energy states within a molecule upon exposure to light of specific wavelengths.[89] Different functional groups exhibit characteristic absorption patterns. A low-intensity band between 250 and 360 nm typically indicates an n→π* transition, observed in groups like N=N, C=O, –COOR, –NO$_2$, and –COOH. Aromatic systems generally display two medium-intensity bands above 200 nm. Molecules such as aldehydes, ketones, amides, and esters, which contain π-electrons along with lone pairs, exhibit two distinct bands: a high-intensity π→π* transition near 250 nm, and a lower-intensity n→π* transition above 300 nm.[104,105] As conjugation increases, both the wavelength and intensity of absorption increase. It primarily provides information on the presence of chromophores (light-absorbing groups) but does not offer detailed structural information, making it necessary to combine with other techniques such as NMR and IR for complete molecular characterization. Additionally, its sensitivity is lower compared to fluorescence spectroscopy, limiting its effectiveness in detecting trace amounts of analytes.[106]
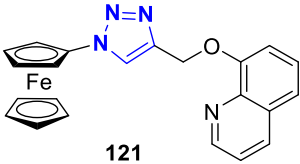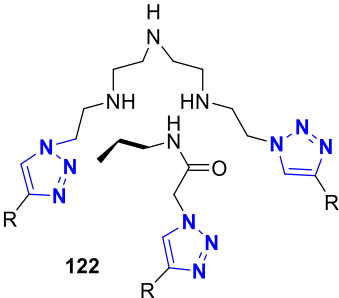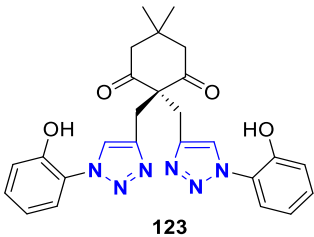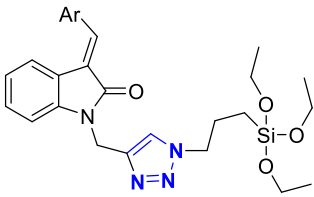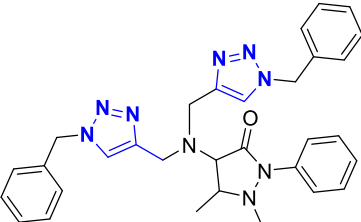
Fluorescence refers to the emission of light that occurs after a fluorescent molecule or fluorophore absorbs ultraviolet (UV) or visible light. Upon absorbing light at a specific wavelength, the fluorophore becomes excited and subsequently releases energy in the form of emitted light at a longer wavelength.[107] The process begins with excitation (i), where the molecule absorbs light and transitions from its ground singlet state (S_0) to an electronically excited singlet state (S_1). This is followed by vibrational relaxation or internal conversion (ii), during which the molecule transitions from a higher to a lower electronically excited state (S_1) without emitting radiation. Finally, emission occurs (iii) typically within 10^{-8} seconds after excitation, as the electron returns to the stable ground state (S_0), releasing light at a wavelength determined by the energy difference between the excited and ground states.[108]

In molecules, each electronic state is associated with multiple vibrational levels. In the ground state, nearly all molecules reside in the lowest vibrational level. When exposed to UV or visible light, the molecule can be excited to one of several vibrational levels within the corresponding electronically excited state. As a result, fluorescence emission does not occur at a single wavelength but spans a range of wavelengths, representing various vibrational transitions within one electronic transition. This is why both excitation and emission spectra are used to capture the fluorescence behaviour of molecules in detail. The use of two distinct wavelength parameters in fluorescence increases its specificity compared to spectroscopic methods based solely on absorption.[109,110]

Table 2.1: Chemosensors integrated with 1,2,3-triazole moiety for the targeted detection of metal ions
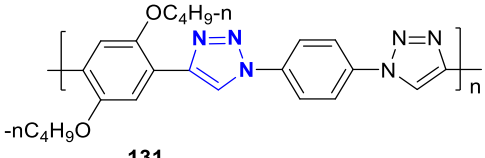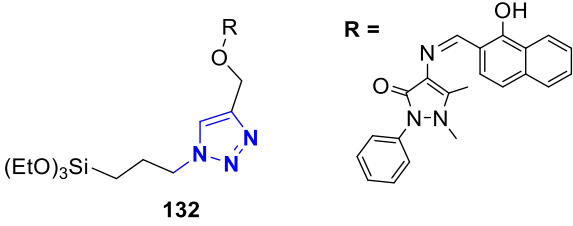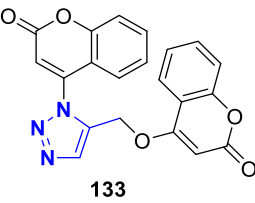
Entry	Metal ion	Structure	Limit of Detection (µM)	Ref.
1.	Fe(II)		2.03	111

Entry	Metal ion	Structure	Limit of Detection (μM)	Ref.
2.	Fe(III)	**101**	0.18	86
3.	Co(II)	**118**	10.0	112
4.	Ni(II)	**119**	0.71	113
5.	Cu(II)	**120**	3.50	114

Entry	Metal ion	Structure	Limit of Detection (μM)	Ref.
6.	Cu(II)	**121**	1.71	[115]
7.	Cu(II)	**122**	2.87	[116]
8.	Cu(II)	**123**	2.00	[117]
9.	Cu(II)	**124**	3.21	[118]
10.	Cu(II)	**125**	3.11	[119]

Entry	Metal ion	Structure	Limit of Detection (μM)	Ref.
11.	Cu(II)	$R_1 = OCH_3$ **126**	9.42	[120]
12.	Zn(II)	**127**	75.0	[121]
13.	Ag(I)	**128**	2.70	[122]
14.	Au(III)	**129**	0.14	[123]
15.	Hg(II)	**130**	1.02	[124]

Entry	Metal ion	Structure	Limit of Detection (μM)	Ref.
16.	Hg(II)	**131**	0.46	[125]
17.	Sn(II)	**132**	0.67×10^3	[126]
18.	Pb(II)	**133**	1.90×10^{-3}	[79]

2.7. Aims and objectives of the thesis

The goal of this thesis **"SYNTHESIS AND CHARACTERIZATION OF CHALCONE BASED 1,2,3-TRIAZOLE VIA CuAAC REACTION AND THEIR APPLICATION AS CHEMOSENSORS"** was to design and synthesize new chalcone based 1,2,3-triazoles and to investigate their practicability as optical sensors tailored for the quantification of metal ions which can be lethal to human body when present above the permissible limits, and hence the detection of transition metal ions has become of paramount importance due to their potential to be either necessary or hazardous to human life. Furthermore, the traditional approaches established for the recognition of these toxic metal ions like atomic absorption spectroscopy (AAS) need expensive analytical equipments and laborious sample preparation. Extensive research demonstrates that the CuAAC methodology can be implemented to synthesize a diverse array of novel chalcone based 1,2,3-triazole derivatives, by modifying functional groups in various organic molecules, including those with

strong fluorophoric properties. After synthesis and characterization, these new compounds can further be applied in ion sensing.

The insights have guided the formulation of objectives for this study as follows:

1) Synthesis of new chalcone based 1,2,3–triazole derivatives via Cu(I) catalysed alkyne azide cycloaddition reaction.

2) Characterization of the synthesized novel compounds by spectroscopic techniques like IR, NMR (^{1}H, ^{13}C) and mass spectrometry.

3) Exploring ion sensing behaviour of the synthesized 1,2,3–triazole derivatives using different spectroscopic techniques.

In recent years, the identification of harmful analytes that negatively impact the environment and living systems has become a major focus worldwide. For example, Cu (II) ion serves as both a vital micronutrient and a potential toxin. While essential for processes like enzymatic activation and iron metabolism, elevated Cu(II) levels from industrial discharge and agricultural runoff can cause bioaccumulation in aquatic ecosystems, leading to the disrupted biodiversity and ecosystem function. In humans, excess Cu(II) can result in neurological abnormalities, liver and kidney damage, gastrointestinal damage.[127,128] Co(II), a trace element essential for vitamin B$_{12}$ can be detrimental when present in excess, leading to serious health issues like heart problems, lungs infection etc.[129] Furthermore, the long-lasting presence of Pb(II) in the human body can severely damage nervous system, increases blood pressure and harms kidneys. Also, it has been linked to memory problems in adults as well as children on exposure to high levels.[130]

Therefore, the development of new, selective chemosensors is crucial, and chalcone-based 1,2,3-triazole sensors have made significant progress in the last decade, particularly for detecting important metal ions in biological and environmental contexts. Over the past decade, chalcone-based 1,2,3-triazole sensors synthesized through click chemistry have shown great versatility, with excellent selectivity and binding abilities.[120] This thesis discusses the synthesis of molecular sensors using the CuAAC methodology, combined with chalcone component that absorb well in the UV-Visible region. Their sensing abilities can be easily studied using reliable methods like absorption and fluorescence spectroscopy. The molecules feature a chalcone backbone with a 1,2,3-triazole ring, providing N atoms for binding to metal ions. When these molecules form complexes with metal ions, changes in their absorption can be analyzed using UV-Visible or fluorescence spectroscopy.

References

1. M. S. Yadav, S. Rajkhowa, S. K. Singh, M. K. Jaiswal and V. K. Tiwari, *ChemistrySelect*, 2024, **9**, e202400776.

2. H. C. Kolb, M. G. Finn and K. B. Sharpless, *Angew. Chem. Int. Ed.*, 2001, **40**, 2004–2021.

3. L. L. Kiessling, *Proc. Natl. Acad. Sci. U S A*, **120**, e2308367120.

4. D. Bauer, S. M. Sarrett, J. S. Lewis and B. M. Zeglis, *Nat. Protoc.*, 2023, **18**, 1659–1668.

5. H. C. Kolb and K. B. Sharpless, *Drug Discov. Today*, 2003, **8**, 1128–1137.

6. S. M. Kondengadan, S. Bansal, C. Yang, D. Liu, Z. Fultz and B. Wang, *Acta Pharm. Sin. B*, 2023, **13**, 1990–2016.

7. X. Li and Y. Xiong, *ACS Omega*, 2022, **7**, 36918–36928.

8. K. R. Venrooij, L. de Bondt and K. M. Bonger, *Top. Curr. Chem. (Z)*, 2024, **382**, 24.

9. K. M. Hartung and E. M. Sletten, *Chem.*, 2023, **9**, 2095–2109.

10. W. H. Binder and R. Sachsenhofer, *Macromol. Rapid Commun.*, 2007, **28**, 15–54.

11. N. Z. Fantoni, A. H. El-Sagheer and T. Brown, *Chem. Rev.*, 2021, **121**, 7122–7154.

12. D. Bauer, M. A. Cornejo, T. T. Hoang, J. S. Lewis and B. M. Zeglis, *Bioconjugate Chem.*, 2023, **34**, 1925–1950.

13. M. González-Lainez, M. Gallegos, J. Munarriz, R. Azpiroz, V. Passarelli, M. V. Jiménez and J. J. Pérez-Torrente, *Organometallics*, 2022, **41**, 2154–2169.

14. H. M. Pineda-Castañeda, Z. J. Rivera-Monroy and M. Maldonado, *ACS Omega*, 2023, **8**, 3650–3666.

15. J. Lauko, P. H. J. Kouwer and A. E. Rowan, *J. Heterocycl. Chem.*, 2017, **54**, 1677–1699.

16. F. Ahmed and H. Xiong, *Dyes Pigments*, 2021, **185**, 108905.

17. B. Schulze and U. S. Schubert, *Chem. Soc. Rev.*, 2014, **43**, 2522–2571.

18. M. M. Matin, P. Matin, Md. R. Rahman, T. Ben Hadda, F. A. Almalki, S. Mahmud, M. M. Ghoneim, M. Alruwaily and S. Alshehri, *Front. Mol. Biosci.*, 2022, **9**, 864286.

19. D. Coelho, Y. Colas, M. Ethève-Quelquejeu, E. Braud and L. Iannazzo, *ChemBioChem*, 2024, **25**, e202400150.

20. M. Bal, M. Tümer and M. Köse, *J. Fluoresc.*, 2022, **32**, 2237–2256.

21. N. George, P. Saini, G. Singh, R. Singh, G. Singh, P. Malik, H. Singh, G. Kaur and J. Singh, *J. Mol. Struct.*, 2024, **1311**, 138288.

22. P. Yadav, K. Lal, A. Kumar, S. K. Guru, S. Jaglan and S. Bhushan, *Eur. J. Med. Chem.*, 2017, **126**, 944–953.

23. M. Yadav, K. Lal, A. Kumar, P. Singh, V. K. Vishvakarma and R. Chandra, *J. Mol. Struct.*, 2023, **1273**, 134321.

24. P. Rajakumar, S. Raja, C. Satheeshkumar, S. Ganesan, P. Maruthamuthu and S. A. Suthanthiraraj, *New J. Chem.*, 2010, **34**, 2247.

25. C. Song, J. Nie, C. Ma, C. Lu, F. Wang and G. Yang, *Appl. Catal. B,* 2021, **287**, 119984.

26. A. Singh, C. Biot, A. Viljoen, C. Dupont, L. Kremer, K. Kumar and V. Kumar, *Chem. Biol. Drug Des.*, 2017, **89**, 856–861.

27. N. Marepu, S. Yeturu and M. Pal, *Bioorg. Med. Chem. Lett.*, 2018, **28**, 3302–3306.

28. Sudheer, V. Kumar, P. Kumar and R. Gupta, *New J. Chem.*, 2020, **44**, 13285–13294.

29. N. A. A. Elkanzi, H. Hrichi, R. A. Alolayan, W. Derafa, F. M. Zahou and R. B. Bakr, *ACS Omega*, 2022, **7**, 27769–27786.

30. H. A. Jasim, L. Nahar, M. A. Jasim, S. A. Moore, K. J. Ritchie and S. D. Sarker, *Biomolecules*, 2021, **11**, 1203.

31. P. Mahesha, N. S. Shetty and S. D. Kulkarni, *J. Fluoresc.*, 2022, **32**, 835–862.

32. S. Kaur, Shalini, B. Ahmad Shiekh, V. Kumar and I. Kaur, *J. Electroanal. Chem.*, 2022, **905**, 115966.

33. A. Gupta, S. Garg and H. Singh, *Anal. Methods*, 2020, **12**, 5022–5045.

34. P. Yadav, K. Lal, L. Kumar, A. Kumar, A. K. Bhan-Khar, A. Paul and R. Kumar, *Eur. J. Med. Chem.,* 2018, **151,** 324–334.

35. K. Bozorov, J. Zhao and H. A. Aisa, *Bioorg. Med. Chem.,* 2019, **27**, 3511–3531.

36. D. P. Vala, R. M. Vala and H. M. Patel, *ACS Omega*, 2022, **7**, 36945–36987.

37. D. Pereira, F. Durães, N. Szemerédi, J. Freitas-da-Silva, E. Pinto, P. Martins-da-Costa, M. Pinto, M. Correia-da-Silva, G. Spengler, E. Sousa and H. Cidade, *Int. J. Mol. Sci.*, 2022, **23**, 14291.

38. K. Sadineni, S. Reddy Basireddy, T. Rao Allaka, S. Yatam, S. Bhoomandla, V. Muvvala and S. Babu Haridasyam, *Chem. Biodivers.*, 2024, **21**, e202400389.

39. N. Rohman, B. Ardiansah, T. Wukirsari and Z. Judeh, *Molecules*, 2024, **29**, 1026.

40. A. A. Ansari, N. A. Oswal, R. S. Nissar, H. S. Chohan and M. S. Khan, *Bioorg. Med. Chem.,* 2018, **26**, 3511–3531.

41. X.-F. Wu, H. Neumann, A. Spannenberg, T. Schulz, H. Jiao and M. Beller, *J. Am. Chem. Soc.*, 2010, **132**, 14596–14602.

42. L.-W. Xu, L. Li, C.-G. Xia and P.-Q. Zhao, *Helv. Chim. Acta*, 2004, **87**, 3080–3084.

43. R. U. Braun, M. Ansorge and T. J. J. Müller, *Chem. Eur. J.*, 2006, **12**, 9081–9094.

44. M. A. Selepe and F. R. Van Heerden, *Molecules*, 2013, **18**, 4739–4765.

45. M. Rueping, T. Bootwicha, H. Baars and E. Sugiono, *Beilstein J. Org. Chem.*, 2011, **7**, 1680–1687.

46. E. Alarcón, N. Romero, H. Aguilar, J. L. Terán, A. Gómez, L. F. Roa, C. E. Lobato and A. Escobar, *10 th Green Chem. Conf., Barcelona -Spain*, 2013, **8**, 10–11.

47. H. Sharma, S. Patil, T. W. Sanchez, N. Neamati, R. F. Schinazi and J. K. Buolamwini, *Bioorg. Med. Chem.*, 2011, **19**, 2030–2045.

48. S. Bunu, E. Awala and E. Deboh, *Saudi Pharm. J.*, 2020, **06**, 379–389.

49. D. Sen, T. S. Easwari, N. A. Farooqui, S. Mahashwari and R. Kumar, *Der Pharm. Lett.*, 2012, **4**, 986–992.

50. R. Shaw, A. Elagamy, I. Althagafi and R. Pratap, *Org. Biomol. Chem.*, 2020, **18**, 3797–3817.

51. M. R. Uehling, A. M. Suess and G. Lalic, *J. Am. Chem. Soc.*, 2015, **137**, 1424–1427.

52. R. J. Ouellette and J. D Rawn, *Organic Chemistry*, 2nd edn, Elsevier, 2019.

53. S. Chandrasekhar, C. Narsihmulu, S.S Kumar, N.R. Reddy, *Tetrahedron Lett.,* 2001, **42**, 80473.

54. A. G. Godfrey and B. Ganem, *J. Am. Chem. Soc.*, 1990, **112**, 3717–3718.

55. X. Cheng, J. Jia and C. Kuang, *Chin. J. Chem.*, 2011, **29**, 2350–2354.

56 . R. M. Singh, D. Nandini, K. C. Bharadwaj, T. Gupta and R. P. Singh, *Org. Biomol. Chem.*, 2017, **15**, 9979–9982.

57. S. Muller, B. Liepold, G.J. Roth and H.J. Bestmann, *Synlett,* 1996, **521,** 521-524.

58. G. F. Zha, W. Y. Fang, Y. G. Li, J. Leng, X. Chen and H. L. Qin, *J. Am. Chem. Soc.,* 2018, **140**, 17666–17673.

59. A. N. Kursunlu and E. Güler, *J. Mol. Struct.,* 2017, **1134**, 345–349.

60. I. H. El Azab, H. S. El-Sheshtawy, R. B. Bakr and N. A. A. Elkanzi, *Molecules*, 2021, **26**, 708.

61. E. M. Guantai, K. Ncokazi, T. J. Egan, J. Gut, P. J. Rosenthal, P. J. Smith and K. Chibale, *Bioorg. Med. Chem.*, 2010, **18**, 8243–8256.

62. A. Singh, S. T. Saha, S. Perumal, M. Kaur and V. Kumar, *ACS Omega*, 2018, **3**, 1263–1268.

63. B. Ngameni, K. Cedric, A. T. Mbaveng, M. Erdoğan, I. Simo, V. Kuete and A. Daştan, *Bioorg. Med. Chem. Lett.*, 2021, **35**, 127827.

64. J. P. Griess and A. W. V. Hofmann, *Philos. Trans. R. Soc. London*, 1997, **154**, 667–731.

65. J. Tat, K. Heskett, S. Satomi, R. B. Pilz, B. A. Golomb and G. R. Boss, *Clin. Toxicol. (Phila)*, 2021, **59**, 683–697.

66. D. S. Treitler and S. Leung, *J. Org. Chem.*, 2022, **87**, 11293–11295.

67. L. Li, P. S. Lopes, V. Rosa, C. A. Figueira, M. A. N. D. A. Lemos, M. T. Duarte, T. Avilés and P. T. Gomes, *Dalton Trans.*, 2012, **41**, 5144–5154.

68. S. H. Kim, S. H. Park, J. H. Choi and S. Chang, *Chem. Asian J.*, 2011, **6**, 2618–2634.

69. L. Godoy Prieto, M. J. Lo Fiego, A. B. Chopa and M. T. Lockhart, *J. Organomet. Chem.*, 2017, **830**, 26–32.

70. K. A. Schnapp, R. Poe, E. Leyva, N. Soundararajan and M. S. Platz, *Bioconjug. Chem.*, 1993, **4**, 172–177.

71. T. Jiang, G. Coin, S. Bordi, P. L. Nichols, J. W. Bode and B. M. Wanner, *J. Org. Chem.*, 2024, **89**, 7962–7969.

72. M. Kitamura, T. Koga, M. Yano and T. Okauchi, *Synlett*, 2012, **23**, 1335–1338.

73. M. Kitamura, M. Yano, N. Tashiro, S. Miyagawa, M. Sando and T. Okauchi, *Eur. J. Org. Chem.,* 2011, **2011**, 458–462.

74. Z.K. Liu, Q. Q. Zhao, Y. Gao, Y.X. Hou and X. Q. Hu, *Adv. Synth. Catal.,* 2020, **363,** 411-424.

75. J. Gavenonis and T. Tilley, *Organometallics*, 2002, **21**, 5549–5563.

76. Y. H. Kim, K. Kim and S. B. Shim, *Tetrahedron Lett.,* 1986, **27**, 4749–4752.

77. M.-C. Ríos, N.-F. Bravo, C.-C. Sánchez and J. Portilla, *RSC Adv.,* 2021, **11**, 34206.

78. E. P. McCarney, C. S. Hawes, S. Blasco and T. Gunnlaugsson, *Dalton Trans.,* 2017, **46**, 1234–1245.

79. Shaily, A. Kumar, I. Parveen and N. Ahmed, *Luminescence*, 2018, **33**, 713–721.

80. S. Ghosh, N. Baildya and K. Ghosh, *New J. Chem.*, 2021, **45**, 10923–10929.

81. A. Ugboya, K. Monroe, U. Ofulue, K. Yates, D. Ghosh, S. M. Landge, R. L. Quirino and K. S. Aiken, *Sensors,* 2020, **20,** 2973.

82. S. Joshi, S. Kumari, R. Bhattacharjee, A. Sarmah, R. Sakhuja and D. D. Pant, *Sens. Actuators B Chem.,* 2015, **220**, 1266–1278.

83. M. Nagaraja, B. Kalluraya, Asma, T. K. Shreekanth and M. S. Kumar, *J. Heterocycl. Chem.*, 2020, **57**, 3642–3652.

84. P. Rajakumar, A. Thirunarayanan, S. Raja and S. Ganesan, *J. Chem. Sci*., 2012, **53**, 1139–1143.

85. P. Yadav, K. Lal, L. Kumar, A. Kumar, A. Kumar, A. K. Paul and R. Kumar, *Eur. J. Med. Chem.,* 2018, **156,** 263-274.

86. G. Singh, Sushma, Priyanka, Pawan, P. Satija, Shilpy, G. Kaur, J. Singh and J. Singh, *Inorg. Chim. Acta*, 2021, **527**, 120576.

87. K. B. Beć, J. Grabska and C. W. Huck, *Molecules*, 2020, **25**, 2948.

88. T. Hong, J.-Y. Yin, S.-P. Nie and M.-Y. Xie, *Food Chem. X*, 2021, **12**, 100168.

89. W. Mäntele and E. Deniz, *Spectrochim. Acta A Mol. Biomol. Spectrosc.*, 2017, **173**, 965–968.

90. T. Claridge, *High-Resolution NMR Techniques in Organic Chemistry*, 2016.

91. P. Charisiadis, V. G. Kontogianni, C. G. Tsiafoulis, A. G. Tzakos, M. Siskos and I. P. Gerothanassis, *Molecules*, 2014, **19**, 13643–13682.

92. M. A. Iron, *J. Chem. Theory Comput.*, 2017, **13**, 5798–5819.

93. W. Kemp, *NMR in Chemistry: A Multinuclear Introduction*, Macmillan Education UK, London, 1986, pp. 1–13.

94. R.M. Silverstein, F. X. Webster, D. J. Kiemle, and D. L. Bryce, *Spectrometeric Identification of Organic Compounds,* 8th ed., Wiley, Hoboken, 1991.

95. G. L. Glish and R. W. Vachet, *Nat. Rev. Drug. Discov.*, 2003, **2**, 140–150.

96. L. V. Schaffer, R. J. Millikin, R. M. Miller, L. C. Anderson, R. T. Fellers, Y. Ge, N. L. Kelleher, R. D. LeDuc, X. Liu, S. H. Payne, L. Sun, P. M. Thomas, T. Tucholski, Z. Wang, S. Wu, Z. Wu, D. Yu, M. R. Shortreed and L. M. Smith, *Proteomics*, 2019, **19**, e1800361.

97. A. C. Leney and A. J. R. Heck, *J. Am. Soc. Mass Spectrom*, 2017, **28**, 5–13.

98. G. T. H. Nguyen, T. N. Tran, M. N. Podgorski, S. G. Bell, C. T. Supuran and W. A. Donald, *ACS Cent. Sci.*, 2019, **5**, 308–318.

99. G. Singh, P. Satija, A. Singh, Diksha, Pawan, Suman, Sushma, Mohit and S. Soni, *Mater. Chem. Phys.*, 2020, **249**, 123005.

100. B. Rathinam, C.-C. Chien, B.-C. Chen and J.-H. Liu, *Tetrahedron*, 2013, **69**, 235–241.

101. B. F. Abdel-Wahab, R. Betz, E. C. Hosten and R. M. Abdelhameed, *J. Mol. Struct.*, 2023, **1294**, 136536.

102. G. Singh, J. Singh, S. S. Mangat, J. Singh and S. Rani, *RSC Adv.*, 2015, **5**, 12644–12654.

103. M. K. Gill, J. A. De Boeck, T. A. H. Le, A. R. H. A. J. L. I. M. F. C. and E. M. T. J. O., *J. Org. Chem.*, 2013, **78,** 6487–6494.

104. W. Feng, L. Li, C. Yang, A. Welle, O. Trapp and P. A. Levkin, *Angew. Chem.*, 2015, **127**, 8856–8859.

105. L. H. Nurani, C. A. Edityaningrum, I. Irnawati, A. R. Putri, A. Windarsih, A. Guntarti and A. Rohman, *Indones. J. Chem.,* 2023, **23**, 542–567.

106. S. Sargazi, I. Fatima, M. Hassan Kiani, V. Mohammadzadeh, R. Arshad, M. Bilal, A. Rahdar, A. M. Díez-Pascual and R. Behzadmehr, *Int. J. Biol. Macromol.,* 2022, **206**, 115–147.

107. J. Marshall and S. Johnsen, *Philos Trans R Soc Lond B Biol Sci*, 2017, **372**, 20160335.

108. Z. Limpouchová and K. Procházka, in *Fluorescence Studies of Polymer Containing Systems*, ed. K. Procházka, Springer International Publishing, Cham, 2016, pp. 91–149.

109. M. H. Penner, in *Food Analysis*, ed. S. S. Nielsen, Springer International Publishing, Cham, 2017, pp. 89–106.

110. R. Wolstenholme, in *Analytical Techniques in Forensic Science*, John Wiley & Sons, 2021, pp. 115–143.

111. K. P. M. J. H. Chai, T. H. T. Nguyen, J. A. M. Huynh, A. K. J. H. Choi and P. D. Huynh, *Chem. Commun.*, 2016, **52**, 4121–4124.

112. P. Kaur, B. Lal, N. Kaur, G. Singh, A. Singh, G. Kaur and J. Singh, *J. Photochem. Photobiol. A Chem.*, 2019, **382**, 111847.

113. J.-H. Zhu, X.-T. Fan and Q.-Y. Cao, *Inorg. Chim. Acta*, 2016, **451**, 111–115.

114. B. Dolai, S. I. Hazarika, S. Giri and A. K. Atta, *Inorgan. Chim. Acta*, 2018, **483**, 496–503.

115. J. Xu, Y. Yang, H. Baigude and H. Zhao, *Spectrochim. Acta A Mol. Biomol. Spect.* 2020, **229**, 117880.

116. J. Sun, X. Xu, G. Yu, W. Li and J. Shi, *Tetrahedron*, 2018, **74**, 987–991.

117. D. Ghosh, S. Rhodes, D. Winder, A. Atkinson, J. Gibson, W. Ming, C. Padgett, S. Landge and K. Aiken, *J. Mol. Struct.*, 2017, **1134**, 638–648.

118. G. Singh, P. Kalra, A. Arora, A. Singh, G. Sharma, S. Sanchita and P. Satija, *New J. Chem.*, 2018, **42**, 16902–16910.

119. G. Singh, B. Lal, R. Singh, N. George, G. Singh, Diksha, G. Kaur, H. Singh, R. K. Tittal, G. Kaur and J. Singh, *Spectrochim. Acta A Mol. Biomol. Spect.* 2023, **302**, 123163.

120. G. Singh, A. Arora, S. Rani, P. Kalra and M. Kumar, *ChemistrySelect*, 2017, **2**, 3637–3647.

121. E. Tamanini, K. Flavin, M. Motevalli, S. Piperno, L. A. Gheber, M. H. Todd and M. Watkinson, *Inorg. Chem.*, 2010, **49**, 3789–3800.

122. L. Y. Hwang, T. H. Yoon, S. J. Lee, S. Y. Kim and C. S. Kim, *J. Am. Chem. Soc.*, 2019, **141,** 13067–13073.

123. B. Dolai, S. Nayim, M. Hossain, P. Pahari and A. Kumar Atta, *Sens. Actuators B Chem.*, 2019, **279**, 476–482.

124. B.-N. Dai, Q.-Y. Cao, L. Wang, Z.-C. Wang and Z. Yang, *Inorg. Chim. Acta*, 2014, **423**, 163–167.

125. X. Huang, J. Meng, Y. Dong, Y. Cheng and C. Zhu, *Polymer*, 2010, **51**, 3064–3067.

126. S. Kaur, H. B. G., A. Sharma and D. K. Gupta, *New J. Chem.*, 2020, **44,** 15686–15699.

127. N. Puentes-Díaz, D. Chaparro, D. Morales-Morales, A. Flores-Gaspar and J. Alí-Torres, *ACS Omega*, 2023, **8**, 4508–4526.

128. D. Luo, X. Wang and W. Feng, *Sci. Rep.*, 2023, **13**, 16554.

129. J.-R. González-Montaña, F. Escalera-Valente, A. J. Alonso, J. M. Lomillos, R. Robles and M. E. Alonso, *Animals (Basel)*, 2020, **10**, 1855.

130. K. Jomova, M. Makova, S. Y. Alomar, S. H. Alwasel, E. Nepovimova, K. Kuca, C. J. Rhodes and M. Valko, *Chem. -Biol. Interact.,* 2022, **367**, 110173.

Chapter III

Synthesis and Characterization
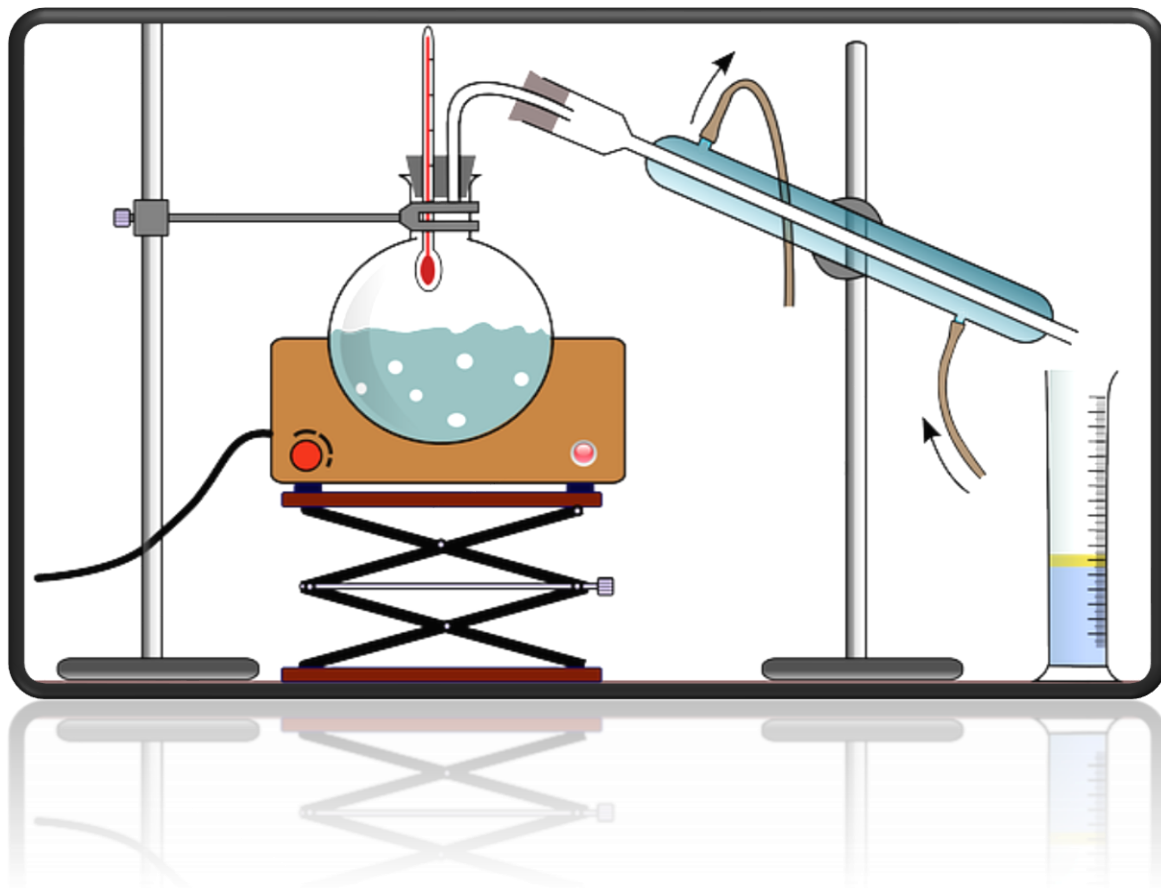
This section provides details of the synthetic methodologies employed in experimental synthesis of compounds, accompanied by thorough structural characterization, using analytical techniques, such as Infrared (IR) Spectroscopy, Nuclear Magnetic Resonance (NMR) Spectroscopy, and Mass Spectrometry.

3.1. General synthetic route for the synthesis of chalcone based 1,2,3-triazole derivatives

The methodology for synthesizing chalcone based 1,2,3-triazole derivatives encompasses series of steps detailed in the following subsections 3.1.1 to 3.1.4. The procedure typically involves the following key stages:

1. Synthesis of chalcone derivatives
2. Synthesis of terminal alkynes from the chalcones
3. Synthesis of organic azide
4. Synthesis of chalcone based 1,2,3-triazole derivatives

The reaction conditions in the synthesis of chalcone-based 1,2,3-triazole derivatives are crucial for obtaining the desired product. Factors such as temperature, solvent, and catalyst type greatly influence the efficiency and outcome of the reaction. The choice of solvent, for example, can affect the solubility of the reactants and the overall reaction rate, while temperature controls the reaction kinetics. The catalyst, typically copper in the case of the CuAAC reaction, is essential for facilitating the cycloaddition between the azide and alkyne groups. Additionally, the specific types of azides and chalcone-tethered alkynes selected also influence the reaction outcome. These parameters can be adjusted based on the desired properties of the final product, ensuring that the reaction proceeds efficiently and yields the intended chalcone-based 1,2,3-triazole derivatives.

3.1.1. Synthesis of chalcone

The synthesis of chalcones from aldehyde and ketone follows a systematic procedure, starting with the preparation of an ethanolic solution of the ketone (1.00 mmol). Potassium hydroxide (KOH) (20% w/v) was then introduced to the ketonic solution in order to speed up the reaction with constant stirring for 10 minutes. Following this, the ethanolic solution of aldehyde (1.00 mmol) is added dropwise gradually to the reaction mixture and left to stir at room temperature. The aldol condensation reaction proceeds via intermediate β-hydroxy ketone to the product **(scheme 3.1.**) The reaction mixture continues to stir until completion, as indicated by TLC monitoring with ethyl acetate and hexane in different ratios. To isolate the desired chalcone product, ice-cold water was added to the reaction mixture, causing the chalcone to precipitate out of solution. The precipitated chalcone was then collected through filtration and thoroughly dried to constant weight, ensuring the removal of any residual solvents or impurities.
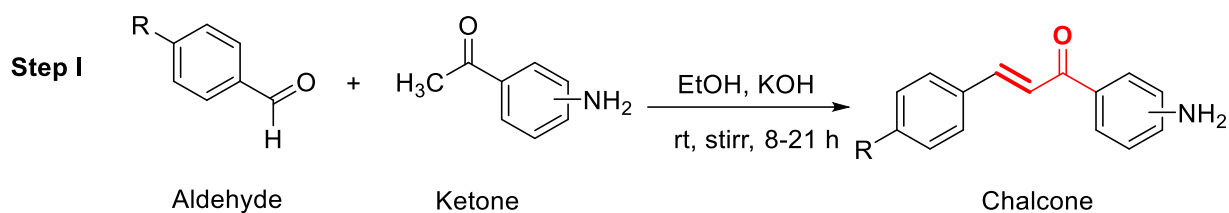
Scheme 3.1: General reaction methodology for the synthesis of chalcones

3.1.2. Synthesis of terminal alkyne from chalcone

The previously synthesised chalcone is used as starting material (1.00 mmol) that was completely dissolved in DMF, followed by the addition of anhydrous potassium carbonate (5.00 mmol) as the base by stirring for 10 minutes. Subsequently, the mixture underwent dropwise addition of propargyl bromide (1.30 mmol) while being stirred at room temperature **(scheme 3.2).** The reaction progress was observed using TLC with ethyl acetate and hexane in different ratios. After confirmation of reaction completion via TLC, ice-cold water was employed to quench the reaction and stirred till precipitate of the desired product was formed.

If the product formed precipitates, it was filtered, washed with copious amounts of cold water (2-3 times) to remove residual solvent, and air-dried until a consistent weight was achieved. In cases where the product was an oil, solvent extraction was performed using a combination of ethyl acetate and water. Ethyl acetate was used to separate the organic layer while the aqueous layer was discarded. The organic phase, containing the product, was then dried over anhydrous sodium sulphate to remove any residual water. Following the drying and vacuum evaporation process, yielding the final product as oil.
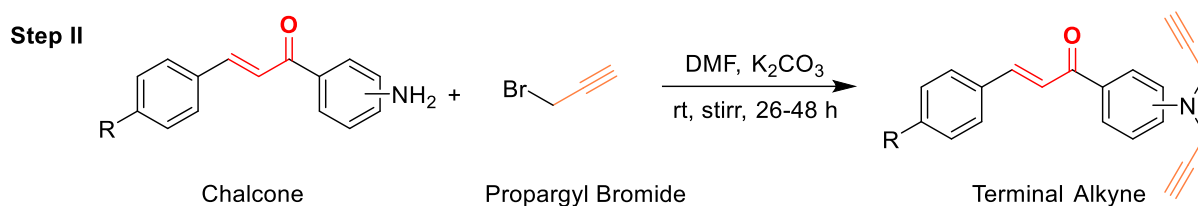
Scheme 3.2: General reaction methodology for the synthesis of chalcone based terminal alkynes

3.1.3. Synthesis of an organic azide

The drying of sodium azide was carried out to remove any residual moisture before use in the reaction. Initially, the sodium azide was placed under a vacuum to ensure thorough removal of moisture. This was done by placing the sodium azide in a vacuum desiccator or vacuum pump under reduced pressure for 3 – 4 hours, until the substance reached a constant

weight, indicating complete drying. Dried sodium azide (5.00 mmol) was carefully added to the solution of organic halide (1.00 mmol) in 25 ml DMF, serving as a solvent medium **(scheme 3.3)**. After that, the reaction mixture was heated and kept between 85 and 90 °C, with continuous stirring for 5 hrs. The nucleophilic substitution reaction proceeds such that azide group is replace with the halide ion. Following the reaction, ice-cold water was added to quench the reaction, once it had cooled to room temperature. The product was subsequently separated through solvent extraction using a combination of ethyl acetate and water. The organic layer was separated using ethyl acetate, while the aqueous layer was discarded. The organic phase, containing the product, was then dried over anhydrous sodium sulphate to remove any residual water. Following the drying process, the final product as oil was obtained by vacuum evaporation, which eliminated the solvent.

Step III

$$R-Cl \quad + \quad NaN_3 \quad \xrightarrow[\substack{85-90\ °C,\ stirr \\ 5h}]{DMF} \quad R-N_3$$

R = Aromatic system Sodium Azide Organic Azide
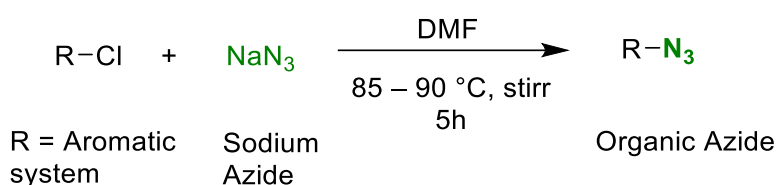
Scheme 3.3: General reaction methodology for the synthesis of organic azides

3.1.4. Synthesis of chalcone based 1,4-disubstituted 1,2,3-triazole derivative

After dissolving the terminal alkyne (1.00 mmol) in a THF and TEA (1:1) solution, the organic azide (1.00 mmol) was added to the reaction mixture. A catalytic quantity of the [CuBr(PPh$_3$)$_3$] complex (0.001 mmol) was then added, and the mixture was stirred while being heated to 55 - 60 °C **(scheme 3.4).** The reaction's progress was tracked using TLC with ethyl acetate and hexane in different ratios. Once the reaction was confirmed to be complete, the mixture was quenched by ice-cold water, causing product to precipitate. Afterwards, the filtration was done to obtain the solid product, thoroughly washed with distilled water, and air-dried until it reached a stable weight. In cases where the product was an oil, solvent extraction was performed using a combination of ethyl acetate and water. The organic layer was separated using ethyl acetate, while the aqueous layer was discarded. The organic phase, containing the product, was then dried over anhydrous sodium sulphate to remove any residual water. Following the drying process, the final product as oil was obtained by vacuum evaporation, which eliminated the solvent. This step ensured the complete removal of the solvent, leaving behind the pure product.

Step IV
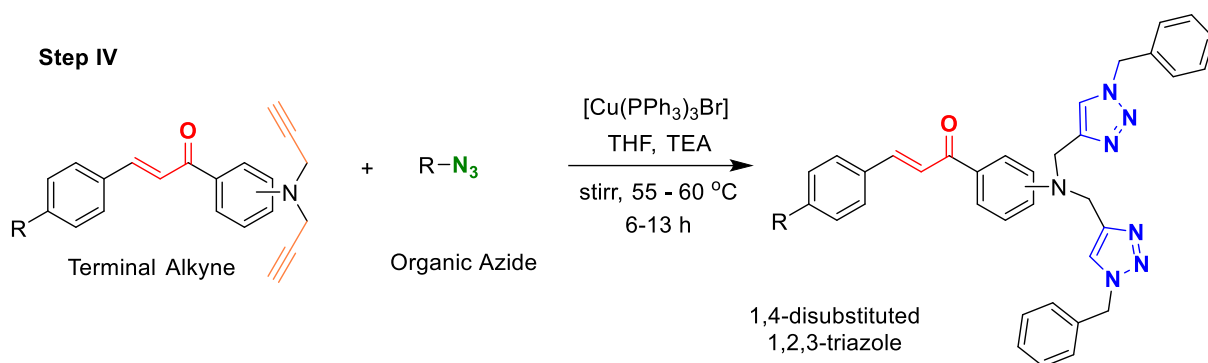
Scheme 3.4: General reaction methodology for the synthesis of chalcone based 1,2,3-triazole derivatives

3.2. Synthesis of organic azide

3.2.1. Synthesis and characterization of benzyl azide (135)

A solution of benzyl chloride **(134)** (5.5 g, 47.8 mmol, 1 equivalent) was prepared by dissolving it in 25 mL of dimethylformamide (DMF). Sodium azide (15.5 g, 238.9 mmol, 5 equivalents) was then introduced into the mixture. The reaction conditions were optimized to ensure efficient conversion while maintaining a controlled environment for the reagents. The reaction mixture was stirred at a temperature of 85 – 90 °C for 5 hours **(scheme 3.5)**. The product **135** was subsequently separated through solvent extraction using a combination of ethyl acetate and water. The organic layer was separated using ethyl acetate, while the aqueous layer was discarded. The organic phase, containing the product, was then dried over anhydrous sodium sulphate to remove any residual water. Following the drying process, Following the drying process, the final product as oil was obtained by vacuum evaporation, which eliminated the solvent.[1]
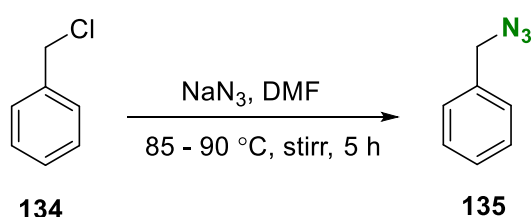
Scheme 3.5: Synthesis of benzyl azide from benzyl chloride

Yield: 61 %

Colour/texture: light yellow oil

M.F.: $C_7H_7N_3$

IR (neat, cm-1): 3032, 2930, 2089, 1452, 1252, 876, 697, 568.

¹H NMR (500 MHz, CDCl₃): δ = 7.22 (d, J = 7.5 Hz, 2H), 7.19 (d, J = 7.2 Hz, 1H), 7.18 - 7.14 (m, 2H), 4.14 (s, 2H).

¹³C NMR (126 MHz, CDCl₃): δ = 135.53, 128.91, 128.37, 127.78, 54.82.

3.3. Synthesis and characterization of 4-benzyloxybenzaldehyde-based ortho, para and meta substituted chalcones, alkynes and their corresponding 1,2,3-triazoles

3.3.1. General synthetic route for the synthesis of ortho-, meta-, and para- substituted chalcones and their characterization

3.3.1.1. ortho-substituted chalcone ((E)-1-(2-aminophenyl)-3-(4-(benzyloxy)phenyl)prop-2-en-1-one) (138)

4-Benzyloxybenzaldehyde (**136**, 2.0 g, 9.4 mmol) and 2-aminoacetophenone (**137**, 1.25 g, 9.4 mmol) were combined in ethanol with continuous stirring to ensure thorough mixing. A 20% (w/v) solution of potassium hydroxide (5.0 mL) was gradually added to the reaction mixture to initiate the reaction. The mixture was stirred at room temperature until the reaction reached completion, which was monitored by TLC using a solvent system of ethyl acetate: hexane (1:9). Once the reaction was complete, it was quenched by the addition of ice-cold water, leading to the precipitation of the product. The precipitated solid was filtered, dried, and purified using ethanol as the solvent.[2] The reaction for the same has been illustrated in scheme **3.6.**
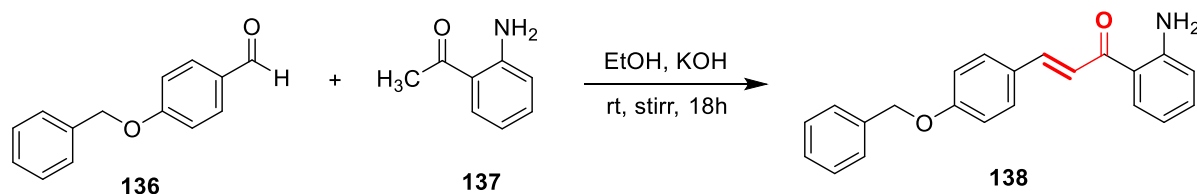
Scheme 3.6: Synthesis of ortho-substituted chalcone from 4-benzyloxybenzaldehyde and 2-aminoacetophenone

Yield: 91%

Colour/texture: bright yellow solid powder

M.F. = C₂₂H₁₉NO₂

Elem. Anal. Calc. (%): C = 80.22; H = 5.81; N = 4.25; **Found (%):** C = 80.27, H = 5.85, N = 4.34

mp: 135 – 136 ℃

IR (neat, cm⁻¹): 3436, 3328, 3044, 1638, 1581, 1502, 1336, 1263, 1205, 1161, 1003.

¹H NMR (500 MHz, CDCl₃) δ = 7.85 (d, J = 8.4 Hz, 1H), 7.71 (d, J = 15.5 Hz, 1H), 7.60 –
7.55 (m, 2H), 7.49 (d, J = 15.5 Hz, 1H), 7.45 – 7.37 (m, 4H), 7.34 (d, J = 7.1 Hz, 1H), 7.29 –
7.22 (m, 1H), 7.03 – 6.96 (m, 2H), 6.74 – 6.64 (m, 2H), 6.29 (s, 2H), 5.10 (s, 2H).

¹³C NMR (126 MHz, CDCl₃) δ = 191.69, 160.42, 150.81, 142.66, 136.43, 134.02, 130.84,
129.89, 128.59, 128.18, 128.07, 127.40, 120.87, 119.25, 117.20, 115.77, 115.17, 70.03.

3.3.1.2. meta-substituted chalcone ((E)-1-(3-aminophenyl)-3-(4-(benzyloxy)phenyl)prop-2-en-1-one) (140)

4-Benzyloxybenzaldehyde **136** (2.0 g, 9.4 mmol) and 3-aminoacetophenone **139** (1.25 g,
9.4 mmol) were dissolved in ethanol under constant stirring. Potassium hydroxide solution (5.0
mL, 20% w/v) was added dropwise, and the reaction mixture was stirred at room temperature
until the formation of the desired product was complete, as confirmed by TLC (ethyl acetate:
hexane, 1:9). The reaction was quenched by adding ice-cold water, and the resulting solid was
collected by filtration, dried, and purified using ethanol as the solvent. The reaction for the
same has been illustrated in scheme **3.7**.
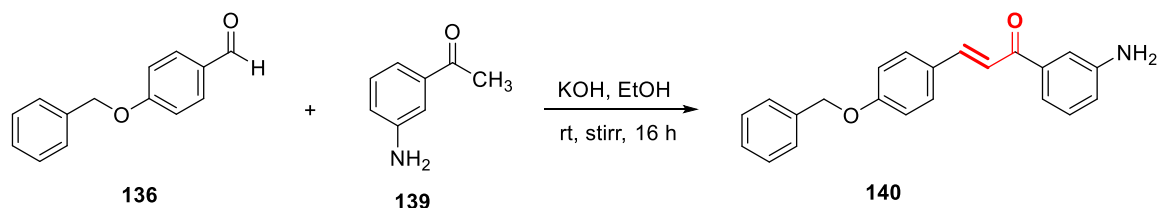
Scheme 3.7: Synthesis of meta-substituted chalcone from 4-benzyloxybenzaldehyde and 3-
aminoacetophenone

Yield: 87 %

Colour/texture: light yellow powder

M.F. = $C_{22}H_{19}NO_2$

Elem. Anal. Calc. (%): C = 80.22; H = 5.81; N = 4.25; **Found (%):** C = 80.29, H = 5.89, N
= 4.31.

mp: 121 – 122 °C

IR (neat, cm⁻¹): 3453, 3358, 3054, 2902, 1653, 1581, 1506, 1453, 1385, 1302, 1250, 1172,
985.

¹H NMR (500 MHz, CDCl₃) δ = 7.88 (d, J = 10.1 Hz, 1H), 7.81 – 7.72 (m, 1H), 7.67 – 7.48 (m, 2H), 7.42 (d, J = 8.3 Hz, 2H), 7.38 (d, J = 9.2 Hz, 2H), 7.35 – 7.30 (m, 3H), 7.27 – 7.23 (m, 1H), 7.07 – 6.86 (m, 3H), 5.16 (s, 2H), 5.10 (s, 2H).

¹³C NMR (126 MHz, CDCl₃) δ = 190.73, 160.77, 146.94, 144.32, 139.64, 136.40, 130.74, 130.20, 129.39, 128.68, 128.18, 127.48, 120.22, 119.21, 118.78, 115.30, 114.42, 70.12.

3.3.1.3. para-substituted chalcone ((E)-1-(4-aminophenyl)-3-(4-(benzyloxy)phenyl)prop-2-en-1-one) (142)

4-Benzyloxybenzaldehyde (2.0 g, 9.4 mmol) **136** and 4-aminoacetophenone (1.25 g, 9.4 mmol) **141** were continuously stirred while dissolved in ethanol. Following a gradual addition of potassium hydroxide (5.0 mL, 20% w/v), the mixture was allowed to stir at room temperature until the reactants were fully transformed into the intended product **142**, as determined by TLC (ethyl acetate: hexane; 1:9). Ice-cold water was added to quench the reaction, and ethanol was used as the eluent to filter, dry, and purify the solid result. The reaction for the same has been illustrated in scheme **3.8.**
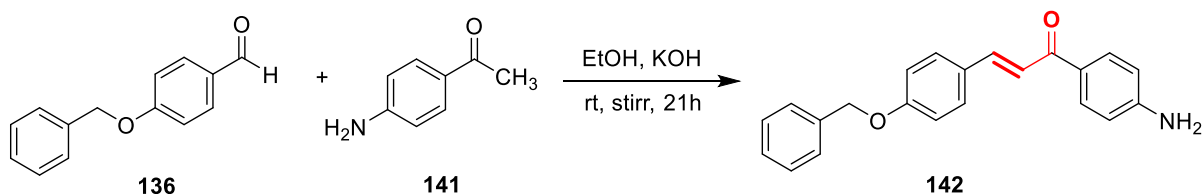
Scheme 3.8: Synthesis of para-substituted chalcone from 4-benzyloxybenzaldehyde and 4-aminoacetophenone

Yield: 90%

Colour/texture: dark yellow powder

M.F. = C₂₂H₁₉NO₂

Elem. Anal. Calc. (%): C = 80.22; H = 5.81; N = 4.25; **Found (%):** C = 80.23, H = 5.83, N = 4.27

mp: 119 – 120 °C

IR (neat, cm⁻¹): 3373, 3336, 3192, 3035, 2912, 1624, 1593, 1505, 1454, 1421, 1382, 1341, 1291, 1247, 1220, 1166, 1078, 1017.

¹H NMR (500 MHz, CDCl₃) δ = 7.92 (d, J = 8.7 Hz, 1H), 7.89 – 7.60 (m, 2H), 7.65 – 7.44 (m, 3H), 7.44 – 7.38 (m, 5H), 7.02 (dd, J = 24.5, 15.0 Hz, 2H), 6.68 (d, J = 8.7 Hz, 2H), 5.15 (s, 2H), 5.10 (s, 2H).

¹³C NMR (126 MHz, CDCl₃) δ = 188.15, 160.48, 150.95, 142.89, 131.01, 130.22, 129.97, 129.87, 129.31, 128.67, 128.32, 128.18, 127.49, 120.98, 119.92, 115.23, 113.93, 70.11.

3.3.2. General synthetic route for the synthesis of ortho-, meta-, and para- substituted chalcone based terminal alkynes and their characterization

3.3.2.1. ortho-substituted chalcone based terminal alkyne ((E)-3-(4-(benzyloxy)phenyl)-1-(2-(di(prop-2-yn-1-yl)amino)phenyl)prop-2-en-1-one) (143)

Chalcone (1.0 g, 3.03 mmol) **138** was dissolved in 20 mL DMF with constant stirring on a magnetic stirrer. Next, anhydrous potassium carbonate (2.1 g, 15.2 mmol) was added, and then propargyl bromide (0.78 g, 6.88 mmol) **50** was added dropwise. 45 hours were spent stirring the reaction mixture at room temperature. The reaction's development was tracked by TLC (ethyl acetate: hexane; 1:9). The product **143** was subsequently separated through solvent extraction using a combination of ethyl acetate and water. The organic layer was separated using ethyl acetate, while the aqueous layer was discarded. The organic phase, containing the product, was then dried over anhydrous sodium sulphate to remove any residual water. Following the drying process, the solvent was removed by vacuum evaporation, yielding the final product as oil. The reaction for the same has been illustrated in scheme **3.9.**
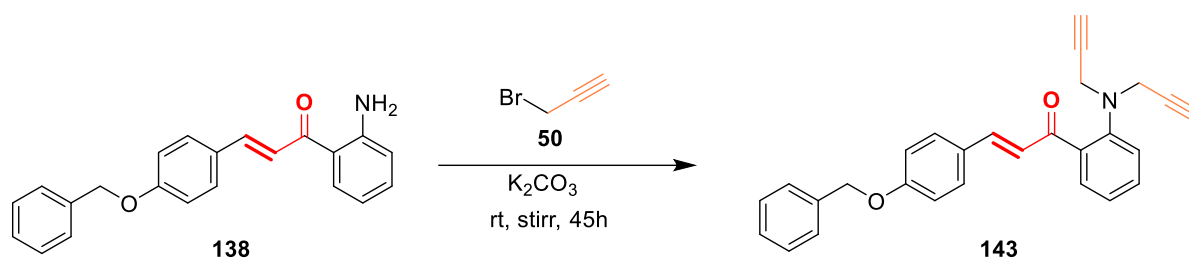
Scheme 3.9: Synthesis of ortho-substituted chalcone based terminal alkyne

Yield: 83%

Colour/texture: brown viscous oil

M.F. = C₂₈H₂₃NO₂

IR (neat, cm⁻¹): 3287, 3029, 2910, 2113, 1684, 1637, 1570, 1504, 1456, 1420, 1293, 1245, 1203, 1161, 1077, 1007.

 ¹H NMR (500 MHz, CDCl₃): δ = 7.91 (d, J = 11.7 Hz, 1H), 7.51 – 7.48 (m, 2H), 7.43 – 7.32 (m, 8H), 6.98 (d, J = 8.9 Hz, 4H), 5.08 (s, 2H), 4.02 (s, 4H), 2.23 (s, 2H).

¹³C NMR (126 MHz, CDCl₃): δ = 191.86, 160.53, 150.44, 142.80, 136.52, 134.73, 134.11, 131.50, 130.01, 128.68, 128.17, 127.50, 120.91, 115.28, 112.04, 80.33, 71.31, 70.12, 32.35.

3.3.2.2. meta-substituted chalcone based terminal alkyne ((E)-3-(4-(benzyloxy)phenyl)-1-(3-(di(prop-2-yn-1-yl)amino)phenyl)prop-2-en-1-one) (144)

Chalcone (1.0 g, 3.03 mmol) **140** was dissolved in 20 mL DMF with constant stirring on a magnetic stirrer. In the reaction mixture, propargyl bromide (0.78 g, 6.88 mmol) was added dropwise **50** and anhydrous potassium carbonate (2.1 g, 15.2 mmol) was added. For 46 hours at room temperature, the reaction mixture was agitated. TLC was used to track the reaction's development (ethyl acetate: hexane; 1:9). After adding ice-cold water to quench the reaction, the solid product **144** was filtered and allowed to dry at room temperature. The reaction for the same has been illustrated in scheme **3.10.**
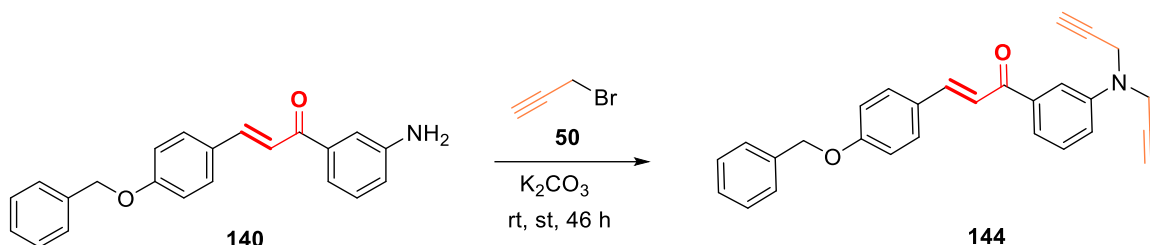
Scheme 3.10: Synthesis of meta-substituted chalcone based terminal alkyne

Yield: 81 %

Colour/texture: light brown powder

M.F. = C₂₈H₂₃NO₂

Elem. Anal. Calc. (%): C = 82.94; H = 5.72; N = 3.45; **Found (%):** C = 82.10; H = 5.81; N = 3.54

mp: 112 – 113 °C

IR (neat, cm^{-1}): 3280, 3056, 2930, 2111, 1656, 1579, 1502, 1446, 1380, 1327, 1239, 1170, 1036.

^{1}H NMR (500 MHz, CDCl$_3$): δ = 7.76 (d, *J* = 15.6 Hz, 1H), 7.57 (d, *J* = 8.2 Hz, 2H), 7.49 (d, *J* = 7.4 Hz, 1H), 7.48 – 7.36 (m, 9H), 6.99 (d, *J* = 8.4 Hz, 2H), 5.09 (s, 2H), 4.17 (s, 4H), 2.27 (s, 2H).

^{13}C NMR (126 MHz, CDCl$_3$): δ = 190.45, 147.90, 143.23, 138.86, 136.17, 133.37, 130.77, 129.49, 129.38, 129.32, 129.15, 122.74, 119.90, 119.78, 114.97, 78.70, 72.98, 40.42.

3.3.2.3. para-substituted chalcone based terminal alkyne ((E)-3-(4-(benzyloxy)phenyl)-1-(4-(di(prop-2-yn-1-yl)amino)phenyl)prop-2-en-1-one) (145)

Chalcone (1.0 g, 3.03 mmol) **142** was dissolved in 20 mL DMF with constant stirring on a magnetic stirrer. To the reaction mixture, anhydrous potassium carbonate (2.1 g, 15.2 mmol) was added, and propargyl bromide (0.78 g, 6.88 mmol) was introduced dropwise **50**. The mixture was stirred at room temperature for 48 hours, with the reaction progress monitored periodically by TLC (ethyl acetate: hexane, 1:9). The ice-cold water was added to quench the reaction and the product **145** was subsequently separated through solvent extraction using a combination of ethyl acetate and water. The organic layer was separated using ethyl acetate, while the aqueous layer was discarded. The organic phase, containing the product, was then dried over anhydrous sodium sulphate to remove any residual water. After the drying process, the final product (oil) was obtained by vacuum evaporation, which eliminated the solvent. The reaction for the same has been illustrated in **scheme 3.11**.
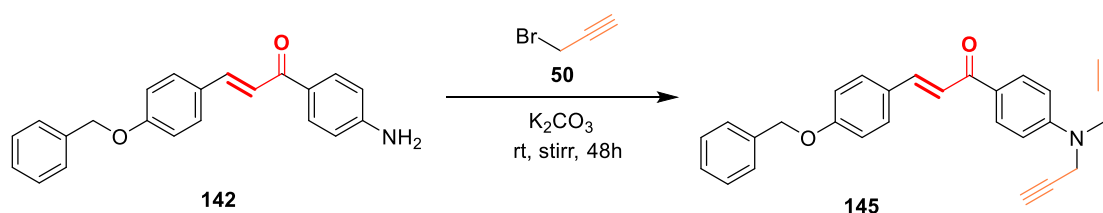
Scheme 3.11: Synthesis of para-substituted chalcone based terminal alkyne

Yield: 85%

Colour/texture: brown viscous oil

M.F. = C$_{28}$H$_{23}$NO$_2$

IR (neat, cm–1): 3286, 2970, 2913, 2115, 1651, 1587, 1505, 1421, 1331, 1293, 1220, 1165, 1017.

^{1}H NMR (500 MHz, CDCl$_3$): δ = 7.82 (d, *J* = 10.8 Hz, 1H), 7.70 (d, *J* = 6.1 Hz, 2H), 7.44 – 7.37 (m, 6H), 7.06 (d, *J* = 8.8 Hz, 2H), 6.82 (d, *J* = 7.2 Hz, 2H), 6.68 (d, *J* = 8.6 Hz, 2H), 5.08 (s, 2H), 3.98 (d, *J* = 2.6 Hz, 4H), 2.25 (t, *J* = 2.5 Hz, 2H).

^{13}C NMR (126 MHz, CDCl$_3$): δ = 190.79, 160.46, 150.70, 142.87, 136.50, 131.99, 130.79, 129.97, 128.65, 128.13, 127.47, 121.92, 119.82, 115.36, 115.29, 115.21, 115.15, 112.32, 79.89, 71.86, 70.08, 33.06.

3.3.3. General synthetic route for the synthesis of ortho-, meta-, and para- substituted chalcone based 1,2,3-triazoles and their characterization

3.3.3.1. ortho-substituted chalcone based 1,2,3-triazole ((E)-3-(4-(benzyloxy)phenyl)-1-(2-(bis((1-benzyl-1H-1,2,3-triazol-4-yl)methyl)amino)phenyl)prop-2-en-1-one) (146)

A chalcone-based alkyne (0.70 g, 1.73 mmol, compound **143**) was dissolved in a THF/TEA mixture (1:1) and combined with an organic azide (0.46 g, 3.46 mmol, compound **135**) and a Cu(I) catalyst (0.001 mmol). The reaction mixture was heated to reflux at 55–60 °C for 8 hours, and the progress was monitored using TLC (ethyl acetate:hexane, 1:4) to ensure the reactants were fully converted. Upon completion, the reaction was quenched by adding ice-cold water. The resulting solid product (compound **146**) was collected through filtration and dried. The reaction for the same has been illustrated in scheme **3.12.**
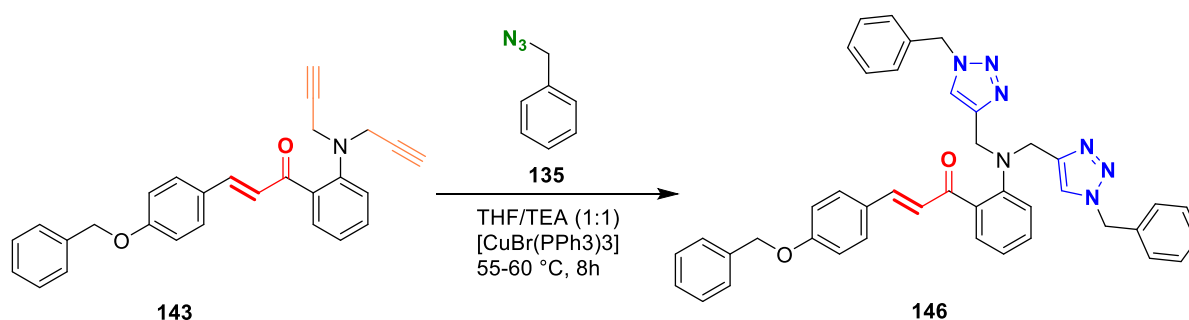
Scheme 3.12: Synthesis of ortho-substituted chalcone based 1,2,3-triazole

Yield: 93 %

Colour/texture: yellow powder

M.F.: C$_{42}$H$_{37}$N$_7$O$_2$

Elem. Anal. Calc. (%): C = 75.09; H = 5.55; N = 14.59, **Found (%):** C = 75.11; H = 5.50; N = 14.57

mp: 165-166 °C

IR (neat, cm⁻¹): 3068, 3033, 2931, 1638, 1570, 1507, 1455, 1419, 1280, 1242, 1198, 1165, 1009.

¹H NMR (500 MHz, CDCl₃): δ = 7.93 (d, *J* = 6.5 Hz, 2H), 7.86 (d, *J* = 16.5 Hz, 1H), 7.72 (s, 1H), 7.69 (s, 1H), 7.59 (d, *J* = 8.8 Hz, 3H), 7.47 – 7.40 (m, 9H), 7.41 – 7.26 (m, 6H), 7.02 (d, *J* = 8.9 Hz, 2H), 6.81 (d, *J* = 8.3 Hz, 2H), 5.49 (s, 4H), 5.12 (s, 2H), 4.61 (d, *J* = 5.6 Hz, 4H).

¹³C NMR (126 MHz, CDCl₃): δ = 190.79, 159.49, 150.06, 141.64, 135.45, 133.84, 133.64, 130.46, 128.94, 128.04, 127.63, 127.17, 127.12, 126.92, 126.45, 119.83, 117.97, 114.23, 113.89, 111.10, 69.06, 53.12, 38.04.

LC-MS: m/z (calculated) = 671.81; m/z (found) = 672.25 (M+1).

3.3.3.2. meta-substituted chalcone based 1,2,3-triazole ((E)-3-(4-(benzyloxy)phenyl)-1-(3-(bis((1-benzyl-1H-1,2,3-triazol-4-yl)methyl)amino)phenyl)prop-2-en-1-one) (147)

A chalcone-based alkyne (0.70 g, 1.73 mmol, compound **144**) was dissolved in a THF/TEA mixture (1:1) and combined with an organic azide (0.46 g, 3.46 mmol, compound **135**) and a Cu(I) catalyst (0.001 mmol). The mixture was refluxed at 55–60 °C for 6 hours, with the reaction progress monitored via TLC (ethyl acetate:hexane, 1:4) to confirm the complete conversion of the reactants. After completion, the reaction was quenched with ice-cold water, and the solid product (compound **147**) was collected by filtration and dried. The reaction for the same has been illustrated in scheme **3.13.**
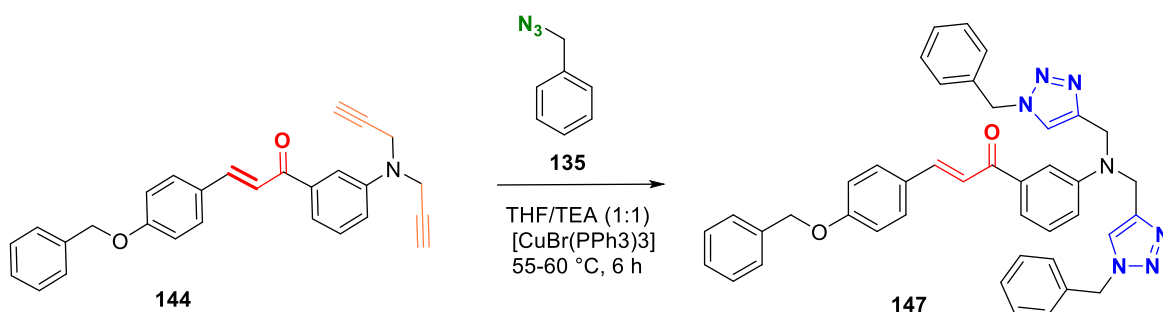
Scheme 3.13: Synthesis of meta-substituted chalcone based 1,2,3-triazole

Yield: 79 %

Colour/texture: light yellow powder

M.F.: $C_{42}H_{37}N_7O_2$

Elem. Anal. Calc. (%): C = 75.09; H = 5.55; N = 14.59, **Found (%):** C = 75.15; H = 5.47; N = 14.52

mp: 161 – 162 °C

IR (neat, cm⁻¹): 3129, 3064, 2916, 1654, 1571, 1511, 1448, 1384, 1333, 1235, 1174, 1121, 1029.

¹H NMR (500 MHz, CDCl₃): δ = 7.62 (d, *J* = 15.7 Hz, 2H), 7.53 – 7.37 (m, 3H), 7.36 – 7.25 (m, 7H), 7.17 (d, *J* = 18.6 Hz, 7H), 7.02 (d, *J* = 47.3 Hz, 6H), 6.89 (d, *J* = 8.3 Hz, 2H), 5.30 (s, 4H), 4.99 (s, 2H), 4.58 (s, 4H).

¹³C NMR (126 MHz, CDCl₃): δ = 190.70, 160.74, 148.04, 144.24, 139.28, 136.40, 134.66, 130.26, 129.38, 129.01, 128.62, 128.58, 128.11, 127.88, 127.78, 127.43, 122.22, 120.10, 117.93, 117.84, 115.27, 113.05, 70.04, 53.98, 46.68.

LC-MS: m/z (calculated): 671.81, **m/z (observed):** 672.30 (M+1).

3.3.3.3. para-substituted chalcone based 1,2,3-triazole ((E)-3-(4-(benzyloxy)phenyl)-1-(4-(bis((1-benzyl-1H-1,2,3-triazol-4-yl)methyl)amino)phenyl)prop-2-en-1-one) (148)

A solution of chalcone-based alkyne (0.70 g, 1.73 mmol) **145** in THF/TEA (1:1) was mixed with the organic azide (0.46 g, 3.46 mmol) **135** and Cu(I) catalyst (0.001 mmol). The reaction mixture was refluxed at 55 – 60 °C for 6 hours until the complete conversion of the reactants monitored by TLC (ethyl acetate: hexane, 1:4). The reaction was then quenched by adding ice-cold water, and the product **148** was subsequently separated through solvent extraction using a combination of ethyl acetate and water. The organic layer was separated using ethyl acetate, while the aqueous layer was discarded. The organic phase, containing the product, was then dried over anhydrous sodium sulphate to remove any residual water. Following the drying process, the solvent was removed by vacuum evaporation, yielding the final product as oil. The reaction for the same has been illustrated in scheme **3.14.**
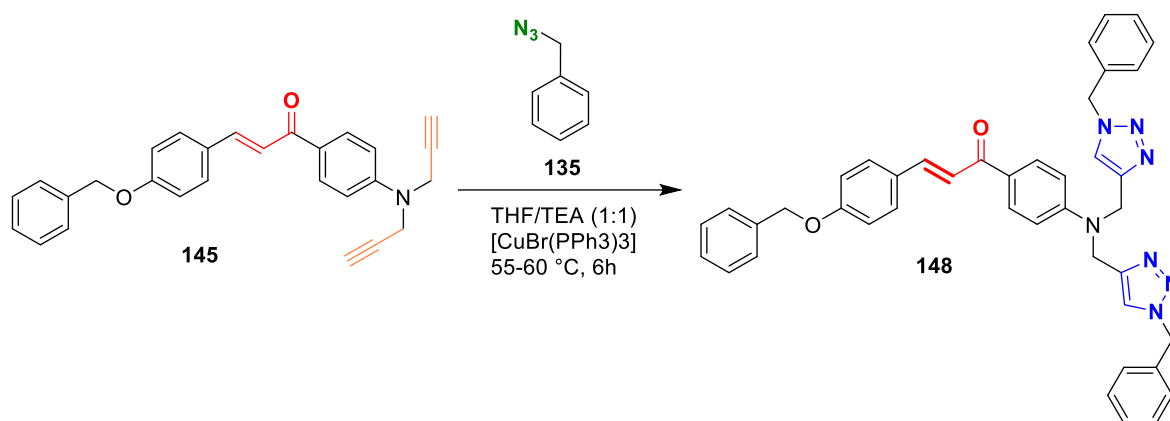
Scheme 3.14: Synthesis of para-substituted chalcone based 1,2,3-triazole

Yield: 86 %

Colour/texture: dark brown viscous oil

M.F.: $C_{42}H_{37}N_7O_2$

IR (neat, cm^{-1}): 3146, 3031, 2958, 2922, 1649, 1590, 1503, 1455, 1327, 1293, 1224, 1169, 1114, 1017.

^{1}H NMR (500 MHz, CDCl$_3$): δ = 7.83 (d, *J* = 8.8 Hz, 1H), 7.72 (d, *J* = 3.4 Hz, 2H), 7.55 (s, 2H), 7.45 – 7.42 (m, 5H), 7.43 – 7.38 (m, 5H), 7.37 – 7.31 (m, 6H), 7.07 (d, *J* = 8.8 Hz, 2H), 6.82 (d, *J* = 9.2 Hz, 2H), 6.68 (d, *J* = 9.7 Hz, 2H), 5.46 (d, *J* = 3.3 Hz, 4H), 5.09 (s, 2H), 4.47 (d, *J* = 3.2 Hz, 4H).

^{13}C NMR (126 MHz, CDCl$_3$): δ = 189.79, 166.75, 159.43, 141.71, 135.48, 130.97, 129.87, 128.94, 128.10, 127.77, 127.70, 127.63, 127.29, 127.11, 127.00, 126.45, 118.79, 114.19, 110.98, 69.06, 67.14, 37.70

LC-MS: m/z (calculated) = 671.81; **m/z (found)** = 672.32 (M+1).

3.4. Synthesis and characterization of 4-chlorobenzaldehyde-based ortho, para and meta substituted chalcones, alkynes and their corresponding 1,2,3-triazoles

3.4.1. General synthetic route for the synthesis of ortho-, meta-, and para- substituted chalcones and their characterization

3.4.1.1. ortho-substituted chalcone ((E)-1-(2-aminophenyl)-3-(4-chlorophenyl)prop-2-en-1-one) (150)

4-chlorobenzaldehyde (2 g, 14.22 mmol) **149** and 2-aminoacetophenone (1.72 mL, 14.22 mmol) **137** were dissolved in ethanol with continuous stirring. Potassium hydroxide (5.0 mL, 20% w/v) was then slowly added to the mixture, which was stirred at room temperature for 12 h until the reactants were completely converted to the desired product **150**, as confirmed by

TLC (ethyl acetate: hexane; 1:9). The reaction was quenched by adding ice-cold water, and the solid product was filtered, dried, and purified using ethanol as the eluent.[3,4] The reaction for the same has been illustrated in scheme **3.15.**
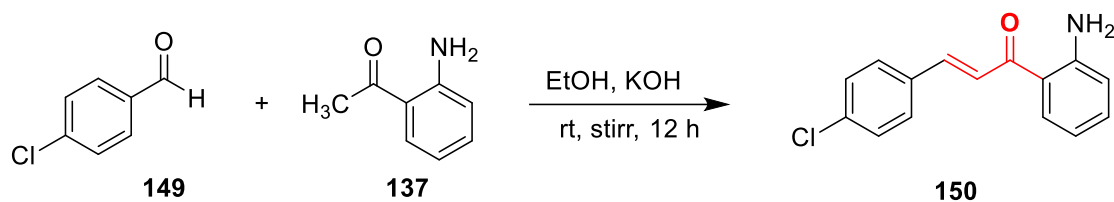
Scheme 3.15: Synthesis of ortho-substituted chalcone from 4-chlorobenzaldehyde and 2-aminoacetophenone

Yield: 90%

Colour/texture: Bright yellow powder

M.F.: $C_{15}H_{12}ClNO$

Elem. Anal. Calc. (%): C = 69.91, H = 4.69, N = 5.44; **Found (%):** C = 69.87, H = 4.71, N = 5.42

mp: 92 – 93 °C

IR (neat, cm⁻¹): 3461, 3295, 3032, 1639, 1606, 1564, 1533, 1484, 1404, 1328, 1280, 1207, 1154, 1083, 994, 822, 747.

¹H NMR (500 MHz, CDCl₃) δ = 7.83 (d, J = 7.2 Hz, 1H), 7.67 (d, J = 15.6 Hz, 1H), 7.61 – 7.53 (m, 3H), 7.37 (d, J = 8.5 Hz, 2H), 7.32 – 7.27 (m, 1H), 6.77 – 6.62 (m, 2H), 6.34 (s, 2H).

¹³C NMR (126 MHz, CDCl₃) δ = 191.17, 151.08, 141.42, 135.92, 134.46, 130.97, 129.40, 129.16, 123.61, 118.90, 117.35, 115.90.

3.4.1.2. meta-substituted chalcone ((E)-1-(3-aminophenyl)-3-(4-chlorophenyl)prop-2-en-1-one) (151)

4-chlorobenzaldehyde (2 g, 14.22 mmol) **149** and 3-aminoacetophenone (1.72 mL, 14.22 mmol) **139** were dissolved in ethanol with continuous stirring. Potassium hydroxide (5.0 mL, 20% w/v) was then slowly added to the mixture, which was stirred at room temperature for 8 h until the reactants were completely converted to the desired product **151**, as confirmed by TLC (ethyl acetate: hexane; 1:9). The reaction was quenched by adding ice-cold water, and the

solid product was filtered, dried, and purified using ethanol as the eluent. The reaction for the same has been illustrated in scheme **3.16.**
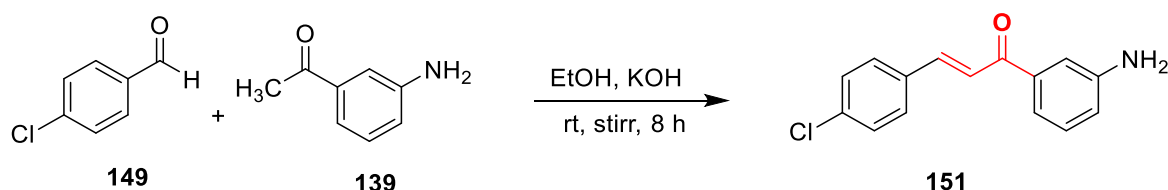
Scheme 3.16: Synthesis of meta-substituted chalcone from 4-chlorobenzaldehyde and 3-aminoacetophenone

Yield: 92%

Colour/texture: clay yellow powder

M.F.: $C_{15}H_{12}ClNO$

Elem. Anal. Calc. (%): C = 69.91, H = 4.69, N = 5.44; **Found (%):** C = 69.87, H = 4.71, N = 5.42

mp: 98 – 99 °C

IR (neat, cm⁻¹): 3449, 3359, 3047, 2868, 1658, 1585, 1487, 1441, 1317, 1215, 1160, 1087, 978, 911, 824, 783, 681, 631.

¹H NMR (500 MHz, CDCl₃) δ = 8.47 (d, J = 12.6 Hz, 1H), 7.89 – 7.75 (m, 4H), 7.60 – 7.48 (m, 2H), 7.45 – 7.37 (m, 2H), 7.28 (dd, J = 38.6, 11.2 Hz, 1H), 2.64 (s, 2H).

¹³C NMR (126 MHz, CDCl₃) δ = 189.82, 159.90, 152.08, 138.18, 134.39, 130.11, 129.66, 129.19, 125.85, 122.36, 120.27, 114.01.

3.4.1.3. para-substituted chalcone ((E)-1-(4-aminophenyl)-3-(4-chlorophenyl)prop-2-en-1-one) (152)

4-chlorobenzaldehyde (2 g, 14.22 mmol) **149** and 4-aminoacetophenone (1.72 mL, 14.22 mmol) **141** were dissolved in ethanol with continuous stirring. Potassium hydroxide (5.0 mL, 20% w/v) was then slowly added to the mixture, which was stirred at room temperature for 9 h until the reactants were completely converted to the desired product **152**, as confirmed by TLC (ethyl acetate: hexane; 1:9). The reaction was quenched by adding ice-cold water, and the

solid product was filtered, dried, and purified using ethanol as the eluent. The reaction for the same has been illustrated in scheme **3.17.**
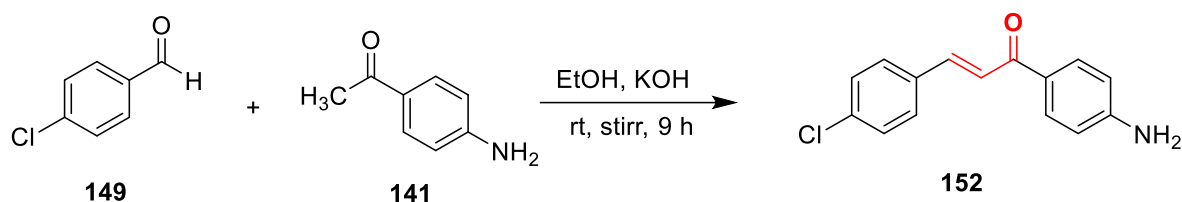
Scheme 3.17: Synthesis of para-substituted chalcone from 4-chlorobenzaldehyde and 4-aminoacetophenone

Yield: 87%

Colour/texture: lemon yellow powder

M.F.: $C_{15}H_{12}ClNO$

Elem. Anal. Calc. (%): C = 69.91, H = 4.69, N = 5.44; **Found (%):** C = 69.87, H = 4.71, N = 5.42

mp: 125 – 126 °C

IR (neat, cm⁻¹): 3457, 3340, 3054, 1635, 1598, 1541, 1490, 1446, 1343, 1224, 1172, 1087, 1017, 980, 811, 672, 597.

¹H NMR (500 MHz, CDCl₃) δ = 7.92 (d, J = 7.6 Hz, 1H), 7.72 (d, J = 15.5 Hz, 2H), 7.53 (dd, J = 23.8, 11.6 Hz, 3H), 7.37 (d, J = 7.5 Hz, 2H), 6.70 (d, J = 7.6 Hz, 2H), 4.19 (s, 2H).

¹³C NMR (126 MHz, CDCl₃) δ = 187.76, 151.24, 141.63, 135.90, 133.86, 131.12, 129.41, 129.14, 128.39, 122.51, 113.81.

3.4.2. General synthetic route for the synthesis of ortho-, meta-, and para- substituted chalcone based terminal alkynes and their characterization

3.4.2.1. ortho-substituted chalcone based terminal alkyne ((E)-3-(4-chlorophenyl)-1-(2-(di(prop-2-yn-1-yl)amino)phenyl)prop-2-en-1-one) (153)

To a solution of chalcone (1.0 g, 3.88 mmol, compound **150**) in 20 mL of DMF, anhydrous potassium carbonate (2.68 g, 19.4 mmol) was added under continuous stirring on a magnetic stirrer. Propargyl bromide (1.06 mL, 9.3 mmol, compound **50**) was then added

dropwise to the mixture. The reaction was allowed to stir at room temperature for 30 hours, and its progress was tracked using TLC (ethyl acetate:hexane, 1:9). The reaction was quenched by adding ice-cold water, and the product **153** was subsequently separated through solvent extraction using a combination of ethyl acetate and water. The organic layer was separated using ethyl acetate, while the aqueous layer was discarded. The organic phase, containing the product, was then dried over anhydrous sodium sulphate to remove any residual water. Following the drying process, the solvent was removed by vacuum evaporation, yielding the final product as oil. The reaction for the same has been illustrated in scheme **3.18.**
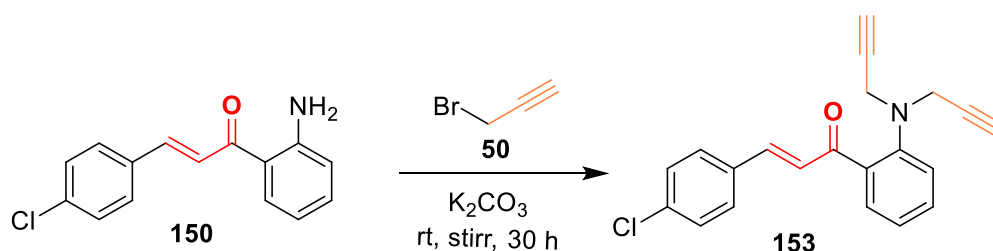
Scheme 3.18: Synthesis of ortho-substituted chalcone based terminal alkyne

Yield: 93%

Colour/texture: brown viscous oil

M.F.: $C_{21}H_{16}ClNO$

IR (neat, cm^{-1}): 3279, 3069, 2925, 2862, 2113, 1640, 1574, 1497, 1411, 1278, 1202, 1153, 1079, 999, 818, 742, 636.

^{1}H NMR (500 MHz, CDCl$_3$): δ = 7.91 (d, J = 7.5 Hz, 1H), 7.83 (s, 1H), 7.65 – 7.54 (m, 3H), 7.46 (d, J = 8.0 Hz, 1H), 7.37 (d, J = 8.4 Hz, 2H), 6.87 (s, 2H), 4.07 (s, 4H), 2.25 (s, 2H).

^{13}C NMR (126 MHz, CDCl$_3$): δ = 191.72, 168.11, 150.84, 141.75, 136.21, 135.36, 134.73, 134.01, 131.85, 131.17, 129.68, 129.43, 123.81, 80.45, 71.64, 38.98.

3.4.2.2. meta-substituted chalcone based terminal alkyne ((E)-3-(4-chlorophenyl)-1-(3-(di(prop-2-yn-1-yl)amino)phenyl)prop-2-en-1-one) (154)

Chalcone (1.0 g, 3.88 mmol, compound **151**) was dissolved in 20 mL of DMF with continuous stirring using a magnetic stirrer. Anhydrous potassium carbonate (2.68 g, 19.4 mmol) was added to the solution, followed by the gradual addition of propargyl bromide (1.06 mL, 9.3 mmol, compound **50**) dropwise. The reaction mixture was stirred at room temperature

for 36 hours, with its progress monitored via TLC (ethyl acetate:hexane, 1:9). Upon completion, the reaction was quenched by adding ice-cold water. The resulting product **(compound 154)** was isolated through solvent extraction using a mixture of ethyl acetate and water. The organic layer was separated using ethyl acetate, while the aqueous layer was discarded. The organic phase, containing the product, was then dried over anhydrous sodium sulphate to remove any residual water. Following the drying process, the solvent was removed by vacuum evaporation, yielding the final product as oil. The reaction for the same has been illustrated in scheme **3.19.**
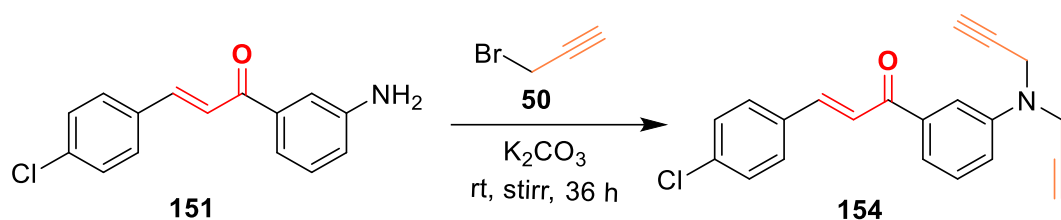
Scheme 3.19: Synthesis of meta-substituted chalcone based terminal alkyne

Yield: 89%

Colour/texture: brown viscous oil

M.F.: $C_{21}H_{16}ClNO$

IR (neat, cm^{-1}): 3289, 3065, 2938, 2112, 1671, 1587, 1488, 1439, 1326, 1261, 1090, 983, 912, 823, 782, 642.

^{1}H NMR (500 MHz, CDCl$_3$): δ = 7.81 (d, J = 8.3 Hz, 1H), 7.73 (d, J = 15.7 Hz, 2H), 7.62 – 7.52 (m, 2H), 7.51 – 7.35 (m, 3H), 7.18 (d, J = 8.3 Hz, 2H), 4.18 (s, 4H), 2.28 (s, 2H).

^{13}C NMR (126 MHz, CDCl$_3$): δ = 190.51, 147.96, 143.20, 138.91, 136.34, 133.42, 130.89, 130.11, 129.55, 129.37, 129.21, 122.79, 115.02, 78.76, 73.03, 40.48.

3.4.2.3. para-substituted chalcone based terminal alkyne ((E)-3-(4-chlorophenyl)-1-(4-(di(prop-2-yn-1-yl)amino)phenyl)prop-2-en-1-one) (155)

Chalcone (1.0 g, 3.88 mmol, compound 152) was dissolved in 20 mL of DMF and stirred continuously on a magnetic stirrer. Anhydrous potassium carbonate (2.68 g, 19.4 mmol) was then added, followed by the slow addition of propargyl bromide (1.06 mL, 9.3 mmol, compound 50). The mixture was stirred at room temperature for 26 hours, and the reaction

progress was monitored using TLC (ethyl acetate:hexane, 1:9). The reaction was quenched by adding ice-cold water, and the product **155** was subsequently separated through solvent extraction using a combination of ethyl acetate and water. The organic layer was separated using ethyl acetate, while the aqueous layer was discarded. The organic phase, containing the product, was then dried over anhydrous sodium sulphate to remove any residual water. Following the drying process, the solvent was removed by vacuum evaporation, yielding the kfinal product as oil. The reaction for the same has been illustrated in scheme **3.20.**
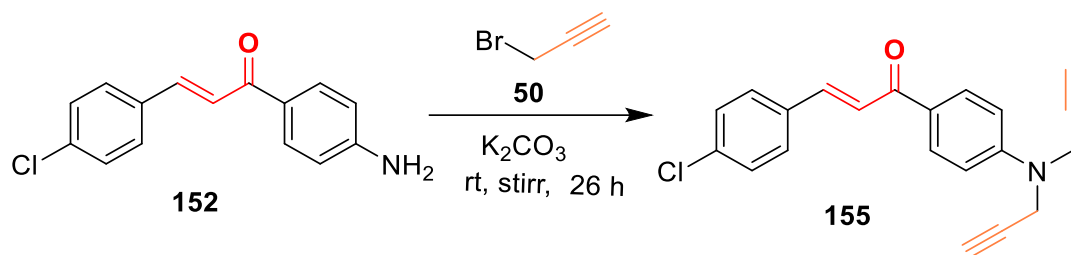
Scheme 3.20: Synthesis of para-substituted chalcone based terminal alkyne

Yield: 90%

Colour/texture: brown viscous oil

M.F.: $C_{21}H_{16}ClNO$

IR (neat, cm⁻¹): 3324, 3067, 2929, 2116, 1656, 1594, 1486, 1407, 1332, 1275, 1225, 1176, 1079, 1019, 975, 811, 743, 663.

¹H NMR (500 MHz, CDCl₃): δ = 7.98 (d, J = 18.5 Hz, 2H), 7.62 (d, J = 8.2 Hz, 3H), 7.32 (d, J = 4.9 Hz, 3H), 6.94 (s, 2H), 4.11 (d, J = 10.8 Hz, 4H), 2.27 (s, 2H).

¹³C NMR (126 MHz, CDCl₃): δ = 187.76, 167.79, 151.04, 141.58, 130.95, 129.42, 129.12, 128.80, 128.16, 122.47, 112.35, 79.83, 68.17, 38.72.

3.4.3. General synthetic route for the synthesis of ortho-, meta-, and para- substituted chalcone based 1,2,3-triazoles and their characterization

3.4.3.1. ortho-substituted chalcone based 1,2,3-triazole ((E)-1-(2-(bis((1-benzyl-1H-1,2,3-triazol-4-yl)methyl)amino)phenyl)-3-(4-chlorophenyl)prop-2-en-1-one) (156)

A chalcone-based alkyne (0.70 g, 1.72 mmol, compound **153**) was dissolved in a mixture of THF and TEA (1:1) and combined with the organic azide (0.43 mL, 3.46 mmol, compound

135) and a Cu(I) catalyst (0.001 mmol). The reaction was heated to reflux at 55–60 °C for 7 hours, and its progress was monitored by TLC (ethyl acetate:hexane, 1:4) to ensure the complete conversion of the reactants. After completion, the reaction was quenched by adding ice-cold water, and the solid product (compound **156**) was isolated by filtration and dried. The reaction for the same has been illustrated in scheme **3.21.**
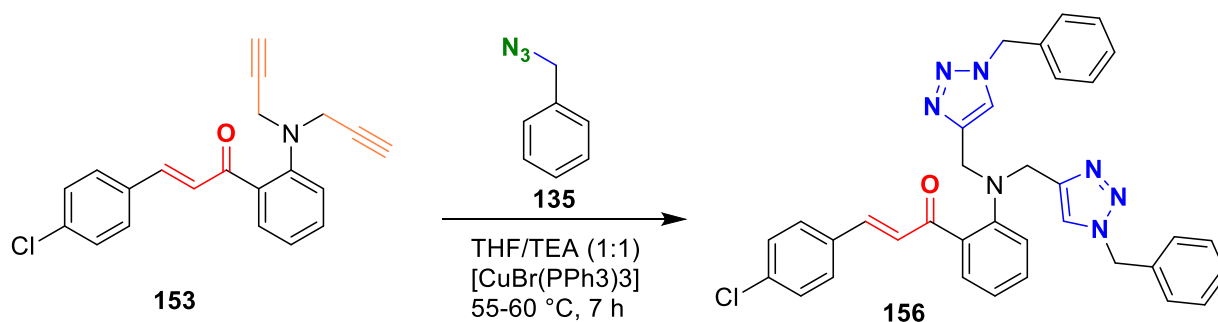
Scheme 3.21: Synthesis of ortho-substituted chalcone based 1,2,3-triazole

Yield: 92%

Colour/texture: yellow powder

M.F.: $C_{35}H_{30}ClN_7O$

Elem. Anal. Calc. (%): C = 75.56, H = 4.83, N = 4.20; **Found (%):** C = 75.55, H = 4.82, N = 4.22

mp: 127 – 128 °C

IR (neat, cm⁻¹): 3071, 2953, 2851, 1642, 1573, 1505, 1413, 1301, 1260, 1200, 1162, 1088, 1046, 1013, 972, 810, 749, 712, 635, 573.

¹H NMR (500 MHz, CDCl₃): δ = 7.88 (d, *J* = 7.8 Hz, 1H), 7.62 (d, *J* = 7.6 Hz, 2H), 7.53 (d, *J* = 8.3 Hz, 3H), 7.37 – 7.31 (m, 9H), 7.23 (d, *J* = 6.2 Hz, 3H), 6.80 (d, *J* = 8.1 Hz, 2H), 6.67 (t, *J* = 7.5 Hz, 2H), 5.48 (s, 4H), 4.60 (s, 4H).

¹³C NMR (126 MHz, CDCl₃): δ = 191.39, 151.24, 141.34, 135.94, 135.22, 134.62, 133.76, 131.57, 129.38, 129.16, 129.09, 128.71, 127.97, 123.57, 114.99, 112.23, 54.22, 39.05.

LC-MS: m/z (calculated) =599.22; **m/z (found)** = 600.12 (M+1).

3.4.3.2. meta-substituted chalcone based 1,2,3-triazole ((E)-1-(3-(bis((1-benzyl-1H-1,2,3-triazol-4-yl)methyl)amino)phenyl)-3-(4-chlorophenyl)prop-2-en-1-one) (157)

A solution of chalcone-based alkyne (0.70 g, 1.72 mmol) **154** in THF/TEA (1:1) was mixed with the organic azide (0.43 mL, 3.46 mmol) **135** and Cu(I) catalyst (0.001 mmol). The reaction mixture was refluxed at 55 – 60 °C for 13 hours until the complete conversion of the reactants monitored by TLC (ethyl acetate: hexane, 1:4). The reaction was then quenched by adding ice-cold water, and the product **157** was subsequently separated through solvent extraction using a combination of ethyl acetate and water. The organic layer was separated using ethyl acetate, while the aqueous layer was discarded. The organic phase, containing the product, was then dried over anhydrous sodium sulphate to remove any residual water. Following the drying process, the solvent was removed by vacuum evaporation, yielding the final product as oil. The reaction for the same has been illustrated in scheme **3.22.**
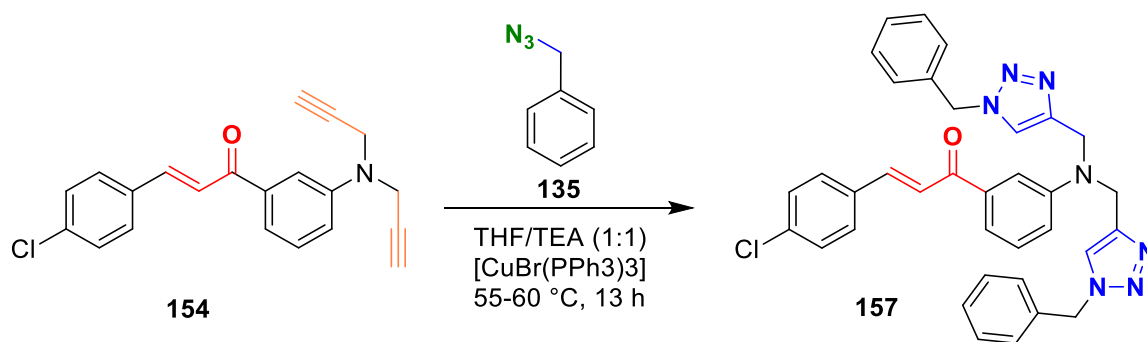
Scheme 3.22: Synthesis of meta-substituted chalcone based 1,2,3-triazole

Yield: 86%

Colour/texture: brown viscous oil

M.F.: $C_{35}H_{30}ClN_7O$

IR (neat, cm⁻¹): 3139, 3060, 2963, 1671, 1590, 1487, 1447, 1327, 1260, 1090, 1016, 798, 700, 540.

¹H NMR (500 MHz, CDCl₃): δ = 7.70 (d, *J* = 15.7 Hz, 1H), 7.62 – 7.54 (m, 2H), 7.54 – 7.47 (m, 1H), 7.47 – 7.40 (m, 2H), 7.40 – 7.34 (m, 6H), 7.25 – 7.21 (m, 1H), 7.21 – 7.18 (m, 2H), 7.18 – 7.12 (m, 6H), 7.10 – 7.02 (m, 1H), 5.39 (d, J = 10.1 Hz, 4H), 4.68 (d, *J* = 12.6 Hz, 4H).

¹³C NMR (126 MHz, CDCl₃): δ = 189.48, 147.11, 141.92, 137.86, 133.68, 133.61, 129.88, 128.66, 128.19, 127.97, 127.65, 126.77, 125.79, 121.77, 121.21, 117.21, 116.89, 115.80, 112.23, 111.57, 53.06, 45.68.

LC-MS: m/z (calculated) = 599.21; **m/z (found)** = 600.22 (M+1).

3.4.3.3. para-substituted chalcone based 1,2,3-triazole ((E)-1-(4-(bis((1-benzyl-1H-1,2,3-triazol-4-yl)methyl)amino)phenyl)-3-(4-chlorophenyl)prop-2-en-1-one) (158)

A solution of chalcone-based alkyne (0.70 g, 1.72 mmol) **155** in THF/TEA (1:1) was mixed with the organic azide (0.43 mL, 3.46 mmol) **135** and Cu(I) catalyst (0.001 mmol). The reaction mixture was refluxed at 55 – 60 °C for 11 hours until the complete conversion of the reactants monitored by TLC (ethyl acetate: hexane, 1:4). The reaction was then quenched by adding ice-cold water, and the product **158** was subsequently separated through solvent extraction using a combination of ethyl acetate and water. The organic layer was separated using ethyl acetate, while the aqueous layer was discarded. The organic phase, containing the product, was then dried over anhydrous sodium sulphate to remove any residual water. Following the drying process, the solvent was removed by vacuum evaporation, yielding the final product as oil. The reaction for the same has been illustrated in scheme **3.23.**
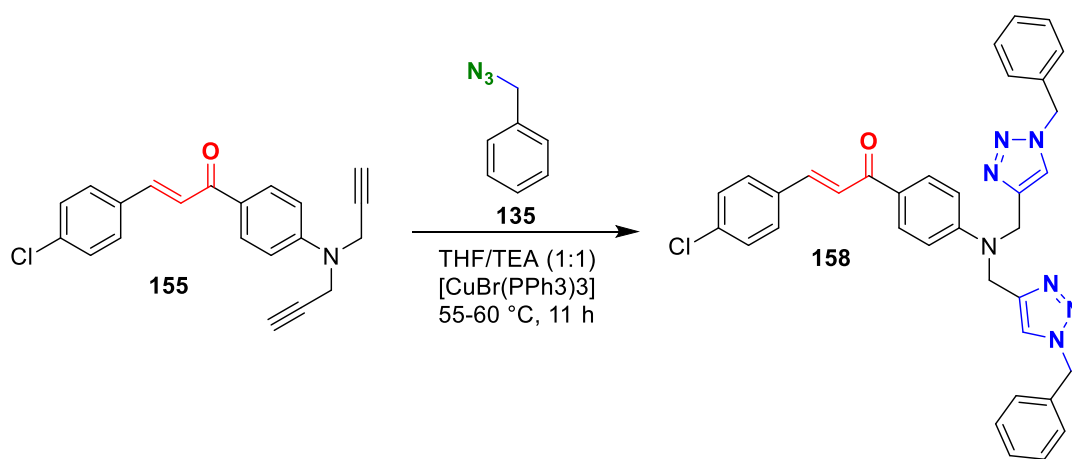
Scheme 3.23: Synthesis of para-substituted chalcone based 1,2,3-triazole

Yield: 88 %

Colour/texture: brown viscous oil

M.F.: $C_{35}H_{30}ClN_7O$

IR (neat, cm⁻¹): 3047, 2926, 1654, 1587, 1509, 1323, 1228, 1168, 1018, 814, 736, 684.

¹H NMR (500 MHz, CDCl₃): δ = 7.95 (s, 1H), 7.73 (d, *J* = 23.5 Hz, 3H), 7.63 (s, 1H), 7.45 (d, *J* = 5.3 Hz, 8H), 7.37 (d, *J* = 2.7 Hz, 7H), 6.95 (s, 2H), 5.46 (s, 4H), 4.22 (s, 4H).

¹³C NMR (126 MHz, CDCl₃): δ = 187.78, 161.13, 141.62, 133.83, 130.96, 130.21, 129.65, 129.42, 129.14, 128.86, 127.70, 127.49, 121.89, 113.93, 112.36, 68.18, 38.73.

LC-MS: m/z (calculated) =599.22; **m/z (found)** = 600.27 (M+1).

References

1. M. De Lourdes G. Ferreira, L. C. S. Pinheiro, O. A. Santos-Filho, M. D. S. Peçanha, C. Q. Sacramento, V. Machado, V. F. Ferreira, T. M. L. Souza and N. Boechat, *Med. Chem. Res.*, 2014, **23**, 1501–1511.

2. J. Kozłowska, B. Potaniec, D. Baczyńska, B. Żarowska and M. Anioł, *Molecules*, 2019, **24**, 4129.

3. R. Abonia, L. Cabrera, J. Quiroga, B. Insuasty, R. Moreno-Fuquen and A. R. Kennedy, *Molbank*, 2016, **2016**, M911.

4. N. A. Jinzeel, *J. Chem. Mater. Res.,* 2015**, 7,** 48-52.

Chapter IV

Results and Discussion
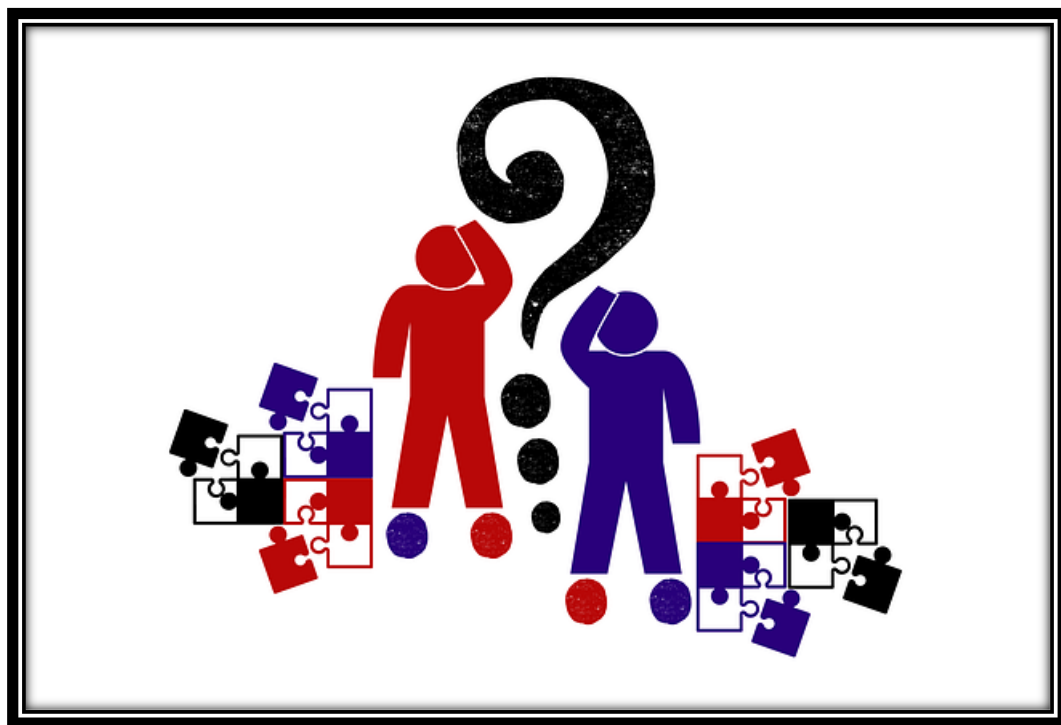
This chapter offers a clear explanation of the spectroscopic and photophysical data. It covers the synthetic and spectroscopic aspects of the compounds and explains the results from the photophysical data.

Chapter IV

Part A

Interpretation and discussion of spectroscopic data

This section discusses the spectroscopic analysis of the synthesized compounds in detail. The results of the analysis, along with the reason for these specific outcomes, are shown through text and figures in this chapter.

4.1 Synthetic approaches for the synthesis of chalcone based 1,2,3-triazoles

Chalcone-based 1,2,3-triazoles represent a unique class of compounds that merge the structural versatility of chalcones with the stability and functional diversity of the 1,2,3-triazole ring.[1,2] By the coupling of chalcones with 1,2,3-triazoles, researchers can harness the potential of conjugated system of the chalcone, enhancing as fluorescence studies leading to the study of metal-ion binding, and their chemical reactivity.[3,4] This synthesis is typically achieved through CuAAC reaction, which connects terminal alkyne-functionalized chalcones with azides, forming the 1,2,3-triazole ring with high selectivity and yield.[5] These 1,2,3-triazole compounds have shown promising applications in chemosensing, medicinal chemistry, and materials science, offering enhanced sensitivity in ion detection, therapeutic potential, and novel optoelectronic properties due to their extended conjugation and structural stability[6–8]. The current research work focuses on the synthesis of chalcone based 1,2,3-triazole derivatives via CuAAC methodology through a series of sequential steps as follows:

4.1.1. Synthesis of chalcone

The synthesis of chalcones involves mixing an ethanolic solution of ketone with potassium hydroxide (KOH) to catalyze the reaction. After stirring for 10 minutes, aldehyde is added gradually, allowing aldol condensation to form the β-hydroxy ketone intermediate. The mixture was stirred until the reactants were fully converted into the desired product, as confirmed by TLC analysis (ethyl acetate: hexane, 1:9). The chalcone was then precipitated by pouring the mixture into ice-cold water, filtered, and dried. The synthesized chalcones were obtained in the yield ranging from 87 % to 92 %.

4.1.2. Synthesis of chalcone based terminal alkyne

The synthesis of chalcone-based terminal alkynes was performed by reacting chalcones with labile protons of -NH$_2$ group with propargyl bromide in the presence of anhydrous potassium carbonate as a base through a nucleophilic substitution reaction, carried out at room temperature in DMF solvent. The reaction time is substrate-dependent, as different chalcone derivatives exhibit varying tendencies to lose protons. The resulting chalcone-based terminal alkynes can be isolated from the reaction mixture either by filtration in case of solid product or through extraction using a combination of ethyl acetate and water solvent system for liquid product. The synthesized alkynes were obtained in the yield ranging from 81 % to 93%.

4.1.3. Synthesis of organic azide

Organic azide was synthesized according to the method outlined by Lourdes *et al.*[9], using a nucleophilic substitution reaction between an aralkyl halide and dried sodium azide. The reaction occured in DMF as a solvent at a temperature range of 85–90 °C. The organic azide was obtained in moderate yield of 61%. Due to the sensitivity of sodium azide to heat and shock, all necessary safety precautions were carefully observed.

4.1.4. Synthesis of chalcone based 1,2,3-triazole

The 1,3-dipolar cycloaddition reaction between chalcone-based terminal alkynes and organic azides was facilitated by Cu(I) catalysis, using TEA as a base and THF as the solvent. By maintaining the reaction at 55–60 °C, depending on the reactants, chalcone-based 1,4-disubstituted 1,2,3-triazole linkers were formed through 'click' cycloaddition. The Cu(I) catalyst played a key role in both accelerating the reaction and ensuring stereospecificity.

4.2. Synthesis and spectral analysis of benzyl azide (135)

4.2.1. Synthesis

Benzyl azide **(135) (figure 4.1)** was prepared by reacting benzyl chloride **(134)** with dried sodium azide (NaN_3) in DMF through a nucleophilic substitution reaction. The reaction was completed after 5 hours of stirring at 85 – 90 °C. Due to the high reactivity and explosive nature of sodium azide, careful monitoring of the reaction conditions was essential to ensure safety. After the reaction, the product was extracted using a solvent extraction process and dried to remove any remaining solvent. The synthesized benzyl azide was then analyzed using infrared (IR) and nuclear magnetic resonance (NMR) spectroscopy to confirm its successful formation.

135
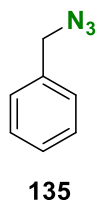
Figure 4.1: Structure of benzyl azide **135**

4.2.2. Analysis of IR spectrum

The IR spectrum of the newly synthesized benzyl azide **(135)** was recorded in the range of 4000-500 cm⁻¹ (neat). A key signal at 2089 cm⁻¹, characteristic of the -N_3 group, confirmed the substitution of the -Cl group in benzyl chloride with the azide group to form benzyl azide

which was previously absent in the IR spectra of the benzyl chloride. The stretching signal for the aromatic C-H bond appeared at 3032 cm⁻¹, while the symmetric stretch of the aliphatic C-H bond from the benzylic carbon was observed at 2930 cm⁻¹. The aromatic C=C stretching was observed at 1452 cm⁻¹ and C-N stretching at 1252 cm⁻¹.

4.2.3. NMR spectral analysis

The ¹H NMR spectrum of benzyl azide **(135)** was recorded at 500 MHz in CDCl₃ with tetramethylsilane as the reference. A singlet at δ = 4.14 ppm was detected in the ¹H NMR spectrum of benzyl azide corresponding to the two protons on the benzylic carbon. In case of benzyl chloride, this singlet is observed around δ = 4.5 - 4.6 ppm as benzylic position is deshielded by chlorine atom, therefore confirm the successful formation of benzyl azide. Additionally, a multiplet in the range of δ = 7.24 - 7.14 ppm was assigned to the five aromatic protons on the benzene ring.

The ¹³C NMR spectrum of benzyl azide **(135)** was also obtained in CDCl₃, providing additional confirmation of the product's synthesis. The carbon atoms in the benzene ring showed signals between δ = 135.53 - 128.31 ppm, while the benzylic carbon gave a signal at δ = 54.82 ppm, which is generally observed at δ = 44 – 46 ppm in the benzyl chloride due to the electronegative atom attached to it.

4.3. Synthesis and spectral analysis of chalcones 138, 140, and 142

4.3.1. Synthesis

The chalcones **(138, 140, 142) (figure 4.2)** were synthesized by reacting the starting materials, i.e., 4-benzyloxybenzaldehyde with o-, m-, and p-aminoacetophenone respectively, which reacted in the presence of potassium hydroxide as the base, deprotonating the alpha-carbon of the aminoacetophenone to form enolate ion. Then enolate ion attacks the carbonyl carbon of 4-benzyloxybenzaldehyde, leading to the formation of an intermediate.
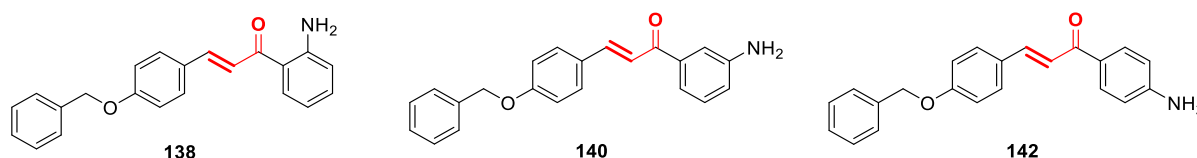
Figure 4.2: Structure of chalcones 138, 140, and 142

Afterwards, intermediate undergoes elimination reaction, losing a water molecule to form the unsaturated system. The products were obtained in solid nature after filtration and air dying. The purification of the obtained products was done using ethanol as eluent, then after

drying the yield of the products **138, 140, 142** were calculated to be 91 %, 87 %, 90 % respectively.

4.3.2. Analysis of IR spectrum

The vibrational spectroscopic data for the synthesized chalcones **138, 140, 142** were recorded as neat spectra within the 4000–400 cm^{-1} range. For compound **138**, a signal at 3436 and 3328 cm^{-1} corresponded to N-H stretching of NH_2 group. Additional signals included 3044 cm^{-1} for alkenyl C-H stretching, 1638 cm^{-1} for carbonyl stretching, 1581 and 1502 cm^{-1} for aromatic C=C stretch, and 1263 cm^{-1} for C-N stretching.

For compound **140**, a signal at 3453 and 3358 cm^{-1} corresponded to N-H stretching of NH_2 group. Additionally, the peaks at 3054 cm^{-1} for alkenyl C-H stretching, 1653 cm^{-1} for carbonyl stretching, 1581 and 1506 cm^{-1} for aromatic C=C stretch, and 1250 cm^{-1} for C-N stretching.

For compound **142**, a signal at 3373 and 3336 cm^{-1} corresponded to N-H stretching of NH_2 group. Additional signals included 3035 cm^{-1} for alkenyl C-H stretching, 1624 cm^{-1} for carbonyl stretching, 1593 and 1505 cm^{-1} for aromatic C=C stretch, and 1247 cm^{-1} for C-N stretching.

4.3.3 Analysis of NMR spectra

The successful synthesis of three 4-benzyloxybenzaldehyde-based chalcones **(138, 140, 142)** was confirmed through both ^1H and ^{13}C NMR spectra. For compound **138**, the ^1H NMR spectrum exhibited a singlet at δ = 5.10 corresponding to the methylene protons of the benzyloxy group, singlet at δ = 6.67 ppm corresponding to the NH_2 protons. The doublet at δ = 7.84 ppm was assigned to alkenyl proton of the C=C attached to the benzene ring. The aromatic protons were attributable to the multiplet in the range of δ = 7.72 - 6.67 ppm. The ^{13}C NMR spectrum further supported the ^1H NMR findings, showing signals at δ = 70.03 ppm corresponding to the methylene carbon (CH_2) attached to the benzyloxy group. The peaks at δ = 120.87 ppm and 142.66 ppm corresponding to the alkenyl carbons. The aromatic carbons are attributable in the range of δ = 160.42 - 115.17 ppm. The peak at δ = 191.69 ppm was attributable to the carbonyl carbon.

For compound **140**, the ^1H NMR spectrum exhibited a singlet at δ = 5.10 corresponding to the methylene protons of the benzyloxy group, singlet at δ = 5.16 ppm corresponding to the NH_2 protons. The doublet at δ = 7.89 ppm was assigned to alkenyl proton of the C=C attached to the benzene ring. The aromatic protons were attributable to the multiplet in the range of δ =

7.87 - 6.99 ppm. The ^{13}C NMR spectrum further supported the ^{1}H NMR findings, showing signals at δ = 70.12 ppm corresponding to the methylene carbon (CH$_2$) attached to the benzyloxy group. The peaks at δ = 120.22 ppm and 144.32 ppm corresponding to the alkenyl carbons. The aromatic carbons are attributable in the range of δ = 160.77 - 114.42 ppm. The peak at δ = 190.73 ppm was attributable to the carbonyl carbon.

For compound **142**, the ^{1}H NMR spectrum exhibited a singlet at δ = 5.10 corresponding to the methylene protons of the benzyloxy group, singlet at δ = 5.15 ppm corresponding to the NH$_2$ protons. The doublet at δ = 7.93 ppm was assigned to alkenyl proton of the C=C attached to the benzene ring. The aromatic protons were attributable to the multiplet in the range of δ = 7.91 - 6.67 ppm. The ^{13}C NMR spectrum further supported the ^{1}H NMR findings, showing signals at δ = 70.11 ppm corresponding to the methylene carbon (CH$_2$) attached to the benzyloxy group. The peaks at δ = 120.98 ppm and 142.89 ppm corresponding to the alkenyl carbons. The aromatic carbons are attributable in the range of δ = 160.48 - 113.93 ppm. The peak at δ = 188.15 ppm was attributable to the carbonyl carbon.

4.4. Synthesis and spectral analysis of terminal alkynes 143, 144, and 145

4.4.1. Synthesis

The terminal alkynes **(143, 144, 145)** were synthesized by reacting the previously synthesized chalcones (138, 140, 142) respectively with 80% propargyl bromide solution in toluene (**figure 4.3**). The reaction was performed at room temperature with constant stirring, using K$_2$CO$_3$ as the base. The base abstracted the labile protons from the amino group on the starting material, allowing the propargyl groups to replace them and form the terminal alkyne derivatives of the chalcones. The resulting brown oily product in the case of 143 and 145 was obtained through solvent extraction, followed by drying the combined organic layers over anhydrous sodium sulphate and evaporating the solvent under reduced pressure. In the case of 144, the product obtained was solid in nature, which was filtered, washed with distilled water and air dried.
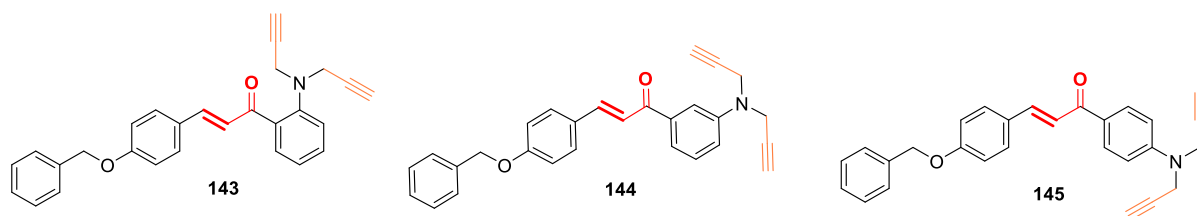
Figure 4.3: Structure of termina alkynes 143, 144, and 145

4.4.2. Analysis of IR spectra

The IR spectra (4000–500 cm^{-1}, neat) were recorded for the chalcone-based terminal alkynes **(143, 144, 145),** with each compound exhibiting characteristic signals. For compound **143,** a signal at 3287 cm^{-1} corresponded to -C≡C-*H* bond stretching, while 2113 cm^{-1} confirmed the presence of the C≡C bond stretch. Additional signals included 3029 cm^{-1} for alkenyl C-H stretching, 2910 cm^{-1} for methylene C-H stretching, 1637 cm^{-1} for carbonyl stretching, 1570 and 1504 cm^{-1} for aromatic C=C stretch, 1452 cm^{-1} for -CH$_2$ bending, and 1293 cm^{-1} for C-N stretching. The absence of a signal around 3400 cm^{-1}, corresponding to N-H stretching, indicated the successful conversion of -NH$_2$ group into the terminal alkyne.

Similarly, for compound **144,** a signal at 3280 cm^{-1} indicated -C≡C-*H* bond stretching, while a signal at 2111 cm^{-1} confirmed the C≡C bond stretch. Additional peaks appeared at 3056 cm^{-1} for alkenyl C-H stretching, 2930 cm^{-1} for methylene C-H stretching, 1656 cm^{-1} for carbonyl stretching, 1579 and 1502 cm^{-1} for aromatic C=C stretching, 1446 cm^{-1} for -CH$_2$ bending, and 1239 cm^{-1} for C-N stretching. The absence of N-H stretching at around 3400 cm^{-1} validated the formation of the terminal alkyne.

For compound **145**, the -C≡C-*H* stretching signal appeared at 3286 cm^{-1}, with a C≡C stretching signal at 2115 cm^{-1}. The methylene C-H stretching was observed at 2970 cm^{-1}, carbonyl stretching at 1651 cm^{-1}, C=C aromatic stretching at 1587 and 1505 cm^{-1}, and C-N stretching was observed at 1293 cm^{-1}. The absence of N-H stretching confirmed the conversion to the terminal alkyne.

4.4.3. Analysis of NMR spectra

The successful synthesis of three 4-benzyloxybenzaldehyde-based terminal alkynes **(143, 144, 145)** was confirmed through both ^{1}H and ^{13}C NMR spectra. For compound **143**, the ^{1}H NMR spectrum exhibited a singlet at δ = 2.23 ppm corresponding to the alkynyl protons (C≡C–*H*). Additionally, a singlet at δ = 4.02 ppm was assigned to methylene protons of the propargyl groups, whereas the single at δ = 5.08 ppm was observed for the methylene protons of the benzyloxy group. The aromatic protons were attributable to the multiplet in the range of δ = 7.91 – 6.97 ppm. The ^{13}C NMR spectrum further supported the ^{1}H NMR findings, showing signals at δ = 71.31 ppm and δ = 80.33 ppm for the C≡C carbons, along with a singlet at δ = 32.35 ppm for methylene carbons of the propargyl groups. Furthermore, the methylene carbon belonging to the benzyloxy group was observed at δ = 70.12 ppm. The aromatic carbons were recorded in the range of δ = 160.53 - 112.04 ppm, and the carbonyl carbon at δ = 191.86 ppm.

For compound **144,** The ¹H NMR spectrum showed a singlet at δ = 2.27 ppm for the alkynyl protons, and another singlet at δ = 4.17 ppm, which corresponded to the methylene protons of the propargyl groups. The methylene protons of the benzyloxy group were represented by a singlet at δ = 5.09 ppm. The aromatic protons were attributable to the multiplet in the range of δ = 7.78 – 6.98 ppm. In the ¹³C NMR spectrum, the C≡C carbons were observed at δ = 72.98 ppm and δ = 78.70 ppm, while the methylene carbons of the propargyl groups appeared as a singlet at δ = 40.42 ppm. Also, the methylene carbon belonging to the benzyloxy group was observed at δ = 70.14 ppm. The aromatic carbons were recorded in the range of δ = 147.90 - 114.97 ppm, and the carbonyl carbon at δ = 190.45 ppm.

In the case of compound **145**, a triplet at δ = 2.25 ppm in the ¹H NMR spectrum was assigned to alkynyl protons, and a doublet at δ = 3.98 ppm corresponded to methylene protons of the propargyl groups. The methylene protons of the benzyloxy group were represented by a singlet at δ = 5.08 ppm The aromatic protons were attributable to the multiplet in the range of δ = 7.83 – 6.67 ppm. The ¹³C NMR spectrum showed signals at δ = 71.86 ppm and δ = 79.89 ppm for the C≡C carbons, while the methylene carbons of the propargyl groups were reflected by a singlet at δ = 33.06 ppm. Additionally, the methylene carbon of the benzyloxy group was observed at δ = 70.08 ppm. The aromatic carbons were recorded in the range of δ = 160.46 – 112.32 ppm, and the carbonyl carbon at δ = 190.79 ppm.

The **table 4.1** highlights the differences in physical and spectroscopic properties of alkyne derivatives **143, 144, 145** at their ortho, meta and para position. The observations revealed that the solid state of the meta isomer can be attributed to its more symmetrical packing, which allow for relatively stronger intermolecular interactions. In contrast, the ortho and para isomers may have disrupted packing due to steric hinderance (ortho) or less favourable interaction (para) resulting in their liquid state at room temperature. The carbonyl stretching appears at lower wavenumber for ortho (1637 cm⁻¹) compared to meta and para isomers which is attributable to the presence of the -NH$_2$ group adjacent to the carbonyl group, thereby resulting in reduced double bond character of the carbonyl group through resonance which can slightly alter the bond strength, leading to shift in IR frequency. In the meta isomer (1656 cm⁻¹), the -NH$_2$ group is not directly conjugated with the carbonyl group which limits the delocalization of the lone pair on -NH$_2$ towards the carbonyl, retaining more of the double-bond character in the carbonyl group.

Table 4.1: Comparison of 4-benzyloxy benzaldehyde based ortho, meta and para substituted alkynes

Alkyne	Structure	Texture	Melting point (°C)	IR (cm⁻¹)		NMR (ppm)			
						¹H		¹³C	
Ortho **143**		Brown viscous oil	N/A	-C≡C-H	3287	-C≡C-**H**	2.23	-**C**≡**C**-H	71.31
				C≡C	2113				80.33
				C=O	1637	N-C**H₂**	4.02	N-**C**H₂	32.35
								C=O	191.86
Meta **144**		Light brown powder	112 – 113	-C≡C-H	3280	-C≡C-**H**	2.27	-**C**≡**C**-H	72.98
				C≡C	2111				78.70
				C=O	1656	N-C**H₂**	4.17	N-**C**H₂	40.42
								C=O	190.45
Para **145**		Brown viscous oil	N/A	-C≡C-H	3286	-C≡C-**H**	2.25	-**C**≡**C**-H	71.86
				C≡C	2115				79.89
				C=O	1651	N-C**H₂**	3.98	N-**C**H₂	33.06
								C=O	190.79

The -NH₂ group exerts an electron-donating inductive effect, which can slightly increase electron density on the carbonyl carbon. However, this effect is less significant compared to the resonance effect observed in the ortho isomer. Consequently, the bond strength of the carbonyl is slightly higher than in the ortho case, leading to a higher stretching frequency. Additionally, the IR frequencies for -C≡C-H and C≡C stretching is observed nearly similar for ortho para and meta isomers.

In ^{1}H NMR of para (3.98 ppm) and ortho (4.02 ppm) isomers, resonance effects dominate due to the favourable positions for delocalization of electrons involving the nitrogen atom. The resonance contributes to greater electron density around the nitrogen, increasing the shielding of the N-CH₂ protons.[10] As a result, the chemical shifts for these isomers appear upfield compared to the meta isomer. In the meta isomer, the electronic effect of the carbonyl group is less effectively delocalized through resonance with the nitrogen due to the position of the substituents on the aromatic ring. However, the inductive electron-withdrawing effect of the carbonyl group is still significant, pulling electron density away from the CH₂ group. This decreases the shielding on the CH₂ protons, resulting in a downfield shift (chemical shift at 4.17 ppm). The peak corresponding to -**C**≡C-H in ^{13}C NMR at shows insignificant variation among all isomers whereas the chemical shift value for N-**C**H₂ varies for ortho (32.35 ppm), meta (40.42 ppm) and para (33.06 ppm) due to the same shielding and resonance effect as attributed in ^{1}H NMR.

4.5. Synthesis and spectral analysis of 1,2,3-triazoles 146, 147, and 148

4.5.1. Synthesis

The three 4-benzyloxybenzaldehyde-based 1,2,3-triazole derivatives **(146, 147, 148) (figure 4.4)** were regioselectively synthesized using their respective terminal alkynes (**143, 144, 145**) and benzyl azide **135** through 1,3-dipolar cycloaddition reactions. These reactions were catalyzed by the [CuBr(PPh₃)₃] complex (0.001 mmol) in a THF (v/v, 3:2) solvent mixture. Triethylamine (TEA) acted as the base, facilitating the deprotonation of the terminal alkynes. The stereoselectivity of the cycloaddition, yielding exclusively 1,4-disubstituted products, was directed by the Cu(I) catalyst. Each reaction, carried out at 55–60 °C for 6-8 hours under stirring, was completed with the formation of solid products in the case of **146** and **147** upon treatment of the reaction mixture with ice-cold water, which was filtered, washed with distilled water and air dried. In the case of compound **148**, the oily product was successfully obtained through a solvent extraction process. This involved extracting the desired

compound from the reaction mixture using an appropriate solvent. The final 1,2,3-triazole derivatives were thoroughly characterized using standard spectroscopic techniques, confirming their successful synthesis.
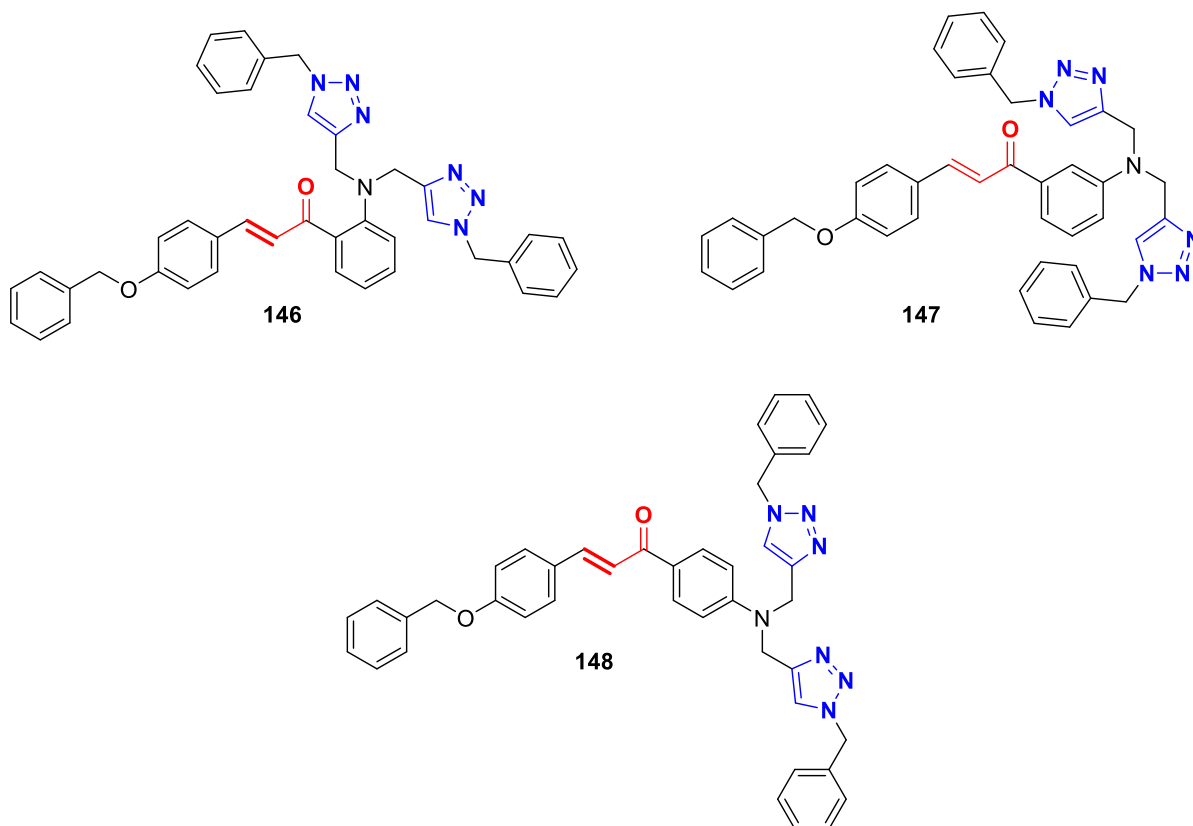
Figure 4.4: Structure of 1,2,3-triazoles 146, 147, and 148

4.5.2. Analysis of IR spectra

The IR spectra (neat, 4000–500 cm^{-1}) for the 4-benzyloxybenzaldehyde-based 1,2,3-triazole derivatives **(146, 147, 148)** provided strong evidence for the successful formation of the target compounds. In all the cases, the absence of signals associated with C≡C-H and C≡C stretching at about 3287 - 3280 cm^{-1} and 2115 - 2111 cm^{-1}, along with the disappearance of the -N=N=N stretching signal at 2089 cm^{-1}, confirmed the modification of the C≡C-H and N$_3$ groups, indicating the formation of the 1,2,3-triazole moiety.

For compound **146,** a signal at 3068 cm^{-1} was attributed to aromatic C-H stretching, while 3033 cm^{-1} indicated the C-H stretching of the triazole ring. A peak at 2931 cm^{-1} was due to methylene C-H stretching, with additional signals at 1638 cm^{-1} for carbonyl stretching, 1570 and 1507 cm^{-1} for aromatic C=C stretching, 1455 cm^{-1} for -CH$_2$ bending, and 1280 cm^{-1} for C-N stretching.

Similarly, for compound **147,** aromatic C-H stretching appeared at 3129 cm^{-1}, with C-H stretching of the triazole ring at 3064 cm^{-1}, and methylene C-H stretching at 2916 cm^{-1}. The carbonyl stretching was observed at 1654 cm^{-1}, whereas the aromatic C=C stretching was attributable to 1571 and 1511 cm^{-1}. The -CH$_2$ bending and C-N stretching were represented by the signals at 1448 cm^{-1} and 1235 cm^{-1} respectively.

For compound **148**, the aromatic C-H stretching signal appeared at 3146 cm^{-1}, with the C-H stretching of the triazole ring at 3031 cm^{-1} and methylene C-H stretching at 2958 cm^{-1}. The carbonyl stretching was observed at 1649 cm^{-1}, while the aromatic C=C stretching was attributable to 1590 and 1503 cm^{-1}. The -CH$_2$ bending was represented by the signal at 1455 cm^{-1}, and the C-N stretching was identified at 1224 cm^{-1}.

4.5.3. Analysis of NMR spectra

At 500 MHz in CDCl$_3$, the ^{1}H NMR spectra of the 4-benzyloxybenzaldehyde-based 1,2,3-triazole derivatives **(146, 147, 148)** were analyzed relative to tetramethylsilane, confirming the conversion of the alkyne moieties into 1,2,3-triazole rings. For all the three compounds, the absence of triplets at about $\delta = 2.23 - 2.27$ ppm, characteristic of the alkynyl protons in the precursors, indicated the successful transformation of the alkyne into the 1,2,3-triazole moiety.

For compound **146,** the doublet at $\delta = 4.61$ ppm was assigned to the methylene protons adjacent to the triazole ring and the nitrogen atoms of the parent structure, while the singlet at $\delta = 5.49$ ppm corresponded to the benzylic protons. The singlet at $\delta = 5.12$ ppm was attributed to the methylene protons of the benzyloxy group, and the aromatic protons appeared as a multiplet in the range of $\delta = 7.93 - 6.81$ ppm. The ^{13}C NMR spectrum further confirmed the successful formation of the 1,2,3-triazole derivative, as no signals were observed for the C≡C carbons, indicating the conversion of the alkyne into the 1,2,3-triazole ring. The signal at $\delta = 38.04$ ppm was assigned to the methylene carbons adjacent to the triazole ring and nitrogen atoms, while the signal at $\delta = 53.12$ ppm was attributed to the benzylic carbons. Additionally, the methylene carbon of the benzyloxy group was represented by the signal at $\delta = 69.06$ ppm. The aromatic carbons were recorded in the range of $\delta = 159.49 - 111.10$ ppm, and the carbonyl carbon at $\delta = 190.79$ ppm.

Similarly, in compound **147**, the methylene protons adjoining the 1,2,3-triazole ring and nitrogen atoms produced a singlet at $\delta = 4.58$ ppm, with the benzylic protons resonating at $\delta = 5.30$ ppm. The methylene protons of the benzyloxy group gave a singlet at $\delta = 4.99$ ppm,

while aromatic protons appeared as a multiplet at δ = 7.64 – 6.89 ppm. The absence of signals corresponding to the C ≡ C carbons in the ^{13}C NMR spectrum provided additional evidence for the successful formation of the 1,2,3-triazole derivative. A distinct signal at δ = 46.68 ppm was attributed to the methylene carbons adjacent to the 1,2,3-triazole ring and nitrogen atoms, whereas a signal at δ = 53.98 ppm was observed for the benzylic carbons, verifying the presence of this functional group. The methylene carbon of the benzyloxy group appeared at δ = 70.04 ppm. The aromatic carbons resonated in the range of δ = 160.74 – 113.05 ppm, consistent with the expected aromatic structure, and the carbonyl carbon was recorded at δ = 190.70 ppm, further validating the successful synthesis of the target compound.

In compound **148,** the methylene protons adjacent to the 1,2,3-triazole ring and nitrogen atoms produced a doublet at δ = 4.47 ppm, while the benzylic protons resonated at δ = 5.46 ppm. The methylene protons of the benzyloxy group appeared as a singlet at δ = 5.09 ppm, with the aromatic protons showing as a multiplet in the range of δ = 7.84 – 6.67 ppm. The ^{13}C NMR spectrum also demonstrated absence of signals for the C ≡ C carbons. A signal at δ = 37.70 ppm corresponded to the methylene carbons adjacent to the 1,2,3-triazole ring and nitrogen atoms, while a signal at δ = 67.14 ppm verified the presence of benzylic carbons. The methylene carbon of the benzyloxy group resonated at δ = 69.06 ppm. The aromatic carbons, appearing within δ = 166.75 – 110.98 ppm, aligned with the anticipated aromatic structure, and the carbonyl carbon recorded at δ = 189.79 ppm further validated the target compound's successful synthesis.

4.5.4. Analysis of mass spectra

The synthesized 1,2,3-triazole derivatives **(146, 147, and 148)** were further subjected to mass spectrometry analysis to confirm their successful synthesis and validate the predicted molecular structures. The mass spectrometric data provided critical evidence for the formation of these compounds, with the observed peaks closely matching the theoretical predictions.

For compound **146**, the calculated molecular mass peak (m/z) was 671.81. The mass spectrum exhibited a prominent peak at m/z = 672.25, which corresponds to the protonated molecular ion [M+H]$^+$. This close agreement between the observed and theoretical values strongly supports the successful synthesis of compound **146**.

Similarly, compound **147** was analyzed, with its predicted molecular mass peak (m/z) also being 671.81. The mass spectrum revealed a significant peak at m/z = 672.30, consistent
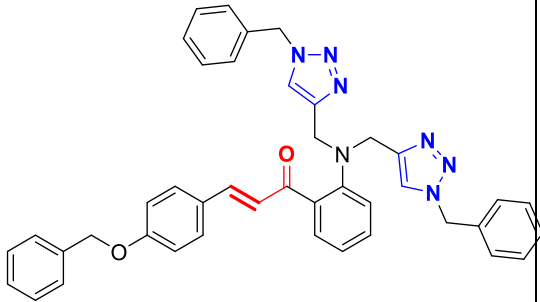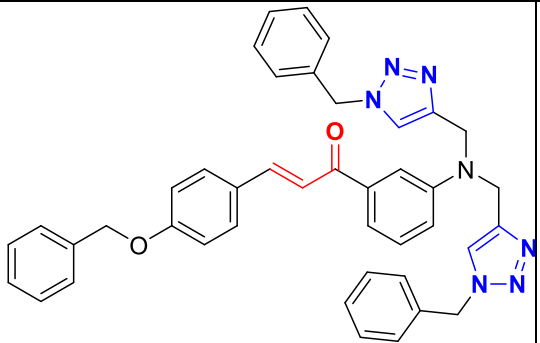
with the expected [M+H]$^{1+}$ ion. This result further corroborates the formation of compound **147** as per the proposed structure.
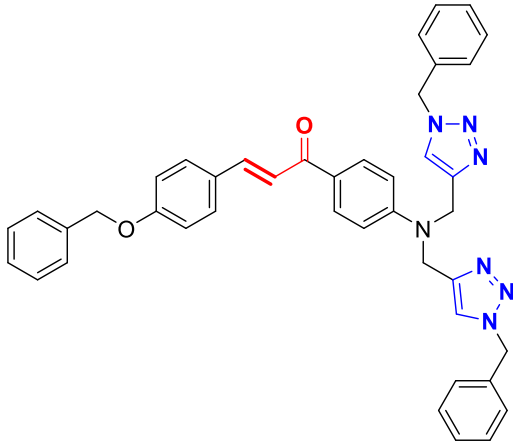
For compound **148,** the theoretical molecular mass peak was again 671.81. The experimental mass spectrum confirmed this prediction by displaying a strong peak at m/z = 672.32, indicative of the protonated molecular ion. This finding validates the successful synthesis of compound **148.**

Table 4.2 presents a comparative analysis of the physical and spectroscopic properties of 1,2,3-triazole derivatives **(146, 147, 148)** at the ortho, meta, and para positions. The ortho and meta isomers are found to exist in solid states, owing to better molecular packing, while the para isomers exhibit a liquid state at room temperature due to less favorable interactions and disrupted packing. The ortho isomer, with a higher melting point, likely benefits from enhanced intramolecular interactions that contribute to its solid state. The lower carbonyl stretching frequency observed for the ortho isomer (1638 cm^{-1}) can be attributed to the proximity of the -NH$_2$ group to the carbonyl group. This adjacency allows for resonance effects that reduce the double bond character of the carbonyl group, weakening the C=O bond strength and shifting the IR frequency. In addition, steric hindrance from the -NH$_2$ group also contributes to this shift.

In the ^{1}H NMR spectra, the chemical shift of the CH$_2$ group for the para isomer appears at 4.47 ppm, where resonance effects dominate due to the favourable positions for electron delocalization involving the nitrogen atom. This results in greater electron density around the nitrogen and enhanced shielding of the N-CH$_2$ protons, leading to an upfield shift of the signal. In contrast, the meta isomer experiences less effective delocalization of electron density due to the positioning of the substituents on the aromatic ring. This decreases the shielding of the CH$_2$ protons, causing a downfield shift to 4.58 ppm. In the ^{13}C NMR spectra, the chemical shift for the N-CH$_2$ group varies for the ortho (38.04 ppm), meta (46.68 ppm), and para (37.70 ppm) isomers. This variation mirrors the shielding and resonance effects observed in the ^{1}H NMR spectra, further supporting the differences in electronic environments across the isomers. These spectroscopic data collectively highlight the impact of substitution position on the molecular structure and electronic properties of the 1,2,3-triazole derivatives.

Table 4.2: Comparison of 4-benzyloxy benzaldehyde based ortho, meta and para substituted chalcone based 1,2,3-triazoles

1,2,3-triazole	Structure	Texture	Melting point (°C)	IR value (cm⁻¹)	NMR (ppm)				Mass (m/z) (LCMS)
					¹H		¹³C		
Ortho 146		Yellow powder	165 –166	C=O 1638	Ph-C**H₂**	5.49	Ph-**C**H₂	53.12	672.25
					N-C**H₂**	4.61	N-**C**H₂	38.04	
					C-**H** (Tz ring)	7.59	**C**-H (Tz ring)	126.45	
							C=O	190.79	
Meta 147		Light yellow powder	161 – 162	C=O 1654	Ph-C**H₂**	5.30	Ph-**C**H₂	53.98	672.30
					N-C**H₂**	4.58	N-**C**H₂	46.68	
					C-**H** (Tz ring)	7.48	**C**-H (Tz ring)	127.43	
							C=O	190.70	

1,2,3-triazole	Structure	Texture	Melting point (°C)	IR value (cm⁻¹)		NMR (ppm)				Mass (m/z) (LCMS)
						¹H		¹³C		
Para 148		Dark brown viscous oil	N/A	C=O	1649	Ph-C**H₂** N-C**H₂** C-**H** (Tz ring)	5.46 4.47 7.54	Ph-**C**H₂ N-**C**H₂ **C**-H (Tz ring) **C**=O	67.14 37.70 126.45 189.79	672.32

4.6. Synthesis and spectral analysis of chalcones 150, 151, and 152

4.6.1. Synthesis

The chalcones **(150, 151, 152) (figure 4.5)** were prepared by reacting 4-chlorobenzaldehyde with o-, m-, and p-aminoacetophenone, respectively, in the presence of potassium hydroxide as a base. Potassium hydroxide deprotonates the alpha-carbon of aminoacetophenone, generating an enolate ion. This enolate then attacks the carbonyl carbon of 4-chlorobenzaldehyde, forming a reaction intermediate. The intermediate subsequently undergoes an elimination reaction, releasing a water molecule and creating the conjugated double bond system characteristic of chalcones. The resulting products (150, 151, 152) were isolated as solids through filtration and air drying.
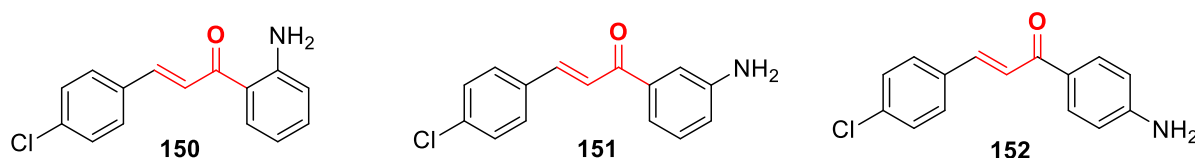
Figure 4.5: Structure of chalcones 150, 151, and 152

4.6.2. Analysis of IR spectra

The vibrational spectroscopic data for the synthesized chalcones **150, 151, 152** were recorded as neat spectra within the 4000–400 cm^{-1} range. For compound **150,** a signal at 3461 and 3295 cm^{-1} corresponded to N-H stretching of NH_2 group. Additional signals included 3032 cm^{-1} for alkenyl C-H stretching, 1639 cm^{-1} for carbonyl stretching, 1564 and 1484 cm^{-1} for aromatic C=C stretch, and 1280 cm^{-1} for C-N stretching.

For compound **151**, a signal at 3449 and 3359 cm^{-1} corresponded to N-H stretching of NH_2 group. Additional signals included 3047 cm^{-1} for alkenyl C-H stretching, 1658 cm^{-1} for carbonyl stretching, 1585 and 1587 cm^{-1} for aromatic C=C stretch.

For compound **152**, a signal at 3457 and 3340 cm^{-1} corresponded to N-H stretching of NH_2 group. Additional signals included 3045 cm^{-1} for alkenyl C-H stretching, 1635 cm^{-1} for carbonyl stretching, 1598 and 1490 cm^{-1} for aromatic C=C stretch.

4.6.3 Analysis of NMR spectra

The successful synthesis of three 4-chlorobenzaldehyde-based chalcones **(150, 151, 152)** was confirmed through both ^1H and ^{13}C NMR spectra. For compound **150**, the ^1H NMR spectrum exhibited a singlet at δ = 6.34 ppm corresponding to the NH_2 protons. The doublet at

δ = 7.84 ppm was assigned to alkenyl proton of the C=C attached to the benzene ring. The aromatic protons were attributable to the multiplet in the range of δ = 7.83 - 6.68 ppm. The ^{13}C NMR spectrum further supported the ^{1}H NMR findings, showing signals at the peaks at δ = 123.61 ppm and 141.42 ppm corresponding to the alkenyl carbons (C=C). The aromatic carbons are attributable in the range of δ = 151.08 - 115.90 ppm. The peak at δ = 191.17 ppm was attributable to the carbonyl carbon.

For compound **151**, the ^{1}H NMR spectrum exhibited a singlet at δ = 2.64 ppm corresponding to the NH_2 protons. The doublet at δ = 8.48 ppm was assigned to alkenyl proton of the C=C attached to the benzene ring. The aromatic protons were attributable to the multiplet in the range of δ = 7.90 – 7.23 ppm. The ^{13}C NMR spectrum further supported the ^{1}H NMR findings, showing peaks at δ = 120.27 ppm and 138.18 ppm corresponding to the alkenyl carbons (C=C). The aromatic carbons are attributable in the range of δ = 159.90 - 114.01 ppm. The peak at δ = 189.82 ppm was attributable to the carbonyl carbon.

For compound **152**, the ^{1}H NMR spectrum exhibited a singlet at δ = 4.19 ppm corresponding to the NH_2 protons. The doublet at δ = 7.93 ppm was assigned to alkenyl proton of the C=C attached to the benzene ring. The aromatic protons were attributable to the multiplet in the range of δ = 7.91 - 6.69 ppm. The ^{13}C NMR spectrum further supported the ^{1}H NMR findings, the peaks at δ = 122.51 ppm and 141.63 ppm corresponding to the alkenyl carbons (C=C). The aromatic carbons are attributable in the range of δ = 151.24 - 113.81 ppm. The peak at δ = 187.76 ppm was attributable to the carbonyl carbon.

4.7. Synthesis and spectral analysis of terminal alkynes 153, 154, 155

4.7.1. Synthesis

The synthesis of terminal alkynes **(153, 154, 155)** involved the reaction of previously synthesized chalcones (150, 151, 152) respectively with an 80% propargyl bromide solution in toluene **(figure 4.6)**. This reaction was conducted at ambient temperature with continuous stirring, utilizing K_2CO_3 as the base. The base effectively abstracted the labile protons from the secondary amino groups present in the starting materials, facilitating the replacement of these protons by the propargyl group, thereby yielding terminal alkyne derivatives of the chalcones. The resulting brown oily product was isolated through solvent extraction, followed by the evaporation of the combined organic layers under reduced pressure. Ultimately, the product solidified upon cooling to room temperature.
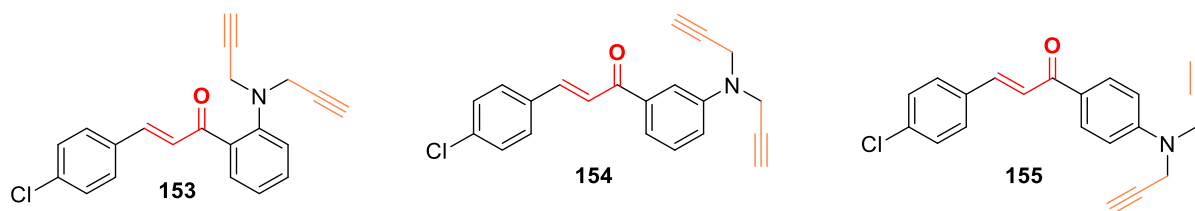
Figure 4.6: Structure of terminal alkynes 153, 154, and 155

4.7.2. Analysis of IR spectra

The IR spectra for the 4-chlorobenzaldehyde-based terminal alkynes **153, 154, and 155** were obtained in the range of 4000–500 cm^{-1} (neat) and revealed specific bands corresponding to the targeted functional groups, verifying the formation of the alkyne derivatives. For compound **153**, the characteristic -C≡C-*H* stretching signal was observed at 3279 cm^{-1}, while a peak at 2113 cm^{-1} indicated the C≡C bond stretch. Other notable signals included alkenyl C-H stretching at 3069 cm^{-1}, methylene C-H stretching at 2925 cm^{-1}, carbonyl stretching at 1640 cm^{-1}, and aromatic C=C stretching at 1574 and 1497 cm^{-1}. Additional peaks were noted at 1411 cm^{-1} for -CH$_2$ bending and 1278 cm^{-1} for C-N stretching. The absence of a signal near 3400 cm^{-1}, typically corresponding to N-H stretching, confirmed the conversion of the -NH$_2$ group into the terminal alkyne.

Similarly, compound **154** showed an IR signal at 3289 cm^{-1} for -C≡C-*H* stretching and a peak at 2112 cm^{-1} for the C≡C bond stretch. Alkenyl C-H stretching appeared at 3065 cm^{-1}, methylene C-H stretching at 2938 cm^{-1}, and carbonyl stretching at 1671 cm^{-1}. Aromatic C=C stretching bands were detected at 1587 and 1488 cm^{-1}, with -CH$_2$ bending at 1439 cm^{-1} and C-N stretching at 1261 cm^{-1}. The absence of the N-H stretches around 3400 cm^{-1} validated the formation of the terminal alkyne derivative.

For compound **155**, the IR spectrum showed the -C≡C-*H* stretching at 3324 cm^{-1}, with a distinct C≡C stretching signal at 2116 cm^{-1}. The alkenyl C-H stretching was attributed to 3067 cm^{-1} whereas the methylene C-H stretching appeared at 2929 cm^{-1}. The carbonyl stretching at 1656 cm^{-1} and aromatic C=C stretching bands at 1594 and 1486 cm^{-1}. Additionally, a C-N stretching signal was observed at 1275 cm^{-1}. As with the other compounds, the absence of an N-H stretching band confirmed the successful transformation of the amino group to the terminal alkyne.

4.7.3. Analysis of NMR spectra
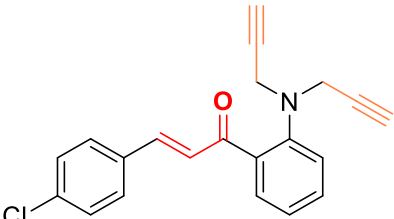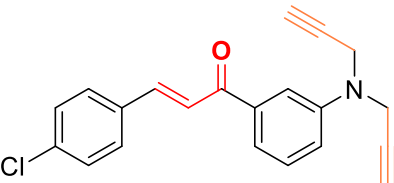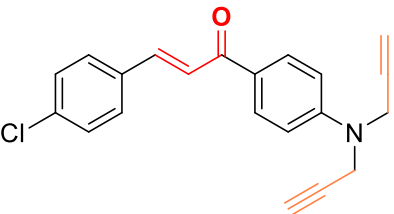
The successful synthesis of 4-chlorobenzaldehyde-based terminal alkynes, **153, 154, and 155,** was confirmed through detailed ¹H and ¹³C NMR spectroscopic analysis. For compound **153,** the ¹H NMR spectrum showed a singlet at δ = 2.25 ppm, corresponding to alkynyl protons (C≡C–H). A singlet at δ = 4.07 ppm was attributed to the methylene protons of the propargyl groups. The aromatic protons were present as a multiplet within the range of δ = 7.92 – 6.87 ppm. Supporting these observations, the ¹³C NMR spectrum displayed signals at δ = 71.64 ppm and δ = 80.45 ppm for the C≡C carbons, along with a singlet at δ = 38.98 ppm for the methylene carbons of the propargyl group. The aromatic carbons appeared in the range of δ = 168.11 – 112.39 ppm, and the carbonyl carbon was observed at δ = 191.72 ppm.

For compound **154,** the ¹H NMR spectrum showed a singlet at δ = 2.28 ppm for the alkynyl protons, and a singlet at δ = 4.18 ppm was assigned to the methylene protons of the propargyl group. The aromatic protons resonated as a multiplet in the δ = 7.82 – 7.17 ppm range. In the ¹³C NMR spectrum, signals at δ = 73.03 ppm and δ = 78.76 ppm confirmed the presence of C≡C carbons, with a singlet at δ = 40.48 ppm for the methylene carbons of the propargyl group. The aromatic carbons appeared in the range of δ = 147.96 – 115.02 ppm, and the carbonyl carbon was noted at δ = 190.51 ppm.

For compound **155,** the ¹H NMR spectrum displayed a singlet at δ = 2.27 ppm, indicating the presence of alkynyl protons, and a doublet at δ = 4.11 ppm, which was attributed to the methylene protons of the propargyl group. The aromatic protons appearing as a multiplet in the range of δ = 7.98 – 6.94 ppm. In the ¹³C NMR spectrum, signals at δ = 71.93 ppm and δ = 79.84 ppm represented the C≡C carbons, and a singlet at δ = 38.74 ppm indicated the methylene carbons of the propargyl group. The aromatic carbons were noted in the range of δ = 167.80 – 112.36 ppm. The carbonyl carbon was present at δ = 187.77 ppm.

The **table 4.3** presents the physical and spectroscopic properties of alkyne derivatives **(153, 154, 155)** at ortho, meta, and para positions. The IR variations are attributed to differences in electronic environments and steric effects induced by substituent positioning. The ortho isomer shows the lowest carbonyl (C=O) stretching frequency (1640 cm⁻¹), is attributable to the presence of the -NH2 group adjacent to the carbonyl group, thereby resulting in reduced double bond character of the carbonyl group through resonance. which can slightly alter the bond strength, experiences steric hindrance and leading to shift in IR frequency.

Table 4.3: Comparison of 4-chloro benzaldehyde based ortho, meta and para substituted alkynes

Alkyne	Structure	Texture	Melting point (°C)	IR value (cm⁻¹)		NMR (ppm)			
						¹H		¹³C	
Ortho **153**				-C≡C-H	3279	-C≡C-**H**	2.25	**-C≡C-H**	71.64
				C≡C	2113				80.45
				C=O	1640	N-C**H₂**	4.07	N-C**H₂**	38.98
								C=O	191.72
Meta **154**		Brown viscous oil	N/A	-C≡C-H	3289	-C≡C-**H**	2.28	**-C≡C-H**	73.03
				C≡C	2112				78.76
				C=O	1671	N-C**H₂**	4.18	N-C**H₂**	40.48
								C=O	190.51
Para **155**				-C≡C-H	3324	-C≡C-**H**	2.27	**-C≡C-H**	71.93
				C≡C	2116				79.84
				C=O	1656	N-C**H₂**	4.11	N-C**H₂**	38.74
								C=O	187.77

The meta and para isomers exhibit higher wavenumbers for C=O, reflecting less steric strain and a stronger bond. The IR frequencies for C≡C stretching is nearly similar for ortho para and meta isomers, whereas the peaks corresponding to -C≡C-H stretching shows variation in para (3324 cm^{-1}) isomer due to the resonance stabilization. Furthermore, in ^{1}H NMR, the chemical shift values for -C≡C-**H** and N-C**H$_2$** are almost same in all isomers. The peak corresponding to -**C**≡**C**-H in ^{13}C NMR at shows insignificant variation among all isomers whereas the chemical shift value for N-**C**H$_2$ varies for ortho (38.98 ppm), meta (40.48 ppm) and para (38.74 ppm) due to the de-shielding of meta electrons. The ortho isomer exhibits the most deshielded carbonyl carbon (191.72 ppm), consistent with increased steric hindrance and electronic withdrawal. Conversely, the para isomer has the least deshielded carbonyl carbon (187.77 ppm), reflecting a more symmetric electronic distribution.

4.8. Synthesis and spectral analysis of 1,2,3-triazoles 156, 157, and 158

4.8.1. Synthesis

The synthesis of 4-chlorobenzaldehyde -based 1,2,3-triazole derivatives **(156, 157, and 158)** was achieved through the reaction of their respective terminal alkynes (**153, 154, and 155**) with benzyl azide **135** in a solvent system of THF (v/v, 1:1), utilizing [CuBr(PPh₃)₃] (0.001 mmol) as the catalyst **(figure 4.7)**.
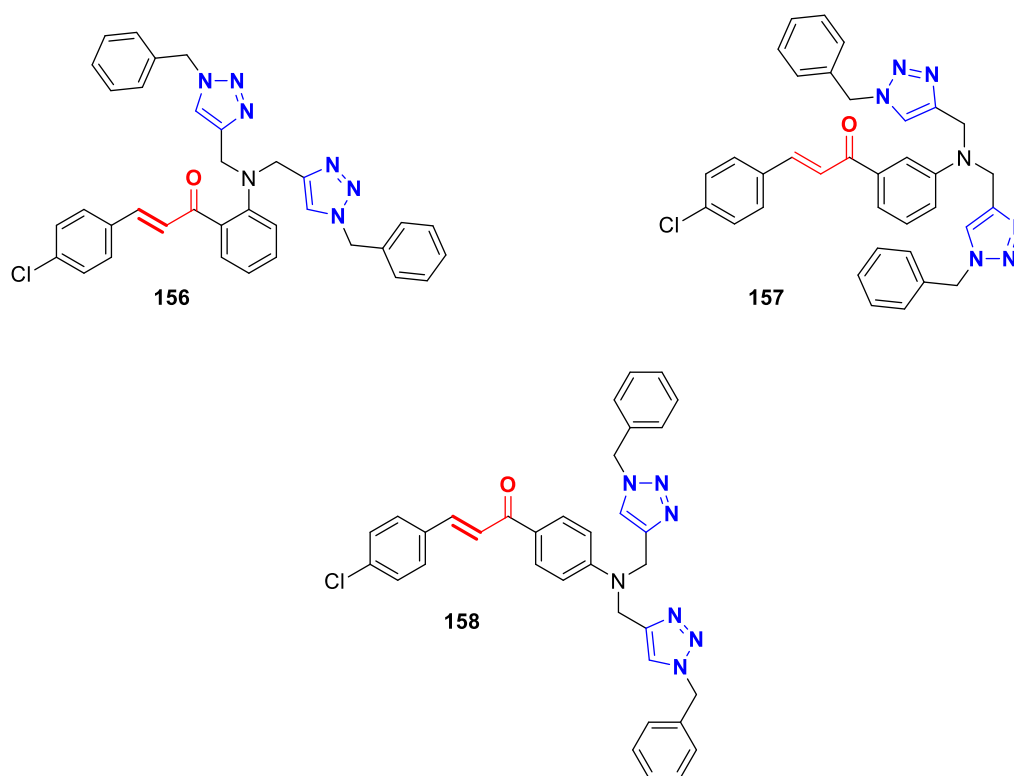
Figure 4.7: Structure of 1,2,3-triazoles 156, 157, and 158

Following 7 - 13 hours of stirring at a temperature range of 55-60 °C, the reactions reached completion. For compounds **157** and **158**, brown oily products were obtained by solvent extraction, with the combined organic layers subsequently dried over anhydrous sodium sulphate. The solvent was then evaporated under reduced pressure, yielding the final product. In contrast, for compound **156**, a solid product was obtained, which was isolated by filtration, washed thoroughly with distilled water, and air-dried to achieve a purified form.

4.8.2. Analysis of IR spectra

The IR spectra (neat, 4000–500 cm^{-1}) of the synthesized 4-chlorobenzaldehyde-based 1,2,3-triazole derivatives **(156, 157, 158)** provided compelling evidence for the successful formation of the target compounds. In all cases, the absence of signals at about 3324 - 3279 cm^{-1}, corresponding to C≡*C-H* stretching, 2116 - 2112 cm^{-1} for C≡C stretching, and 2089 cm^{-1} associated with -N=N=N stretching, indicated the modification of C≡C-H and N$_3$ groups, confirming the synthesis of the 1,2,3-triazole moiety.

For compound **156,** a signal at 3071 cm^{-1} was attributed to aromatic C-H stretching, while the C-H stretching of the methyl groups appeared at 2953 cm^{-1}. The carbonyl group corresponded to 1642 cm^{-1}; additional peaks at 1573 cm^{-1} and 1505 cm^{-1} corresponded to aromatic C=C stretching while the peak at 1413 cm^{-1} was associated with the bending vibrations of the methylene groups.

In the case of compound **157**, the IR spectrum showed similar trends. The disappearance of the C≡C-H and C≡C stretching signals confirmed the formation of the triazole ring. Aromatic C-H stretching was exhibited at 3139 cm^{-1}, and C-H stretching of the 1,2,3-triazole moiety was observed at 3060 cm^{-1}. The methylene group C-H stretching appeared at 2963 cm^{-1}, while peaks at 1590 cm^{-1} and 1487 cm^{-1} indicated aromatic C=C stretching. Bending vibrations of the -CH$_2$ were also demonstrated with signal at 1447 cm^{-1}.

For compound **158,** the spectrum displayed an aromatic C-H stretching peak at 3047 cm^{-1}, while the methylene C-H stretching was recorded at 2926 cm^{-1}. The other significant peaks were displayed at 1587 cm^{-1} and 1509 cm^{-1}, indicating the presence of aromatic C=C stretching.

4.8.3. Analysis of NMR spectra

At 500 MHz in CDCl$_3$, the ^{1}H NMR spectra of the 4-chlorobenzaldehyde-based 1,2,3-triazole derivatives **(156, 157, 158)** were recorded with tetramethylsilane as the reference, providing clear evidence for the successful conversion of alkyne moieties into 1,2,3-triazole

rings. For all three compounds, the absence of the characteristic triplet at around $\delta = 2.25 - 2.28$ ppm, which would indicate alkynyl protons in the precursors, confirmed the complete transformation into the 1,2,3-triazole structure.

For compound **156,** a singlet at $\delta = 4.60$ ppm was assigned to the methylene protons adjacent to the 1,2,3-triazole moiety and nitrogen atoms, while a singlet at $\delta = 5.48$ ppm was observed for the benzylic protons. Additionally, the aromatic protons displayed a multiplet between $\delta = 7.88 - 6.67$ ppm. In the ^{13}C NMR spectrum, the lack of C≡C carbon signals further confirmed the conversion of the alkyne moiety into the 1,2,3-triazole ring. A signal at $\delta = 39.05$ ppm was attributed to the methylene carbons adjacent to the 1,2,3-triazole ring and nitrogen atoms, while the signal at $\delta = 54.22$ ppm corresponded to the benzylic carbons. The aromatic carbons resonated between $\delta = 151.24 - 112.23$ ppm, with the carbonyl carbon at $\delta = 191.39$ ppm, aligning with expected values for this derivative.

For compound **157,** the methylene protons adjacent to the 1,2,3-triazole ring and nitrogen atoms produced a doublet at $\delta = 4.68$ ppm, while benzylic protons resonated at $\delta = 5.39$ ppm. The aromatic protons appeared as a multiplet between $\delta = 7.70 - 7.12$ ppm. In the ^{13}C NMR spectrum, a signal at $\delta = 45.68$ ppm was attributed to the methylene carbons adjacent to the 1,2,3-triazole moiety and nitrogen atoms, with the benzylic carbons at $\delta = 53.06$ ppm, confirming their presence. The aromatic carbons ranged from $\delta = 147.11 - 111.57$ ppm, with the carbonyl carbon at $\delta = 189.48$ ppm.

In compound **158,** the methylene protons adjacent to the 1,2,3-triazole ring and nitrogen atoms appeared as a singlet at $\delta = 4.22$ ppm, while the benzylic protons resonated at $\delta = 5.46$ ppm. The aromatic protons were observed as a multiplet within $\delta = 7.95 - 6.95$ ppm. The ^{13}C NMR spectrum showed methylene carbons adjacent to the 1,2,3-triazole ring at $\delta = 38.73$ ppm, with benzylic carbons at $\delta = 68.18$ ppm. The aromatic carbons resonated within $\delta = 161.13 - 112.36$ ppm, with the carbonyl carbon at $\delta = 187.78$ ppm, supporting the successful synthesis of the target compound.

4.8.4. Analysis of mass spectra

The successful synthesis of the 1,2,3-triazole **derivatives (156, 157, and 158)** was confirmed through mass spectrometry analysis. The observed mass spectra provided strong evidence for the formation of the desired compounds by revealing prominent [M+H]+ peaks closely aligned with their predicted molecular masses.

For compound **156,** the theoretical molecular mass was calculated as m/z = 599.22. The mass spectrum displayed a strong [M+H]+ peak at m/z = 600.12, indicating the addition of a proton and validating the successful synthesis of the compound. The close match between the predicted and observed values supports the proposed molecular structure.
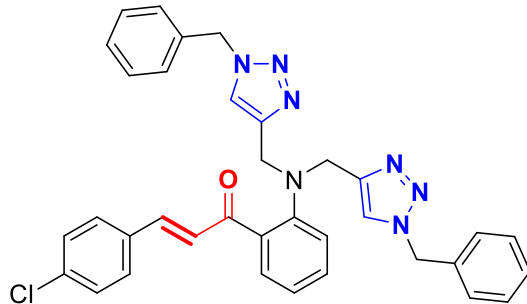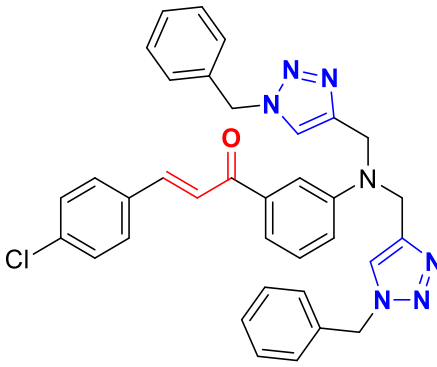
In the case of compound **157**, the expected molecular mass was m/z = 599.21. The mass spectrum confirmed its successful formation by showing a prominent [M+H]+ peak at m/z = 600.22, further corroborating the structural integrity of the synthesized derivative.
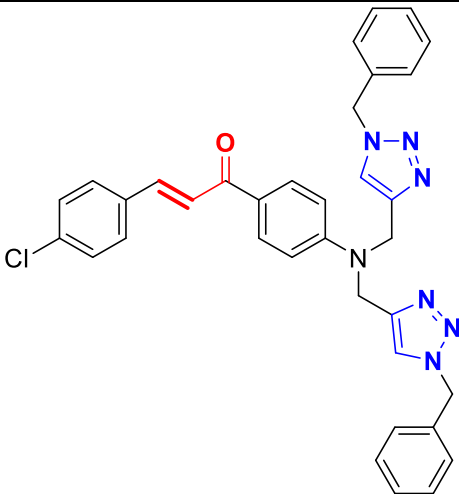
Similarly, for compound **158**, the predicted molecular mass was m/z = 599.22. The mass spectrum revealed a strong [M+H]+ peak at m/z = 600.27, providing definitive evidence of its successful synthesis and alignment with the expected molecular architecture.

The **table 4.4** provides a comparative analysis of the physical and spectroscopic properties of 1,2,3-triazole derivatives **(156, 157, 158)** at the ortho, meta, and para positions. The ortho isomers exhibit solid state due to better molecular packing, meta and para isomers may have disrupted packing due to less favourable interactions resulting in their liquid state at room temperature. The lower carbonyl stretching frequency for ortho isomer (1642 cm^{-1}), is due to its proximity to substituents, is attributable to the presence of the -NH$_2$ group adjacent to the carbonyl group, thereby resulting in reduced double bond character of the carbonyl group through resonance, which can slightly alter the bond strength, experiences steric hindrance and leading to shift in IR frequency. The meta and para isomers have relatively less steric strain, leading to higher frequencies. The ortho isomer exhibits the most downfield shifts for protons (Ph-CH$_2$ (5.48 ppm), likely due to deshielding caused by nearby electronegative groups or steric hindrance. The meta and para isomers experience less electronic interaction, resulting in slightly upfield shifts. The proton of N-C**H$_2$** (4.22 ppm) shoes significant upfield shift on para position due to the more shielding effect. The protons attached to the 1,2,3-triazole ring resonate at higher frequency due to the pronounced shielding effect on the para position as compared to the meta and ortho position. In ^{13}C NMR, the para isomer shows the most significant shifts in the Ph-CH$_2$ region (68.18 ppm), likely due to enhanced electronic delocalization in the para configuration.

Table 4.4: Comparison of 4-chloro-benzaldehyde based ortho, meta and para substituted chalcone based 1,2,3-triazoles

1,2,3-triazole	Structure	Texture	Melting point (°C)	IR value (cm⁻¹)	NMR (ppm)				Mass (m/z) (LCMS)
					¹H		¹³C		
Ortho **156**		Yellow powder	127 – 128	C=O 1642	Ph-C**H₂** N-C**H₂** C-**H** (Tz ring)	5.48 4.60 7.62	Ph-**CH₂** N-**CH₂** **C**-H (Tz ring) **C**=O	54.22 39.05 123.57 191.39	600.12
Meta **157**		Brown viscous oil	N/A	C=O 1671	Ph-C**H₂** N-C**H₂** C-**H** (Tz ring)	5.42 4.68 7.54	Ph-**CH₂** N-**CH₂** **C**-H (Tz ring) **C**=O	53.06 45.68 121.21 189.48	600.22

1,2,3-triazole	Structure	Texture	Melting point (°C)	IR value (cm⁻¹)		NMR (ppm)				Mass (m/z) (LCMS)
						^{1}H		^{13}C		
Para 158		Brown viscous oil	N/A	C=O	1654	Ph-C**H₂** N-C**H₂** C-**H** (Tz ring)	5.46 4.22 7.45	Ph-**C**H₂ N-**C**H₂ **C**-H (Tz ring) **C**=O	68.18 38.73 121.89 187.78	600.27

References

1. P. Yadav, K. Lal, L. Kumar, A. Kumar, A. K. Bhan-Khar, A. Paul and R. Kumar, *Eur. J. Med. Chem.*, 2018, **157**, 62-73.

2. F. Ahmed and H. Xiong, *Dyes Pigm.*, 2021, **185**, 108905.

3. A. Gupta, S. Garg and H. Singh, *Anal. Methods*, 2020, **12**, 5022–5045.

4. S. Kaur, Shalini, B. Ahmad Shiekh, V. Kumar and I. Kaur, *J. Electroanal. Chem.*, 2022, **905**, 115966.

5. I. H. El Azab, H. S. El-Sheshtawy, R. B. Bakr and N. A. A. Elkanzi, *Molecules*, 2021, **26**, 708.

6. S. Bunu, E. Awala and E. Deboh, *Saudi Pharma. J.*, 2020, **06**, 379–389.

7. N. A. A. Elkanzi, H. Hrichi, R. A. Alolayan, W. Derafa, F. M. Zahou and R. B. Bakr, *ACS Omega*, 2022, **7**, 27769–27786.

8. J. J. Bryant and U. H. F. Bunz, *Chem. Asian J.*, 2013, **8**, 1354–1367.

9. M. De Lourdes G. Ferreira, L. C. S. Pinheiro, O. A. Santos-Filho, M. D. S. Peçanha, C. Q. Sacramento, V. Machado, V. F. Ferreira, T. M. L. Souza and N. Boechat, *Med. Chem. Res.*, 2014, **23**, 1501–1511.

10. R.M. Silverstein, F. X. Webster, D. J. Kiemle, and D. L. Bryce, *Spectrometeric Identification of Organic Compounds,* 8th ed., Wiley, Hoboken, 1991.

Chapter IV

Part B

Analysis of photophysical data

In this section of chapter 4, the photophysical properties of the newly synthesized chalcone based 1,4-disubstituted 1,2,3-triazole derivatives are comprehensively discussed. UV-Visible and fluorescence spectroscopic techniques were employed to investigate the photophysical behaviour of these compounds.

4.9. Introduction to electronic spectroscopy

4.9.1. UV-Visible spectroscopy

UV-Visible spectroscopy is an essential analytical technique for examining the interaction of ultraviolet (UV, λ = 200–400 nm) and visible (λ = 400 –700 nm) light with molecules. This method is based upon the absorption of light, which corresponds to the excitation of electrons from lower-energy molecular orbitals (ground states) to higher-energy molecular orbitals (excited states).[1,2] The resulting absorption spectra provide valuable insights into the electronic structure of molecules, making this technique fundamental in ion recognition studies. The process of light absorption in UV-Visible spectroscopy is governed by the Beer-Lambert law, which establishes that absorbance (A) is directly proportional to the concentration (c) of the absorbing species and the path length (l) of the medium through which the light travels. The electronic energy levels probed by UV-Visible spectroscopy primarily involve transitions of π-electrons, non-bonding (n) electrons, and σ-electrons.[3,4] An electron is moved from a lower-energy orbital to a higher-energy orbital by the energy of photon of light that a molecule absorbs. The common electronic transitions observed include:

- $\sigma \rightarrow \sigma^*$: Electrons in σ bonds are excited to their antibonding sigma σ^* orbitals. These transitions require high energy and occur predominantly in alkanes and other molecules with strong covalent bonds, typically absorbing light in the far-UV region (below 200 nm).
- $n \rightarrow \sigma^*$: Non-bonding electrons, often associated with atoms like oxygen, nitrogen, or halogens, are excited to antibonding σ^* orbitals. This transition occurs at slightly lower energies compared to $\sigma \rightarrow \sigma^*$ and is characteristic of saturated compounds containing lone electron pairs.
- $\pi \rightarrow \pi^*$: Electrons in π bonds are promoted to antibonding π^* orbitals. These transitions are commonly observed in unsaturated systems, including alkenes, alkynes, and aromatic compounds, and they typically absorb light within the UV-Visible spectrum.
- $n \rightarrow \pi^*$: Non-bonding electrons are excited to antibonding π^* orbitals. This transition is prevalent in molecules with conjugated systems, carbonyl groups, or other chromophores, often absorbing in the visible or near-UV region.

The absorption spectrum produced during UV-Visible spectroscopy is unique to each molecule, reflecting the specific energy gaps (ΔE) between its electronic states. The energy difference between ground and excited states governs the wavelength of light absorbed, with smaller energy gaps resulting in the absorption of light at longer wavelengths.[5] Conjugation and

resonance significantly influence these energy gaps, as extended conjugated systems and delocalized electrons lower ΔE, shifting absorption from the UV region to the visible range. This shift, often referred to as a bathochromic or red shift, is a hallmark of systems with high degrees of conjugation or aromaticity.[6] Consequently, UV-Visible spectroscopy is particularly effective in studying chromophores and other molecular systems where electronic transitions occur within accessible energy ranges.

In ion sensing, the binding of transition metals with ligands is a crucial interaction that can be effectively studied using UV-Visible spectroscopy. Transition metals, due to their partially filled d-orbitals, exhibit coordination behaviour with organic ligands having donor atoms like O, N, S etc., leading to measurable changes in the electronic structure of the ligand.[7,8] These changes is often manifested as shifts in absorption peaks (hyperchromic/ hypochromic or bathochromic/ hypsochromic shifts) or the appearance of new absorption bands in the UV-Visible spectrum.[9,10]

4.9.2. Fluorescence spectroscopy

Fluorescence spectroscopy, an emission-based technique, is instrumental in the study of molecular luminescence following excitation by UV or visible light. This technique operates on the principle that molecules absorb photons, become excited to higher electronic states, and subsequently emit light as they return to their ground state. The emitted light, a result of a radiative relaxation process, typically occurs at a longer wavelength than the absorbed light due to energy dissipation during relaxation.[11] This phenomenon, characterized by the Stokes shift, is a cornerstone of fluorescence spectroscopy, enabling its application in sensitive and selective detection methodologies, including transition metal ion sensing. The electronic energy levels in fluorescence spectroscopy resemble those of UV-Visible spectroscopy but encompass both absorption and emission processes.[12]

In the context of metal ion sensing, fluorescence spectroscopy provides critical insights into metal-ligand interactions. Transition metals, often possessing unfilled d-orbitals, exhibit unique coordination chemistry with fluorescent ligands, inducing measurable changes in the ligand's photophysical properties.[13] Binding with a metal ion can lead to fluorescence enhancement (turn-on), quenching (turn-off), or shifts in the emission wavelength, driven by mechanisms such as photoinduced electron transfer (PET), energy transfer, or changes in electronic structure.[14] The significance of fluorescence spectroscopy in ion sensing lies in its high sensitivity, enabling the detection of trace amounts of metal ions, and its ability to provide real-time information about metal-ligand interactions. This technique also allows for the elucidation

of complexation mechanisms, making it a powerful tool in designing and optimizing fluorescent chemosensors for transition metals. By exploiting the principles of fluorescence and the unique optical properties of transition metal complexes, researchers can develop robust and selective systems for environmental monitoring, biological assays, and industrial applications.[15,16]

4.10. Chemosensing analysis of 4-benzyloxybenzaldehyde based 1,2,3-triazoles 146, 147, and 148

The ion recognition abilities of the synthesized 1,2,3-triazole derivatives were evaluated using UV-Vis and fluorescence spectroscopy for various metal ions, where the design of the probes was based on the incorporation of a chalcone backbone known for their reliable UV-Vis spectral performance. The chalcone structure was strategically modified by linking it to a benzyl group, which served as the transducer unit, through a 1,2,3-triazole bridge that not only acted as a spacer but also provided receptor sites for electron-deficient metal ions due to the nitrogen atoms bearing lone pairs. Consequently, the synthesized derivatives exhibited a robust aromatic framework that reinforced their molecular stability and enhanced their potential as chemosensing agents.

4.10.1. Ion recognition analysis of 1,2,3-triazole derivative 146

Dimethylsulfoxide (DMSO) was selected as the solvent medium for UV-Vis and fluorescence spectroscopic investigations due to the excellent solubility and favourable spectral properties of probe **146**. After optimizing the solution concentrations for the UV-Vis examinations, it was determined that 0.05 mM concentration would be used to monitor the sensing behavior of probe **146,** owing to the presence of well-defined absorption bands. The maximum absorbance (λ_{max}) of probes **146** was recorded at 340 nm.

The ion sensing characteristics of the probe were next investigated using 1 mM solutions of Ca(II), Mg(II), Ba(II), Cr(III), Mn(II), Fe(II), Fe(III), Co(II), Ni(II), Cu(II), Zn(II), Cd(II), and Pb(II) chlorides, which were dissolved in DMSO. Upon titration of each of the probe solutions with 1 mM metal chloride solutions in separate experiments, it was observed that the absorption spectra showed no significant changes in the absorption maxima or intensity, except for Pb(II) and Cu(II), which exhibited the most pronounced variations in absorbance peaks. The relative chemosensing response of the probes **146** towards these metal ions is depicted in **figure 4.8**, which indicates a higher sensitivity of the probe to Pb(II) and Cu(II) compared to other metal ions of equimolar concentrations.
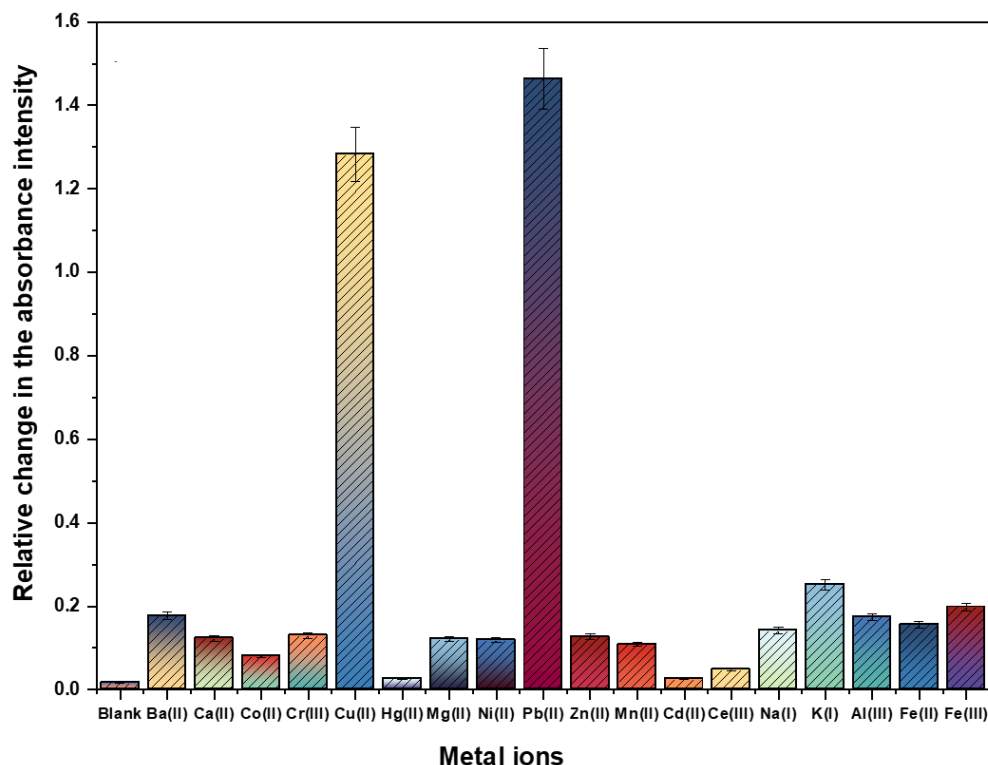
Figure 4.8: Relative chemosensing behaviour of probe **146** with different metal ions in DMSO

4.10.2. Chemosensing response of probe 146 for Pb(II) and Cu(II) via UV-Vis spectroscopy

The interactions of probe **146** with Pb(II) and Cu(II) ions was investigated through UV-Vis spectroscopy, wherein solution of the probe was titrated with 1 mM solutions of these metal ions in separate experiments. With the gradual addition of Pb(II) ions, the absorption peaks at 340 nm and 414 nm, corresponding to n→π* transitions, showed a hypochromic shift, indicating a decrease in absorption intensity. At the same time, the absorption band at 269 nm, which is attributed to π→π* transitions, experienced a significant hyperchromic shift, reflecting an increase in absorption intensity. This led to the formation of an isosbestic point at 293 nm, suggesting a clear interaction between the probe and Pb(II) ions, due to complexation or coordination between the metal and the probe. This phenomenon can be attributed to an increased electronic transition, wherein a greater number of electrons are promoted from the ground state to the excited state. In contrast, the successive addition of Cu(II) ions to the probe solution caused a hypochromic shift in the absorption peak at 414 nm, while the peak at 340 nm remained largely unaffected. Additionally, a new broad and intense peak appeared at 284

nm, accompanied by the formation of an isosbestic point at 337 nm, thereby confirming the effective sensing of these metal ions by the probe **(figure 4.9 (a) and (b))**.

Furthermore, the inset plots in **figure 4.9 (a) and (b)** illustrate the relative changes in maximum absorbance (A_n/A_o) for probe **146** where A_n represents the absorption maxima recorded after successive additions of the metal ions, and A_o corresponds to the initial absorption maxima of the probe. Additionally, the Benesi-Hildebrand (B-H) equation **(A)** was employed to determine the association constant (K_a) for the 1:1 host-guest complexation. The B-H plots for the complexation of probe **146** with Pb(II) as well as Cu(II) are presented in **figure 4.10 (a) and (b).** The K_a values for probe **146** for Pb(II) and Cu(II) ions were 6.18×10^3 M^{-1} and 7.57×10^3. Moreover, the binding ratio of 1:1 (M:L) were established probe based on the Job's plot analysis, as depicted in **figure 4.11 (a) and (b).**

$$\frac{1}{A - Ao} = \frac{1}{A' - Ao} + \frac{1}{Ka(A' - Ao)[M^{n+}]} \qquad (A)$$

Where Ao = initial absorption intensity

A = absorption intensity with a specific concentration of metal ions

A' = final absorption intensity

$[M^{n+}]$ = concentration of metal ions, and

K_a = association constant
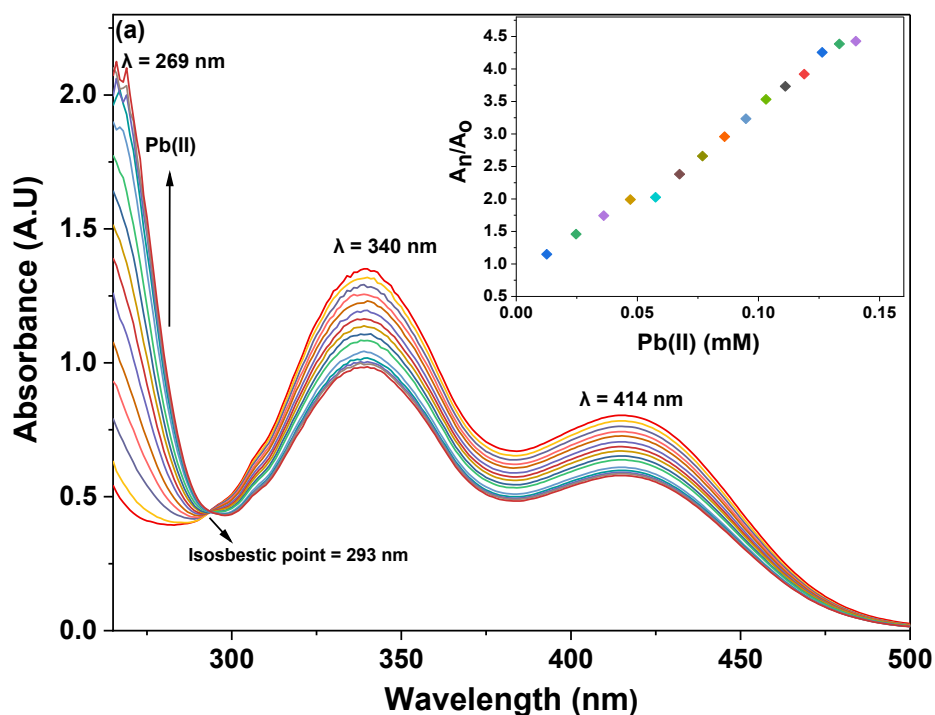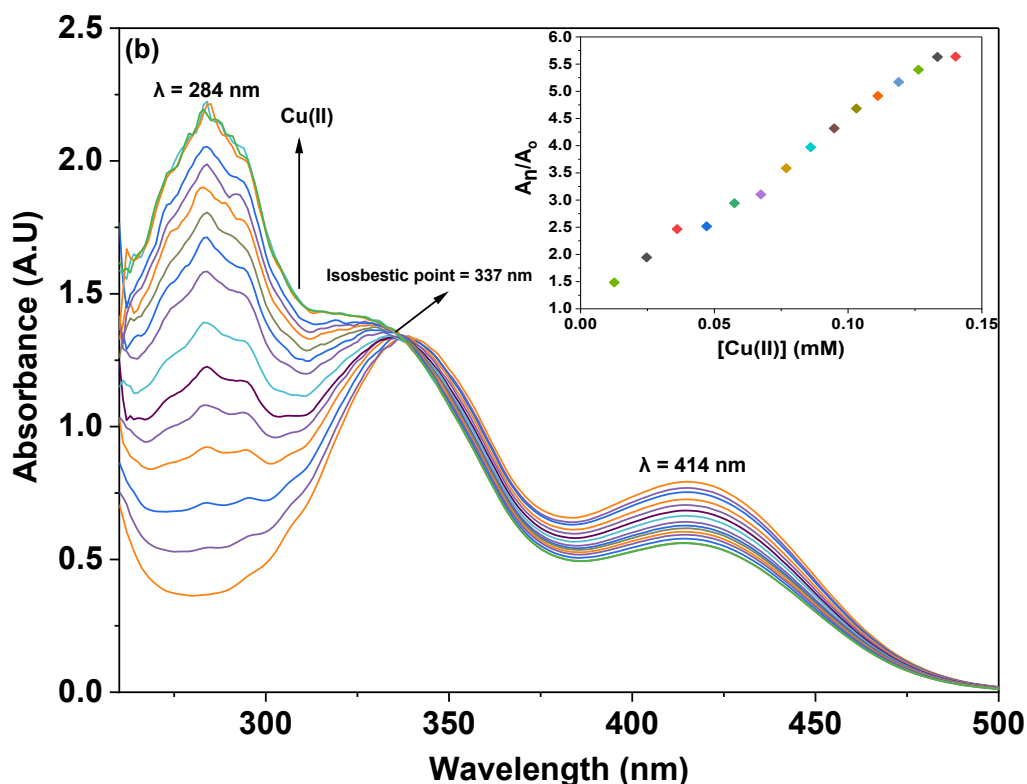
Figure 4.9: The changes in the absorption maxima of probe **146** were recorded during titration with (a) Pb(II) ions and (b) Cu(II) ions in DMSO, highlighting the spectral shifts indicative of metal-probe interactions. The inset graphically represents the variation in the relative absorbance of probe **146** (A_n/A_o) plotted against the concentration of the metal ions (mM),
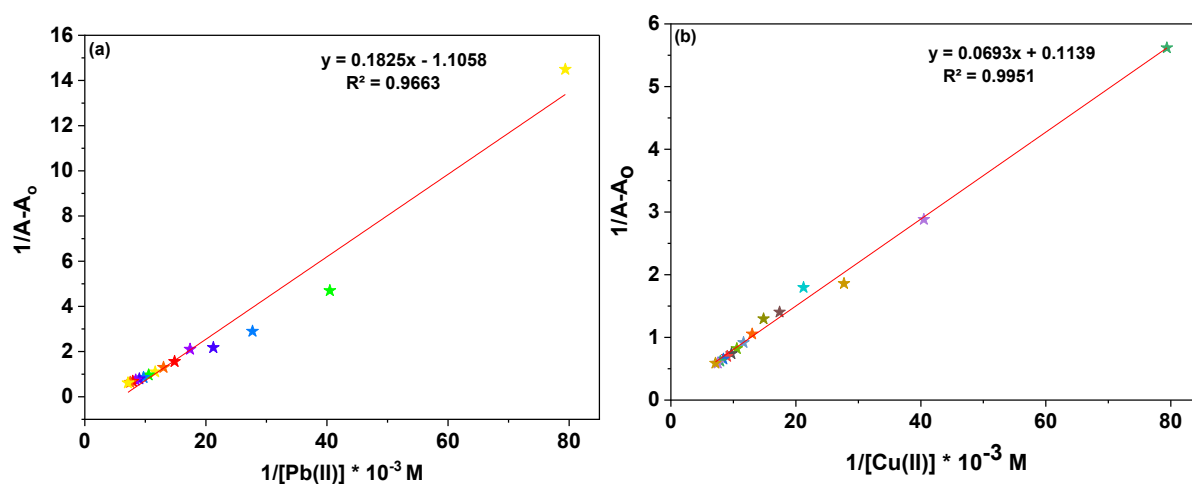
Figure 4.10: B-H plots representing the complexation behaviour of the synthesized probe **146** with (a) Pb(II) ions and (b) Cu(II) ions, demonstrating the interaction profiles and binding affinities between the probe and the respective metal ions
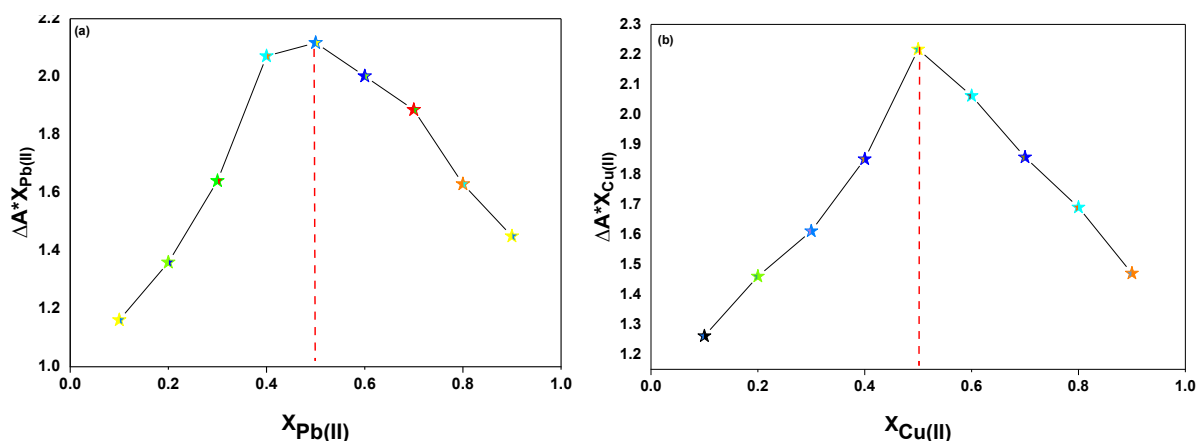
Figure 4.11: Job's plot analysis of probe **146** on interaction with metal ion (a) Pb(II) (b) Cu(II)

4.10.3. Chemosensing response of probe 146 Pb(II) and Cu(II) via fluorescence spectroscopy

The interactions of probe **146** with Pb(II) and Cu(II) ions were also examined through fluorescence spectroscopy, where solution (30 µM) of the probe was titrated with 30 µM solutions of the metal ions in separate experiments. When excited at 350 nm (λ_{ex}), probe 146 displayed a strong emission peak at 438 nm (λ_{em}), along with a smaller shoulder at 412 nm. Separate titrations with Pb(II) and Cu(II) ions, as shown in **figure 4.12 (a) and (b),** revealed an increase in fluorescence emission intensity upon the addition of either metal ion to the solution. This enhancement in fluorescence is likely due to a photoinduced electron transfer (PET) process, which occurs upon metal ion interaction with the probe.[14]
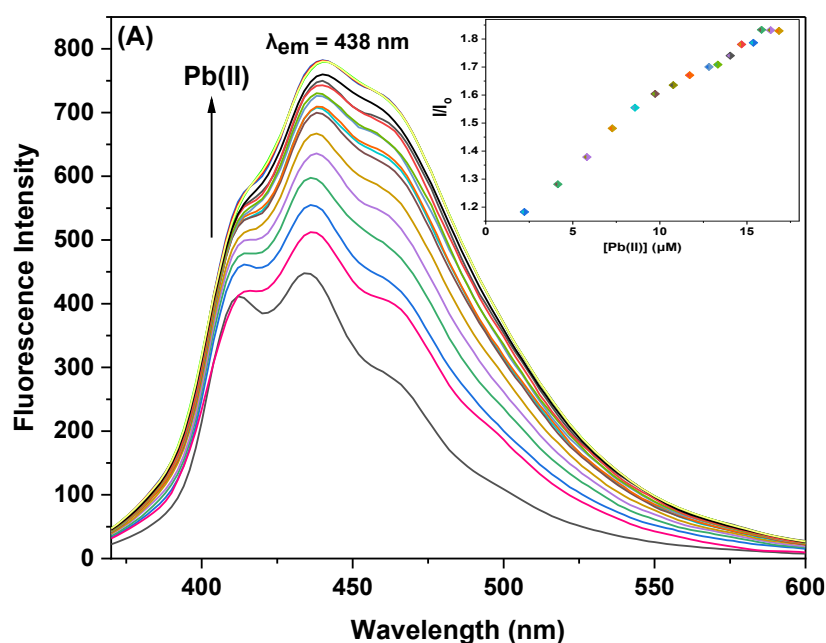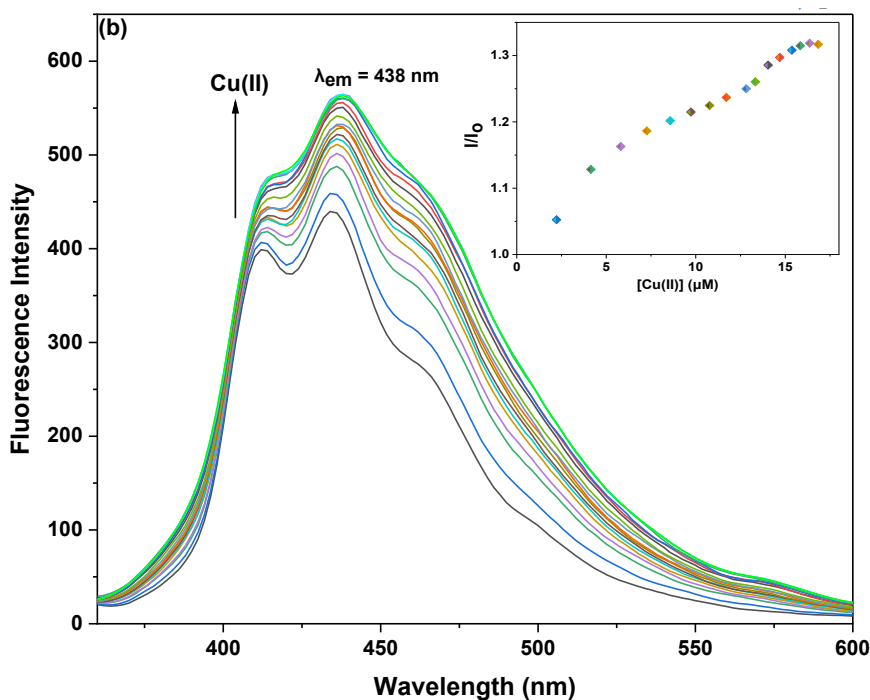
Figure 4.12: Changes in the fluorescence emission of probe **146** were observed with the gradual addition of **(a)** Pb(II) and **(b)** Cu(II) ions in DMSO. The inset shows the relative change in the emission intensity of probe **146** as a function of metal ion concentration (µM).

Furthermore, to evaluate the sensitivity of the probe towards Pb(II) and Cu(II) ions, correlation plots **figure 4.13 (a) and (b)** were used to calculate the limits of detection (LoD) and quantification (LoQ). The LoD values for probe **146** for detecting Pb(II) were determined to be 5.69 µM, while for detecting Cu(II) ions, the LoD values were 6.55 µM. The LoQ values for the probe **146** for the recognition of Pb(II) ions were found to be 18.97 µM, whereas for Cu(II) ions, the values were 21.85 µM. The values for LoD, LoQ, K_a, and stoichiometric ratio for the probe have been compiled and presented in **table 4.5**.
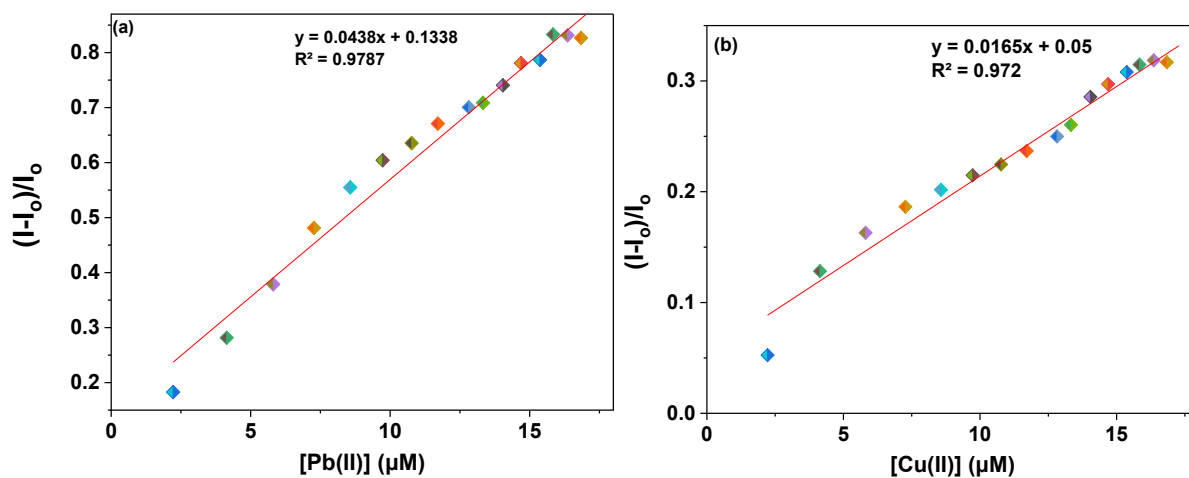
Figure 4.13: Correlation plot of probe **146** illustrating $(I-I_n)/I_o$ vs. (a) [Pb(II)] and (b) [Cu(II)]

4.10.4. Competitive metal ion interaction analysis of probes 146

In addition to the selective ion recognition analysis, the selectivity of probes **146** was also evaluated in the presence of all metal ions simultaneously in an equimolar ratio. In this experiment, a single solution containing an equimolar ratio of various metal ions was prepared and subsequently the titration of each probe solution was done, wherein it was observed that the UV-Vis spectra obtained in each separate titration closely resembled those obtained when Pb(II) was used alone for the aforementioned probes, thereby indicating that each probe selectively sensed Pb(II) even in the presence of other metal ions **figure 4.14** These experiments effectively demonstrated that Pb(II) was selectively detected by all the three probes, confirming that the presence of other metal ions did not interfere with their chemosensing properties.
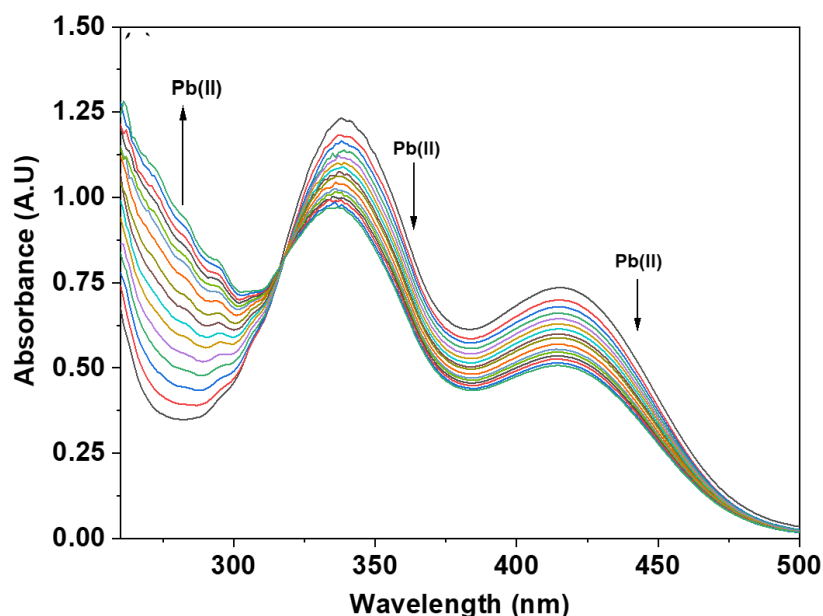
Figure 4.14: UV-Vis spectrum of probe **146**, in DMSO, highlighting the selective detection of Pb(II) among various metal ions at equimolar concentrations

4.10.5. Time dependence analysis of probe-metal ion complexation for 146

The examination of the time-based response of the metal-bound probe **146** provided valuable insights into their sensitivity to metal ions. To investigate the effect of time on the behaviour of these metal-bound probe, absorption spectroscopy was utilized. The results, presented in **figure 4.15 (a) and (b)**, demonstrated that the absorbance of Pb(II)-bound and Cu(II)-bound solution of probe **146** did not exhibit any significant changes, even after prolonged periods of standing. This indicates that probe **146** possessed a high degree of stability and a robust affinity for the metal ions.

133
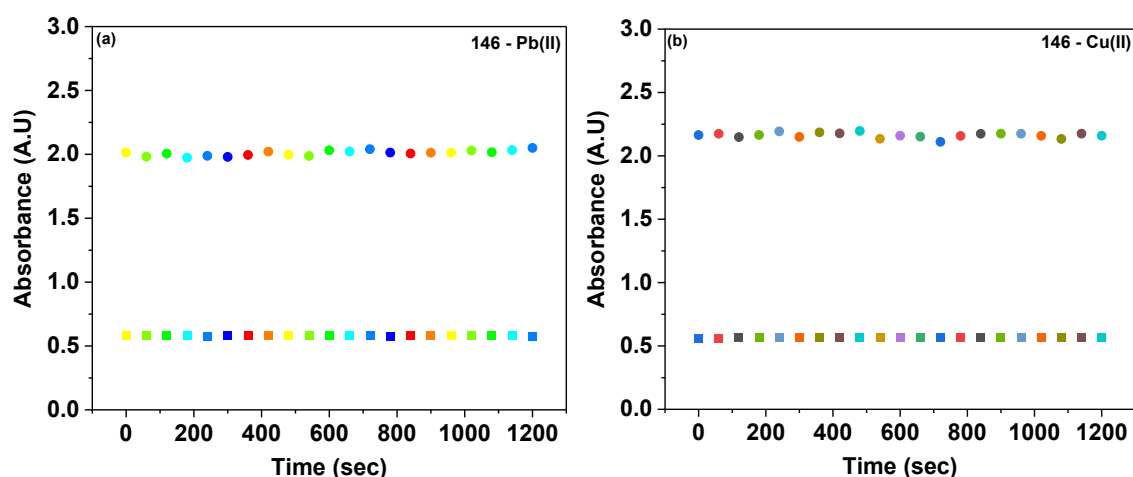
Figure 4.15: The time-dependent absorption spectrum of (a) probe **146**-Pb(II) and (b) probe **146**-Cu(II) complex solution demonstrating a consistent absorbance over time

4.10.6. Temperature dependence analysis of probe-metal ion complexation for 146

The influence of temperature on the binding properties of probe 146 was investigated over a range of temperatures, wherein the absorption spectra of the metal-bound probe solution was recorded at 2 °C intervals from 20 °C to 50 °C for each probe. The results, as depicted in **figure 4.16 (a) and (b)**, revealed that temperature variations had no significant effect on the binding abilities of probe **146**. This indicated that the interactions between the probe and the metal ions were highly stable and robust, even under varying thermal conditions.
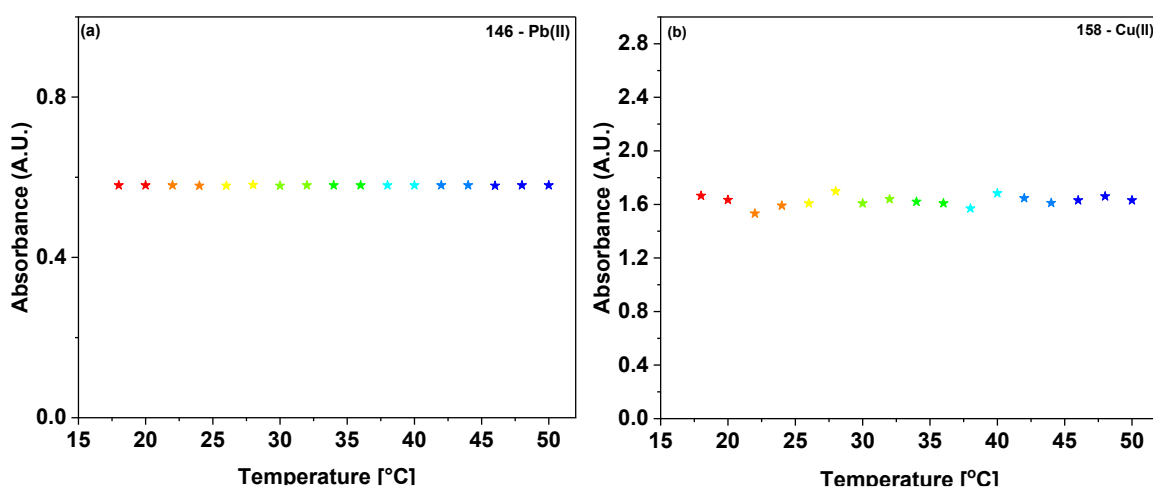
Figure 4.16: Variation in maximum absorbance of (a) probe **146**-Pb(II) complex and (b) probe **146**-Cu(II) complex showing minimal variation in absorbance across a range of temperatures.

4.10.7. Ion recognition analysis of 1,2,3-triazole derivatives 147

After optimizing the solution concentration for UV-Vis analysis, a concentration of 0.05 mM was selected for monitoring the sensing behavior of probe **147**, as it exhibited well-defined absorption bands, wherein, DMSO was chosen as the solvent. The maximum absorbance (λ_{max}) of probe **147** was recorded at 348 nm. These probes' ion detecting capabilities were then examined using 1 mM solutions of Ca(II), Mg(II), Ba(II), Cr(III), Mn(II), Fe(II), Fe(III), Co(II), Ni(II), Cu(II), Zn(II), Cd(II), and Pb(II) dissolved in DMSO. Titration experiments were performed by incrementally adding the metal chloride solutions to the probe solution. For most metal ions, the absorption spectra showed negligible changes in the absorption maxima or intensity. However, significant variations in absorbance peaks were observed specifically for Pb(II) and Cu(II), indicating a pronounced chemosensing response. The relative sensitivity of probe 147 toward these metal ions is illustrated in **figure 4.17**, which highlights its superior selectivity for Pb(II) and Cu(II) compared to other tested ions at equimolar concentrations.
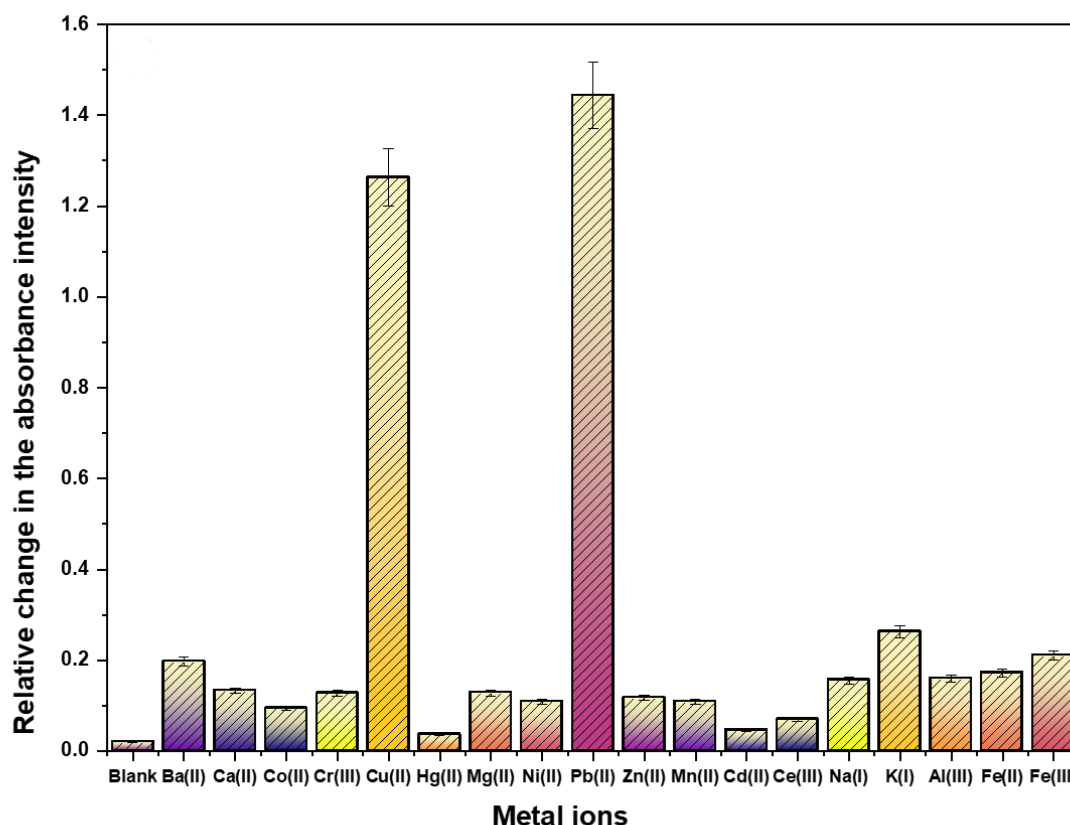
Figure 4.17: Relative chemosensing behaviour of probe **147** with different metal ions in DMSO

4.10.8. Chemosensing response of probe 147 for Pb(II) and Cu(II) via UV-Vis spectroscopy

Using UV-Vis spectroscopy, the interaction of probe **147** with Pb(II) and Cu(II) ions was investigated. Wherein, 1 mM solutions of each metal ion were gradually added to separate probe solutions. When Pb(II) was introduced, the absorption peak at 348 nm experienced a reduction in intensity (hypochromic shift), while a smaller shoulder at 264 nm showed an increase in intensity (hyperchromic shift), leading to the appearance of an isosbestic point at 283 nm, as illustrated in **figures 4.18 (a) and (b).**
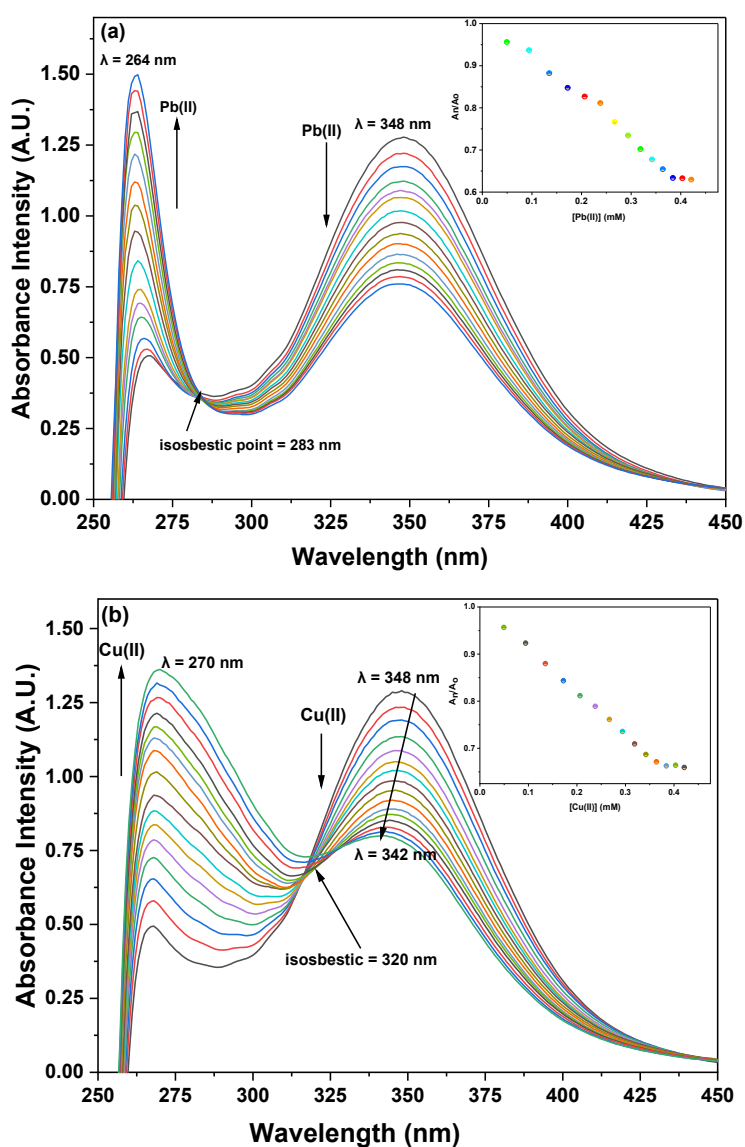
Figure 4.18: Changes in the absorption maxima of probe **147** were observed during titration with (a) Pb(II) and (b) Cu(II) ions in DMSO. The inset shows the relative change in absorbance of probe **147** (An/Ao) as a function of the metal ion concentration (mM).

In the case of Cu(II), the absorption peak shifted approximately 6 nm toward shorter wavelengths, from 348 nm to 342 nm, likely due to the metal-to-ligand charge transfer (MLCT)[17,18] interaction. This shift was accompanied by a decrease in absorption intensity and a notable increase in intensity at 270 nm, suggesting a higher probability of electronic transitions. As a result, peak broadening occurred, and an isosbestic point appeared at 320 nm. The inset plots in **figures 4.18 (a) and (b)** illustrate the relative changes in maximum absorbance (A_n/A_o) for probe **147**, where A_n represents the absorbance after successive additions of the metal ions, and A_o corresponds to the initial absorbance of the probe. The Benesi-Hildebrand plots for probe **147** with Pb(II) and Cu(II) are presented in **figures 4.19 (a) and (b),** yielding K_a values of 2.18×10^3 M^{-1} and 2.35×10^3 M^{-1}, respectively. Additionally, the 1:1 binding stoichiometry was confirmed through Job's plot analysis, as depicted in **figures 4.20 (a) and (b).**
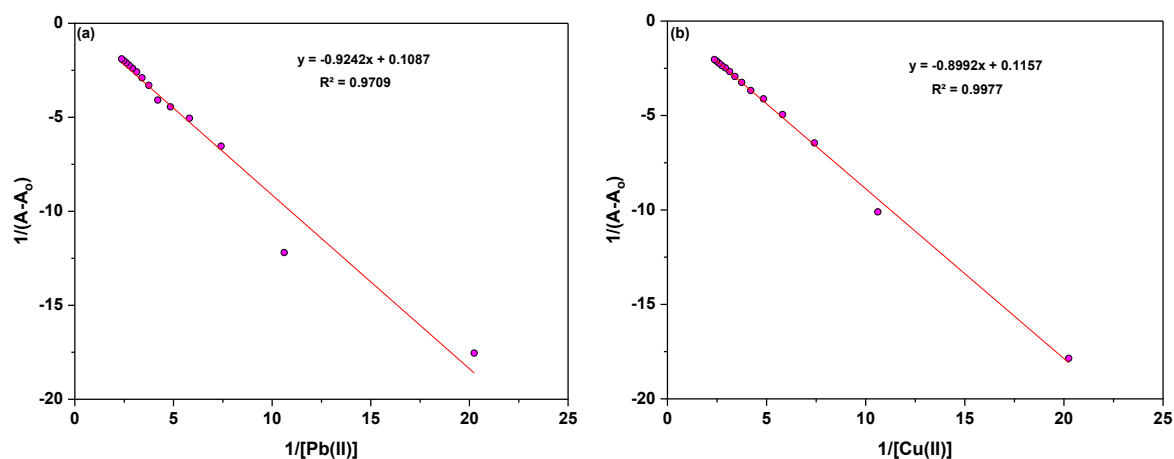
Figure 4.19: B-H plot for the complexation of probe **147** with (a) Pb(II) and (b) Cu(II)
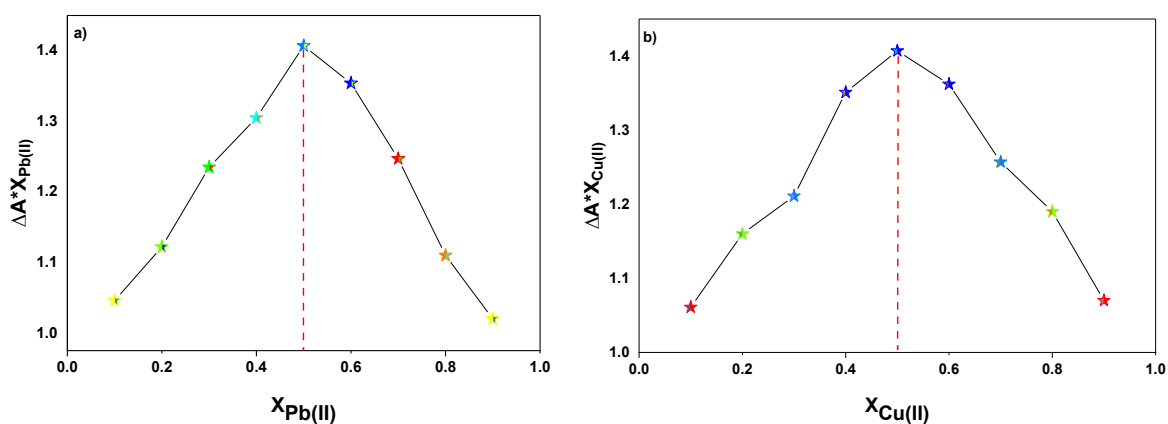
Figure 4.20: Job's plot analysis of probe **147** on interaction with metal ion (a) Pb(II) (b) Cu(II)

4.10.9. Chemosensing response of probe 147 for Pb(II) and Cu(II) via fluorescence spectroscopy

The interactions of probe **147** with Pb(II) and Cu(II) ions were further investigated using fluorescence spectroscopy. Solutions of the probe were titrated with 30 µM solutions of the metal ions in separate experiments. Upon excitation at 340 nm (λ_{ex}), probe **147** displayed a distinct fluorescence emission peak at 437 nm (λ_{em}) with a minor shoulder peak at 413 nm. The fluorescence intensity of probe 147 showed a significant enhancement upon the addition of Pb(II) and Cu(II) ions **figures 4.21 (a) and (b)**, can be attributed to the PET phenomenon. This increase in emission intensity indicates a strong interaction between the probe and the metal ions, likely due to coordination or complexation.

To assess the sensitivity of probe **147** toward Pb(II) and Cu(II) ions, correlation plots **(figure 4.22 (a) and (b))** were utilized to calculate the limits of detection (LoD) and quantification (LoQ). The LoD for detecting Pb(II) was determined to be 3.64 µM, while for Cu(II) detection, it was 1.37 µM. Similarly, the LoQ values for Pb(II) and Cu(II) detection were calculated to be 12.15 µM and 4.58 µM, respectively. A comprehensive summary of the LoD, LoQ, association constant (K_a), and stoichiometric ratio for all the probes is presented in **Table 4.5.**
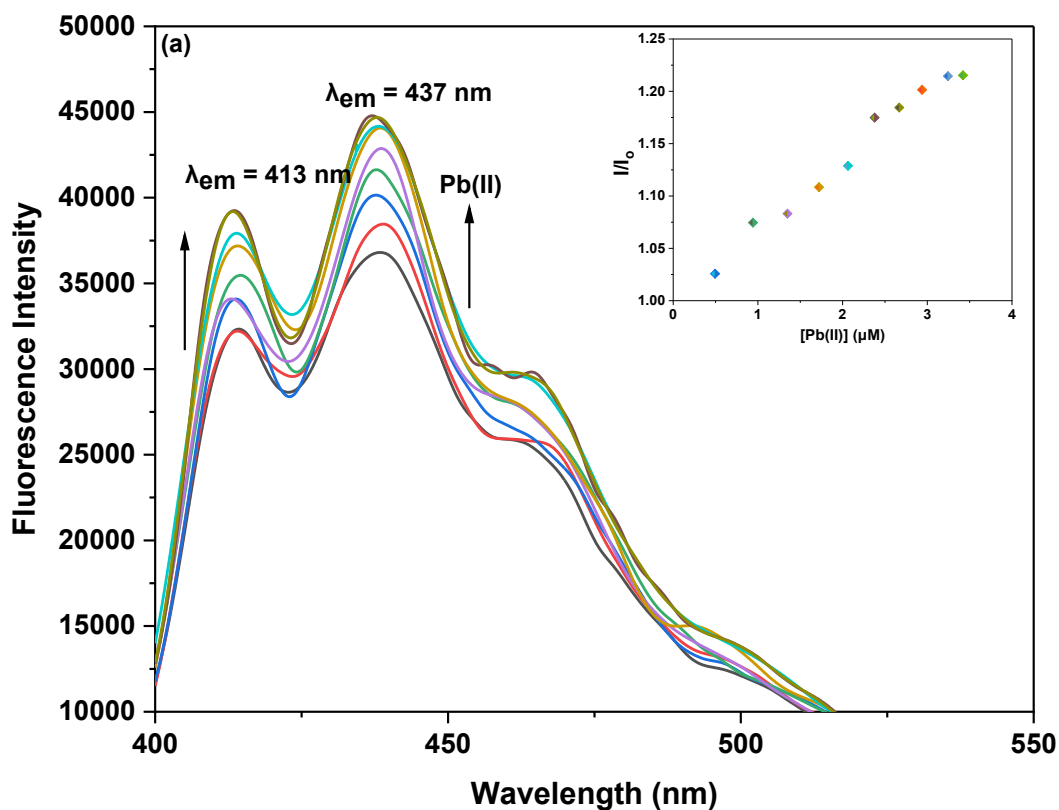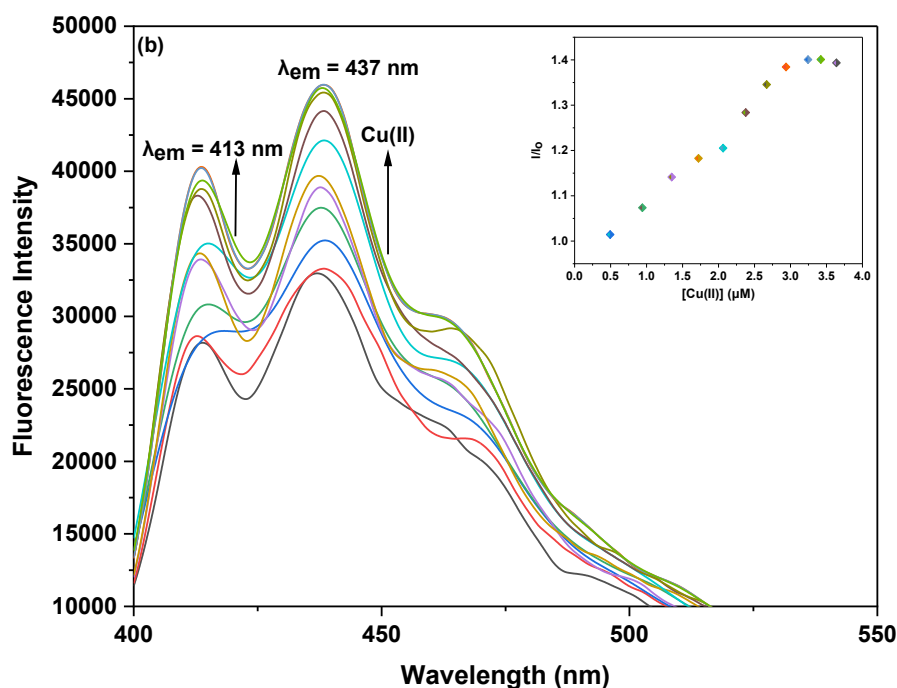
Figure 4.21: Variations in the emission of probe **147** upon the gradual addition of (a) Pb(II) and (b) Cu(II) ions in DMSO; the inset illustrates the relative change in emission of probe **147** versus metal ion concentration (μM)
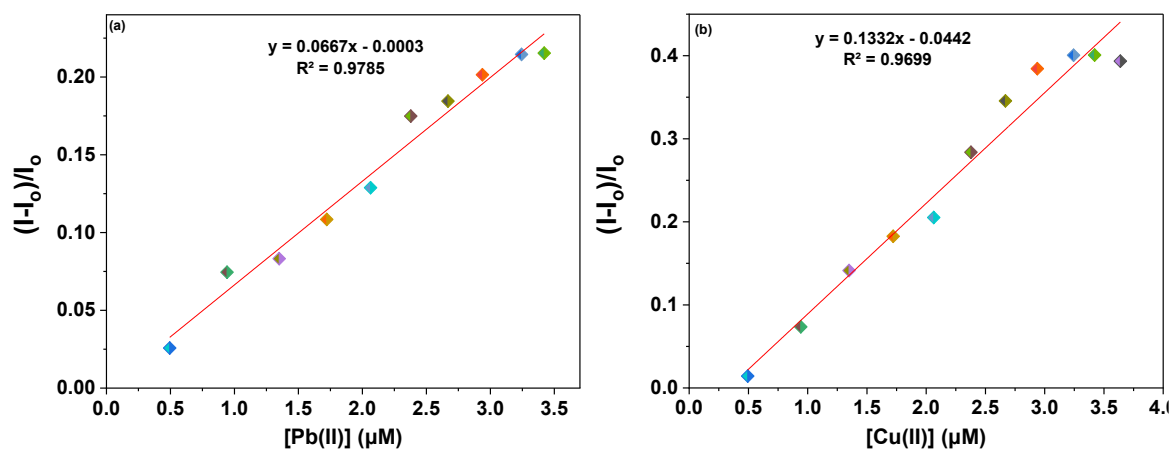
Figure 4.22: Correlation plot of probe **147** illustrating $(I-I_n)/I_o$ vs. (a) [Pb(II)] and (b) [Cu(II)]

### 4.10.10. Competitive metal ion interaction analysis of probes 147

To further investigate the selective ion recognition capabilities, the selectivity of probe **147** was assessed in the presence of all metal ions simultaneously at equimolar concentrations. A solution containing equimolar ratios of various metal ions was prepared, and the probe solution was titrated with this mixed metal ion solution. The resulting UV-Vis spectra closely resembled those obtained when Pb(II) was tested individually with the probe. This observation, depicted in **figure 4.23**, indicates that probe **147** selectively detects Pb(II) even in the presence

of other competing metal ions. These experiments conclusively demonstrated the high selectivity of probe **147** for Pb(II), confirming that the presence of other metal ions does not interfere with its chemosensing properties. This selective recognition highlights the potential of probe **147** as an effective and reliable sensor for Pb(II) in complex mixtures.
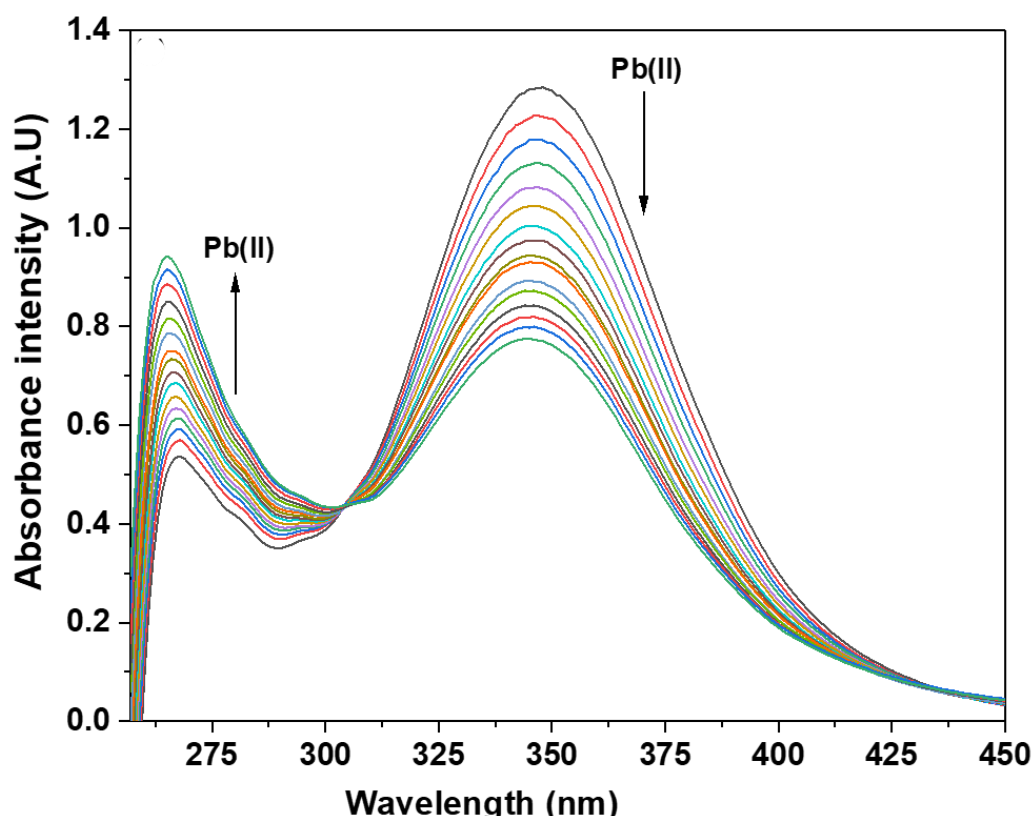
Figure 4.23: UV-Vis spectrum of probe **146**, in DMSO, highlighting the selective detection of Pb(II) among various metal ions at equimolar concentrations

4.10.11. Time dependence analysis of probe-metal ion complexation for 147

The time-dependent response of the metal-bound probe **147** was thoroughly investigated to evaluate its stability and sensitivity toward metal ions. Absorption spectroscopy was employed as the analytical technique to monitor the behavior of the metal-bound complexes over prolonged durations. The results, as depicted in **figure 4.24 (a) and (b),** demonstrated that the absorbance of Pb(II)-bound and Cu(II)-bound solutions of probe 147 remained steady, with no significant variations observed even after extended periods of standing. These findings emphasize the remarkable stability of probe **147** in its metal-bound state and its robust and enduring affinity for Pb(II) and Cu(II) ions. This exceptional stability underscores the reliability of probe **147** for long-term chemosensing applications, making it a promising candidate for the development of durable and efficient sensing systems.
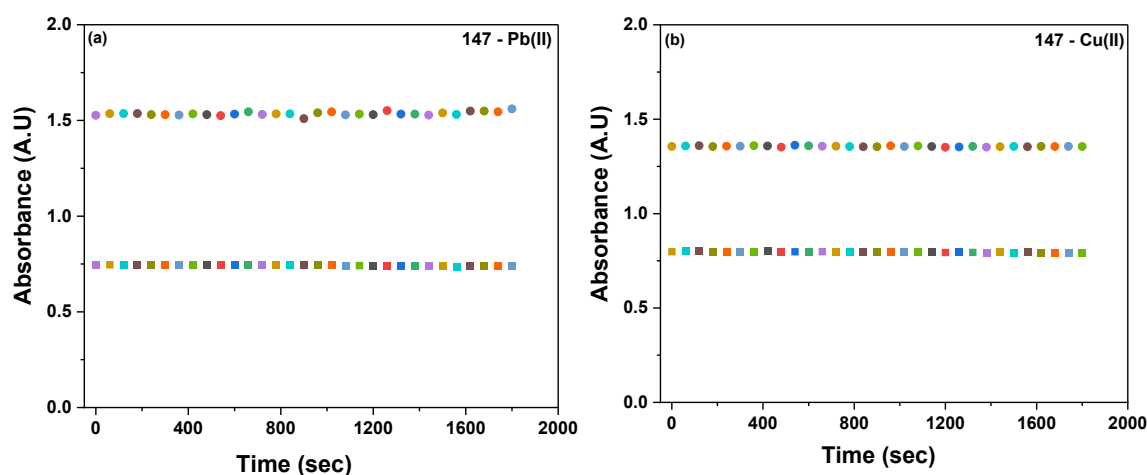
Figure 4.24: The time-dependent absorption spectrum of (a) probe **147**-Pb(II) and (b) probe **147**-Cu(II) complex solution demonstrating a consistent absorbance over time

4.10.12. Temperature dependence analysis of probe-metal ion complexation for 147

The influence of temperature on the binding capabilities of probe **147** was evaluated by recording the absorption spectra of its metal-bound solutions across a temperature range from 20 °C to 50 °C, with measurements taken at 2 °C intervals. The results, presented in **figure 4.25 (a) and (b),** demonstrated that temperature variations had no discernible impact on the binding behavior of probe **147.** These findings indicate that the interactions between the probe and the metal ions are highly stable and resilient, maintaining robust binding affinity even under varying thermal conditions. This stability underscores their potential for applications in diverse environmental and operational settings.
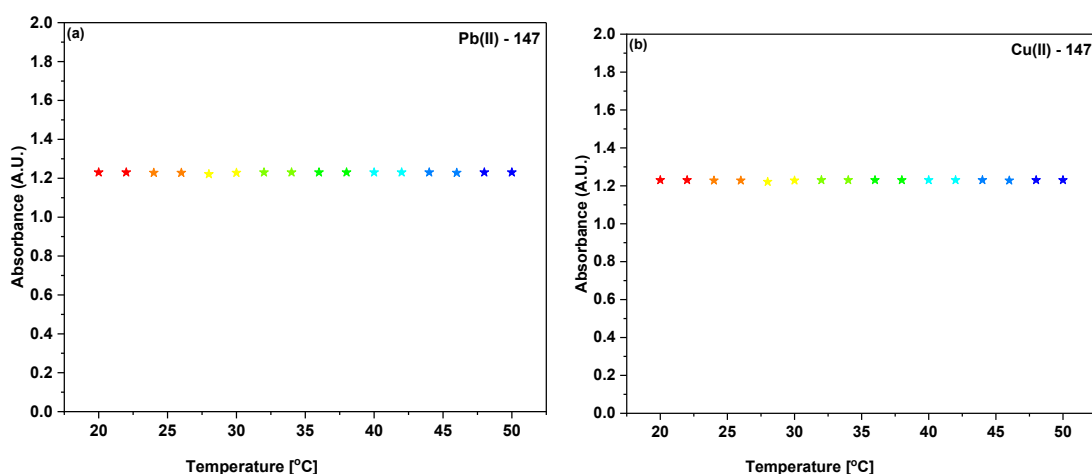
Figure 4.25: Variation in maximum absorbance of (a) probe **147**-Pb(II) complex and (b) probe **147**-Cu(II) complex showing minimal variation in absorbance across a range of temperatures.

4.10.13. Ion recognition analysis of 1,2,3-triazole derivatives 148

Dimethyl sulfoxide (DMSO) was chosen as the solvent medium for UV-Vis and fluorescence spectroscopic studies of probe **148** due to its excellent solubility and compatible spectral characteristics. To optimize the experimental conditions for UV-Vis analysis, a concentration of 0.03 mM was selected for probe **148**, as this concentration provided distinct and well-defined absorption bands. The maximum absorbance (λ_{max}) for probe **148** was observed at 368 nm. Subsequently, the ion sensing properties of the probe was analyzed using 1 mM solutions of Ca(II), Mg(II), Ba(II), Cr(III), Mn(II), Fe(II), Fe(III), Co(II), Ni(II), Cu(II), Zn(II), Cd(II), and Pb(II) chlorides dissolved in DMSO. After titrating the probe solution with these metal ion solutions individually, the absorption spectra showed minimal changes in both maxima and intensity for most metal ions. However, pronounced alterations in the absorbance peaks was observed specifically with Pb(II) and Cu(II). The comparative chemosensing response of probe **148** toward these metal ions, shown in **figure 4.26,** demonstrates its significantly higher sensitivity to Pb(II) and Cu(II) compared to other tested ions at the same concentration.
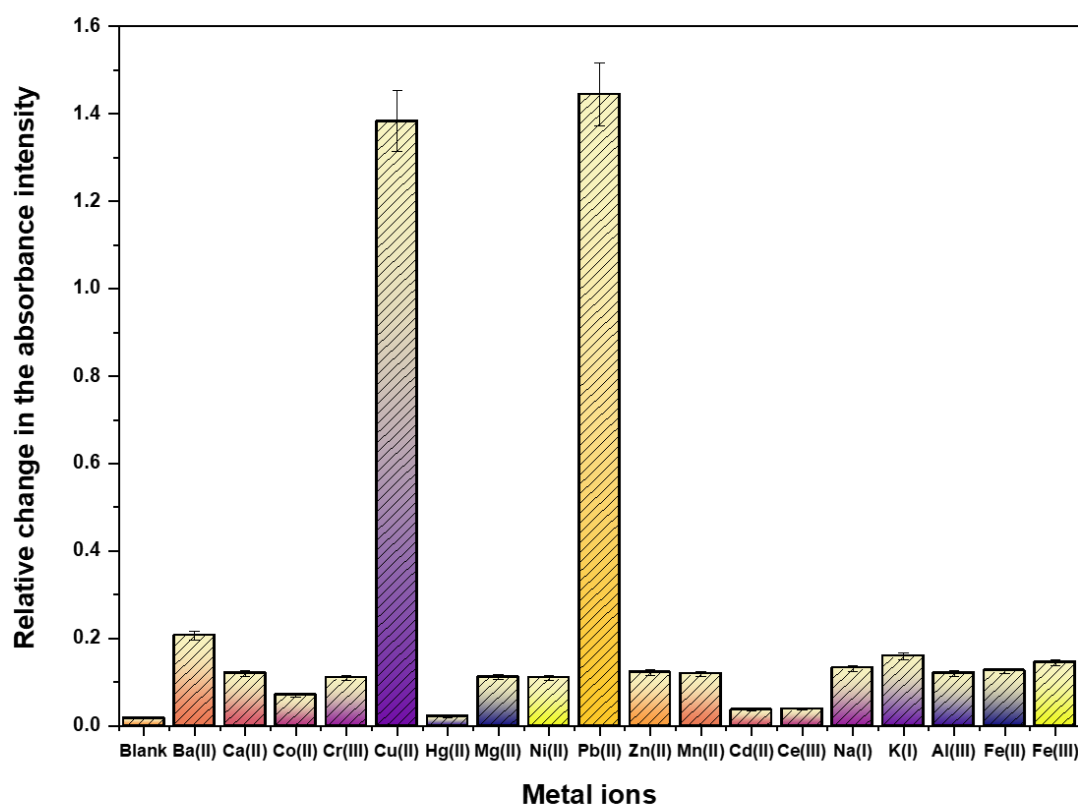
Figure 4.26: Relative change in the absorbance intensity of the probe **148** on addition of different metal ions

4.10.14. Chemosensing response of probe 148 for Pb(II) and Cu(II) via UV-Vis spectroscopy

The interactions of probe **148** with Pb(II) and Cu(II) ions were investigated through UV-Vis spectroscopy, wherein solutions of the probe was titrated with 1 mM solutions of Pb(II) and Cu(II) ions in separate experiments. When Pb(II) ions were gradually added to the probe **148** solution, the peak at 368 nm underwent a hypochromic shift, attributed to n→π* transitions. At the same time, a pronounced hyperchromic shift was seen at 268 nm, linked to an increased probability of electronic transitions related to π→π* transitions. This resulted in a ratiometric change, with the formation of an isosbestic point at 298 nm.
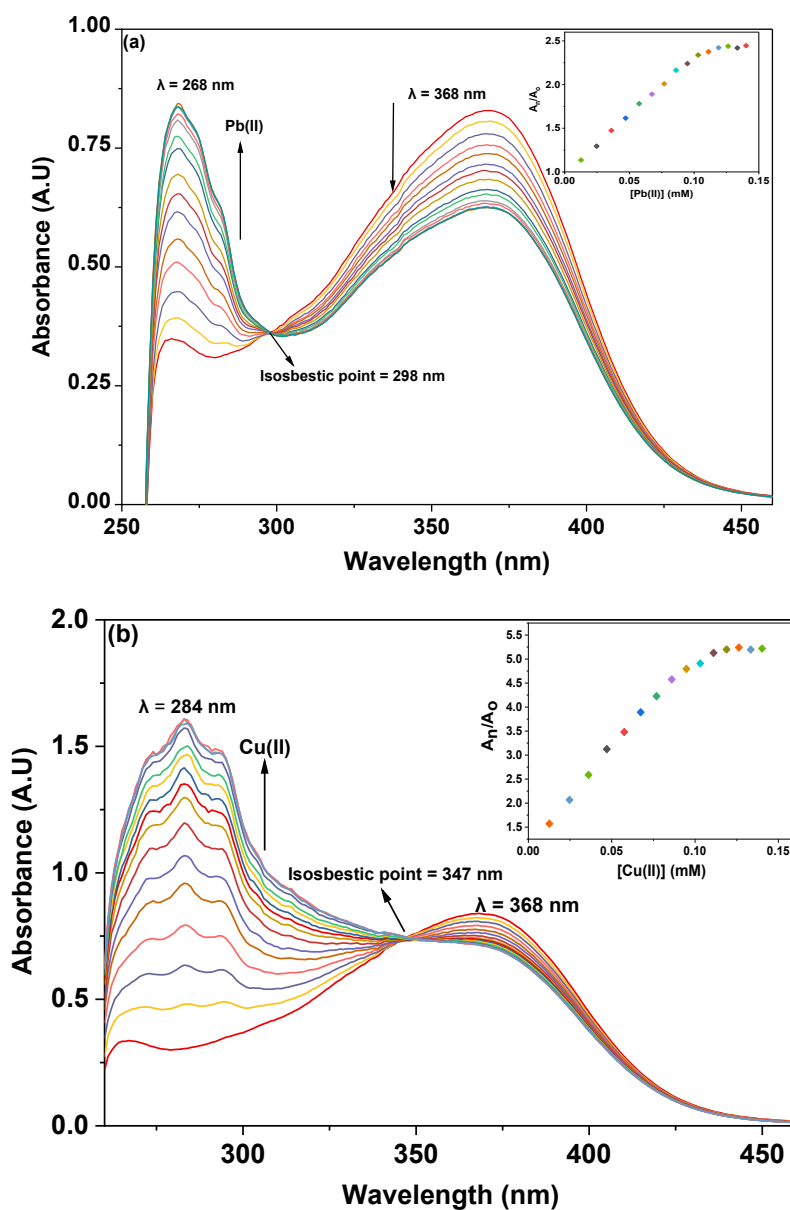
Figure 4.27: Shifts in the absorption maxima of probe **148** with (a) Pb(II) and (b) Cu(II) in; the inset exhibits the relative absorbance change of probe **148**

A hypochromic shift was observed in the 368 nm peak upon titration with Cu(II) ions, while the peak initially observed at 284 nm shifted significantly, both intensifying in absorption (hyperchromic shift) and shifting 16 nm to shorter wavelengths, forming a new peak at 284 nm. The appearance of an isosbestic point at 347 nm further confirmed the selective sensing of Cu(II) ions by probe **148,** which displayed a ratiometric response and a blue shift, as shown in **figure 4.27 (a) and (b).**
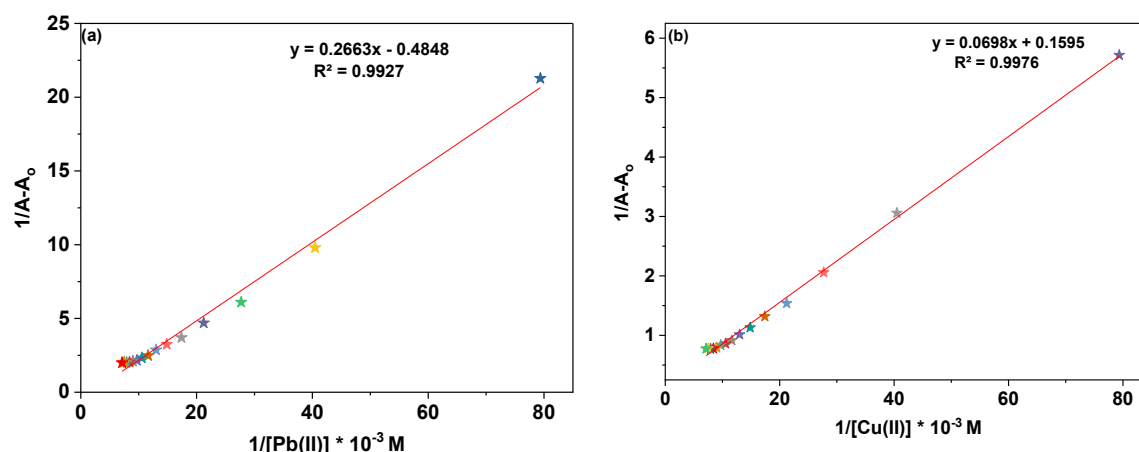
Figure 4.28: B-H plot for the complexation of probe **148** with (a) Pb(II) and (b) Cu(II)

Furthermore, the inset plots in **figure 4.27 (a) and (b)** illustrate the relative changes in maximum absorbance (A_n/A_o) for probe **148,** where A_n represents the absorption maxima recorded after successive additions of the metal ions, and A_o corresponds to the initial absorption maxima of each probe. The corresponding Benesi-Hildebrand plots for the complexation of probe **148** with Pb(II) as well as Cu(II) are presented in **figure 4.28 (a) and (b)**. The K_a values for probe **148** for Pb(II) and Cu(II) ions were 8.54×10^3 M^{-1}, 9.37×10^3 M^{-1}, respectively. Moreover, the binding ratio of 1:1 (M:L) were established for the probe based on the Job's plot analysis, as depicted in **figure 4.29 (a) and (b).**
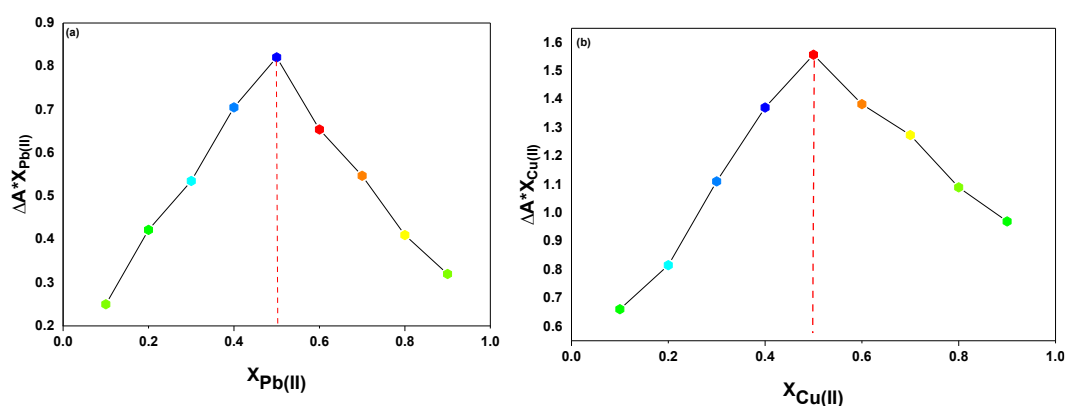
Figure 4.29: Job's plot analysis of probe **148** on interaction with metal ion (a) Pb(II) (b) Cu(II)

4.10.15. Chemosensing response of probe 148 for Pb(II) and Cu(II) via fluorescence spectroscopy

The interaction of probe **148** with Pb(II) and Cu(II) ions was further explored using fluorescence spectroscopy. In separate experiments, solutions of probe 148 were titrated with 30 μM solutions of each metal ion, and the resulting fluorescence emission was measured. When excited at 370 nm (λ_{ex}), probe **148** displayed a strong emission peak at 436 nm (λ_{em}), accompanied by a smaller shoulder at 412 nm, suggesting a characteristic fluorescence profile of the probe in the absence of metal ions. Upon incremental addition of Cu(II) and Pb(II) ions, the fluorescence intensity of probe 148 increased significantly, indicating a strong interaction between the probe and the metal ions. The metal ion binding likely alters the electronic environment of the probe, leading to enhanced fluorescence emission. This behaviour is depicted in **figure 4.30 (a) and (b),** where the increase in fluorescence intensity is shown as a function of metal ion concentration. Furthermore, to evaluate the sensitivity of the probes towards Pb(II) and Cu(II) ions, correlation plots **figure 4.31 (a) and (b),** were used to calculate the limits of detection (LoD) and quantification (LoQ). The LoD values for probe **148** for detecting Pb(II) were determined to be 5.06 μM, while for detecting Cu(II) ions, the LoD values were 7.52 μM. The LoQ values for the probe **148** for the recognition of Pb(II) ions were found to be 16.89 μM, whereas for Cu(II) ions, the values were 25.08 μM. The values for LoD, LoQ, K_a, and stoichiometric ratio for all the probes have been compiled and presented in **table 4.5**.
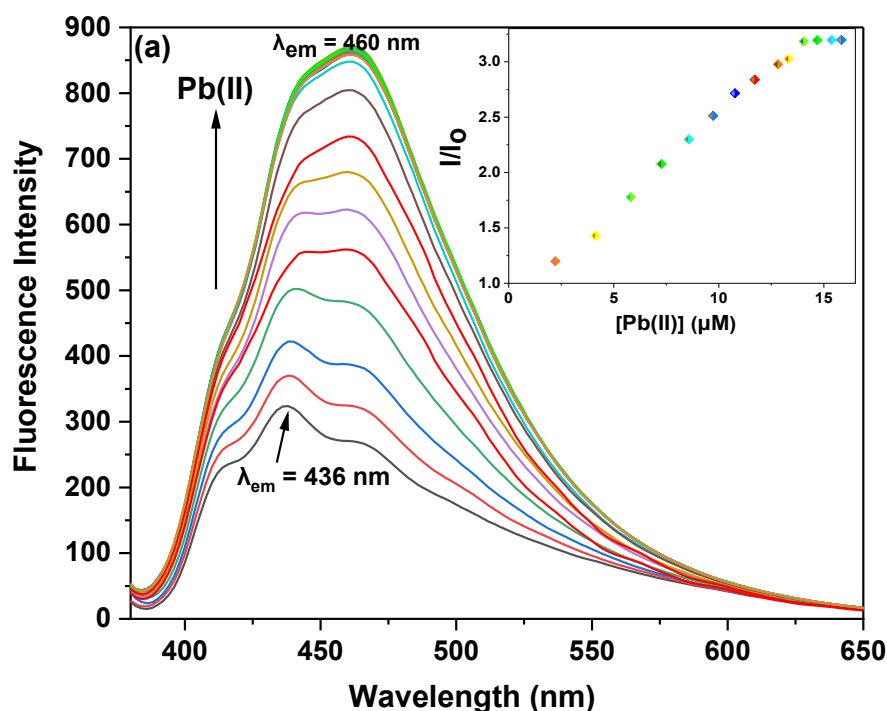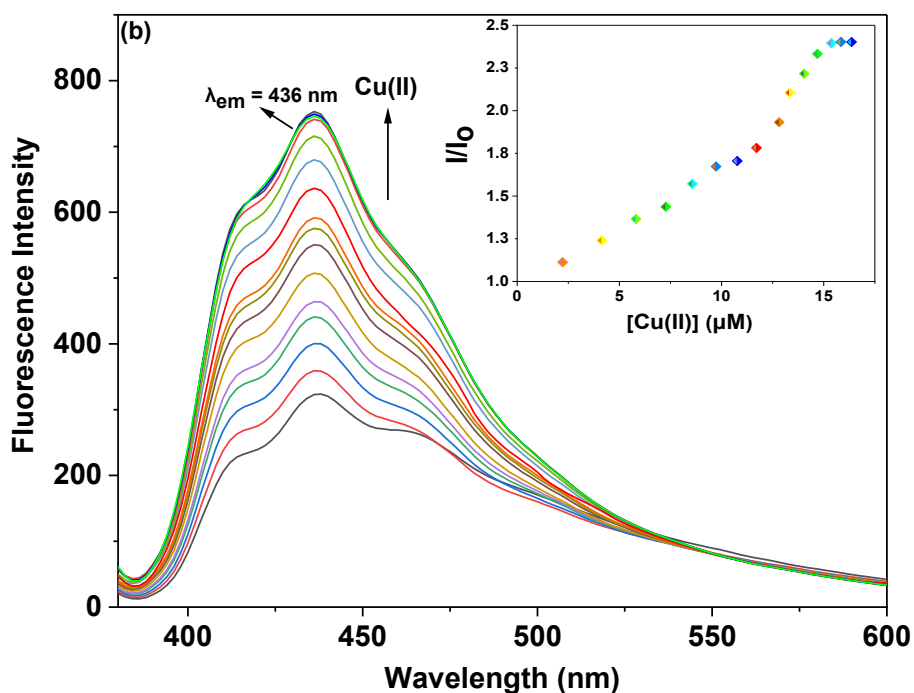
Figure 4.30: Variations in the fluorescence emission of probe **148** upon the incremental addition of (a) Pb(II) and (b) Cu(II) ions in DMSO; the inset illustrates the relative change in emission of probe **148** versus metal ion concentration (μM)
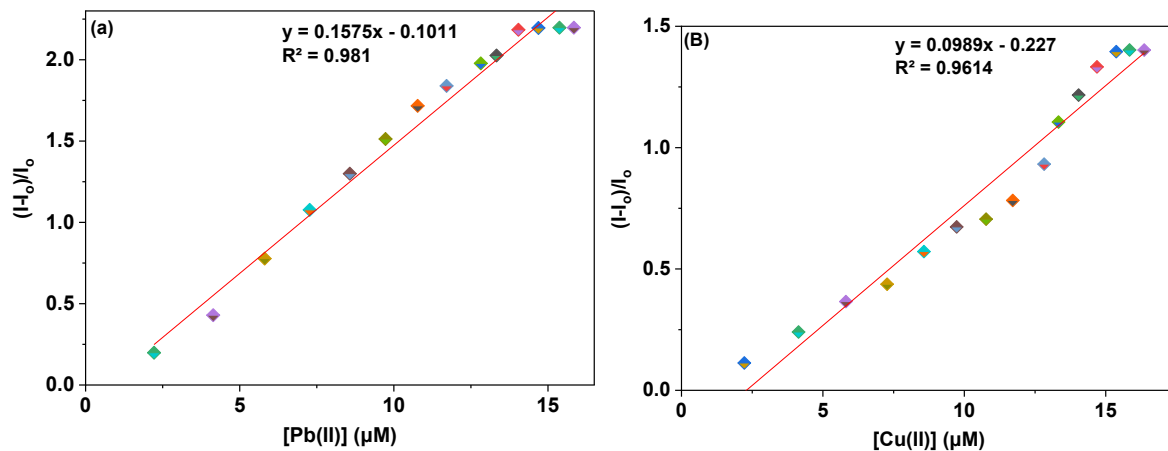
Figure 4.31: Correlation plot of probe **148** illustrating $(I-I_n)/I_o$ vs. (a) [Pb(II)] and (b) [Cu(II)]

4.10.16. Competitive metal ion interaction analysis of probe 148

In addition to the selective ion recognition analysis, the selectivity of probe **148** was also evaluated in the presence of all metal ions simultaneously in an equimolar ratio. In this experiment, a single solution containing an equimolar ratio of various metal ions was prepared and subsequently the titration of probe solution was done, wherein it was observed that the UV-

Visible spectra obtained in each separate titration closely resembled those obtained when Pb(II) was used alone for the probe, thereby indicating that probe selectively sensed Pb(II) even in the presence of other metal ions (**figure 4.32)**, confirming that the presence of other metal ions did not interfere with their chemosensing properties.
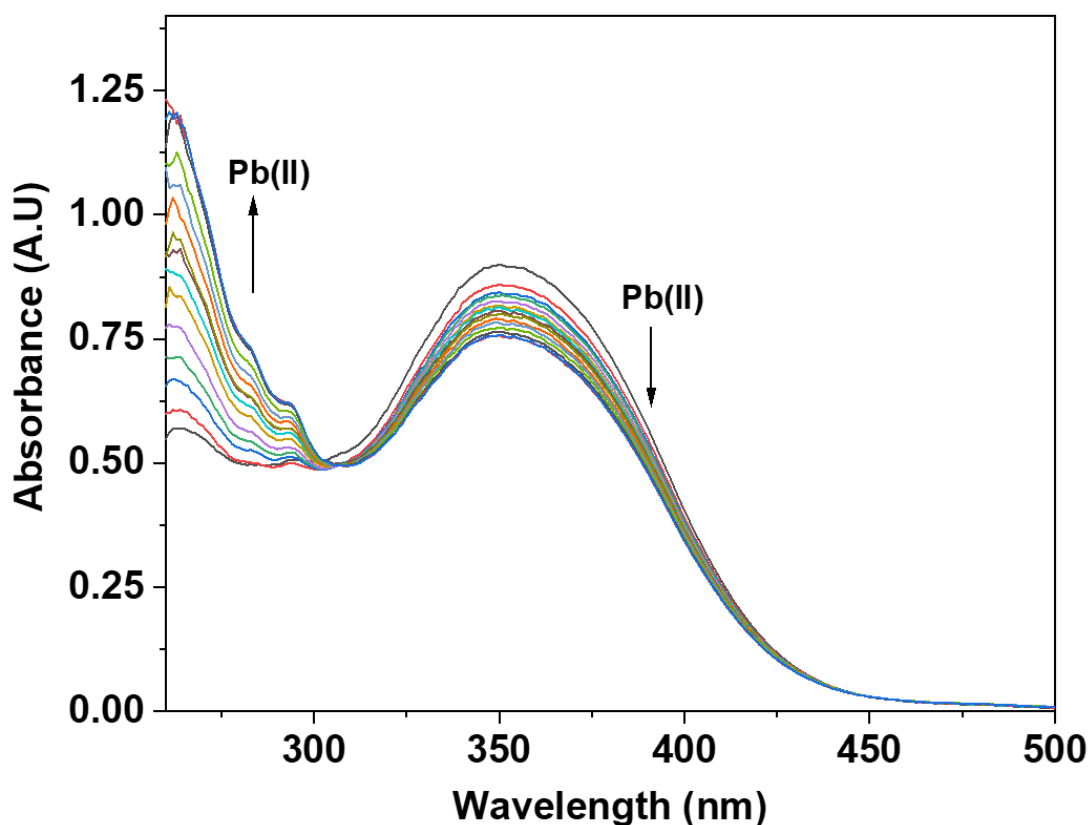
Figure 4.32: UV-Vis spectrum of probe **148** in DMSO, highlighting the selective detection of Pb(II) among various metal ions at equimolar concentrations

4.10.17. Time dependence analysis of probe-metal ion complexation for 148

The time-dependent response of the metal-bound probe **148** was thoroughly examined to gain deeper insights into its sensitivity, stability, For this purpose, absorption spectroscopy was utilized to assess the influence of prolonged standing time on the behavior of the probe in its metal-bound state. The results, depicted in **figure 4.33 (a) and (b),** clearly demonstrate that the absorbance of both Pb(II)-bound and Cu(II)-bound solutions of probe **148** remained remarkably stable over extended periods, showing no notable variations. These findings suggest that probe 148 exhibits a high degree of stability when complexed with these metal ions, along with a robust and enduring affinity for them.
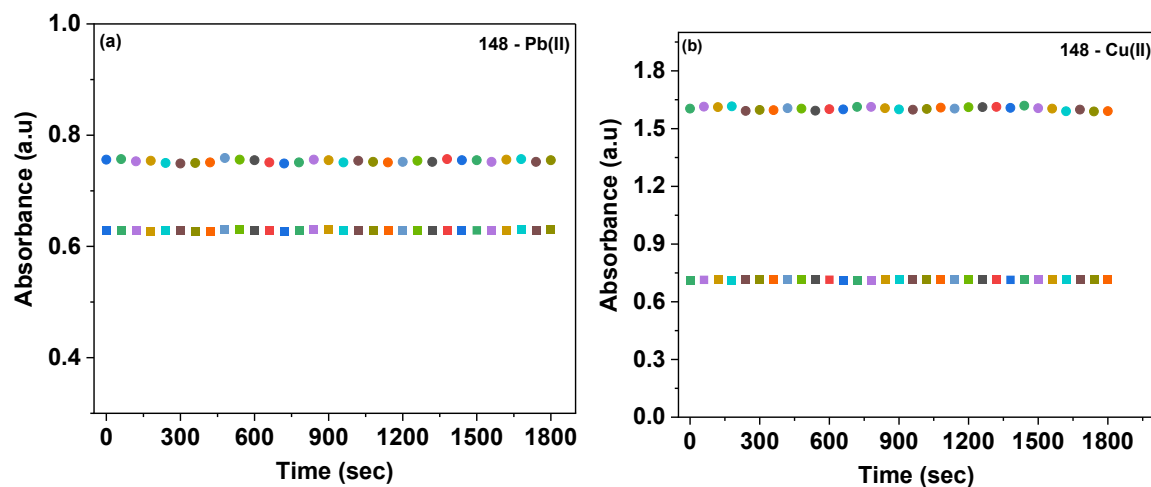
Figure 4.33: The time-dependent absorption spectrum of (a) probe **148**-Pb(II) and (b) probe **148**-Cu(II) complex solution demonstrating a consistent absorbance over time

4.10.18. Temperature dependence analysis of probe-metal ion complexation for 148

The influence of temperature on the binding properties of probe 148 was investigated over a range of temperatures. wherein the absorption spectra of the metal-bound probe solution were recorded at 2 °C intervals from 20 °C to 50 °C for each probe. The results, as depicted in **figure 4.34 (a) and (b)**, revealed that temperature variations had no significant effect on the binding abilities of probe 148. This indicated that the interactions between these probes and the metal ions were highly stable and robust, even under varying thermal conditions.
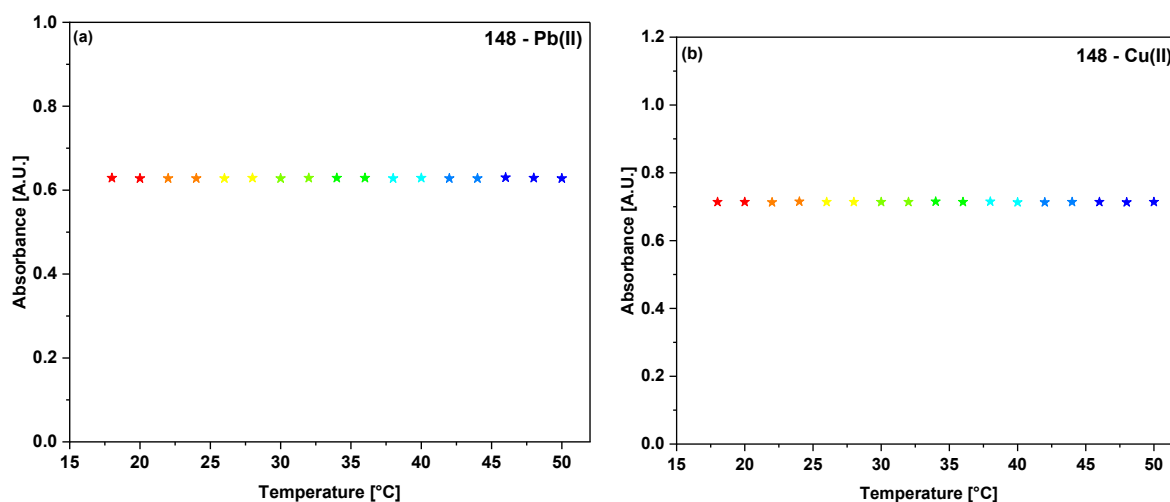
Figure 4.34: Variation in maximum absorbance of (a) probe **148**-Pb(II) complex and (b) probe **148**-Cu(II) complex showing minimal variation in absorbance across a range of temperatures.

Table 4.5: A comprehensive summary of the LoD, LoQ, association constant (K_a), and stoichiometric ratio for probe **146. 147, 148**

Probe	Metal ion	UV-Visible λ_{max}	Type of shift	Fluorescence λ_{em}	Type of shift	LoD (μM)	LoQ (μM)	Association Constant (K_a)	Binding Ratio
146	Pb(II)	340	Hyperchromic	438	Fluorescence enhancement	5.69	18.97	$6.18 \times 10^3 \ M^{-1}$	1:1
	Cu(II)					6.55	21.85	$7.57 \times 10^3 \ M^{-1}$	
147	Pb(II)	348	Hyperchromic	437	Fluorescence enhancement	3.64	12.15	$2.18 \times 10^3 \ M^{-1}$	
	Cu(II)					1.37	4.58	$2.35 \times 10^3 \ M^{-1}$	
148	Pb(II)	368	Hyperchromic	436	Fluorescence enhancement	5.06	16.89	$8.54 \times 10^3 \ M^{-1}$	
	Cu(II)					7.52	25.08	$9.37 \times 10^3 \ M^{-1}$	

The **table 4.5** provides insight into the influence of positional isomerism (ortho, meta, and para) of the chalcone based 1,2,3-triazole moiety in probes **146, 147, and 148** on their binding properties. All the three probes detected Pb(II) and Cu(II) ions. For probe **146**, the ortho configuration, exhibited λ_{max} value 340 nm due to the influence of its structural arrangement. The ortho positioning of the 1,2,3-triazole moiety can lead to enhanced electronic interactions between the 1,2,3-triazole and adjacent groups in the molecule. These interactions can create distinct electronic transitions, likely involving both π-π* and n-π* transitions, resulting in two observable absorption peaks in **146**. In contrast, probes **147** (meta) and **148** (para) showed only a single peak, as their configurations provide a more symmetric environment. Probe **147**, the meta isomer showed slightly lower LoD values for both metal ions but its binding constant is less which is suggestive of unstable binding of probe **147** with the metal ions. This trend suggests that the meta-arrangement may result in a less favorable spatial orientation for strong metal coordination. Probe **148,** the para configuration demonstrated superior performance, for both metal ions as it is having highest association constant for both the metal ions. The enhanced binding affinity and sensitivity can be attributed to the para-arrangement, which likely provides an optimal spatial arrangement for metal ion coordination.

4.10.19. Plausible mode of interaction

According to the HSAB theory, both Pb(II) and Cu(II) are classified as weak acids. These metal ions can form coordination bonds with atomic groups possessing lone pairs, such as nitrogen, oxygen, and sulfur atoms. The ability of probes **146, 147, and 148** to capture the incoming electron deficient metal ions can be attributed to the presence of lone pairs on the nitrogen atoms of the 1,2,3-triazole moiety integrated into their respective structures. Furthermore, it was also determined from the Job's plots that all the three probes form a 1:1 metal-ligand complex with both Pb(II) and Cu(II). These observations provided insights into the binding mechanism between the receptor probes 146, 147, and 148 and the metal ions, as illustrated in **figure 4.35**, wherein it was hypothesized that the probe was able to bind with the metal ions through both the 1,2,3-triazole ring-containing arms, thereby forming a claw like structure to capture the metal ion. The binding interactions were further supported by ^{1}H NMR spectroscopic analysis, focusing on the complexation of probes 146, 147, and 148 with Pb(II). The ^{1}H NMR data for probe **146** showed a significant downfield shift in the proton signal corresponding to the 1,2,3-triazole ring, from δ = 7.59 ppm to δ = 7.77 ppm, indicating

coordination between the nitrogen atoms of the triazole moiety and the Pb(II) ion. Similarly, probe **147** exhibited a shift in the triazole proton peak from δ = 7.48 ppm to δ = 7.79 ppm, confirming its interaction with the metal center. For probe **148**, a comparable downfield shift from δ = 7.59 ppm to δ = 7.71 ppm was observed upon complexation with Pb(II), further corroborating the involvement of the triazole moiety in metal binding. These ^{1}H NMR observations are consistent with the proposed binding mode, where the triazole rings act as key binding sites for both Pb(II) and Cu(II). The similarity in binding behavior for Pb(II) and Cu(II) is inferred due to their comparable chemical properties as soft acids, further validating the proposed claw-like binding mechanism of the probes.
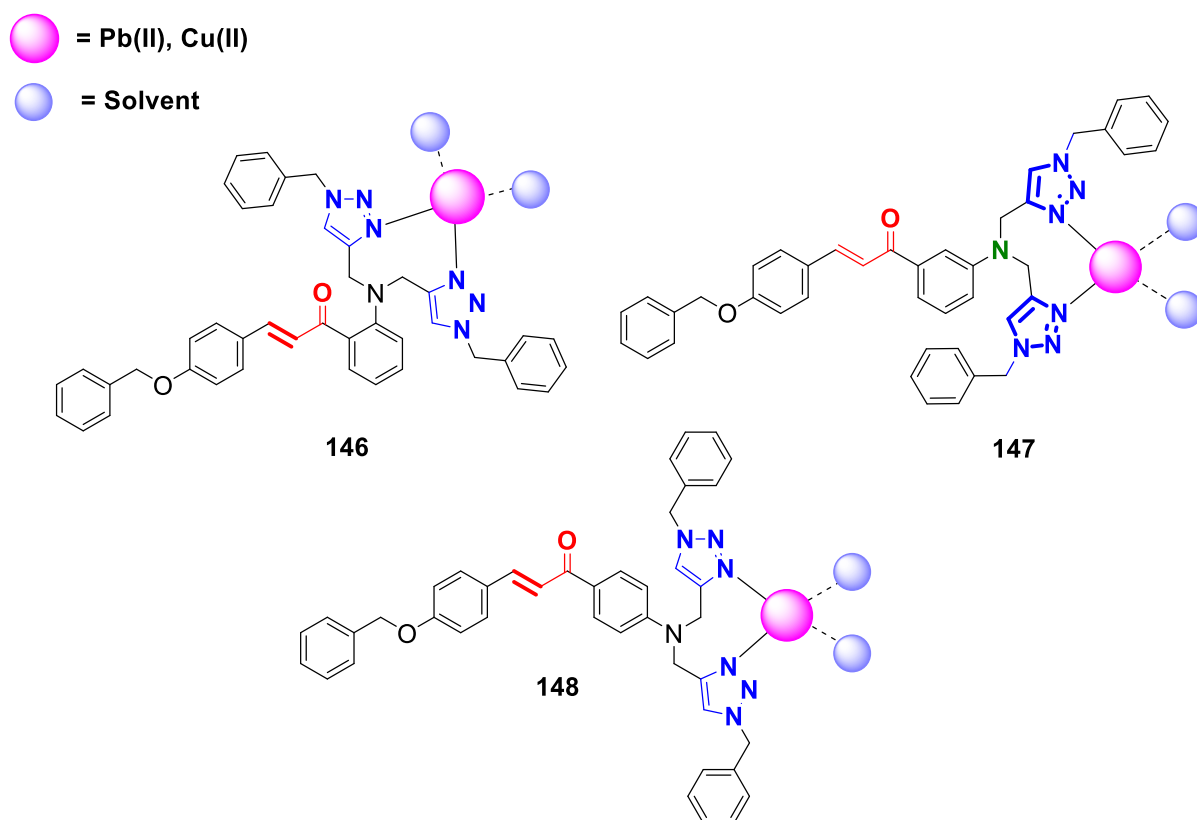
Figure 4.35: Plausible binding mode of probe **146**, **147**, and **148** with Pb(II)/Cu(II)

4.11. Chemosensing analysis of 4-chlorobenzaldehyde based 1,2,3-triazoles 156, 157, and 158

The ion recognition capabilities of the synthesized 1,2,3-triazole derivatives were assessed using UV-Vis and fluorescence spectroscopy with various metal chlorides. The design of these probes were also based on the incorporation of a chalcone backbone, selected for its well-established performance in UV-Vis spectral analysis. The chalcone structure was purposely modified by introducing a benzyl group, functioning as the transducer unit, via a 1,2,3-triazole bridge. This bridge not only served as a spacer but also provided receptor sites

for electron-deficient metal ions due to the lone pairs present on the nitrogen atoms. As a result, the synthesized derivatives displayed a stable aromatic framework, which enhanced their effectiveness as chemosensing agents.

4.11.1. Ion recognition analysis of 1,2,3-triazole derivative 156

Tetrahydrofuran (THF)/water (4:1) was selected as the solvent media for conducting UV-Vis and fluorescence spectroscopic studies due to the excellent ability of THF to dissolve the probes and the favourable impact of H_2O keeping in mind its biological relevance. To optimize the conditions for UV-Vis analysis, the concentrations of the probe solutions were adjusted at 0.02 mM would be used for probe **156** respectively, as these concentrations provided well-defined and distinct absorption bands suitable for monitoring their sensing behavior. The maximum absorbance (λ_{max}) for probe **156** was observed at 311 nm, the distinct spectral properties as depicted in a **figure 4.36**.
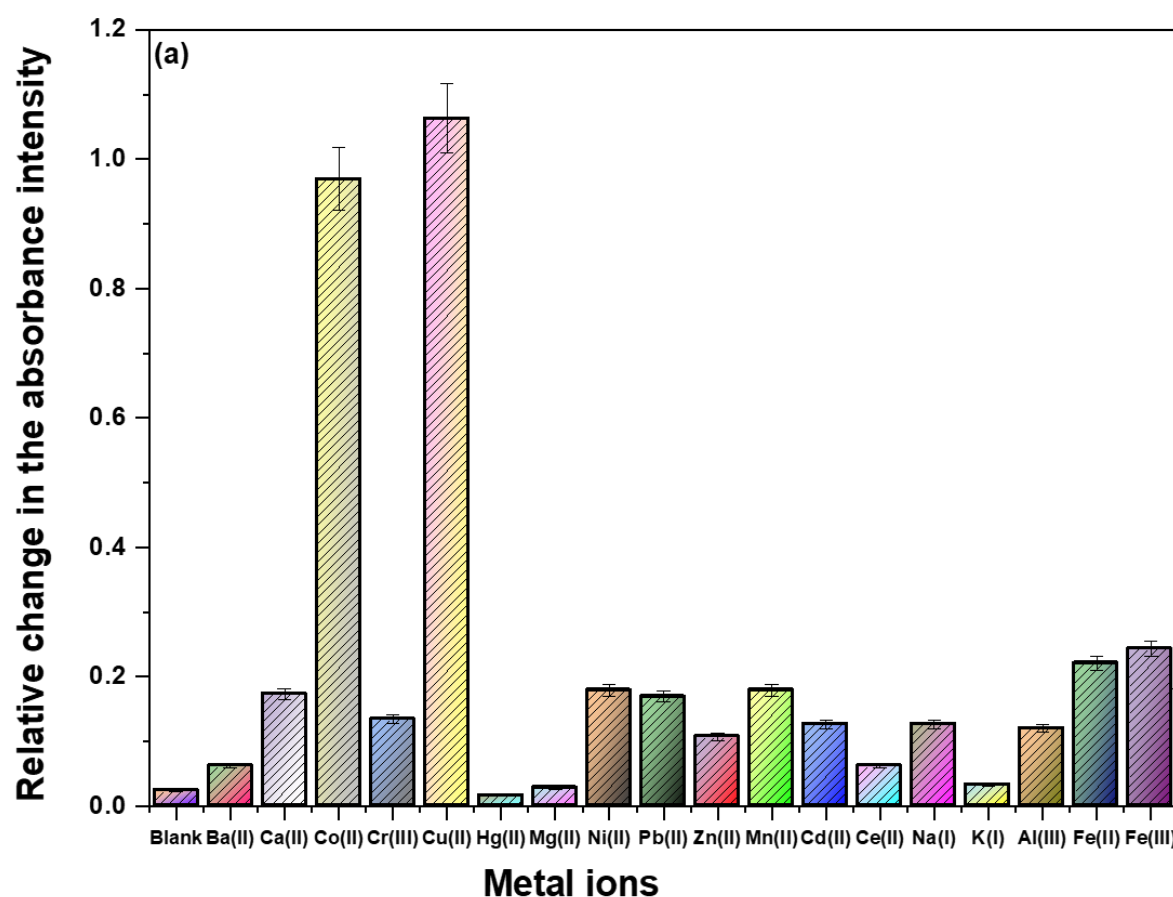
Figure 4.36: Relative chemosensing behaviour of probe **156** with different metal ions in THF: water (4:1)

4.11.2. Chemosensing response of probe 156 for Co(II) and Cu(II) via UV-Visible spectroscopy

The interactions of probe **156** with Co(II) and Cu(II) ions were systematically investigated using UV-Vis spectroscopy. In these experiments, solutions of probe were titrated with 1 mM solutions of Co(II) and Cu(II) ions in separate titrations. The corresponding spectral changes are depicted in **figure 4.37 (a) and (b)**. For probe **156**, the addition of Co(II) ions resulted in a significant hyperchromic shift in the absorption peak observed at 311 nm, attributable to the increased probability of electronic transitions form ground state to excited state, accompanied by a smaller hyperchromic shift at 425 nm. These changes are attributed to $n \rightarrow \pi*$ transitions, indicating a strong interaction between the probe and Co(II) ions. Similarly, titration with Cu(II) ions led to pronounced hyperchromic shifts at 311 nm and minor hyperchromic changes at 425 nm. Furthermore, the inset plots in **figure 4.37 (a) and (b)** illustrate the relative changes in maximum absorbance (A_n/A_o) for probe **156,** where A_n represents the absorption maxima recorded after successive additions of the metal ions, and A_o corresponds to the initial absorption maxima of the probe. The corresponding Benesi-Hildebrand plots for the complexation of probe 156 with Co(II) as well as Cu(II) are presented in **figure 4.38 (a) and (b)**. The K_a values for probe **156** for Co(II) and Cu(II) ions were 8.80×10^3 M^{-1}, 5.99×10^3 M for the aforementioned metal ions, respectively. Moreover, the binding ratio of 1:1 (M:L) were established based on the Job's plots analysis **(figure 4.39 (a) and (b))**.
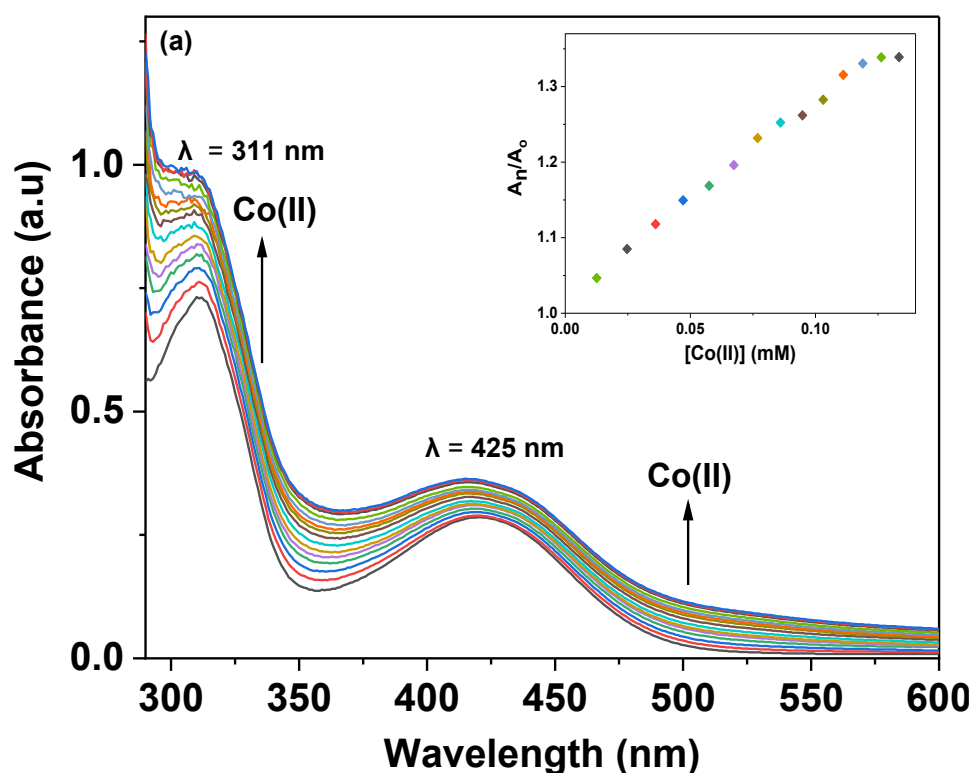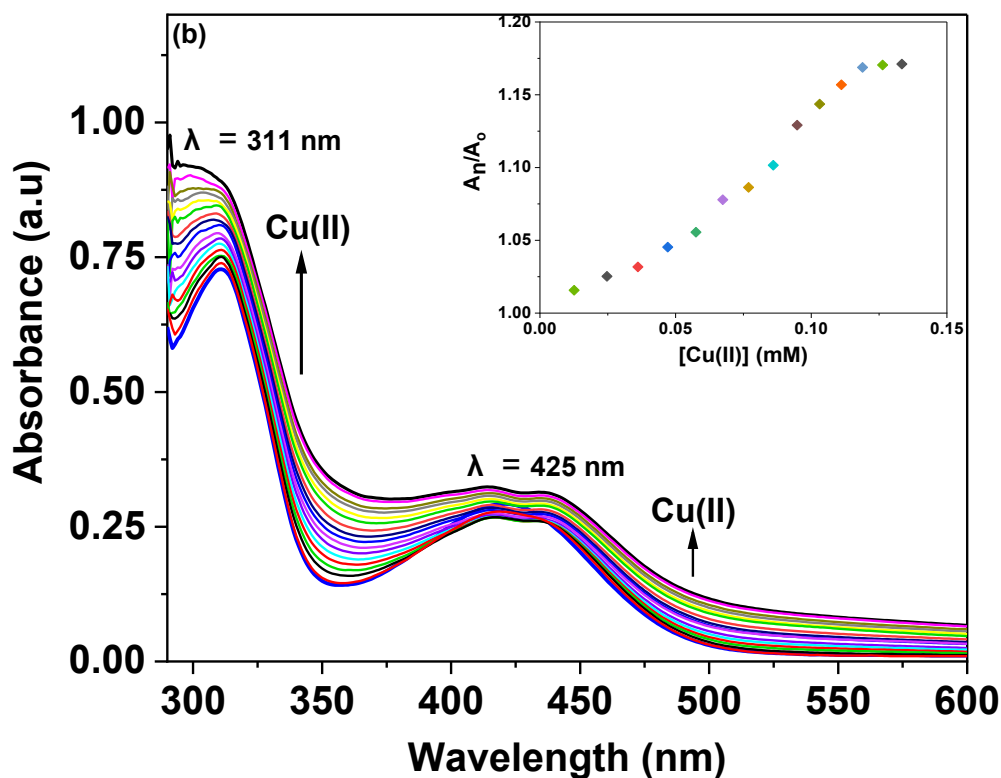
Figure 4.37: Shifts in the absorption maxima of probe **156** observed during titration with (a) Co(II) and (b) Cu(II) in THF: H_2O (4:1) as the solvent; the inset exhibits the relative absorbance change of probe **156** (A_n/A_o) and metal ion concentration (mM)
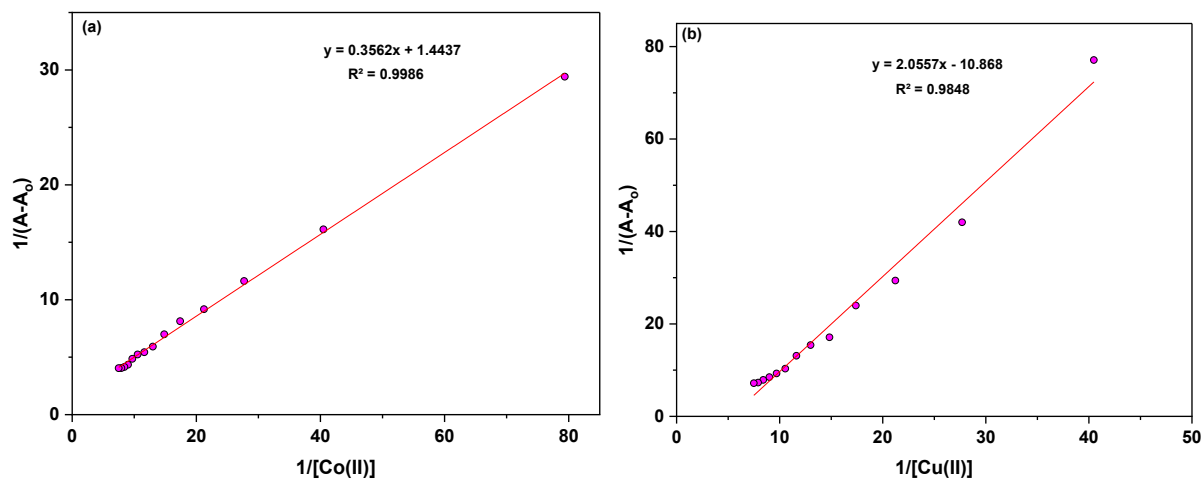
Figure 4.38: B-H plots representing the complexation behaviour of the synthesized probe **156** with (a) Co(II) ions and (b) Cu(II) ions, demonstrating the interaction profiles and binding affinities between the probe and the respective metal ions
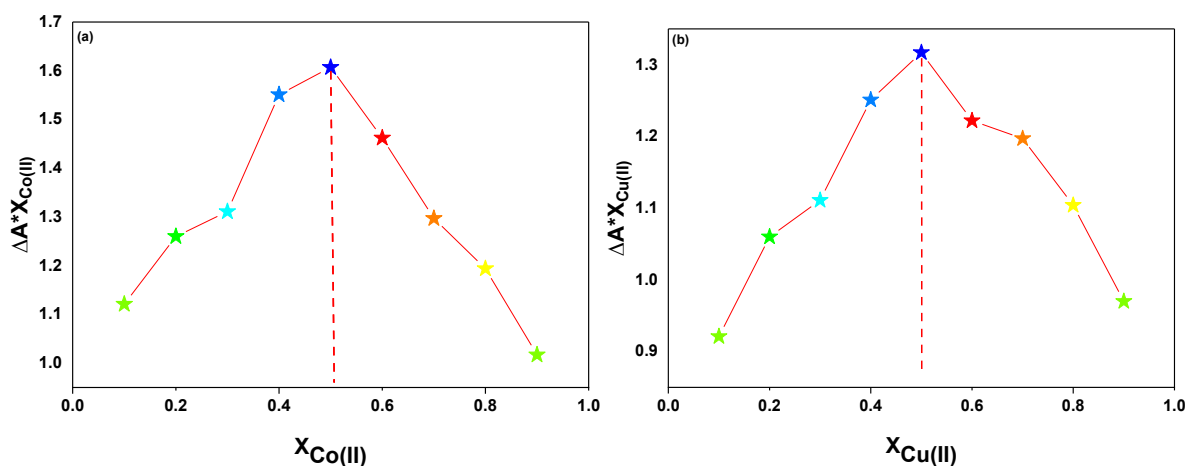
Figure 4.39: Job's plot analysis of probe **156** on interaction with metal ion (a) Co(II) (b) Cu(II)

4.11.3. Chemosensing response of probe 156 for Co(II) and Cu(II) via fluorescence spectroscopy

The interactions of probe **156** with Co(II) and Cu(II) ions were investigated using fluorescence spectroscopy, where probe solutions were titrated with 10 µM solutions of each metal ion in separate experiments. Upon excitation at 295 nm (λ_{ex}), probe **156** displayed a strong emission peak at 355 nm (λ_{em}). Titrations with both Co(II) and Cu(II) ions, as shown in **figure 4.40 (a) and (b),** revealed that the fluorescence emission intensity of probe **156** increased with the addition of either metal ion to the solution. Throughout the experiment, the metal ion concentration was progressively raised to a maximum of 15 equivalents, while the probe concentration remained constant at 5 µM.
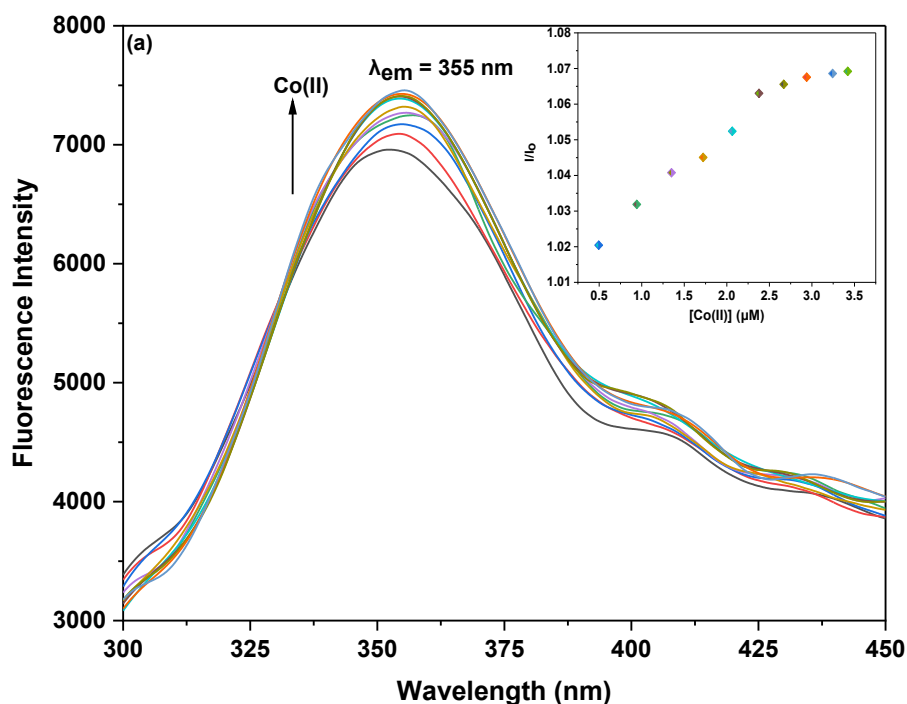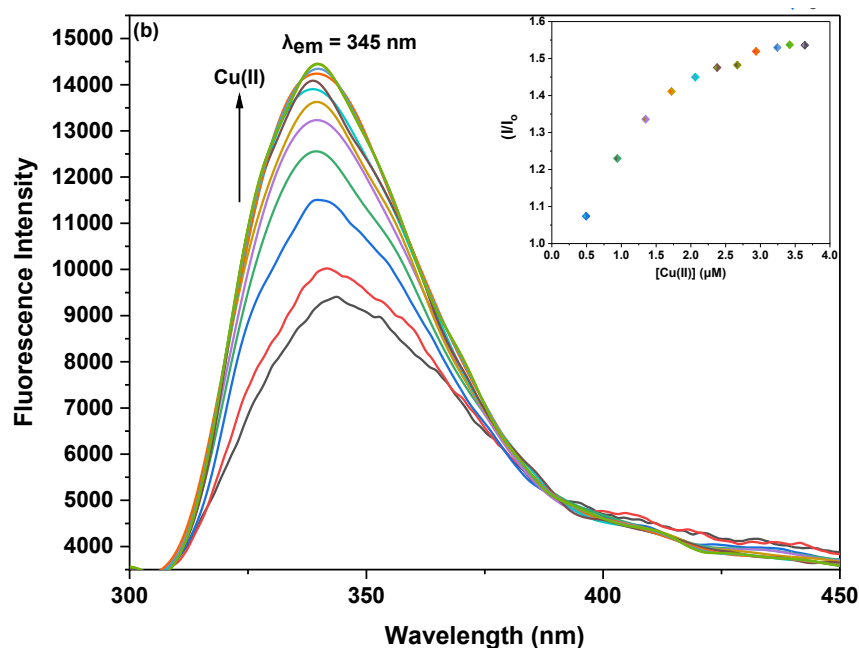
Figure 4.40: Variations in the fluorescence emission of probe **156** upon the incremental addition of (a) Co(II) and (b) Cu(II) ions in THF: H_2O (4:1); the inset illustrates the relative change in emission of probe **156** versus metal ion concentration (μM)

Furthermore, to evaluate the sensitivity of the probe towards Pb(II) and Cu(II) ions, correlation plots (**figure 4.41 (a) and (b)**) were used to calculate the limits of detection (LoD) and quantification (LoQ). The LoD values for probe **156** for detecting Co(II) were determined to be 1.64 μM, while for detecting Cu(II) ions, the LoD values were 3.19 μM. The LoQ values for the probe **156** for the recognition of Co(II) ions were found to be 5.46 μM, whereas for Cu(II) ions, the values were 10.64 μM, respectively. The values for LoD, LoQ, K_a, and stoichiometric ratio for all the probes have been compiled and presented in **table 4.6**.
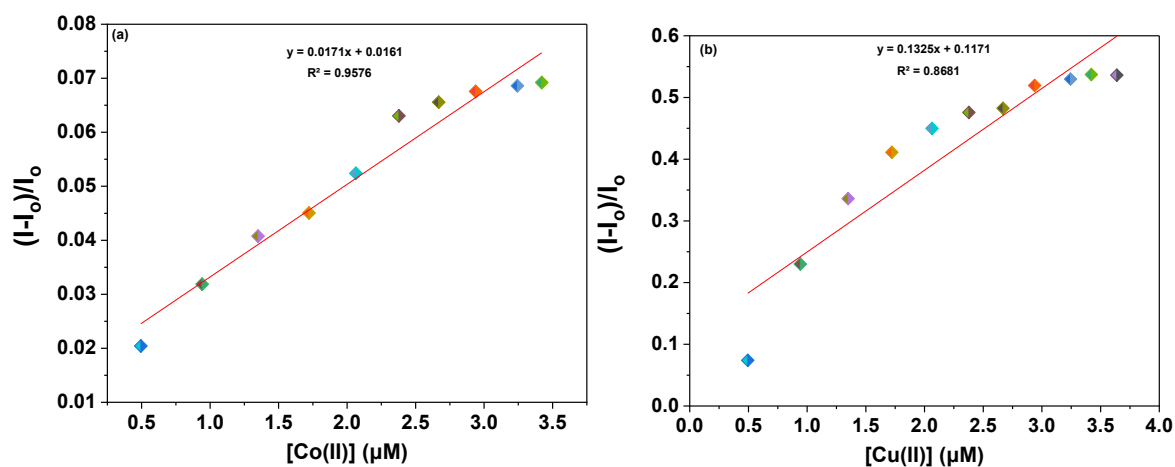
Figure 4.41: Correlation plot of probe **156** illustrating $(I-I_n)/I_o$ vs. (a) [Co(II)] and (b) [Cu(II)]

156

4.11.4. Competitive metal ion interaction analysis of probes 156

The selectivity of probe **156** was further assessed in the presence of all metal ions simultaneously, prepared in an equimolar ratio. A single solution containing an equimolar mixture of various metal ions was titrated with each probe, and the resulting UV-Vis spectra were analyzed **(figure 4.42)**. It was observed that the spectra obtained during these titrations closely matched those recorded when Co(II) was used alone with the probe. This finding indicates that each probe selectively recognized Co(II) even in the presence of other competing metal ions. These results conclusively demonstrate that probe exhibit high selectivity for Co(II), with no interference from other metal ions, thereby confirming their robust chemosensing properties.
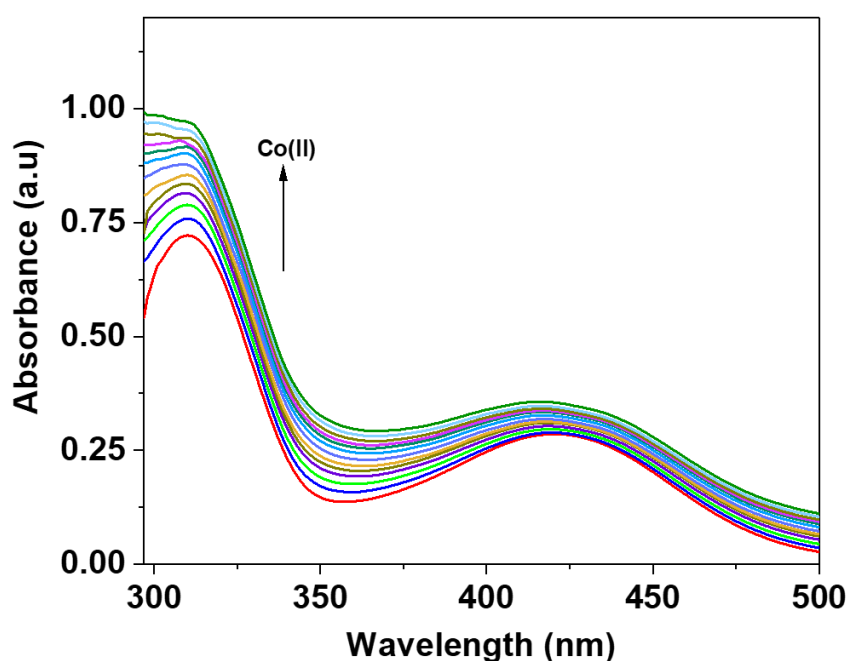
Figure 4.42: UV-Vis spectrum of probe **156** in THF: H_2O (4:1), highlighting the selective detection of Co(II) among various metal ions at equimolar concentrations

4.11.5. Time dependence analysis of probe-metal ion complexation for 156

The time-dependent behaviour of the metal-bound probes **156** was evaluated to gain insights into their stability and sensitivity toward metal ions. Absorption spectroscopy was employed to monitor the effect of time on these metal-bound probe. As depicted in the corresponding **figure 4.43 (a) and (b)**, the absorbance of Co(II)- and Cu(II)-complexed solutions of probe **156** remained consistent, showing no significant variation even after extended periods of standing. These findings confirm that the probe exhibit excellent stability and maintain a strong, robust affinity for the respective metal ions over time.

157
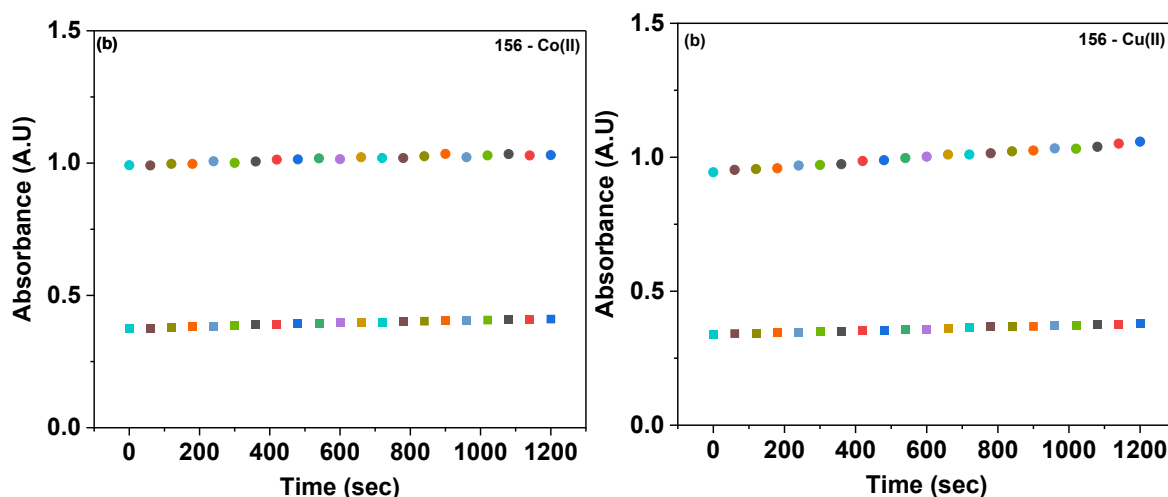
Figure 4.43: The time-dependent absorption spectrum of (a) probe **156**-Co(II) and (b) probe **156**-Cu(II) complex solution demonstrating a consistent absorbance over time

4.11.6. Temperature dependence analysis of probe-metal ion complexation for 156

The influence of temperature on the binding efficiency of probe **156** was investigated by recording the absorption spectra of their metal-bound complexes at 2 °C intervals over a temperature range of 20 °C to 50 °C. As illustrated in the accompanying **figure 4.44 (a) and (b)**, no significant changes were observed in the binding behaviour of the probe across the tested temperatures. These results highlight the thermal stability and robustness of the interactions between the probe and the metal ions, demonstrating their consistent performance under varying thermal conditions.
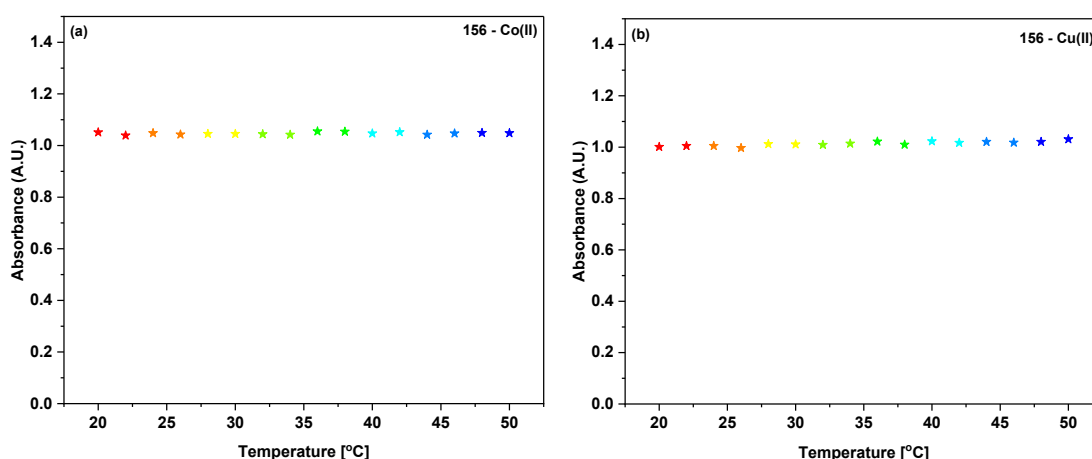
Figure 4.44: Variation in maximum absorbance of (a) probe **156**-Co(II) complex and (b) probe **156**-Cu(II) complex showing minimal variation in absorbance across a range of temperatures.

4.11.7. Ion recognition analysis of 1,2,3-triazole derivatives 157

Tetrahydrofuran (THF)/H_2O (4:1) was selected as the solvent media for conducting UV-Vis and fluorescence spectroscopic studies due to the excellent ability of THF to dissolve the probe and the favourable impact of H_2O keeping in mind its biological relevance. To optimize the conditions for UV-Vis analysis, the concentrations of the probe solutions were adjusted at 0.05 mM would be used for probe **157,** as these concentrations provided well-defined and distinct absorption bands suitable for monitoring their sensing behaviour. The maximum absorbance (λ_{max}) for probes 157 was observed at 317 nm, highlighting their distinct spectral properties as depicted in a **figure 4.45.**
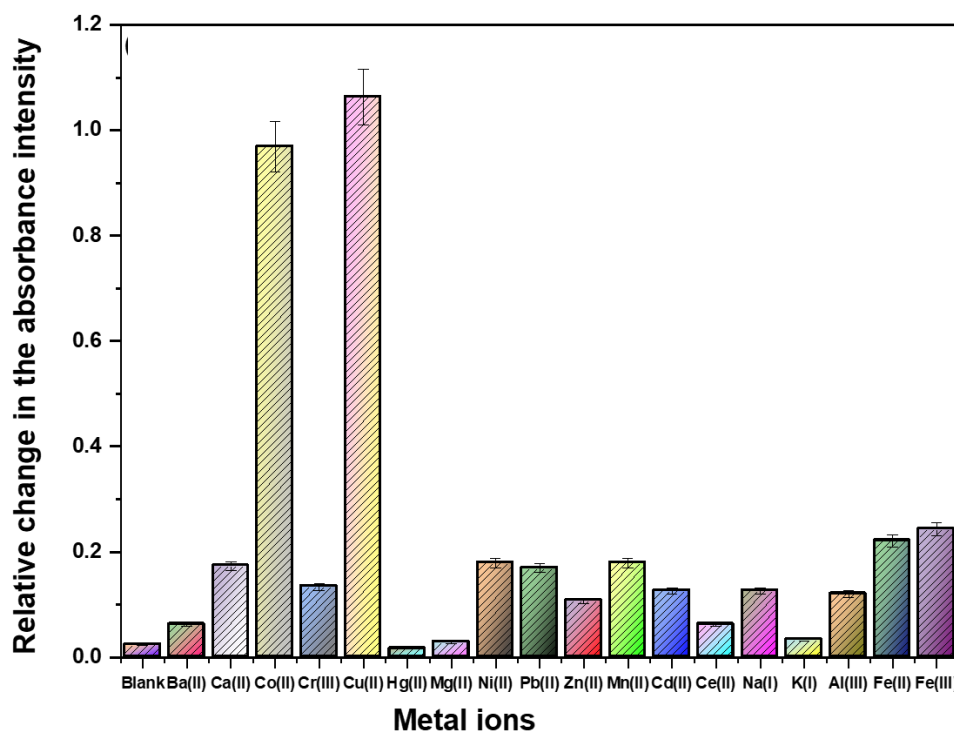
Figure 4.45: Relative chemosensing behaviour of probe **157** with different metal ions in THF: water (4:1)

4.11.8. Chemosensing response of probe 157 for Co(II) and Cu(II) via UV-Visible spectroscopy

The interactions of probe **157** with Co(II) and Cu(II) ions were analyzed in detail using UV-Vis spectroscopy. In these studies, the probe solution was titrated separately with 1 mM solutions of Co(II) and Cu(II) ions, allowing the observation of distinct changes in the absorption spectra corresponding to its interaction with each metal ion. Upon the stepwise addition of Co(II) ions, a significant reduction in the intensity of the absorption peak at 317 nm was observed, indicating a hypochromic effect. Notably, an isosbestic point emerged at 370

nm, suggesting a transition between two distinct species in solution are illustrated in **figure 4.46 (a) and (b).**
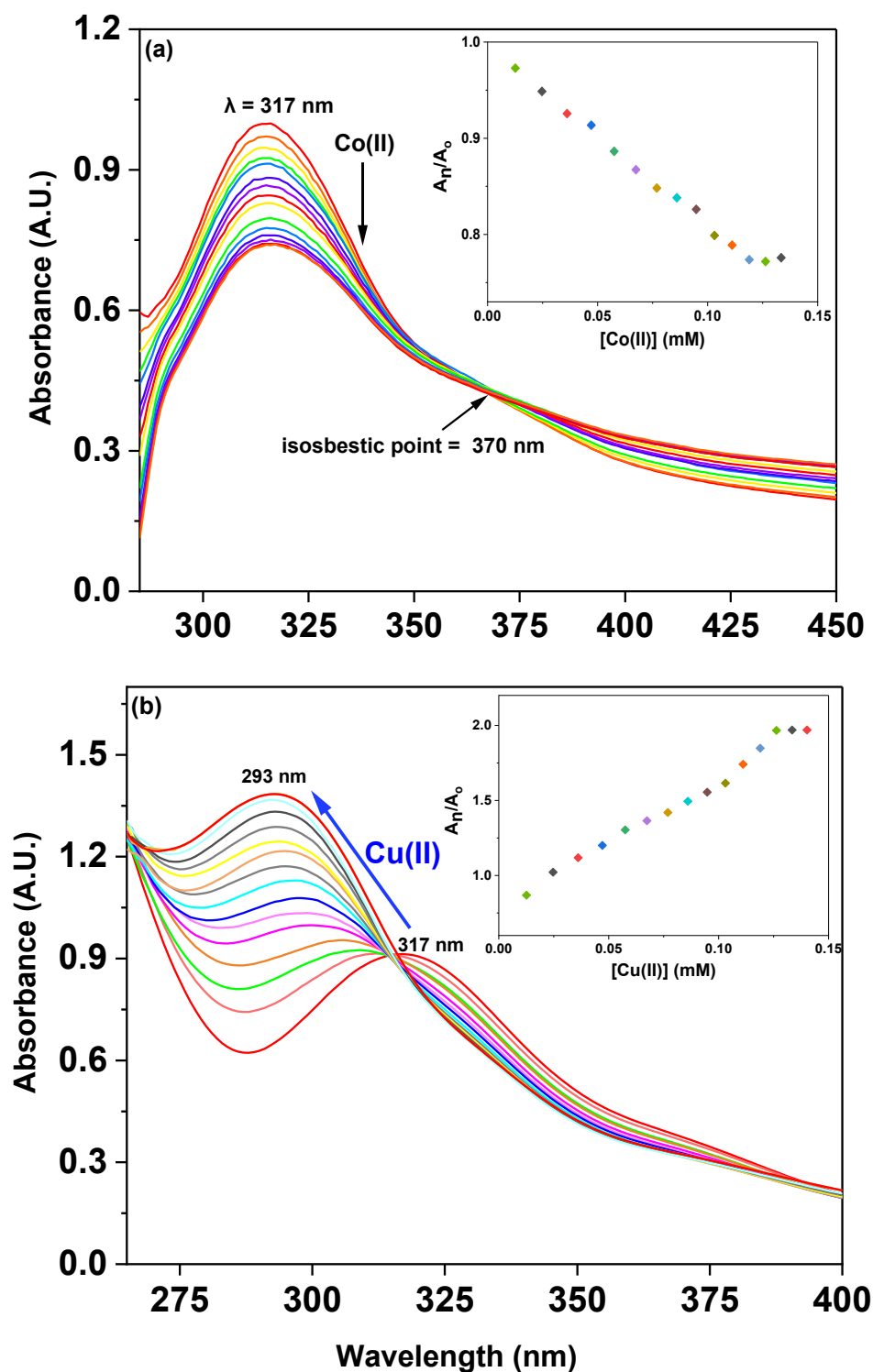
Figure 4.46: Shifts in the absorption maxima of probe **157** observed during titration with (a) Co(II) and (b) Cu(II) in THF: H_2O (4:1) as the solvent; the inset exhibits the relative absorbance change of probe **157** (A_n/A_o) and metal ion concentration (mM)

Conversely, the titration of probe **157** with Cu(II) ions elicited a different response. The absorption maximum at 317 nm underwent a notable blue shift, decreasing by approximately 24 nm to 293 nm. This spectral shift was accompanied by a hyperchromic effect, as evidenced by a marked increase in absorbance intensity at the new maximum. These variations in spectral behaviour upon interaction with Co(II) and Cu(II) ions point to the probe's selective and differential binding properties for these metal ions.
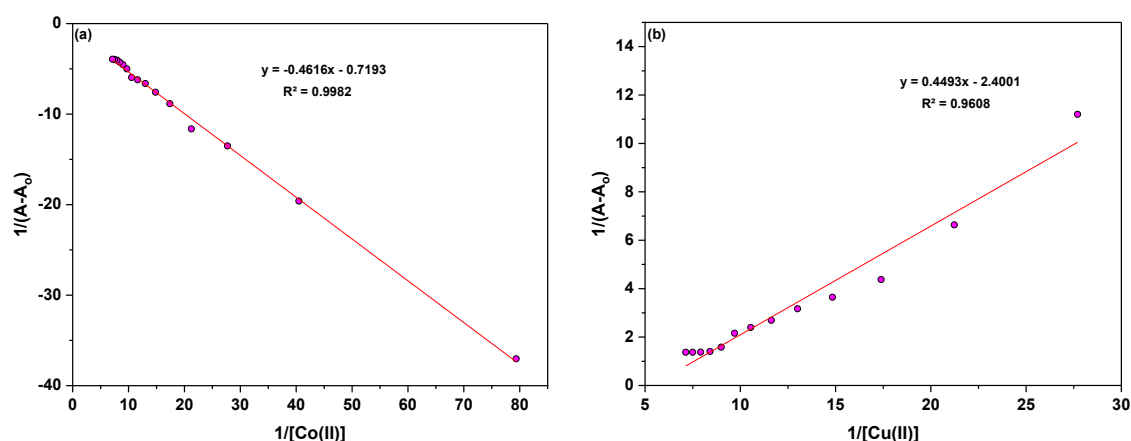
Figure 4.47: B-H plot for the complexation of probe **157** with (a) Co(II) and (b) Cu(II)
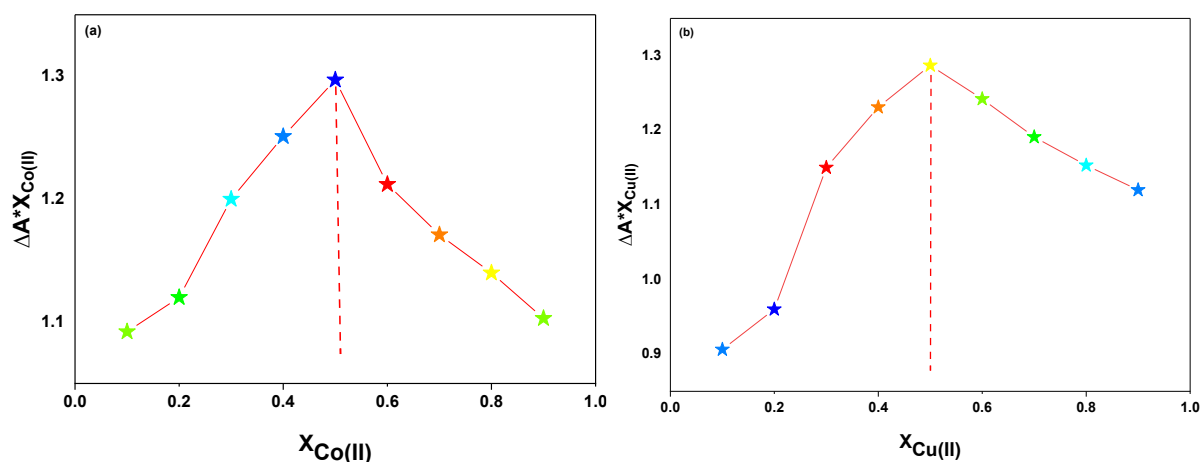
Figure 4.48: Job's plot analysis of probe **157** on interaction with metal ion (a) Co(II) (b) Cu(II)

Furthermore, the inset plots in **figure 4.46 (a) and (b)**. illustrate the relative changes in maximum absorbance represented by A_n/A_o for probe **157** where A_n represents the absorption maxima recorded after successive additions of the metal ions, and A_o corresponds to the initial absorption maxima of each probe. The corresponding Benesi-Hildebrand plots for the complexation of probe **157** with Co(II) as well as Cu(II) are presented in **figure 4.47 (a) and (b)**. The K_a values for probe **157** for the aforementioned metal ions were 7.66×10^3 M^{-1}, 4.74

$\times 10^3$ M^{-1}, respectively. Moreover, the binding ratio of 1:1 (M:L) were established for probe based on the Job's plots analysis **(figure 4.48 (a) and (b)).**

4.11.9. Chemosensing response of probe 157 for Co(II) and Cu(II) via fluorescence spectroscopy

The interactions of probe **157** with Co(II) and Cu(II) ions were also examined through fluorescence spectroscopy, where solutions of each probe were titrated with 10 µM solutions of the metal ions in separate experiments. For probe **157,** upon excitation at a wavelength of (λ_{ex}) 320 nm, a distinct fluorescence emission peak was observed at (λ_{em}) 442 nm. The fluorescence intensity of probe **157** significantly increased upon the addition of Co(II) and Cu(II) ions, as depicted in the corresponding **figure 4.49 (a) and (b)**.

Furthermore, to evaluate the sensitivity of the probes towards Pb(II) and Cu(II) ions, correlation plots (**figure 4.50 (a) and (b))** were used to calculate the limits of detection (LoD) and quantification (LoQ). The LoD values for probe **157** for detecting Co(II) were determined to be 2.08 µM, while for detecting Cu(II) ions, the LoD values were 2.30 µM. The LoQ values for the probe **157** for the recognition of Co(II) ions were found to be 6.94 µM, whereas for Cu(II) ions, the values were 7.68 µM. The values for LoD, LoQ, K$_a$, and stoichiometric ratio for all the probes have been compiled and presented in **table 4.6**.
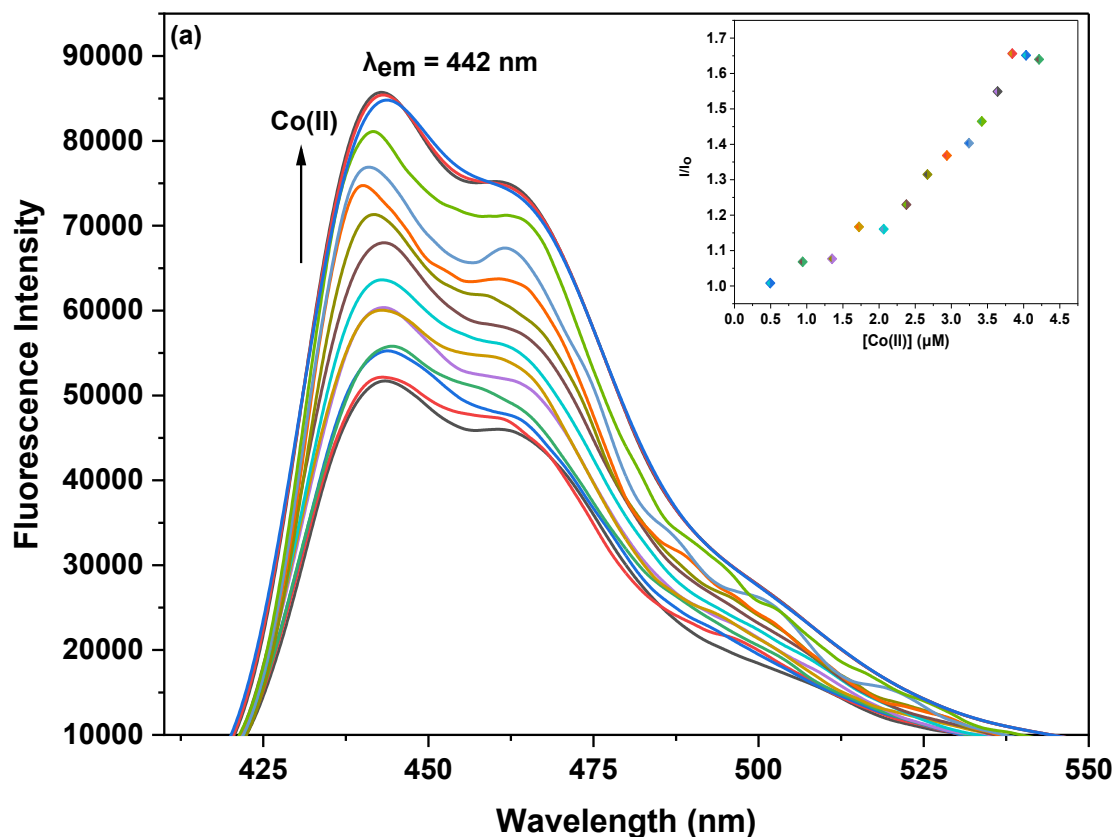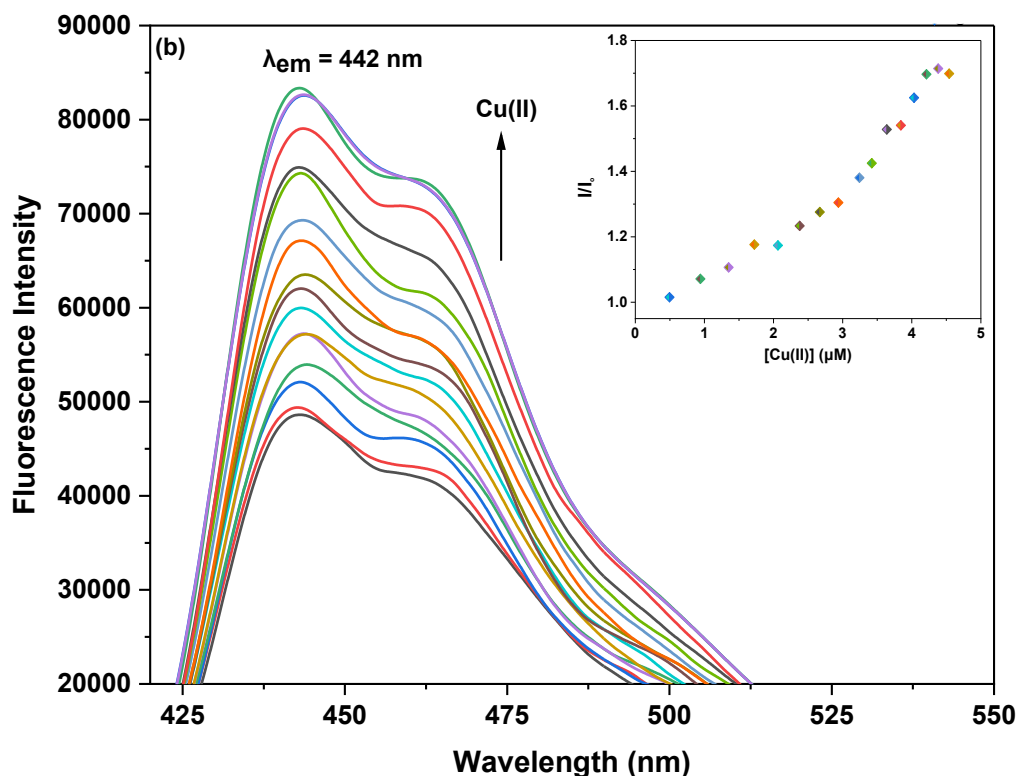
Figure 4.49: Variations in the fluorescence emission of probe **157** upon the incremental addition of (a) CoII) and (b) Cu(II) ions in THF: H_2O (4:1); the inset illustrates the relative change in emission of probe **157** versus metal ion concentration (μM)
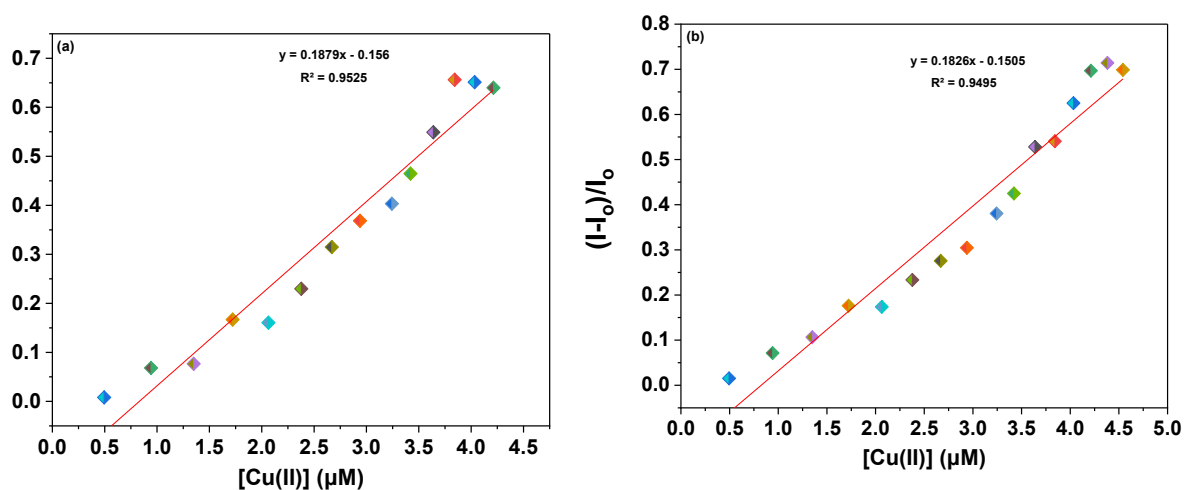
Figure 4.50: Correlation plot of probe **157** illustrating $(I-I_n)/I_o$ vs. (a) [Co(II)] and (b) [Cu(II)]

4.11.10. Competitive metal ion interaction analysis of probe 157

The selectivity of probe **157** was further assessed in the presence of all metal ions simultaneously, prepared in an equimolar ratio. A single solution containing an equimolar mixture of various metal ions was titrated with each probe, and the resulting UV-Vis spectra

were analyzed **(figure 4.51)**. It was observed that the spectra obtained during these titrations closely matched those recorded when Co(II) was used alone with the probe. This finding indicates that the probe selectively recognized Co(II) even in the presence of other competing metal ions. These results conclusively demonstrate that the probe exhibit high selectivity for Co(II), with no interference from other metal ions, thereby confirming their robust chemosensing properties.
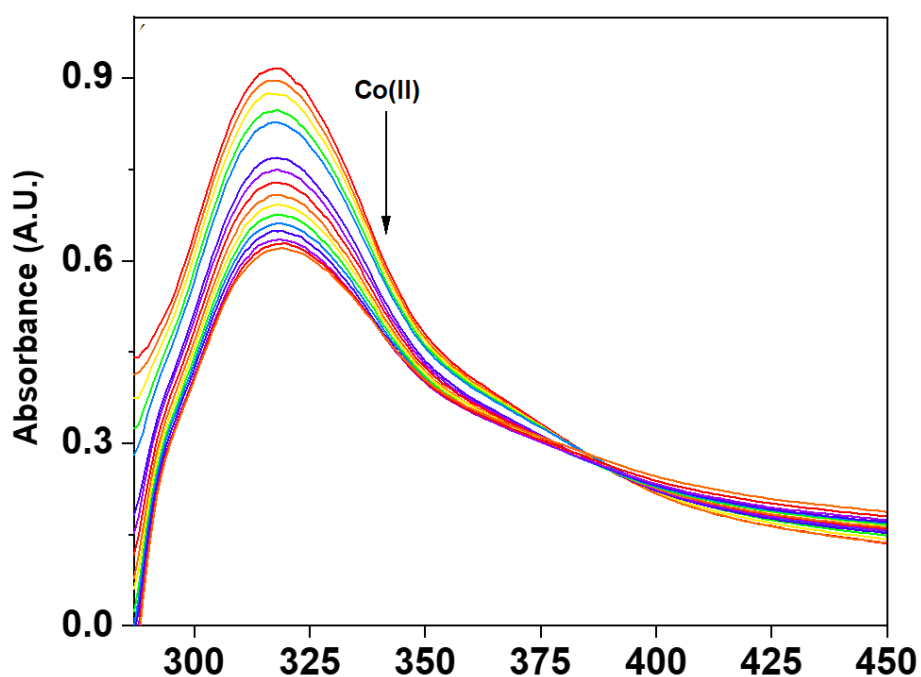
Figure 4.51: UV-Vis spectrum of probe **157** in THF: H_2O (4:1), highlighting the selective detection of Co(II) among various metal ions at equimolar concentrations

4.11.11. Time dependence analysis of probe-metal ion complexation for 157

The time-dependent behavior of the metal-bound probe **157** was comprehensively evaluated to gain valuable insights into its stability, durability, and sensitivity toward metal ions. Absorption spectroscopy was employed as a key analytical technique to monitor the effect of prolonged standing on the performance and integrity of the metal-bound probe. The corresponding results, illustrated in **figure 4.52 (a) and (b),** reveal that the absorbance of Co(II)- and Cu(II)-complexed solutions of probe 157 remained stable and consistent, exhibiting no significant variations even after extended periods of time. These observations unequivocally confirm that probe **157** demonstrates exceptional stability when bound to these metal ions and retains its strong and robust affinity for them over prolonged durations.
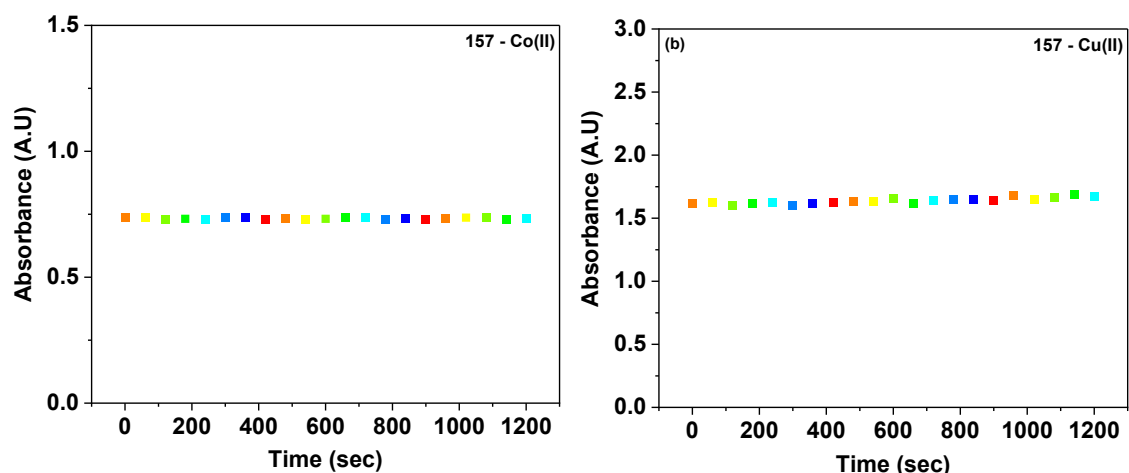
Figure 4.52: The time-dependent absorption spectrum of (a) probe **157**-Co(II) and (b) probe **157**-Cu(II) complex solution demonstrating a consistent absorbance over time

4.11.12. Temperature dependence analysis of probe-metal ion complexation for 157

The influence of temperature on the binding efficiency of probe **157** was investigated by recording the absorption spectra of their metal-bound complexes at 2 °C intervals over a temperature range of 20 °C to 50 °C. As illustrated in the accompanying **figure 4.53 (a) and (b)**, no significant changes were observed in the binding behaviour of the probe across the tested temperatures. These results highlight the thermal stability and robustness of the interactions between the probe and the metal ions, demonstrating their consistent performance under varying thermal conditions.
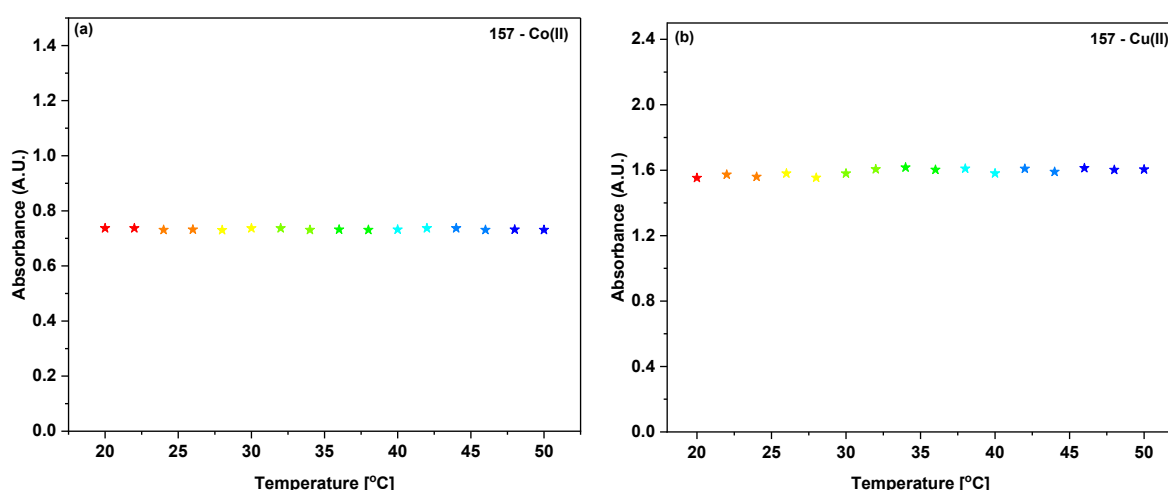
Figure 4.53: Variation in maximum absorbance of (a) probe **157**-Co(II) complex and (b) probe **157**-Cu(II) complex showing minimal variation in absorbance across a range of temperatures.

4.11.13. Ion recognition analysis of 1,2,3-triazole derivatives 158

The ion recognition capabilities of the synthesized 1,2,3-triazole derivatives **158** were assessed using UV-Vis and fluorescence spectroscopy with various metal chlorides. Wherein, THF/water (4:1) was selected as the solvent media for conducting UV-Vis and fluorescence spectroscopic studies due to the excellent ability of THF to dissolve the probe and the favourable impact of H_2O keeping in mind its biological relevance. To optimize the conditions for UV-Vis analysis, the concentration of the probe solutions were adjusted at 0.02 mM, would be used for probe **158**, as these concentrations provided well-defined and distinct absorption bands suitable for monitoring their sensing behavior. The maximum absorbance (λ_{max}) for probe 158 was observed at and 362 nm, highlighting their distinct spectral properties as depicted in a **figure 4.54.**
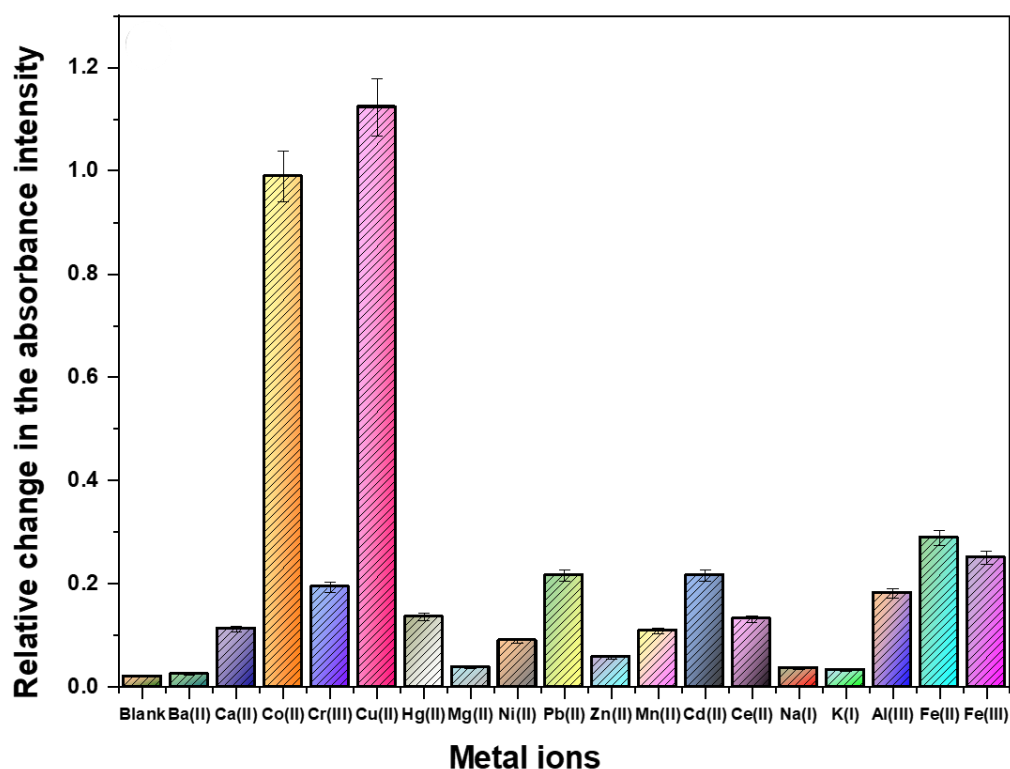
Figure 4.54: Relative chemosensing behaviour of probe **158** with different metal ions in THF: H_2O (4:1)

4.11.14. Chemosensing response of probe 158 for Co(II) and Cu(II) via UV-Visible spectroscopy

The interactions of probe **158** with Co(II) and Cu(II) ions were systematically investigated using UV-Vis spectroscopy. In these experiments, solutions of the probe were titrated with 1 mM solutions of Co(II) and Cu(II) ions in separate titrations. The stepwise

addition of Co(II) ions to the solution of probe **158** induced a significant hyperchromic effect at the absorption peak at 362 nm, which is characteristic of n→π∗ electronic transitions.
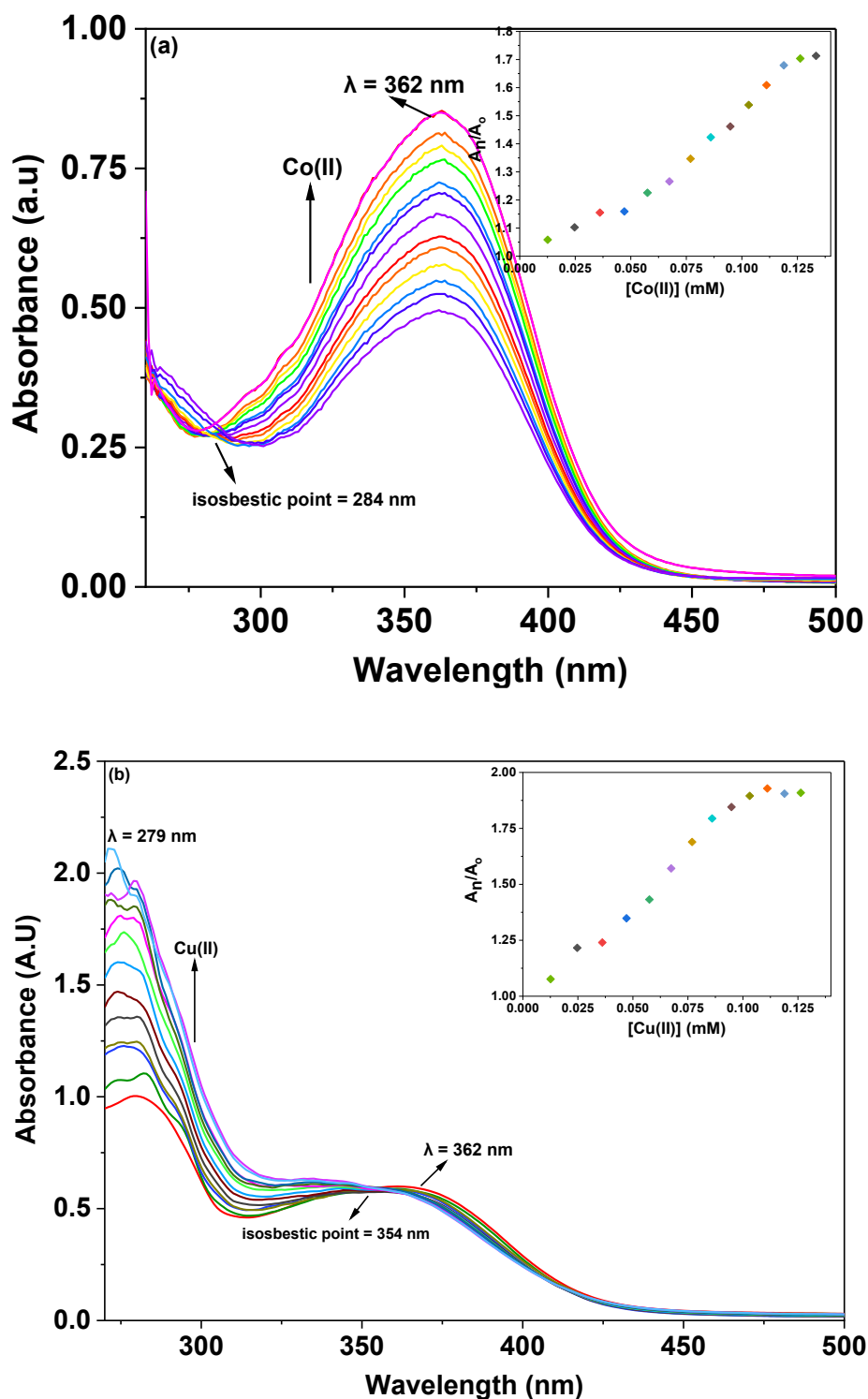
Figure 4.55: Shifts in the absorbance peak of probe **158** observed during titration with (a) Co(II) and (b) Cu(II) in THF: H_2O (4:1) as the solvent; the inset exhibits the relative absorbance change of probe **158** (A_n/A_o) and metal ion concentration (mM)

This spectral change was further highlighted by the appearance of an isosbestic point at 284 nm, suggesting a well-defined interaction and equilibrium between the free and metal-bound forms of the probe. In contrast, the titration of probe **158** with a 1 mM Cu(II) solution produced a prominent hyperchromic shift in the absorption band at 279 nm. This effect was accompanied by the formation of an isosbestic point at 354 nm, further indicating a distinct binding interaction between the probe and Cu(II) ions depicted in **figure 4.55 (a) and (b).** Furthermore, the inset plots in **figure 4.55 (a) and (b)** illustrate the relative changes in maximum absorbance. Additionally, the association constant (K_a) for probe **158** for the aforementioned metal ions were 6.61×10^3 M^{-1}, 1.00×10^4 M^{-1}, respectively. The corresponding Benesi-Hildebrand plots for the complexation of probe **158** with Co(II) as well as Cu(II) are presented in **figure 4.56 (a) and (b)**. Moreover, the binding ratio of 1:1 (M:L) were established for probe based on the Job's plots analysis **(figure 4.57 (a) and (b)).**
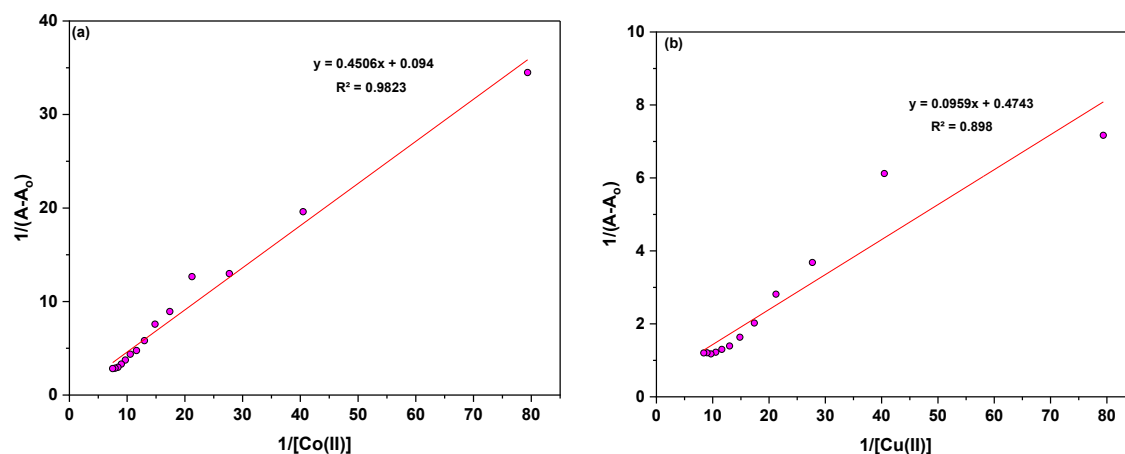
Figure 4.56: B-H plot for the complexation of probe **158** with (a) Co(II) and (b) Cu(II)
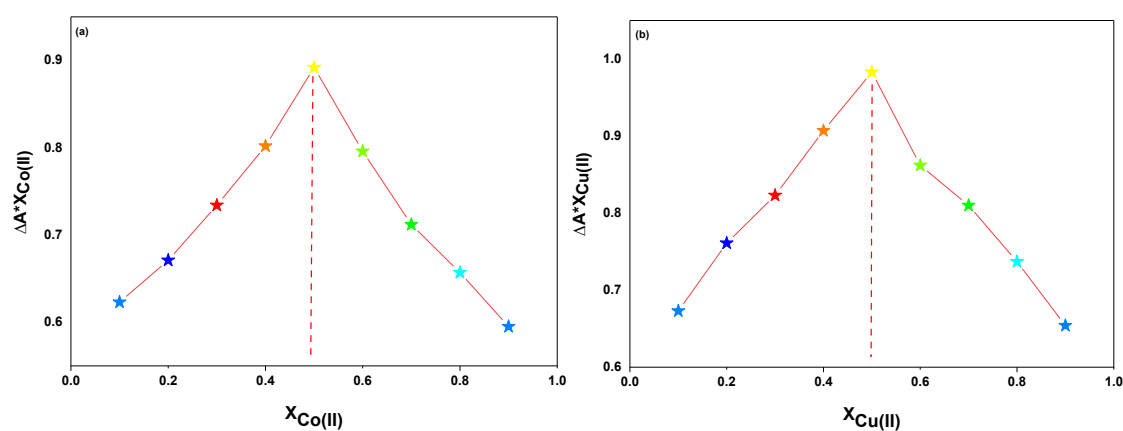
Figure 4.57: Job's plot analysis of probe **158** on binding with metal ion (a) Co(II) (b) Cu(II)

4.11.15. Chemosensing response of probe 158 for Co(II) and Cu(II) via fluorescence spectroscopy

Using fluorescence spectroscopy, the interactions of probe **158** with Co(II) and Cu(II) ions were also investigated, where solutions of probe were titrated with 10 µM solutions of the metal ions in separate experiments. In the case of probe **158**, when exposed to an excitation wavelength (λ_{ex}) of 360 nm, a pronounced emission peak (λ_{em}) at 438 nm was observed. The fluorescence emission intensity of probe **158** for both Co(II) and Cu(II) (**figure 4.58 (a) and (b)**) increased with the addition of metal ions to the solution.

Furthermore, to evaluate the sensitivity of the probe towards Pb(II) and Cu(II) ions, correlation plots (**figure 4.59 (a) and (b)**) were used to calculate the limits of detection (LoD) and quantification (LoQ). The LoD values for probe **158** for detecting Co(II) were determined to be 1.81 µM, while for detecting Cu(II) ions, the LoD values were 1.17 µM. The LoQ values for the probes **158** for the recognition of Co(II) ions were found to be 6.04 µM, whereas for Cu(II) ions, the values were 3.92 µM. The values for LoD, LoQ, K_a, and stoichiometric ratio for all the probes have been compiled and presented in **table 4.6**.
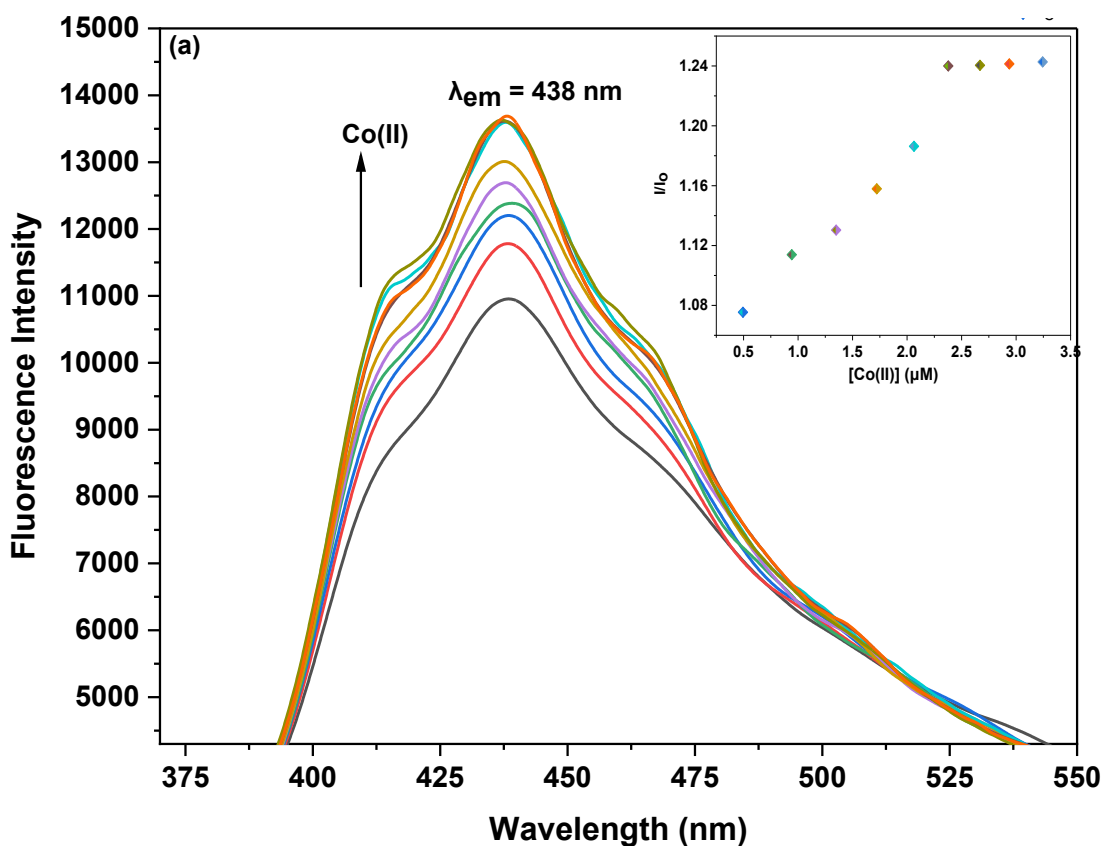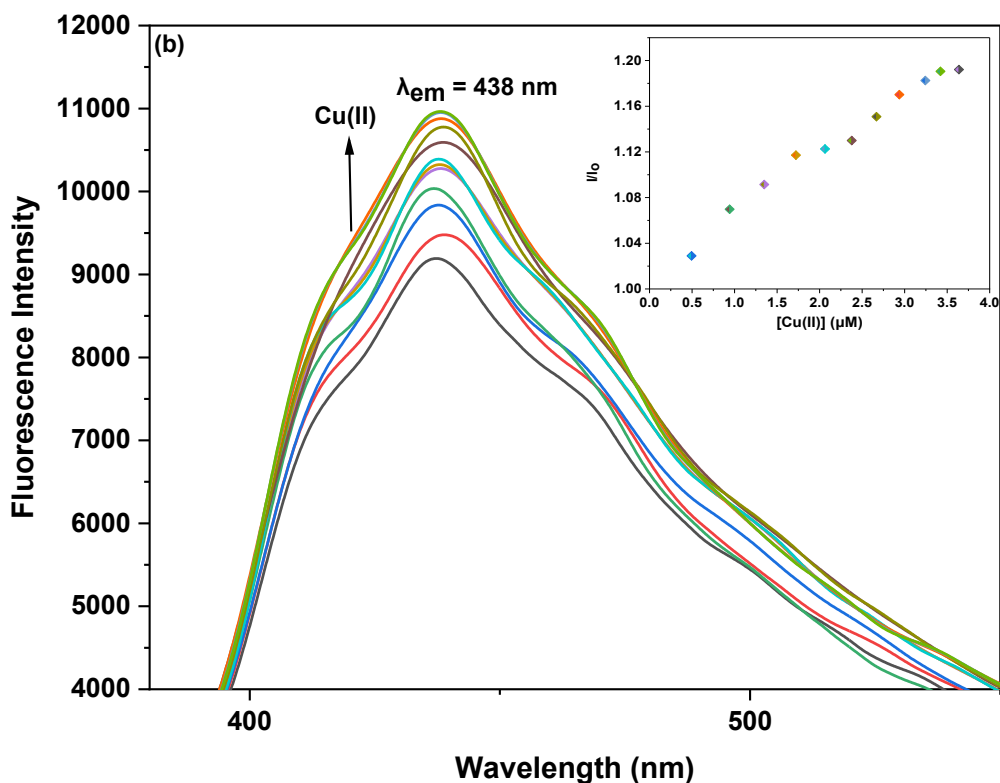
Figure 4.58: Changes in the emission of the probe **158** with the gradual addition of (a) Co(II) and (b) Cu(II) ions in a THF: H_2O (4:1) mixture. The inset shows the relative emission change of probe **158** as a function of metal ion concentration (μM).
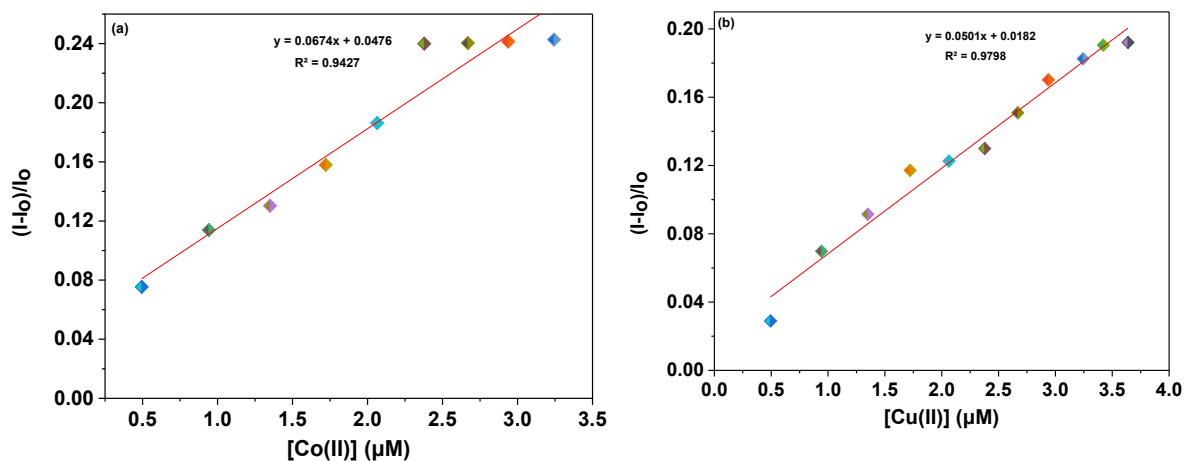
Figure 4.59: Correlation plot of probe **158** illustrating $(I-I_n)/I_o$ vs. (a) [Co(II)] and (b) [Cu(II)]

4.11.16. Competitive metal ion interaction analysis of probe 158

The selectivity of probe **158** was further assessed in the presence of all metal ions simultaneously, prepared in an equimolar ratio. A single solution containing an equimolar mixture of various metal ions was titrated with each probe, and the resulting UV-Vis spectra were analyzed **(figure 4.60)**. It was observed that the spectra obtained during these titrations

closely matched those recorded when Co(II) was used alone with the probe. This finding indicates that the probe selectively recognized Co(II) even in the presence of other competing metal ions. These results conclusively demonstrate that the probe exhibit high selectivity for Co(II), with no interference from other metal ions, thereby confirming their robust chemosensing properties.
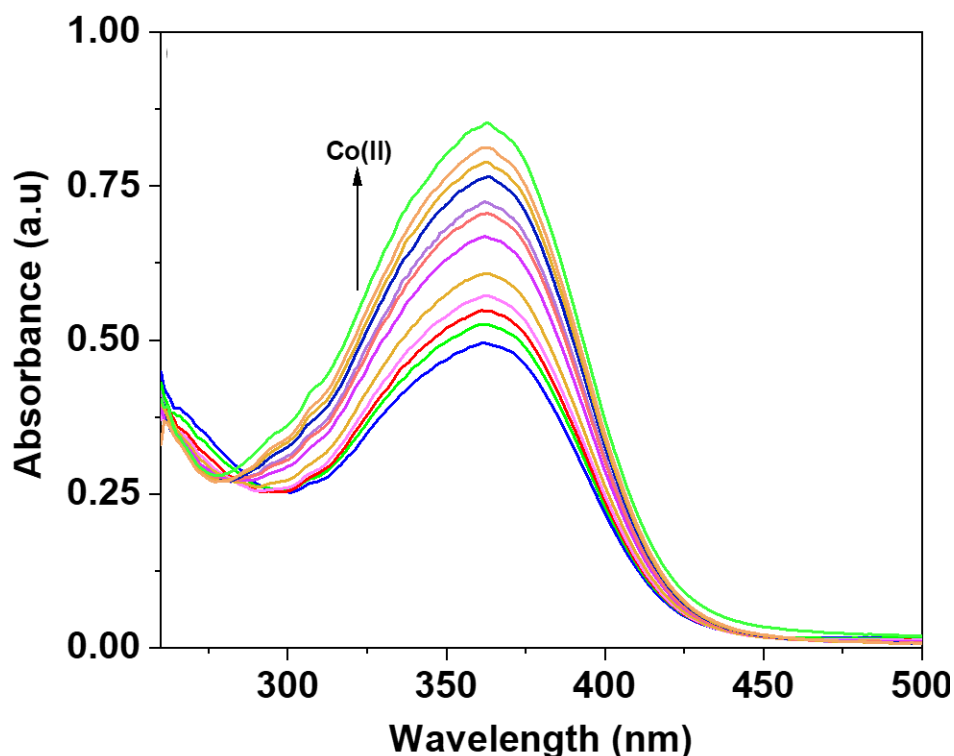
Figure 4.60: UV-Vis spectrum of probe **158** in THF: H$_2$O (4:1), highlighting the selective detection of Co(II) among various metal ions at equimolar concentrations

4.11.17. Time dependence analysis of probe-metal ion complexation for 158

The time-dependent behavior of the metal-bound probe **158** was systematically evaluated to gain valuable insights into its stability and sensitivity toward metal ions. Absorption spectroscopy was utilized as the analytical tool to monitor the effect of time on the metal-bound probe's performance and integrity. The results, illustrated in **figure 4.61 (a) and (b),** reveal that the absorbance of Co(II) and Cu(II)-complexed solutions of probe **158** remained stable and consistent, with no significant variations observed even after extended periods of standing. These findings demonstrate that probe **158** exhibits excellent stability in its metal-bound form and maintains a strong and robust affinity for Co(II) and Cu(II) ions over time. This high level of stability highlights its potential for reliable and long-term applications in metal ion detection and chemosensing, ensuring consistent performance without degradation.
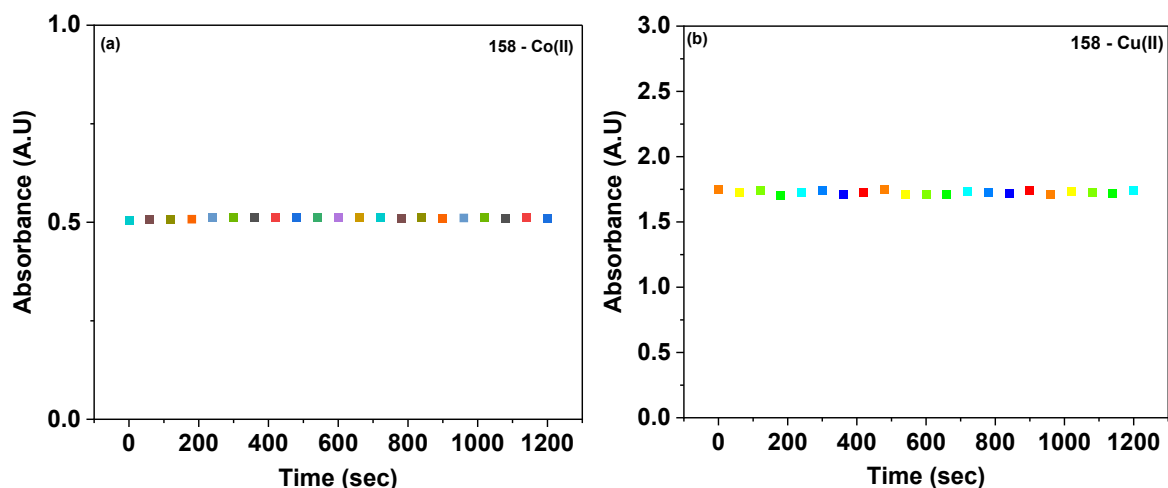
Figure 4.61: The time-dependent absorption spectrum of (a) probe **158**-Co(II) and (b) probe **158**-Cu(II) complex solution demonstrating a consistent absorbance over time

4.11.18. Temperature dependence analysis of probe-metal ion complexation for probe 158

The influence of temperature on the binding efficiency of probe **158** was investigated by recording the absorption spectra of their metal-bound complexes at 2 °C intervals over a temperature range of 20 °C to 50 °C. As illustrated in the accompanying **figure 4.62 (a) and (b)**, no significant changes were observed in the binding behaviour of the probe across the tested temperatures. These results highlight the thermal stability and robustness of the interactions between the probe and the metal ions, demonstrating their consistent performance under varying thermal conditions.
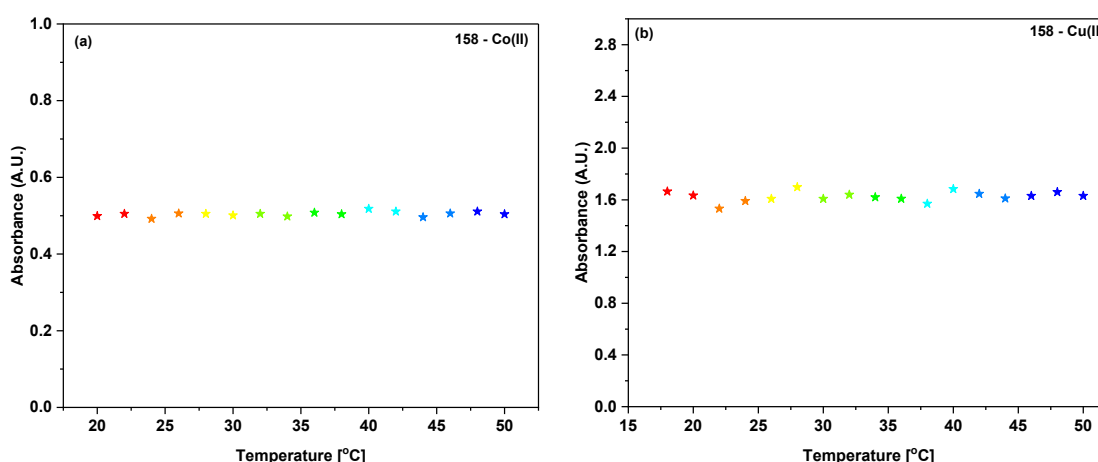
Figure 4.62: Variation in maximum absorbance of (a) probe **158**-Co(II) complex and (b) probe **158**-Cu(II) complex showing minimal variation in absorbance across a range of temperatures.

Table 4.6: A comprehensive summary of the LoD, LoQ, association constant (K_a), and stoichiometric ratio for probe **156, 157, 158**

Probe	Metal ion	UV-Visible λ_{max}	Type of shift	Fluorescence λ_{em}	Type of shift	LoD (µM)	LoQ (µM)	Association Constant (K_a)	Binding Ratio
156	Co(II)	311	Hyperchromic	445	Fluorescence enhancement	1.64	5.46	8.80×10^3 M^{-1}	
	Cu(II)					3.19	10.64	5.99×10^3 M^{-1}	
157	Co(II)	317	Hypochromic	442	Fluorescence enhancement	2.08	6.94	7.66×10^3 M^{-1}	1:1
	Cu(II)		Hyperchromic			2.30	7.68	4.74×10^3 M^{-1}	
158	Co(II)	362	Hyperchromic	438	Fluorescence enhancement	1.81	6.04	6.61×10^3 M^{-1}	
	Cu(II)					1.17	3.92	1.00×10^4 M^{-1}	

The **table 4.6** provides insight into the influence of positional isomerism (ortho, meta, and para) of the chalcone based 1,2,3-triazole moiety in probes **156, 157, and 158** on their binding properties, wherein all the three probes sensed Co(II) and Cu(II). For probe **156**, the ortho configuration exhibited moderate sensitivity and binding affinity for both Co(II) and Cu(II), suggesting that steric hindrance in the ortho position might partially restrict optimal binding interactions. Also, the probe **156** (ortho configuration) exhibited two peaks at 311 nm and 425 nm due to the influence of its structural arrangement. The ortho positioning of the 1,2,3-triazole moiety can lead to enhanced electronic interactions between the 1,2,3-triazole and adjacent groups in the molecule. These interactions can create distinct electronic transitions, likely involving both π-π* and n-π* transitions, resulting in two observable absorption peaks. In contrast, probes **157** (meta) and **158** (para) showed only a single peak, as their configurations provide a more symmetric environment.

Probe **157**, the meta isomer showed slightly reduced sensitivity, with higher LoD values for both metal ions. This trend suggests that the meta-arrangement may result in a less favorable spatial orientation for strong metal coordination. Probe **158,** the para configuration demonstrated superior performance, particularly for Cu(II) detection, with the lowest LoD (1.17 μM) and the highest association constant (1.00×10^4 M^{-1}). The enhanced binding affinity and sensitivity can be attributed to the para-arrangement, which likely provides an optimal spatial arrangement for metal ion coordination.

The enhanced fluorescence emission observed in all six probes **(146, 147, 148, 156, 157, and 158)** upon metal ion addition is attributed to the photoinduced electron transfer (PET) mechanism. In the metal-free state, the lone pairs of electrons on the nitrogen atoms within the 1,2,3-triazole moiety are likely involved in PET, facilitated by their proximity to the benzyl groups. This PET activity introduces a non-radiative de-excitation pathway, effectively quenching the fluorescence emission.

However, upon coordination of metal ions to the nitrogen atoms of the 1,2,3-triazole group, a notable structural reorganization occurs. The benzyl groups are displaced from their proximity to the 1,2,3-triazole structure, as illustrated in **figure 4.63**. This displacement disrupts the PET mechanism by restricting the involvement of the nitrogen lone pairs in electron transfer, thereby favoring radiative pathways. Consequently, the fluorescence emission is significantly enhanced, showcasing the role of metal ion coordination in modulating the photophysical properties of these probes.[19]
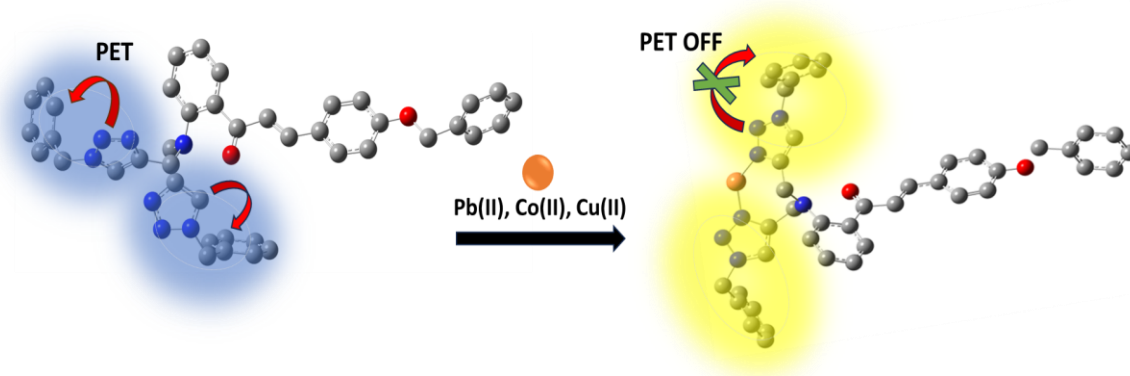
Figure 4.63: A representative picture depicting the PET mechanism of probe on binding with metal ions

4.11.19. Plausible mode of interaction

According to the Hard and Soft Acids and Bases (HSAB) theory, Co(II) is categorized as a borderline acid, while Cu(II) is classified as a weak acid. Both metal ions can form coordination bonds with donor atoms, such as nitrogen, oxygen, and sulfur, which possess lone electron pairs. The binding affinity of probes **156, 157, and 158** for electron-deficient metal ions is predominantly attributed to the presence of lone electron pairs on the nitrogen atoms within the 1,2,3-triazole moiety integrated into their molecular frameworks. This functional group provides an electron-rich site, enabling effective coordination with metal ions. Job's plot analyses confirmed the formation of 1:1 metal-ligand complexes for all three probes with both Co(II) and Cu(II), offering a deeper understanding of their coordination mechanisms. As depicted in **figure 4.64**, the proposed binding model reveals that the probes interact with the metal ions through the nitrogen atoms of the 1,2,3-triazole rings. This interaction results in a claw-like structural conformation, which efficiently encapsulates the metal ion. This structural arrangement underscores the role of the 1,2,3-triazole moiety in facilitating selective and stable metal ion coordination. The binding site for Co(II) and Cu(II) ions in probes **156, 157, and 158** demonstrates a significant degree of consistency with the binding sites observed for Pb(II) and Cu(II) ions in previously studied probes **146, 147, 148**. This similarity is due to the preserved structural integrity of the 1,2,3-triazole moiety, which remains a central feature in the design of these probes. The conserved structural framework of the 1,2,3-triazole moiety ensures that its binding properties remain unchanged across various probes, irrespective of slight modifications in other parts of the probe structure.
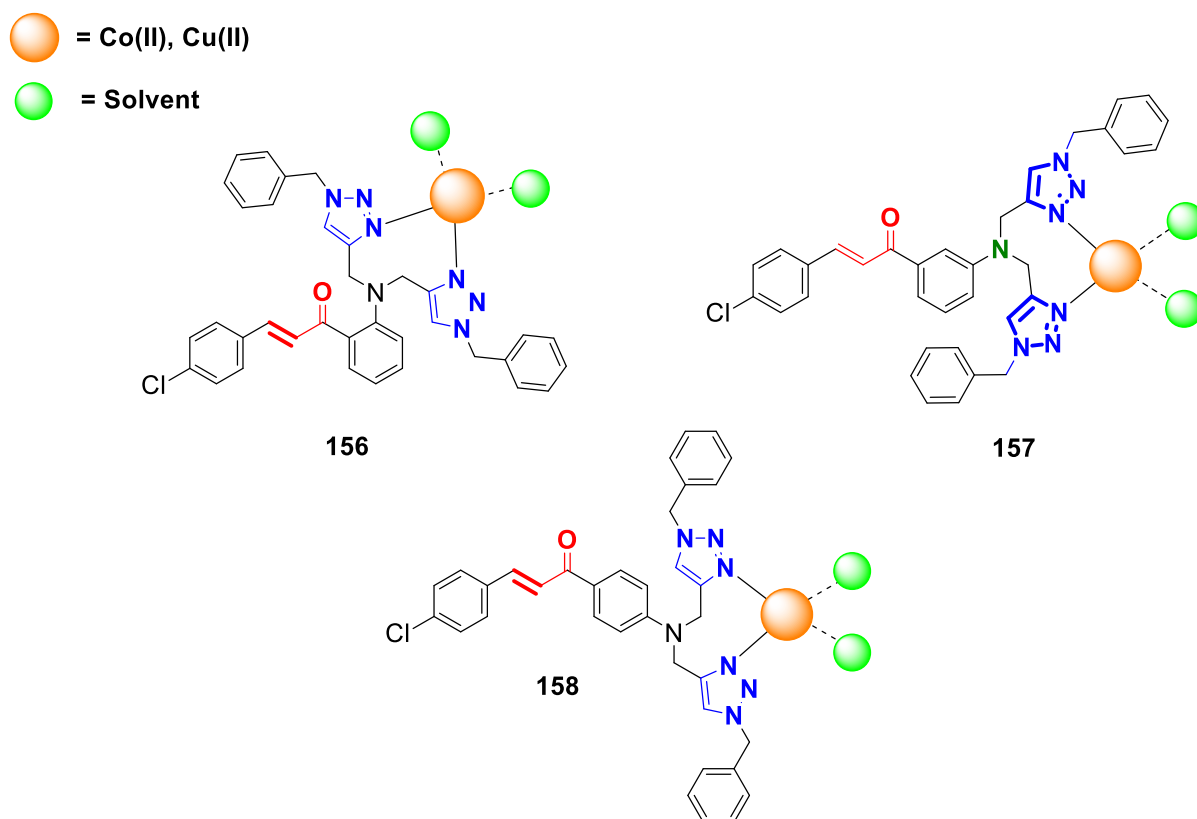
Figure 4.64: Plausible binding mode of probe **156**, **157**, and **158** with Co(II)/Cu(II)

4.12. Conclusion

In this section, chalcone-based 1,2,3-triazole-tethered frameworks are highlighted as pivotal structural motifs in chemosensing due to their facile synthesis and pronounced selectivity for specific analytes. These compounds were developed as selective recognition agents for various ecologically and physiologically relevant metal ions. The molecular design incorporated chalcone as a core scaffold, chosen for its labile protons and aromatic framework, which was subsequently functionalized via nucleophilic substitution with propargyl groups to introduce terminal alkynes. These alkynes underwent CuAAC reactions to yield 1,2,3-triazole derivatives equipped with chromogenic and fluorogenic units. These functional groups enhanced the optical properties of the derivatives, enabling precise absorption and emission measurements upon metal ion binding to evaluate their selective recognition behaviour.

The sensing selectivity was observed to vary with changes in the structural configuration of the probes, which influenced the size and flexibility of the receptor cavity and, consequently, the specificity for different metal ions. The stability and robustness of the probe-metal ion complexes were assessed through absorption studies conducted over extended

durations and across varying temperature ranges. Quantitative analysis of the interactions was performed, including the determination of critical parameters such as the limit of detection (LoD), limit of quantification (LoQ), association constant (K_a), and the stoichiometric ratio of probe-metal ion complexation. This systematic evaluation underscored the potential of these chalcone-triazole ensembles as reliable and selective chemosensors for targeted metal ion detection.

Variations in the substitution pattern of the benzoyl unit—ortho, meta, and para—were systematically evaluated to understand their impact on sensing efficiency. Despite these positional changes, the probes retained consistent recognition capabilities for target metal ions. This consistency can be attributed to the preservation of the triazole ring's nitrogen atoms as the primary binding site, maintaining an effective interaction with the analytes. However, subtle differences were observed in LoD, LoQ, and binding constant values, reflecting the influence of steric and electronic factors associated with the substituent's position. The para configuration showed slightly enhanced binding affinity due to reduced steric hindrance, while the ortho and meta derivatives exhibited comparable yet distinct behaviors. These findings emphasize the importance of molecular design in optimizing probe performance and demonstrate the potential of these chalcone-triazole scaffolds as adaptable and efficient platforms for selective metal ion sensing.

References

1. W. Feng, L. Li, C. Yang, A. Welle, O. Trapp and P. A. Levkin, *Angew. Chem.*, 2015, **127**, 8856–8859.

2. R. A. Pratiwi and A. B. D. Nandiyanto, *Indones. J. Edu. Res. Tech.*, 2022, **2**, 1–20.

3. W. Mäntele and E. Deniz, *Spectrochim. Acta A Mol. Biomol. Spectrosc.*, 2017, **173**, 965–968.

4. L. H. Nurani, C. A. Edityaningrum, I. Irnawati, A. R. Putri, A. Windarsih, A. Guntarti and A. Rohman, *Indones. J. Chem.*, 2023, **23**, 542–567.

5. K. Gupta, P. Joshi, R. Gusain and O. P. Khatri, *Coord. Chem. Rev.*, 2021, **445**, 214100.

6. R. Joseph, *ACS Omega*, 2020, **5**, 6215–6220.

7. M. Bal, M. Tümer and M. Köse, *J. Fluoresc.*, 2022, **32**, 2237–2256.

8. F. Caroleo, G. Magna, M. L. Naitana, L. Di Zazzo, R. Martini, F. Pizzoli, M. Muduganti, L. Lvova, F. Mandoj, S. Nardis, M. Stefanelli, C. Di Natale and R. Paolesse, *Sensors*, 2022, **22**, 2649.

9. J. Baranwal, B. Barse, G. Gatto, G. Broncova and A. Kumar, *Chemosensors*, 2022, **10**, 363.

10. N. Bereli, D. Çimen, H. Yavuz and A. Denizli, 2021, pp. 1–21.

11. G. Das, B. Garai, T. Prakasam, F. Benyettou, S. Varghese, S. K. Sharma, F. Gándara, R. Pasricha, M. Baias, R. Jagannathan, N. Saleh, M. Elhabiri, M. A. Olson and A. Trabolsi, *Nat. Commun.*, 2022, **13**, 3904.

12. C. Guo, A. C. Sedgwick, T. Hirao and J. L. Sessler, *Coord. Chem. Rev.*, 2021, **427**, 213560.

13. V. Kumar, H. Kim, B. Pandey, T. D. James, J. Yoon and E. V. Anslyn, *Chem. Soc. Rev.*, 2023, **52**, 663–704.

14. H. Niu, J. Liu, H. M. O'Connor, T. Gunnlaugsson, T. D. James and H. Zhang, *Chem. Soc. Rev.*, 2023, **52**, 2322–2357.

15. B. Rathinam, C.-C. Chien, B.-C. Chen and J.-H. Liu, *Tetrahedron*, 2013, **69**, 235–241.

16. M. H. Penner, in *Food Analysis*, ed. S. S. Nielsen, Springer International Publishing, Cham, 2017, pp. 89–106.

17. F. Ahmed and H. Xiong, *Dyes Pig.*, 2021, **185**, 108905.

18. A. Ramdass, V. Sathish, E. Babu, M. Velayudham, P. Thanasekaran and S. Rajagopal, *Coord. Chem. Rev.*, 2017, **343**, 278–307.

19. A. Ganguly, S. Ghosh, S. Kar and N. Guchhait, *Spectrochim. Acta A: Mol. Biomol. Spectrosc.*, 2015, **143**, 72–80.

Summary

This chapter provides a concise summary of the entire thesis, presenting an overview of the methodology, experimental findings and key outcomes.

This thesis presents the synthesis of chalcone based 1,2,3-triazole derivatives, accompanied by their characterization through an array of spectroscopic techniques, with an emphasis on their applications in chemosensing for the selective detection of metal ions via UV-Visible and fluorescence spectroscopy. The research is systematically organized into four sections: Chapter I provides an **introduction** to the context of the study, Chapter II is the **review of literature,** Chapter III details the **synthesis and characterization,** and chapter IV presents the **results and discussion.**

Chapter I: Introduction

This chapter of the thesis serves as a comprehensive introduction to the key concepts underlying the research on chalcone-based 1,2,3-triazole derivatives. The chapter begins by exploring the revolution of organic chemistry towards the heterocyclic compounds and their classification, emphasizing the critical role of heterocycles in various biological, pharmaceutical, and materials science applications. The subsequent subsection detailed about, click chemistry, a revolutionary approach introduced by Sir Karl Barry Sharpless. This methodology focuses on highly efficient and selective reactions that yield specific products with minimal byproducts. Click chemistry is particularly relevant for its modular nature, allowing for the easy assembly of complex molecular architectures from simpler building blocks. CuAAC facilitates the formation of 1,4-disubstituted 1,2,3-triazoles through the cycloaddition of terminal alkynes and azides in the presence of a copper (I)-catalyst **(figure S1)**. A detailed mechanistic analysis of CuAAC is presented, discussing both mononuclear and binuclear pathways. The chapter further explores the applications of 1,2,3-triazoles, focusing on their strong coordination capabilities with various metal ions due to the presence of nitrogen heteroatoms in the ring. This property makes them suitable as chemosensors for detecting toxic heavy metal ions, addressing the pressing issue of environmental contamination. Finally, the chapter briefly discusses UV-Visible and fluorescence spectroscopy, emphasizing their applications in evaluating the chemosensing capabilities of chalcone based 1,2,3-triazoles.
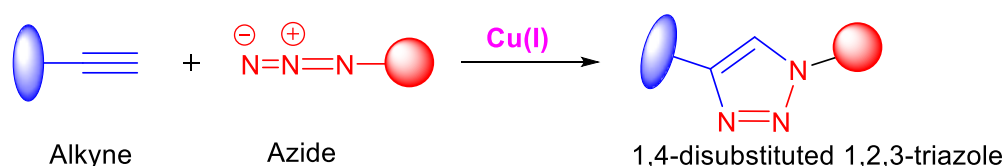
Figure S1: A schematic representation of synthesis of 1,4-disubstituted 1,2,3-triazole via CuAAC reaction

Chapter II: Review of Literature

The first section of this chapter describes about the Click Chemistry, its potential applications in polymer science, drug delivery, bioconjugation, cell biology, proteomics, pharmaceutical science, material science and environmental chemistry. Among various notable click reactions, Cu(I) catalyzed alkyne azide cycloaddition reaction have gained popularity due to its key features of modularity, wide scope, high yields, stereospecific nature. The subsequent section highlights CuAAC reaction for the synthesis of 1,2,3 triazole derivatives with complete conversion and exceptional purity. The literature presents numerous methodologies for synthesizing 1,4-disubstituted 1,2,3-triazole derivatives utilizing various structural frameworks, including Schiff bases, chalcones, dendrimers, polymers, and other organic derivatives, to achieve diverse functional properties. Among these frameworks, the chalcone scaffold stands out due to its ease of modification, strong π-conjugation, and intrinsic ability to improve interactions with metal ions. These properties make chalcones particularly well-suited for the design of highly sensitive and selective chalcone-based 1,2,3-triazole metal ion sensors. In the next section the literature about the synthesis of chalcone based 1,2,3-triazole derivatives is discussed and divided into four subsections:

➢ Synthesis of chalcone
➢ Synthesis of chalcone based terminal alkyne
➢ Synthesis of organic azide
➢ Synthesis of chalcone based 1,2,3 triazole

Firstly, the synthesis of chalcone from various methodologies is described such as, carbonylated heck coupling reaction, Sonogashira isomerization coupling, solid acid catalyst mediated reaction, Claisen-Schmidt reaction etc. Similarly, various chemical strategies for synthesizing terminal alkynes are outlined, highlighting the diverse reactants and reaction conditions employed in each synthetic route, such as α,β-eliminations, carbene rearrangement, the use of Ohira–Bestmann reagent, and chalcone-based alkynes. The following section explores the different synthetic strategies used for creating both aliphatic and aromatic organic azides. It then presents an overview of the [3+2] cycloaddition reaction between organic azides and terminal alkynes to produce 1,4-disubstituted 1,2,3-triazoles, utilizing various Cu(I) catalytic systems and solvent conditions. Several studies highlight the direct application of Cu(I) salts as catalysts, as well as multicomponent systems where Cu(I) is generated from Cu(II) salts. Consequently, this study utilizes the [CuBr(PPh3)3] complex as a Cu(I) catalyst to synthesize new 1,2,3-triazole derivatives.

The next section provides a concise overview of several spectroscopic methods, including IR, NMR, and mass spectrometry, that are employed to characterize the synthesized molecules. Lastly, the chapter details about the applications of 1,2,3-triazole derivatives, with a particular focus on their use in chemosensing. In conclusion, the literature review on 1,2,3-triazoles as ion sensors emphasizes their promising potential in developing highly selective and sensitive ion detection systems. These sensors are capable of accurately detecting a wide range of metal ions across diverse solvent environments.

Chapter III: Synthesis and characterisation

This chapter outlines the complete experimental work performed to achieve the research objectives, including the synthesis and characterization of novel chalcone based 1,2,3-triazole derivatives. It begins with a thorough overview of the general synthetic procedures used to synthesize chalcones, chalcone based terminal alkynes, organic azide, and chalcone-based 1,2,3-triazole derivatives. Following this, the chapter presents the actual experimental method for synthesizing organic azide (benzyl azide) **(figure S2)**, along with analytical data, including yields, physical descriptions (color/texture), and IR and NMR (^{1}H, ^{13}C) characterizations. In the next subsection, the synthesis of chalcone is presented **(figure S3)** and the synthesis of novel chalcone based terminal alkynes from initial substrates (chalcone) is then described **(figure S4)**. For each synthesis, the experimental conditions, yields, color, and melting points are detailed. Additionally, IR and NMR data for each alkyne are provided to confirm successful synthesis.

The Cu(I)-catalyzed 3+2 cycloaddition reaction was used for the synthesis of chalcone based 1,2,3-triazole derivatives **(figure S5)**, which is presented in the subsequent section after the synthesis of chalcone based alkynes, including all required experimental conditions. Each 1,2,3-triazole derivative was evaluated for product yield, colour/texture, melting point, IR, NMR (^{1}H and ^{13}C), mass spectrum for the successful confirmation, with data presented immediately after the reaction schemes. Appendix A outlines the material, procedures, and instrumentation used in the analysis of the synthesized compounds, while the appendices B, C, and D contains IR, NMR and mass spectra, respectively.

Chapter IV: Results and Discussion

This chapter presents a comprehensive analysis and interpretation of the data obtained from spectroscopic techniques, providing an in-depth discussion on the successful synthesis of chalcones, chalcone based terminal alkynes, organic azides and chalcone based 1,2,3-triazole

derivatives. additionally, the chapter elaborated on the UV-Visible and fluorescence studies conducted to evaluate the chemosensory potential of the synthesized chalcone based 1,2,3-triazole compounds, specifically their ability to detect metal ions. This chapter is structured into two sections based on the nature of the spectral data: Part A focuses on IR, NMR, and mass spectroscopic analysis, confirming the successful synthesis of the target compounds, while Part B details the UV-Visible and fluorescence studies, highlighting the selective ion recognition capabilities of the synthesized probes.

Part A

Benzyl chloride (134) was converted to benzyl azide **(135)** by stirring with sodium azide in DMF at 85–90 °C. The resulting product was oily at room temperature, and its structure was confirmed using infrared (IR) and nuclear magnetic resonance (NMR) spectroscopy. In the IR spectrum (recorded neat within the 4000–450 cm^{-1} range), a characteristic absorption peak for the azide group (-N$_3$) was observed at 2089 cm^{-1}, along with other peaks consistent with the expected azide structure. The benzyl azide was further characterized by ^{1}H NMR spectroscopy at 500 MHz in CDCl$_3$, showing a singlet at δ = 4.14 ppm corresponding to the methylene (-CH$_2$) group attached to the azide functionality. Peaks in the range δ = 7.22–7.14 ppm were attributed to aromatic protons. Similarly, the ^{13}C NMR spectrum aligned well with the predicted structure. Signals from aromatic carbons appeared in the range δ = 135.53–127.78 ppm, while the methylene carbon of the azide group was observed at δ = 54.82 ppm.

135
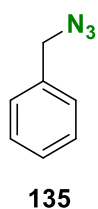
Figure S2: Representation of the synthesized organic azide (benzyl azide)

Chalcones were synthesized by reacting 4-benzyloxybenzaldehyde and 4-chlorobenzaldehyde with o-, m-, and p-aminoacetophenone, respectively. The reactions were carried out in the presence of potassium hydroxide, which acted as a base to deprotonate the α-carbon of aminoacetophenone, forming an enolate ion. The resulting chalcones were obtained as solid products. A signal at 3461 - 3295 cm^{-1} corresponded to N-H stretching of NH$_2$ group. the ^{1}H NMR spectrum exhibited a singlet at δ = 6.67 – 2.64 ppm corresponding to the NH$_2$ protons. The doublet at δ = 8.84 - 7.84 ppm was assigned to alkenyl proton of the C=C attached

to the benzene ring. The aromatic protons were attributable to the multiplet in the range of δ = 7.91 - 6.67 ppm. The ¹³C NMR spectrum further supported the ¹H NMR findings, the peaks at δ = 123.61 – 120.22 ppm and 144.32 – 138.18 ppm corresponding to the alkenyl carbons (C=C). The aromatic carbons are attributable in the range of δ = 160.77 – 113.81 ppm. The peak at δ = 191.69 – 187.76 ppm was attributable to the carbonyl carbon.
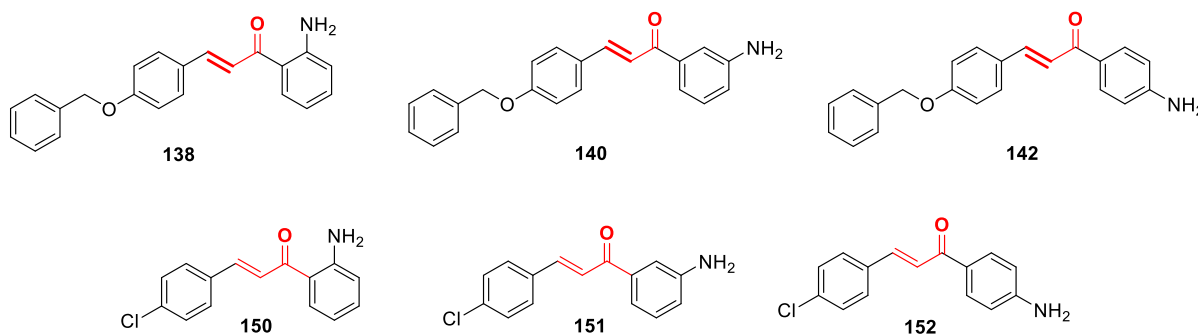
Figure S3: Representation of all the synthesized chalcones

To synthesize terminal alkynes, 1 mmol of a starting material containing labile proton(s) was reacted with 1.30 mmol of an 80% propargyl bromide solution in toluene and an appropriate base. The reaction, conducted at room temperature in DMF, involved stirring the mixture with the base, which facilitated the extraction of the labile proton(s) from the starting material and their replacement with propynyl group(s) via a nucleophilic substitution mechanism. The reaction time varied depending on the substrate's propensity to lose a proton. The formation of the desired alkynes was confirmed by comparing their IR spectra (4000–450 cm⁻¹) with those of the starting materials.
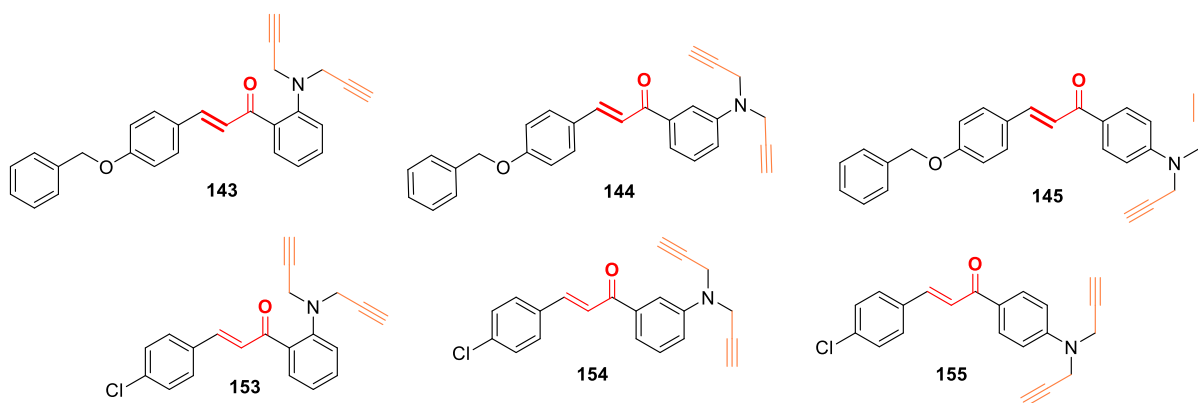
Figure S4: Representation of all the synthesized chalcone-based terminal alkynes

The characteristic -C≡C-H stretch was observed at approximately 3324–3279 cm⁻¹, while the -C≡C stretch appeared at around 2111–2116 cm⁻¹. ¹H NMR spectra further validated the synthesis, showing a peak for the alkyne proton (≡C-H) at δ = 2.28–2.23 ppm and a peak for methylene protons attached to nitrogen (N-CH₂) at δ = 4.57–4.18 ppm. Peaks corresponding to aromatic protons were observed between δ = 7.98–6.67 ppm. In the ¹³C NMR spectra, signals attributed to the C≡C carbons appeared at δ = 73.03–71.31 ppm, confirming the successful synthesis of the alkyne.

To synthesize the 1,2,3-triazole-derived chemosensor probes, the precursor alkynes underwent [3+2] cycloaddition with organic azides using [CuBr(PPh₃)₃] as the catalyst in a THF:TEA solvent mixture (v/v, 1:1). Characterization by IR, NMR, and mass spectrometry confirmed the successful cycloaddition process. In the IR spectra, a strong absorption peak observed at 2089 cm⁻¹ for azides and in the range of 2111–2116 cm⁻¹ for terminal alkynes disappeared completely in the products, indicating full cyclization of the precursors. NMR analysis further validated this, with the disappearance of the alkyne proton signal at δ = 2.28–2.23 ppm in the 1H NMR spectrum, confirming the formation of 1,2,3-triazole derivatives.
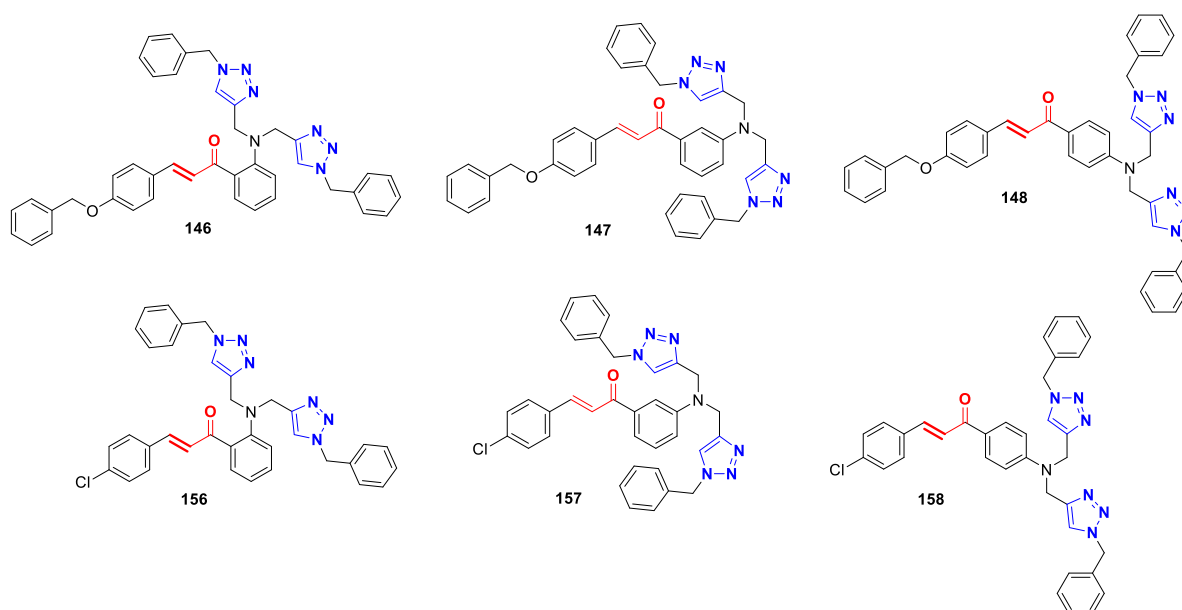
Figure S5: Representation of all the synthesized chalcone-based 1,2,3-triazole derivative

Additionally, the methylene (-CH₂) protons in the alkyne molecules showed a downfield shift to δ = 4.57–4.18 ppm, reflecting the deshielding effect from the newly formed triazole ring. In the ¹³C NMR spectra, the signals at δ = 73.03–71.31 ppm, attributed to the terminal alkyne carbons, were absent in the spectra of the triazole derivatives, further indicating successful ring formation. Mass spectrometry data corroborated these findings, with the

observed molecular ions matching the expected structures of the 1,2,3-triazole compounds, confirming their synthesis via the CuAAC reaction.

Part B

To evaluate the ion-sensing properties of the synthesized 1,2,3-triazole derivatives, their photophysical characteristics were systematically studied using UV-Vis and fluorescence spectroscopy, as detailed in Part B of Chapter IV. The presence of 1,2,3-triazole moieties in their structure, featuring nitrogen atoms as optimal coordination sites for specific metal ions, makes these derivatives promising candidates for ion recognition. Accordingly, their sensing capabilities were assessed through UV-Vis and/or fluorescence titrations performed with selected metal ions.

The interactions of probe **146** with Pb(II) and Cu(II) ions were analyzed using UV-Vis and fluorescence spectroscopy. UV-Vis titration with 1 mM metal ion solutions revealed hypochromic shifts at 340 nm and 414 nm and a hyperchromic shift at 269 nm for Pb(II), forming an isosbestic point at 293 nm. For Cu(II), a hypochromic shift at 414 nm, a new peak at 284 nm, and an isosbestic point at 337 nm were observed **(figure S6)**. Job's plot confirmed a 1:1 binding ratio for both ions. In fluorescence studies, excitation at 350 nm resulted in a strong emission peak at 438 nm with a shoulder peak at 412 nm. Titration with Pb(II) and Cu(II) ions enhanced fluorescence intensity as their concentrations increased to 15 equivalents (probe concentration: 30 µM) **(figure S7)**. The K_a values for probe for Pb(II) and Cu(II) ions were 6.18×10^3 M^{-1} and 7.57×10^3. The LoD values were 5.69 µM for Pb(II) and 6.55 µM for Cu(II), with LoQ values of 18.97 µM and 21.85 µM, respectively.
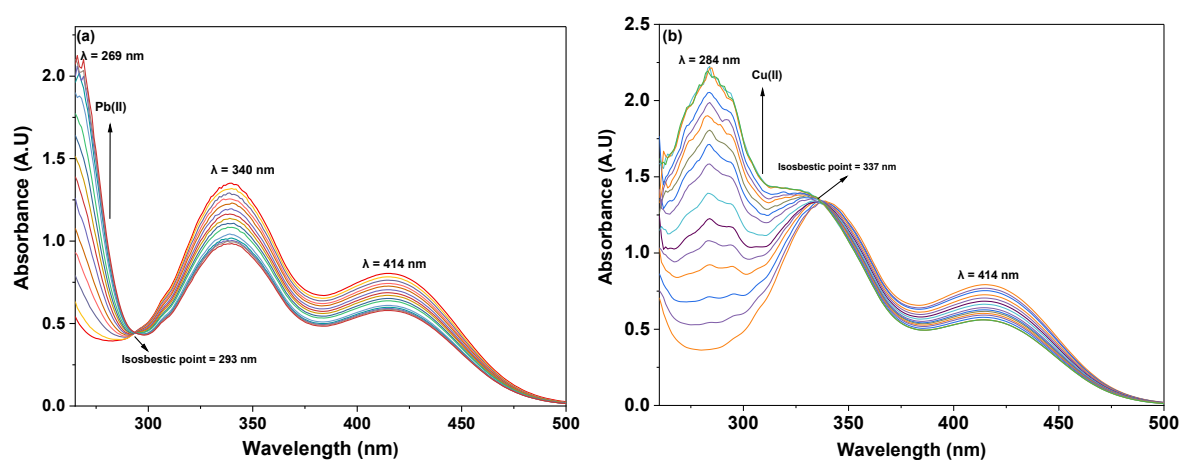
Figure S6: Shifts in absorption maxima of probe **146** on titration with (a) Pb(II) (b) Cu(II) in DMSO
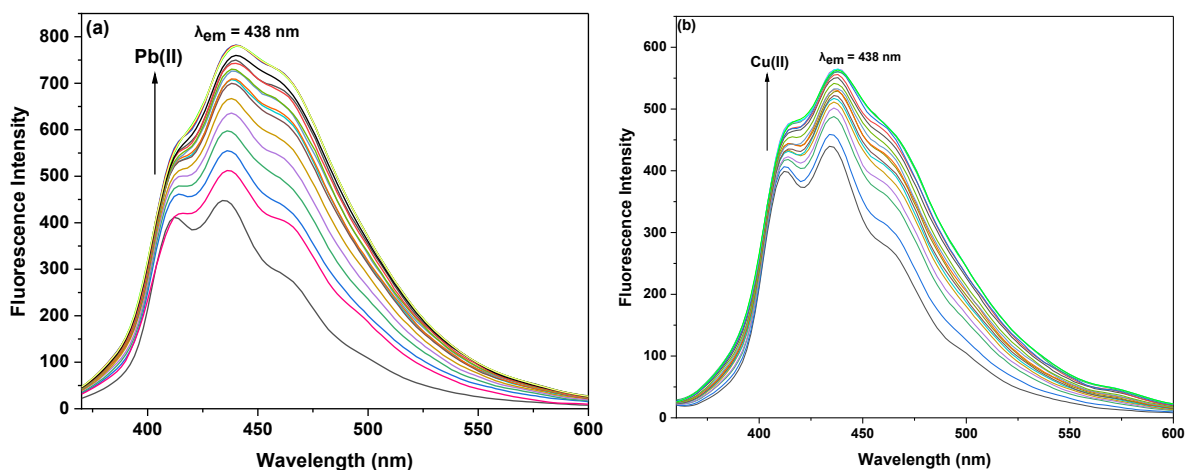
Figure S7: Incremental increase in the fluorescence emission of probe **146** on titration with (a) Pb(II) (b) Cu(II) in DMSO

For probe **147,** Upon the gradual addition of Pb(II), the absorption peak at 348 nm showed a hypochromic shift, while a shoulder at 264 nm underwent a pronounced hyperchromic shift, forming an isosbestic point at 283 nm. For Cu(II), incremental addition caused a blue shift of ~6 nm (348 nm to 342 nm) with a hypochromic effect and significant hyperchromic broadening at 270 nm, leading to an isosbestic point at 320 nm **(figure S8)**. Job's plot confirmed a 1:1 binding ratio for both ions. In fluorescence studies, probe **147,** upon excitation at 340 nm, exhibited a prominent emission peak at 437 nm with a minor shoulder at 413 nm. Fluorescence intensity significantly increased with the addition of Pb(II) and Cu(II) ions (probe concentration: 30 μM) **(figure S9)**. The Benesi-Hildebrand plots for probe with Pb(II) and Cu(II), yielding K_a values of 2.18×10^3 M^{-1} and 2.35×10^3 M^{-1}, respectively. The LoD values for Pb(II) and Cu(II) were 3.64 μM and 1.37 μM, with LoQ values of 12.15 μM and 4.58 μM, respectively.

Figure S8: Shifts in absorption maxima of probe **147** on titration with (a) Pb(II) (b) Cu(II) in DMSO

Figure S9: Incremental increase in the fluorescence emission of probe **147** on titration with (a) Pb(II) (b) Cu(II) in DMSO

The incremental addition of Pb(II) ions to probe **148** caused a hypochromic shift at 368 nm (n→π* transitions) and a hyperchromic shift at 268 nm (π→π* transitions), forming an isosbestic point at 298 nm. For Cu(II), a hypochromic shift at 368 nm and a hyperchromic, hypsochromic shift to 284 nm were observed, with an isosbestic point at 347 nm, confirming selective sensing and ratiometric responses **(figure S10)**. Fluorescence studies (λ_{ex} = 370 nm) showed a strong emission peak at 436 nm with a shoulder at 412 nm. Emission intensity increased with the addition of Pb(II) or Cu(II) ions (probe concentration: 30 μM; metal ion: up to 15 equivalents) **(figure S11)**. Benesi-Hildebrand plots provided K_a values of 8.54×10^3 M^{-1} for Pb(II) and 9.37×10^3 M^{-1} for Cu(II), with a 1:1 binding ratio confirmed by Job's plot. LoD values were 5.06 μM for Pb(II) and 7.52 μM for Cu(II), with LoQ values of 16.89 μM and 25.08 μM, respectively.
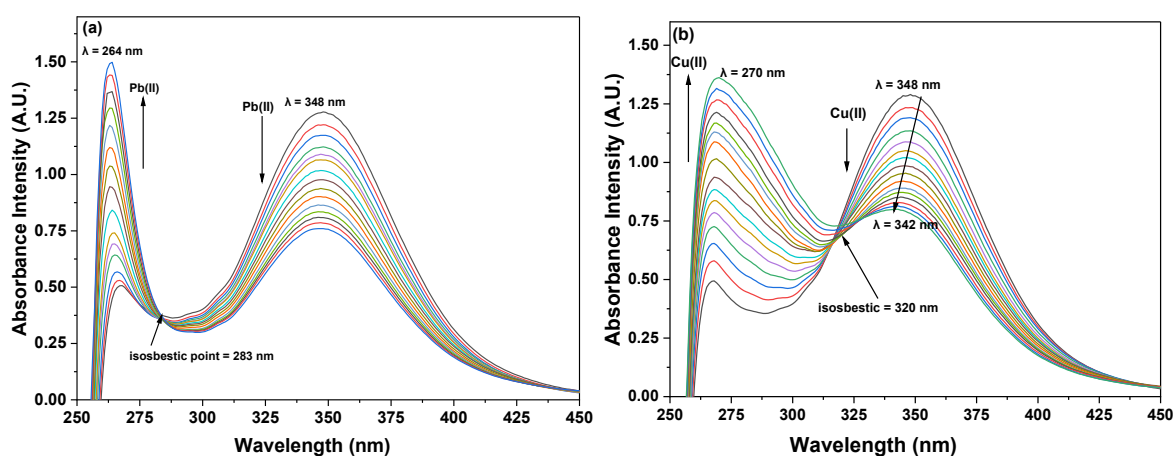

Figure S10: Shifts in absorption maxima of probe **148** on titration with (a) Pb(II) (b) Cu(II) in DMSO

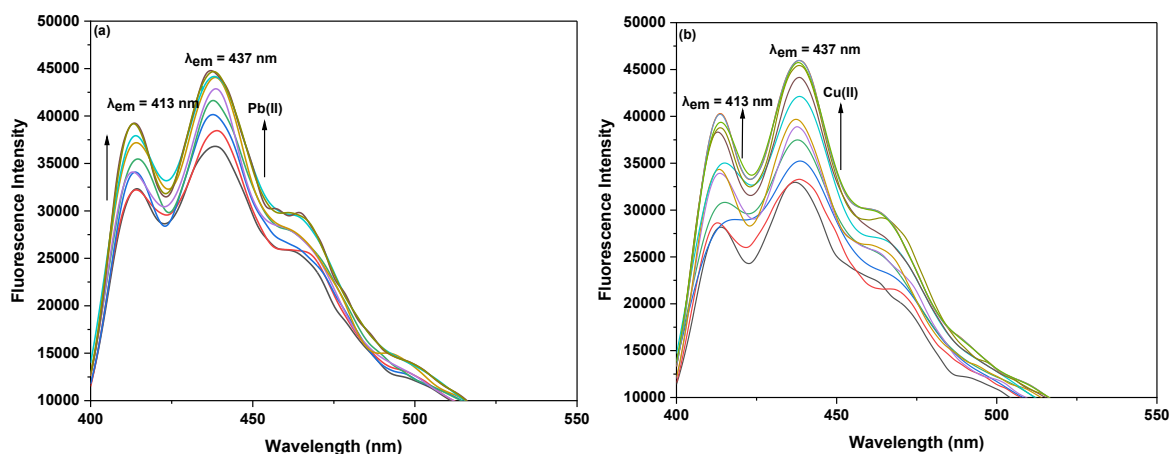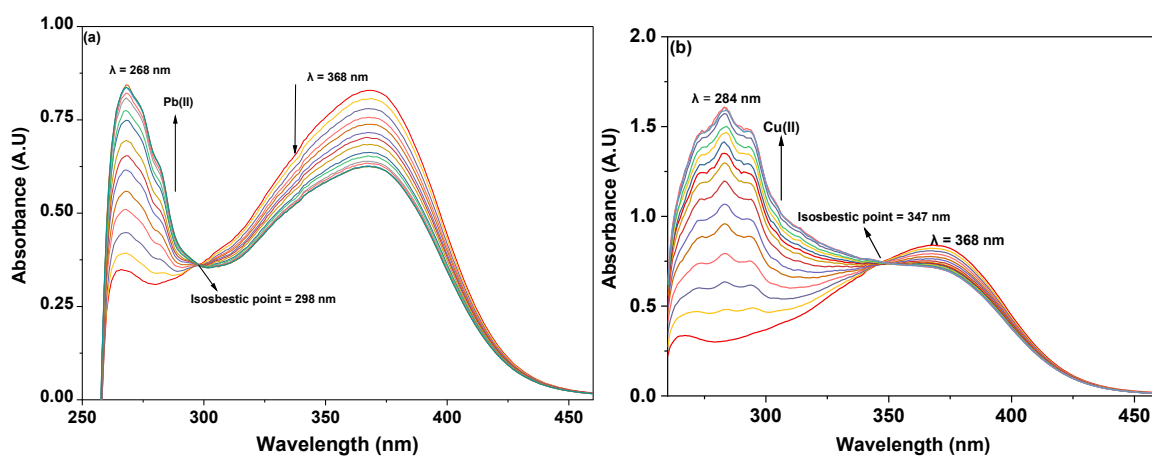**Figure S11:** Incremental increase in the fluorescence emission of probe **148** on titration with (a) Pb(II) (b) Cu(II) in DMSO

The interactions of probe **156** with Co(II) and Cu(II) ions were systematically investigated using UV-Vis spectroscopy. The addition of Co(II) ions resulted in a significant hyperchromic shift in the absorption peak observed at 311 nm, accompanied by a smaller hyperchromic shift at 425 nm. These changes are attributed to $n \rightarrow \pi*$ transitions, indicating a strong interaction between the probe and Co(II) ions. Similarly, titration with Cu(II) ions led to pronounced hyperchromic shifts at 311 nm and minor hyperchromic changes at 425 nm **(figure S12)**. The interactions of probes **156** with Co(II) and Cu(II) ions were also examined through fluorescence spectroscopy, where solutions of each probe were titrated with 10 μM solutions of the metal ions in separate experiments. When exposed to an excitation wavelength (λ_{ex}) of 295 nm, probe **156** exhibited a prominent emission peak (λ_{em}) at 445 nm.
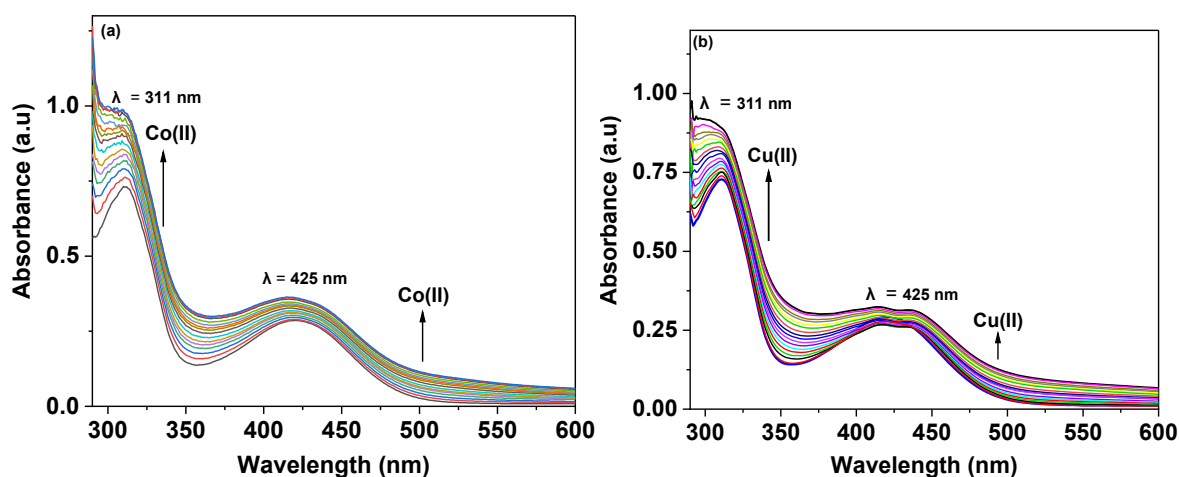
Figure S12: Incremental increase in the absorption maxima of probe **157** on titration with (a) Co(II) (b) Cu(II) in THF/H$_2$O (4:1)

Independent titrations for both Co(II) and Cu(II) ions demonstrated that the fluorescence emission intensity of probe **156** increased upon the introduction of either of the metal ions into the solution **(figure S13)**. The K_a values for probe **156** for Co(II) and Cu(II) ions were 8.80×10^3 M^{-1}, 5.99×10^3 M^{-1} for the aforementioned metal ions, respectively. Moreover, the binding ratio of 1:1 (M:L) were established based on the Job's plots analysis. The LoD value for probe **156** for detecting Co(II) was determined to be 1.64 µM, while for detecting Cu(II) ions, the LoD value was 3.19 µM. The LoQ values for the probe **156** for the recognition of Co(II) ions was found to be 5.46 µM, whereas for Cu(II) ions, the value was 10.64 µM.
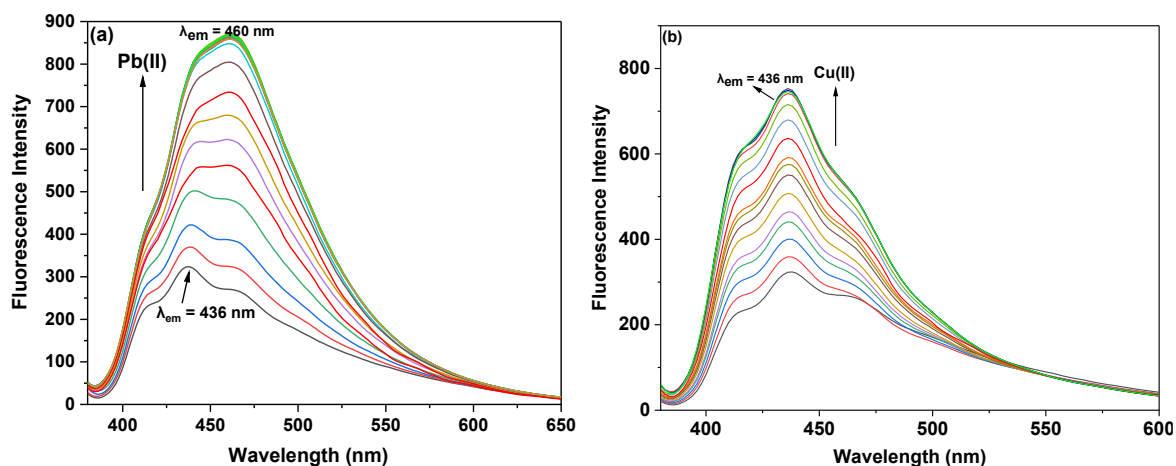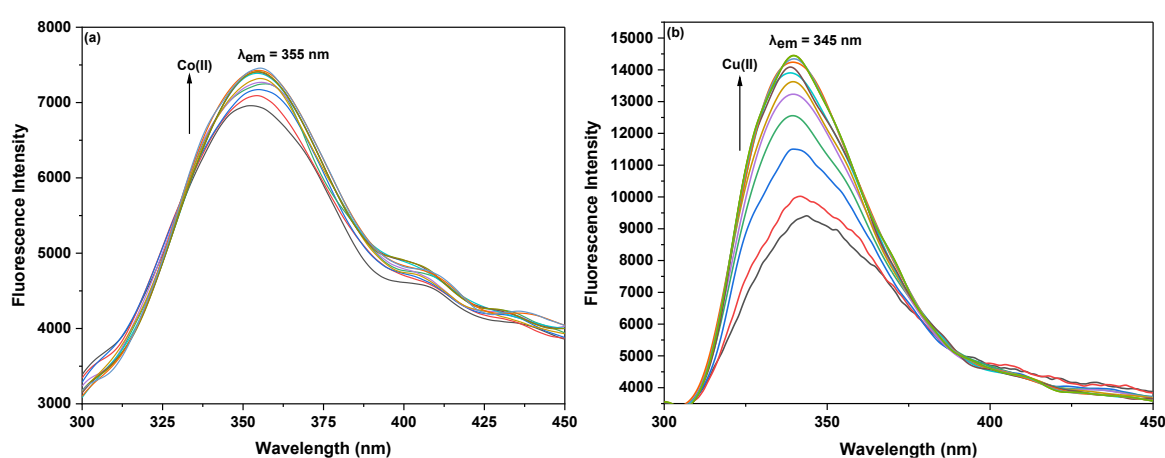

Figure S13: Incremental increase in the fluorescence emission of probe **156** on titration with (a) Co(II) (b) Cu(II) in THF/H$_2$O (4:1)

The interactions of probes **157** with Co(II) and Cu(II) ions were systematically investigated using UV-Vis spectroscopy. Distinct spectral changes were observed upon titration with Co(II) and Cu(II) ions, indicating specific interactions with the metal ions. During the gradual addition of a 1 mM Co(II) solution to the probe, the absorption peak at 317 nm exhibited a pronounced hypochromic shift, characterized by a decrease in intensity. This shift was accompanied by the emergence of an isosbestic point at 370 nm. In contrast, the incremental addition of a 1 mM Cu(II) solution induced a notable blue shift of approximately 24 nm in the absorption maximum, shifting it from 317 nm to 293 nm. This shift was further accompanied by a significant hyperchromic effect at 293 nm, highlighting an increase in absorbance intensity **(figure S14)**. The contrasting spectral responses to Co(II) and Cu(II) ions reflect the probe's differential binding behaviour. The interactions of probes **157** with Co(II) and Cu(II) ions were also examined through fluorescence spectroscopy, upon excitation at a wavelength of (λ_{ex}) 320 nm, a distinct fluorescence emission peak was observed at (λ_{em}) 442

nm. The fluorescence intensity of probe **157** significantly increased upon the addition of Co(II) and Cu(II) ions **(figure S15)**. The K_a values for probe **157** for the aforementioned metal ions were 7.66×10^3 M^{-1}, 4.74×10^3 M^{-1}, respectively. Moreover, the binding ratio of 1:1 (M:L) were established for probe based on the Job's plots analysis. The LoD value for probe **157** for detecting Co(II) were determined to be 2.08 µM, while for detecting Cu(II) ions, the LoD values were 2.30 µM. The LoQ values for the probe **157** for the recognition of Co(II) ions was found to be 6.94 µM, whereas for Cu(II) ions, the value was 7.68 µM.

Figure S14: Incremental increase in the absorption maxima of probe **157** on titration with (a) Co(II) (b) Cu(II) in THF/H$_2$O (4:1)
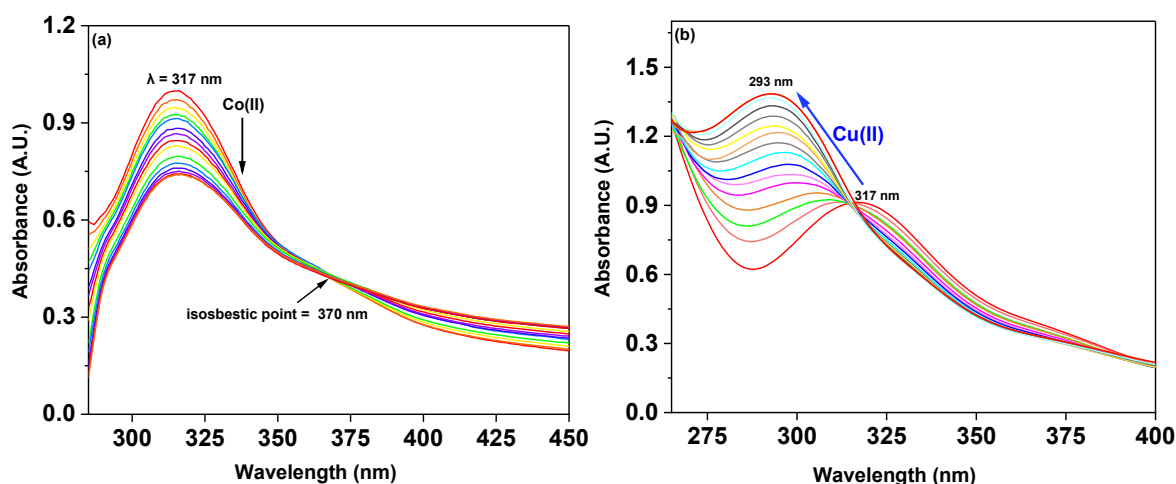

Figure S15: Incremental increase in the fluorescence emission of probe **157** on titration with (a) Co(II) (b) Cu(II) in THF/H$_2$O (4:1)

The interactions of probe **158** with Co(II) and Cu(II) ions were systematically investigated using UV-Vis spectroscopy. In these experiments, solutions of each probe were titrated with 1 mM solutions of Co(II) and Cu(II) ions in separate titrations. The stepwise addition of Co(II) ions to the solution of probe **158** resulted in a pronounced hyperchromic shift

in the absorption peak at 362 nm, indicative of $n \rightarrow \pi*$ transitions. This spectral change was accompanied by the emergence of an isosbestic point at 284 nm. In case of Cu(II) , the incremental addition of a 1 mM Cu(II) solution induced a notable hyperchromic shift at 279 nm accompanied by the formation of an isosbestic point 354 nm **(figure S16)**. The K_a values for probe **158** for the aforementioned metal ions were 6.61×10^3 M^{-1}, 1.00×10^4 M^{-1}, respectively.
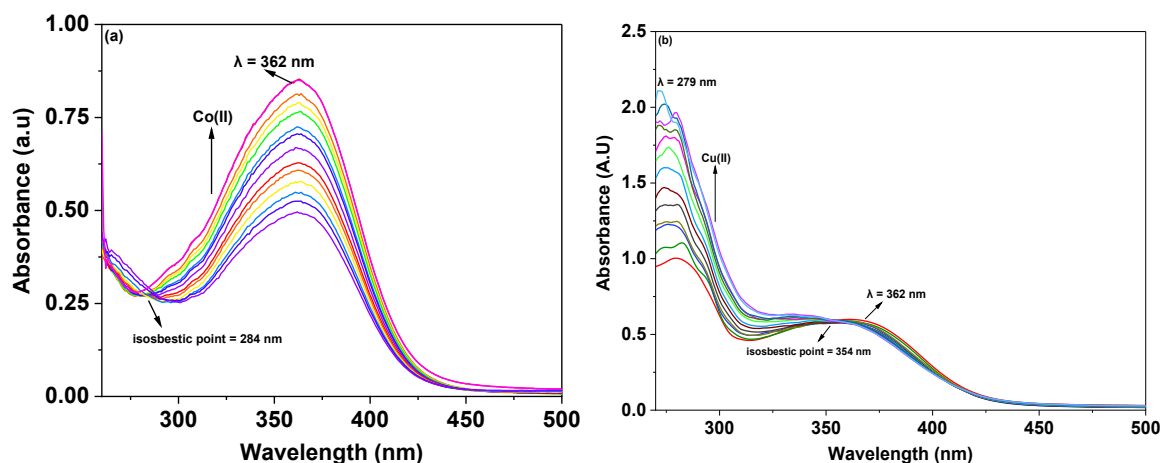
Figure S16: Incremental increase in the absorption maxima of probe **158** on titration with (a) Co(II) (b) Cu(II) in THF/H$_2$O (4:1)
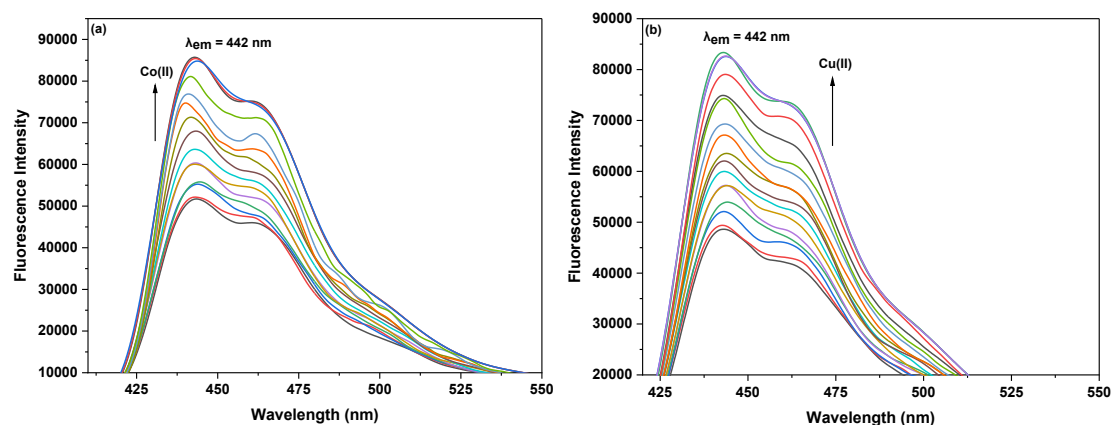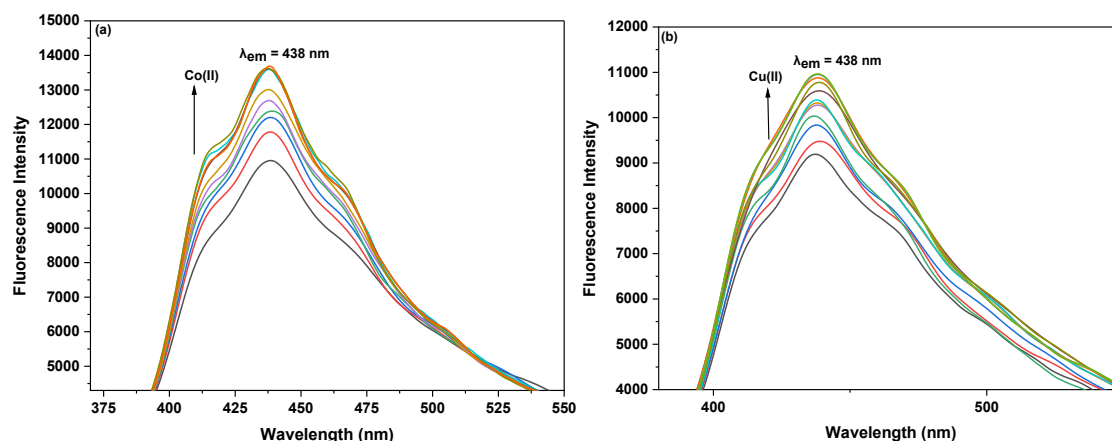

Figure S17: Incremental increase in the fluorescence emission of probe **158** on titration with (a) Co(II) (b) Cu(II) in THF/H$_2$O (4:1)

Moreover, the binding ratio of 1:1 (M:L) were established for probe based on the Job's plots analysis. The interactions of probe **158** with Co(II) and Cu(II) ions were also examined through fluorescence spectroscopy, where solutions of each probe were titrated with 10 µM solutions of the metal ions in separate experiments. In the case of probe **158**, when exposed to

an excitation wavelength (λ_{ex}) of 360 nm, a pronounced emission peak (λ_{em}) at 438 nm was observed. The increase in fluorescence emission intensity of probe **158** for both Co(II) and Cu(II) is depicted in **figure S17**. The LoD value for probe **158** for detecting Co(II) was determined to be 1.81 µM, while for detecting Cu(II) ions, the LoD value was 1.17 µM. The LoQ values for the probes **158** for the recognition of Co(II) ions was found to be 6.04 µM, whereas for Cu(II) ions, the value was 3.92 µM.

Annexure A
Instrumentation and Chemicals

Annexure A details the instruments utilized for the spectroscopic analysis of the synthesized compounds and lists the various reagents, catalysts, and solvents employed in their chemical synthesis and analytical evaluation.

General experimental techniques

- ### Infrared Spectra

  The infrared spectra of the synthesized compounds were recorded in the range of 4000–450 cm^{-1} using a SHIMADZU FTIR-8400S spectrophotometer, accessed at the Central Instrumentation Facility (CIF), Lovely Professional University, Phagwara, Punjab.

- ### NMR Spectra

  The ^{1}H and ^{13}C NMR spectra of the synthesized compounds were obtained using a Bruker Advance Neo FT NMR spectrophotometer, with tetramethylsilane (TMS) as the internal reference and CDCl$_3$ and DMSO-d6 as solvents. The analyses were conducted at the Sophisticated Analytical Instrumentation Facility (SAIF), Panjab University, Chandigarh.

- ### Mass Spectra

  Mass spectrometric analyses (LCMS) of the synthesized 1,2,3-triazoles were performed using a Bruker Esquire 3000 mass spectrometer, accessed at the Sophisticated Analytical Instrumentation Facility (SAIF), Panjab University, Chandigarh.

- ### UV-Vis Spectra

  UV-Vis spectroscopic measurements were carried out using a SHIMADZU UV-1900 spectrophotometer, accessed at the School of Chemical Engineering and Physical Sciences, Lovely Professional University, Phagwara, Punjab.

- ### Fluorescence Spectra

  Fluorescence spectroscopic studies were conducted using a Perkin Elmer FL 6500 spectrophotometer, accessed at the Central Instrumentation Facility (CIF), Lovely Professional University, Phagwara, Punjab.

- ### Melting Point

  The melting points of the synthesized compounds were determined using a Mel Temp II apparatus with sealed capillaries, performed at the School of Chemical Engineering and Physical Sciences, Lovely Professional University, Phagwara, Punjab.

- ### General Materials

  The following materials were utilized in the study: Bromotris(triphenylphosphine)copper(I) [CuBr(PPh$_3$)$_3$] (Aldrich), propargyl bromide (80% solution in toluene) (Spectrochem), N,N-dimethylformamide (DMF) (LOBA Chemie), benzyl

chloride (LOBA Chemie), sodium azide (LOBA Chemie), tetrahydrofuran (THF) (SDFCL), triethylamine (TEA) (LOBA Chemie), potassium carbonate (LOBA Chemie), ethyl acetate (LOBA Chemie), n-hexane (LOBA Chemie), dimethyl sulfoxide (DMSO) (LOBA Chemie), acetonitrile (SDFCL), 4-benzyloxybenzaldehyde (LOBA Chemie), 4-chlorobenzaldehyde (LOBA Chemie), 2-aminoacetophenone (LOBA Chemie), 3-aminoacetophenone (LOBA Chemie), and 4-aminoacetophenone (LOBA Chemie).

Annexure B

Annexure B includes the IR, ¹H and ¹³C NMR, for all the synthesized chalcones, terminal alkynes, organic azides, and also mass spectrums for chalcone-based 1,2,3-triazole derivatives.

IR spectrum of benzyl azide 135
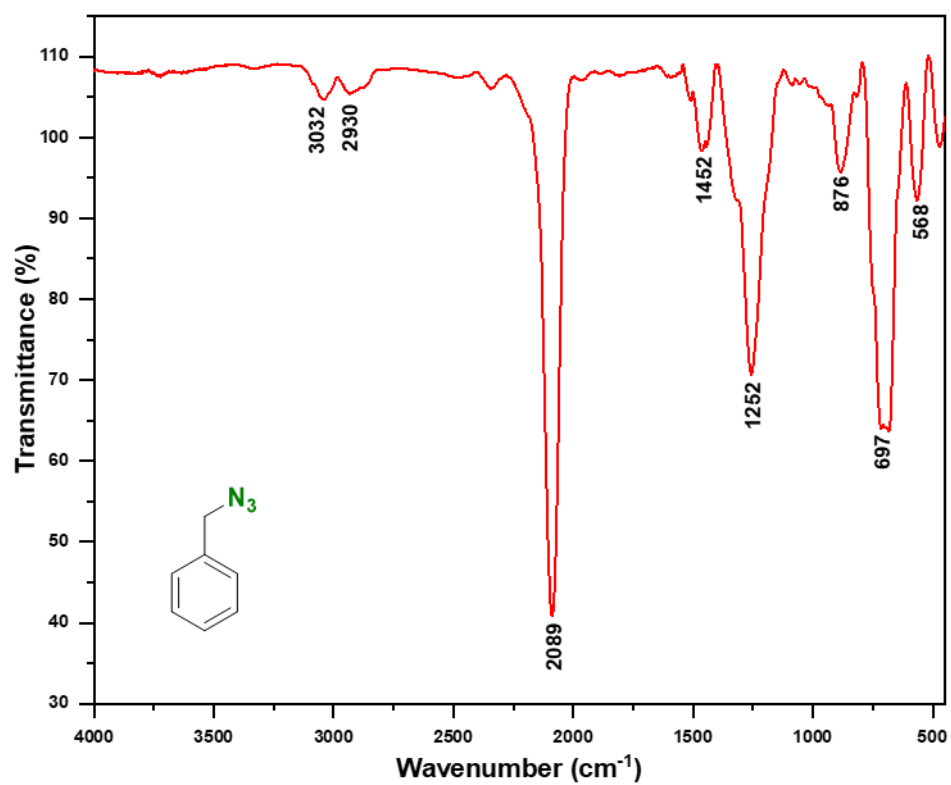
IR spectrum of chalcone 138
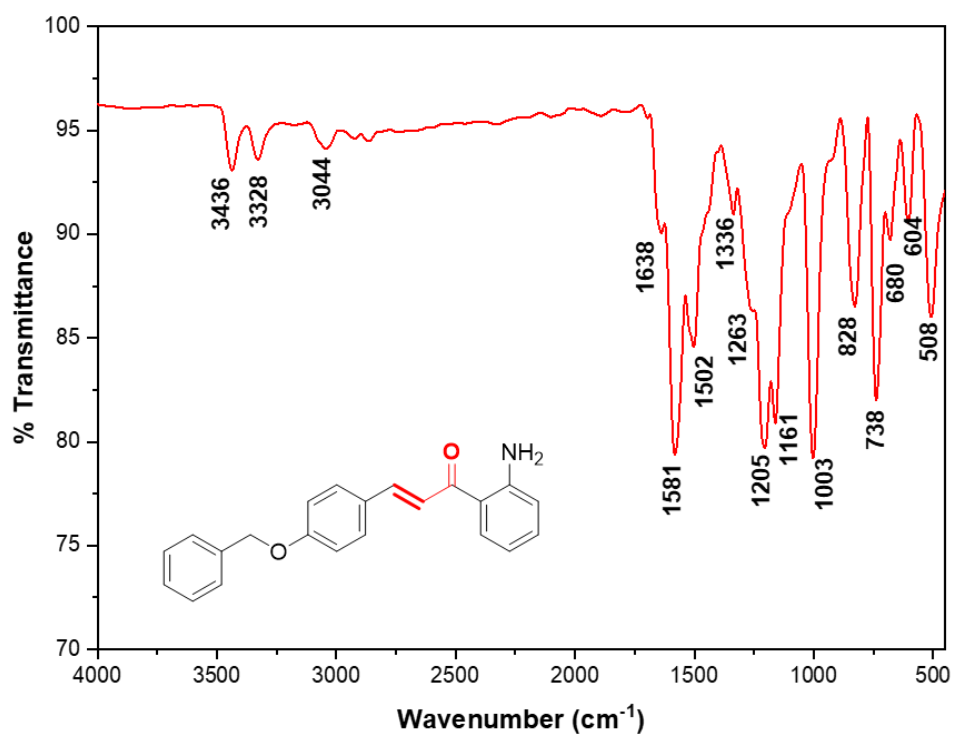
IR spectrum of chalcone 140
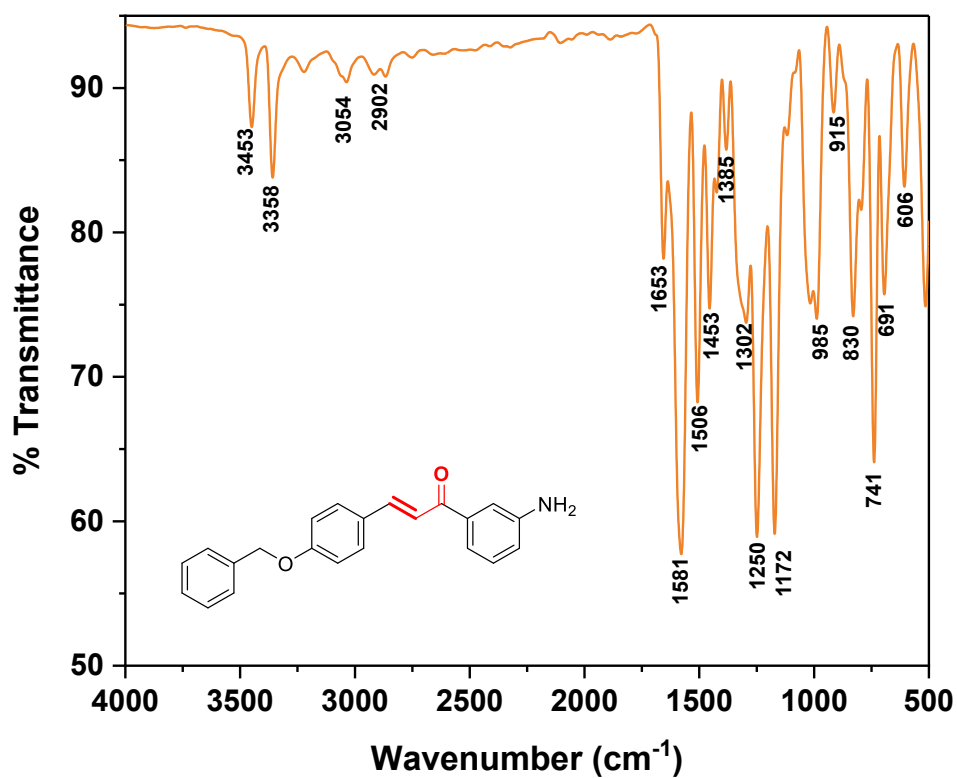
IR spectrum of chalcone 142
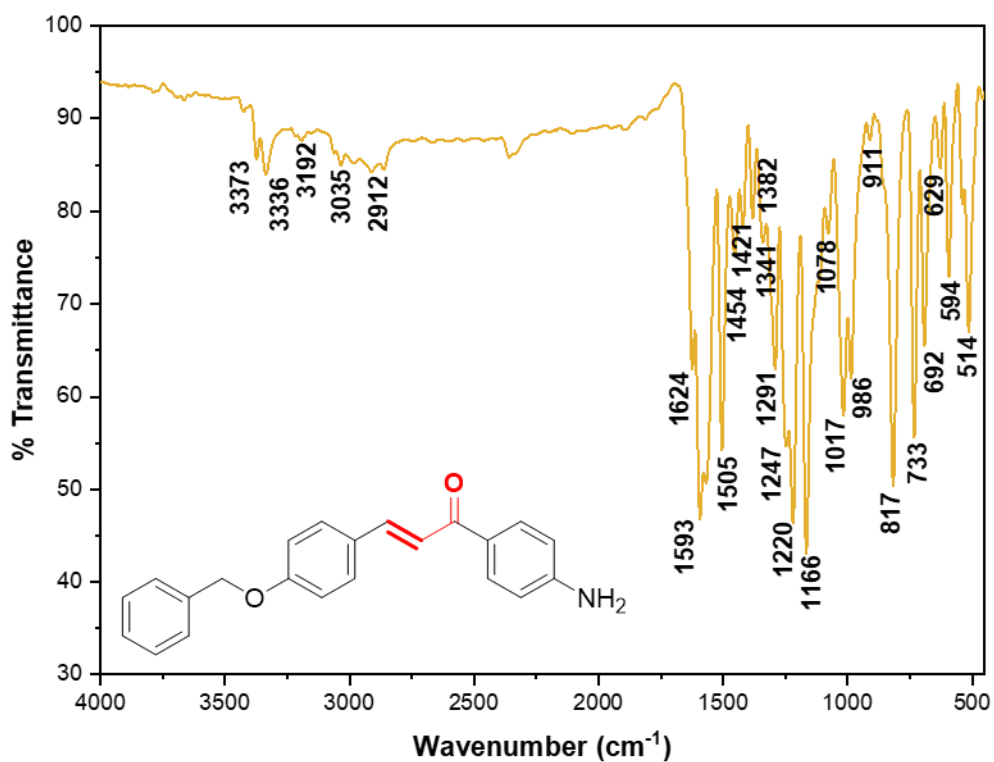
IR spectrum of alkyne 143
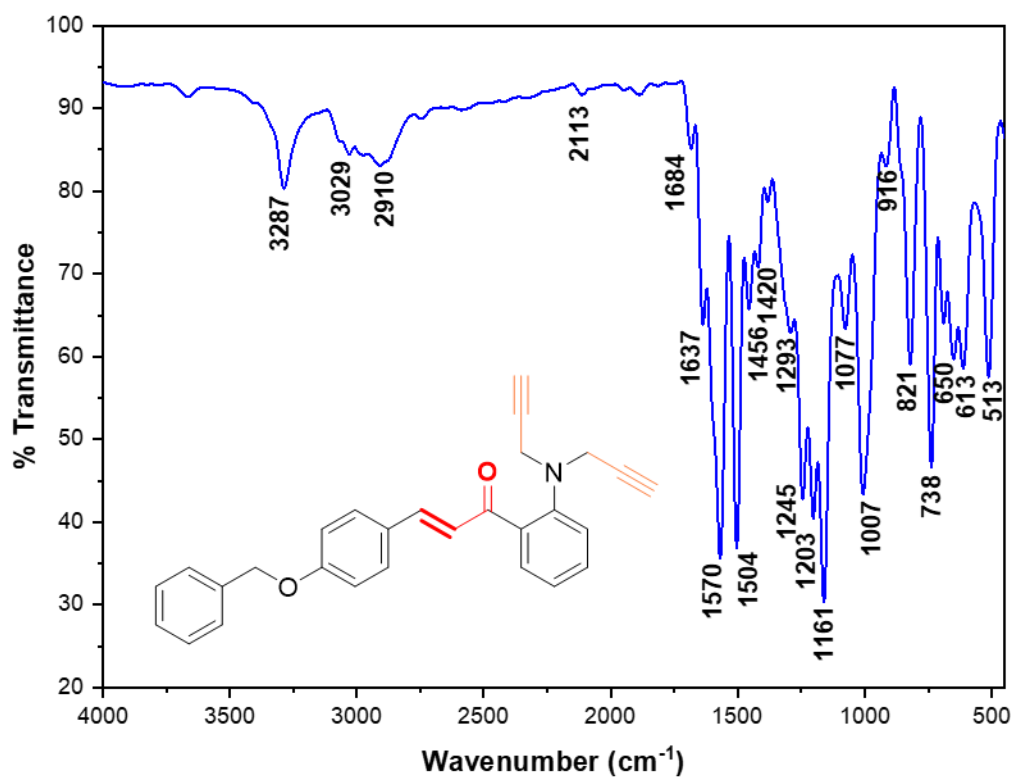
IR spectrum of alkyne 144
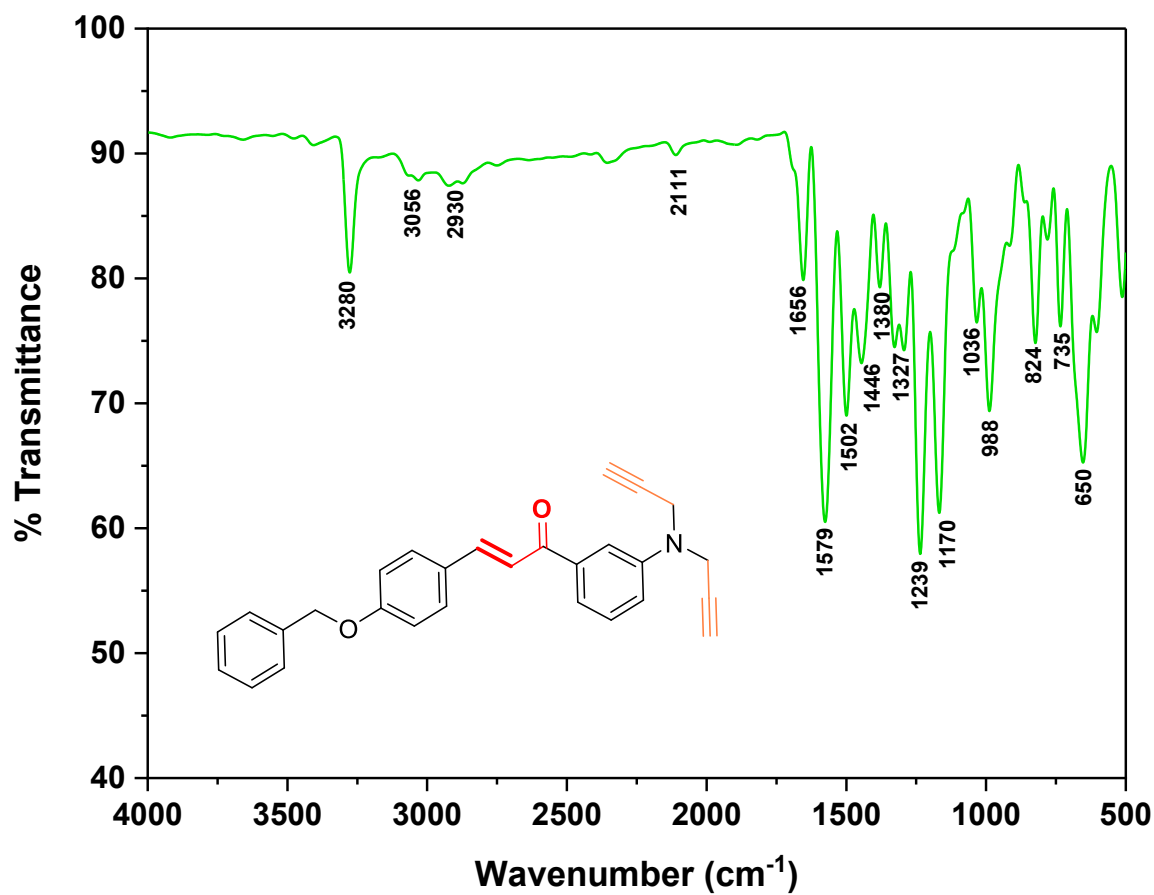
IR spectrum of alkyne 145
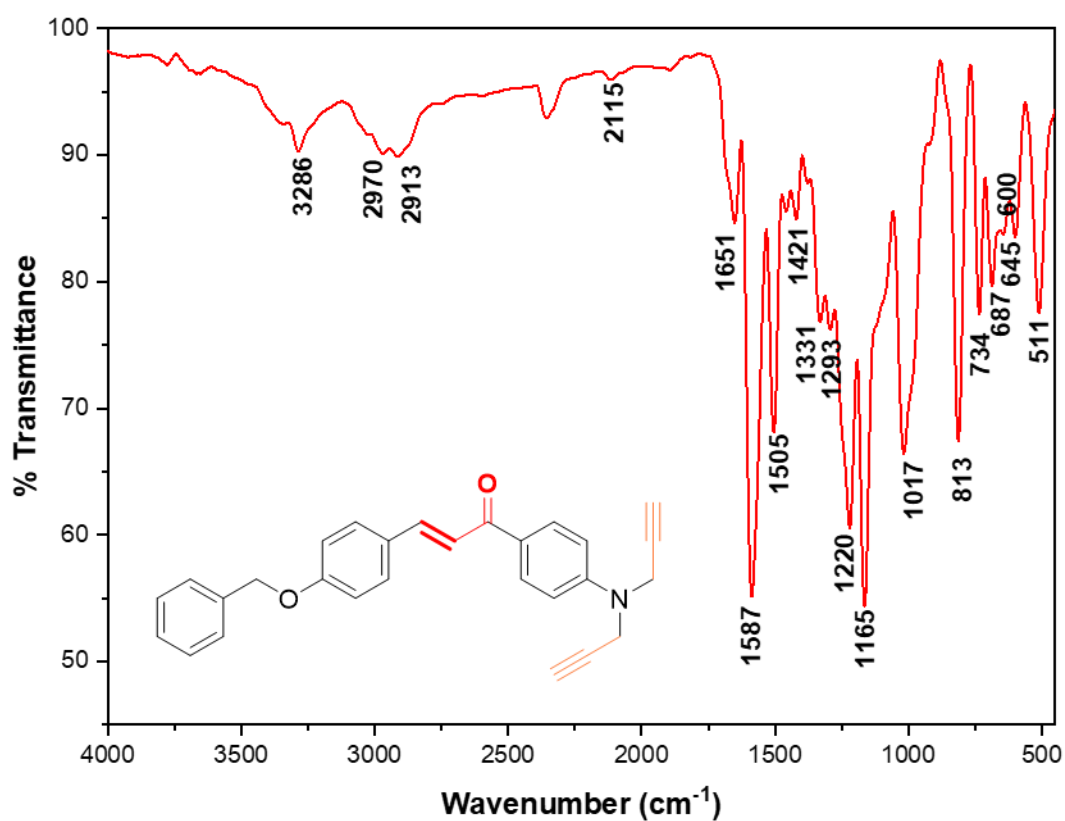
IR spectrum of 1,2,3-triazole 146
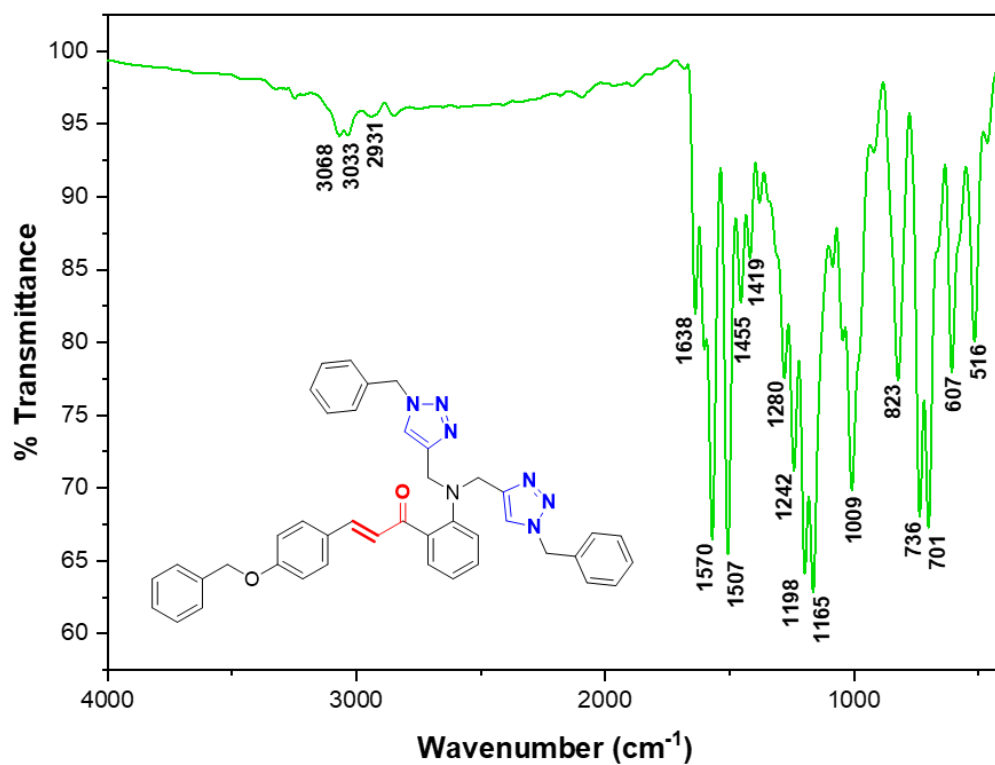
IR spectrum of 1,2,3-triazole 147
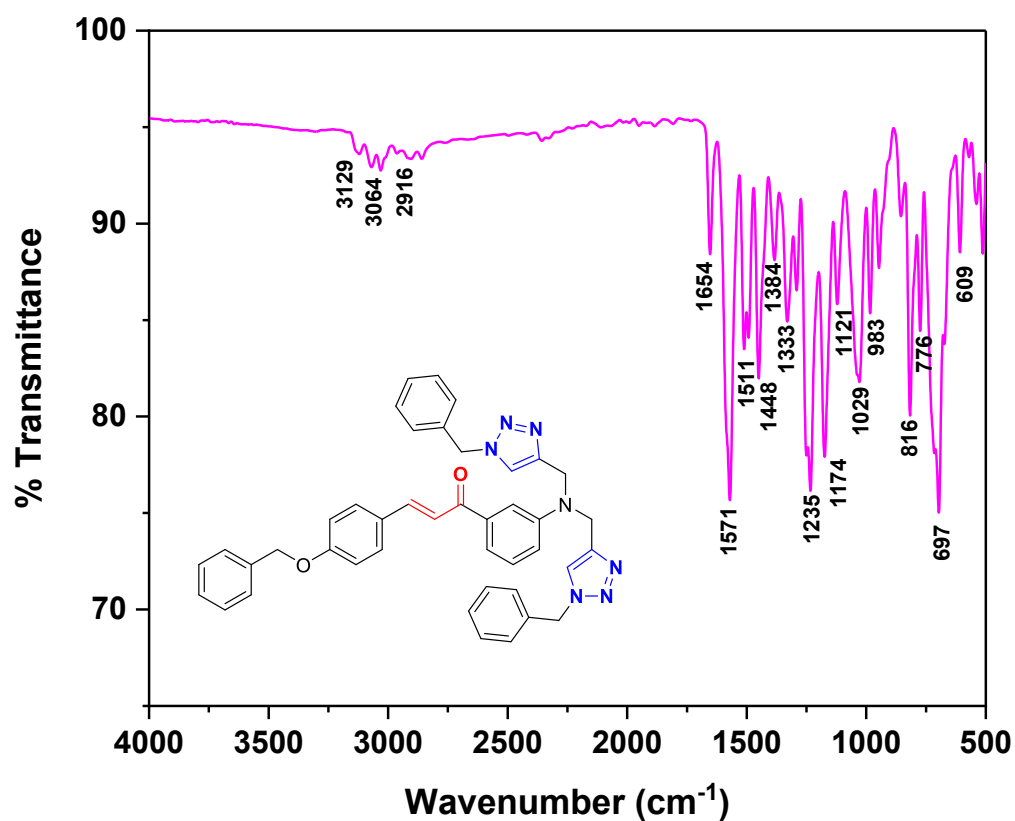
IR spectrum of 1,2,3-triazole 148

IR spectrum of chalcone 150
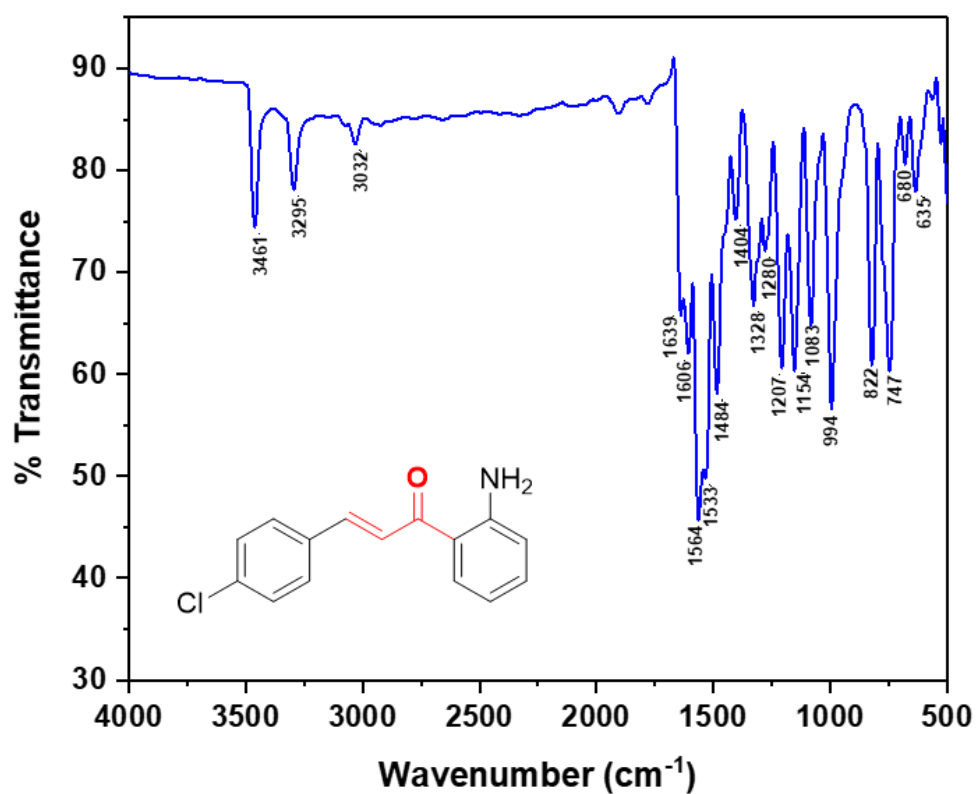
IR spectrum of chalcone 151
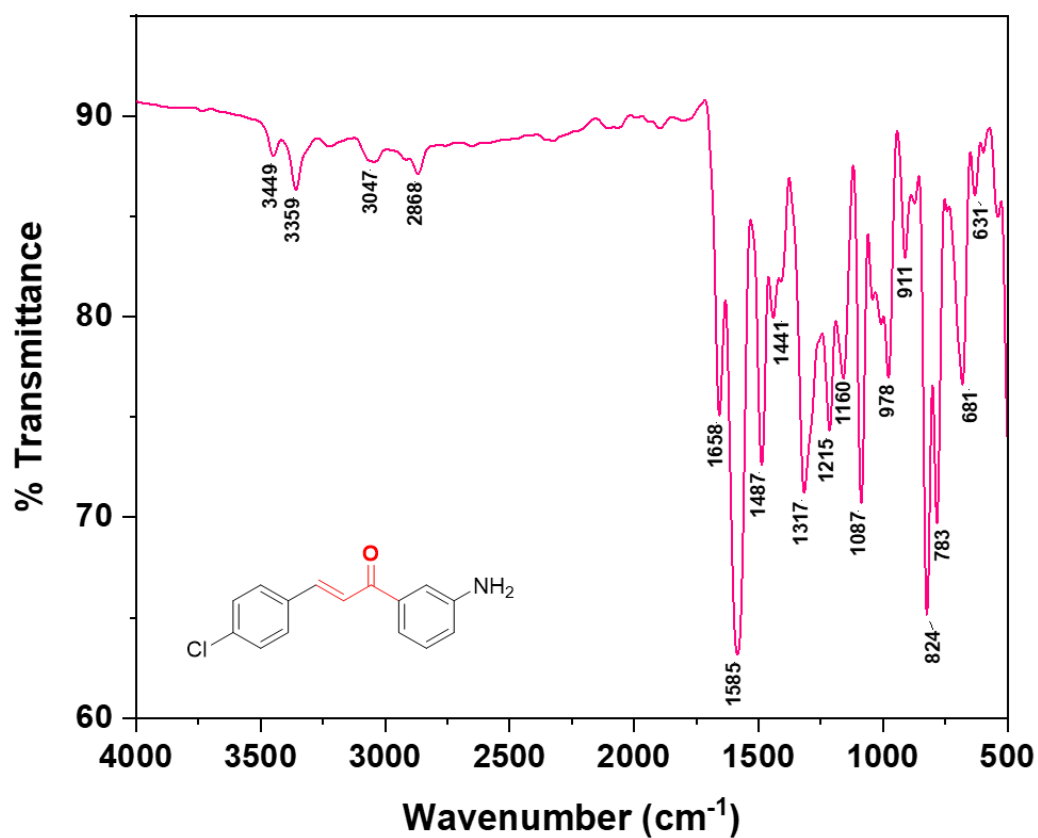
IR spectrum of chalcone 152

IR spectrum of alkyne 153
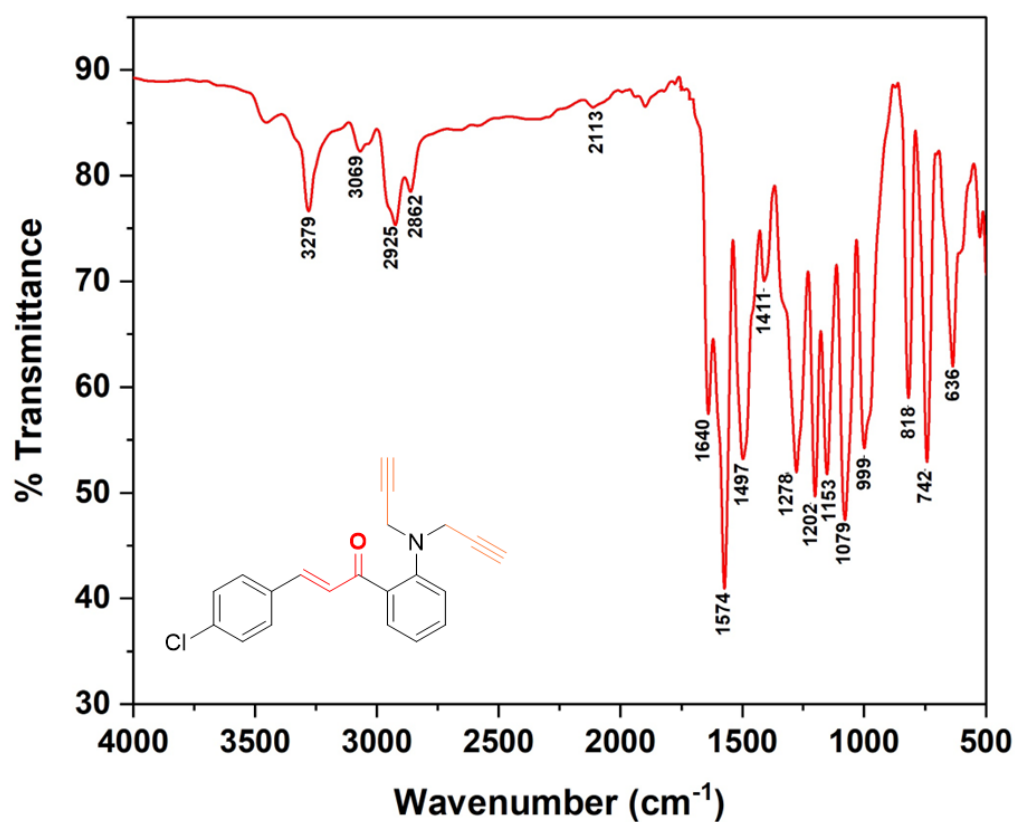
IR spectrum of alkyne 154
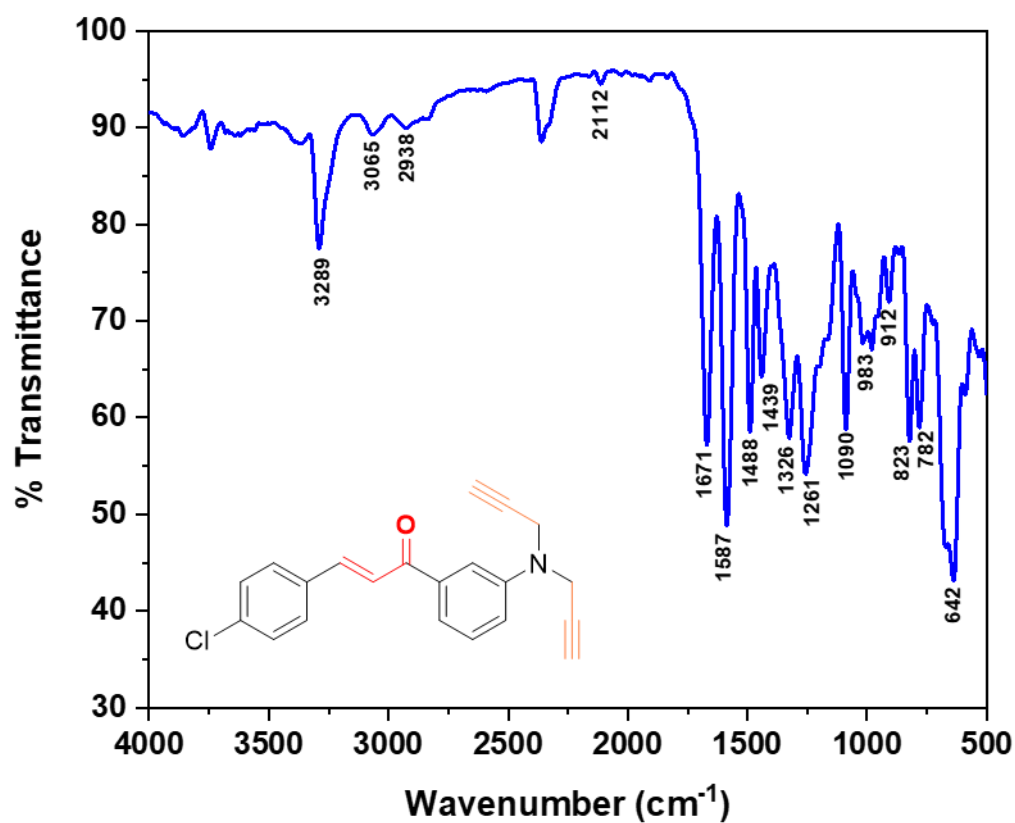
IR spectrum of alkyne 155
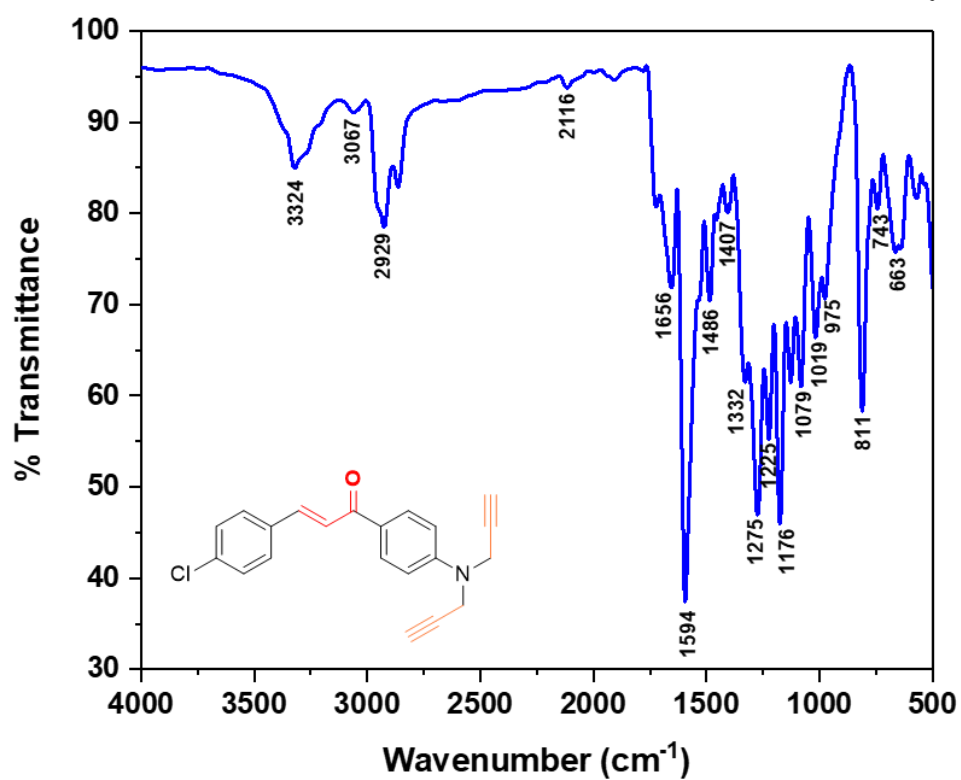
IR spectrum of 1,2,3-triazole 156
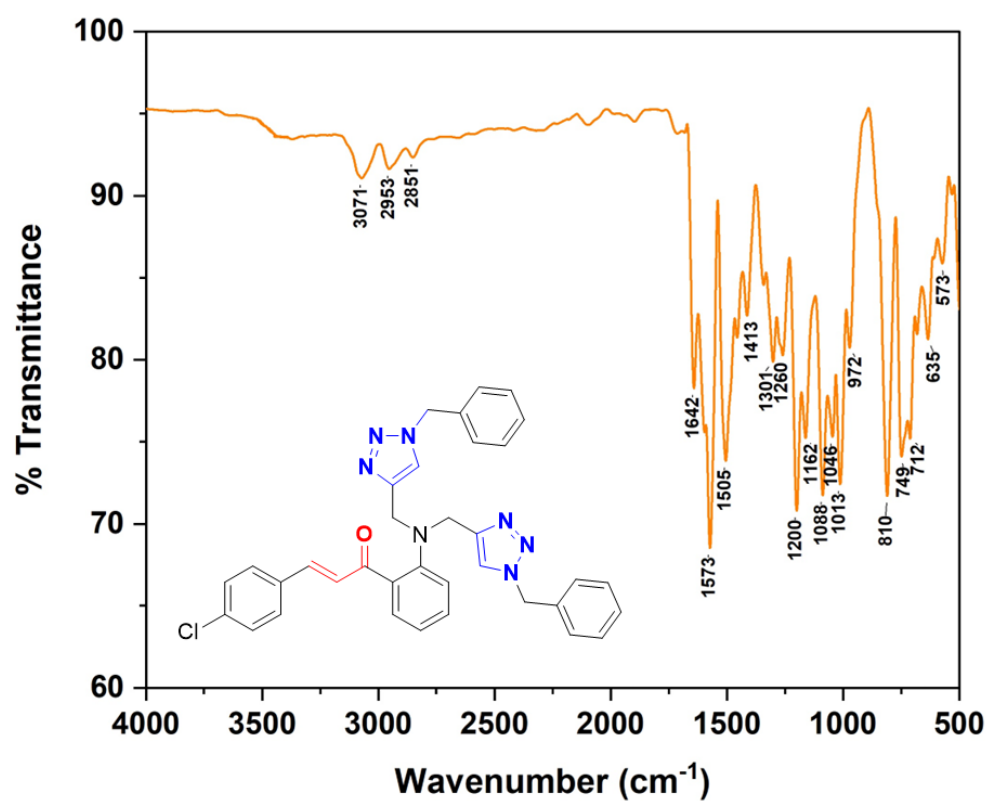
IR spectrum of 1,2,3-triazole 157
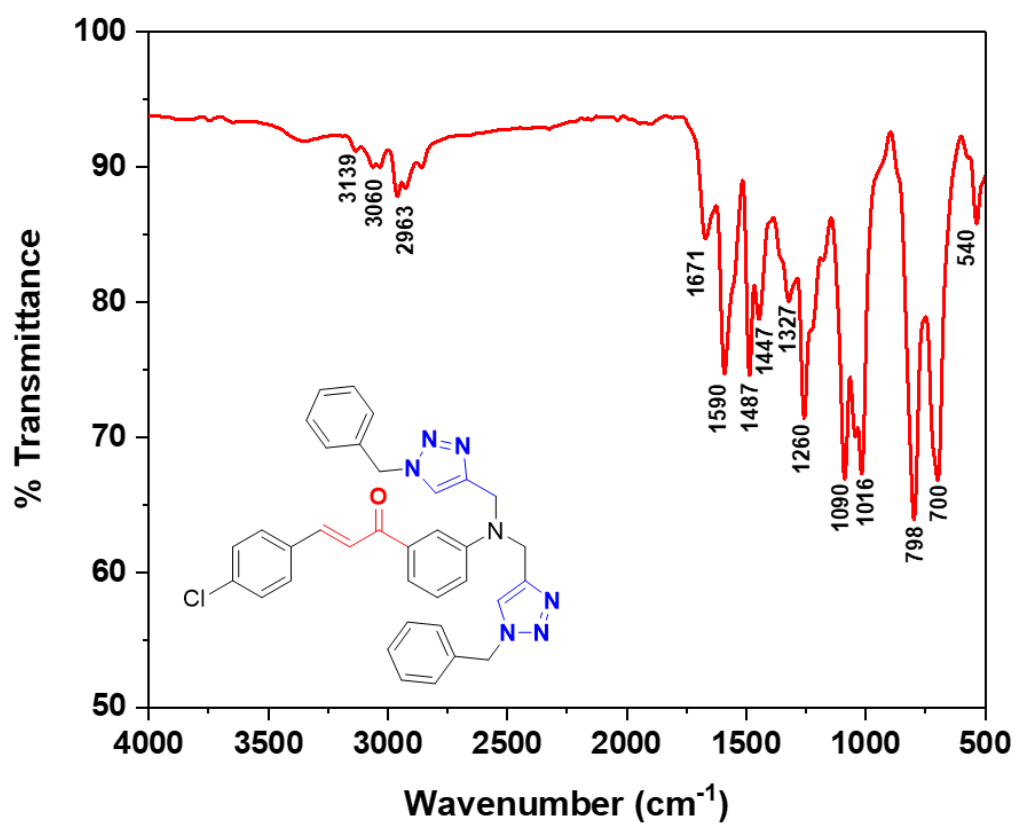
IR spectrum of 1,2,3-triazole 158
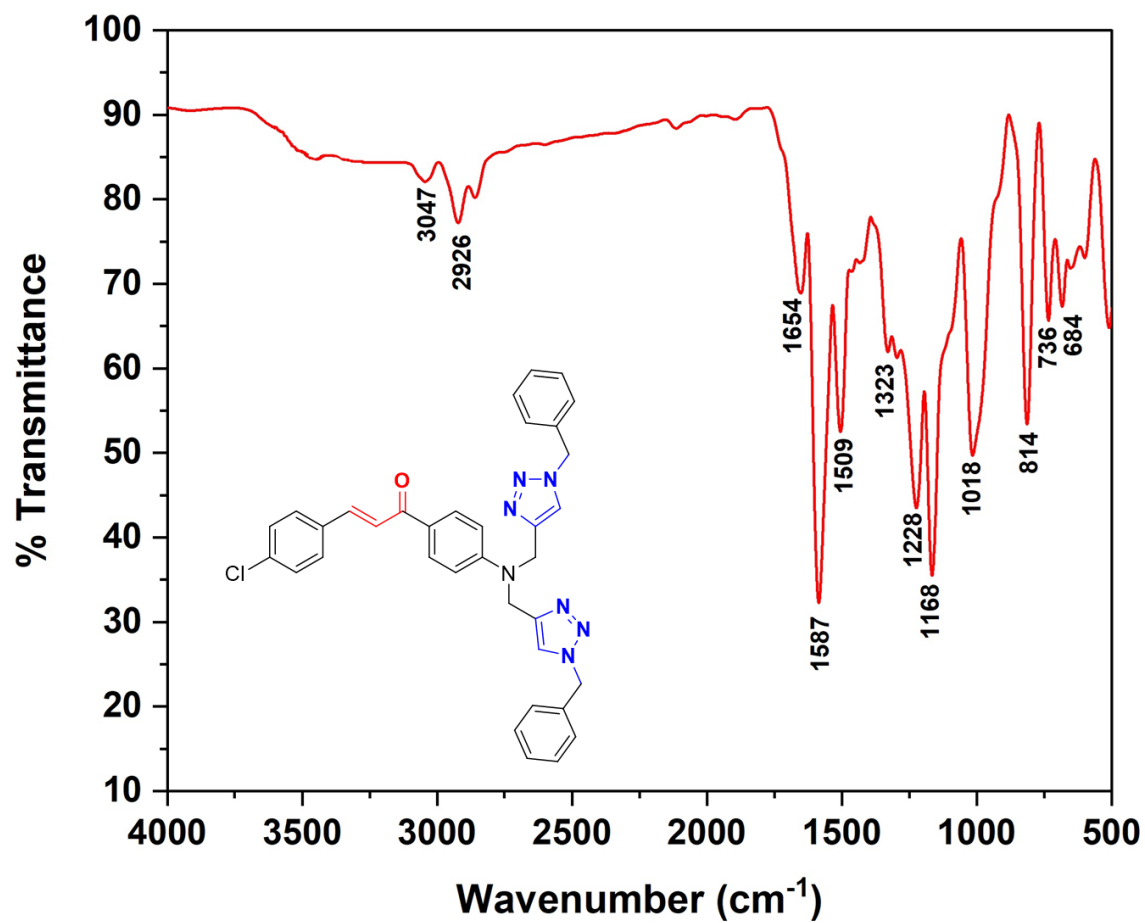
^{1}H NMR spectrum of benzyl azide 135
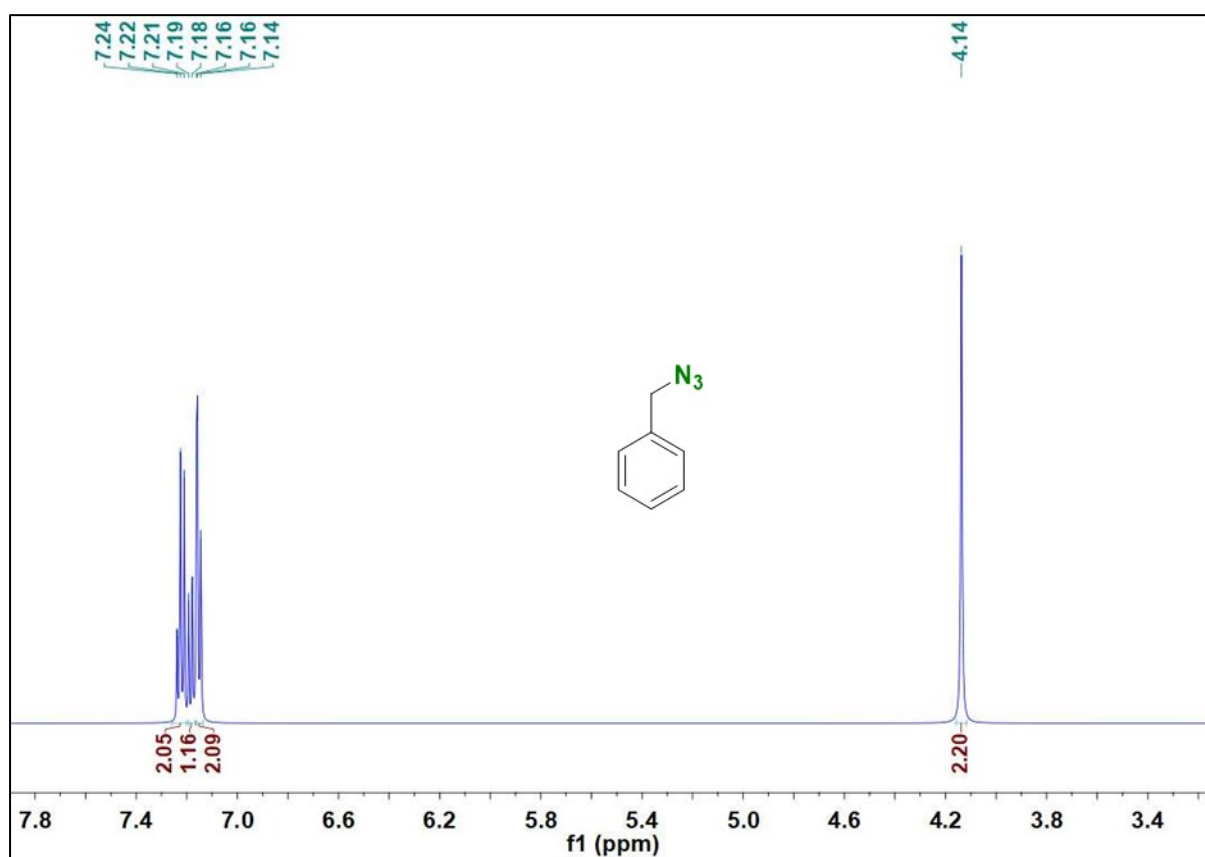
^{13}C NMR spectrum of benzyl azide 135
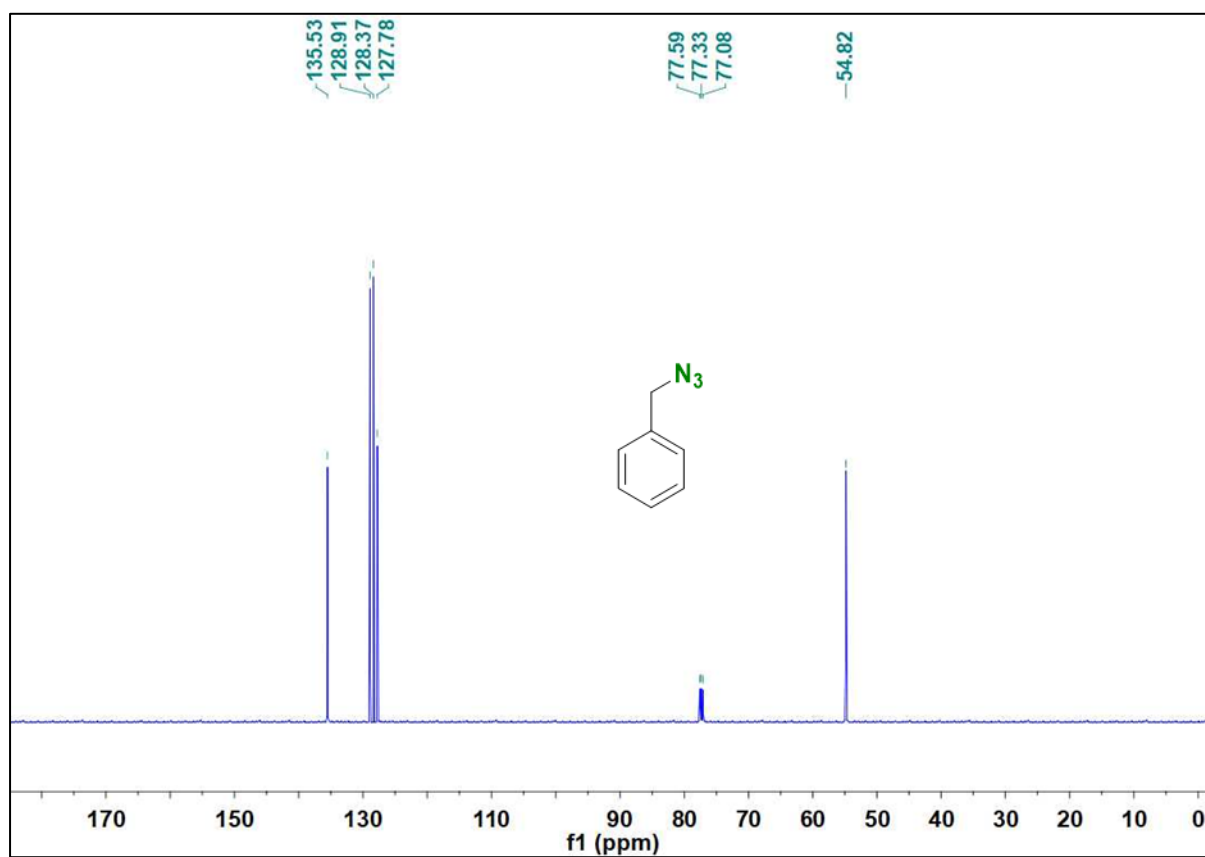
^{1}H NMR spectrum of chalcone 138
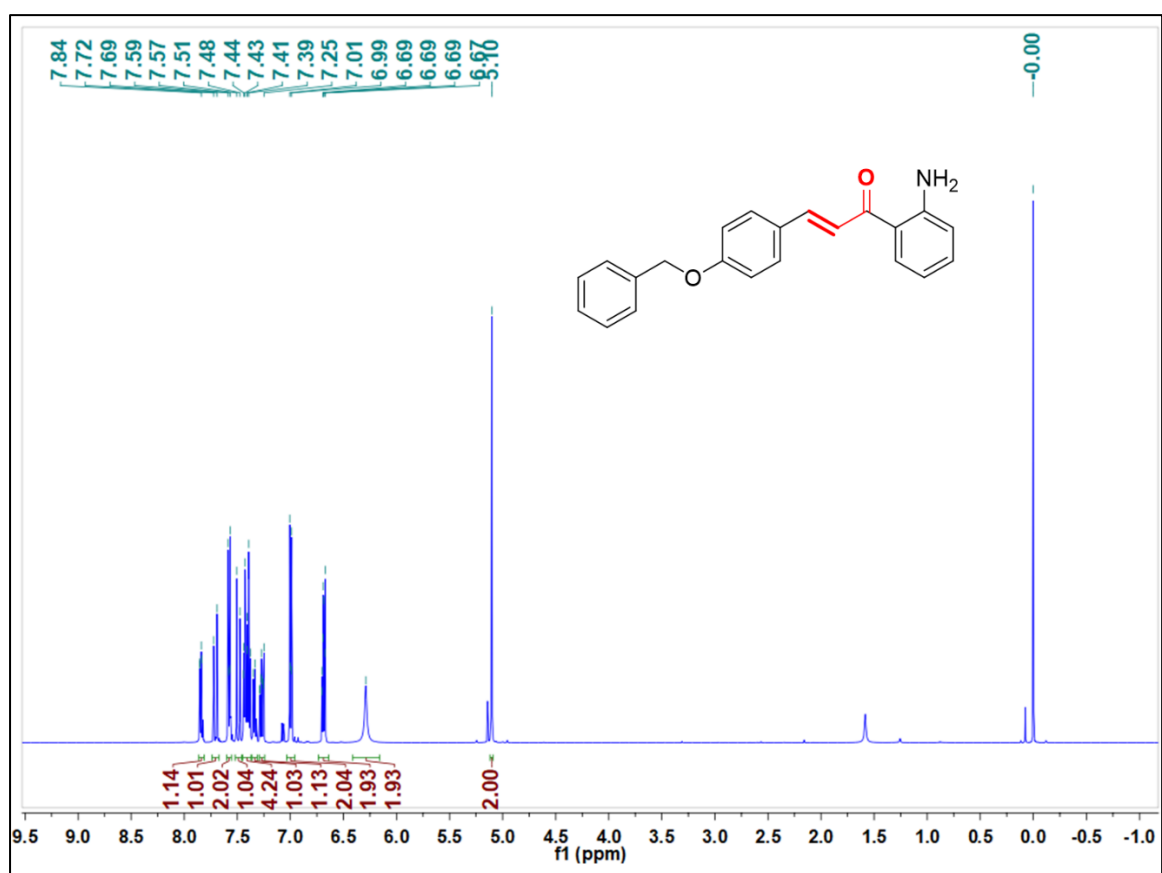
^{13}C NMR spectrum of chalcone 138
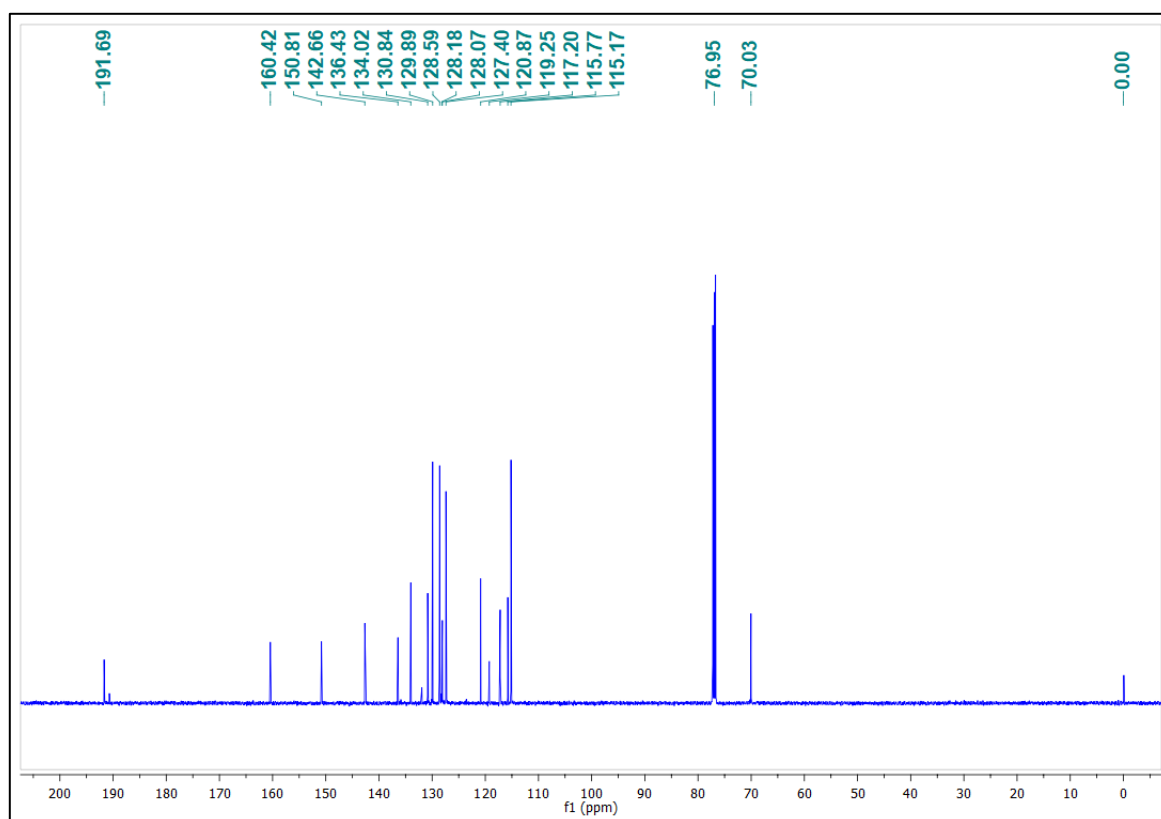
¹H NMR spectrum of chalcone 140

^{1}H NMR spectrum of chalcone 140

¹³C NMR spectrum of chalcone 140
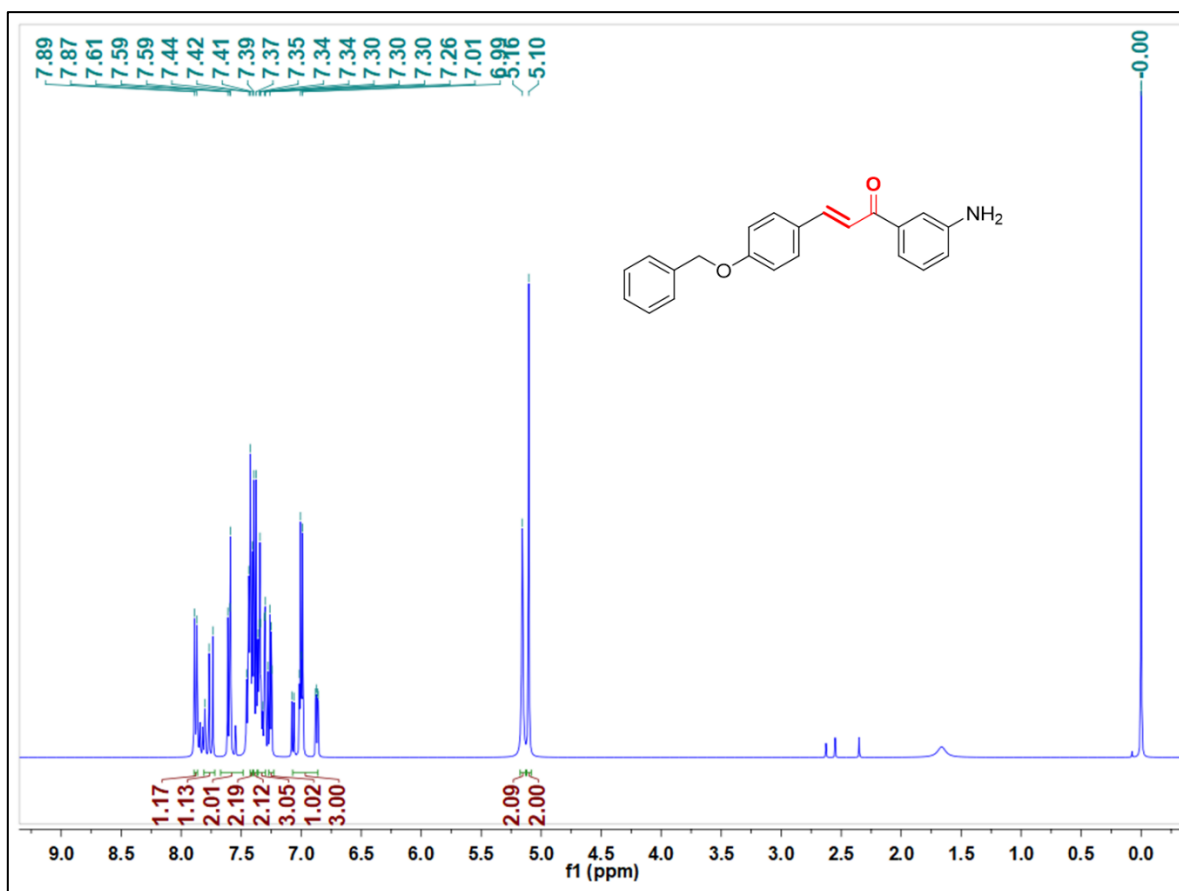
^{13}C NMR spectrum of chalcone 140
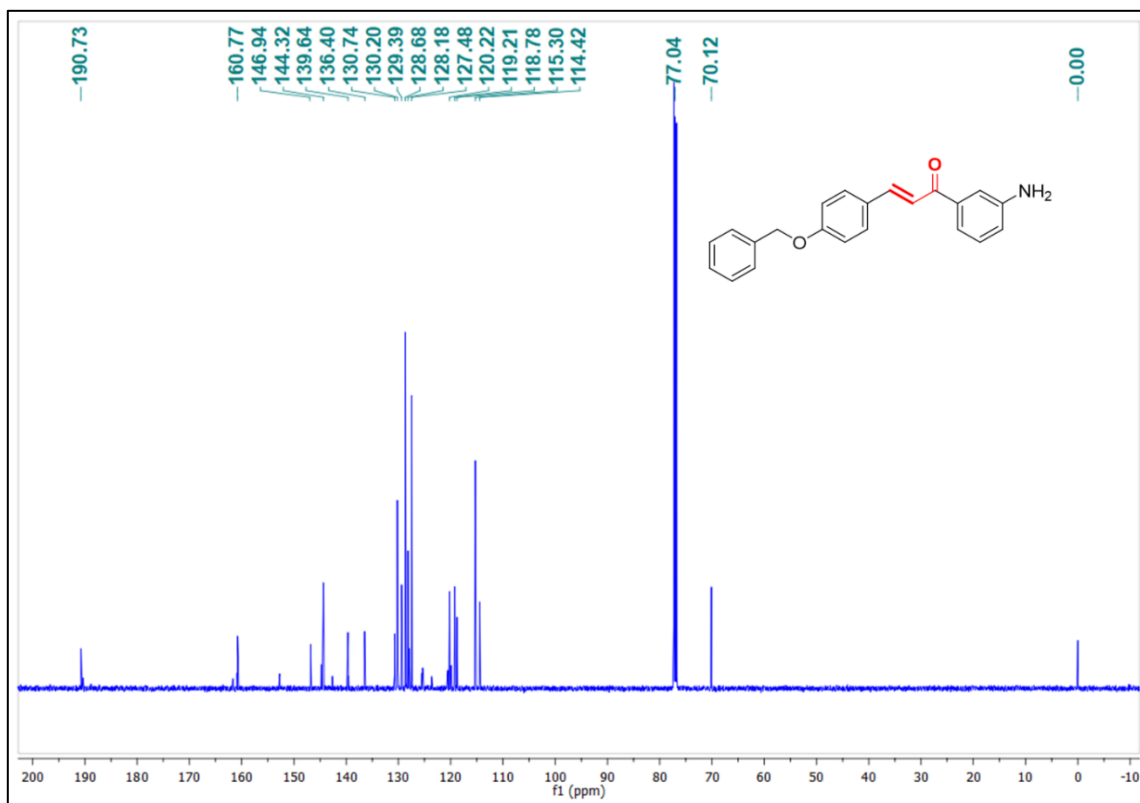
¹H NMR spectrum of chalcone 142
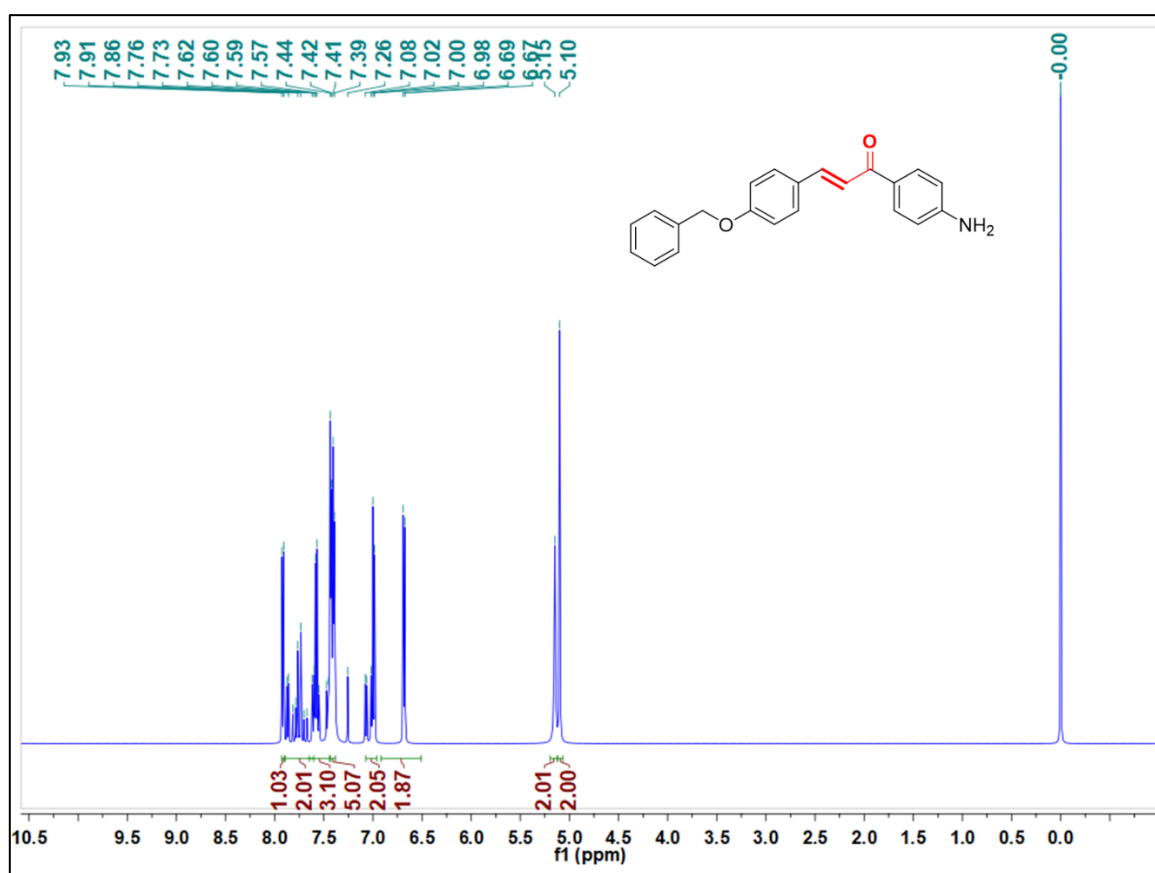
¹³C NMR spectrum of chalcone 142
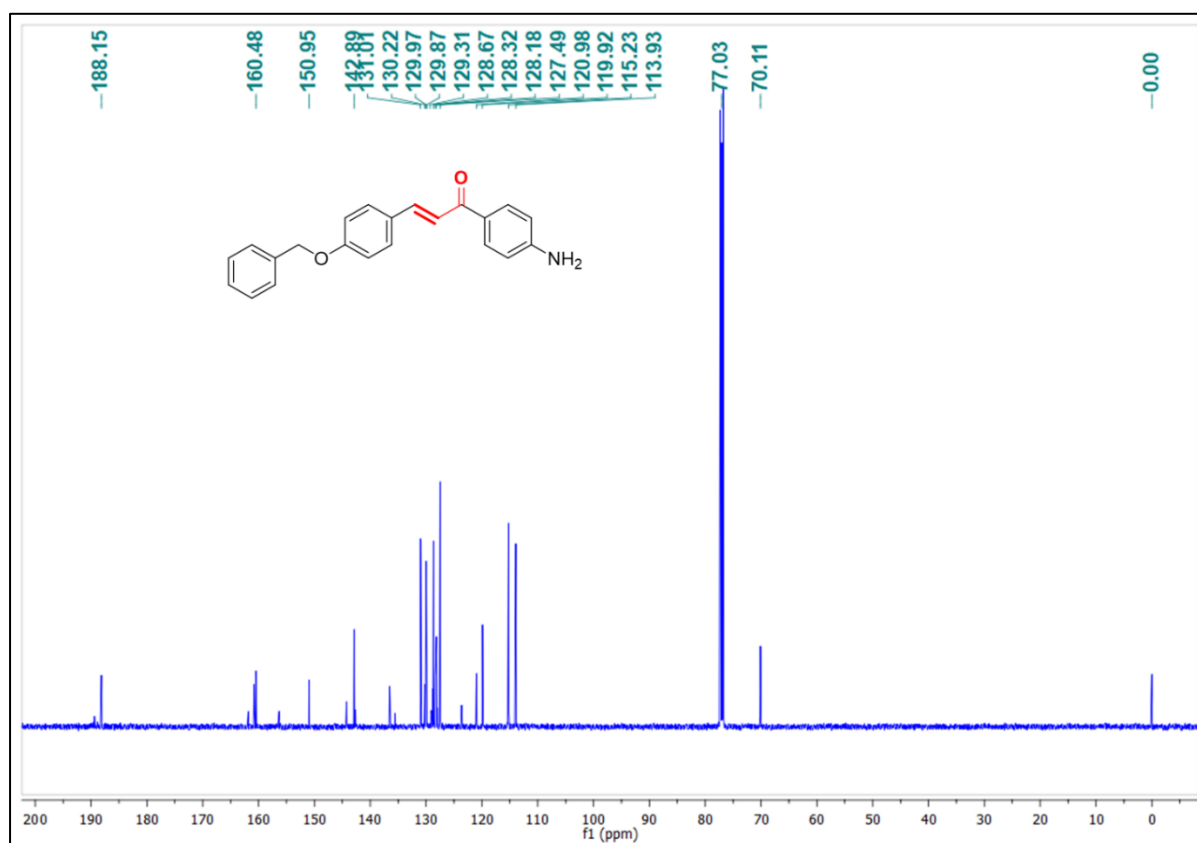
¹H NMR spectrum of alkyne 143
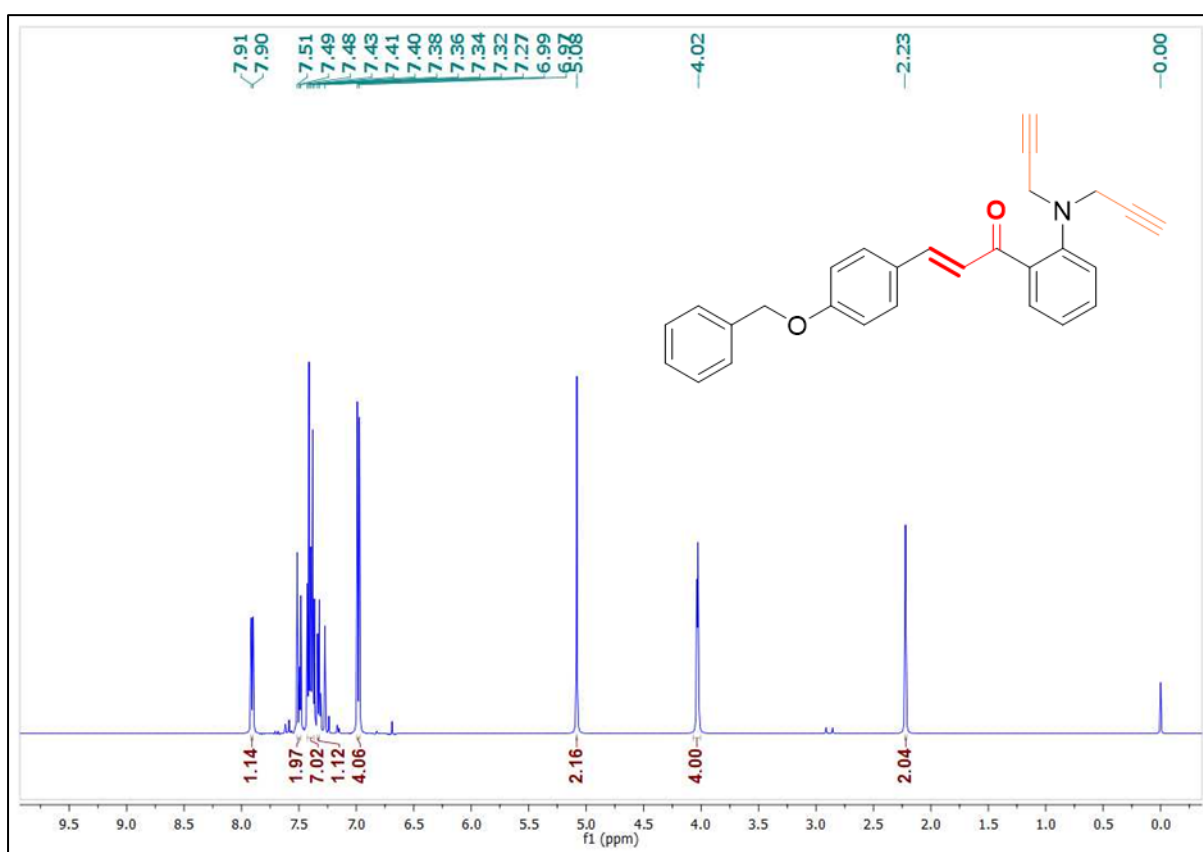
¹³C NMR spectrum of alkyne 143
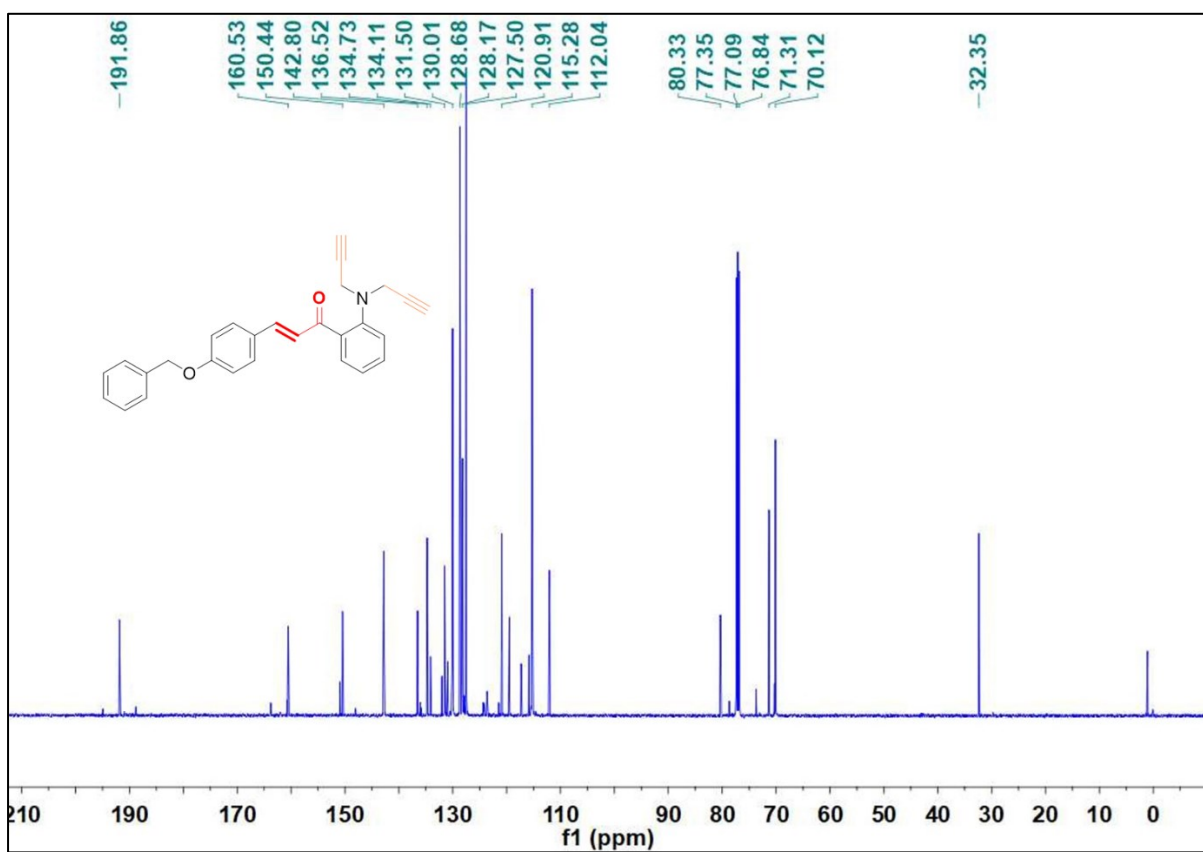
^{1}H NMR spectrum of alkyne 144
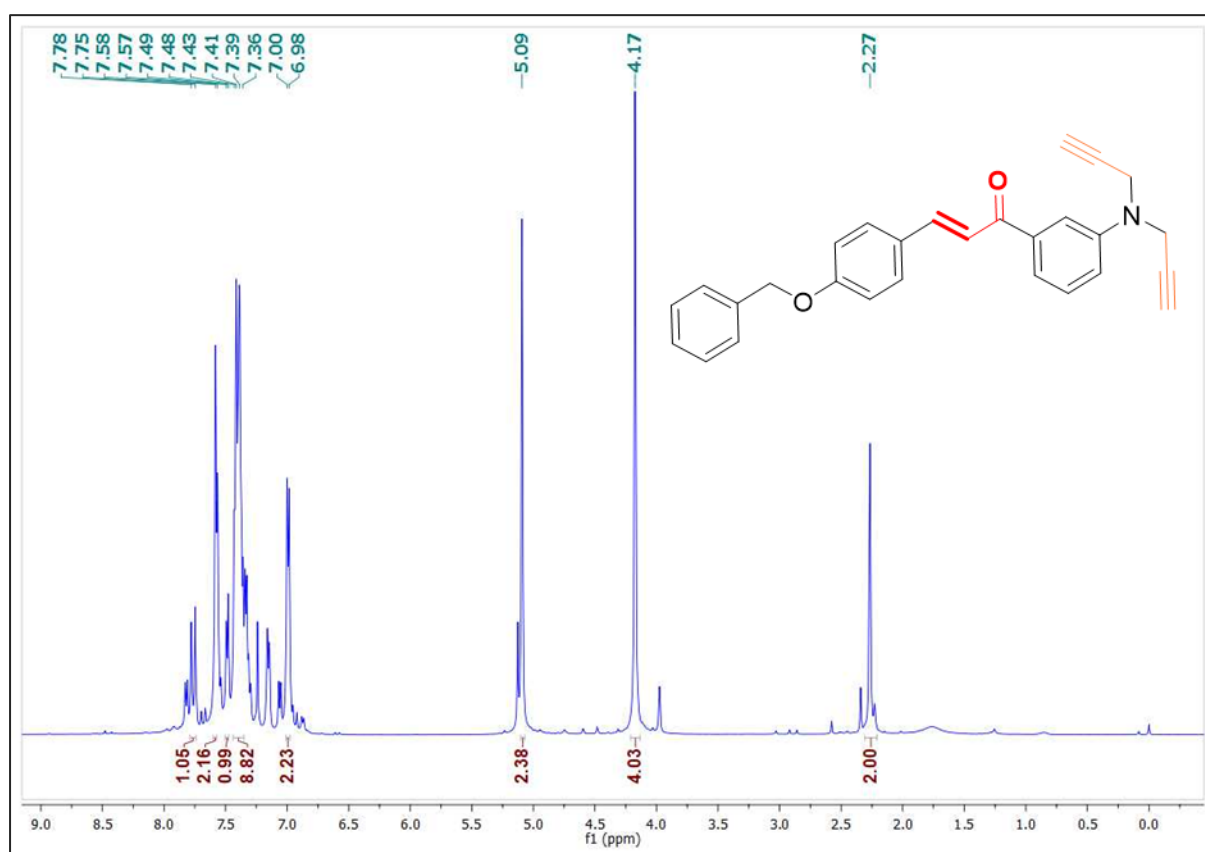
^{13}C NMR spectrum of alkyne 144
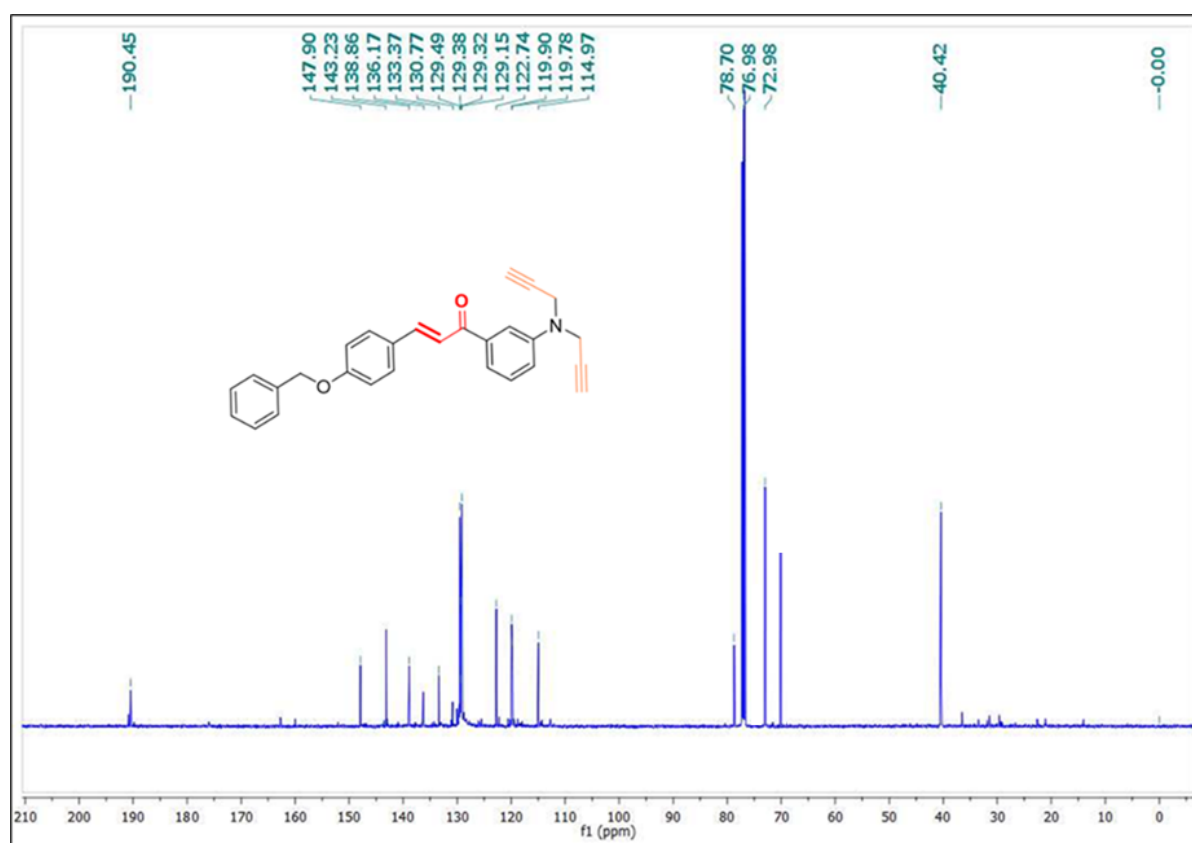
^{1}H NMR spectrum of alkyne 145
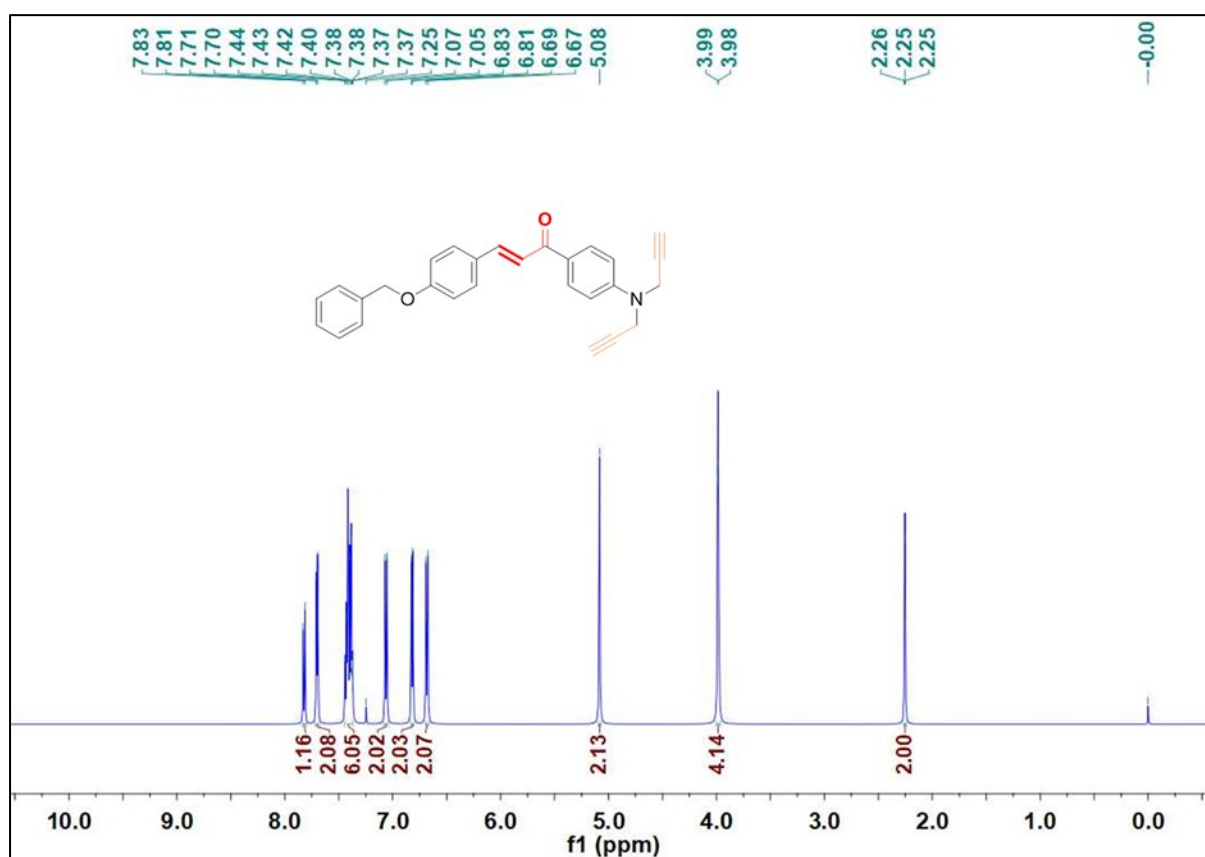
^{13}C NMR spectrum of alkyne 145
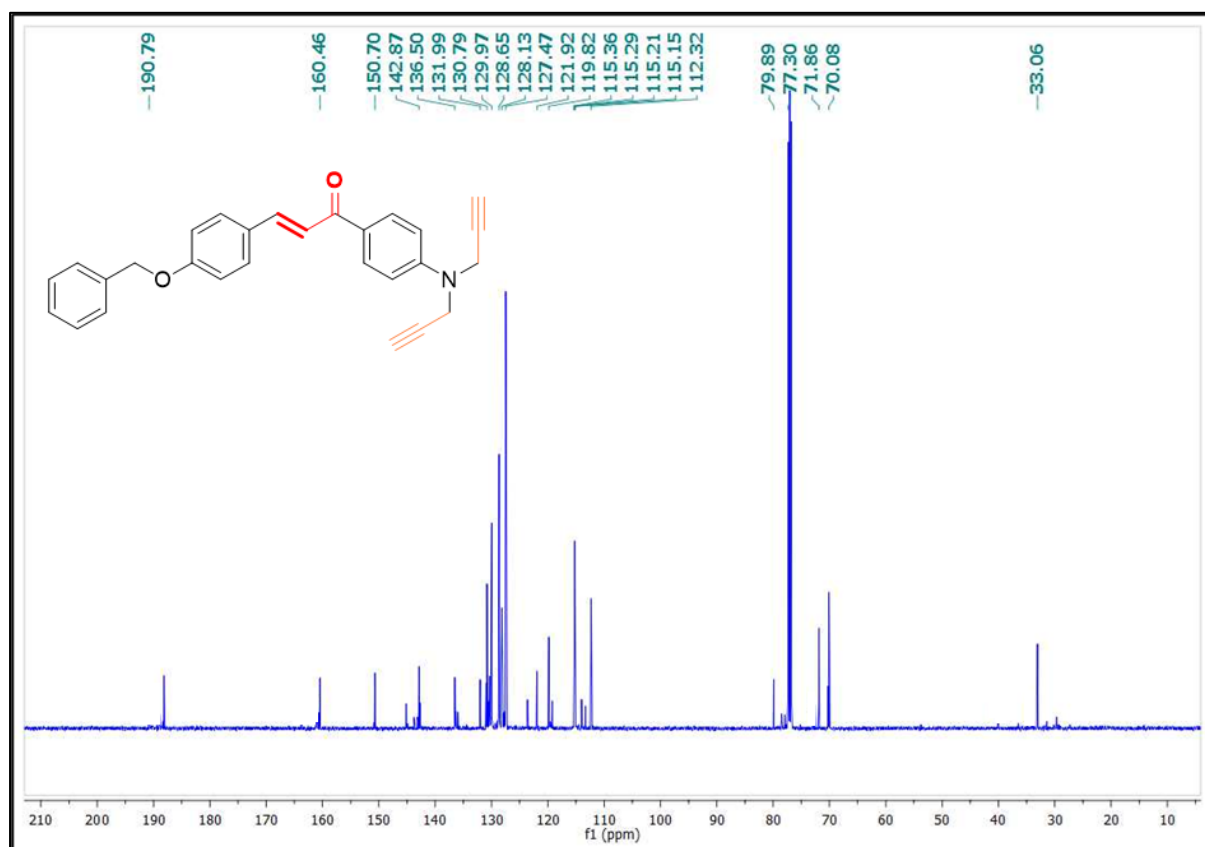
¹H NMR spectrum of 1,2,3-triazole 146

¹H NMR spectrum of 1,2,3-triazole 146

¹³C NMR spectrum of 1,2,3-triazole 146
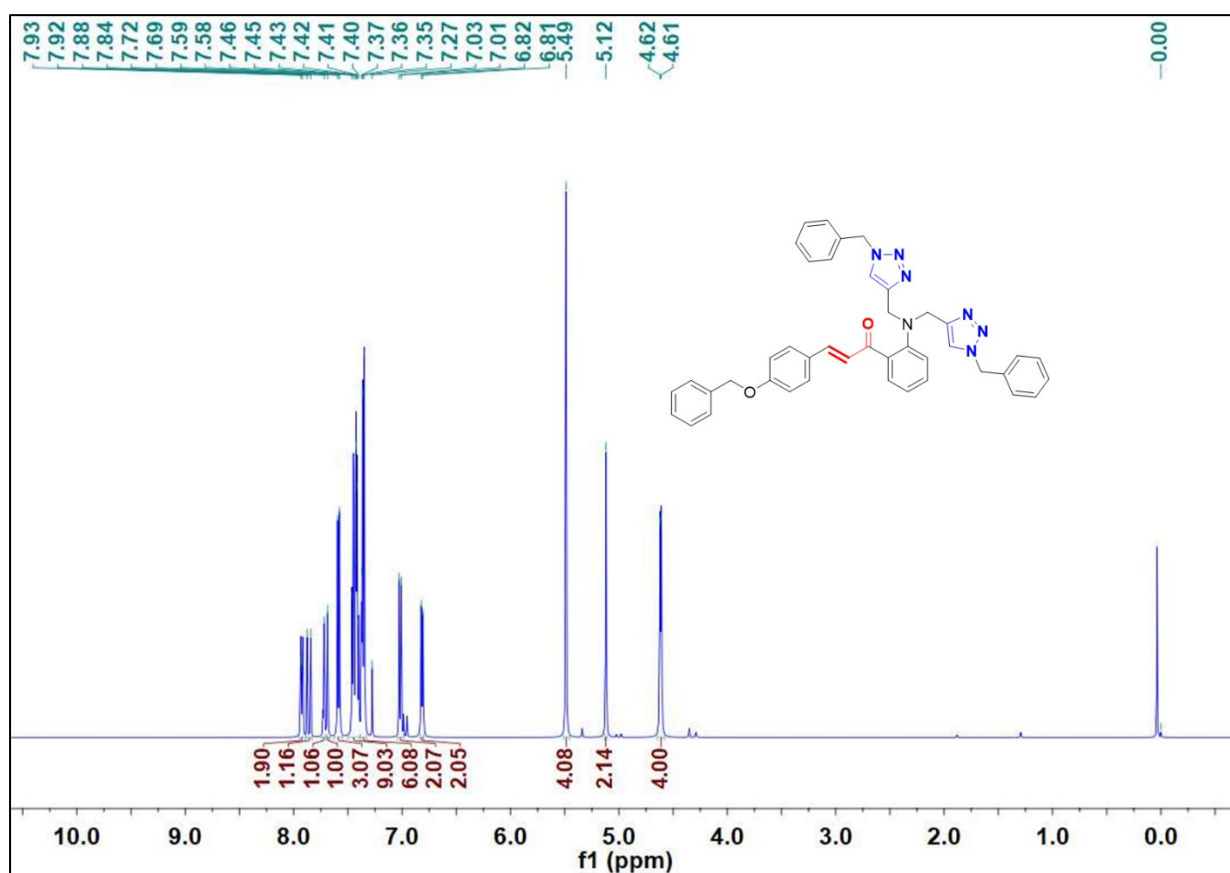
¹³C NMR spectrum of 1,2,3-triazole 146
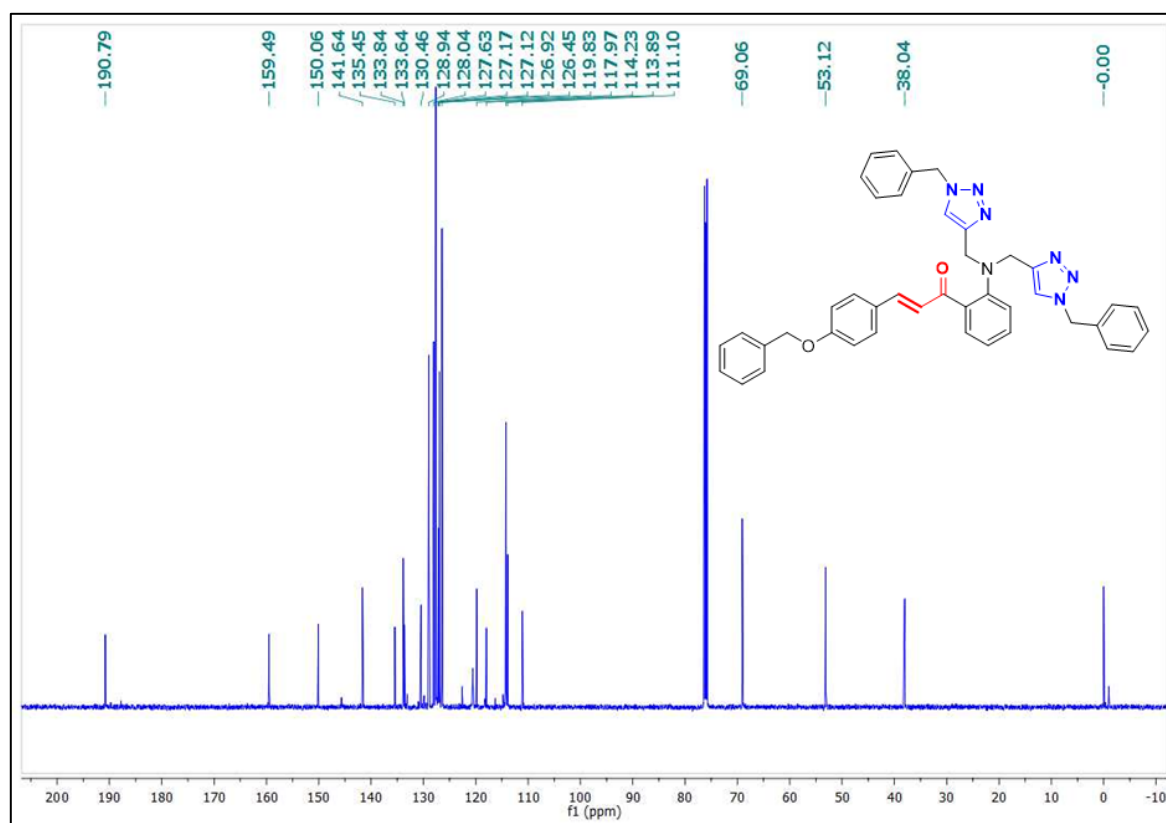
^{1}H NMR spectrum of 1,2,3-triazole 147
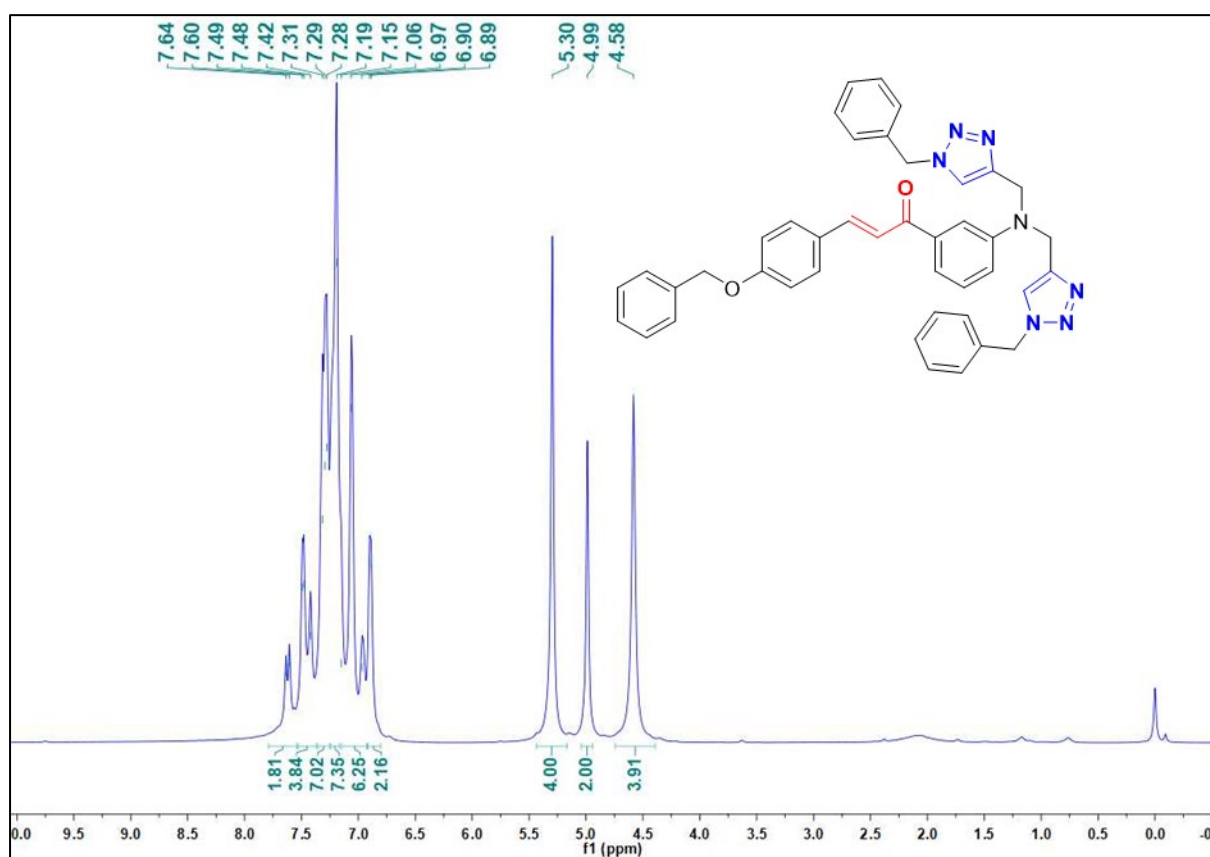
^{13}C NMR spectrum of 1,2,3-triazole 147
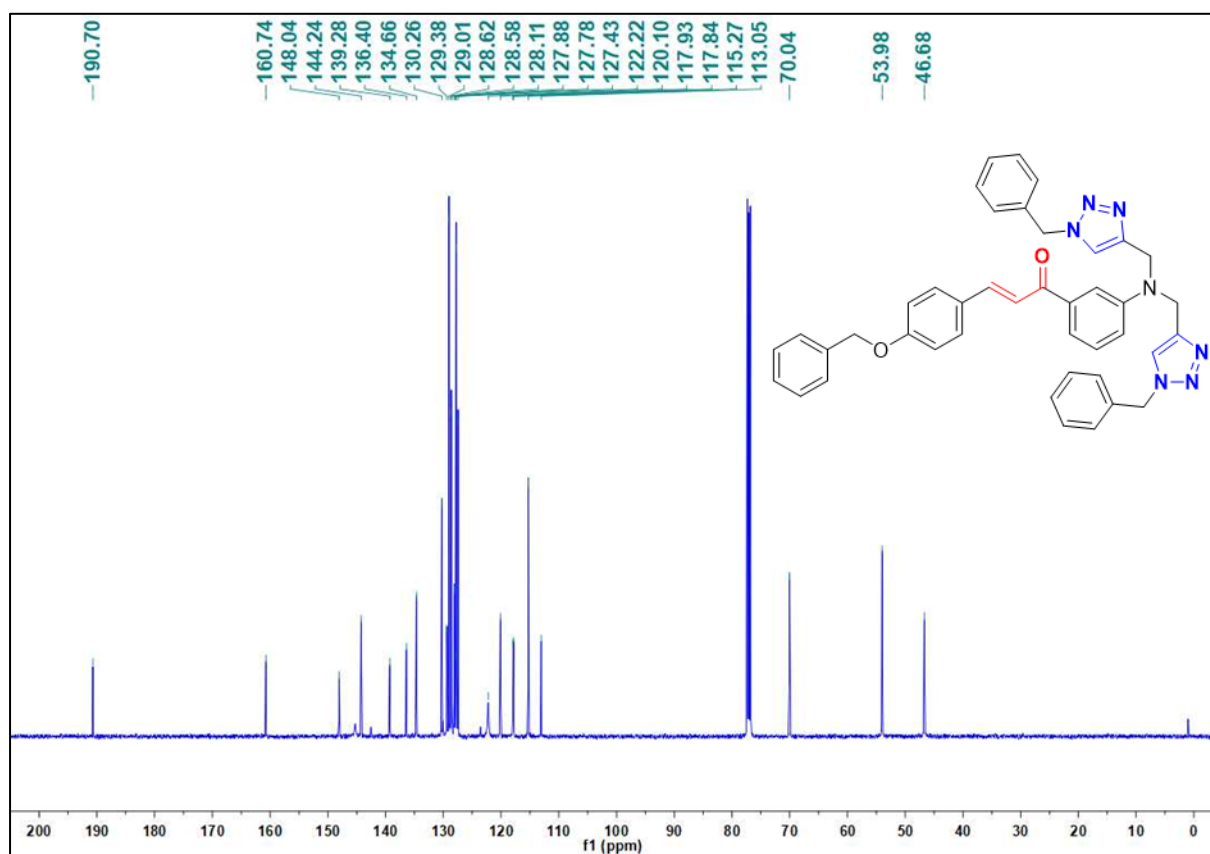
^{1}H NMR spectrum of 1,2,3-triazole 148
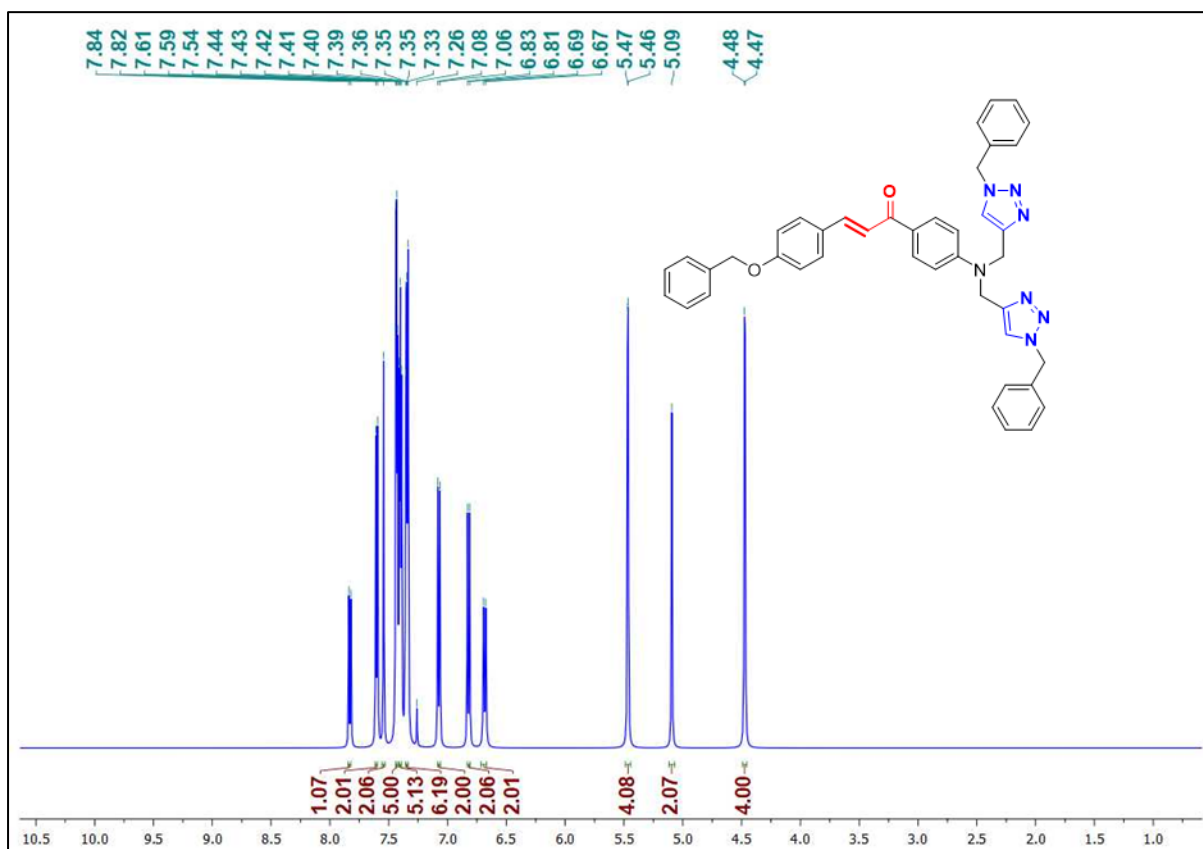
^{13}C NMR spectrum of 1,2,3-triazole 148
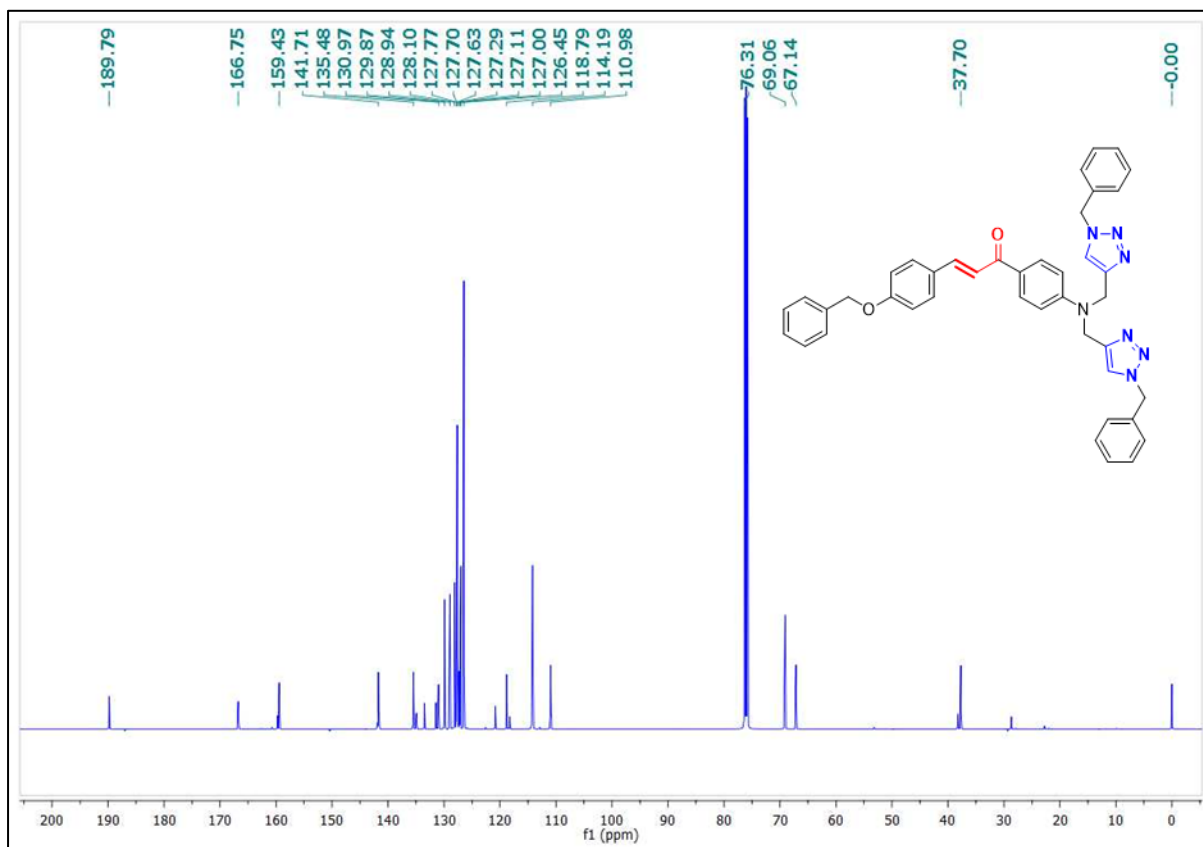
^{1}H NMR spectrum of chalcone 150
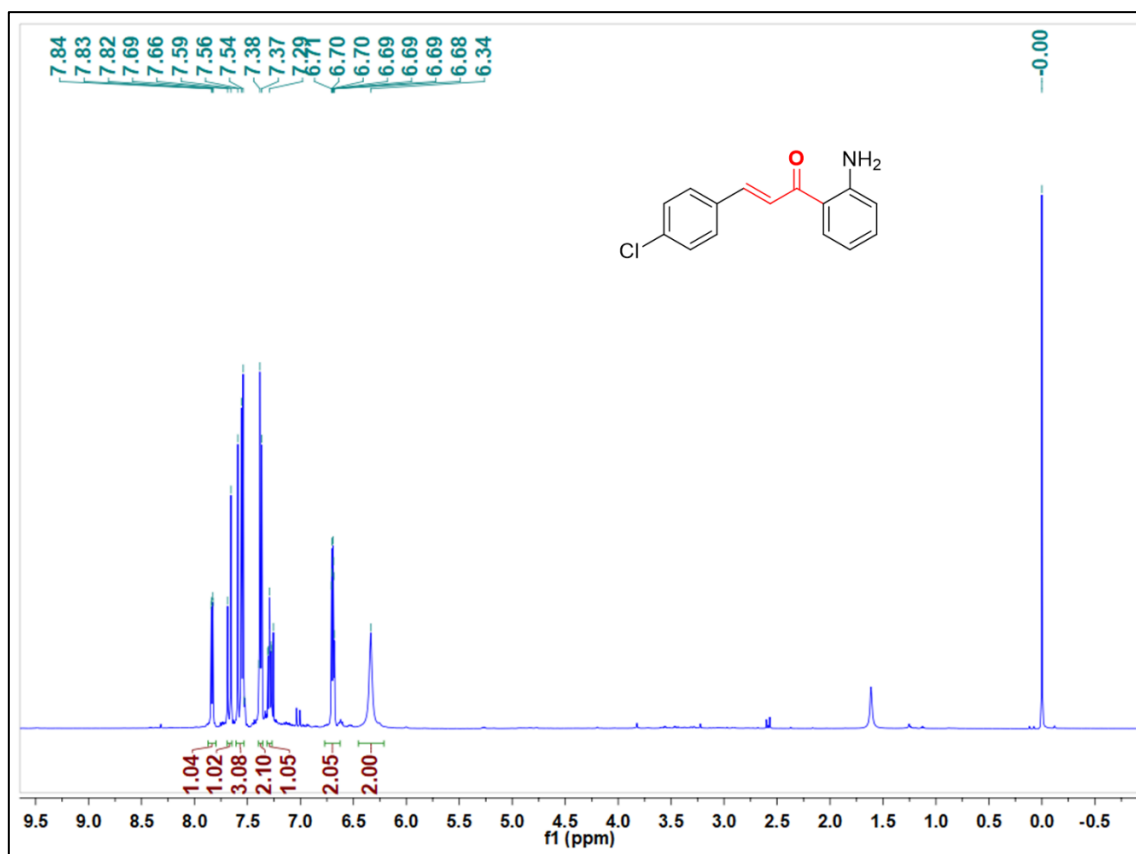
^{13}C NMR spectrum of chalcone 150
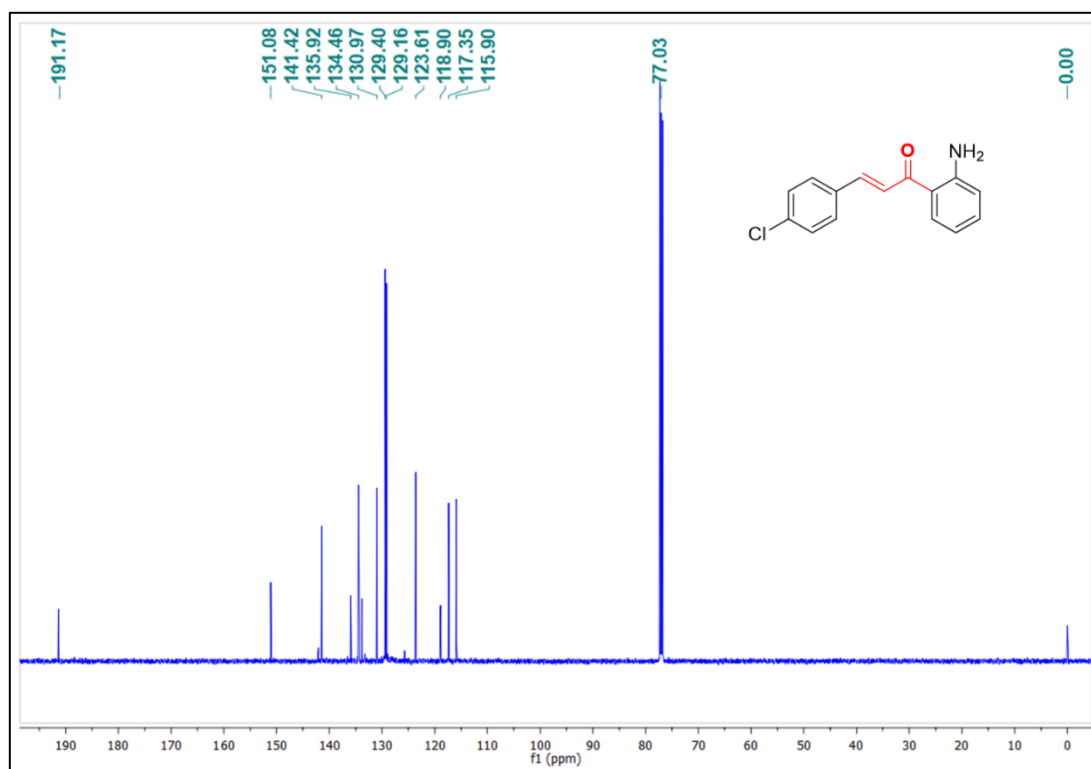
¹H NMR spectrum of chalcone 151
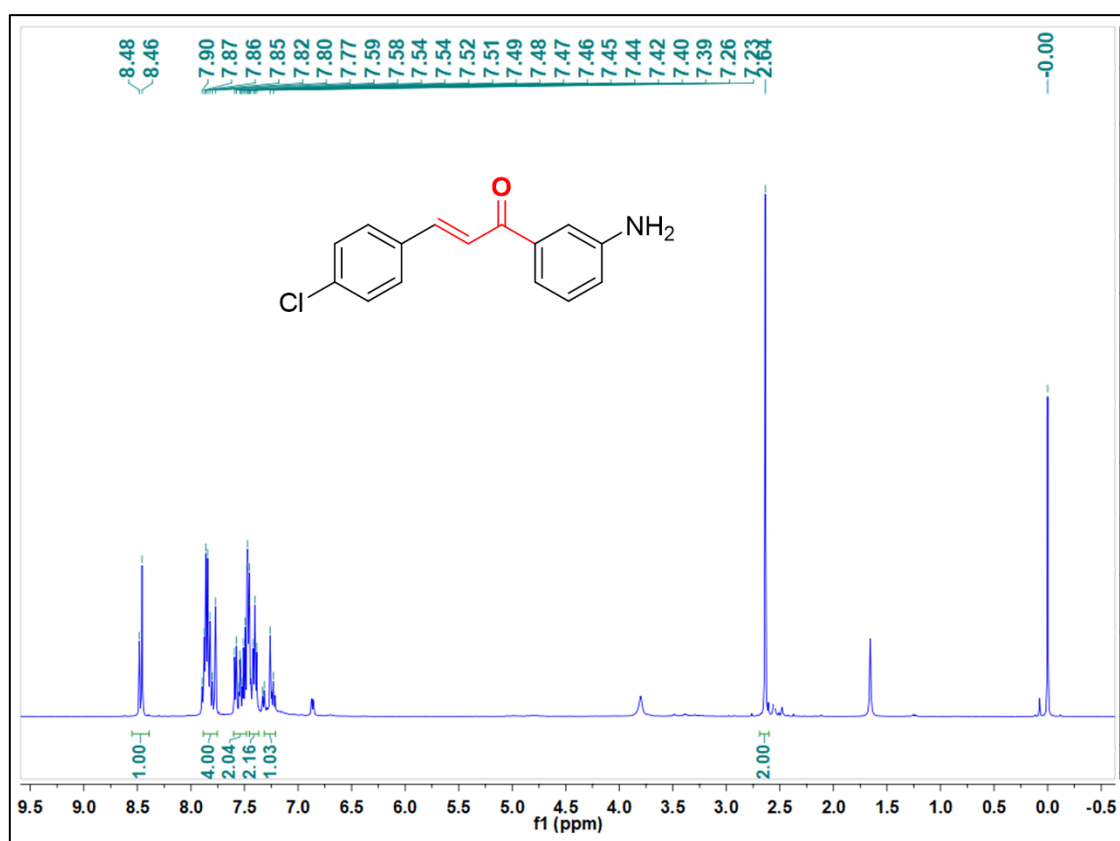
¹³C NMR spectrum of chalcone 151
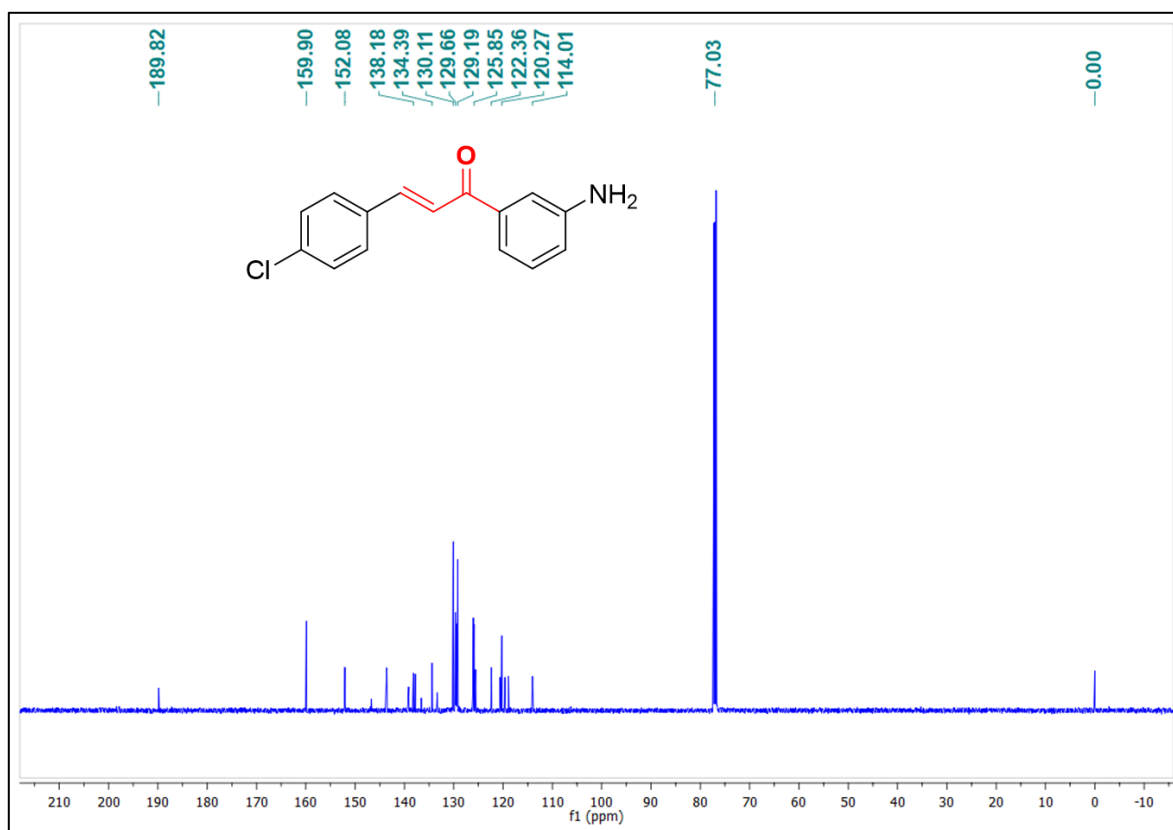
^1H NMR spectrum of chalcone 152
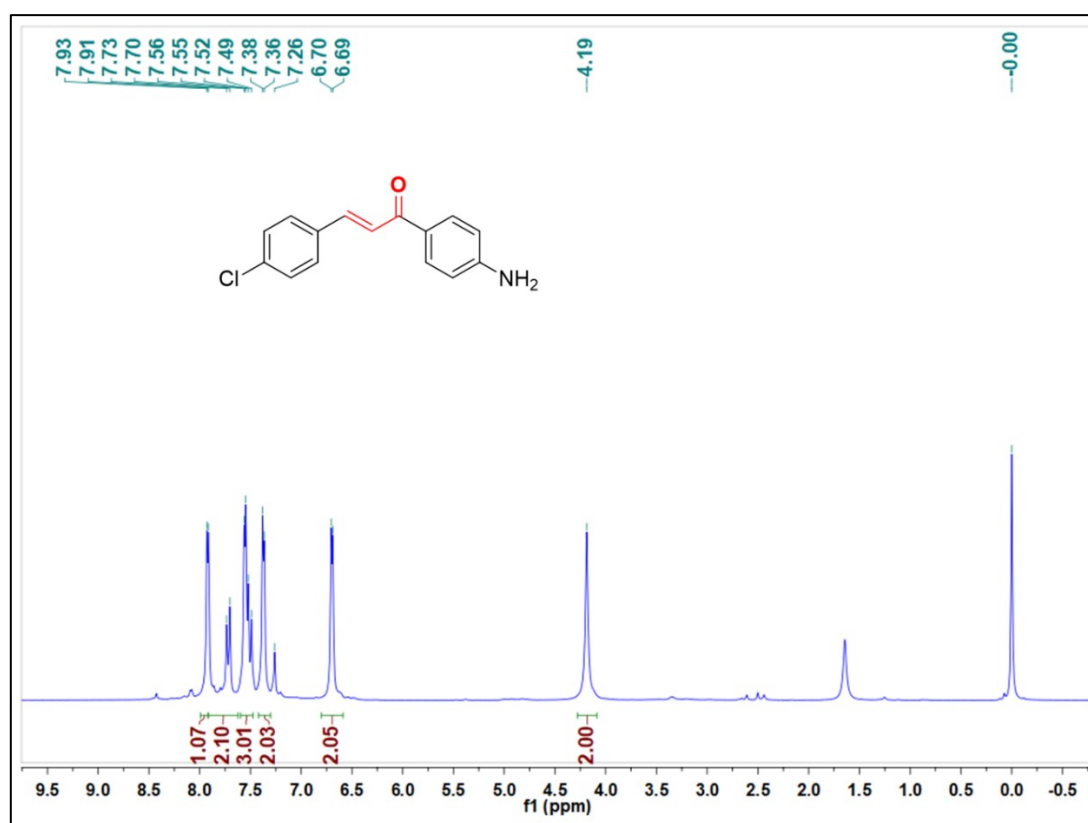
^{13}C NMR spectrum of chalcone 152

¹H NMR spectrum of alkyne 153

¹H NMR spectrum of alkyne 153
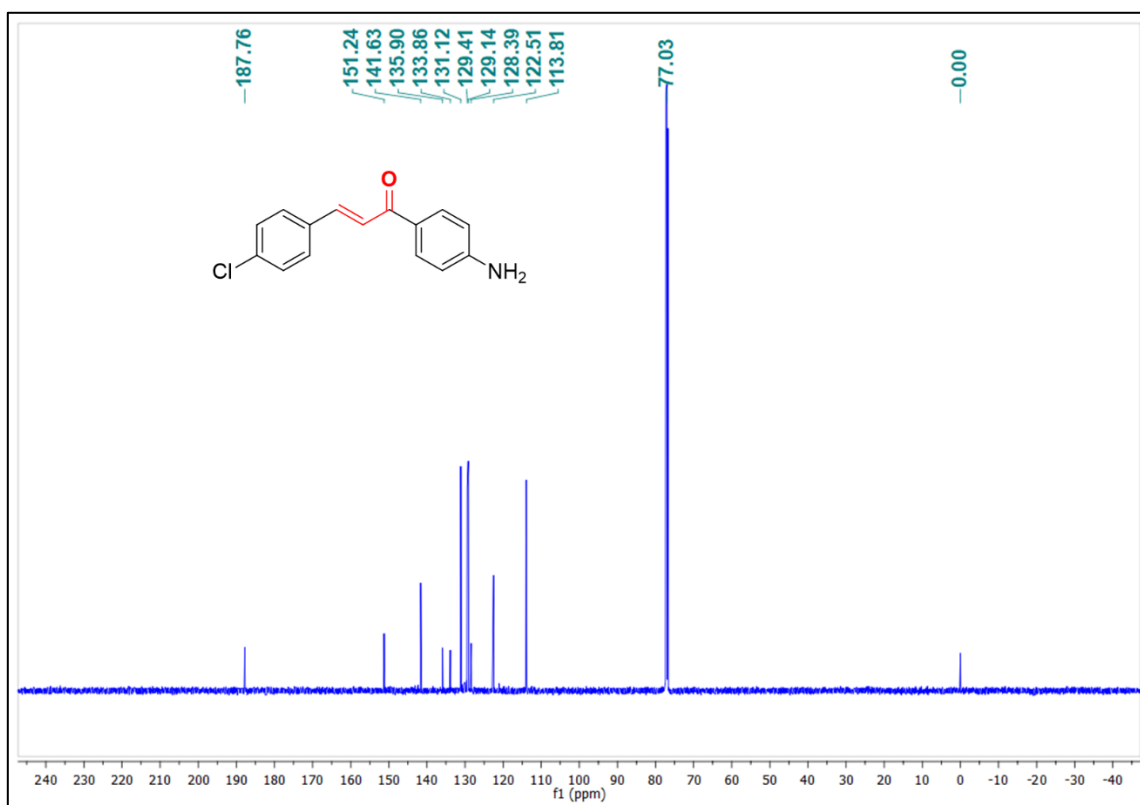
¹³C NMR spectrum of alkyne 153
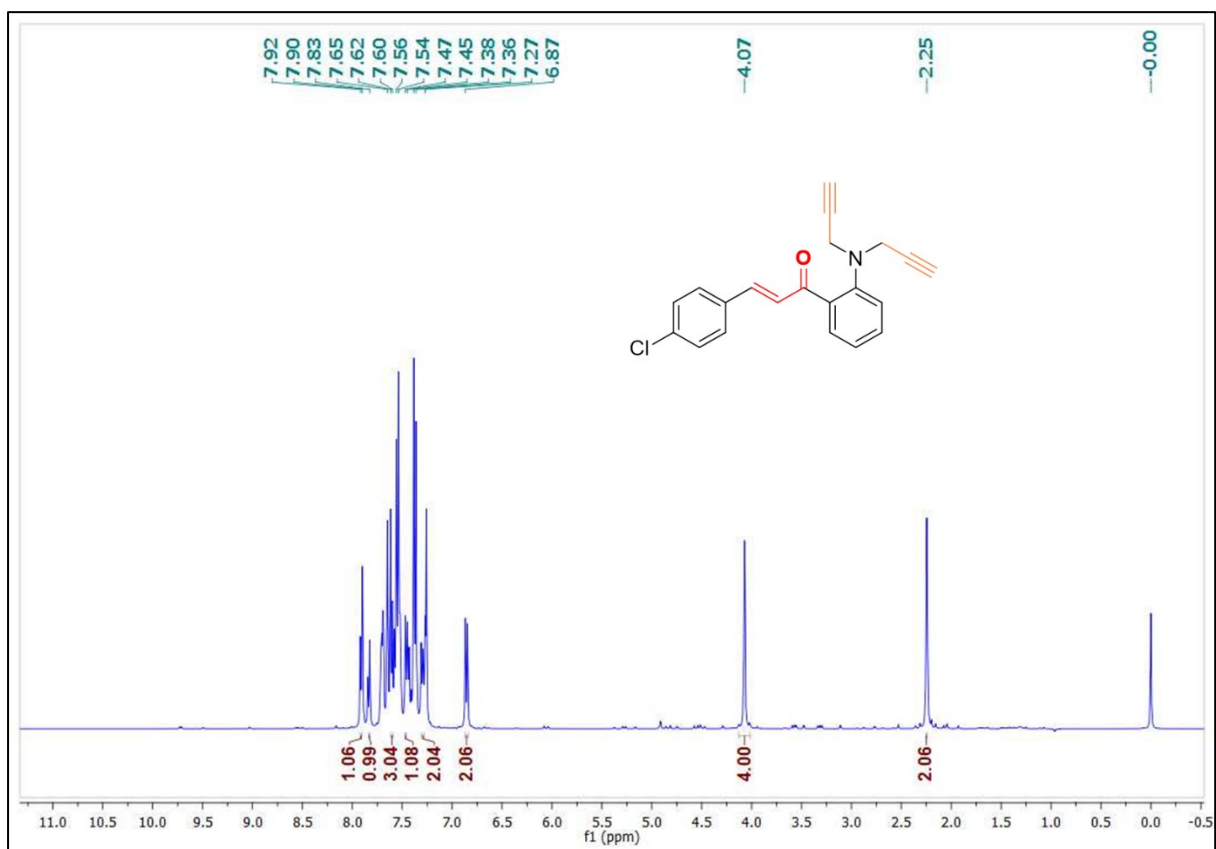
¹³C NMR spectrum of alkyne 153
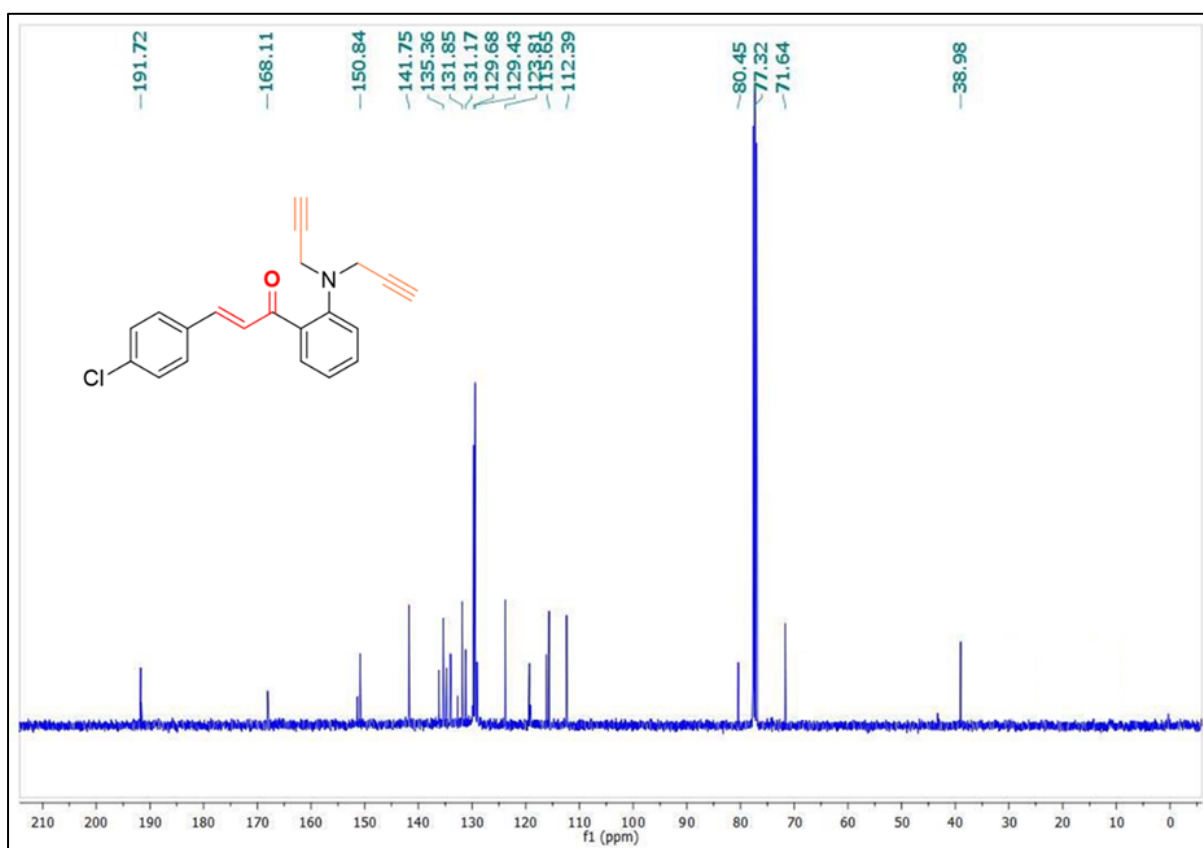
¹H NMR spectrum of alkyne 154
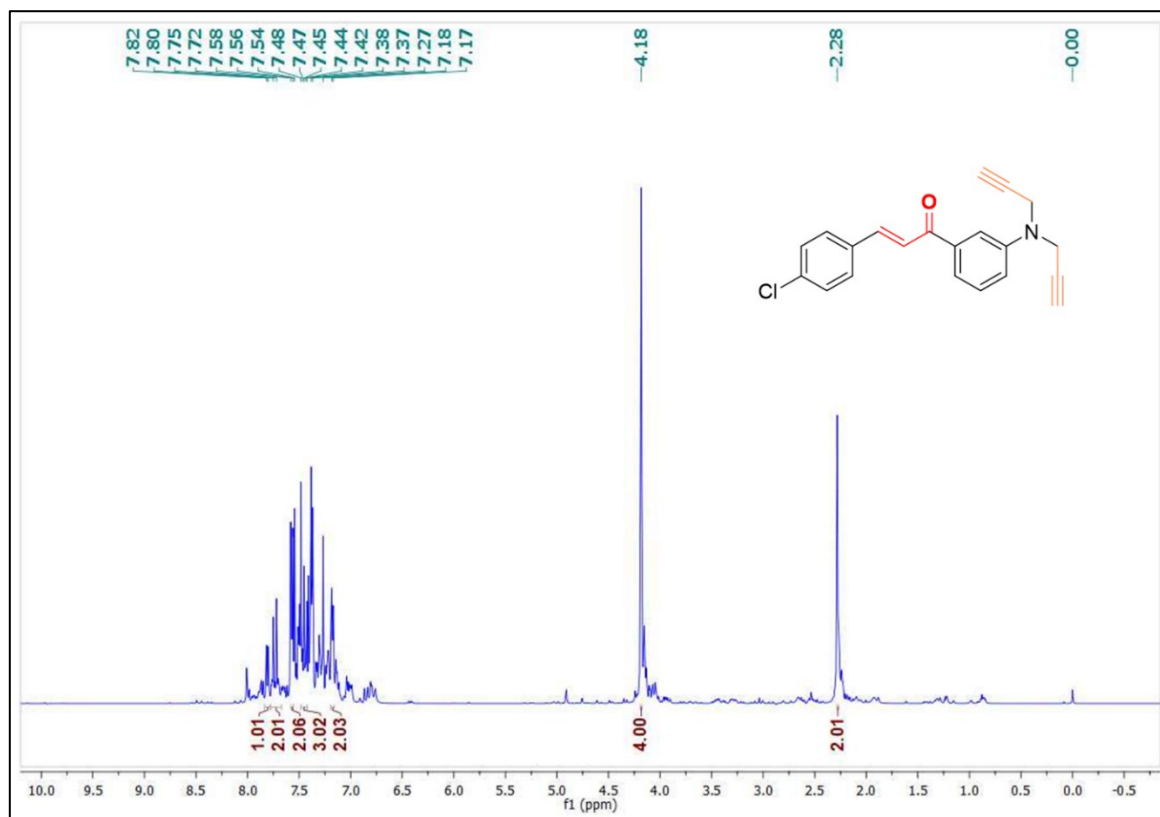
¹³C NMR spectrum of alkyne 154
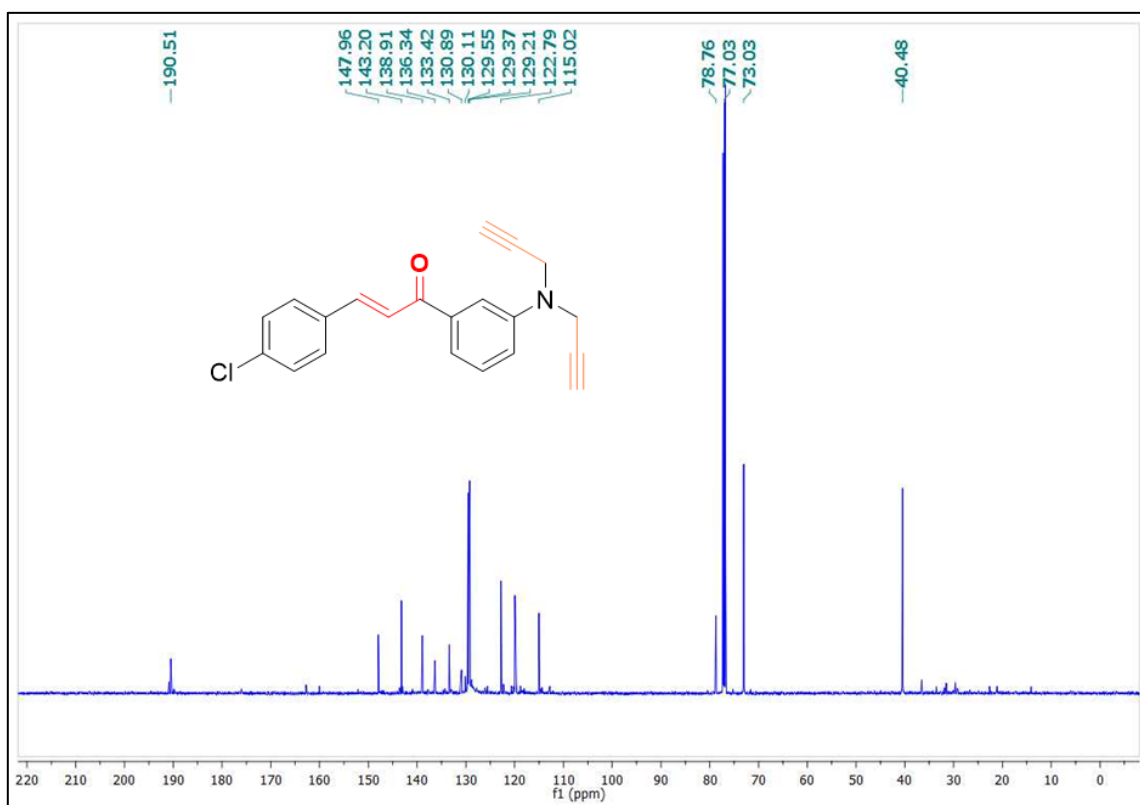
^{1}H NMR spectrum of alkyne 155
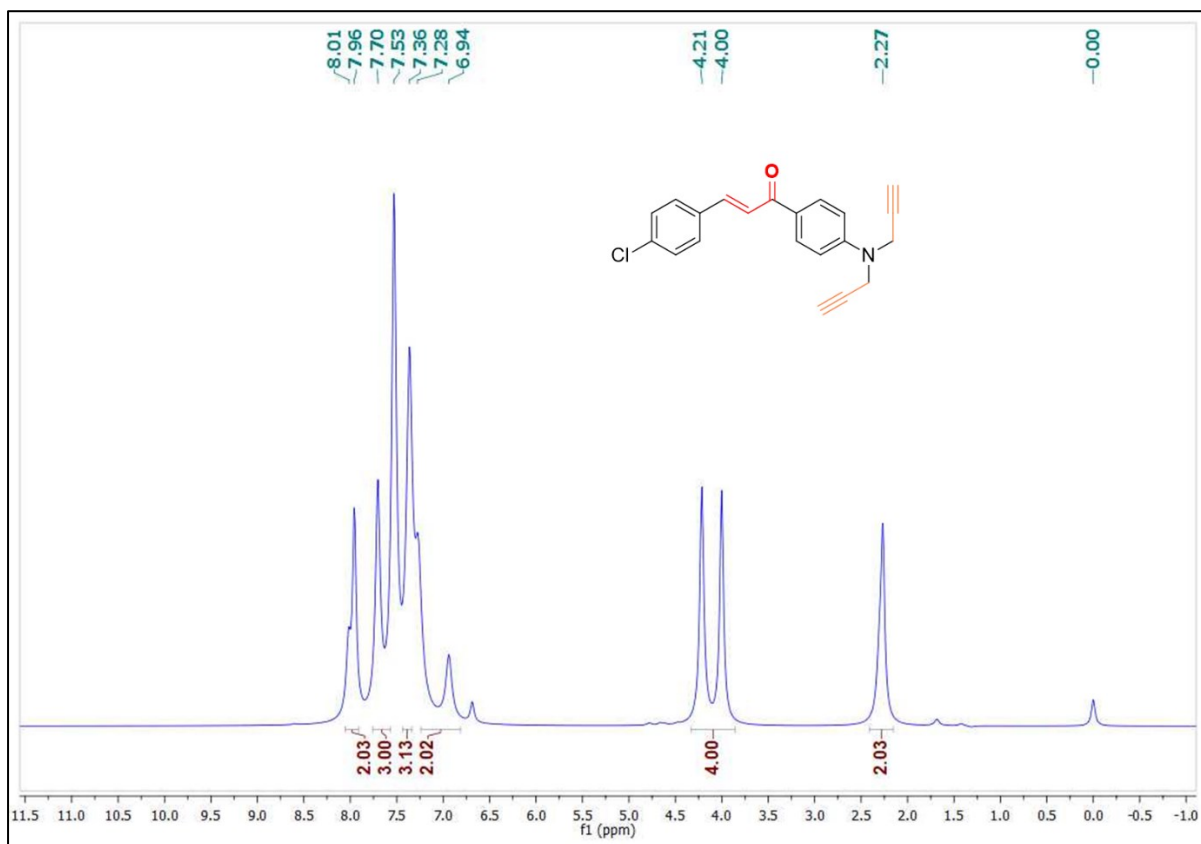
^{13}C NMR spectrum of alkyne 155
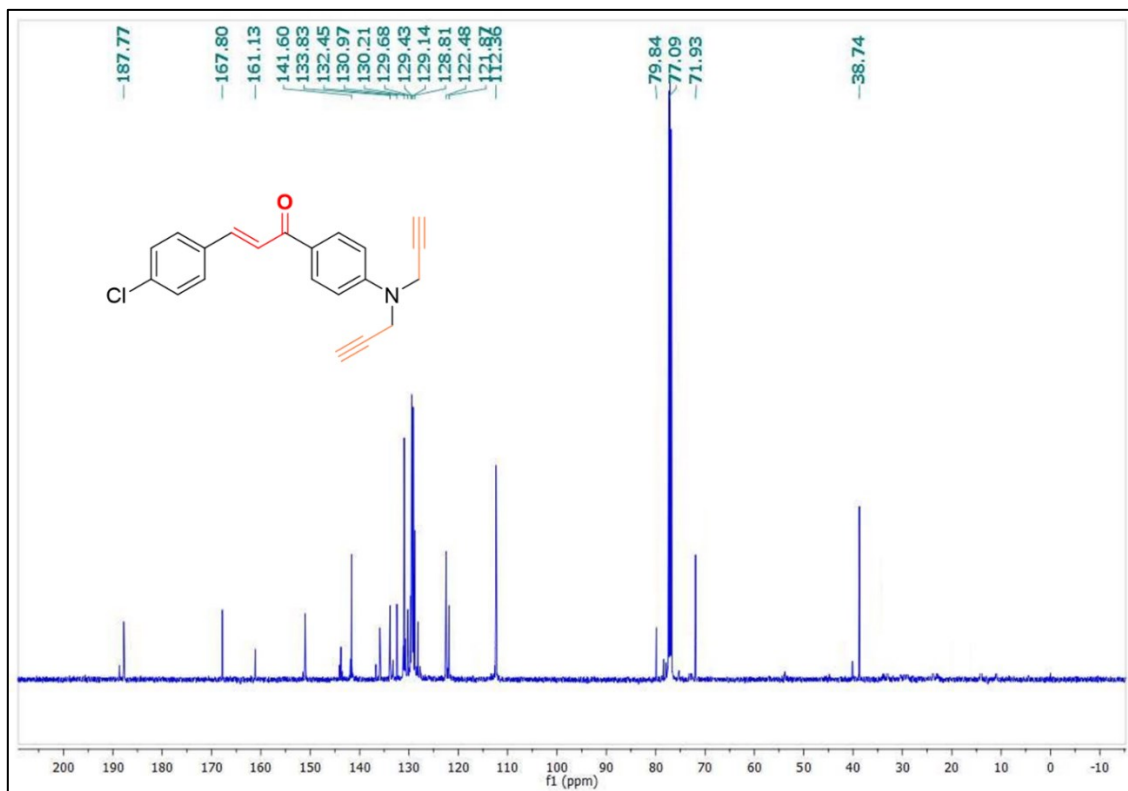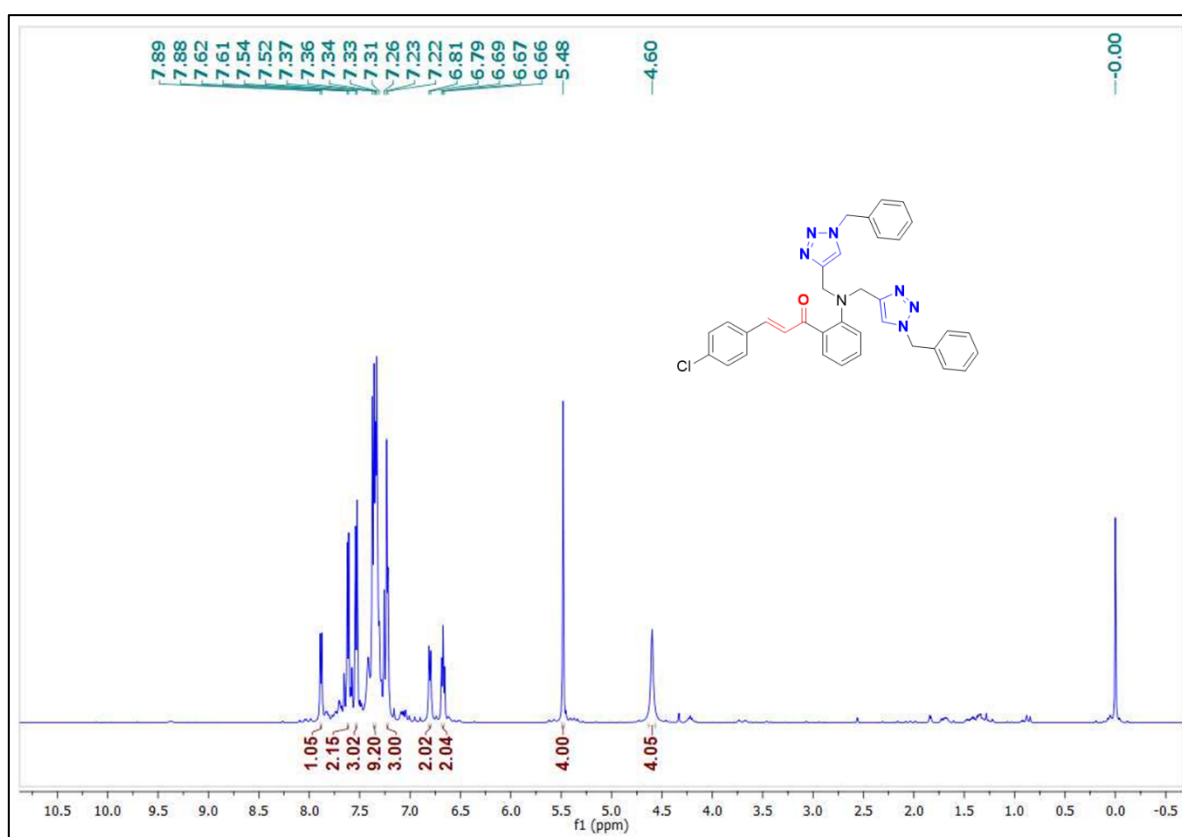
¹H NMR spectrum of 1,2,3-triazole 156

¹H NMR spectrum of 1,2,3-triazole 156

7.89
7.88
7.62
7.61
7.54
7.52
7.37
7.36
7.34
7.33
7.31
7.26
7.23
7.22
6.81
6.79
6.69
6.67
6.66
5.48
4.60
0.00

1.05
2.15
3.02
9.20
3.00
2.02
2.04
4.00
4.05

¹³C NMR spectrum of 1,2,3-triazole 156

191.39
151.24
141.34
135.22
129.38
129.16
129.09
128.71
127.97
114.59
112.23
77.05
54.22
39.05
0.00
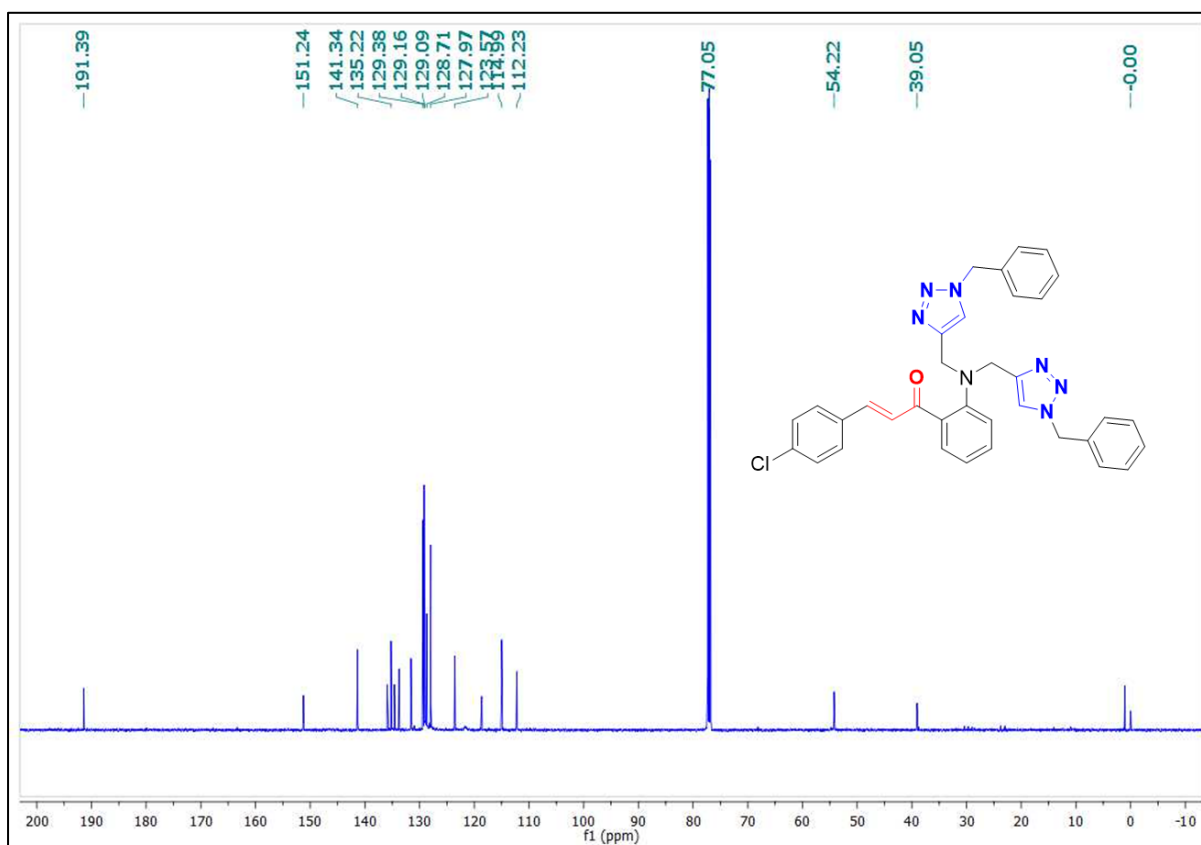
^{1}H NMR spectrum of 1,2,3-triazole 157
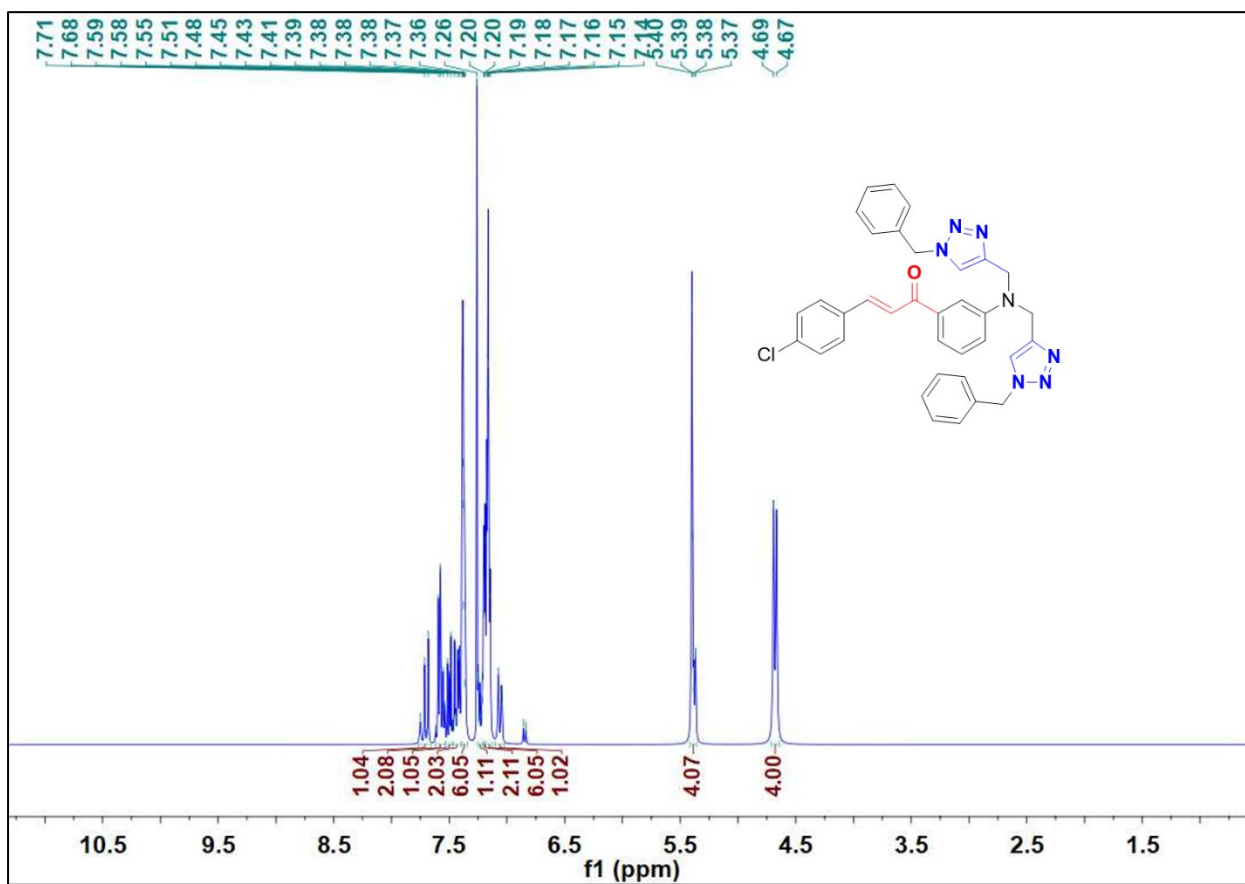
^{13}C NMR spectrum of 1,2,3-triazole 157
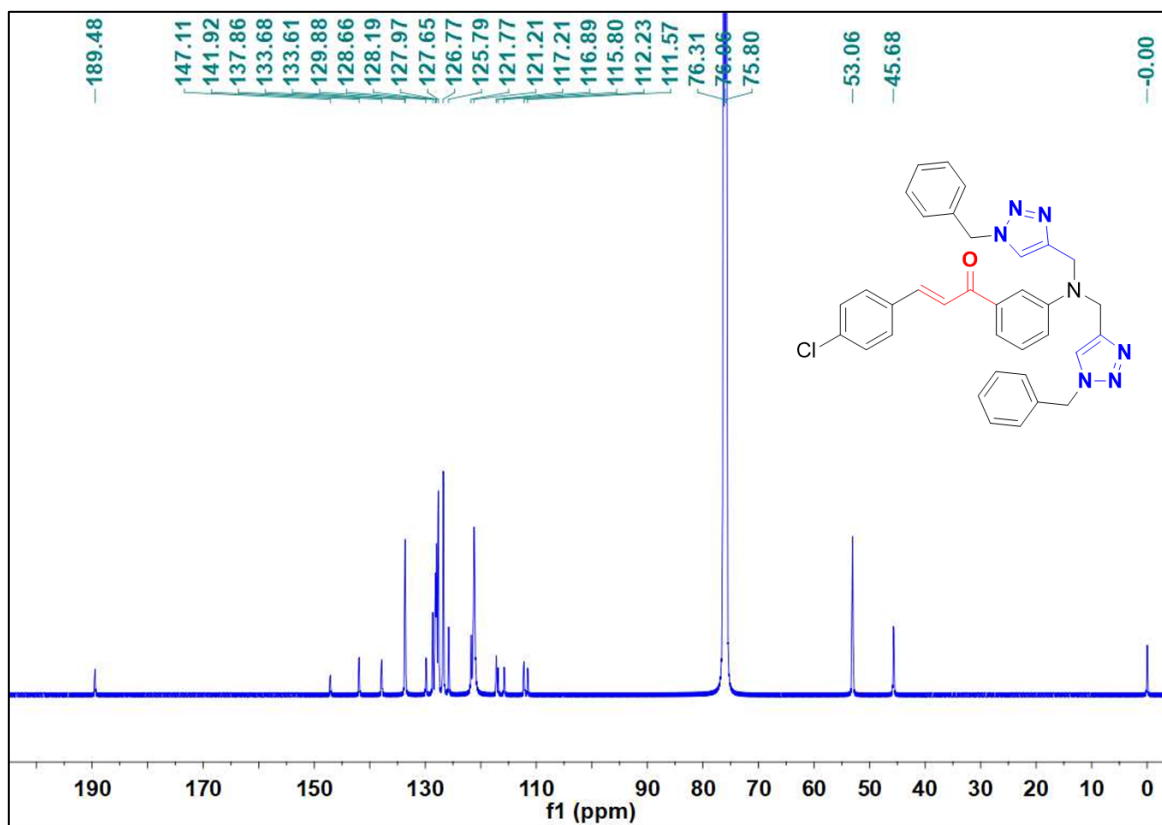
^{1}H NMR spectrum of 1,2,3-triazole 158
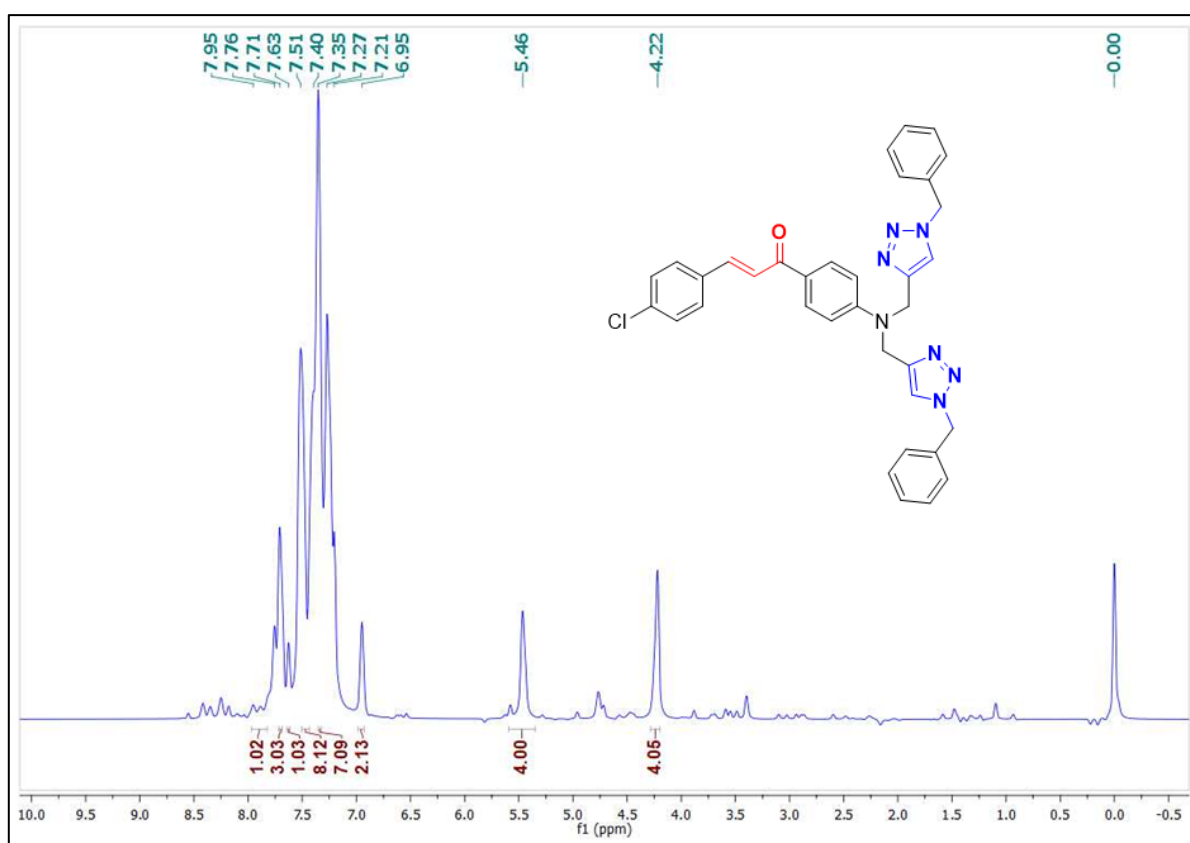
^{13}C NMR spectrum of 1,2,3-triazole 158
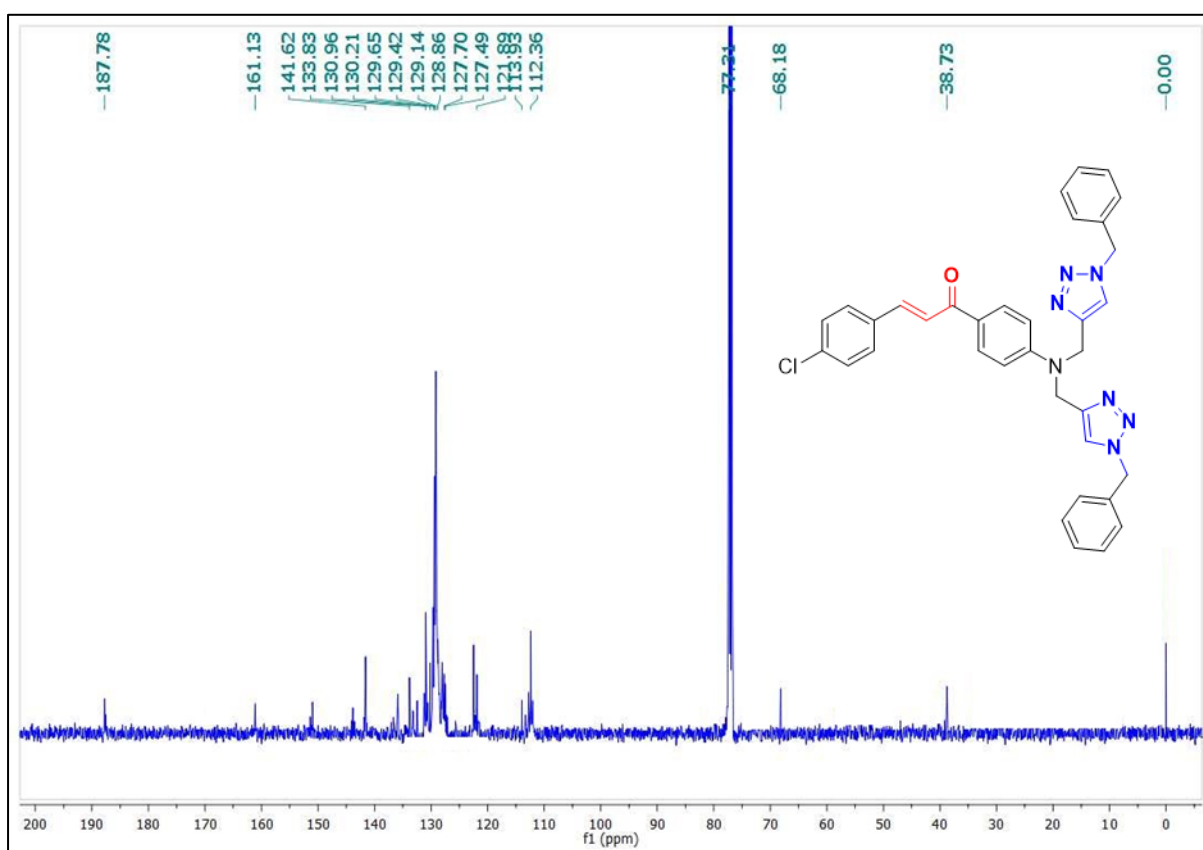
^{1}H NMR spectrum of 1,2,3-triazole 146 – Pb(II) complex
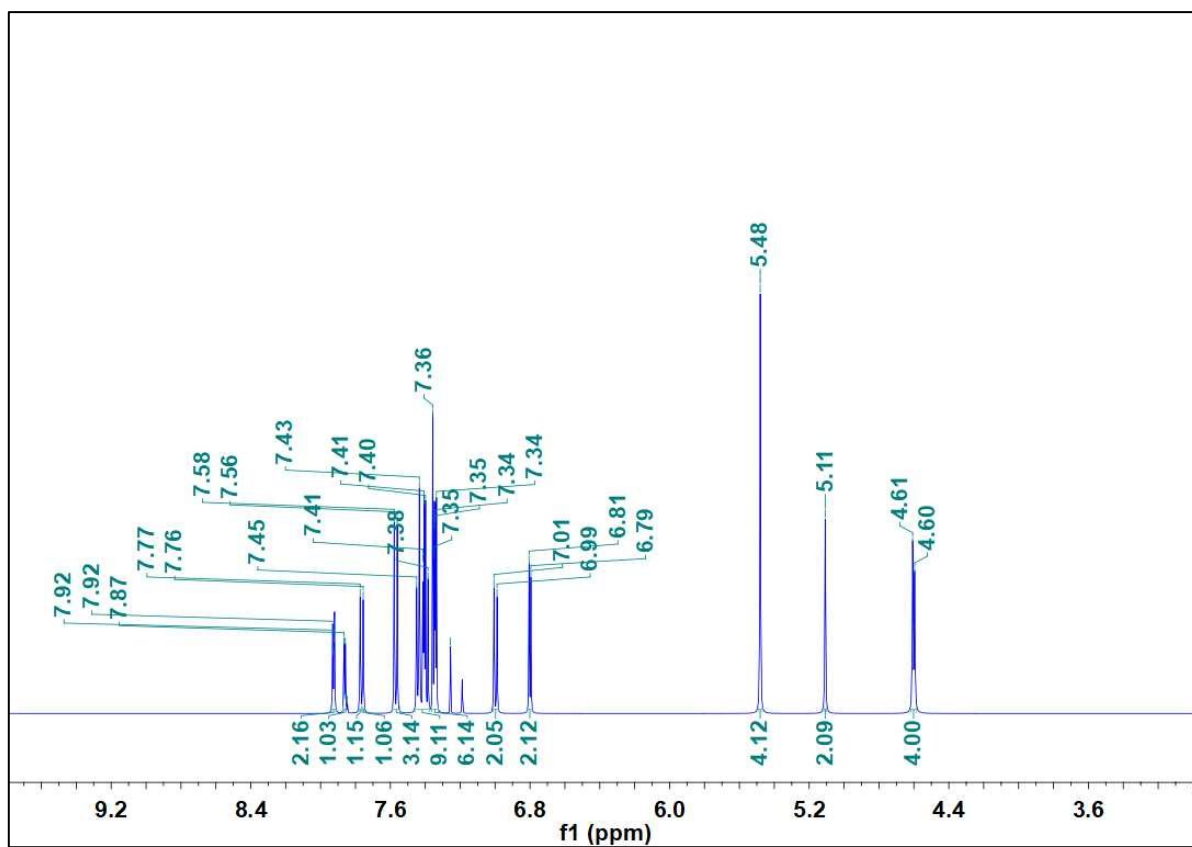
^{1}H NMR spectrum of 1,2,3-triazole 147 – Pb(II) complex
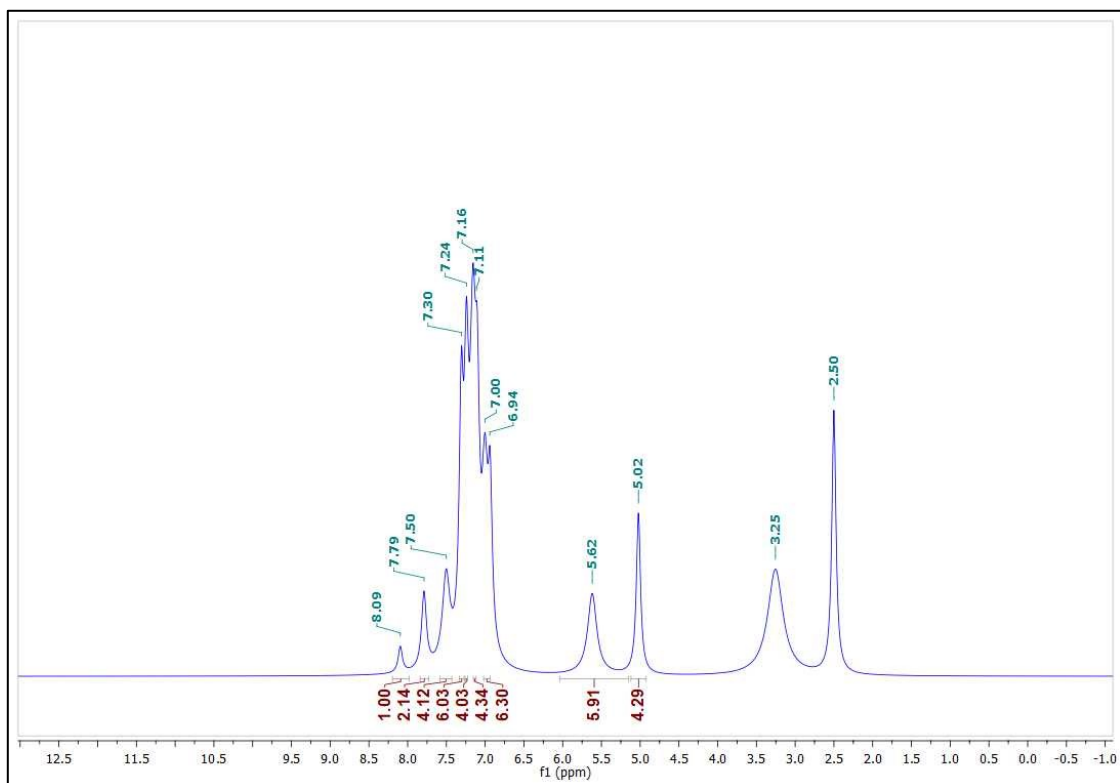
^{1}H NMR spectrum of 1,2,3-triazole 148 – Pb(II) complex
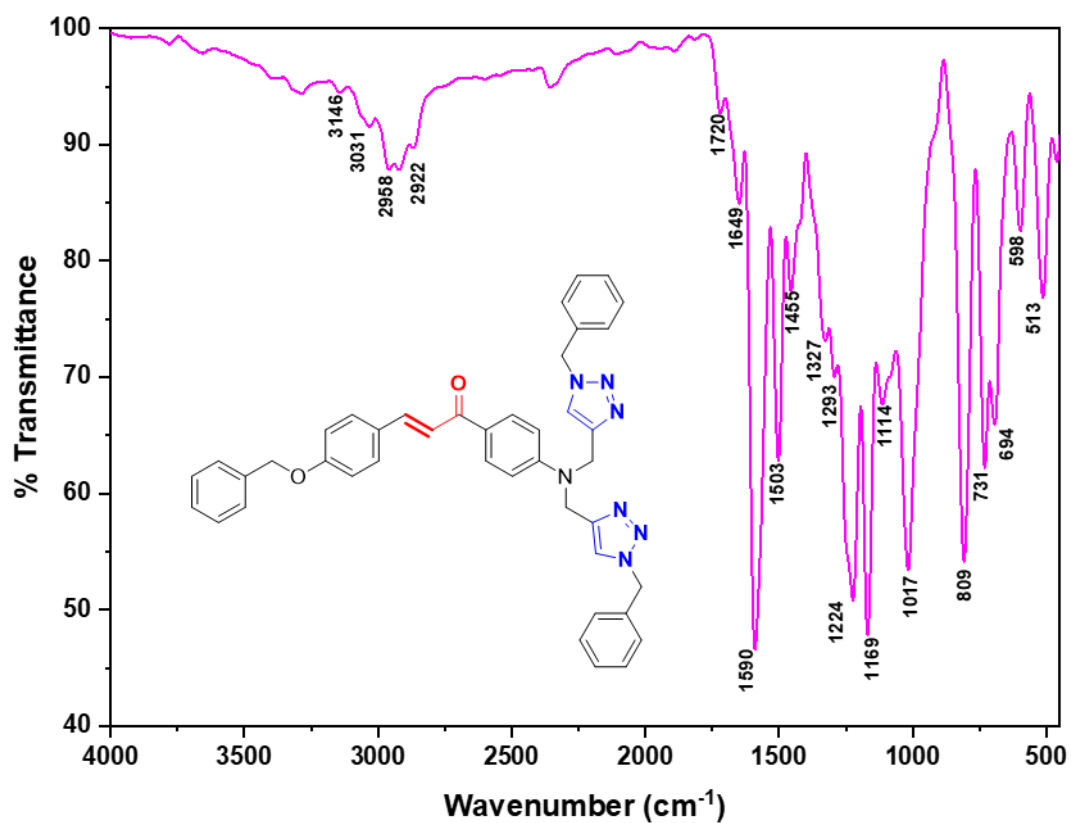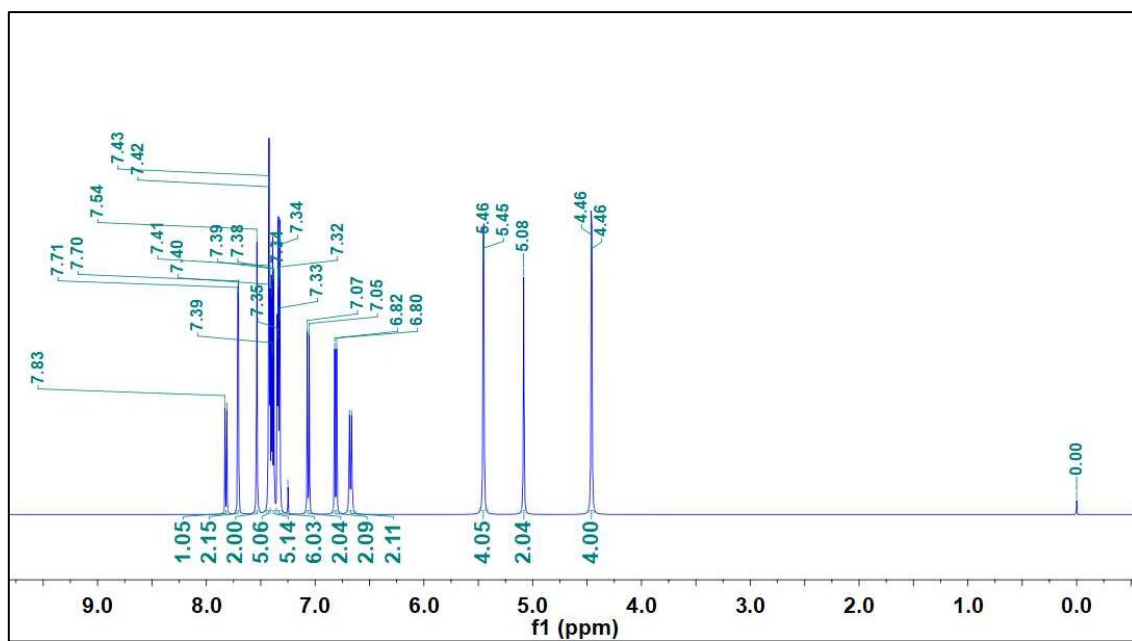

Mass spectrum of 1,2,3-triazole 146
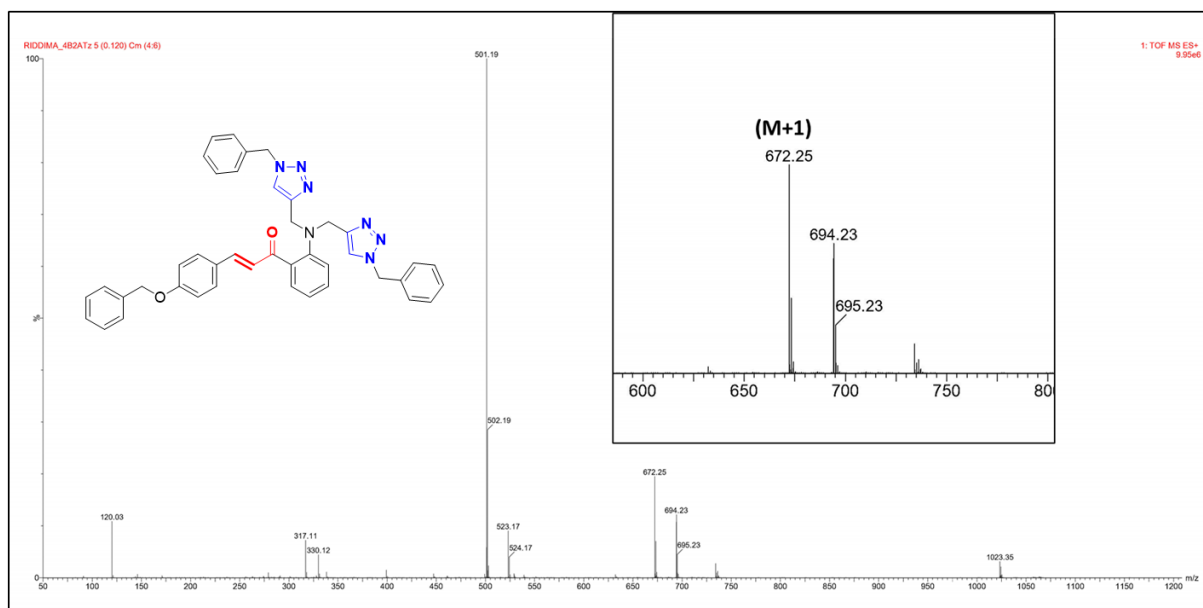
Mass spectrum of 1,2,3-triazole 147

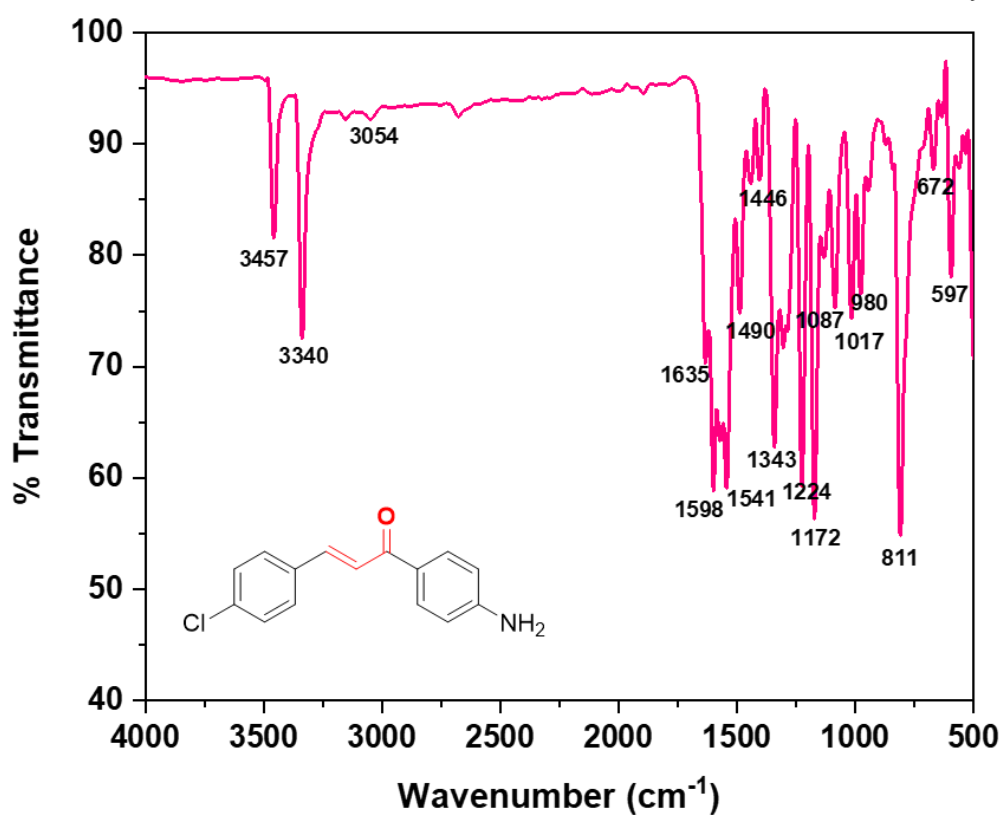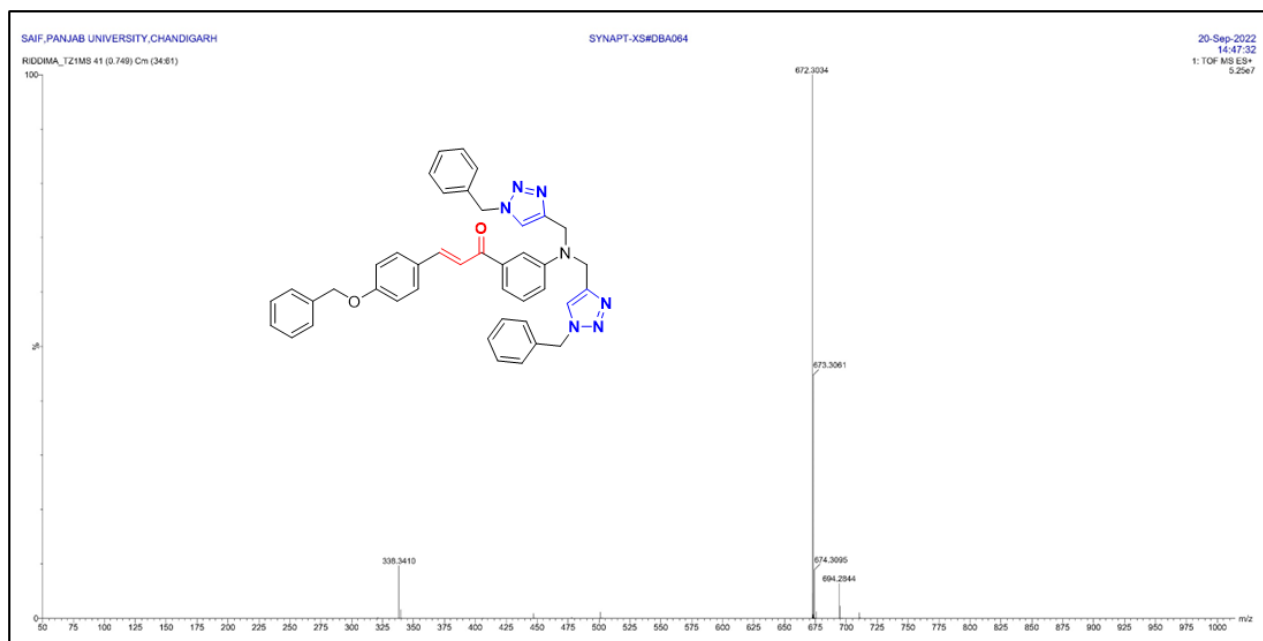
Mass spectrum of 1,2,3-triazole 148
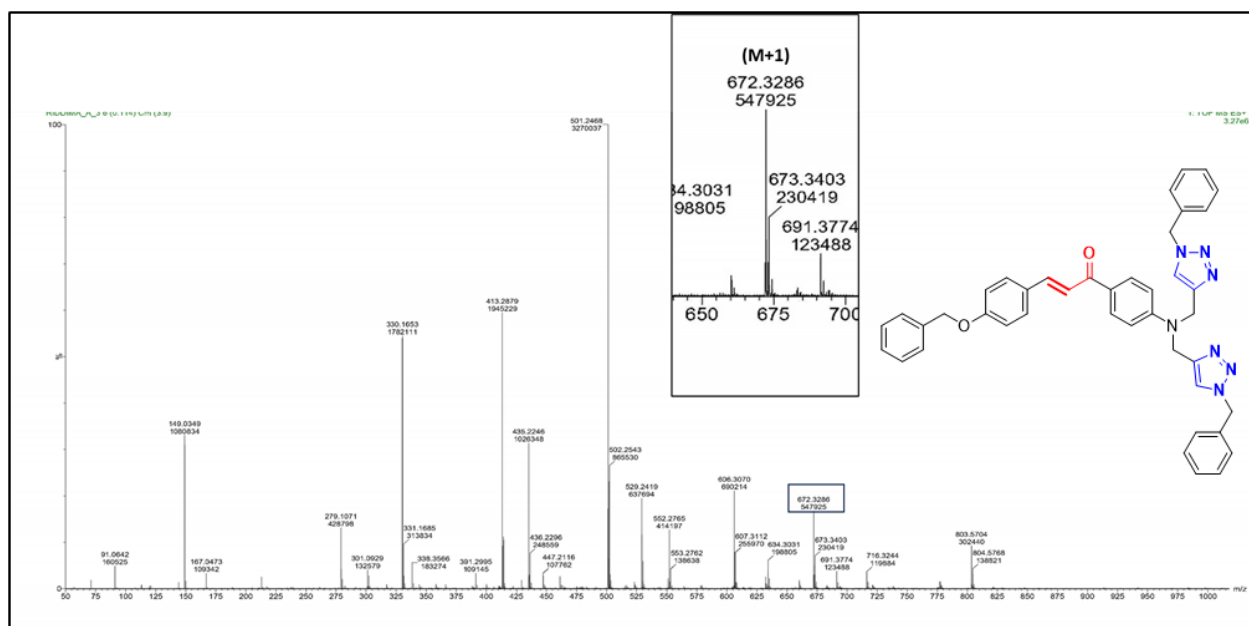
Mass spectrum of 1,2,3-triazole 156
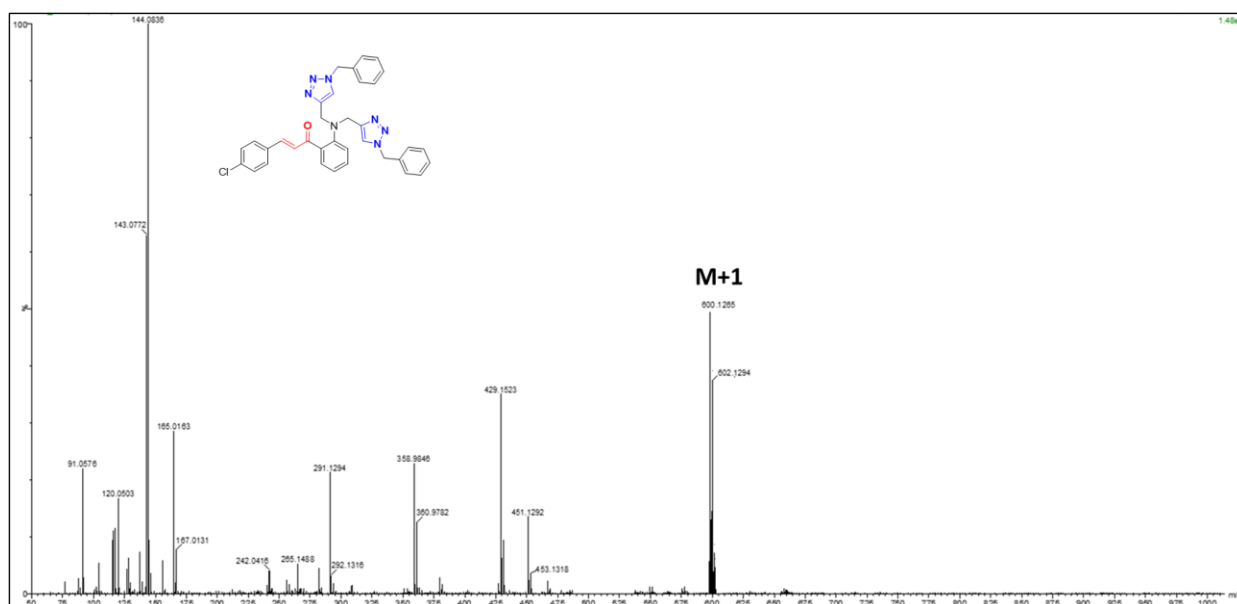
Mass spectrum of 1,2,3-triazole 157
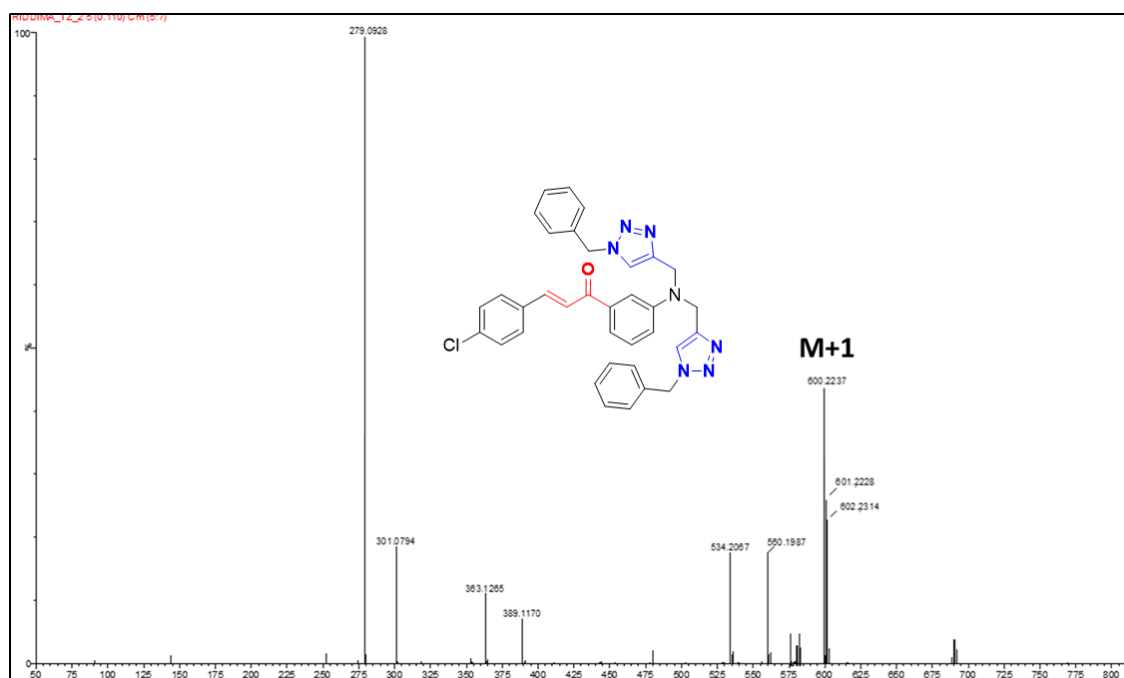
Mass spectrum of 1,2,3-triazole 158
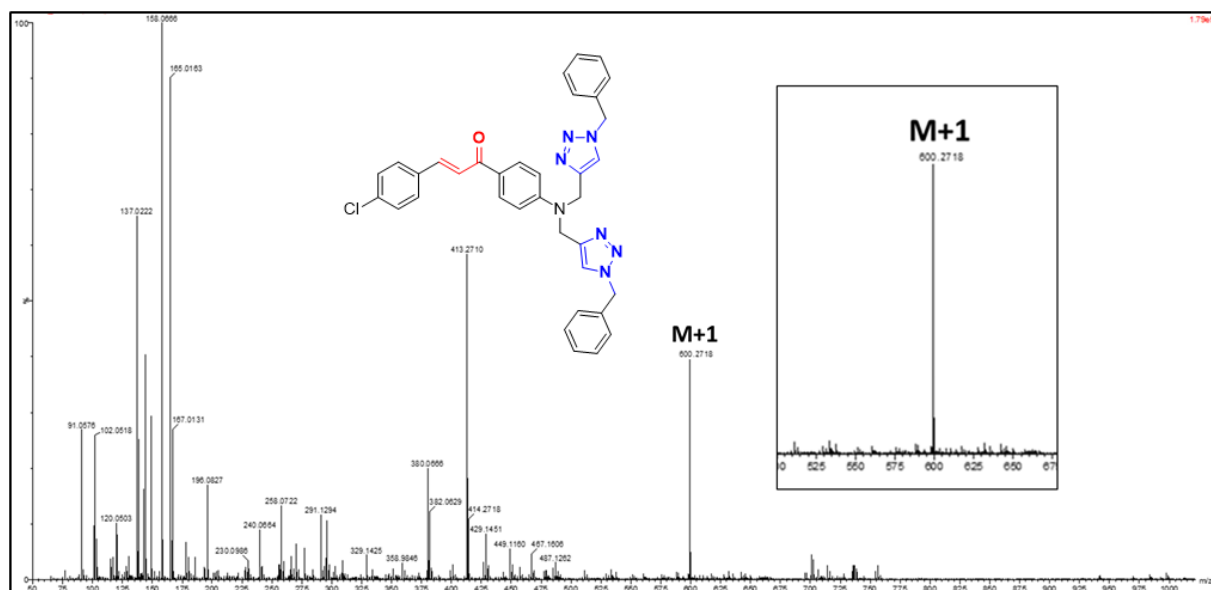
List of Publications

Singh, R.; Singh, G.; George, N.; Singh, G.; Gupta, S.; Singh, H.; Kaur, G.; Singh, J. Copper-Based Metal–Organic Frameworks (MOFs) as an Emerging Catalytic Framework for Click Chemistry. *Catalysts,* **2023**, *13*, 130–159.

R Singh, G Singh, N George, G Singh, A Devi, H Singh, G Kaur, J Singh.; Cu (i)-catalysed 1, 2, 3-triazole stitched chalcomer assembly as Pb (ii) and Cu (ii) ion sensor: DFT and docking scrutiny. *RSC advances,* **2023**, 13 (46), 32399-32412.

R Singh, G Singh, N George, G Singh, P Malik, H Singh, G Kaur, J Singh.; Unveiling the ion sensing capabailities of 'click' derived chalcone-tailored 1,2,3-triazolic isomers for Pb(ii) and Cu(ii) ions: DFT analysis. *RSC advances,* **2024,** 14 (22), 15374-15390.

R. Singh, G. Singh, N. George, G. Singh, A. Dalal, H. Singh, G. Kaur, J. Singh, Chalcone-ensembled 1,2,3-triazole via click chemistry: Selective 'Turn-On' detection of Cu(II) ions via photoinduced electron transfer in real water samples and computational analysis, *Journal of Molecular Structure,* **2025,** 1325, 140921.

R. Singh, G. Singh, N. George, H. Singh, G. Kaur, and J. Singh, in Click Chemistry in Polymer Science Designs to Applications, ed. N. K. Singha, P. Mondal, and R. Hoogenboom, Royal Society of Chemistry, 2024, vol. 39, ch. 16, pp. 428-450.

Singh, G.; **Singh, R.;** Singh, H.; Singh, J. Hydrogels Using Click Chemistry. In Click Chemistry Volume 1: Fundamentals and Synthesis, Gupta, R. K., Ed.; CRC Press: Boca Raton, **2024;** Vol. 1, pp 227-253.

Mehak; Singh, G.; **Singh, R**.; Singh, G.; J Stanzin; Kaur, G.; Kaur, G.; Singh, H.; Singh, J. Clicking in harmony: exploring the bio-orthogonal overlap in click chemistry, *RSC advances,* **2024**, 14 (11), 7383-7413

Singh, G.; Lal, B,; **Singh, R**.; George, N.; Singh, G.; Diksha; Kaur, G.; Singh, H.; Tittal, R,; Kaur, G.; Singh, J., Ampyrone appended 1,2,3-triazole as selective fluorescent Cu(II) ion sensor: DFT and docking findings, *Spectrochimica Acta Part A: Molecular and Biomolecular Spectroscopy,* 302, **2023**, 123163.

Singh, G.; **Singh, R.**; George, N.; Singh, G.; Sushma; Kaur, G.; Kaur, G.; Singh, H.; Singh, J. 'Click'-Synthesized PET Based Fluorescent Sensor for Hg(II), Pb(II) and Cr(III) Recognition: DFT and Docking Studies. *J Photochem Photobiol A Chem* **2023**, *441*, 114741.

Singh, G.; **Singh, R.**; George, N.; Singh, G.; Satija, P.; Kaur, G.; Singh, H.; Singh, J. Selective Recognition of Pb(II) and Cr(III) by Novel Maleic Hydrazide-Based 1,2,3-Triazole Linked Derivatives. *J Mol Struct* **2023**, *1277*, 134823.

Singh, G.; George, N.; **Singh, R.**; Singh, G.; Sushma; Kaur, G.; Singh, H.; Singh, J. Ion Recognition by 1,2,3-Triazole Moieties Synthesized via "Click Chemistry." *Appl Organomet. Chem* **2023**, *37*, e6897.

George, N.; Singh, G.; **Singh, R.**; Singh, G.; Anita Devi; Singh, H.; Kaur, G.; Singh, J. Microwave Accelerated Green Approach for Tailored 1,2,3–Triazoles via CuAAC. *Sustain Chem Pharm* **2022**, *30*, 100824.

Singh, G.; George, N.; **Singh, R.**; Singh, G.; Kaur, J. D.; Kaur, G.; Singh, H.; Singh, J. CuAAC-Derived Selective Fluorescent Probe as a Recognition Agent for Pb(II) and Hg(II): DFT and Docking Studies. *ACS Omega* **2022**, *7*, 39159–39168.

Singh, G.; Majeed, A.; **Singh, R.**; George, N.; Singh, G.; Sophia, N.; Singh, H.; Kaur, G.; Singh, J. CuAAC Ensembled 1,2,3-Triazole Linked Nanogels for Targeted Drug Delivery: A Review. *RSC Adv* **2023**, *13*, 2912–2936.

George, N.; Singh, G.; Saini, P.; **Singh, R.**; Singh, G.; Singh, H.; Kaur, G.; Singh, J. Detection of copper in tea and water sample: A click-oriented azomethine-based 1,2,3-triazole fluorescent chemosensor with reversible INHIBIT logic gate behavior and computational aspects, *J Mol Struct*, 1311, **2024**, 138288.

George, N.; Singh, G.; **Singh, R.**; Singh, G.; Singh, H.; Kaur, G.; Singh, J. Click Modified Bis-Appended Schiff Base 1,2,3-Triazole Chemosensor for Detection of Pb(II)Ion and Computational Studies. *J Mol Struct* **2023**, *1288*, 135666.

George, N.; Singh, G.; **Singh, R.**; Singh, G.; Sushma; Singh, H.; Kaur, G.; Singh, J. Schiff base functionalized 1,2,3-triazole derivative for Fe(III) ion recognition, as N,O,O-Fe-O,O,N sandwich complex: DFT analysis. *Polyhedron* **2023**, *242*, 116496.

Singh, G; Gupta, S; Kaur, J; Markan, P; Vikas; Yadav, R; Sehgal, R; Singh, J; **Singh, R**. Highly selective Schiff base functionalized silatrane based receptor as Sn(II) ion chemosensor: Synthesis, photophysical, DFT and docking studies. *J Mol Struct* **2023**, *1288*, 135687.

Singh, G.; **Singh, R**.; Singh, H.; Singh, J, Hydrogels Using Click Chemistry, *CRC Press,* 1st edition, **2024, 27.**

List of conference Presentations

1. Paper presented in the **9th HSCA International Conference on Recent Trends in Bio and Material Sciences** held on September 23-24, 2022, organized by the Him Science Congress Association in collaboration with Sardar Patel University, Mandi, Himachal Pradesh, India.

2. Paper presented in the **International Conference in Chemistry – 2024 on Recent advances in applied chemical sciences** held on February 23-24, 2024, organized by the chemistry section, Maulana Azad National Urdu University Hyderabad, India.

3. Poster presented in the **International Conference on Molecules and Materials Technology (MMT-2023)** held on April 21-22, 2023, organized by the Department of Chemistry, National Institute of Technology (NIT) Kurukshetra, Haryana, India.

Workshops

1. Completed one-week workshop in **'Skill development program on sophisticated research instruments'** held from 12th May - 18th May 2023, conducted by H.N.B.G.U Garhwal (Uttrakhand), under the auspices of Department of chemistry, Government of India, under Synergistic Training Program Utilizing Scientific and Technological Infrastructure (STUTI).

2. Completed three-day workshop and hands on training on **'Spectroscopy, Separation, and Surface Characterization Techniques'** held from March 04 – 06, 2024, organized by department of Chemistry and Biochemistry (DCBC), at Thapar Institute of Engineering and Technology (TIET), Patiala, Punjab.

Published papers and Certificates

Copper-Based Metal–Organic Frameworks (MOFs) as an Emerging Catalytic Framework for Click Chemistry

Riddima Singh [1], Gurleen Singh [1], Nancy George [1], Gurjaspreet Singh [2], Sofia Gupta [2], Harminder Singh [1], Gurpreet Kaur [3,*] and Jandeep Singh [1,*]

1. School of Chemical Engineering and Physical Sciences, Lovely Professional University, Phagwara 144411, India
2. Department of Chemistry and Centre of Advanced Studies in Chemistry, Panjab University, Chandigarh 160014, India
3. Department of Chemistry, Gujranwala Guru Nanak Khalsa College, Civil Lines, Ludhiana 141001, India
* Correspondence: chemgurpreet5@gmail.com (G.K.); singhjandeep@gmail.com (J.S.)

Abstract: In the extensive terrain of catalytic procedures for the synthesis of organic molecules, metal–organic frameworks (MOFs) as heterogenous catalysts have been investigated in a variety of chemical processes, including Friedel–Crafts reactions, condensation reactions, oxidations, and coupling reactions, and utilized owing to their specific properties such as high porosity, tuneability, extraordinary catalytic activity, and recyclability. The eminent copper-tailored MOF materials can be exceptionally dynamic and regioselective catalysts for click reactions (1,3-dipolar cycloaddition reaction). Considering the fact that Cu(I)-catalyzed alkyne–azide cycloaddition (CuAAC) reactions can be catalyzed by several other copper catalysts such as Cu (II)-β-cyclodextrin, $Cu(OAc)_2$, $Fe_3O_4@SiO_2$, picolinimidoamide–Cu(II) complex, and Cu(II) porphyrin graphene, the properties of sorption and reusability, as well as the high density of copper-MOFs, open an efficient and robust pathway for regimented catalysis of this reaction. This review provides a comprehensive description and analysis of the relevant literature on the utilization of Cu-MOFs as catalysts for CuAAC 'click' reactions published in the past decade.

Keywords: metal–organic frameworks (MOF); Cu-MOF; catalyst; 1,4-disubstituted 1,2,3-triazole; click chemistry; heterogenous catalysis

1. Introduction

Click chemistry is one of the most robust and versatile methodologies currently known to researchers, capable of synthesizing large complex compounds from relatively smaller moieties [1,2]. Due to its advantageous features and facile pathway of synthesis, the methodology has received significant interest globally. Carolyn R. Bertozzi, Morten Meldal, and K. Barry Sharpless in 2022 were awarded the Nobel Prize in Chemistry for their ground-breaking contribution, which was a big step in advancement. The advent of click chemistry has led to the discovery of nitrogen-rich azole heterocycles, which have been shown to be fascinating compounds with broad potential significantly with their pharmacological [3] and chemosensing [4] properties. 'Click' reactions, specifically Cu(I)-catalyzed cycloaddition involving a terminal alkyne and an organic azide to synthesize 1,4-disubstituted-1,2,3-triazole, have received a large amount of consideration in the fields of material science, polymer science, peptide chemistry [5], and synthetic organic chemistry over the past few decades. However, due to the fact that alkynes are poor 1,3-dipole acceptors, this reaction cannot proceed regioselectively without a suitable catalyst. Significantly, the presence of Cu(I), which forms bonds with terminal alkynes, greatly enhances the pace, selectivity, and overall efficiency of click reactions [6].

The catalysts tailored from transition metals have the potential to act as fabricators in the assemblage of supplementary intricate structures, yielding complex organic structures

Check for updates

Cu(ɪ)-catalysed 1,2,3-triazole stitched chalcomer assembly as Pb(ɪɪ) and Cu(ɪɪ) ion sensor: DFT and docking scrutiny†

Riddima Singh, [a] Gurleen Singh, [a] Nancy George,[a] Gurjaspreet Singh, [b] Anita Devi,[b] Harminder Singh, [a] Gurpreet Kaur*[c] and Jandeep Singh *[a]

Herein, a 1,2,3-triazole derivative (CBT), synthesized using the Copper(ɪ) catalyzed Alkyne Azide Cycloaddition (CuAAC) procedure, based on a chalcone skeleton has been reported, that was implemented as an effective sensor for Pb(ɪɪ) and Cu(ɪɪ) ions. The synthesized CBT was characterized using spectroscopic techniques such as FTIR, NMR (^{1}H and ^{13}C), and mass spectrometry. The sensing behaviour of CBT was analyzed using UV-Vis spectroscopy, demonstrating selective sensing for Pb(ɪɪ) and Cu(ɪɪ) ions, competitively. The correlation plot revealed the detection limit for Pb(ɪɪ) and Cu(ɪɪ) ions to be 100 μM and 110 μM respectively. In addition, DFT simulations and molecular electrostatic potential (MEP) studies scrutinized the binding strategy of the free CBT and its orientation towards the metal ions in the metal–ligand complex. The probe CBT was predicted *via* the online platform Way2drug for its pharmacological properties, investigating the possibility to inhibit early atherosclerosis. CBT was subsequently docked to the TRIB1 protein using AutoDock Vina and demonstrated a high binding affinity with a value of −6.2 kcal mol^{-1}.

1. Introduction

The environmental accumulation of metal ions above the permissible concentrations has led to their substantial upsurge, which has put forward the need to explore efficient and robust research alternatives for their instantaneous detection even in low concentrations. The emphasis on analytical cation detection is due to their well-documented pervasive toxic effects on both the terrestrial as well as aquatic living systems,[1–3] thereby rendering their qualitative as well as quantitative recognition as the need of the hour.[4] Due to the unregulated use of lead *via* mining, smelting, ceramics, paint, automobile exhaust emissions, *etc.*, its accumulation in the environment has undergone an exponential ascent since the latter years of the 'bygone century'.[5] Also, exposure to lead can denature DNA and proteins, is detrimental to bone health, and may result in cell transformation, thereby rendering the cells to become malignant.[6] Copper ions, though involved in biological processes in electron and oxygen transport in the body's soft tissues, can be toxic in higher concentrations where they can interfere with biological functioning by altering essential proteins/enzymes.[7–9] This can pose serious health risks like anaemia, interstitial nephritis, oxidative damage, hypertension, cardiovascular disease, severe neurological disease, *etc.*[10,11] Therefore, the detection of these metal ions above the threshold limit needs immediate attention to address environmental pollution and minimize impacts on biological systems.[12,13] This leads to the importance of metal ion sensors based on organic frameworks for selective recognition.

In this pursuit, *O*-chalcones and N-heterocycles have been potential sensors due to their selective cation binding capabilities.[14] The chalcones have a backbone of unsaturated carbonyl groups with conjugation and have the potential to exhibit chemosensing.[15–17] The combination of these motifs with the 1,2,3-triazole moiety *via* 'Click' (CuAAC) methodology has emerged as the most preferred synthetic route to form chalcone appended 1,4-disubstituted-1,2,3-triazole derivatives.[18] There is an increased demand for these moieties owing to their extensive selectivity for ion detection,[19,20] in addition to their significant biological properties such as antibacterial, antioxidative, antifungal activities *etc.*

The ion detecting property of a fluorescent chemosensor is based on a host–guest relationship, wherein the interaction of the receptor with the analyte induces photophysical changes in the fluorophore which indicates successful ion recognition.[21] Besides, exclusivity of a sensor is attributable to the cavity size, wherein the N-rich 1,2,3-triazole ring helps in the recognition

[a]School of Chemical Engineering and Physical Sciences, Lovely Professional University, Phagwara-144411, Punjab, India. E-mail: singhjandeep@gmail.com

[b]Department of Chemistry and Centre of Advanced Studies in Chemistry, Panjab University, Chandigarh-160014, Punjab, India

[c]Department of Chemistry, Gujranwala Guru Nanak Khalsa College, Civil Lines, Ludhiana-141001, Punjab, India

† Electronic supplementary information (ESI) available. See DOI: https://doi.org/10.1039/d3ra05760g

Unveiling the ion sensing capabailities of 'click' derived chalcone-tailored 1,2,3-triazolic isomers for Pb(II) and Cu(II) ions: DFT analysis†

Riddima Singh, [ID] [a] Gurleen Singh, [ID] [a] Nancy George,[a] Gurjaspreet Singh,[b] Pooja Malik,[b] Harminder Singh, [ID] [a] Gurpreet Kaur*[c] and Jandeep Singh [ID] *[a]

In this study, two novel chalcone-derived 1,2,3-triazole-appended positional isomers (probe **6** and probe **9**) were synthesized *via* the 'CuAAC' (Cu(I) – catalysed alkyne azide cycloaddition) methodology for the purpose of metal ion detection. The synthesized probes underwent characterization utilizing standard spectroscopic methodologies including FTIR, NMR (^{1}H and ^{13}C), and mass spectrometry. Subsequently, the sensing capabilities of these probes were explored using UV-Vis and fluorescence spectroscopy, wherein their selective recognition potential was established for Pb(II) and Cu(II), both of which can pose serious health hazards when prevalent in the environment above permissible limits. Both the probes exhibited fairly low limits of detection (LoD), determined as 5.69 μM and 6.55 μM in the case of probe **6** for Pb(II) and Cu(II) respectively; whereas the probe **9** exhibited an LoD of 5.06 μM and 7.52 μM for Pb(II) and Cu(II), respectively. The job's plot for the probe demonstrates the formation of a 1 : 1 complex between the metal and ligand. Furthermore, the interaction of the free probes with the metal ions in the metal–ligand complex was elucidated through ^{1}H NMR analysis and validated theoretically using Density Functional Theory (DFT) simulations with the B3LYP/6-311G++(d,p) and B3LYP/LANL2DZ basis sets for geometry optimization of the probes and their corresponding metal complexes. These findings offer a reliable approach to Cu(II) and Pb(II) ion detection and can be further used for the potential applications in environmental monitoring and analytical chemistry.

1. Introduction

The toxic heavy metal ions, such as copper (Cu) and lead (Pb), pose significant ecological concerns due to their persistence in the environment and the capacity to accumulate within various ecosystems.[1,2] These metal ions are primarily released into the environment through anthropogenic activities such as industrial processes, mining, and improper waste disposal.[3] Once introduced, they undergo complex biogeochemical cycles and can accumulate in soils, sediments, and aquatic systems, thereby proving challenging as they tend to biomagnify through the food chain, leading to higher concentrations in organisms at higher trophic levels.[4,5] The adverse effects of copper and lead accumulation in living organisms are manifold. Copper, an essential micronutrient at low concentrations, becomes toxic when present in excess, leading to oxidative stress, cellular damage, and disruption of enzyme functions.[6] On the other hand, Lead is a non-essential metal but can still interfere with calcium metabolism, disrupt nerve transmission, impair reproductive and developmental processes, and even at low levels, pose severe neurological risks, especially to children.[7] The ecological and physiological impacts of copper and lead accumulation underscore the critical importance of sensing and monitoring these toxic heavy metal ions in the environment to preserve the health of ecosystems and safeguard living organisms.[8] For this purpose, 1,2,3-triazole-based chemosensors, synthesized *via* 'click chemistry' provide a reliable alternative that is simple to implement and yields accurate findings with high selectivity and sensitivity.[9–11]

Click chemistry constitutes a methodological paradigm within chemical synthesis, characterized by its expeditious and high-yield generation of products.[12] Among its diverse modalities, the Copper(I)-catalyzed Azide–Alkyne Cycloaddition (CuAAC) has emerged as a preeminent avenue for constructing 1,2,3-triazoles.[13] This transformative reaction involves the cyclization of an azide and alkyne moiety, mediated by a copper(I) catalyst, culminating in the regioselective and efficient formation of the 1,2,3-triazole scaffold. The versatility of CuAAC in producing 1,2,3-triazoles has found remarkable applications,

[a]School of Chemical Engineering and Physical Sciences, Lovely Professional University, Phagwara–144411, Punjab, India. E-mail: singhjandeep@gmail.com

[b]Department of Chemistry and Centre of Advanced Studies in Chemistry, Panjab University, Chandigarh–160014, India

[c]Department of Chemistry, Gujranwala Guru Nanak Khalsa College, Civil Lines, Ludhiana–141001, Punjab, India

† Electronic supplementary information (ESI) available. See DOI: https://doi.org/10.1039/d4ra01471e

236

Chalcone-ensembled 1,2,3-triazole via click chemistry: Selective 'Turn-On' detection of Cu(II) ions via photoinduced electron transfer in real water samples and computational analysis

Riddima Singh [a], Gurleen Singh [a], Nancy George [a], Gurjaspreet Singh [b], Anurag Dalal [b], Harminder Singh [a], Gurpreet Kaur [c,*], Jandeep Singh [a,*]

[a] School of Chemical Engineering and Physical Sciences, Lovely Professional University, Phagwara 144411 Punjab, India
[b] Department of Chemistry and Centre of Advanced Studies in Chemistry, Panjab University, Chandigarh 160014, India
[c] Department of Chemistry, Gujranwala Guru Nanak Khalsa College, Civil lines, Ludhiana 141001, Punjab, India

ABSTRACT

A 'Turn-On' fluorescent chalcone based 1,2,3 triazole derivative (BRT) was synthesised using the Copper(I) catalysed alkyne-azide cycloaddition (CuAAC) reaction. The probe BRT was characterized using FTIR, ^{1}H and ^{13}C NMR spectroscopy and mass spectrometry. The ion sensing capabilities of BRT were evaluated through UV–Visible and fluorescence spectroscopy utilizing DMSO/H_2O (9:1) solvent system. The probe demonstrated the exclusive recognition of Cu(II) ions, as evidenced through the substantial hyperchromic shifts in UV–Vis as well as fluorescence spectra, attributed to a photo-induced electron transfer (PET) mechanism. A 1:1 binding ratio between BRT and Cu(II) ions was determined via a Job's plot, and the limit of detection and limit of quantification were calculated to be 1.77 μM and 5.91 μM respectively, from fluorescence spectroscopy. Additionally, the association constant (Ka) was calculated as 1.81×10^3 M^{-1} using the Benesi-Hilderbrand equation. Furthermore, real-time water sample testing validated the practical applicability of the probe for environmental monitoring. DFT was employed to optimize the molecular structures and generate HOMO – LUMO density plots of BRT and its Cu(II) complex.

1. Introduction

The detection and quantification of toxic metal ions in environmental water sources are critical for public health and environmental protection [1,2]. Metal ions, due to their widespread industrial usage and natural occurrence, often find their way into water bodies, posing significant risks when accumulated in excess [3,4]. Among various metal ions, copper (II) ion is of particular concern due to its dual role as both a vital nutrient and a potential toxicant [5,6]. While trace amounts of Cu(II) are essential for biological functions including enzyme activation, iron metabolism, and the formation of connective tissue, its excessive concentrations can lead to severe environmental issues including water contamination via industrial discharges, agricultural runoff, and toxicity to aquatic life through bioaccumulation and biomagnification in the food chain [7–9]. This can result in detrimental effects on aquatic ecosystems, such as impaired growth and reproduction in fish and invertebrates, and can alter the biodiversity and functioning of aquatic environments [10,11]. For humans, excessive Cu (II) intake can cause gastrointestinal distress, liver and kidney damage, and neurological disorders [12]. Furthermore, chronic exposure has been linked to conditions such as Wilson's disease and other copper-related metabolic disorders [13]. Over the past few years, fluorescent chemical probes have gained widespread application in detecting various analytes such as amino acids, metal cations, and anions, due to their simplicity, ease of use, and high sensitivity [14–16]. Therefore, the development of efficient and selective sensors for copper in aqueous environments is of significant interest.

Chalcones, a class of natural or synthetic compounds with a characteristic α,β-unsaturated carbonyl system, have garnered attention for their versatile chemical reactivity and biological activity [17,18]. Their structural framework offers a robust platform for further functionalization, enabling the development of sophisticated chemosensing materials [19,20]. Recently, the click chemistry approach, particularly the CuAAC, has turned out as a powerful tool for synthesizing 1,2,3-triazole

Check for updates

Selective metal ion recognition *via* positional isomers: fluorescent chalcone-1,2,3-triazole hybrids for Co(II) and Cu(II) detection†

Riddima Singh, [a] Gurleen Singh, [a] Nancy George,[b] Gurjaspreet Singh,[c] Pallavi Markan,[c] Harminder Singh, [a] Gurpreet Kaur*[d] and Jandeep Singh *[a]

This study reports the synthesis of three positional isomers (**6a–6c**) of chalcone-tethered 1,2,3-triazoles *via* the Cu(I)-catalyzed alkyne–azide cycloaddition (CuAAC) reaction. The synthesized probes were comprehensively characterized using FTIR, ^{1}H and ^{13}C NMR, and mass spectrometry. Their potential as metal ion sensors was evaluated through UV-vis and fluorescence spectroscopy, revealing high selectivity and sensitivity toward Co(II) and Cu(II) ions. The probes **6a–c** exhibited low limits of detection (LoD): 1.64 μM (Co(II)) and 3.19 μM (Cu(II)) for ortho isomer (**6a**), 2.08 μM (Co(II)) and 2.30 μM (Cu(II)) for meta substituted (**6b**), and 1.81 μM (Co(II)) and 1.17 μM (Cu(II)) for para-substituted (**6c**) 1,2,3-triazole derivatives. Job's plot analysis confirmed a 1:1 metal–ligand complex formation. To further elucidate binding interactions, Density Functional Theory (DFT) calculations were conducted, employing B3LYP/6-31G+(d,p) for free probes and B3LYP/LANL2DZ for their metal complexes. The combined experimental and theoretical results establish a robust and selective sensing platform for Cu(II) and Co(II) detection, with promising applications in environmental monitoring and analytical chemistry.

1. Introduction

The pervasive integration of heavy metals in contemporary industries, coupled with cutting-edge technological advancements, has introduced profound risks that threaten both humans and the environment.[1–3] Notably, cobalt, although necessary in small quantities for the production of vitamin B12 and many enzymatic reactions, can also be very poisonous when present in excessive amounts.[4] Exposure to cobalt in the workplace, which is often found in mining, alloy production, and battery manufacturing sectors, may result in significant health problems. Prolonged exposure to elevated amounts of cobalt may lead to respiratory issues, such as asthma and interstitial

Copper plays a crucial role in several biological processes, such as serving as a cofactor for enzymes engaged in redox reactions, facilitating the creation of connective tissue, and aiding in the manufacture of neurotransmitters.[7,8] Excessive buildup of copper may result in hazardous consequences because it can produce reactive oxygen species *via* Fenton-like processes, leading to oxidative stress and harm to cells.[9,10] Prolonged exposure to elevated quantities of copper may lead to severe health issues, including Wilson's disease.[11] Moreover, the occurrence of acute copper poisoning may result in gastrointestinal discomfort, destruction of red blood cells, renal failure, and potentially fatal consequences.[12] Copper pollution resulting from industrial operations, mining, and agricultural

CHAPTER 16

Photoclick Chemistry in Polymer Science

RIDDIMA SINGH[a], GURLEEN SINGH[a], NANCY GEORGE[a], HARMINDER SINGH[a], GURPREET KAUR[b*] AND JANDEEP SINGH[a*]

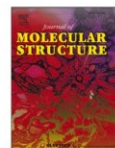[a]School of Chemical Engineering and Physical Sciences, Lovely Professional University, Phagwara–144411, Punjab, India; [b]Department of Chemistry, Gujranwala Guru Nanak Khalsa College, Civil Lines, Ludhiana–141001, Punjab, India
*E-mail: singhjandeep@gmail.com

16.1   Introduction

Sir Karl B. Sharpless and his research group formalized the "click chemistry" paradigm and stated that click reactions are notably modular, simple and quick, and produce significantly high yields,[1] providing stereospecific products and only generating inoffensive byproducts that may be eliminated using non-chromatographic techniques.[2,3] The extensive use of click reactions through metal catalyzed 1,3-dipolar cycloadditions, thiol–ene reactions, Diels–Alder cycloadditions, and Michael additions has attracted considerable global interest in current research, particularly in polymer chemistry, drug discovery, and materials science.[4] The click chemistry concept extends and enhances the existing reaction techniques by focusing on the most efficient reactions, thereby complementing combinatorial chemistry and structure-based design approaches. By selecting the right building blocks, click

ROYAL SOCIETY OF CHEMISTRY

Check for updates

Organosilane based magnetic silica nanoparticles for the detection of Al(III) ions and construction of a molecular logic gate†

Gurjaspreet Singh, ✱[a] Anita Devi,✱[a] Anamika Saini,[a] Diksha,[a] Yamini Thakur,[a] Riddima Singh, [b] Jandeep Singh, [b] Pooja Kalra[c] and Brij Mohan ✱[d]

Here, organosilane based magnetic silica nanoparticles were developed by grafting synthesized organosilane onto the surface of magnetic silica nanoparticles and used as a turn-on fluorescent sensor for Al(III) ions. The resulting nanohybrids $Fe_3O_4@SiO_2@silane$ were characterized using a variety of analytical methods, including FTIR, TGA, EDX, XRD, VSM and SEM. The fluorescence spectra changes revealed that $Fe_3O_4@SiO_2@silane$ is highly selective for Al(III) *via* the photoinduced electron transfer (PET) mechanism. The sensor $Fe_3O_4@SiO_2@silane$ was also capable of specifically sensing 4-nitrophenol (4-NP). The detection limits were determined to be 2.23×10^{-8} M for Al(III) and 1.83×10^{-6} M for 4-NP. Furthermore, the changes in fluorescence exhibited by $Fe_3O_4@SiO_2@silane$ upon the addition of Al(III) and 4-NP serve as the basis for an IMPLICATION-type logic gate. The pharmacokinetic profile of the synthesized compound **3** was examined using MOLINSPIRATION and ADMET software, and the findings were favourable.

1. Introduction

Magnetic materials have gained popularity in recent years due to their broad range of applications, which include data storage, biotechnology, and catalysis.[1–4] In order to produce magnetic materials with desired magnetic characteristics, the assembly of magnetic nanoparticles is often needed. The modification of magnetic nanoparticles (MNPs) has received increased focus in materials science due to their unique capabilites in magnetic targeting, magnetic resonance imaging, chemotherapy, hyperthermia, bioseparation, gene therapy, enzyme immobilization and controlled drug release.[5–8] Iron oxide nanoparticles (IONPs) have received a lot of interest in various biomedical and industrial sectors due to their distinctive physicochemical and magnetic properties.[9] In the biomedical sector, IONPs are being created for enzyme/protein immobilization, cell labelling, DNA detection and tissue engineering.[10–12] Additionally, the silica coating on iron oxide nanoparticles increases their stability and protects them in an acidic environment.[13] Silane is frequently employed to alter and endow the functionalized end groups directly to the surface of bare IONPs for post-connecting with metal ions, polymers, biomolecules or other biological entities.[14–18] Furthermore, as seen in earlier research, 3-aminopropyltriethyloxysilane aided in the preservation of IONP morphology. Silane functionalized magnetic IONPs have recently emerged as a popular and effective approach in biological separation, detection, sensor, and other bio-applications.[19,20]

Modern industrial wastes are primarily high in toxic heavy metal ions, which can cause adverse effects in living organisms.[21] As is well known, Al(III) is the third most abundant metal ion in the earth's crust ($\sim 8.3\%$ by weight) and is widely used in fabrics, medicine, papermaking, food additives, cookware and wrapping paper.[22–24] However, an increased level of Al(III) in the brain can result in conditions like Parkinson's disease, osmotic encephalopathy and Alzheimer's disease.[25–27] According to WHO standards, the daily consumption of Al(III) ions should be less than 3–10 mg, and the maximum Al(III) concentration in drinking water should not exceed 7.41 μM.[28] On the other hand, 4-nitrophenol (4-NP), a nitroaromatic, is commonly used in the production of dyes, pesticides, paper, petroleum, explosives, hair pigment, drugs and other natural pollutants that endanger public safety and health.[29–31] In

[a] *Department of Chemistry & Centre of Advanced Studies, Panjab University, Chandigarh, 160014, India. E-mail: gjpsingh@pu.ac.in, anitadevi0025@gmail.com*
[b] *School of Chemical Engineering and Physical Sciences, Lovely Professional University, Phagwara, 144411, Punjab, India*
[c] *Department of Chemistry and Biochemistry, School of Basic Sciences and Research, Sharda University, Greater Noida, 201306, U.P., India*
[d] *Centro de Química Estrutural, Institute of Molecular Sciences, Instituto Superior Técnico, Universidade de Lisboa, Av. Rovisco Pais, 1049-001 Lisboa, Portugal. E-mail: brizharry17@gmail.com*
† Electronic supplementary information (ESI) available. See DOI: https://doi.org/10.1039/d3nj02095a

REVIEW

Check for updates

Clicking in harmony: exploring the bio-orthogonal overlap in click chemistry

Mehak,†[a] Gurleen Singh, †[a] Riddima Singh, [a] Gurjaspreet Singh,[b] Jigmat Stanzin,[b] Harminder Singh, [a] Gurpreet Kaur*[c] and Jandeep Singh *[a]

In the quest to scrutinize and modify biological systems, the global research community has continued to explore bio-orthogonal click reactions, a set of reactions exclusively targeting non-native molecules within biological systems. These methodologies have brought about a paradigm shift, demonstrating the feasibility of artificial chemical reactions occurring on cellular surfaces, in the cell cytosol, or within the body – an accomplishment challenging to achieve with the majority of conventional chemical reactions. This review delves into the principles of bio-orthogonal click chemistry, contrasting metal-catalyzed and metal-free reactions of bio-orthogonal nature. It comprehensively explores mechanistic details and applications, highlighting the versatility and potential of this methodology in diverse scientific contexts, from cell labelling to biosensing and polymer synthesis. Researchers globally continue to advance this powerful tool for precise and selective manipulation of biomolecules in complex biological systems.

1. Introduction

Biological systems are accompanied by delicate networks of native biomolecules, vital for conventional functioning. For scrutinizing and modifying the biological systems, scientists have introduced a fresh set of reactions, namely bio-orthogonal

[a]School of Chemical Engineering and Physical Sciences, Lovely Professional University, Phagwara-144411, Punjab, India. E-mail: singhjandeep@gmail.com

[b]Department of Chemistry and Centre of Advanced Studies in Chemistry, Panjab University, Chandigarh-160014, India

[c]Department of Chemistry, Gujranwala Guru Nanak Khalsa College, Civil Lines, Ludhiana–141001, Punjab, India

† The authors contributed equally to this work.

click reactions, which exclusively alter non-native target molecules in the biological system, heretofore introduced, making it an ideal reaction for employing *in vitro*.[1–3] Bio-orthogonal chemistry enables the execution of organic synthesis typically conducted in a laboratory within living organisms and cells.[4] In contrast to numerous laboratory reactions, bio-orthogonal reactions are not designed for the bulk production of materials. Rather, their purpose is to covalently modify biomolecules with non-native functional groups under biological conditions, facilitating their examination and manipulation.[5,6] The roots of bio-orthogonal chemistry can be traced way back to the Huisgen 1,3-dipolar cycloaddition of organic azide and terminal alkyne to yield a racemic mixture of 1,4-disubstituted and 1,5-disubstituted 1,2,3-triazoles (Fig. 1).[7] The versatility of this reaction

Check for updates

CuAAC ensembled 1,2,3-triazole linked nanogels for targeted drug delivery: a review

Gurleen Singh,[a] Ather Majeed,[a] Riddima Singh,[a] Nancy George,[a] Gurjaspreet Singh,[b] Sofia Gupta,[b] Harminder Singh, [ID] [a] Gurpreet Kaur*[c] and Jandeep Singh [ID] *[a]

Copper(I) catalyzed alkyne azide cycloaddition (CuAAC), the quintessential example of 'click chemistry', provides an adaptable and adequate platform for the synthesis of nanogels for sustained drug release at targeted sites because of their better biocompatibility. The coupling of drugs, carried out *via* various synthetic routes including CuAAC, into long-chain polymeric forms like nanogels has exhibited considerable assurance in therapeutic advancements and intracellular drug delivery due to the progression of water solubility, evacuation of precocious drug release, and improved upthrust of the pharmacokinetics of the nanogels, thereby rendering them as better and efficient drug carriers. The inefficiency of drug transmission to the target areas due to the resistance of complex biological barriers *in vivo* is a major hurdle that impedes the therapeutic translation of nanogels. This review compiles the data of nanogels synthesized specifically *via* CuAAC 'click' methodology, as scaffolds for targeted drug delivery and their assimilation into nanomedicine. In addition, it elaborates the ability of CuAAC to graft specific moieties and conjugating biomolecules like proteins and growth factors, onto orthogonally functionalized polymer chains with various chemical groups resulting in nanogels that are not only more appealing but also more effective at delivering drugs, thereby enhancing their site-specific target approach and initiating selective therapies.

1. Introduction

In the domains of biomedicine, bio-nanotechnology, and pharmaceutics, polymer-based drug nanocarriers have always been fascinating drug therapies for targeted site-specific drug delivery.[1–3] A wide range of diseases including neurological disorders, cardiovascular diseases, and malignancies can be treated and healed in a better and more efficient manner using polymeric drug delivery systems owing to the targeted and controlled release of therapeutics,[4–6] thereby reducing the side effects of drugs, especially those for cancer which is a major threat to human health after cardiovascular diseases which are the leading cause of human fatality.[7–10] It was reported by the International Agency for Research on Cancer (IARC), in 2018, that there were 18.1 million cancer diagnoses globally, with a projected increase to 29.5 million by 2040.[10] Cancer therapy still has high side effects of anti-cancerous drugs, while damaging the fast-growing cells of the body as well as the tumor sites in adequate immune responses resulting in adverse side effects,[11,12] To tackle such issues, researchers have focused on

the development of nanocarriers to transport the drugs for high intracellular drug delivery.[13,14]

The design and expansion of nanocarriers play a key role in the development of new advanced therapeutic ways as the nanotechnology implied for their synthesis additionally empowers the drugs of concern to enhance their vital properties like solubility and increased concentration at the target site for higher potency and reduced side effects.[15] These desirable traits of drugs in consideration with the stealth behavior of the nanocarriers towards the immune system are being explored for the treatment of many chronic and acute disorders, as the nanoparticles potentially improve the therapeutic index, decrease off-target toxicity, and change the pharmacokinetic profile of pharmaceuticals[16] so that the desirable drug gets incorporated into the body and accumulates at the required site while exhibiting pharmacophoric properties exclusively towards the target cells, known as 'targeted drug delivery'. A variety of nanocarriers have been reported in the literature for applications in targeted drug delivery such as mesoporous nanocarriers, dendrimers, carbon nanotubes, gold nanoparticles, quantum dots, nanogels, *etc.*, and are represented in Fig. 1.[17]

Nanogels have proved to be apt agents for targeted drug delivery due to their high biocompatibility and beneficial dimensions ranging from human organs, and cells to viruses.[18,19] Nanogels essentially are submicron-sized hydrogels

[a]School of Chemical Engineering and Physical Sciences, Lovely Professional University, Phagwara 144411, Punjab, India. E-mail: singhjandeep@gmail.com

[b]Department of Chemistry and Centre of Advanced Studies in Chemistry, Panjab University, Chandigarh 160014, India

[c]Department of Chemistry, Gujranwala Guru Nanak Khalsa College, Civil Lines, Ludhiana 141001, Punjab, India. E-mail: chemgurpreet5@gmail.com

'Click'-synthesized PET based fluorescent sensor for Hg(II), Pb(II) and Cr (III) recognition: DFT and docking studies

Gurleen Singh [a], Riddima Singh [a], Nancy George [a], Gurjaspreet Singh [b], Sushma [c], Gagandeep Kaur [d], Gurpreet Kaur [e], Harminder Singh [a], Jandeep Singh [a,*]

[a] School of Chemical Engineering and Physical Sciences, Lovely Professional University, Phagwara 144411, Punjab, India
[b] Department of Chemistry and Centre of Advanced Studies in Chemistry, Panjab University, Chandigarh 160014, Punjab, India
[c] Chitkara College of Pharmacy, Chitkara University, Punjab 140401, India
[d] Material Application Research Lab. (MARL), Department of Nano Science and Materials, Central University of Jammu, Jammu 181143, Punjab, India
[e] Department of Chemistry, GGN Khalsa College, Civil Lines, Ludhiana 141001, Punjab, India

ABSTRACT

In this study, a novel photoinduced electron transfer (PET) based 1,2,3-triazole appended chemosensor probe (PRT) for the recognition of toxic heavy metal ions has been developed via Cu(I)-catalyzed alkyne-azide cycloaddition (CuAAC), a quintessential example of 'click chemistry' for which the 2022 Nobel prize in chemistry was awarded to Prof. K.B. Sharpless, Prof. M. Meldal and Prof. C. Bertozzi. The synthesized probe was successfully characterized via IR spectroscopy, NMR (^{1}H and ^{13}C) spectroscopy, and mass spectrometry; and additionally demonstrated to selectively sense the highly toxic Hg(II), Pb(II), and the biologically essential Cr(III) ions via absorption and fluorescence spectroscopy. The Job plot of PRT suggested the stoichiometric ratio of 1:1 with the sensed metal ions, whereas the association constant values determined through Benesi-Hildebrand (B-H) equation indicated the strongest binding of PRT with Cr(III) followed by Pb(II) and Hg(II) respectively, even though the competitive metal ion titration revealed the selectivity of PRT for Pb(II) over the other metal ions. The density functional theory (DFT) approach as implemented in the Gaussian 09 package with B3LYP/6-311G++(d, p) and B3LYP/LANL2DZ was used to perform geometry optimization and quantum chemical computations. Above and beyond, PRT was also docked with Interleukin (IL)-6 protein, thereby providing glimpses of its anti-inflammatory potential.

1. Introduction

The notion of environmental contamination, an exponentially augmenting threat to nature as well as all life forms, has grabbed the attention of the global research community due to its distressing state [1–3]. Laying a special emphasis on this contamination factor by the non-biodegradable and persistent entities such as the heavy metal ions, researchers have significantly ventured to resolve this menace via discrete methodologies [4,5]. However, the ever-evolving challenges such as bioaccumulation and the need for real-time analysis consistently require researchers to find contemporary and sturdy courses of action to curb such hazards. Due to the protein binding potential and enzyme inactivation capabilities of heavy metal ions [6,7] resulting in detrimental effects on the vital body metabolic processes [8], their accumulation in the environment is one such problem that has posed a serious threat since the industrial revolution, largely due to their upsurged release as a result of anthropogenic activities like mining, metallurgy, pesticide production, nuclear and thermal power plants, etc. [9]. Out of the various heavy metals, mercury and lead are two of the most pernicious elements having no biological function but capable of earnest subversance [10,11]. Both the elements in their divalent form are reported to cause impairment of several biological functions like enzymatic and redox reactions; and soft tissues such as the brain, kidneys, heart, etc. [12–15] leading to pervasive and irreversible toxic effects. Also, chromium in its trivalent form is essential for the human body to perform multiple functions including glucose metabolism regulation, facilitation of macronutrient metabolism, stimulation of insulin synthesis, etc. However, its overabundance is linked with irritation of the respiratory tract, irritant dermatitis, carcinogenicity, etc. whereas lower levels in the body tend to induce peripheral neuropathy,

* Corresponding author.
E-mail addresses: harminder_env@yahoo.com (H. Singh), singhjandeep@gmail.com (J. Singh).

Detection of copper in tea and water sample: A click-oriented azomethine-based 1,2,3-triazole fluorescent chemosensor with reversible INHIBIT logic gate behavior and computational aspects

Nancy George [a], Parveen Saini [b], Gurleen Singh [a], Riddima Singh [c], Gurjaspreet Singh [c], Pooja Malik [c], Harminder Singh [a], Gurpreet Kaur [d,*], Jandeep Singh [a,*]

[a] School of Chemical Engineering and Physical Sciences, Lovely Professional University, Phagwara 144411, Punjab, India
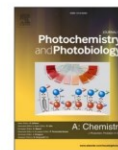[b] Department of Chemistry, Shanti Devi Arya Mahila College, Dinanagar 143531, Punjab, India
[c] Department of Chemistry and Centre of Advanced Studies in Chemistry, Panjab University, Chandigarh 160014, India
[d] Department of Chemistry, Gujranwala Guru Nanak Khalsa College, Civil lines, Ludhiana 141001, Punjab, India

ARTICLE INFO

ABSTRACT

A fluorescent azomethine-scaffolded-1,2,3-triazole linked chemosensor was synthesized utilizing alkyne and azidomethylbenzene via Cu(I)-catalyzed click chemistry. The compounds (3–5 and **L6**) were analyzed using FTIR, ^1H NMR, ^{13}C NMR, and GCMS–. The exploration of ion sensing ability of **L6** complex, using UV–Vis and fluorescence spectroscopy in $ACN:H_2O$ (4:1) medium resulted in detection of Cu(II) ions, exclusively. Further **L6**-Cu(II) complex was characterized via FTIR, FE-SEM, LCMS and supported by DFT studies. A significant structural modification has rendered the current probe as highly selective for Cu^{2+} ions, with 'Turn-On' response. The chemical receptor (**L6**) establishes 1:1 molar ratio with Cu(II) ions with binding constant of 6.0×10^4 M^{-1} and excellent detection limit of 20 nM. In addition, the sensitive reversible behavior of probe (**L6**) with two chemical inputs (Cu^{2+} and EDTA) contributes to the construction of an INHIBIT logic circuit. The Copper ion detection was effectively monitored for real-world samples like Black Tea with precise quantification of Copper(II) ions.

1. Introduction

The ever-evolving field of ion-sensors, serving as selective probes for detection of charged species exemplifies a highly promising domain within applied supramolecular chemistry. Copper remains an indispensable trace element ubiquitously found in cells and organs, critical for cellular respiration, antioxidant defense, connective tissue formation, neurotransmitter biosynthesis, peptide hormone maturation, pigmentation, keratinization, and iron homeostasis [1] Copper ions form integral microelement with occurrence in most oxidases, including cytochrome C and copper oxidase, and aids in the structural integrity and orientation of the enzymes, ensuring appropriate in vivo redox processes [2–4]. However, copper dysregulation in homo-sapiens can develop Menkes, Wilson's diseases and/or lead to neurogenetic disorders such as Alzheimer's, Huntington's, Prion, and Parkinson's syndrome, as well as amyotrophic lateral sclerosis, and metabolic disorders including diabetes mellitus and adiposity. Consequently, copper has been recognized to modulate malignancies that function via renowned oncogenic BRAF mutations and influence tumorigenesis [5–9]. The permissible tolerable limit of copper within a human body is 1.0–1.5 ppm, with recommended dietary intake in adults of 0.9 ppm, set forth by FDA [10]. EPA has established a regulatory threshold, specifically known as the maximum contaminant level goal for copper in potable drinking water at 1.3 ppm [11]. Owing to the pivotal role of Cu^{2+} and its profound impact on metabolic pathways, it is imperative to employ a forthright, selective and highly perceptive approach for the precise quantification and identification of Cu^{2+} in various matrices such as drinking water, industrial settings, environmental contexts, and food samples [12,13].

Despite the precision and sensitivity of atomic absorption spectroscopy (AAS), inductively coupled plasma mass spectrometry (ICP-MS), mass spectroscopy (MS), and time-of-flight mass spectrometry (TOFMS), their utilization requires expensive instrumentation, meticulous sample preparation, and expertise skill [14,15]. Subsequently, fluorescent detection of metal ions is enticing a great deal of attentiveness for applications in optical imaging and analytical sensing owing to their

Detection of copper in tea and water sample: A click-oriented azomethine-based 1,2,3-triazole fluorescent chemosensor with reversible INHIBIT logic gate behavior and computational aspects

Nancy George [a], Parveen Saini [b], Gurleen Singh [a], Riddima Singh [c], Gurjaspreet Singh [c], Pooja Malik [c], Harminder Singh [a], Gurpreet Kaur [d,*], Jandeep Singh [a,*]

[a] School of Chemical Engineering and Physical Sciences, Lovely Professional University, Phagwara 144411, Punjab, India
[b] Department of Chemistry, Shanti Devi Arya Mahila College, Dinanagar 143531, Punjab, India
[c] Department of Chemistry and Centre of Advanced Studies in Chemistry, Panjab University, Chandigarh 160014, India
[d] Department of Chemistry, Gujranwala Guru Nanak Khalsa College, Civil lines, Ludhiana 141001, Punjab, India

ABSTRACT

A fluorescent azomethine-scaffolded-1,2,3-triazole linked chemosensor was synthesized utilizing alkyne and azidomethylbenzene via Cu(I)-catalyzed click chemistry. The compounds (**3–5** and **L6**) were analyzed using FTIR, ^1H NMR, ^{13}C NMR, and GCMS–. The exploration of ion sensing ability of **L6** complex, using UV–Vis and fluorescence spectroscopy in ACN:H_2O (4:1) medium resulted in detection of Cu(II) ions, exclusively. Further **L6**-Cu(II) complex was characterized via FTIR, FE-SEM, LCMS and supported by DFT studies. A significant structural modification has rendered the current probe as highly selective for Cu^{2+} ions, with 'Turn-On' response. The chemical receptor (**L6**) establishes 1:1 molar ratio with Cu(II) ions with binding constant of 6.0×10^4 M^{-1} and excellent detection limit of 20 nM. In addition, the sensitive reversible behavior of probe (**L6**) with two chemical inputs (Cu^{2+} and EDTA) contributes to the construction of an INHIBIT logic circuit. The Copper ion detection was effectively monitored for real-world samples like Black Tea with precise quantification of Copper(II) ions.

1. Introduction

The ever-evolving field of ion-sensors, serving as selective probes for detection of charged species exemplifies a highly promising domain within applied supramolecular chemistry. Copper remains an indispensable trace element ubiquitously found in cells and organs, critical for cellular respiration, antioxidant defense, connective tissue formation, neurotransmitter biosynthesis, peptide hormone maturation, pigmentation, keratinization, and iron homeostasis [1] Copper ions form integral microelement with occurrence in most oxidases, including cytochrome C and copper oxidase, and aids in the structural integrity and orientation of the enzymes, ensuring appropriate in vivo redox processes [2–4]. However, copper dysregulation in homo-sapiens can develop Menkes, Wilson's diseases and/or lead to neurogenetic disorders such as Alzheimer's, Huntington's, Prion, and Parkinson's syndrome, as well as amyotrophic lateral sclerosis, and metabolic disorders including diabetes mellitus and adiposity. Consequently, copper has been recognized to modulate malignancies that function via renowned oncogenic BRAF mutations and influence tumorigenesis [5–9]. The permissible tolerable limit of copper within a human body is 1.0–1.5 ppm, with recommended dietary intake in adults of 0.9 ppm, set forth by FDA [10]. EPA has established a regulatory threshold, specifically known as the maximum contaminant level goal for copper in potable drinking water at 1.3 ppm [11]. Owing to the pivotal role of Cu^{2+} and its profound impact on metabolic pathways, it is imperative to employ a forthright, selective and highly perceptive approach for the precise quantification and identification of Cu^{2+} in various matrices such as drinking water, industrial settings, environmental contexts, and food samples [12,13].

Despite the precision and sensitivity of atomic absorption spectroscopy (AAS), inductively coupled plasma mass spectrometry (ICP-MS), mass spectroscopy (MS), and time-of-flight mass spectrometry (TOFMS), their utilization requires expensive instrumentation, meticulous sample preparation, and expertise skill [14,15]. Subsequently, fluorescent detection of metal ions is enticing a great deal of attentiveness for applications in optical imaging and analytical sensing owing to their

* Corresponding authors.
E-mail addresses: chemgurpreet5@gmail.com (G. Kaur), singhjandeep@gmail.com (J. Singh).
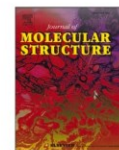
Click modified bis-appended Schiff base 1,2,3-triazole chemosensor for detection of Pb(II)ion and computational studies

Nancy George [a], Gurleen Singh [a], Riddima Singh [a], Gurjaspreet Singh [b], Priyanka [b], Harminder Singh [a], Gurpreet Kaur [c], Jandeep Singh [a],[*]

[a] School of Chemical Engineering and Physical Sciences, Lovely Professional University, Phagwara, Punjab 144411, India
[b] Department of Chemistry and Centre of Advanced Studies in Chemistry, Panjab University, Chandigarh 160014, India
[c] Department of Chemistry, Gujranwala Guru Nanak Khalsa College, Civil lines, Ludhiana, Punjab 141001, India

ARTICLE INFO

ABSTRACT

A novel 1,2,3-triazole linked schiff base chemosensor was stitched via Cu(I) catalyzed click reaction with excellent yield, high selectivity, sensitivity and characterized using fourier transform infrared spectroscopy (FTIR), NMR (^{1}H and ^{13}C), mass spectrometry (MS), CHN analysis, thermal gravimetric analysis (TGA) and differential scanning calorimetry (DSC). The developed chemosensor was investigated for it's optical properties using UV–visible and fluorescent spectroscopy. The detected limit of the synthesized probe was estimated 0.25 μM from fluorescence spectroscopy, which is particularly below the WHO guidelines. The binding stoichiometric (2:1) of ligand was confirmed by the job's plot and the binding constant was determined to be $4.1 \times 10^6 \ M^{-1}$ and $1.4 \times 10^5 \ M^{-1}$ from the B-H plot and the Stern-Volmer curve, respectively. These results establish the developed chemosensor as a potent probe for analytical and practical applications. The optimized geometrical structure of the probe (4) was run on Gaussian 09 program using DFT method with (B3LYP)/6–311G++(d,p) basis set of hybrid density functional theory.

1. Introduction

Metal ion pollution has become a worldwide ecological concern in recent years due to rapid development and increasing industrialization. The pervasive use of lead ions in particular has resulted in massive environmental pollution, posing grave health concern to individuals and biological systems. Petrol, paints, pigments, lead batteries, alloys, ceramics, glass, chemicals, toys, electronics, water pipes, and other consumer items are the most prevalent anthropogenic sources of lead contamination in environmental matrices (water, soil, air, and food). Excessive lead exposure causes a variety of health problems in humans, affecting the kidneys, gastrointestinal, hematological, cardiac, reproductive, and neurological systems. Furthermore, Pb^{2+} is far more dangerous than those other metals since it is a neurotoxin that may accumulate in muscles and bones, causing nervous system damage as well as brain and blood disorders [1–5]. The United States Environmental Protection Agency (USEPA) and the World Health Organization (WHO) have precisely specified permitted concentration limits of Pb^{2+} metal ions in drinking water as 16 ppb (16 μg L^{-1}) and 10 ppb (48 nM),

respectively. Similarly, the US Food and Drug administration had established an action level of 2.5 μM for Pb^{2+} in goods intended for use by newborns and children. As a result, determining and monitoring the level of the lead metal ion is critical to ensure that heavy metal lead concentrations remain below the designated hazardous limit [6–8].

Schiff bases are widely recognized as tunable compounds with an azomethine bond, and they are developing as a prominent class in chemical and medicinal chemistry due to their distinguishing characteristics and diverse biological activities. Schiff bases have been widely explored as flexible ligands for analyte detection, and their facile interactions with metal due to changes in electrical characteristics have been intensively researched [9–13]. Synthetically achievable and structurally versatile, 1,2,3-triazole derivatives are primarily produced via 1,3-dipolar cycloaddition of organic azides and substituted alkynes [10,14]. Recently, Carolyn R. Bertozzia, Morten Meldal, and K. Barry Sharpless were awarded 2022 Nobel Prize in Chemistry for discovering click chemistry, an ecologically benign approach for swiftly combining molecules to produce cancer treatments and generate materials. The potential of the generated 1,2,3-triazole system to behave as a binding
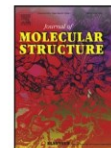
Selective recognition of Pb(II) and Cr(III) by novel maleic hydrazide-based 1,2,3-triazole linked derivatives

Gurleen Singh[a], Riddima Singh[a], Nancy George[a], Gurjaspreet Singh[b], Pinky Satija[c], Gurpreet Kaur[d], Harminder Singh[a,*], Jandeep Singh[a,*]

[a] School of Chemical Engineering and Physical Sciences, Lovely Professional University, Phagwara 144411 Punjab, India
[b] Department of Chemistry and Centre of Advanced Studies in Chemistry, Panjab University, Chandigarh 160014, India
[c] School of Advanced Chemical Sciences, Shoolini University, Solan 173212, India
[d] Department of Chemistry, Gujranwala Guru Nanak Khalsa College, Civil lines, Ludhiana 141001 Punjab, India

A R T I C L E   I N F O

A B S T R A C T

The present report describes the application of versatile and stereospecific Copper(I) catalyzed alkyne-azide cycloaddition (CuAAC) reaction to synthesize two novel maleic hydrazide appended 1,2,3-triazole based chemosensors (**5** and **6**) as selective probes for Pb(II) and Cr(III) recognition. Maleic hydrazide is a plant growth regulator known to prevent cell division. The probes were characterized via IR, NMR (^{1}H and ^{13}C) spectroscopy and mass spectrometry; and subsequently explored for their ion sensing behavior in DMSO as solvent media via UV–Vis spectroscopy. The probe **5** displayed peak at 312 nm accompanied by a smaller peak at 258 nm; whereas the probe 6 exhibited peaks at 274 nm, 284 nm and 294 nm. Furthermore, the association constants for probe **5** were determined to be 0.61×10^5 M^{-1} and 0.20×10^6 M^{-1} for Pb(II) and Cr(III) respectively; and for probe **6** the association constant values for Pb(II) and Cr(III) were 0.46×10^6 M^{-1} and 0.76×10^6 M^{-1} respectively. Structural optimization of both the probes was carried out using DFT with hybrid density functional (B3LYP)/6–311G++(d,p)basis set of theory and LANL2DZ basis set was utilized to optimize the representative **5**+metal complex . Subsequent docking analysis of **5** and **6** was carried out with leukotriene b4 via AutoDock Vina to get perceptions about their potential anti-inflammatory properties, wherein the binding energies of the probes **5** and **6** were observed to be -8.3 and -9.6 kcal/mol respectively.

1. Introduction

Selective recognition of biologically relevant metal ions is of paramount interest among the research community at present owing to their importance in diverse physiological processes and environmental toxicity [1–3]. Transition elements present in living systems in trace amounts and other heavy metal ions, in particular, have received great attention in modern-day research [4–6] due to their involvement and/or interference in various metabolic, enzymatic, and redox reactions taking place in the human body [7,8]. In addition to that, fluctuations in their levels from the prescribed levels lead to health complications [9]. Lead is a significant element that has no known function in the human body but in its divalent form is insidiously toxic, affecting almost every organ and system in the body, with the most affected systems being the central nervous system, cardiovascular system, liver, kidneys and reproductive systems [10–12]. Since the twentieth century has witnessed an exponential increase in the use of leaded gasoline and other lead-based products, therefore environmental accretion of lead [13] has posed a great health hazard. Among trivalent ions, Cr(III) is known to perform an imperative part in certain biotic events viz glycometabolism improvement [14] and carbohydrates, proteins, fats and nucleic acid metabolism [15]. Deficiency of Cr(III) is related to increased risks of cardiovascular diseases and diabetes [16] whereas its overabundance is linked with carcinogenicity [17]. Industrial utilization of metallic chromium is also widespread [18] and hence its improper disposal poses a potential threat of its environmental accumulation and subsequent oxidation to the immensely toxic hexavalent state [19]. Hence, there is a constant need of developing new methodologies for quantitative as well as qualitative recognition of such metal ions. Scheme 1

Imposing advantages over other reported methodologies for ion recognition such as atomic absorption spectroscopy (AAS) and inductively coupled plasma-mass spectrometry (ICPMS) [20–22], development of highly selective and sensitive chemosensors as metal ion recognition ensembles has been immensely explored

Short communication

'Turn On' fluorescent imine linked 1,2,3-triazole based chemosensor for detection of mercuric ions

Nancy George [a], Gurleen Singh [a], Riddima Singh [a], Gurjaspreet Singh [b], Sudha Malik [b], Harminder Singh [a], Gurpreet Kaur [c,*], Jandeep Singh [a,*]

[a] School of Chemical Engineering and Physical Sciences, Lovely Professional University, Phagwara 144411, Punjab, India
[b] Department of Chemistry and Centre of Advanced Studies in Chemistry, Panjab University, Chandigarh 160014, India
[c] Department of Chemistry, Gujranwala Guru Nanak Khalsa College, Civil Lines, Ludhiana 141001, Punjab, India

A B S T R A C T

The exorbitant use or erroneous management of metal ions has been incurred with catastrophic pollution of our ecological system, particularly in soil and water bodies, resulting in significant repercussions. Hence, precise identification and analysis of heavy-metal ions in intricate hydrological environments is imperative. Therefore, an imine conjugated 1,2,3-triazole derivative **VPT** was synthesized, characterized via FTIR, NMR (^{1}H & ^{13}C), LCMS spectroscopic techniques and was employed for the exclusive identification of Hg^{2-} ions in the presence of various other metal ions via UV–Visible and fluorescence spectroscopy. The sensor **VPT** exhibited binding constant (K_a) value of 2.93×10^4 M^{-1} and detection limit value of 0.5×10^{-9} M in the ACN:H$_2$O::4:1 medium. The stoichiometric ratio was determined using Job's plot, which revealed a (1:1) ratio of **VPT** with Hg^{2+} ions. In addition, time-dependent, temperature-dependent, and pH titration studies were conducted via U.V-Visible spectroscopy to expand the sensor's applicability. The viable configurations of probe **VPT** and its 1:1 stoichiometric with Hg^{2-} ion were optimized using the B3LYP/6-311G++(d,p)/LANL2DZ levels of theory in the Gaussian 09 program respectively and this semi-empirical quantum mechanics approach demonstrated a reduction in the energy gap confirming the stable formation of [**VPT**-Hg^{2-}] complex. These insights facilitate the design of fluorescent probe **VPT** for detecting Hg^{2+} in both environmental and biological context.

1. Introduction

Mercury is a relentless bio-accumulative, hazardous metal that possesses distinct physicochemical properties, which are of significant global health concern. The natural and anthropogenic dispersal of Hg continues to pose a substantial risk to both human and environmental well-being [1,2]. Mercury finds extensive application in various sectors such as domestic items (cutlery, culinary pots, skin lotions), the electrical industry (switches, thermostats, and batteries) dentistry (dental amalgams), and numerous industrial processes, including the production of caustic soda, its use in nuclear reactors, as antifungal agents for wood processing, as a solvent for reactive and metallic substances, and as a preservative for pharmaceutical products. However, humans are exposed to several sources of mercury including accidental incidents, environmental pollution, food adulteration, orthodontic treatments, preventative healthcare measures, industrial, agricultural activities, and occupational practices [3]. Therefore, excessive mercury accumulation may cause mental retardation, cognitive impairment, and prolong exposure may accelerate the development of disorders including Parkinson's, Alzheimer's, and multiple sclerosis, subsequently damage the neurological system, respiratory tract, and cardiovascular system [4,5]. The World Health Organization (WHO) has established guidelines for the acceptable levels of Hg^{2+} in drinking water, stipulating that it should not exceed 6 parts per billion (30 nM) [6]. Consequently, developing a method to accurately analyze the qualitative and quantitative aspects of Hg^{2+} metal ions is crucial for studying their role in life activities and timely monitoring their prevalence in the ecological environment [7].

Photophysical mechanism such as Atomic absorption spectroscopy (AAS), Gas chromatography-mass spectrometry (GC–MS), Inductively coupled plasma atomic emission spectroscopy (ICP-AES), and X-ray or laser-induced breakdown spectrometry (LIBS) remain as well recognized, predominant techniques for heavy metal detection [8]. However, the aforementioned procedures tend to incur high costs and lack portability, since they need lengthy measurement durations, substantial sample quantities, and the expertise personnel [9,10]. Alternatively, prevalence of absorbance and emission-based techniques has surged in several fields as these approaches have attained prominence owing to their ease of implementation and their ability to provide ameliorated levels of sensitivity and specificity. Chemosensors have shown

Chapter **11**

Hydrogels Using Click Chemistry

Gurleen Singh, Riddima Singh,
Harminder Singh and Jandeep Singh*

School of Chemical Engineering and Physical Sciences,
Lovely Professional University, Phagwara, Punjab - 144411 (India)

11.1 INTRODUCTION

Hydrogels are three-dimensional, hydrophilic polymer networks composed of polymer chains that are interconnected through crosslinking and can absorb large amounts of water or biological fluids, even retaining them while maintaining their structural integrity. The crosslinking points in the hydrogels create a porous structure that enables the hydrogels to imbibe aqueous solutions, resulting in a swollen state [1]. The presence of water within the hydrogels gives them a gel-like consistency and a high degree of flexibility and elasticity. Due to these unique abilities, they are widely recognized in several fields, including biomedical, pharmaceutical, and materials sciences [2].

The hydrogels can be fine-tuned for specific functions by regulating their chemical composition, crosslinking density, and network architecture. The precursors for hydrogel synthesis include various natural or synthetic polymers, such as polyacrylates, polyacrylamides,

*For Correspondence: Jandeep Singh (singhjandeep@gmail.com)

REVIEW

Applied Organometallic Chemistry   **WILEY**

Ion recognition by 1,2,3-triazole moieties synthesized via "click chemistry"

Gurleen Singh[1] | Nancy George[1] | Riddima Singh[1] |
Gurjaspreet Singh[2] | Sushma[2] | Gurpreet Kaur[3] | Harminder Singh[1] |
Jandeep Singh[1]

[1]School of Chemical Engineering and Physical Sciences, Lovely Professional University, Phagwara, Punjab, India

[2]Department of Chemistry and Centre of Advanced Studies in Chemistry, Panjab University, Chandigarh, India

[3]Department of Chemistry, Gujranwala Guru Nanak Khalsa College, Ludhiana, Punjab, India

Correspondence

Jandeep Singh and Harminder Singh, School of Chemical Engineering and Physical Sciences, Lovely Professional University, Phagwara 144411, Punjab, India.
Email: jandeep.19394@lpu.co.in, singhjandeep@gmail.com and harminder_env@yahoo.com, harminder.singh@lpu.co.in

Funding information

There is no funding for this project.

1,2,3-Triazole-based ligands obtained through copper(I)-catalyzed azide-alkyne cycloaddition (CuAAC) have been exploited in vast array of research domains owing to the stitching of simpler molecules through a needle of Cu(I) catalyst. The numerous reports on ion(s) detection capabilities of synthesized 1,4-disubstituted 1,2,3-triazole ligands using absorption and fluorescence spectroscopy are accessible. This review enlists substituted 1,2,3-triazole-based sensor probes, since 2010, synthesized selectively by CuAAC, having the ability to sense either a single ion or multiple ions under specific set of conditions along with their detection limits. The review also apprehends the different techniques and sensing mechanisms involved in the detection of ions by chemosensor probes.

KEYWORDS

alkyne-azide cycloaddition, chemosensor, fluorescence spectroscopy, ion sensing, UV–Vis spectroscopy

1 | INTRODUCTION

Click chemistry is a vital synthetic tool that facilitates an efficient and relatively simple method for construction of large fragments using smaller molecules. The term "click chemistry" was first coined by Karl Barry Sharpless in 1998, in lieu for the discovery of Cu(I)-catalyzed alkyne-azide cycloaddition (CuAAC) reaction on account of the high efficiency, excellent yields, and regioselective product, with inoffensive by-products.[1] The series of "click reactions," which share common trajectories,[2] include metal-catalyzed azide-alkyne cycloaddition,[3–12] strain-promoted azide-alkyne cycloaddition (SPAAC),[13–15] strain-promoted alkyne-nitrone cycloaddition,[16,17] inverse electron demand Diels–Alder reaction (IEDDA),[18,19] and Staudinger ligation,[20–22] as the most

widely performed and studied reactions. Amidst the aforementioned reactions, CuAAC (categorized under metal-catalyzed azide-alkyne cycloaddition) has been extensively utilized in pursuit of synthesis of wide variety of complexes attributable to its exceptional thermodynamic and kinetic profile,[23] in addition to high functional group tolerance[24] wherein an azide binds irreversibly with an alkynyl group in a highly regioselective manner[25] to give a five-membered 1,4-disubstituted 1,2,3-triazole ring,[26,27] as illustrated in Figure 1. Cu(I) catalyst[28] enhances the reaction rate by almost 10^7 times in comparison with uncatalyzed Huisgen cycloaddition wherein no regioselective control yields 1,4- and 1,5-triazoles in nearly equal proportions.[29–31] Click chemistry has been extensively exploited in drug discovery and delivery,[32–34] photodynamic therapy,[35,36] solid-

CuAAC-Derived Selective Fluorescent Probe as a Recognition Agent for Pb(II) and Hg(II): DFT and Docking Studies

Gurleen Singh, Nancy George, Riddima Singh, Gurjaspreet Singh, Jashan Deep Kaur, Gurpreet Kaur, Harminder Singh,* and Jandeep Singh*

ACCESS | 📊 Metrics & More | 📖 Article Recommendations | 🗂 Supporting Information

ABSTRACT: Copper(I)-catalyzed alkyne−azide cycloaddition (CuAAC) is a resourceful and stereospecific methodology that has considerably yielded promising 1,2,3-triazole-appended "click" scaffolds with the potential for selective metal ion recognition. Based on "click" methodology, this report presents a chemosensor probe (TCT) based on 4-*tert*-butylcatechol architecture, via the CuAAC pathway, as a selective and efficient sensor for Pb(II) and Hg(II) ions, categorized as the most toxic and alarming environmental contaminants among the heavy metal ions. The synthesized probe was successfully characterized by spectroscopy [IR and NMR (^{1}H and ^{13}C)] and mass spectrometry. The chemosensing study performed in acetonitrile/water (4:1) solvent media, via UV−vis and fluorescence spectroscopy, established its selective sensitivity for Pb(II) and Hg(II) species among the list of explored metal ions with the limits of detection being 8.6 and 11 μM, respectively. Additionally, the ^{1}H NMR and IR spectra of the synthesized TCT−metal complex also confirmed the metal−ligand binding. Besides, the effect of time and temperature on the binding ability of TCT with Pb(II) and Hg(II) was also studied via UV−vis spectroscopy. Furthermore, density functional theory studies put forward the structural comprehension of the sensor by availing the hybrid density functional (B3LYP)/6311G++(d,p) basis set of theory which was subsequently utilized for investigating its anti-inflammatory potential by performing docking analysis with human leukotriene b4 protein.
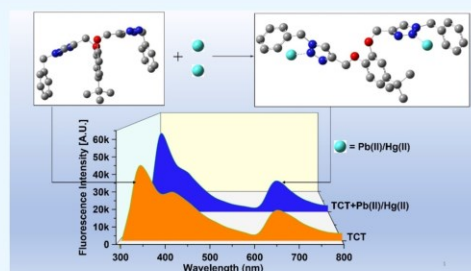
1. INTRODUCTION

The consistent search for efficient and suitable scaffolds for toxic heavy metal ion(s) recognition has been the core idea of ongoing research among the various researchers worldwide owing to their potential deleterious effects on humans and their ecotoxicological presence in the environment.[1−3] The presence of toxic ions such as Pb(II), Hg(II), and so forth above the permissible threshold value can alter the biomolecules mainly via oxidative damage and diminishing of enzymatic activities,[4,5] thereby interfering with the vital processes occurring inside the body to sustain life. Lead has become a ubiquitous heavy metal globally.[6] On accumulation in significant quantities in the soft tissues such as the brain, kidneys, heart, and so forth, it can interact with the physiologically active groups of different proteins and hence incapacitate their biological functions, which result in serious health hazards such as hematological effects (anemia), nephrotoxicity (interstitial nephritis), cardiovascular effects (hypertension), neurological effects (lead encephalopathy), and so forth.[7−11] Mercury in its inorganic form [Hg(II)] is severely toxic to living organisms, and the startling consideration that other forms of mercury are convertible to the insidiously toxic divalent form via "biomethylation" keeps the researchers on their toes for controlling mercury accretion in the environment.[12] Significant concentrations of mercury in the body impairs enzymatic activity and causes mitochondrial dysfunction and increased oxidative stress, thereby resulting in complications such as hypertension, cardiac arrhythmia, coronary heart disease, atherosclerosis, and so forth.[12−16] Therefore, a constant need to confirm the presence of such toxic and non-biodegradable heavy metal ions in the environment becomes indispensable to keep their accumulation in the environment well within the permissible limits.

The archetypal click reaction, that is, CuAAC[17] methodology, provides a well-organized, robust, and efficient pathway to synthesize 1,2,3-triazole-based compounds for addressing the research problem of metal ion toxicity in addition to other sensing devices such as supramolecular polymers.[18−20] The development of new 1,2,3-triazole-linked compounds by
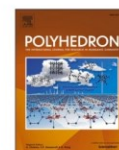
Schiff base functionalized 1,2,3-triazole derivative for Fe(III) ion recognition, as N,O,O-Fe-O,O,N sandwich complex: DFT analysis

Nancy George [a], Gurleen Singh [a], Riddima Singh [a], Gurjaspreet Singh [b], Sushma [c], Harminder Singh [a], Gurpreet Kaur [d,*], Jandeep Singh [a,*]

[a] School of Chemical Engineering and Physical Sciences, Lovely Professional University, Phagwara 144411, Punjab, India
[b] Department of Chemistry and Centre of Advanced Studies in Chemistry, Panjab University, Chandigarh 160014, India
[c] Chitkara College of Pharmacy, Chitkara University, Patiala 140417, Punjab, India
[d] Department of Chemistry, Gujranwala Guru Nanak Khalsa College, Civil Lines, Ludhiana 141001, Punjab, India

ARTICLE INFO

ABSTRACT

The present research aims to synthesize Schiff base tethered 1,2,3-triazole derivative using Cu(I) catalyzed click reaction as a highly sensitive and selective optical chemosensor for the recognition of ferric ions. The synthesized probe was characterized using Fourier transform infrared spectroscopy (FTIR), NMR (^{1}H and ^{13}C), mass spectrometry, CHN analysis, and Thermal gravimetric analysis (TGA). The UV–vis spectroscopy was employed in eco-friendly EtOH:H$_2$O (9:1 v/v) solvent media to investigate the optical properties of the developed chemosensor **SBT**, the association constant and limit of detection of Fe^{3+} was determined to be 2.6×10^4 M^{-1} and 1.3×10^{-7} M establishing the designed **SBT** as a potent probe for analytical and practical applications. Additionally, the time-dependent study and pH sensitivity of the developed probe **SBT** and metal–ligand complex were also studied via UV–visible spectroscopy. Besides, FTIR spectra and TGA curve of the synthesized (**SBT**-metal complex) confirmed the binding of the metal–ligand complex. Furthermore, the real sample application for detection of Fe^{3+} in spinach (food rich in Iron) was analysed, and the **SBT**-based sensing system yielded a recovery rate of greater than 99.07%. The synthesized probe was also explored for its computational-based DFT studies via Gaussian 09 programs using the DFT method with (B3LYP)/-311G (d,p) basis set of hybrid density functional theory.

1. Introduction

Among the most persistent challenges for scientists is to develop extremely sensitive and selective metal-ion responsive chemosensors for the effective tracking of physiologically and ecologically relevant metal ions. Although, Iron is a substantial transition metal that plays a requisite role in oxygen transport in the human body, and subsequently act as a cofactor in the enzymatic activities involved in biochemical reactions [1]. However, excessive deposition of iron in ferritin proteins can cause metabolic imbalance resulting in the disruption of cellular processes, and hinders the biosynthetic activity. Iron in a trivalent state is predominant owing to its capacity to oxidise during aerobic oxidation photosynthesis [2]. But the concomitant accumulation of Fe^{3+} can be fatal to human beings, causing respiration syndrome, convulsions, skin ailments, dysfunction of organs, Parkinson's and Alzheimer's diseases, cardiac arrest and can lead to cancer [3-5]. Meanwhile, the daily requirement of iron uptake in adult male and the female body is 9.1 and

19.6 (mg/d) respectively as recommended by the World Health Organization (WHO) and exceeding these levels can lead to deterioration of human's health if left untreated [2,6,7]. Therefore, development of versatile, precise and efficient Fe^{3+} ion responsive chemosensor, below the permissible levels, is essential [8-10]. Recently, the development of Fe^{3+} selective sensors feature drawbacks such as turn-off responses and interferences with other metal ions. Additionally, these detectors are structurally intricate and need a tedious multistep chemical synthesis, resulting in excessively expensive costs. Most of the chemosensors reported have the inability to clearly distinguish between Fe^{3+} and Fe^{2+} oxidation states. Subsequently, various oxidation states have distinct features, it is vital to identify one from the other in order to analyse their course of action [11-14].Table 1.Table 2..

'Click chemistry' has allured enormous research attention due to the synthetic simplicity for synthesis of 1,2,3-triazole linkers, that act as binding pockets in diverse applications in chemical biology, agrochemical, dyes, pigments and so forth. The CuAAC Meldal–Sharpless

Microwave accelerated green approach for tailored 1,2,3–triazoles via CuAAC

Nancy George [a], Gurleen Singh [a], Riddima Singh [a], Gurjaspreet Singh [b], Anita Devi [b], Harminder Singh [a], Gurpreet Kaur [c,**], Jandeep Singh [a,*]

[a] School of Chemical Engineering and Physical Sciences, Lovely Professional University, Phagwara, 144411, Punjab, India
[b] Department of Chemistry and Centre of Advanced Studies in Chemistry, Panjab University, Chandigarh, 160014, India
[c] Department of Chemistry, Gujranwala Guru Nanak Khalsa College, Civil Lines, Ludhiana, 141001, Punjab, India

ARTICLE INFO

ABSTRACT

The persistent deterioration of our environmental assets has initiated 'a push' among the scientific community for increased reliance on eco-friendly methodologies minimizing the utilization of hazardous materials. As an outcome, there is a paradigm shift in the synthetic modules of organic reactions from conventional techniques to the parameters of green principles. Therefore, the demand for microwave (μw) tailored reactions has witnessed substantial and exponential growth in the last two decades. In accordance, the employment of green methodology in Cu(I) catalyzed alkyne-azide cycloaddition reaction (CuAAC) for the synthesis of 1,2,3–triazole derivatives have reared fruitful results with the reduction of synthetic time, superior yields without benign solvents. The use of the microwave technique has been amplified with its implementation of a range of green methodologies by contributing to solvent-less, catalyst-free, use of ionic liquids and aqueous medium. This review puts forward the microwave synthesis of 1,2,3–triazoles through Cu(I) mediated click chemistry.

1. Introduction

Heterocyclic compounds have emerged as a special class of compounds owing to their numerous medicinal properties such as DNA-virus inhibitors, anti-hepatotoxic, anti-microbial agents and industrial applications like the synthesis of dyes, cosmetics, weed killers, reprography, antioxidants, and plastics, leading to the advancement in scientific research (Mishra et al., 2021; Dharavath et al., 2020; Ashok et al., 2020a). The stitching of a terminal alkyne with an organic azide in a cycloadditive manner is one of the most extensive techniques for the synthesis of N-heterocycles (Hernández-López et al., 2020; SinghSanchita et al., 2018; M'Hamed, 2015; Kumar et al., 2021). and utilizing this methodology, particularly the 5-membered 1,2,3–triazole linked molecules can be effectively synthesized. Huisgen in the 1960's laid down the path for 1,3 dipolar cycloaddition reaction under uncatalyzed and prolonged thermal conditions giving a mixture of 1,4 and 1,5-disubstituted products. However, the reaction methodology suffered from the serious drawbacks of non-regioselectivity, long reaction time, and poor product yields (Bräse et al., 2005; T.-S. L. and Prusoff, 1978; Singh et al., 2018a; Tiwari et al., 2016; Huisgen, 1963; Huisgen et al., 1967; Kanemasa and Kanai, 2000; Bhuyan et al., 2018; Dheer et al., 2017; Hein and Fokin, 2010).

---

* Corresponding author.
** Corresponding author.
  E-mail addresses: chemgurpreet5@gmail.com (G. Kaur), singhjandeep@gmail.com (J. Singh).

Certificates

मौलाना आज़ाद नेशनल उर्दू यूनिवर्सिटी
MAULANA AZAD NATIONAL URDU UNIVERSITY
(A Central University established by an Act of Parliament in 1998. Accredited with 'A+' Grade by NAAC)

CERTIFICATE
OF PARTICIPATION
This is to certify that

Riddima Singh

School of Chemical Engineering and Physical Sciences, Lovely Professional University,
Phagwara–144411 (Punjab)

has participated in the **International Conference In Chemistry - 2024 on Recent Advances In Applied Chemical Sciences**, organized by the Chemistry Section, School of Sciences, Maulana Azad National Urdu University, Hyderabad, India, on 23-24 February, 2024 and presented paper entitled (Oral/Poster): "Click derived Chalcone based 1,2,3-Triazole Derivative as Metal on Sensor"

Dr. Qasim Ullah
Convener

Prof. Salman Ahmad Khan
Dean, School of Sciences

Under Diamond Jubilee Celebration
International Conference
on
Molecules and Materials Technology (MMT-2023)
21st - 22nd April, 2023

आज़ादी का
अमृत महोत्सव

Certificate of Presentation

This is to certify that Dr./Mr./Ms. RIDDIMA SINGH
of LOVELY PROFESSIONAL UNIVERSITY has Presented POSTER
in International Conference on Molecules and Materials Technology (MMT-2023) organized by, Department of Chemistry National Institute of Technology, Kurukshetra held in 21st - 22nd April, 2023.

Conference Secretary
MMT-2023

Chairman
MMT-2023

CERTIFICATE
OF PARTICIPATION

International Conference on
Recent Trends in Bio and Material Sciences

This certificate is awarded to

Riddima Singh

of Lovely Professional University for **Oral/Poster Presentation** of research paper titled **Synthesis and characterization of anthraquinone based 1,2,3-triazole linker via 'CuAAC' methodology for selective detection of Fe (II) ions** in the International Conference on Recent Trends in Bio and Material Sciences October 10 - 11, 2022 organised by **Him Science Congress Association** at **Sardar Patel University**, Mandi, Himachal Pradesh

Dr. Deepak Pathania
HSCA - President

Dr. Rajesh Kumar Sharma
HSCA - Vice President

Dr. Jagdeep Verma
Conference Chairman

SKILL DEVELOPMENT PROGRAM ON SOPHISTICATED RESEARCH INSTRUMENTS

Under the scheme of
Synergistic Training program Utilizing the Scientific and Technological Infrastructure (**STUTI**) supported by Department of Science and Technology, Government of India.

CERTIFICATE
of Participation

Riddima Singh

This is to certify that ....

has participated in "SKILL DEVELOPMENT PROGRAM ON SHOPHISTICATED RESEARCH INSTRUMENTS from **May 12th** to **18th** , 2023 organized by Department of Chemistry, H.N.B. Garhwal University, Srinagar (Garhwal), Uttarakhand(A Central University) in association with Banasthali Vidyapith, Rajasthan.

Convener
Dr. Bhaskaran
Department of Chemistry
H.N.B. Garhwal University

Chairman
Prof. D. S. Negi
Department of Chemistry
H.N.B. Garhwal University

PMU Coordinator
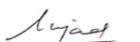Dr. Parvej A.Alvi
Banasthali Vidyapith
Rajasthan

255

CERTIFICATE OF PARTICIPATION

This acknowledges that

RIDDIMA SINGH

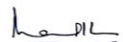from **LOVELY PROFESSIONAL UNIVERSITY, PHAGWARA, JALANDHAR**

has attended DST-PURSE sponsored three-day workshop & hands-on training on *"Spectroscopy, Separation, and Surface Characterization Techniques"*, organized by Department of Chemistry and Biochemistry (DCBC), during March 04-06, 2024 at Thapar Institute of Engineering and Technology (TIET), Patiala, Punjab

Prof. Amjad Ali
Organizer of Workshop
TIET, Patiala, Punjab

Prof. Soumen Basu
Organizer of Workshop
TIET, Patiala, Punjab

Prof. Manmohan Chhiber
Head DCBC
TIETPatiala, Punjab